

University of London
Imperial College of Science, Technology and Medicine
Department of Medicine Division of Surgery, Oncology,
Reproductive Biology and Anaesthetics (SORA)

A THEORETICAL INVESTIGATION
OF THE RADIOBIOLOGICAL
RATIONALE FOR HIGH-LET
RADIOTHERAPY

Alejandro Cárabe Fernández

Submitted in part fulfilment of the requirements for the degree of Doctor of
Philosophy in Radiobiology of the University of London and the Diploma of
Imperial College, October 2007

To my wife, whom I love immensely

Contents

<i>Acknowledgements</i>	<i>vi</i>
<i>Abbreviations</i>	<i>viii</i>
<i>Abstract</i>	<i>ix</i>
1. <i>Introduction</i>	<i>1</i>
2. <i>Radiobiological rationale of high-LET radiotherapy and clinical applications</i>	<i>4</i>
2.1. <i>The RBE concept and its modifying factors</i>	<i>4</i>
2.2. <i>Clinical implementation of RBE</i>	<i>8</i>
2.2.1. <i>The reference RBE</i>	<i>8</i>
2.2.2. <i>The clinical RBE</i>	<i>10</i>
2.3. <i>Non-conventional radiation therapy modalities: rationale, technical aspects and short survey of clinical data</i>	<i>13</i>
2.3.1. <i>Fast Neutron Therapy</i>	<i>13</i>
2.3.2. <i>Proton Therapy</i>	<i>20</i>
2.3.3. <i>Ion Therapy</i>	<i>29</i>
2.4. <i>Summary</i>	<i>36</i>
2.5. <i>Bibliography</i>	<i>40</i>
3. <i>Classical Radiobiology: Principles of the Linear-Quadratic Model</i>	<i>45</i>
3.1. <i>The origins of the Linear-Quadratic model</i>	<i>45</i>
3.2. <i>The BED formulation and its natural evolution with clinical Practice</i>	<i>51</i>
3.2.1. <i>Time factors in fractionated radiotherapy</i>	<i>52</i>
3.2.2. <i>Considerations of fractionation effects in non-conventional Radiotherapy</i>	<i>55</i>
3.3. <i>Summary</i>	<i>58</i>
3.4. <i>Bibliography</i>	<i>60</i>
4. <i>Quantitative and qualitative aspects of radiation: Microdosimetric Considerations</i>	<i>62</i>
4.1. <i>Quantitative and qualitative parameters at a macroscopic scale: Absorbed Dose (D) and Linear Energy Transfer (L)</i>	<i>64</i>
4.1.1. <i>LET distributions</i>	<i>68</i>
4.2. <i>Quantitative and qualitative parameters at a microscopic</i>	

	<i>scale: Classical Microdosimetry.</i>	<i>71</i>
4.3.	<i>Brief introduction to mechanistic models based on microdosimetric magnitudes</i>	<i>76</i>
	4.3.1. <i>The theory of dual radiation action (TDRA).</i>	<i>76</i>
	4.3.2. <i>The kinetic-microdosimetric model.</i>	<i>81</i>
	4.3.3. <i>The Local Effect Model (LEM).</i>	<i>87</i>
4.4.	<i>Summary</i>	<i>93</i>
4.5.	<i>Bibliography</i>	<i>95</i>
5.	<i>Time and dose fractionation effects in non-conventional Radiotherapy</i>	<i>98</i>
	5.1. <i>Revision of time-dose relationships in non-standard radiotherapy</i>	<i>98</i>
	5.2. <i>Development of the theory supporting the evidences to prove the working hypothesis</i>	<i>111</i>
	5.3. <i>Example of the derivation of RBE_{max} and RBE_{min} from fractionated data on mouse oesophagus exposed to neutrons</i>	<i>116</i>
	5.4. <i>Repercussions of the present theory on RBE calculations at clinically relevant fraction sizes in non-conventional radiotherapy</i>	<i>118</i>
	5.5. <i>Potential problems that may rise from the proposed method of analysis.</i>	<i>122</i>
	5.6. <i>Bibliography</i>	<i>129</i>
6.	<i>Results and conclusions relevant to Chapter 5</i>	<i>132</i>
	6.1. <i>Neutron data</i>	<i>134</i>
	6.1.1. <i>Early reactions on pig skin from exposure to neutrons. . .</i>	<i>134</i>
	6.1.2. <i>Early skin reaction on the feet of mice</i>	<i>137</i>
	6.1.3. <i>Mouse small intestine</i>	<i>140</i>
	6.1.4. <i>Mice jejunal mucosa</i>	<i>144</i>
	6.1.5. <i>Mice central nervous system</i>	<i>147</i>
	6.1.6. <i>Radiation pneumonitis mice lung</i>	<i>150</i>
	6.1.7. <i>Lung damage in mice as measured from increased breathing rate and lethality</i>	<i>155</i>
	6.1.8. <i>Reaction from different normal tissues of pig to neutrons: skin, kidney and lung</i>	<i>162</i>

6.1.8.1.	<i>Effects on epidermis and dermal vascular/connective tissues</i>	162
6.1.8.2.	<i>Effects on cutaneous and subcutaneous tissue.</i>	166
6.1.8.3.	<i>Effects on lung function.</i>	170
6.1.8.4.	<i>Effects on renal function.</i>	174
6.1.8.5.	<i>RBE comparisons for early and late reacting tissues as predicted when considering $RBE_{min}=1$ and $RBE_{min}\neq 1$.</i>	178
6.1.9.	<i>Renal damage in mice.</i>	180
6.1.10.	<i>Colo-rectal injury in mice.</i>	184
6.1.10.1.	<i>RBE curve comparisons between early and late effects for each type of end points</i>	193
6.2.	<i>Heavier Ion data.</i>	195
6.2.1.	<i>Skin reactions on mouse legs.</i>	195
6.2.2.	<i>Tumour growth delay (TGD) versus skin reactions (ASR) on mouse legs.</i>	204
6.2.2.1.	<i>RBE curve comparisons between early (ASR) and late effects (TGD) for each LET value.</i>	216
6.2.3.	<i>Survival of intestinal crypt cells.</i>	217
6.3.	<i>Tabulated data of calculated (α/β) ratios, BED, RBE_{max}, RBE_{min} and ΔRBE_{2Gy}.</i>	223
6.3.1.	<i>Neutrons.</i>	223
6.3.1.1.	<i>Analysis of the variation of RBE_{max} and RBE_{min} with (α/β).</i>	225
6.3.1.1.1.	<i>Early reactions.</i>	225
6.3.1.1.2.	<i>Late reactions.</i>	226
6.3.1.2.	<i>Analysis of the variation of ΔRBE_{2Gy} with (α/β)</i>	227
6.3.2.	<i>Carbon Ions.</i>	228
6.3.2.1.	<i>Analysis of variation of RBE_{max} and RBE_{min} with LET.</i>	230
6.3.2.1.1.	<i>Normal Tissues.</i>	230
6.3.2.1.2.	<i>Tumour tissues.</i>	232
6.3.2.2.	<i>Analysis of variation of ΔRBE_{2Gy} with LET.</i>	233

6.4.	<i>Analysis of threshold doses where the therapeutic index changes when considering $RBE_{min}=1$ and $RBE_{min}\neq 1$.</i>	235
6.4.1.	<i>Neutrons.</i>	235
6.4.2.	<i>Carbon ions.</i>	236
6.5.	<i>Statistical analysis.</i>	236
6.5.1.	<i>Neutros.</i>	237
6.5.2.	<i>Carbon ions.</i>	238
6.6.	<i>Conclusions.</i>	239
6.7.	<i>Bibliography.</i>	241
7.	<i>High-LET repair kinetics: predictions from standard repair models</i>	243
7.1.	<i>General revision of standard repair models.</i>	243
7.2.	<i>The reciprocal repair (RR) model: model revision and preliminary analysis</i>	249
7.2.1.	<i>Theoretical considerations relating to the Reciprocal Repair model</i>	251
7.3.	<i>Bibliography.</i>	260
8.	<i>Extension of the Reciprocal Repair Model to high-LET radiations.</i>	263
8.1.	<i>General Considerations.</i>	263
8.1.1.	<i>Single Strand Breaks production and repair for high-LET radiations.</i>	263
8.1.2.	<i>Double Strand Breaks production and repair for high-LET radiations.</i>	267
8.2.	<i>Assumptions and working hypotheses of the proposed repair model for high-LET radiations</i>	284
8.3.	<i>Generalisation of the Reciprocal Repair Model to all LET.</i>	287
8.3.1.	<i>Experimental analysis of δ</i>	289
8.3.2.	<i>Theoretical analysis of δ</i>	292
8.4.	<i>Bibliography.</i>	303
9.	<i>Results and conclusions relevant to Chapter 8</i>	310
9.1.	<i>Neutron data.</i>	312
9.1.1.	<i>Repair of mouse cells exposed to gamma rays and neutrons.</i>	312
9.2.	<i>Heavier ion data.</i>	317

9.2.1. Induced chromosomal damage by X-rays and Neon ions	317
9.2.2. Induced chromatin damage in human cells irradiated with accelerated carbon ions.	320
9.2.3. Rejoining of DNA fragments produced by radiations of different linear energy transfer.	324
9.2.4. DNA DSB induction and rejoining in V79 cells irradiated with light ions	331
9.3. Analysis of the proportions of unrepaired DNA damage produced by each type of radiation	341
9.4. Statistical analysis.	342
9.5. Conclusions.	343
9.6. Bibliography.	345
10. General discussion and Conclusions	346
10.1. Bibliography.	357
11. The way forward	358
11.1. Bibliography.	362
Appendix A. Derivation of Equation 4.28.	
Appendix B. Solution to the system of differential equations 4.39 and 4.40	
Appendix C. Scientific Papers	
Appendix D. Curriculum Vitae	

Acknowledgements

This project would have never been possible without the enthusiastic support of **The Cyclotron Trust** and more specifically of **Mr Don Grocott**, who has always been extremely helpful and actively involved in helping in the search for the necessary data for our modelling.

I would like to express my profound gratitude to the entire **Department of Radiation Physics and Radiobiology** at the Imperial College Healthcare NHS Trust (London) for their continuous support and sympathy to the very last minute of this project, and most especially to the team of physicist working there as well as to **Miss Elena Antoniou** for her continuous and unconditional help.

I am also extremely grateful to **Professor Bleddyn Jones** who was one of the main promoters of this project and who spent with me countless hours reviewing the fundamentals of that fascinating science called Radiobiology. I sincerely hope this work fulfils his expectations and that it will provide even more opportunities for us to work together in the years to come.

Very special thanks to **Dr John Gueulette** and **Dr Blanche De Coster** for their warm welcome every time I visited them in Brussels, where I had the most enriching conversations on neutron radiobiology and the most delicious oysters I have ever tasted.

I would like to thank also **Professor John W Hopewell** for the interest shown in this work and for his extremely useful comments and ideas relevant to the concept of RBE_{min} .

If there is anyone I feel especially indebted to, it is my parents, **Antonio y Esperanza**, whose effort, diligence and love, shown to me since I was born, has made me the person

I am today. I offer to them this work as a sign of my eternal and profound gratitude for all their effort, patience and loving kindness.

I have left the last acknowledgements to those whom I consider as being the two most important persons in enabling me to carry out the work for this PhD. These are the two people I have felt walking hand in hand with me all along the path of this project, making me feel as a companion and showing their kindness, sympathy and support in moments of darkness and desperation:

Professor Roger G Dale, my supervisor, colleague and friend, whose support and presence I have felt in every minute of this long intellectual journey. His enthusiasm, constructive advice and perseverance provided for me the ideal model for a PhD supervisor.

My wife, Vanessa, whose patience, care and love has allowed me to ‘keep the eye on the ball’, not only for the duration of this project, but since the day we met for the first time. They say that behind a great man there is always a great woman... well, I am not a great man, but I am lucky enough to realise I am married to a great woman.

Abbreviations

<i>IMRT</i>	<i>Intensity Modulated Radiotherapy</i>
<i>IGRT</i>	<i>Image Guided Radiotherapy</i>
<i>3D-CRT</i>	<i>3D – Conformal Radiotherapy</i>
<i>TCP</i>	<i>Tumour Control Probability</i>
<i>NTCP</i>	<i>Normal Tissue Complication Probability</i>
<i>MLC</i>	<i>Multi-leaf collimator</i>
<i>NIRS</i>	<i>National Institute of Radiobiological Sciences (Japan)</i>
<i>GSI</i>	<i>Gesellschaft für Schwerionenforschung (Germany)</i>
<i>LQ</i>	<i>Linear quadratic model</i>
<i>BED</i>	<i>Biologically Effective Dose</i>
<i>ERD</i>	<i>Extrapolated Response Dose</i>
<i>ETD</i>	<i>Extrapolated Total Dose</i>
<i>Fe</i>	<i>Fractionation Effect equation</i>
<i>RBE</i>	<i>Relative Biologically Effectiveness</i>
<i>RBE_{max}</i>	<i>Maximum RBE at infinitesimally small doses</i>
<i>RBE_{min}</i>	<i>Minimum RBE at infinitely large doses</i>
<i>LET</i>	<i>Linear Energy Transfer</i>
<i>ICRP</i>	<i>International Commission on Radiological Protection</i>
<i>ICRU</i>	<i>International Commission on Radiation Units and Measurements</i>
<i>MK</i>	<i>Microdosimetric-Kinetic model</i>
<i>LEM</i>	<i>Local Effect model</i>
<i>NSD</i>	<i>Nominal Standard Dose</i>
<i>RMR</i>	<i>Repair Miss-Repair model</i>
<i>LPL</i>	<i>Lethal-Potentially Lethal model</i>
<i>RR</i>	<i>Reciprocal Repair model</i>
<i>IR</i>	<i>Incomplete Repair</i>
<i>TDRA</i>	<i>Theory of Dual Radiation Action</i>
<i>AIC</i>	<i>Akaike's Information Criteria</i>
<i>SSB</i>	<i>Single Strand Break</i>
<i>DSB</i>	<i>Double Strand Break</i>
<i>DNA</i>	<i>Deoxyribonucleic Acid</i>

Abstract

The growing interest in the use of high-LET radiations for cancer therapy, now becoming more readily available as technology becomes cheaper, means that it is necessary to review the principles of conventional clinical radiobiology and to re-interpret and extend them so they are applicable to alternative and less conventionally used types of radiations. Current formulations of the Linear–Quadratic (LQ) model of dose-effect assume that, due to the quasi-exponential survival curves obtained from experiments with high-LET radiations, fractionation effects are quite marginal in high-LET radiotherapy and therefore allow simpler treatment regimes, with a general trend towards the use of hypo-fractionation. However, by comparison with clinical data, it has been observed that, at large doses per fraction, the neglect of accumulation of sublethal damage effects can potentially result in an over- or under estimation of the Relative Biological Effectiveness (RBE) value. In this thesis an extension of the current LQ formulation for high-LET radiotherapy is proposed whereby a new parameter, the asymptotic minimum RBE at high dose per fraction (RBE_{\min}), is introduced to take account of the possible effects produced by accumulation of the sublethal damage created by high-LET radiations. This effect may be expressed in terms of the Biologically Effective Dose (BED) as:

$$BED_H = n_H d_H \left(RBE_{\max} + RBE_{\min}^2 \frac{d_H}{(\alpha/\beta)_L} \right)$$

where $RBE_{\min} = \sqrt{\beta_H/\beta_L}$ and β_H and β_L are the respective high- and low-LET quadratic radiosensitivity coefficients. According to the new formulation, the total dose required to produce a high-LET treatment which is isoeffective to a conventional (low-LET) treatment could be wrongly predicted if RBE_{\min} is assumed to be 1 (i.e. $\beta_H = \beta_L$). To further quantify this effect, an existing model of RBE was extended to study the variation of RBE with changing dose per fraction when sublethal damage is either

considered to be negligible ($RBE_{\min} = 1$), or sufficiently prominent to affect the dose per fraction ($RBE_{\min} \neq 1$). The associated relationship is:

$$RBE = 0.5 \cdot \frac{(\alpha/\beta)_L RBE_{\max} + \sqrt{(\alpha/\beta)_L^2 RBE_{\max}^2 + 4d_L RBE_{\min}^2 ((\alpha/\beta)_L + d_L)}}{(\alpha/\beta)_L + d_L}$$

This model has been tested on neutron data assuming $RBE_{\min} = 1$ and $RBE_{\min} \neq 1$, and a simple statistical analysis (t-test, $p_{\text{two-tailed}} < 0.05$) reveals that 56% of the investigated cases for early reacting tissue and 86% of the cases for late reacting tissues show a better fit to the data when $RBE_{\min} \neq 1$. Similarly, carbon ion data has also been examined and, in this case, 100% of the datasets used are better fitted when values of $RBE_{\min} \neq 1$ are assumed. Although the amount of available data is limited, the results are sufficiently encouraging to suggest extending the study to other tissues and to a wider range of laboratory conditions in order to more accurately gauge the validity of the proposed formulation.

As one of the main factors determining the design of fractionation regimes (and which in turn will influence the overall RBE of a given radiation type) is the inter-fractional repair time, a novel repair kinetic model based on second order repair is proposed for application in fractionation design for high-LET radiations. Within this model formulation, the number of undamaged targets at time t [$n(t)$] from an initial population of N_0 targets, is expressed as:

$$\frac{n(t)}{N_0} - \frac{\delta}{N_0} = \frac{1 - \frac{\delta}{N_0}}{zt + 1}$$

where the repair half-time is expressed as $1/z$ and is related to the fraction of unreparable damage (δ) produced by the particular high-LET radiation in question. The proportion of unreparable damage predicted by the model can be readily obtained, and a good correlation is observed between the changing proportion of unreparable damage and the production of complex Double Strand DNA Breaks (DSB) with changing LET. This implies that some of the current formulations used for calculating BED, and which

are based on first order repair kinetics, may need to be reconsidered. A comparison between three different repair models (mono-exponential, bi-exponential and the model proposed here) reveals that the new model provides a better fit to the data than the mono-exponential repair model, but is not as close as the bi-exponential model. However, the bi-exponential model requires a larger number of assumed parameter values and that makes it more impractical to use at the clinical level. That could justify the adoption of the new repair model as the best practical alternative to the currently used mono-exponential model.

The thesis concludes by discussing the potential implications of the above findings in the future design and analysis of high-LET treatment schedules and suggests some further work.

Introduction

The *precise* delivery of dose has always been the main driver of technological advances in radiotherapy. While radiotherapy treatments a century ago involved single doses of low-energy X-rays in single fields, current delivery techniques involve sophisticated mechanisms that allow to convolving the dose to the treatment volume with less than 3-5% uncertainty. Intensity modulated (IMRT) and image guided (IGRT) radiotherapy are good examples of three-dimensional conformal radiotherapy (3D-CRT). While these techniques allow a very high level of normal tissue sparing, there is still a ‘dose bath’ to large volumes outside the target region which might be considered a disadvantage. More ‘exotic’ techniques use alternative types of radiation characterised by dose depth curves with a Bragg peak, which allow the deposition of very high doses in the tumour while maintaining a high level of normal tissue sparing due to the lower entrance dose and sharp dose cut-off beyond the tumour, and also to the small number of beams involved in the treatment.

The therapeutic effectiveness of a specific type of treatment is normally represented in terms of the difference between the Tumour Control Probability (TCP) and the Normal Tissue Complication Probability (NTCP). The process of treatment optimization consists of using all the necessary means to increase the therapeutic gain of the treatment by increasing TCP and/or decreasing NTCP. There are several different ways of doing this, but all involve physical means and/or biological means. Physical means of treatment optimization encompass those techniques where the dose is deposited in the treatment volume using physical restrictors (e.g. MLCs). The use of these techniques in conjunction with Monte Carlo simulations of radiation transport can have a high impact on the therapeutic gain of the treatment.

Alternatively to the optimization of the treatment by physical means, the difference between TCP and NTCP can be increased by considering the different radiobiological properties of the tissues involved in the treatment field. Radiobiology is the science of the response of living systems to radiation and seeks to establish laws of behaviour under different macroscopic and microscopic environmental conditions. These laws are expressed in the form of models that include both fundamental and user-controllable parameters, the latter of which can be adjusted in order to predict the optimal situations in which the therapeutic gain of a treatment can be maximised.

The ideal source of radiation would be one that combines both of the ways of treatment optimisation techniques mentioned above, and this is the case with certain high-LET radiations, e.g. fast neutrons, protons and carbon ions. Fast neutrons are a source of high-LET radiation that have been used for more than 40 years and neutron therapy is still in use in a number of centres around the world for tumours with poor prognosis to conventional radiotherapy. Proton and carbon ions are relatively new techniques currently gathering a strong momentum as the technology involved to produce them becomes cheaper. The amount of pre-treatment experimental work with neutrons to characterise their radiobiological properties was very extensive and allowed the establishment of clinically relevant values of important radiobiological parameters, in particular their relative biological effectiveness (RBE) with respect to photons. A great deal of effort was devoted in the UK, the pioneer country in the use of high-LET particles to treat cancer, to obtain experimental values of RBE for different tissues (normal and tumour) in order to convert clinical doses of photons into “equivalent” doses of neutrons.

Experimental work with protons has been performed in order to establish the RBE applicable to different tissues for proton therapy, as a result of which an overall RBE of 1.1 has been accepted by many clinical centres. This implies that the radiobiological properties of photons and protons are broadly similar (causing protons to be considered as low-LET particles with a Bragg peak as the depth dose curve) and that protons represent the ultimate source of radiation for conformal radiotherapy. Radiobiological experiments with carbon ions were also performed prior to their clinical implementation in Japan (NIRS) and Germany (GSI) and these showed that carbon ions have RBE

values much greater than 1. This means that carbon ions have similar radiobiological properties to neutrons but with the conformal advantage of protons.

The available database for radiobiological parameters is fairly extensive for conventional radiotherapy, but it is much more restricted in the case of high-LET particles, with the possible exceptions of neutrons. With the increasing number of high-LET radiotherapy centres being commissioned worldwide, it becomes necessary to construct models that extend the existing radiobiological theory of conventional radiotherapy to the new frontiers of high-LET radiations. This will allow more reliable prediction of the instances in which the use of high-LET radiations is more beneficial for cancer treatment and the correct fractionation to use in each of those instances.

The purpose of this thesis is to provide an extension of the Linear Quadratic dose-effect model to take into account accumulation of sublethal damage effects which, it is suggested, could have a major impact on the design of fractionation regimes with high-LET particles. Similarly, the repair kinetics of such particles are reviewed through a proposed new model which could potentially help to establish the correct inter-fractional time to allow full repair or, alternatively, to correct total treatment doses in order to avoid exceeding normal tissue tolerance.

The thesis can be considered as being in two parts, the first part (chapters 2 to 6) dealing with RBE, its meaning and formulation, and the second part (chapters 7 to 9), dealing with the repair kinetics of high-LET particles. The new models proposed in this thesis are comprehensively explained in chapter 5 (RBE) and chapter 8 (repair kinetics) and start from hypotheses respectively formulated in sections 5.1 and 8.2. In order to assess the validity of both new models, their predictions were analysed using published data obtained from different centres. The results of these analyses are in chapter 6 (RBE) and 9 (repair kinetics). Finally, chapters 10 and 11 respectively assess all of the results and suggest further work which would develop the ideas further. The three chapters which follow this Introduction provide the required theoretical background for the thesis.

Radiobiological rationale of high-LET radiotherapy and clinical applications

The main clinical rationale for high-LET radiotherapy is the higher therapeutic gain of this type of radiation under certain irradiation conditions compared to conventional (low-LET) radiotherapy. Two aspects of this assertion will be dealt with in this chapter: what is understood by therapeutic gain and what are the irradiation conditions under which each type of radiations is most favourable?

2.1. The RBE concept and its modifying factors

The following figure illustrates the difference in dose necessary to produce a given biological effect using different types of radiation (Goodhead, 1987).

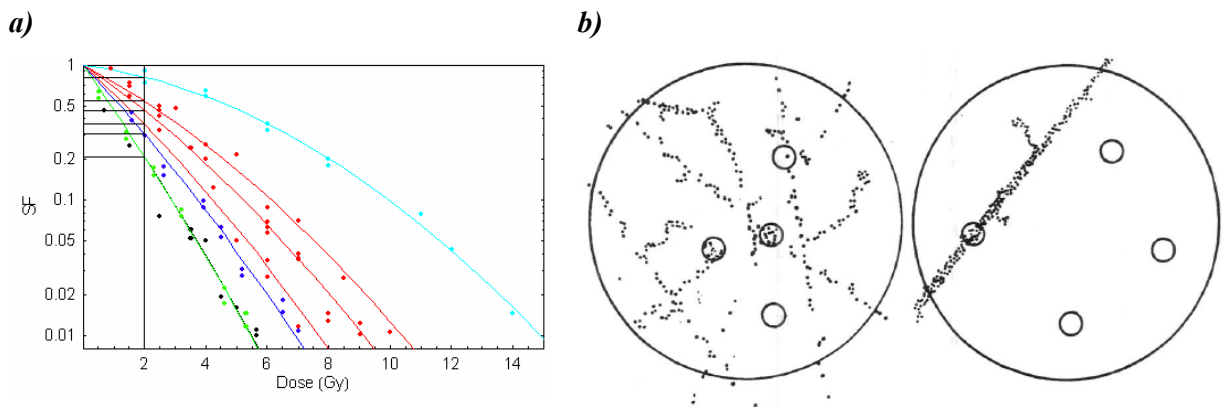


Figure 2.1: (a) Change of survival level (i.e. radiation effectiveness) obtained for the same dose of radiations with different LET. Data by Barendsen et al. (1963); (b) Change in pattern of energy deposition between low- and high-LET radiations (Wambersie et al., 2003).

The differences in survival obtained in Figure 2.1a for the same absorbed dose delivered by different types of radiation suggest different biological effectiveness for each type of radiation. The reason for this change of effectiveness is found at the microscopic level, where the energy is deposited in different patterns for each of these radiations (see Figure 2.1b). These differences in energy distribution at the microscopic level lead to the concept of Relative Biological Effectiveness (RBE). This concept was defined for the first time by the ICRP (1963) and ICRU (1979) as: ‘*A ratio of the absorbed dose of a reference radiation to the absorbed dose of a test radiation to produce the same level of biological effect, other conditions being equal. When two radiations produce an effect that is not of the same extent and/or nature, an RBE cannot be specified*’. More specifically, if ‘A’ is the *test* (high-LET) radiation quality and ‘B’ is the *reference* (low-LET) radiation quality, and if D_A and D_B are the doses necessary to produce the effect of interest with radiation *A* and *B* respectively, then the RBE of radiation *A* relative to radiation *B* is

$$RBE = \frac{D_B}{D_A} \quad (2.1)$$

A more in-detail review of the RBE formulation will be given in Chapter 5, whereas, in this chapter, the more fundamental aspects of RBE and its modifying factors in clinical use are discussed.

According to the way RBE is defined, it is clear that it is a quantity which is derived from experimental data. It is thus subject to an experimental uncertainty that can be reduced by specifying the biological system used in the experiment, the type and level of effect, along with the experimental conditions used. However, there are a number of factors that will strongly affect the value of RBE and these are:

- (i) *Dose per fraction*, because RBE increases with decreasing dose per fraction (see Figure 2.2).

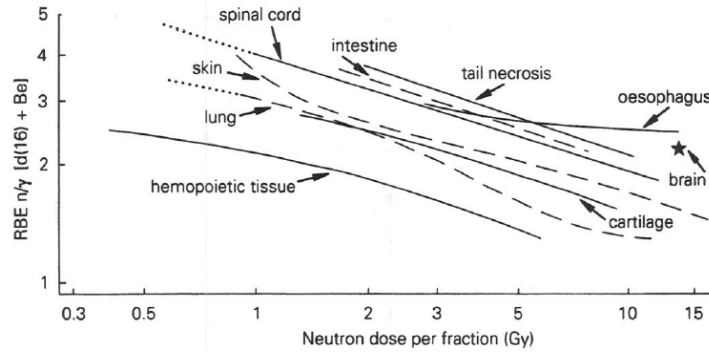


Figure 2.2: RBE changes with doses per fraction. In this figure, RBE has been plotted against neutron dose per fraction; however, it is conventionally believed that RBE changes with dose (and therefore with survival level) due to the shoulder on the survival curve of the reference radiation, and it is for this reason that RBE tend to be more commonly plotted against the reference dose per fraction (Bewley, 1989).

- (ii) *Tissue type*, because RBE values for late effects are significantly higher than for early effects (see Chapter 6).
- (iii) *Particle energy*, because, as can be seen in the following plot, this variation is quite noticeable in the case of neutrons (see Figure 2.3).

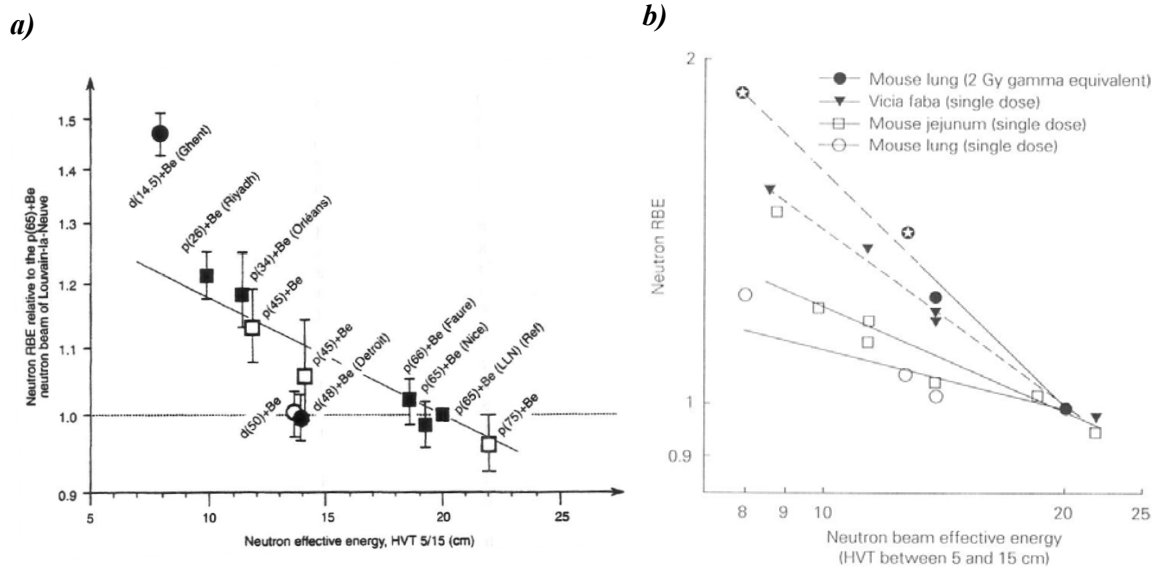


Figure 2.3: (a) RBE is lower for neutrons with higher energy (Wambersie, 1999); (b) Variation of neutron RBE as a function of neutron beam effective energies expressed by their half value thickness for different biological systems and irradiation conditions (Wambersie et al., 1993).

- (iv) *Particle LET*, because increased clustering of radiation is known to produce higher radiation lethality. The next figure shows how this effectiveness increases with increasing LET up to a turnover point.

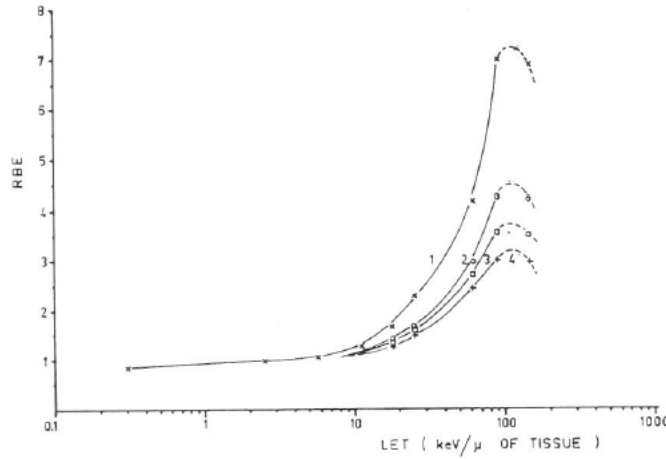


Figure 2.4: Change of RBE with LET (Barendsen, 1968) at different survival levels, i.e. 1 – 80% survival, 2 – 20% survival, and 3 – 5% survival.

- (v) *Cell cycle*, because data for the survival of synchronous populations of mammalian cells exposed to densely ionising particulate radiations show that, for radiations of sufficiently high LET, the differences in radiosensitivity from stage-to-stage in the cell cycle disappear (Sinclair, 1968; Berry *et al.*, 1972). For the fast neutron energies used in experimental radiotherapy, however, the variations in sensitivity through the cell cycle appear to be similar and almost as large in magnitude as the variations in sensitivity to X- and γ -rays (Berry *et al.*, 1972) (see Figure 2.5).

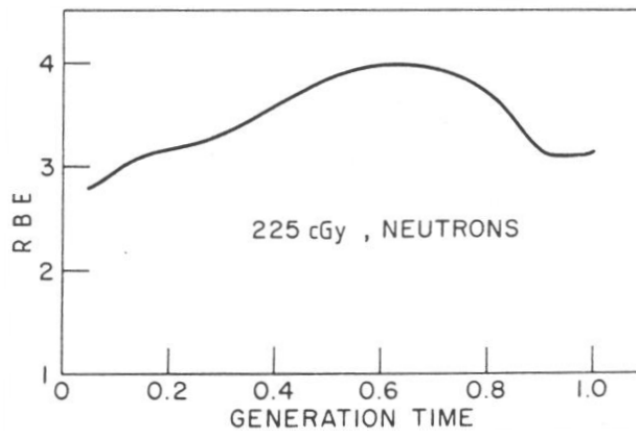


Figure 2.5: Changes of radiosensitivity during cell cycle for different types of radiations (Bewley, 1989).

All the plots used to illustrate the dependence of RBE with the modifying factors mentioned above have been produced using fast neutrons as the RBE variations for this type of particle is significant and well documented. In general, it is observed that RBE increases with decreasing dose per fraction, that RBE values for late effects are usually higher than for early effects, and that they decrease significantly with increasing neutron energy (Gueulette *et al.*, 1997). There have been proposed numerous mechanistic and empirical models with which to predict the effectiveness of any given type of radiation under well-defined irradiation conditions, but the number of parameters required in such models is usually so large that they are of little (if any) help used in clinical practice. For this reason, as we will see in the following section, reliable values of clinical RBE can be only derived at present from experiments and clinical experience.

2.2. Clinical implementation of RBE

When a new type of radiation modality is introduced in therapy, it is necessary to determine its RBE relative to the radiation beams already in use and for which the radiation-oncologist has accumulated clinical experience. The aim of the RBE calculations is of course to help the radiation oncologist to prescribe the right dose with the new type of radiation and these calculations are performed using different biological systems, and different experimental conditions. Different steps, implying different concepts, can be identified between, on the one hand, the radiobiological RBE determinations and, on the other hand, the final selection of what will be called the ‘clinical RBE’ (Wambersie, 1999).

2.2.1. The reference RBE

The variability of RBE with the factors enumerated above makes it very difficult to select a particular value of RBE when comparing the effectiveness of two radiation qualities on a specific biological system (or tissue type). No single RBE value is appropriate to every combination of system, effect and experimental condition. Therefore, if two experiments performed with the same radiation qualities give different RBE values, one needs to ensure that the set up and the experimental conditions on both of them are the same. The difference between the observed RBEs does not necessarily

imply that there is disagreement or that one result is wrong, it could simply reflect the variation of RBE with dose, biological system and biological effect.

The selection of a reference value of RBE for a particular *test* radiation quality (assuming as a general agreement that 250kV X-rays represents the *reference* radiation) will require the specification of a well defined dose at which this reference RBE is measured, the biological system used for this measurement and the exact experimental conditions in which it is measured. These reference conditions should be as representative as possible of the clinical situations in order to allow easy intercomparisons between experimental work and clinical practice.

However, a general and formal agreement does not yet exist on the choice of the radiobiological system for radiobiological intercomparisons. Most of the RBE determinations performed during the pre-therapeutic phase in the case of fast neutrons and protons, or radiobiological experimentation in the case of heavy nuclei (C, He, H, etc...) used biological systems chosen because they were suitable for RBE determination. These systems were well codified, reliable, easy to transport, providing rapidly reproducible results (e.g. mammalian cell *in vitro*, *Vicia faba*, intestinal crypt cell systems, etc...).

Similarly, there is no general agreement on the optimal dose at which to report reference values of RBE. The chosen doses and doses per fraction should normally coincide with those used in clinical protocols established to treat different tissue types. But, as there a variety of dose-fractionation schemes (that also differ among different countries) it is remarkably difficult to set a general reference dose level from which clinical intercomparisons could be made straightforward.

Wambersie (1999) proposed the following conditions to report reference levels of RBE:

- Dose level: 2 Gy (photon equivalent) per fraction.
- Biological system: a system endpoint 'representative' of the RBE average or overall late tolerance of normal tissues.

The *reference* RBE is one possible radiobiological approach since, in principle, there should be only one reference RBE value for a given particle beam. This implies the assumption that a single RBE value can be defined for an ‘overall’ or ‘average’ late tolerance for the normal tissues in patients. The fact that the alpha/beta ratios normally used in the clinic for early and late reactions (respectively 10 and 3Gy) represent average (or reference) values taken from a range of possibilities (Fowler, 1989) supports the practice of selecting average (or reference) values of RBE for late tolerance of normal tissues in patients.

2.2.2. *The clinical RBE*

When a new type of radiation beam for which clinical observations does not yet exist, the reference RBE should logically be taken as a first indication of the likely clinical RBE. Later on, as clinical experience is build up (in particular with dose escalation studies or via comparison of dose-effect curves for tumour control and normal tissue complications), the clinical RBE can be progressively adjusted. The adjustments on the reference RBE to achieve the relevant clinical RBE need to reflect several influences:

- (i) The clinical RBE should take into account the variability of RBE values along the test radiation depth dose curve (except for the case of neutrons not produced by incident protons with no additional polyethylene filtration (Hornsey *et al.*, 1988; Hall, 1989), as for this case the RBE remains constant with depth). At each point of the hadron or particle depth dose curve (i.e. at each depth), a different dose is deposited, and different tissue types may be involved. According to the factors mentioned above which cause RBE to change, the common situation is that, along the depth dose curve of the non-conventional radiation, RBE does not remain the same. As seen in the following figure, for Carbon ions there is a significant variation of RBE with depth with values ranging from 1.2 and 2.0 (Gueulette *et al.*, 2004) or even 3.0 to 5.0 (Weyrather *et al.*, 2004), whereas in the case of protons this variations are much smaller with values ranging between 1.1 and 1.2 (Gueulette *et al.*, 1996; 1997). This small variation of RBE with depth of

proton has supported the general agreement of selecting a fixed RBE of 1.1 when using protons (Paganetti *et al.*, 2002).

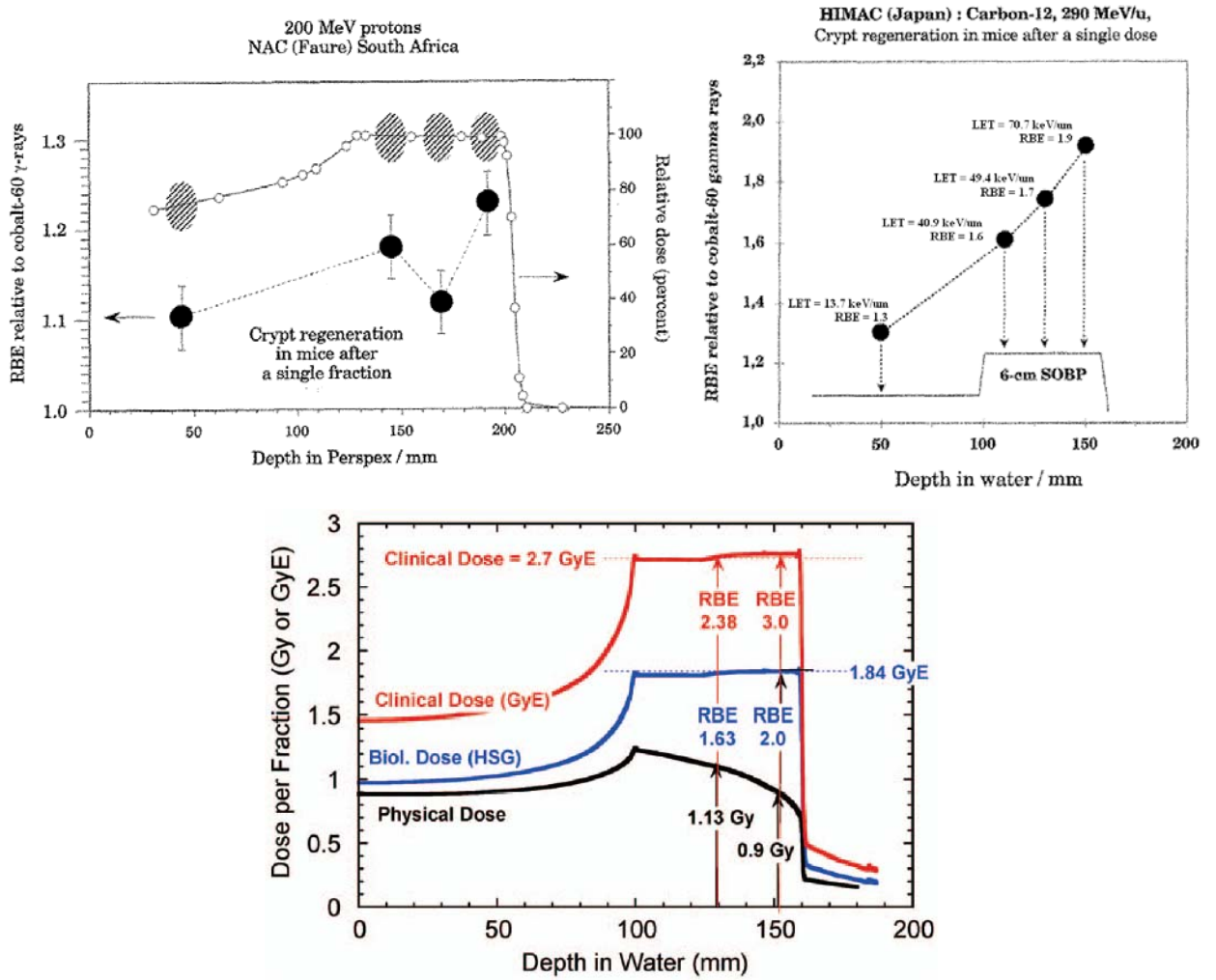


*Figure 2.6: Change of biological effectiveness along the path of a particle beam, for different types of particles: top left, 200MeV protons (Wambersie *et al.*, 1999); top right, 290MeV/u carbon ions (Gueulette *et al.*, 2004); bottom, comparison between absorbed dose, biological dose and clinical dose for human salivary gland (HSG) cells exposed to a carbon ion beam of 290MeV/u (Matsufuji *et al.*, 2007). It is worth to read an in depth explanation of this comparison in a review paper by Gueulette *et al.* (2007).*

The variability of RBE with depth dose in the case of carbon ions has interesting therapeutic implications, especially for tissues which are radioresistant to photons and protons.

Finally, to link this discussion with the ‘overall average RBE’ idea discussed above for the reference RBE value, we can say that this reference value

should incorporate the average of the values of RBE found on the depth dose curve. Then, if the clinical RBE value selected for any specific treatment is obtained from the reference RBE value, it would imply that the clinical RBE will account (to some extent at least) for the variability of the RBE with depth dose.

The physical selectivity¹ of proton and carbon ions is always greater than photons, but this is not always the case with fast neutrons, e.g. the physical selectivity of fast neutrons produced by 16MeV cyclotron or (d+T) generator is significantly inferior to that of photons of any energy and a dose reduction factor must be introduced when prescribing the target dose in order to avoid exceeding the tolerance level of tissues at risk. Alternatively, if increasing the neutron beam energy is an option (as RBE decreases with increasing neutron energy), it might improve the therapeutic ratio and consequentially the clinical potential of the treatment.

- (ii) In the case of fast neutrons, there is a significant gamma contamination of the beam that has to be taken into account when assessing reference RBE values. Similarly, for carbon ions and heavy nuclei, nuclear fractionation tends to extend the depth dose curve of the beam which in turn may affect the value of the reference RBE. In both of these cases, the clinical RBE value selected may include an additive RBE effect of the different radiation components constituting the clinical beam.

- (iii) When a clinical RBE value for a particular type of treatment is taken directly from a different centre, or chosen according to a specific protocol, it is extremely important to ensure that the beam set-up coincides with the original beam where the reference and the clinical RBE were measured. If this is not possible, weighting factors will be required to compensate for differences in the physical selectivity of both beams, different energy spectra, and any other differences in the clinical set-up.

¹ Beams of particles with greater 'physical selectivity' are those that produce a more conformal dose distribution around the planned treatment volume.

In conclusion, the *clinical RBE* is the quantity the radiation oncologist has to make use of when prescribing the treatment and although it is a dose ratio of the two radiation qualities under comparison, it is not in a strict sense the RBE, but the *reference RBE* empirically weighted by:

1. Past personal experience
2. Clinical experience reported from other centres
3. Volume effects related to the beam characteristics, geometry, or technical conditions

Therefore,

$$RBE_{clinical} = W_{RBE} \times RBE_{reference} \quad (2.2)$$

Where W_{RBE} is the RBE weighting factor, the value of which must be ultimately decided by the radiation oncologist in charge of the patient.

2.3. Non-conventional radiation therapy modalities: rationale, technical aspects and short survey of clinical data

2.3.1. Fast Neutron Therapy

Rationale: Historical and Radiological basis

Historically, the *oxygen effect* was the main rationale for introducing fast neutrons in radiotherapy. It was Swartz in Germany who, by 1912, noted that the skin reaction produced in his forearm by radium applicator was reduced if the applicator was pressed hard onto the skin, which he initially attributed to interruption of the blood supply. But it was Mottram in 1935 who realised that the interruption of blood supply to the cells was not the critical factor determining their radiosensitivity but the consequent reduction in the oxygen transferred to these cells through the blood stream which was making them more radioresistant. In 1949 and 1950 Thoday, Gray and Read

confirmed Mottram's conclusion by studying the growth inhibition of the primary root of the broad bean *Vicia faba* exposed to radiation (Sheline *et al.*, 1971).

In 1940 Stone and Larkin (Stone *et al.*, 1940; 1942) reported their results of a very preliminary study of neutron therapy on 34 head and neck patients exposed between 26 September 1938 and June 1939 using the 37 inches cyclotron available at Berkeley, University of California (Brennan, 1977). Their conclusions were promising enough to encourage the continuation of the study, which by December 1939, was based on a 60 inch cyclotron capable of producing 16 MeV deuterons with a neutron spectrum very much like that which was to be produced later at Hammersmith Hospital, in 1955. Between December 1939 and September 1941, 120 head and neck patients were treated and, although the results were still considered promising, some serious side effects began to be noted. In 1943 the trial was terminated because of the advent of World War II, and four years later, in a report published in 1948 in the form of the Janeway Lecture, Stone reviewed all 226 patients treated on the 60 inch cyclotron, of which 17 were alive, and concluded that the severe late effects in these patients were not in keeping with the relatively mild early effects being observed and for this reason he discouraged any further use of neutrons in radiotherapy (Stone, 1948).

It was now 1955 and the idea of starting a new neutron trial at Hammersmith Hospital was well under way. Out of the radiobiology work done in England (presented during the Annual Congress of the British Institute of Radiology in London on April 27th, 1962 (Bewley *et al.*, 1963; Field *et al.*, 1967; 1968) and also by Barendsen *et al* in Holland (1968), came the realization that the RBE of neutrons increases as fraction size decreases. This led to a re-examination of Stone's cases and raised the possibility that he had underestimated the effectiveness of his neutron beam. The idea was based on the fact that Stone's RBE figures were derived mainly from single fraction exposures of skin using relatively high doses. Dr Stone conferred with the Hammersmith group and the discussions lent support to the idea that Stone might have inadvertently over-dosed his patients by not knowing about the influence of small fraction size.

Two ideas were at that stage fairly well established. Firstly, an explanation was at hand to explain why Stone had trouble with late effects; and secondly, there was a positive

reason (the oxygen effect) for believing that neutrons might be superior to photons in radiotherapy. Three sets of data were available at this point to support the latter notion:

- i. Hypoxic cells are present in malignant tumours; they result from the fast proliferation of the cancer cells.
- ii. Hypoxic cells are approximately three times more radio-resistant than well-oxygenated cells for low-LET radiation. The difference in radio-sensitivity between aerobic and hypoxic cells is measured in terms of the Oxygen Enhancement Ratio (OER), given by the ratio of doses required in the well-oxygenated and hypoxic cells to achieve the same effect, i.e.

$$OER = \frac{d_{hypoxic}}{d_{air}} \quad (2.3)$$

The presence of a small percentage of hypoxic cells (1% or even 0.1%) can thus make the tumour radio-resistant.

- iii. The OER for X-rays in the case of HeLa cells exposed to X-rays and 14 MeV fast neutrons in air and nitrogen is about 1.51 (Nias *et al.*, 1967).

On the basis of the emerging understanding of late- and oxygen- effects, the radiobiology work carried out on pigs at Hammersmith from 1955 to 1963 was extended in 1965 to include study of the effects of neutrons on normal human skin (lateral thigh) in patients with terminal malignancies elsewhere in the body. The objective was to find out if late effects were consonant with early effects as they were shown to be in pig skin. The results were positive and, if allowance is made for difference in fraction size, the results supported the idea that the late effects of neutrons would be clinically acceptable. For these reasons, in the 1970s, neutron therapy once more became available as a therapeutic modality, initially at the Hammersmith Hospital in 1967, and later in the U.S. at centres such as the University of Washington in Seattle, UCLA, M.D. Anderson Cancer Center in Houston, Fermilab near Chicago, and the Cleveland Clinic. In Europe other neutron facilities were developed: in the UK, at Edinburgh and Clatterbridge; in Germany at Dresden, Heidelberg and Essen; and, in Belgium, at Louvain. Several randomised clinical trials were undertaken at these centres

during the 1970s and the 1980s and the overall consensus was that, although fast-neutrons therapy yielded a slightly higher local control rate for some tumours, this gain was offset by higher morbidity that was at least partly attributable to the poorer physical dose distributions achievable with the neutron beams used in the randomised trials (Laramore, 1997).

Technological Aspects

Neutron beams can be generated in several ways and which can be schematically distributed into four groups:

- Reactors, using fast neutrons in the beam
- ‘Low-energy’ cyclotrons, usually accelerated deuterons with energies ranging from 13 to 16 MeV (d + Be reaction)
- (d + T) generators
- ‘High-energy’ cyclotrons or linear accelerators (d/p + Be reaction)

It is only in the fourth group that the physical selectivity and the technical conditions be considered to be sufficiently acceptable for adequate treatments, especially in comparison with modern linear accelerators.

In some centres, large clinical programs were completed from which important radiobiological and clinical conclusions could be derived. In some other centres, the facilities were shut down abruptly for the following reasons:

- Usually due to technical difficulties; for example, all (d + T) generators are now shut down.
- In other centres, due to patient recruitment problems
- In general, due to ‘suboptimal’ physical selectivity

Today, in the majority of centres still active in neutron therapy, the technical conditions are becoming progressively comparable to those in modern photon beam therapy. In

addition, a few new high-energy facilities have been proposed (e.g. in China, Germany, Poland, Slovakia, and South Africa).

Clinical Aspects (Short Survey)

Salivary Gland Tumours. Neutron beam therapy should be considered as the treatment of choice in patients with unresectable salivary gland tumours or in patients where radical resection would require facial nerve sacrifice (See Table I) (Krüll *et al.*, 1998).

Reference	No. of Patients	Local Control
<i>Catterall (1987)</i>	65	48 (74%)
<i>Battermann and Mijnheer (1986)</i>	32	21 (66%)
<i>Duncan et al (1987)</i>	22	12 (55%)
<i>Prott et al (1996)</i>	64	39 (61%)
<i>Kovacs et al (1987)</i>	15	13 (87%)
<i>Krull et al (1995)</i>	74	44 (59%)
<i>Skolyszweski et al (1982)</i>	3	2
<i>Overall</i>	275	179 (65%)

Table 2.1: Pooled European Data of Local Control in Advanced Salivary Gland Tumour

For inoperable primary or recurrent tumours, a randomised cooperative study showed, at two years, a significant advantage for neutrons compared to photons for loco-regional control (76% vs. 17%, $P < 0.005$) and a trend towards improved survival (62% vs. 25%). Ten-year analysis continued to show a striking difference in loco-regional control (56% for neutrons vs. 17% for photons, $P = 0.009$), but both groups experienced a high rate of metastatic failure (see next figure) (Lindsey *et al.*, 1996).

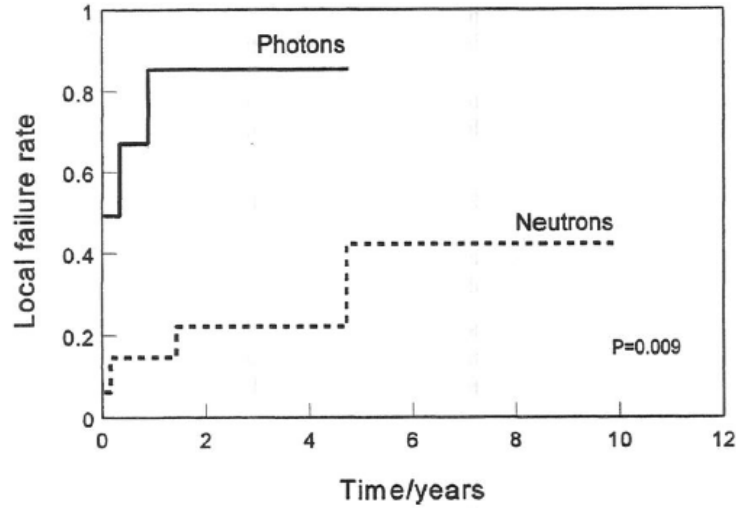


Figure 2.7: Probability of local-regional failure for unresectable salivary gland tumours treated with neutrons (Lindsey et al., 1996).

Prostatic Adenocarcinoma. For prostatic adenocarcinomas, their typical slow growth rate and low cycling fraction are strong indications for exploring neutrons (high LET) in the treatment of this disease.

The Radiation Therapy Oncology Group (RTOG), 1997, compared mixed (photon + neutron) beams to conventional photons for locally advanced prostatic cancer. Loco-regional control as well as survival was significantly superior after mixed-beam irradiation.

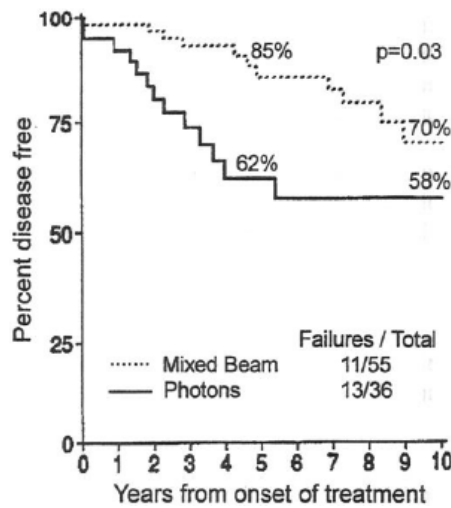
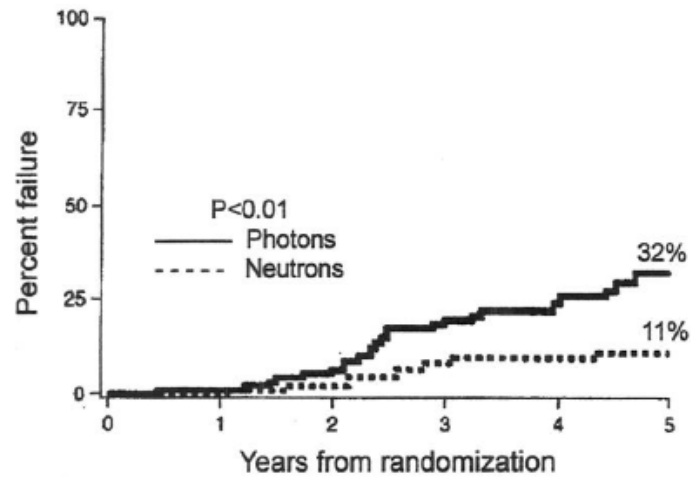


Figure 2.8: Loco-regional control in patients treated with mixed (neutron/photon) beams or photons only (RTOG randomised trial) for locally extended prostatic adenocarcinoma (Lindsey et al., 1996).

In 1986, the Neutron Therapy Collaborative Working Group (NTCWG) compared neutrons (alone) and conventional photons. As shown in the next figure, a significant difference ($P < 0.01$) was observed in ‘clinical’ loco-regional failure, with respective actuarial 5-year failure rates of 11% vs. 32% after neutrons and photons (Lindsey *et al.*, 1996). Inclusion of routine post-treatment biopsies resulted in 5-year ‘histological’ local-regional failure rates of 13% and 32%, respectively ($P = 0.01$).



*Figure 2.9: Loco-regional failure in patients with locally advanced prostate cancer (Lindsey *et al.*, 1996).*

Due to the long natural history of recurrent prostate cancer, longer follow-up is required to assess the ultimate impact of the improved local control on survival. However, prostate specific antigen (PSA) levels could provide an indication: at 5 years, 17% of the neutron patients showed elevated PSA levels compared to 45% for the photon patients ($P < 0.001$).

Late effects (mainly large bowel complications) were worse in the neutron-treated group (11% vs. 3%). However, no colostomy was required in 51 patients treated with a multileaf collimator at the University of Washington, while 6/38 patients, from other centres using movable jaw or fixed cone collimator, did require colostomy.

The data from Louvain-la-Nueve suggest that mixed neutron-photon therapy is particularly efficient in patients with unfavourable prognostic factors, such as $PSA > 20\text{ng/mL}$ (Scalliet *et al.*, 1998).

2.3.2. Proton Therapy

Rationale: Improved physical selectivity at no radiobiological cost

Two are the main principles driving proton radiotherapy are summarised in the following figures:

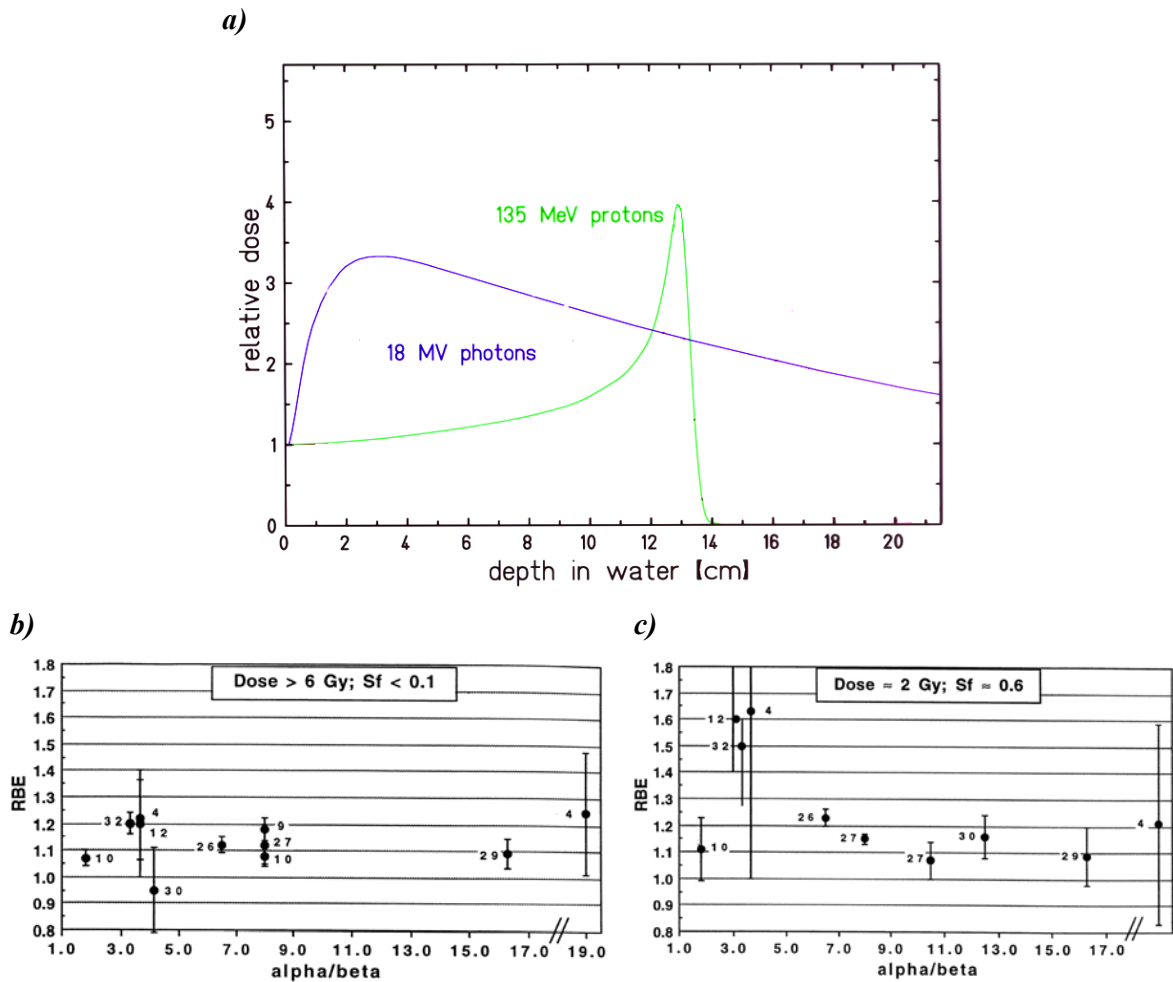


Figure 2.10: (a) Comparison of depth dose curves for a 18MV photon beam and a 135MeV proton beam; (b) RBE values against $(\alpha/\beta)_L$ values for cells (in vitro) or tissues (in vivo) exposed to doses >6Gy of protons; (c) RBE values against $(\alpha/\beta)_L$ values for cells or tissues exposed to doses ≈ 2 Gy of protons (Gerweck et al., 1999).

- Figure 2.10a, shows the characteristic depth-dose curve of a proton beam:
 - o Low entrance dose ('initial plateau'),
 - o Dose increases with depth more and more steeply to reach a maximum at the 'Bragg peak'. The depth of the Bragg peak in tissue depends on the energy of the beam.
 - o Zero exit dose as there is no dose distribution beyond the depth of the Bragg peak and thus there is full sparing of the tissues behind the target volume.
- Figure 2.10b & c, on the other hand, shows why proton beams have no radiobiological advantages as they are characterised by average RBE values of 1.0-1.2 for all tissues². If a constant value of RBE [i.e. 1.1 (Paganetti *et al.*, 2002; Gueulette *et al.*, 2001)] is assumed, the vast clinical experience accumulated with photons can thus be transferred directly to proton therapy.

The main advantage of proton therapy is that, with a single beam, it is possible to localise the dose not only in the lateral direction but also as a function of the depth in the patient. Compared to photons one can achieve with protons a general reduction of the integral dose outside of the target volume by a factor of 2 or 3, which represent a clinically significant dose sparing for the surrounding healthy tissues. Protons are expected to produce superior results mainly for the treatment of large tumours with complex shape.

The disadvantage of proton therapy is the large size and cost of the accelerator and of the beam lines needed for the transport of the beam (Pedroni, 2000).

An up-to-date review of the current centres using protons as part of their clinical treatment protocols can be found on <http://ptcog.web.psi.ch/ptcentres.html>

² An increase of RBE values is however observed at doses ≈ 2 Gy (clinically relevant doses) for cells/tissues of low $(\alpha/\beta)_L$, where the RBE ~ 1.6 (average RBE($d\approx 2$ Gy)) $=1.28\pm 0.07$ (SE); average RBE($d>6$ Gy)) $=1.13\pm 0.03$ (SE).

Technological Aspects: Beam Delivery

Two methods can be used to deliver proton beam therapy: passive scattering and beam scanning.

- *The passive scattering technique*

This technique is the traditional beam delivery method. It is illustrated in the following figure:

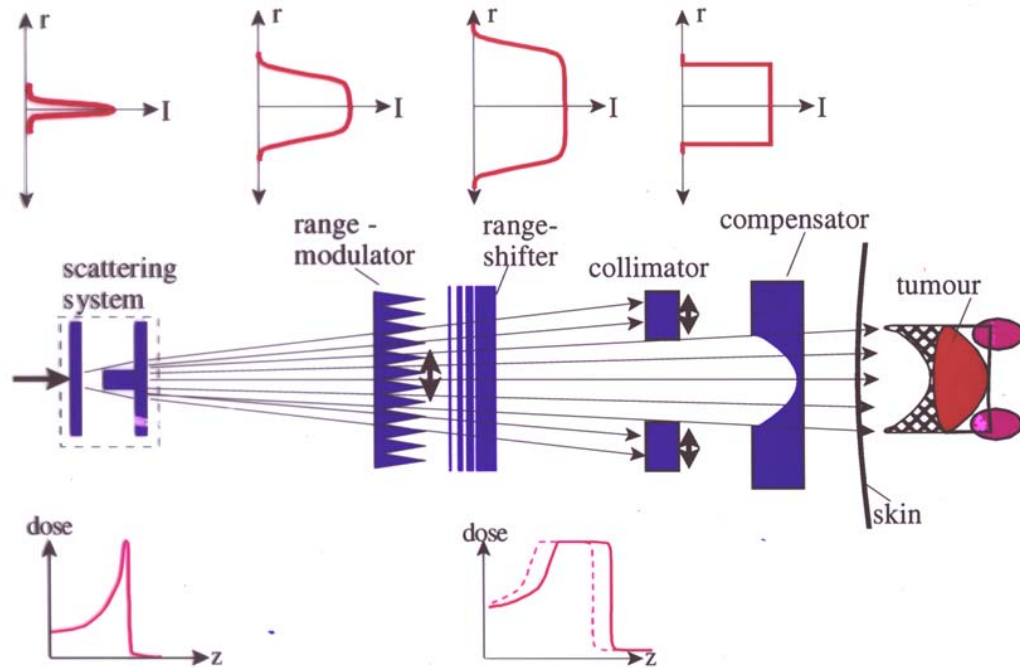


Figure 2.11: Representation of a purely passive system. Starting with a single Bragg peak and extended to a Spread-Of-Bragg-Peak (SOBP) after beam traverses the range-shifter.

In step 1 of the above diagram the proton beam is scattered by material in the beam ahead of the patient in such a way as to produce a homogenous flux of protons in the solid angle used for the irradiation. The dose is then shaped in the lateral direction using collimators (step 2). A fast spinning wheel of variable thickness (the ‘range shifter wheel’) in step 3 introduces a variable amount of absorbing material in the beam as a function of time. The resulting modulation of the proton range can be chosen such as to produce a homogeneous region of dose throughout a given range of depth (the spread-

out Bragg peak, SOBP). At the end of step 3, there is a multi-leaf collimator to shape the field conformingly to the target volume. In step 4 an individual compensator bolus can be optionally added to this set-up to shift the distal edge of the dose field to conform more closely to the deepest side of the target volume. All the necessary hardware must be adapted and in part created individually for each single field. This makes the beam delivery with multiple dose fields on a scattering gantry rather laborious. The passive scattering method produces by default a homogeneous dose field with a fixed SOBP thickness in depth (fixed range modulation). To be able to change the modulation and create an intensity modulated beam a completely different approach has to be taken, which is achieved by the beam scanning technique.

Hall (2006) has recently indicated that passive scattering techniques, a technique widely used in many proton therapy centres, have the disadvantage of producing neutrons after the proton beam traverses the scattering foil which results in a total-body dose to the patient (Yan *et al.*, 2002) (see Figure 2.11a). The consequence of this exposure is that passive modulation results in different doses at different distances from the field edge that are 10 times higher than those characteristic of IMRT with X-rays. For this reason it would be very difficult to defend the case of the benefit of protons imparted by passive scattering methods against the use of IMRT. The full benefit of protons is achieved only if a scanning beam is used in which doses are 10 times lower than the doses from IMRT (see Figure 2.11b).

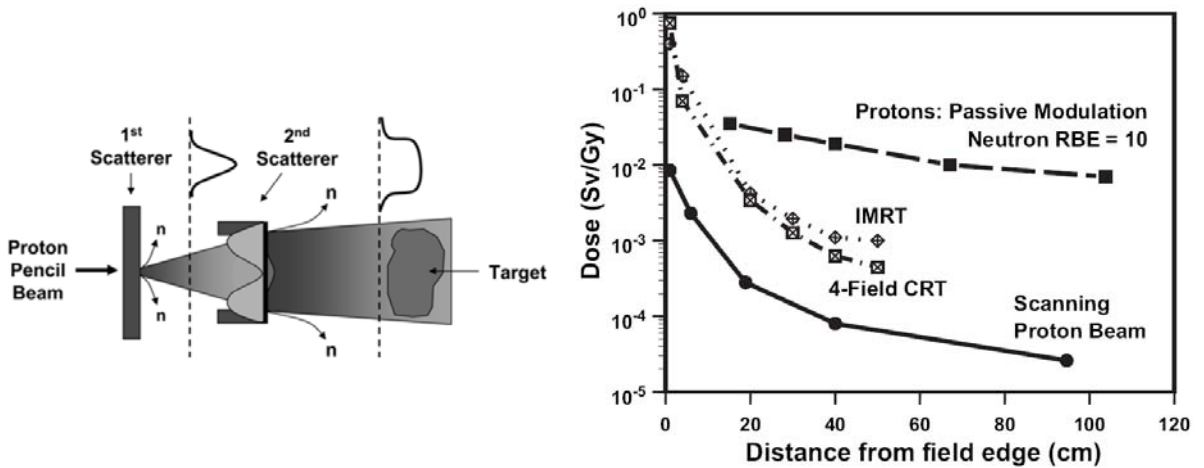


Figure 2.12: Neutron contamination on a proton beam after beam traverses scattering foil and radiobiological consequences (Hall, 2006).

- *The Beam Scanning technique*

In this case the proton pencil beam coming from the accelerator is delivered directly into the patient. Individual pencil beams are aimed so as to sequentially position the associated Bragg peaks at specified (x,y,z) coordinates under computer control. A high conformity is thus achieved by changing the dosage and the position of each pencil beam. In the lateral direction the beam is usually scanned through magnetic deflection of the beam ahead of the patient. The modulation in depth is achieved by changing dynamically the energy of the protons. The range can be adjusted as a function of the beam position in both transverse directions (variable range modulation).

The major advantages of the spot scanning technique compared to passive scattering are the additional dose sparing due to the variable modulation of the range, the dose delivery without patient specific hardware and the capability to deliver intensity modulated therapy (without additional modifications). Also, as a difference to the passive scattering technique, the absence of the scattering foil on the beam means no contamination inside or outside of the treatment field. The major disadvantage is the higher sensitivity of this method to organ motion during the scanning process.

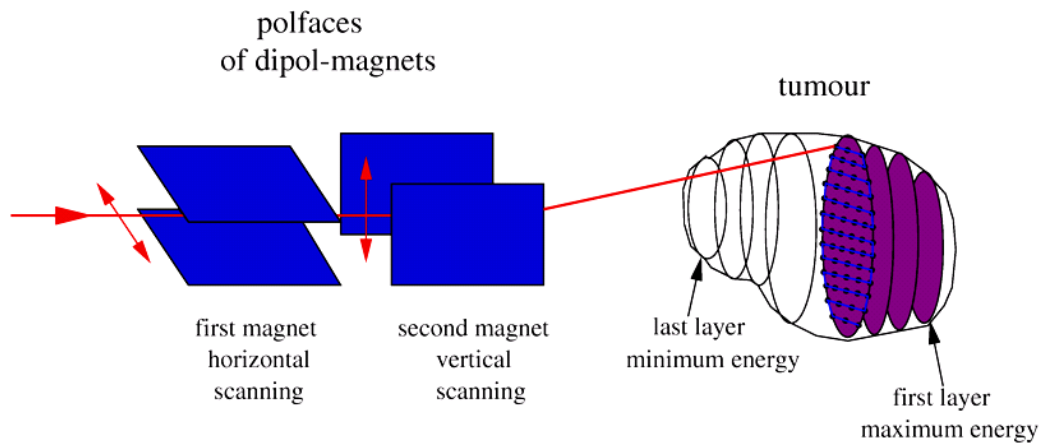


Figure 2.13: Illustration of the beam scanning technique to deliver protons.

Clinical Aspects (Short Survey)

Wambersie *et al.* (2003) prepared a summary of an extended survey (Wambersie *et al.* 1992a; 2001) on the clinical results obtained from different centres using protons to treat certain types of tumours.

- Uveal Melanoma

According to the depth deposition curve shown above (Figure 2.10a), proton beams are ideal for treating intraocular lesions since they can be made to deposit their absorbed dose in the target volume, while significantly limiting the irradiation of the non-involved ocular and orbital structures.

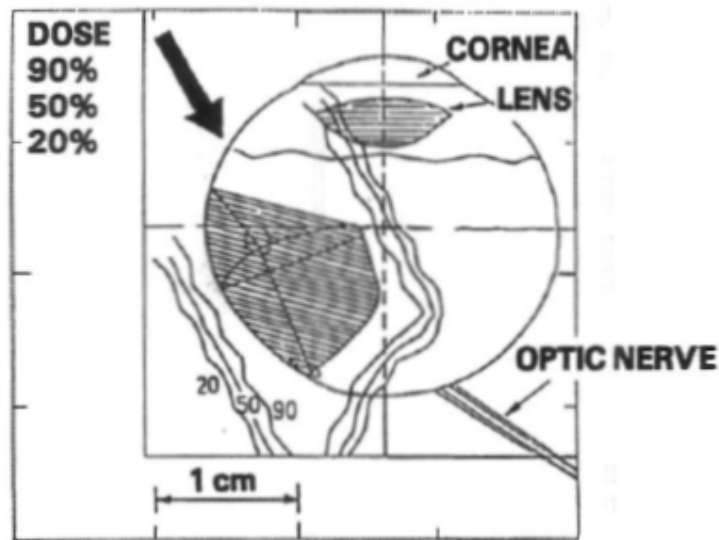


Figure 2.14: Treatment of uveal melanoma with a 60MeV-SOBPs proton beam.

Large series of patients with uveal melanoma were treated with protons in several centres worldwide. The Massachusetts General Hospital/Harvard Cyclotron Laboratory (MGH/HCL) in Boston played a pioneering role, and 2568 uveal melanoma patients were treated up until September 1998 (Munzenrider *et al.*, 1999).

Good local tumour control (96% and 95% at 60 and 84 months respectively), was reported. Eye retention probability after proton therapy depends on tumour size, being

respectively 97%, 93%, and 78% for patients with small, intermediate and large tumours. 5-year survival for patients treated with either protons or enucleation is similar (about 80%).

- Tumours of the base of Skull and Cervical Spine

Proton (or other charged particle beams) are the treatment of choice for skull base and cervical spine tumours: beam energy can be focused in the target volume, while achieving significant sparing of the brain, brain stem, cervical cord, optical nerves and chiasma.

At HCL/MGH in Boston, 621 patients with chordomas and low-grade chondrosarcomas of the skull base and cervical spine were treated with protons between 1975 and 1998. For skull base tumours, with follow-up ranging from 1 to 254 months (median of 41 months), local recurrence-free survival is significantly better for chondrosarcomas than for chordomas. It is 98% at 5 years and 94% at 10 years for chondrosarcomas and 73% at 5 years and 54% at 10 years for chordomas (Munzenrider *et al.*, 1999). Overall survival is also significantly better: 91% vs. 80% at 5 years and 88% vs. 54% at 10 years, respectively.

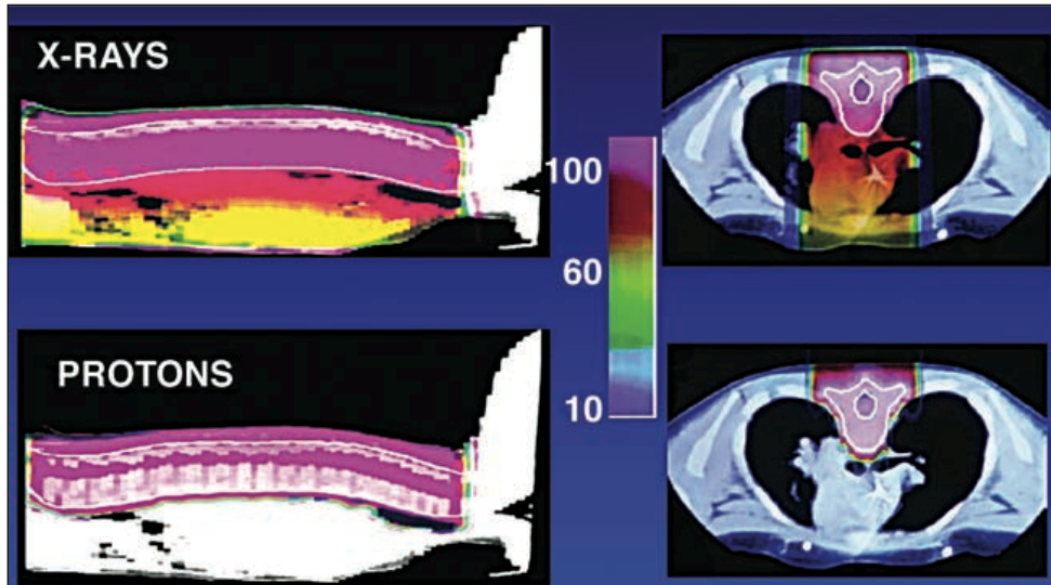
For cervical spine tumours, with follow-up ranging from 1 to 172 months (median of 36 months), local recurrence-free survival was not significantly different for chondrosarcomas and chordomas: 54% vs. 69% at 5 years and 54% vs. 48% at 10 years, respectively. The overall survival at 5 years for chondrosarcomas and chordomas were 48% and 80%, respectively, but at 10 years, 48% and 33%, respectively (Munzenrider *et al.*, 1999).

- CNS Tumours in Children

Paediatric tumours located in the CNS are particular challenging and require highly refined techniques of radiation therapy and proton therapy is thus ideal (Habrand *et al.*, 1999; Wambersie *et al.*, 1992b; Jones *et al.*, 1999). The preliminary results from the centres in Loma Linda, MGH/HCL, and Orsay are promising and show an excellent

immediate and late tolerance. The main reason for this is, as expected, a reduced integral dose as can be seen in the following figure.

a)



b)

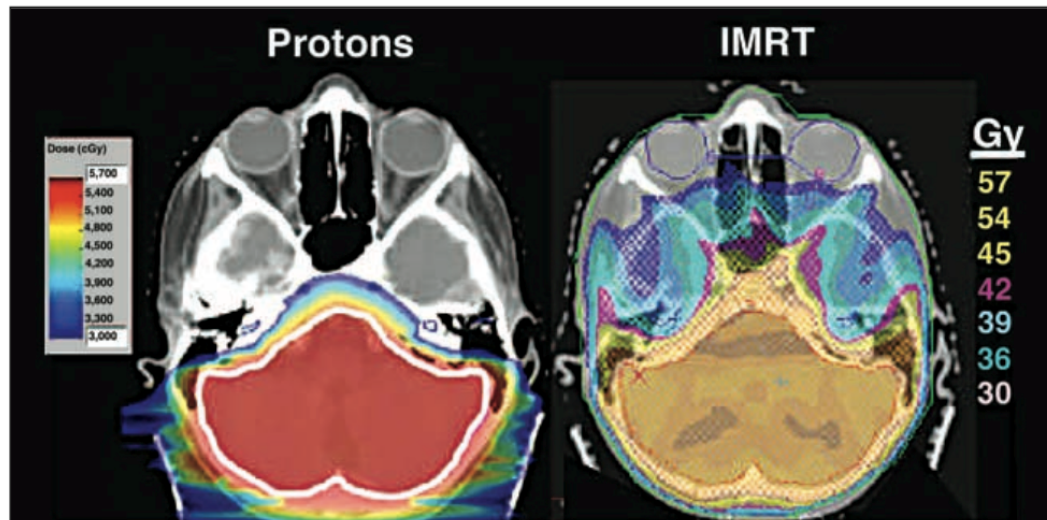


Figure 2.15: Improved conformity of paediatric CNS tumours when treated with protons compared with photons. a) Comparison of spinal fields for medulloblastoma (Kirsch et al., 2004); b) Comparison of whole-brain irradiation and posterior fossa boost using protons with IMRT (Kirsch et al., 2004).

- Other Locations

Results of proton beam therapy for other tumour types and localizations have been reported, in particular, for retinoblastoma and age-related macular degeneration (Wambersie *et al.*, 1992a).

A different survey, independent to that produced by Wambersie (1992a; 2001) has been recently published (Lodge *et al.*, 2007; Olsen *et al.*, 2007). While the earlier work reported an overall improvement of the treatment of the different sites mentioned with protons relative to photons, the later work concludes that, based on an extensive literature revision that did not discriminate between languages or study design, proton therapy is not superior to conventional radiotherapy. The following table summarises these conclusions.

Tumour Site	N studies/N	Result
<i>Head and Neck</i>	2/62	No firm conclusions
<i>ACC (locally advance)</i>	-	-
<i>Prostate cancer</i>	3/1751	Similar
<i>Ocular Tumours</i>	10/7708	Superior
<i>Gastro-intestinal cancer</i>	5/369	No firm conclusions
<i>Lung cancer (no-small cell)</i>	3/156	No firm conclusions
<i>CNS</i>	10/839	Similar
<i>Chordomas of skull base</i>	3/302	Superior
<i>Sarcoma's</i>	1/47	No firm conclusions
<i>Pelvic tumours</i>	3/80	No firm conclusions

Table 2.2: Results literature review in comparison with conventional therapy classified by tumour site. Abbreviations: N, number of patients; ACC, adenoid cystic carcinomas; CNS, central nerve system tumours, inclusive skull base, spinal cord chordoma and chondrosarcomas.

It is interesting, however, to observe how the reported treatment success of protons compared to photons increases as the number of patients included in the study increases. Nonetheless, it is difficult to assess if this phenomenon is due to the protons themselves being more advantageous than photons or if the higher success is related to the greater experience accumulated when treating larger population of patients.

2.3.3. Ion Therapy

As the main particles used in ion therapy are carbon ions, this section will focus on this type of radiation. Carbon ions are recognised by the physics community as a light-ion whereas the radiation oncology (or radiobiology) community recognises it as a heavy-ion radiation. They combine the advantages of an excellent physical selectivity with the radiobiological advantages of high-LET radiations for some types of tumours.

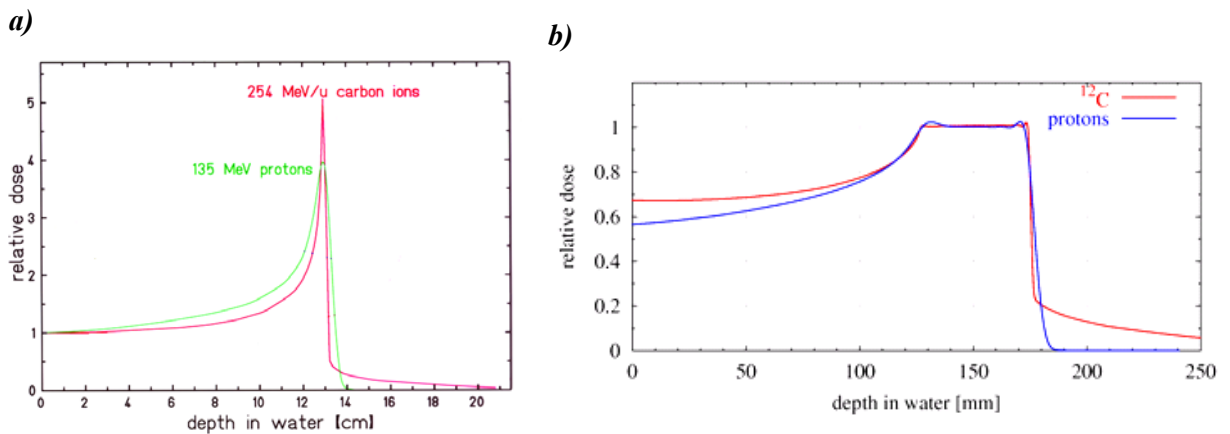


Figure 2.16: (left) comparison of a 135MeV proton depth dose curve with that of a 254MeV/u carbon ion beam; (right) comparison of a SOBP for a proton beam with that for a carbon ion beam.

The depth dose curve (DDC) of a carbon ion beam includes, as with the case of protons, a Bragg peak (Figure 16a). There are three main features of a carbon ion DDC when compared to that of a proton beam: (i) the peak is narrower, which improves the precision of dose deposition (i.e. physical selectivity) when using active beam scanning techniques; also (ii), the penumbra is somewhat narrower with carbon ions than with protons as the particles are heavier; and finally (ii), the existence of nuclear fragmentation at the tail of the curve. This can, to some extent, represent a disadvantage as some energy is deposited beyond the primary Bragg peak but it is probably not clinically relevant as the associated doses are low and the fragments are low- or high-LET particles, depending on the nature of the target nuclei (See Figure 2.17).

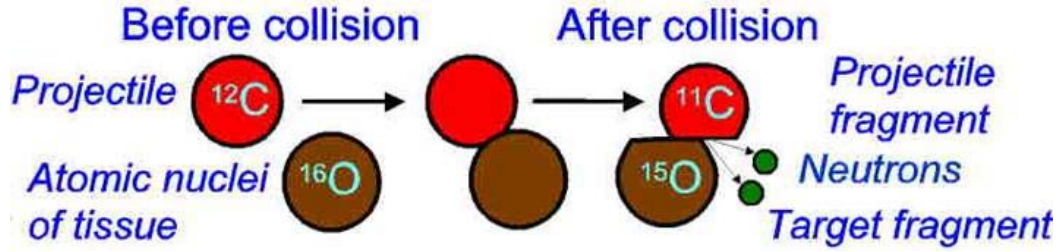


Figure 2.17: Fragmentation after collision between a carbon and an oxygen ion.

The physical and biological advantages of carbon ions in radiotherapy were summarised by Amaldi (Amaldi *et al.*, 2005) as follows:

1. Carbon ions deposit their maximum energy density in the Bragg peak at the end of their range, where they can produce severe damage to the cells while sparing both the transversely adjacent and deeper located healthy tissues.

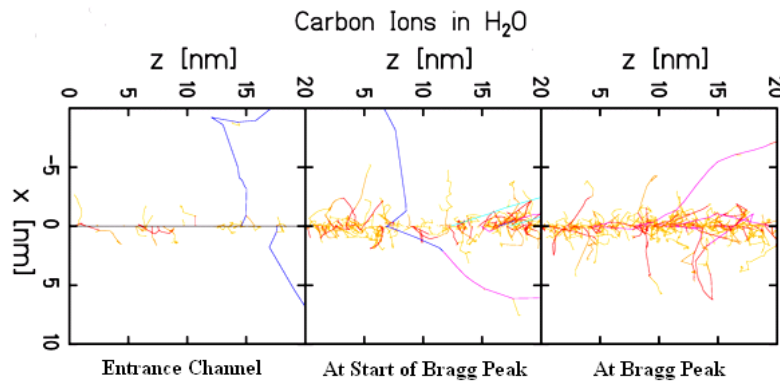


Figure 2.18: Change of energy deposition pattern (i.e. LET) at different points of a carbon ion beam.

2. Beams of carbon ions can easily be formed as narrow focused and delivered using scanning pencil beams of variable penetration depth, so that any part of a tumour can be accurately irradiated with optimal precision. They penetrate the patient with minor lateral scattering and longitudinal straggling. Indeed, lateral and longitudinal scattering is about 3 times less than for protons. Being charged, carbon ions can easily be formed as narrow focused and scanning pencil beams of variable penetration depth, so that any part of a tumour can be accurately irradiated with optimal precision.

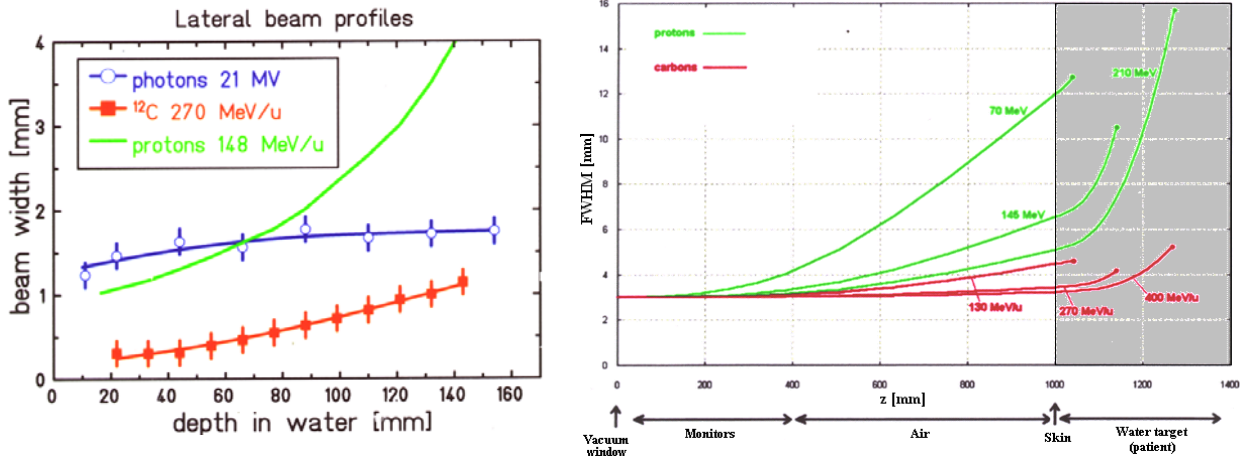


Figure 2.19: (left) Lateral scattering present on a 21MV photon, 148 MeV/u proton and a 270 MeV/u carbon ion beam; (right) beam scattering from a real scanning setup (exit window, monitors, air, patient).

- Carbon beams have a favourable depth profile of the RBE. This is the main advantage with respect to protons: at high energies, in the entrance channel mostly repairable damage is produced, corresponding to low RBE values, while in the last 2–3 cm of the range the RBE significantly increases to values between 2 and 5, depending on the type of tumour. Moreover very radio-resistant tumours show the largest increase in RBE.

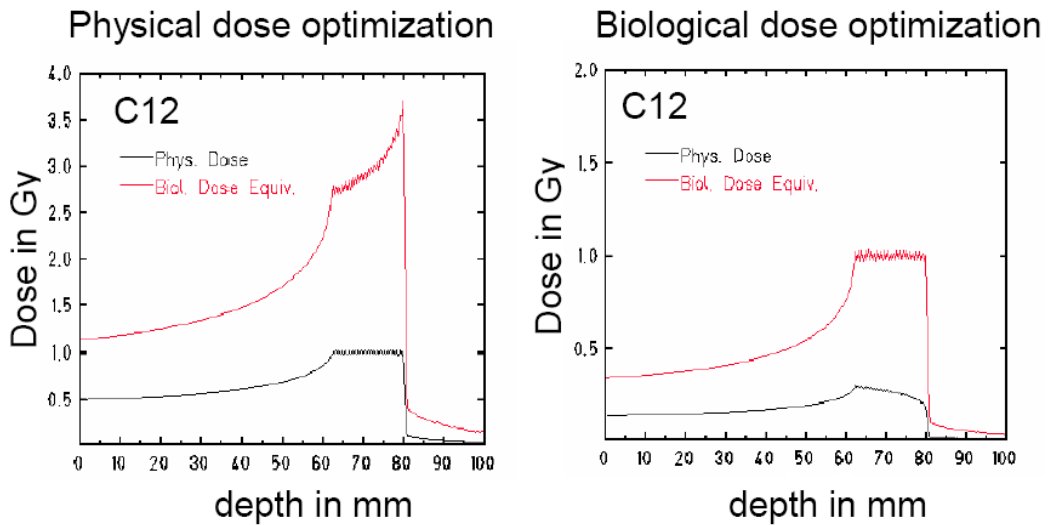


Figure 2.20: Difference between physical dose optimization and biological dose optimization.

4. The location where the dose is deposited by carbon ions can be determined by means of on-line positron emission tomography (PET). The on-line PET control permits exploitation of the millimetre precision of a focused carbon beam, with its high biological effectiveness for targets that are close to or inside a critical structure, such as optical nerves and spinal cord.

In terms of beam delivery techniques, passive and active beam scanning may be used as with protons. When combined with the possibility of rotating gantries this makes the carbon ion modality a very precise tool for treatment.

Clinical Results (Short Survey)

There are currently four centres worldwide using carbon ions in a fully dedicated clinical setup: HIMAC (Heavy Ion Medical Accelerator in Chiba) and HIBMC (Hyogo Ion Beam Medical Centre) in Japan and HIT (Heidelberg Ion-Beam Therapy Centre) in Germany. A fourth centre is planned to be opened by the end of 2007 in Pavia (Italy), the CNAO (Centro Nazionale di Adroterapia Oncologica), which together with HIT and GSI (Gesellschaft für Schwerionenforschung Darmstadt - Germany) are part of the European Network for Light Ion Therapy (ENLIGHT) project. It was at GSI where the German project for clinical implementation of ion therapy was piloted until the construction of the HIT facility early this year. Other centres exist capable of delivering carbon ions for radiotherapy purposes, but the beam availability is not fully dedicated to clinical use.

Up to 2007, the two pioneering centres conducting clinical trials, GSI and HIMAC, treated with carbon ions a total of more than 3,300 patients (>3,000 patients in HIMAC and 300 in GSI) (Schulz-Ertner *et al.*, 2004; Schardt, 2007; NIRS, 2005-2006):

Site	Centre		Number of patients treated			
<i>Head & Neck</i>	NIRS	GSI	352		21 ⁱ	
<i>CNS - spine</i>	NIRS	GSI	89		17	
<i>Base of Skull</i>	NIRS	GSI	42	54 ⁱⁱ	33 ⁱⁱⁱ	15 ^{iv}
<i>Lung</i>	NIRS		420			
<i>Liver</i>	NIRS		200			
<i>Prostate</i>	NIRS		431			
<i>Uterus</i>	NIRS		107			
<i>Bone & soft tissue</i>	NIRS		291			
<i>Oesophagus</i>	NIRS		41			
<i>Pancreas</i>	NIRS		64			
<i>Rectum</i>	NIRS		67			
<i>Eye Melanoma</i>	NIRS		59			
<i>Lacrimal gland</i>	NIRS		12			
<i>Miscellaneous</i>	NIRS		454			
TOTAL			2629		140	

Table 2.3: Current status of patient treated with carbon ions at HIMAC (Japan) and GSI (Germany); (i) Adenoid cystic carcinoma; (ii) Chordoma; (iii) Chondrosarcoma; (iv) Other skull base tumours.

The results for the pilot/trial projects conducted at NIRS (Tsuji *et al.*, 2002) and GSI (Schulz-Ertner *et al.*, 2004) have been reported recently. The GSI reported their results obtained between 1997-2002 (156 patients in total) and concluded that, for those patients with chordomas, chondrosarcomas and other skull base tumours treated with 20 daily fractions of median total dose of 60GyE³, the three-year local control rates were 81% for chordomas, 100% for chondrosarcomas and 62% for adenoid cystic carcinomas (Schardt, 2007). In the case of NIRS, the following table summarises the results obtained over the period 1994-2006 (2867 patients in total) (Tsuji *et al.*, 2007).

³ For a definition of Gray-equivalent dose (GyE), see (Wambersie *et al.*, 2006).

Protocol	Pha-se	Tumors	GyE/frs/wk	No. Pats	3-year Local Control	Overall Survival		Comments
						3-yr	5-yr	
Head&Neck-1+2	I / II	Locally advanced	49~70/16~18/4~6	34	81%	48%	37%	
Head&Neck-3(9602)	II	Locally advanced	57.6/16/4	224	77%	57%	43%	
		- Adenoid cystic ca		64	82%	76%	68%	
		- Adenoca		26	72%	64%	64%	
		- Malignant melanoma		80	88%	49%	30%	
		- Others		54	55%	46%	27%	
Head & Neck-4	I / II	Sarcoma	70.4/16/4	16	100%	56%	56%*	*4-yr survival
Head&Neck-5	II	Malignant melanoma	57.6/16/4	57	82%	42%	35%*	
		- C-ion +Chemotherapy		48	92%	45%	45%*	
Skull base/ cervical spine	I / II	Skull base/cervical spine	48.0~60.8/16/4	40	93%	94%	87%	
		- Chordoma		25	88%	100%	86%	
Lung-1(9303)	I / II	Stage I (Peripheral type)	59.4~95.4/18/6	47	65%	-	42%(61%)*	* Figures in () indicate
Lung-2(9701)	I / II	Stage I (Peripheral type)	72.0~79.2/9/3	34	91%	-	41%(60%)*	cause-specific survival
Lung-3(9802)	II	Stage I (Peripheral type)	72.0/9/3	50	95%	-	50%(76%)*	
Lung-4(0001)	I / II	Stage I (Peripheral type)	52.8~60.0/4/1	79	90%	-	41%(62%)*	
Lung-3+4	-	Stage I (Peripheral type)	4 and 9 fractions	129	93%	-	44%(71%)*	
		- I A (\leq 3 cm)		71	99%	-	56%(88%)*	
		- I B (> 3 cm)		58	85%	-	30%(48%)*	
Lung-5(0201)**	I / II	Stage I (Peripheral type)	28~44 (Single irrad)	116	-	-	-	** On-going dose-
Lung-6(9801)	I / II	Stage I (Central type)	57.6~61.2/9/3	23	91%	-	21%(39%)*	escalation study
Lung-7(9903)	I / II	Locally advanced	68~76/16/4	37	88%	-	38%(55%)*	
Liver-1	I / II	T2~4 MONO	49.5~79.5/15/5	24	81%	50%	25%	
Liver-2	I / II	T2~4 MONO	48~70/4~12/1~3	82	87%	48%	26%	
Liver-3	II	T2~4 MONO	52.8/4/1	44	95%	58%	35%	* Pats with good liver
Liver-2+3	-	All cases treated with 4 frs	52.8/4/1	61	94%	57%	33%	function: single, 3~5 cm
		- with localized tumor*	52.8/4/1	21	-	71%	67%	
Liver-4	I / II	T2~4 MONO	/2fr/2days	40	-	-	-	
5-yr bNED Survival								
Prostate-1	I / II	B2~C	54~72/20/5	35	97%	94%	89%	----91%
Prostate-2	I / II	A2~C	60~66/20/5	61	100%	97%	90%	----78%
Prostate-3	II	T1C~C	66/20/5	333	99%	94%	91%	----87%
Prostate-2+3	Total	A2~C	66/20/5	374	99%	95%	92%	----88%
		- Low risk		68	98%	98%	93%	----87%
		- High risk		306	100%	94%	91%	----89%
		- PSA \leq 20		216	99%	96%	91%	----89%
		- PSA > 20		158	100%	94%	92%	----88%
Cervix-1	I / II	III~IVa (Sq Cell Ca)	53~72/24/6	30	49%	40%	37%	
Cervix-2+3	I / II	II~IVa (Sq Cell Ca)	64~72/20~24/5	36	69%	52%	43%	
		- Stage III			72%	57%	45%	
		- Stage IVa			63%	38%	38%	
Uterus(Adenoca)	I / II	II~IVa (Adenoca)	62.4~71.2/20/5	39	74%	70%	53%	
Bone/Soft Tissue-1	I / II	Unresectable	53~74/16/4	57	63%	47%	36%	Eligibility criteria include
Bone/Soft Tissue-2	II	Unresectable	70.4/16/4	190	82%	67%	54%	the tumor located in the pelvis
Bone/Soft-1+2	-	Osteosarcoma	70.4/16/4	48	69%	51%	34%	and para-spinal region.
		Chordoma	70.4/16/4	69	98%	91%	80%	
Rectum-1	I/II	Pelvic recurrence	67.2~73.6/16/4	65	82%	65%	55%	
Pancreas:								
Proepo C-ion-1	I/II	Resectable All	44.8~48.0/16/4	22	-	23.8% (36.3)*	*2-yr Survival	
Proepo C-ion-2	I/II	Resectable All	30.0~33.2/8/2	11	-	18.0%(40.0)*	**1-yr Survival	
Radical C-ion	I/II	Unresectable All	38.4~48.0/12/3	31	-	44.0%**	Figures in () are for resected pats	

Table 2.4: Patients treated with carbon ions on different sites at NIRS.

Although the result here presented indicate a high tumour control probability for most of the cases studied (49%-100%) with a high overall survival, (Lodge *et al.*, 2007) highlighted, similarly to the case with protons, the necessity to be cautious when estimating the possible benefits of carbon ion therapy versus conventional radiotherapy. Their results in this case are summarised in the following table.

Tumour site	Ions	
	<i>n</i> studies/ <i>N</i>	Result
Head and neck	2/65	Similar to protons
ACC (locally advanced)	1/29	Superior
Prostate cancer	4/201	No firm conclusions
Ocular tumours	2/1343	Similar to protons
Gastro-intestinal cancer	2/73	No firm conclusions
Lung cancer (non-small cell)	3/205	Similar to SRT
CNS ^a	3/405	Similar to protons
Chordomas of skull base	2/107	Similar to protons
Sarcoma's	1/57	No firm conclusions
Pelvic tumours	2/49	No firm conclusions

Table 2.5: Results literature review in comparison with conventional therapy classified by tumour site. N, number of patients; ACC, adenoid cystic carcinomas; SRT, stereotactic radiotherapy; CNS, central nerve system tumours, inclusive skull base, spinal cord chondroma and chondrosarcoma.

At present, randomised trials proving the superiority of carbon ion RT in comparison to photon IMRT and protons are lacking, but Debus *et al.* (2000) and Schulz-Ertner *et al.* (2004) have recently reported a much better local control probability for Chordoma and Chondrosarcoma when using Carbon ions than when using IMRT.

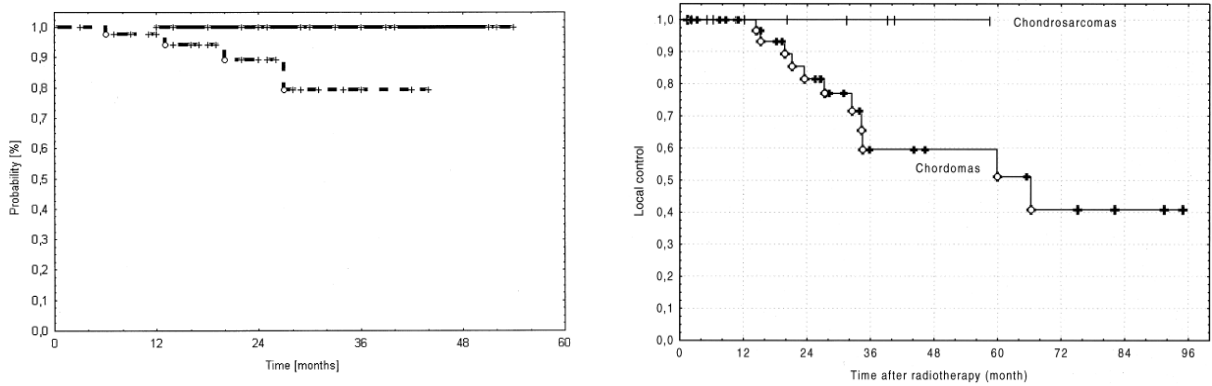


Figure 2.21: Kaplan-Meier curves for C12 (left) and IMRT (right) of chordomas and chondrosarcomas.

control rate was 77% for patients treated with mixed schedules (55 patients) and only 31% for patients receiving photons alone (36 patients) ($P < 0.01$). Actuarial survival rates at 8 years ('determinantal' survivals, i.e. adjusted by exclusion of intercurrent deaths) were 82% and 54% respectively ($P = 0.02$).

Remarkably good results have also been reported with neutron therapy for locally extended tumours of the paranasal sinuses. In the series treated at the Hammersmith Hospital, 86% (37/43) of the patients showed complete remission and relief of symptoms was noticed in all cases (Errington, 1986). For soft tissue sarcomas, the results reported from the different centres indicate an overall local control rate after neutron therapy of 53% for inoperable tumours, which is higher than the 38% control rate observed after low-LET radiation for similar patient series. For primary bone tumours and differentiated chondrosarcomas, better results have also been observed after neutron therapy compared to the current photon therapy results (Laramore *et al.*, 1989).

The value of fast neutrons has been assessed in other tumour types or sites but no definitive conclusions could be drawn (Schmitt *et al.*, 1990; Tsunemoto *et al.*, 1989). In fact, the general conclusion which emerges from the review of the clinical results is in agreement with what could be expected from the radiobiological data: replacement of X-rays by neutrons – or more generally of low-LET by high-LET radiation – brings a benefit for some types of tumours and, on the contrary, a loss for other tumours. The tumours for which fast neutrons were found to be superior to conventional X-rays are, in general, slowly growing and well differentiated.

However, negative results have been obtained for brain tumours (Schmitt *et al.*, 1990). Similarly, the value of fast neutrons for tumours in the head and neck area has been questioned (Griffin *et al.*, 1989). In general, it has been suggested that fast neutrons will only be highly effective in only 10 to 20% of tumours, with the disadvantage of possibly inducing higher normal tissue morbidity (Britten *et al.*, 2001; Wambersie, 1990).

The respective advantages and disadvantages of proton and ion therapy have also been discussed in this chapter. In the case of protons, it is clear that the improved physical selectivity of the beam without any significant change in the RBE effects is an advantage, as all the knowledge accumulated from conventional radiotherapy is still valid. But for tumours which are radioresistant to photons, and therefore to protons also, it is necessary to consider even more powerful alternatives to protons, such as the one offered by carbon ions.

To select the optimal clinical value of RBE in the case of carbon ions, the trials carried out at HIMAC have used dose escalation techniques starting from single fraction doses during phase I studies and, once the optimal overall time and fraction number was found, they maintained them during phase II studies. The average number of fractions they used was 12 which is approximately half the fraction number required for X-ray and proton beam therapy, and the treatment time they used was 3 weeks (Tsuji *et al.*, 2007).

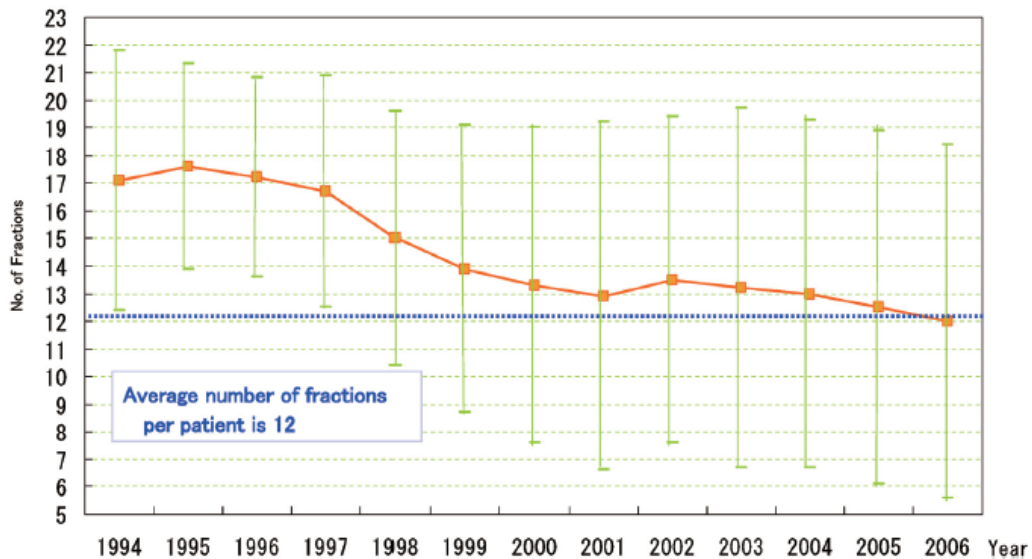


Figure 2.23: Average number of fractions in carbon ion radiotherapy

Although the adoption of hypofractionation regimes is the correct and safe option to select during dose escalation trials, (because RBE will not then be at its highest values) the use of appropriate radiobiological models could help to select fractionation

schedules which would ultimately optimise the therapeutic window available for the site treated with carbon ions. A model is proposed in Chapter 5 for this purpose, which explains a method for deriving values of RBE at different doses per fraction, taking into account direct and accumulative effects of high-LET radiations. A new formulation of the classical radiobiological concept BED (Biologically Effective Dose) will also be introduced in order to obtain isoeffective fractionation schemes with low- and high-LET treatments.

2.5. Bibliography

- Amaldi U., Kraft G. *Report on Progress in Physics* 68:1861-1882 (2005).
- Barendsen G.W., Walter H.M., Fowler J.F., Bewley D.K. *Radiation Research* 18:106-119 (1963).
- Barendsen G.W. *Current Topics in Radiation Research (Nether) Quarterly* 4:293-356 (1968).
- Battermann J.J. *Thesis, University of Amsterdam* (The Netherlands, 1981).
- Berry R.J., Partridge S., Harper K.H. *In: Conference on particle accelerators in radiation therapy. Report LA-5180-C, pp.108-112* (1973).
- Bewley D.K., Fowler J.F., Morgan R.L., Silvester J.A., Turner B.A. *British Journal of Radiology* 36(422):107-115 (1963).
- Bewley D.K. *In: The physics and radiobiology of fast neutron beams, pp.106. Ed. Adam Hilger, Bristol and New York* (1989).
- Brennan J.T. *International Journal Radiation Oncology Biology Physics* 3:143-148 (1977).
- Britten R.A., Peters L.J., Murray D. *Radiation Research* 156(2):125-135 (2001).
- Debus J., Schulz-Ertner D., Schad L., Essig M., Rhein B., Thillmann C.O., Wannenmacher M. *International Journal of Radiation Oncology Biology Physics* 47(3):591-596 (2000).
- Errington R.D. *Bulletin du Cancer* 73(5):569-576 (1986).
- Field S.B., Thomlinson R.H., Jones T. *British Journal of Radiology* 40, 834-842 (1967); and 41, 597-607 (1968).
- Fowler, J.F. *British Journal of Radiology* 62(740):679-694 (1989).
- Gerweck L.E., Kozin S.V., Relative biological effectiveness of proton beams in clinical therapy, *Radiotherapy and Oncology* 50:135-142 (1999).
- Goodhead, D.T. *In: Nuclear and atomic data for radiotherapy and related radiobiology, pp.37-54. IAEA: Viena* (1987).
- Griffin B.R., Laramore G.E., Russell K.J., Griffin T.W., Eenmaa J. *Radiotherapy and Oncology* 12(2):105-111 (1988).
- Griffin T.W., Pajak T.F., Maor M.H., Laramore G.E., Hendrickson F.R., Parker R.G., Thomas F.J., Davis L.W. *International Journal of Radiation Oncology Biology Physics* 17(5):959-965 (1989).

- Gueulette J., Gregoire V., Octave-Prignot M., Wambersie A. *Radiation Research* 145(1):70-74 (1996).
- Gueulette J., Böhm L., De Coster B.M., Vynckier S., Octave-Prignot M., Schreuder A.N., Symons J.E., Jones D.T.L., Wambersie A., Scalliet P. *Radiotherapy and Oncology* 42:303-309 (1997).
- Gueulette J., Slabbert J.P., Böhm L., De Coster B.M., Rosier J.F., Octave-Prignot M., Ruifrok A., Schreuder A.N., Wambersie A., Scalliet P. *Radiotherapy and Oncology* 61(2):177-184 (2001).
- Gueulette J., Octave-Prignot M., De Costera B.M., Wambersie A., Gregoire V. *Radiotherapy and Oncology* 73 (Suppl 2):S148-S154 (2004).
- Gueulette J., Wambersie A. *Journal of Radiation Research* 48(Suppl):A97-A102 (2007).
- Habrand J.L., Mammari H., Ferrand R., Pontvert D., Bondiau P.Y., Kalifa C., Zucker J.M. *Strahlentherapie und Onkologie* 175 (Suppl II):91-94 (1999).
- Hall E.J. *British Journal of Radiology* 62(740):765 (1989).
- Hall E.J. *International Journal of Radiation Oncology Biology Physics* 65(1):1-7 (2006).
- Hornsey S., Myers R., Parnell C.J., Bonnett D.E., Blake S.W., Bewley D.K., *British Journal of Radiology* 61(731):1058-62 (1988).
- ICRP. *Health Physics* 9(4):357-384 (1963).
- International Commission on Radiation Units and Measurements (ICRU), Report 30.* International Commission on Radiation Units and Measurements, Bethesda, MD. pp13-14 (1979).
- Jones D.T., Schreuder A.N., Symons J.E., de Kock E.A., Vernimmen F.J., Stannard C.E., Wilson J., Schmitt G. *Strahlentherapie und Onkologie* 175 (Suppl II):30-32 (1999).
- Kirsch D.G., Tarbell N.J. *The Oncologist* 9:442-450 (2004).
- Krüll A., Schwarz R., Brackrock S., Engenhardt-Cabillic R., Huber P., Prott F.J., Breteau N., Favre A., Lessel A., Koppe H., Auberger T. *In: Fast Neutrons and High-LET Particles in Cancer Therapy.* Engenhardt-Cabillic R., Wambersie A. Eds., pp.88. Springer: Heidelberg (1998).
- Laramore G.E., Griffith J.T., Boespflug M., Pelton J.G., Griffin T., Griffin B.R.,

- Russell K.J., Koh W., Parker R.G., Davis L.W. *American Journal of Clinical Oncology* 12(4):320-326 (1989).
- Laramore G.E. *Seminars in Oncology* 24:672-685 (1997).
- Lindsley K.L., Cho P., Stelzer K.J., Koh W.J., Austin-Seymour M., Russell K.J. *Bulletin du Cancer. Radiothérapie* 83 (Suppl 1): 78s-86s (1996).
- Lodge M., Pijls-Johannesma M., Stirk L., Munro A.J., De Ruyscher D., Jefferson T. *Radiotherapy and Oncology* 83(2):110-122 (2007).
- Matsufuji N., Kanai T., Kanematsu N., Miyamoto T., Baba M., Kamada T., Kato H., Yamada S., Mizoe J., Tsujii H. *Journal of Radiation Research* 48(Suppl):A81-A86 (2007).
- Munzenrider J.E., Liebsch N.J. *Strahlentherapie und Onkologie* 175 (Suppl II):57-63 (1999).
- Nias A. H. W., Greene D., Fox M., Thomas R. L. *International Journal of Radiation Biology* 13(5):449-456 (1967).
- NIRS *Annual Report*, NIRS-45, pp.49 (2005-2006). See:
<http://www.nirs.go.jp/ENG/publications/2005/05.pdf>
- Olsen D.R., Bruland Ø.S., Frykholm G., Norderhaug I.N. *Radiotherapy and Oncology* 83(2):123-132 (2007).
- Paganetti H., Niemierko A., Ancukiewicz M., Gerweck L.E., Goitein M., Loeffler J.S., Suit H.D. *International Journal of Radiation Oncology Biology Physics* 53(2):407-21 (2002).
- Pedroni E. *In: Proceedings of the 7th European Particle Accelerator Conference, EPAC 2000, Vienna, Austria, pp.240-245 (2000).*
- Richard F., Renard L., Wambersie A. *Bulletin du Cancer* 73(5):562-568 (1986).
- Russell K.J., Laramore G.E., Krall J.M., Thomas F.J., Maor M.H., Hendrickson F.R., Krieger J.N., Griffin T.W. *Prostate* 11(2):183-193 (1987).
- Scalliet P., Remouchamps V., Lhoas F., Van Glabbeke M., Curran D., Ledent T., Wambersie A., Richard F., Van Cangh P. *In: Proceedings of the XXIX PTCOG Meeting, DKFZ, Heidelberg and GSI, Darmstadt, Germany (1998).*
- Schardt D. *Nuclear Physics A* 787:633c-641c (2007).
- Sinclair W.K. *In: Biophysical Aspects of Radiation Quality, Second Panel Report, pp.39-56. Vienna, STI/PUB/171 IAEA (1968).*

- Schulz-Ertner D., Nikoghosyan A., Thilmann C., Haberer T., Jäkel O., Karger C., Kraft G., Wannemacher M., Debus J. *International Journal of Radiation Oncology Biology Physics* 58(2):631-640 (2004).
- Schmitt G., Wambersie A. *Radiotherapy and Oncology* 17:47-56 (1990).
- Sheline G.E., Phillips T.L., Field S.B., Brennan J.T., Raventos A. *American Journal of Roentgenology, radium therapy and nuclear medicine* 111(1):31-41 (1971).
- Stone R.S., Lawrence J.H., Aebersold P.C. *Radiology* 35:322-327 (1940).
- Stone R.S., Larkin J.C. *Radiology* 39:608-620 (1942).
- Stone R.S. *American Journal of Roentgenology Radium Therapy* 59:771-785 (1948).
- Tsujii H., Morita S., Miyamoto T., Mizoe J.-E., Kamada T., Kato H., Tsuji H., Yamada S., Yamamoto N., Murata H. *Annual Report NIRS*; National Institute of Radiological Sciences: Chiba-shi, Japan; pp.61 (2002).
- Tsujii H., Mizoe J., Kamada T., Baba M., Tsuji H., Kato H., Kato S., Yamada S., Yasuda S., Ohno T., Yanagi T., Imai R., Kagei K., Kato H., Hara R., Hasegawa A., Nakajima M., Sugane N., Tamaki N., Takagi R., Kandatsu S., Yoshikawa K., Kishimoto R., Miyamoto T. *Journal of Radiation Research* 48 (Suppl A):A1-A13 (2007).
- Tsunemoto H., Morita S., Satoh S., Iino Y., Yoo Y. *Strahlentherapie und Onkologie* 165(4):330-336 (1989).
- Wambersie A. *In: Radiobiological and Clinical Bases of Particle Therapy (Review), Proceedings of the 2nd European Particle Accelerator Conference, Nice (France), pp.268 (1990).*
- Wambersie A., Chauvel P., Gademann G., Gérard J.-P., Sealy R. EULIMA, Final Report, European Commission, Rue de la Loi, 200, B-1049: Brussels, Belgium, pp.2 (1992a).
- Wambersie A., Gregoire V., Brucher J.M. *International Journal of Radiation Oncology Biology Physics* 22(2):275-286 (1992b).
- Wambersie A., Menzel H.G. *Strahlentherapie und Onkologie* 169:57-64 (1993).
- Wambersie A. *Strahlentherapie und Onkologie* 175 (suppl II):39-43 (1999).
- Wambersie A. *Radiochimica Acta* 89, 245-253 (2001).
- Wambersie A., Gueulette J., Jones D.T.L. and Gahbauer R. *In: Charged particle and photon interactions with matter, pp. 743-784. Eds. Mozumber A. and Hatano Y. Marcel Dekker Inc, New York (2003).*

- Wambersie A., Hendry J. H., Andreo P., DeLuca P. M., Gahbauer R., Menzel H., Whitmore G. *Radiation Protection Dosimetry* 122(1-4):463-470 (2006).
- Weyrather W.K., Kraft G. *Radiotherapy and Oncology* 73 (Suppl 2):S161-S169 (2004).
- Yan X., Titt U., Koehler A. M. *Nuclear Instruments and Methods in Physics Research* A476, 429-434 (2002).

Classical Radiobiology: Principles of the Linear-Quadratic Model

The Linear-Quadratic (LQ) model represents the foundation of contemporary Radiobiology and all the models proposed in this thesis are derived from it. Hence this chapter introduces a review of its origins as well as its use in predicting final effects of some of the most common clinical situations encountered in conventional Radiotherapy.

3.1. The origins of the Linear-Quadratic model

Before the determination of the first *in-vitro* (Puck *et al.*, 1956) and *in-vivo* (Hewitt *et al.*, 1959) X-ray survival curves, several mathematical models were developed to predict survival levels at different doses for different types of radiation. One of the first and, for a long time, most accepted theories on cell survival was the Target Theory (Lea, 1946), which assumed the existence of specific sensitive targets within the cell, such that the survival or non-survival of a cell after radiation exposure would be related to the number of targets inactivated. The general version of the theory proposed that just one hit by radiation on each of n sensitive targets in the cell would lead to its death. The theory was fundamentally based on Poisson statistics and, more specifically, the presumption that during irradiation there is a very large number of hits taking place, but the probability of hitting any one cellular target is very small. Thus, for each cell,

$$P(0 \text{ hits on a specific target}) = \exp(-D/D_0) \quad (3.1)$$

Thus,

$$P(\text{specific target inactivated}) = 1 - \exp(-D/D_0) \quad (3.2)$$

As there are n targets in the cell:

$$P(\text{all } n \text{ targets inactivated}) = [1 - \exp(-D/D_0)]^n \quad (3.3)$$

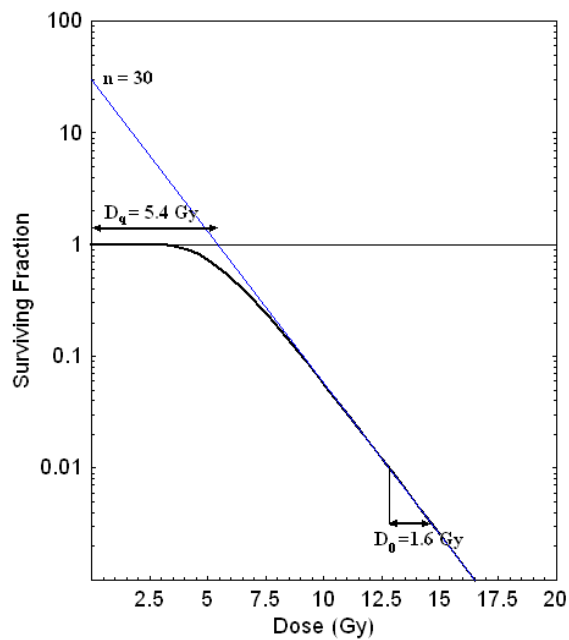
Thus, the final survival equation is:

$$P(\text{survival}) = P(\text{not all targets inactivated}) = 1 - [1 - \exp(-D/D_0)]^n \quad (3.4)$$

Figure 3.1a shows a survival curve obtained for $n=30$ and $D_0=1.6\text{Gy}$. These two parameters, n and D_0 , are related by a third parameter, D_q called the quasi-threshold dose which, in approximate terms, represents the dose below which there is no effect. It is given by:

$$D_q = D_0 \log_e n \quad (3.5)$$

a)



b)

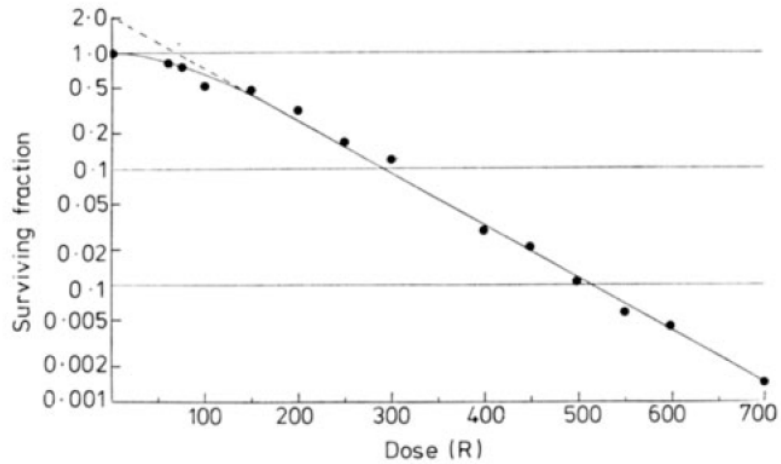


Figure 3.1: Comparison between a survival curve predicted by the Target Theory (showed in a) and the first survival curve experimentally measured by in-vitro by Puck et al. (1956) (showed in b). The experimental survival curve showed a finite initial slope (at $d \approx 0$ Gy) not predicted by the Target Theory.

When the first survival data was obtained, it became obvious that the general expression of the Target Theory derived above had the shortcoming of predicting a response that is flat for very low radiation doses whereas the data suggested that this was not the case, and that most mammalian cells had survival curves with a finite initial slope. To take account of this, Equation (3.4) was adjusted by adding an additional single-target component (i.e. $\exp(-D/D_1)$), resulting in a new equation:

$$P(\text{survival}) = \exp(-D/D_1) \times \left(1 - \{1 - \exp[-D(1/D_0 - 1/D_1)]\}^n\right) \quad (3.6)$$

According to this expression, four parameters are required to specify the survival curve associated with a given cell: n , D_0 , D_1 and D_q . This makes the model too complicated to be of much use in the clinical environment and of little value in helping to understand the fundamental mechanisms determining radiation effects.

After the discovery of the DNA structure by Watson, Crick, Wilkins and Franklin (Watson *et al.*, 1953a and 1953b), the idea of sensitive sites that had to be inactivated by radiation was abandoned and substituted by the belief that assaults to the DNA structure and their repair were the main determinant of the final effects expressed by cells after

exposure to radiation. Under this assumption, a new model evolved to predict radiation effect on cells. This, the Linear-Quadratic (LQ) model, fitted the continuously downward bending form of the cell survival much better than the Target theory as it predicted a finite initial slope. Two different approaches, an experimental and a mechanistic one, were used to derive the equation of the model, which may be expressed most simply as:

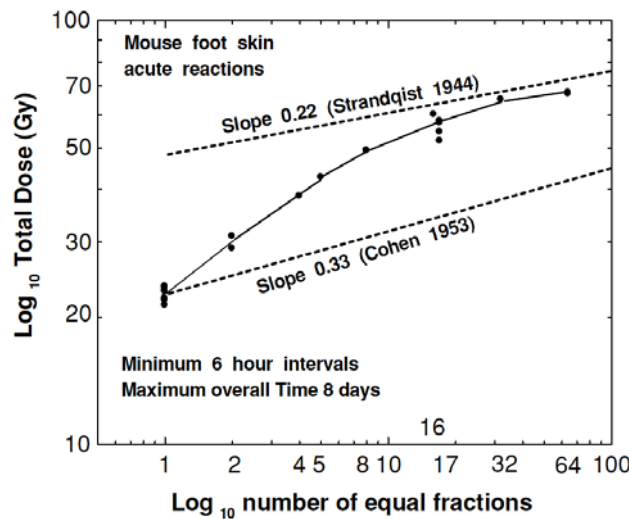
$$P(\text{survival}) = \exp(-\alpha d - \beta d^2) \quad (3.7)$$

The mechanistic approach to the LQ model will be dealt with in Chapter 4. The first experimental evidence that survival data from mammalian cells exposed to X-rays could be fitted by a linear-quadratic equation was found by Douglas and Fowler (Douglas *et al.*, 1976). In their experiments, they irradiated the legs of a number of mice simultaneously with X-rays and measured acute skin reactions on the legs in order to identify isoeffective fractionation regimes using 1 to 64 fractions. They then plotted the total isoeffective dose for each regime versus the number of fractions, showing that this plot was not a straight log-log line as predicted by the Ellis' NSD (Nominal Standard Dose) formula (Ellis, 1969), but a curving line (see Figure 3.2a). Then Douglas plotted the reciprocal of the total isoeffective dose versus dose per fraction, as simple algebra demonstrated that this data would only be a straight line if the cell survival curve of the critical (basal) cells had a linear-quadratic form. The data did indeed demonstrate a straight line relating reciprocal total dose to dose per fraction, which Douglas called *Fe* (fraction effective) plot, and it allowed the calculation of values of the parameters of the LQ formula, α and β , directly from experimental data (See Figure 3.2b) by using Equation (3.8). Further, reconstruction of the resulting iso-effect doses, divided by the fraction number for each fraction size, showed a very large shoulder, continuously bending which could be fitted with a linear quadratic equation (see Figure 3.2c).

$$Fe = \frac{1}{nd} = \frac{\alpha}{E} + \frac{\beta}{E} \cdot d \quad (3.8)$$

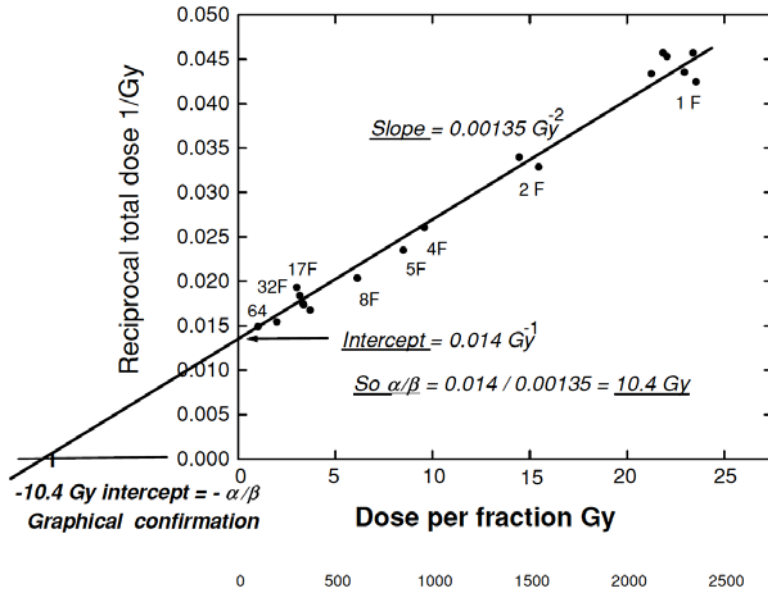
In Equation (3.8) n represents the number of fractions, d represents the dose per fraction and E represents the final intended effect. This demonstrated that the linear-quadratic formula applied to gross reactions in tissue *in situ* came from the mouse experiments, but its application to clinical radiotherapy did not materialised until four or five years later when Barendsen (1982), published his work on a formalism (called the ‘Extrapolated Tolerance Dose’ – ETD¹) based on the assumption that the frequency of a given radiation effect involve linear and quadratic dose-dependent terms. The ETD was based, as the Fe concept, on dose per fraction (d) as the basic parameter to describe iso-effective treatment schedules, but one of the main advantages of the ETD concept over the Fe concept was that it did not require the knowledge of specific values of α and β (which could only be obtained from experiments) but the knowledge of the ratios of α and β (α/β) for each type of tissue involved in the treatment. The α/β ratios were much easier to work with and, as a rule of thumb in clinical radiobiology, a general value of 3Gy and 10Gy were adopted to represent the α/β ratio of late-normal and tumour tissue respectively. The ETD concept was then ultimately developed and clinically justified by other people such as Dale (1985), Thames (1985), and Fowler (1989) the last of whom renamed ETD as the ‘Biological Effective Dose’ (BED) and produced an extensive review of α/β values for a large variety of tissues.

a)



¹ Later called ERD – Extrapolated Response Dose – by Barendsen (1982) to take into account the fact that ‘not all types of damage involved are actually related to tolerance, but rather to specific responses of the tissues considered’.

b)



c)

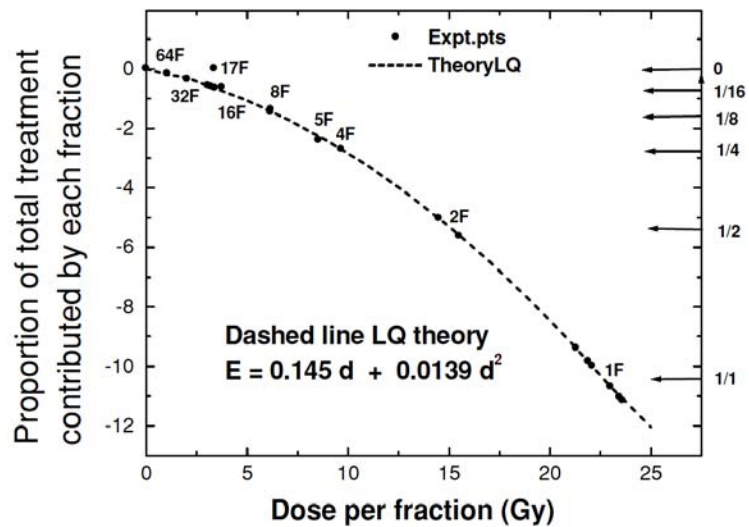


Figure 3.2: Results of the fractionation experiments carried out by Douglas and Fowler (1976) on mice skin reactions to different fractions of X-rays. Observe how, in figure (a), data could easily be confused for linear if only 8 fractions had been used, which overstates the importance when producing fractionation data of using very large number of fractions to study the departure from linearity on time-dose curves.

3.2. The BED formulation and its natural evolution with clinical practice

To derive the value of BED for a given fractionation scheme, it is necessary to specify the tissue involved (in terms of the α/β ratio) and the end point of interest (E). In this case, the ‘log cell kill’ (i.e. E) from n fractions of d Grays is given by:

$$E = n(\alpha d + \beta d^2) \Rightarrow BED = E/\alpha = nd \left(1 + \frac{d}{\alpha/\beta} \right) \tag{3.9}$$

It is useful to provide an explanation of BED by thinking of it as the total dose corresponding to the limiting case of the effect produced by a fractionation scheme of an infinite number of infinitesimally small doses per fraction, i.e.

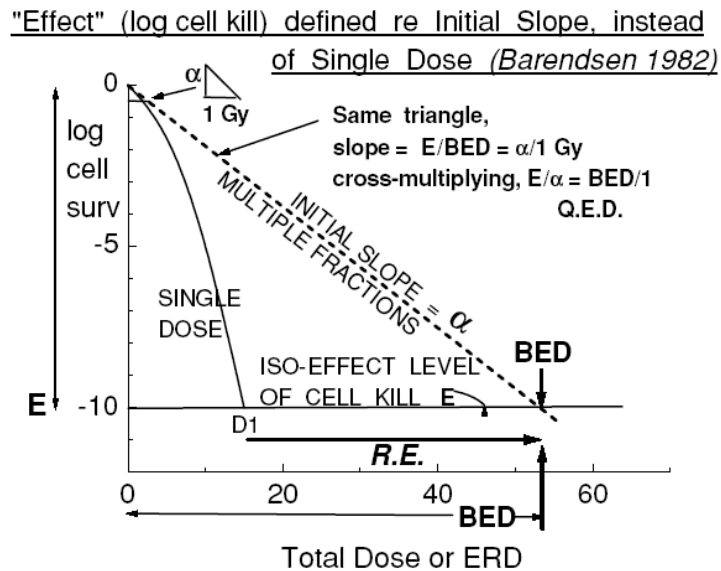


Figure 3.3: Graphical explanation of the BED concept (Fowler, 2006).

Equation (3.9) has been extended to account for a number of relevant clinical situations, such as changes in fractionation schemes to compensate unplanned gaps during radiotherapy treatments, change in radiation quality, etc... which will be discussed in the following subsections.

3.2.1. Time factors in fractionated radiotherapy

Fowler and Stern (1963) compared the respective influences of overall treatment time, fraction size and fraction number on the total isoeffective dose. In their initial observations, which are explained in more detail in Chapter 5, they concluded that the overall treatment time played a relatively minor role in the increase of the total dose required to produce the same effect when the number of fractions was increased. Accordingly, the observed increase of total isoeffective dose with number of fractions must be almost entirely due to the non-linear response of survival as the doses per fraction increase. This conclusion had to be reconsidered more carefully when Denekamp (1973) observed that the total dose increment necessary to counteract tissue repopulation in mice skin after different overall treatment times (one, two and three weeks) of daily irradiation changed quite dramatically. In particular, Denekamp observed that repopulation began about 12 days after the start of irradiation and it was then equivalent to an extra dose of approximately 1.3Gy per day (See Figure 3.4a). In the case of human tissue, the delay in the onset of repopulation was found to be longer (up to 4 weeks) (Fowler, 1984) due to the slower response of human tissue and the longer cell cycle of its individual cells. Although the existence of an onset time suggests a discontinuous (biphasic (Withers *et al.*, 1988; Maciejewski 1991) or even multiphasic) pattern for tumour repopulation, current views on repopulation models (Fowler, 1991; Jones *et al.*, 1995; 1999) suggest that repopulation may occur on a progressive pattern (one repopulation rate) as shown in Figure 3.4b instead of the discontinuous (more than one repopulation rate) one shown in Figure 3.4a.

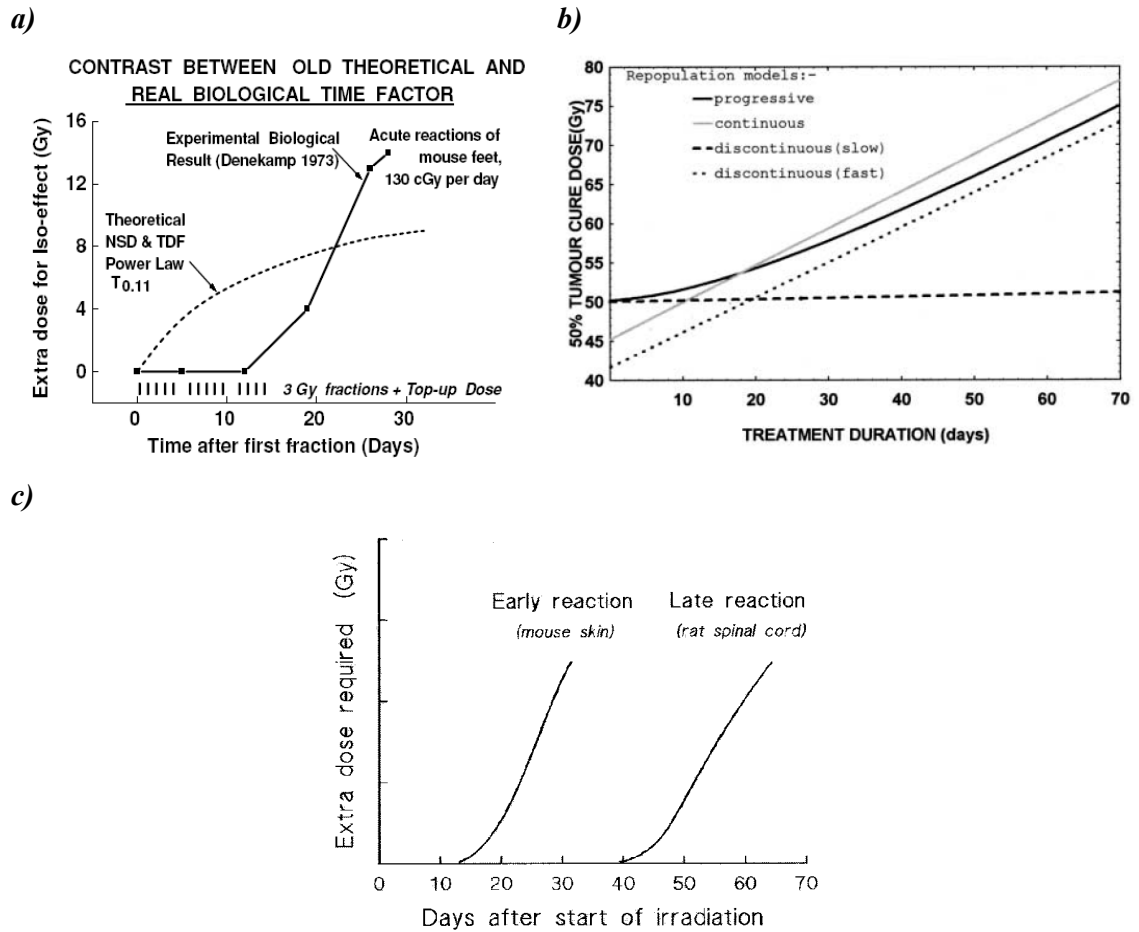


Figure 3.4: Study of repopulation effects from two different models perspectives: (a) considering there is an onset time (T_k) before repopulation does not exist; (b) considering a continuous repopulation effect always present but negligible at short overall treatment times; (c) Differences of repopulation capability between early and late reacting tissues.

Fowler (1983) also realised the important fact that different types of tissue had different onset times of repopulation (Figure 3.4c). Two tissue-type groups thus came to be recognised: those with a shorter onset time of repopulation, called *early reacting tissues* (e.g. skin, mucosa and intestinal epithelium) and those with a long onset times of repopulation, called *late reacting tissues* (e.g. like the case of spinal cord). Tumours are usually considered as behaving like early reacting tissues with short repopulation times, so the extension of the overall treatment time due to unplanned gaps during treatment, for instance, would require an extra amount of dose to counteract for repopulation². This

² As a corollary to this it could be inferred that late reacting tissues are not affected by repopulation in the event of an unplanned gap and therefore Equation (3.10) would not apply to late reacting tissues.

extra amount of dose has to be incorporated when calculating schedule variations to allow for unplanned gap during treatment. This is done by introducing a time factor ($e^{-\gamma T}$) in the survival formula representing the amount of cells not been killed by the lack of radiation, i.e.

Survival after treatment gap:

$$S = \exp[-n(\alpha d + \beta d^2) + \gamma T] \quad (3.10)$$

So that the total effect is given by:

$$E = n(\alpha d + \beta d^2) - \gamma T \quad (3.11)$$

and the biologically effective dose is then given by:

$$BED = \frac{E}{\alpha} = nd \left(1 + \frac{1}{(\alpha/\beta)} \right) - \frac{\gamma T}{\alpha} \quad (3.12)$$

A number of authors (Travis *et al.*, 1987; van de Geijn, 1989; Yaes, 1991; Dale, 1989; Amin *et al.*, 1993) have suggested that Equation (3.12) can be more precisely presented as:

$$BED = \frac{E}{\alpha} = nd \left(1 + \frac{1}{(\alpha/\beta)} \right) - \frac{0.693(T - T_K)}{\alpha T_{eff}} \quad (3.13)$$

Where T_K is the time at which repopulation effectively begins after the start of treatment, and T_{eff} corresponds to the effective doubling time of the tumour. According to Equation (3.13), four parameters are now required to predict effects of radiation on tumours when treatment time is considered, i.e. α/β , T_K , T_{eff} and α . Therefore, and similarly to the situation described in Equation (3.6), the introduction of a time factor in the LQ model diminishes its predicting power (or ‘innocence’ as Fowler (1989) puts it) (Dale, 1990).

3.2.2. Considerations of fractionation effects in non-conventional Radiotherapy

The BED formulation presented so far is traditionally used to design isoeffective fractionation schedules in conventional radiotherapy (i.e. that employing electrons or X-rays). In the present section the applicability and extension of this formulation to non-conventional radiotherapy (e.g. hadron or particle therapy) is presented.

When the survival curves of a biological system exposed to low- and high-LET radiations are plotted and compared, the main feature is that the survival curves as LET increases become more and more steep, i.e. more-closely exponential.

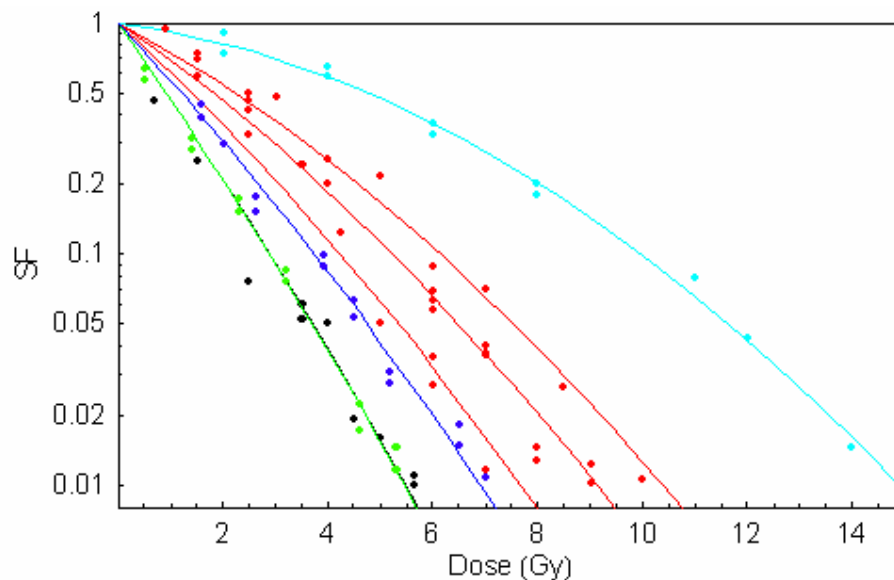


Figure 3.5: Comparison of survival curves produced with different types of radiation (Barendsen *et al.*, 1963).

This change of the shape of the survival curve is due to the higher efficiency of high-LET radiations in producing double strand DNA breaks, which are more difficult to repair. As indicated before (and later in Chapters 5 and 7), this type of damage (called Type A by Dale (1985)) is represented by the linear component of the LQ model, which at high-LET becomes much more predominant over the quadratic term in determining the shape of the survival curve. The exponential character of high-LET survival curves has always been understood as the main reason to assume high-LET radiations to be

less sensitive to fractionation effects than low-LET radiations, as cumulative radiation effects (two or more separate events leading to a double strand break) seem to be playing a minor role in attaining the final biological end point. This, together with the fact that the predominance of α at high-LET makes very difficult the measurement of β , has given rise to the assumption that β remains constant with changing LET. Assuming that this is the case, two fractionation regimes carried out with different radiation qualities will produce the same biological effect only if:

$$n_L(\alpha_L d_L + \beta d_L^2) = n_H(\alpha_H d_H + \beta d_H^2) \quad (3.14)$$

The question to answer is what extension/s have/s to be made on the BED formulation to adapt it to high-LET radiotherapy. For this purpose let us divide both sides of Equation (3.14) by α_L arriving to the expression:

$$n_L d_L \left(1 + \frac{d_L}{(\alpha/\beta)_L} \right) = n_H \left(RBE_{\max} d_H + \frac{d_H^2}{(\alpha/\beta)_L} \right) = n_H d_H \left(RBE_{\max} + \frac{d_H}{(\alpha/\beta)_L} \right) \quad (3.15)$$

where RBE_{\max} represents the value of RBE at the limit case of $d=0Gy$ and is given by

$$\alpha_L d_L = \alpha_H d_H \Rightarrow RBE \Big|_{d \approx 0Gy} = \frac{d_L}{d_H} = \frac{\alpha_H}{\alpha_L} = RBE_{\max} \quad (3.16)$$

Hence,

$$BED_H = n_H d_H \left(RBE_{\max} + \frac{d_H}{(\alpha/\beta)_L} \right) \quad (3.17)$$

Although repair effects have a relatively low impact when using high-LET radiations (see Chapter 7), repopulation may still be a factor to consider when extended overall treatment times are involved. Koike *et al.* (2002) found evidences of the existence of repopulation in NFSa fibrosarcoma grown in C3H/HeMsNrsf male mice legs after irradiation with 74 keV/ μ m carbon ions, using fractionation regimes ranging from single to 6 fractions.

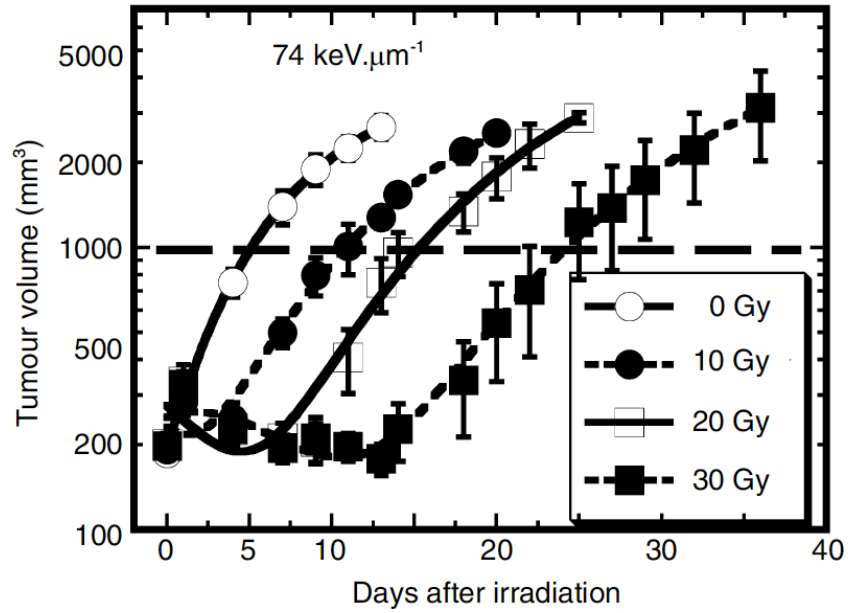


Figure 3.6: NFSa fibrosarcomas growing in mice legs irradiated with a 6cm SOBPs of carbon ions of $74 \text{ keV}/\mu\text{m}$ using 0 to 6 daily fractions.

Jones *et al.* (2006) have postulated that the same formulation presented in Equation (3.12) is still applicable, the only change being that, due to the higher efficiency of high-LET doses, the daily dose correction factors should be much lower than $K\left(\frac{0.693}{\alpha_L T_{pot}}\right)$ value doses (see Figure 3.7). In this case, isoeffective extended fractionation schedules with high-LET radiations will be obtained applying:

$$BED_H = n_H d_H \left(RBE_{\max} + \frac{d_H}{(\alpha/\beta)_L} \right) - K_H (T_H - T_K) \quad (3.18)$$

where $K_H = \frac{0.693}{\alpha_H T_{pot}} \ll K_L = \frac{0.693}{\alpha_L T_{pot}}$, which holds from the simple fact that $\alpha_H \gg \alpha_L$.

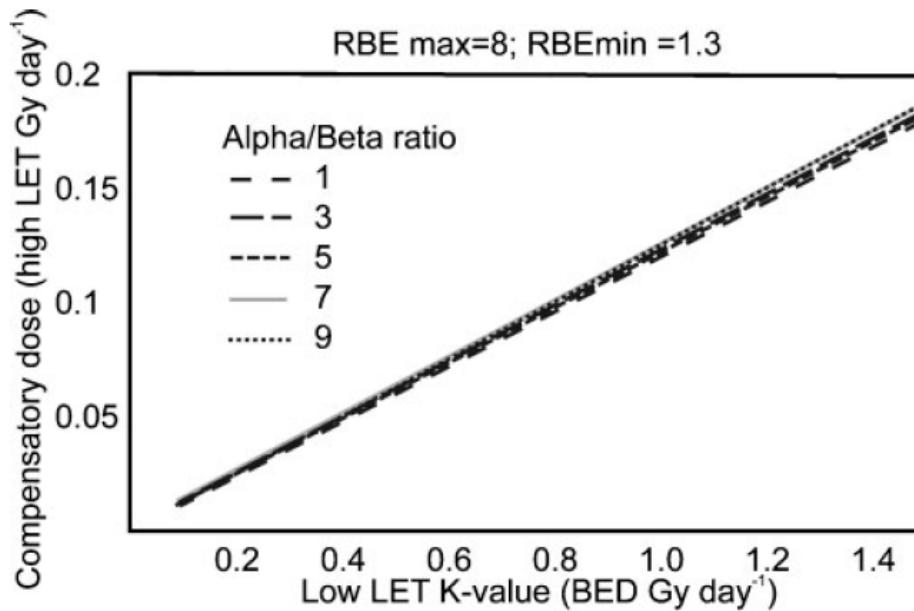


Figure 3.7: Relationship between low-LET K value and the calculated single fraction compensatory per day for a high-LET radiation with an $RBE_{max} = 8$ and $RBE_{min} = 1.3$ (Jones *et al.* 2006).

3.3. Summary

In this section we have briefly revised the experimental origin and the required extensions of the Linear-Quadratic model in order to incorporate effects such as repopulation and changes in radiation quality. Other factors can also be included in the model to account for different effects but these two offer, in my opinion, the chance to see how LQ can be adapted and use in different clinical situations in a simple and amenable way.

In the subsection dealing with fractionation effects with high-LET radiations, the classical formulation has been presented with the generally accepted assumption that accumulation effects have little impact and β is constant for different radiation qualities. These assumptions are specifically challenged in Chapter 5 of this thesis and the results of the alternative theory (where β is assumed to change with LET) are presented in Chapter 6. The impact of this revised theory on current practises of applying RBE weighting factors instead of a changing RBE value with dose per fraction is also discussed. This has special relevance in particular centres where there is a tendency to use large fraction sizes with high-LET radiotherapy (Tsujii *et al.*, 2004; 2007) as the use

of fixed RBE factors at high fraction doses can underestimate some important underlying effects and could lead to under- or over-estimation of the RBE for each individual tissue involved in the treatment field.

3.4. Bibliography

- Amin A.E., Wheldon T.E., O'Donoghue J.A., Barrett A. *Journal of Radiation Oncology Biology Physics* 27(2):323-330 (1993).
- Barendsen G.W., Walter H.M., Fowler J.F., Bewley D.K. *Radiation Research* 18:106-119 (1963).
- Barendsen G.W. *International Journal of Radiation Oncology Biology Physics* 8(11):1981-1997 (1982).
- Dale R.G. *British Journal of Radiology* 58(690):515-528 (1985).
- Dale R.G. *Radiotherapy and Oncology* 15(4):371-381 (1989).
- Dale R.G. *Radiotherapy and Oncology* 19(3):245-255 (1990).
- Denekamp J. *British Journal of Radiology* 46(545):381-387 (1973).
- Douglas B.G., Fowler J.F. *Radiation Research* 66(2):401-426 (1976).
- Ellis F. *Clinical Radiology* 20(1):1-7 (1969).
- Fowler J.F., Stern B.E. *British Journal of Radiology* 36(423):163-173 (1963).
- Fowler J.F. *Radiotherapy and Oncology* 1(1):1-22 (1983).
- Fowler J.F. *Acta Radiologica. Oncology* 23(4):209-216 (1984).
- Fowler J.F. *British Journal of Radiology* 62(740):679-694 (1989).
- Fowler J.F. *Radiotherapy and Oncology* 22(3):156-8 (1991).
- Fowler J.F. *Physics in Medicine and Biology* 51(13):R263-R286 (2006).
- Hewitt H.B., Wilson C.W. *Nature* 183(4667):1060-1061 (1959).
- Jones B., Dale R.G. *Radiotherapy and Oncology* 37(2):136-139 (1995).
- Jones B., Dale R.G. *Acta Oncologica (Stockholm, Sweden)* 38(7):883-893 (1999).
- Jones B., Carabe-Fernandez A., Dale R.G. *British Journal of Radiology* 79(939):254-257 (2006).
- Koike S., Ando K., Uzawa A., Takai N., Kukawa T., Furusawa Y., Oohira C., Monobe M., Lee R., Suzuki M., Nojima K. *Radiation Protection Dosimetry* 99(1-4):405-408 (2002).
- Lea D.E. *In: Actions of Radiations on Living Cells*. Cambridge University Press, 2nd Ed. (1946).
- Maciejewski B., Majewski S. *Radiotherapy and Oncology* 21(3), 163-170 (1991).
- Puck T.T., Marcus P.I. *Journal of Experimental Medicine* 103(5):653-666 (1956).

- Thames H.D. *International Journal Radiation Biology* 47(3):319-339 (1985).
- Travis E.L., Tucker S.L. *International Journal of Radiation Oncology Biology Physics* 13(2):283-287 (1987).
- Tsuji H., Mizoe J.E., Kamada T., Baba M., Kato S., Kato H., Tsuji H., Yamada S., Yasuda S., Ohno T., Yanagi T., Hasegawa A., Sugawara T., Ezawa H., Kandatsu S., Yoshikawa K., Kishimoto R., Miyamoto T. *Raditherapy and Oncology* 73 (Suppl 2):S41-S49 (2004).
- Tsuji H., Mizoe J., Kamada T., Baba M., Tsuji H., Kato H., Kato S., Yamada S., Yasuda S., Ohno T., Yanagi T., Imai R., Kagei K., Kato H., Hara R., Hasegawa A., Nakajima M., Sugane N., Tamaki N., Takagi R., Kandatsu S., Yoshikawa K., Kishimoto R., Miyamoto T. *Journal of Radiation Research* 48 (Suppl A):A1-A13 (2007).
- van de Geijn J. *British Journal of Radiology* 62(735):296-298 (1989).
- Watson J.D., Crick F.H.C. *Nature* 171(4356):737-738 (1953a); and
— *Nature* 171(4356): 964-967 (1953b).
- Withers H.R., Taylor J.M., Maciejewski B. *Acta Oncologica (Stockholm, Sweden)* 27(2):131-146 (1988).
- Yaes R.J. *Radiotherapy and Oncology* 21(2):143-144 (1991).

Quantitative and qualitative aspects of radiation: Microdosimetric considerations

The irradiation of matter and, more particularly, tissue, can be characterised in a variety of ways but basically one is dealing with measures of radiation quantity and radiation quality. When measuring either of these two aspects it is important to remember that the interaction between radiation and matter is random and chaotic at a microscopic scale, while at a macroscopic scale the fluctuation of energy deposited at a specific point is mostly minimal. Therefore, the quantitative and qualitative aspects of radiation should be characterised by parameters of differing nature (depending on the scale of interest) but defined in such a way that the integration of the discrete (microscopic) parameters leads the way to the continuous (macroscopic) parameters and vice-versa. This continuity between microscopic and macroscopic magnitudes is reflected in the following figure, where energy density is plotted as a function of the mass (or the track length) within which energy density is determined. As an example, the dosimetric variables absorbed dose (D) and linear energy transfer¹ (LET or L) have been plotted along with their corresponding microdosimetric variables *specific energy* (z) and *linear energy* (y).

¹ This discussion is restricted to L_{∞} . Utilization of a finite cut-off for delta-ray energy increases the complexity without significantly altering the conclusions made here. The case of L_{Δ} will be considered later in this chapter.

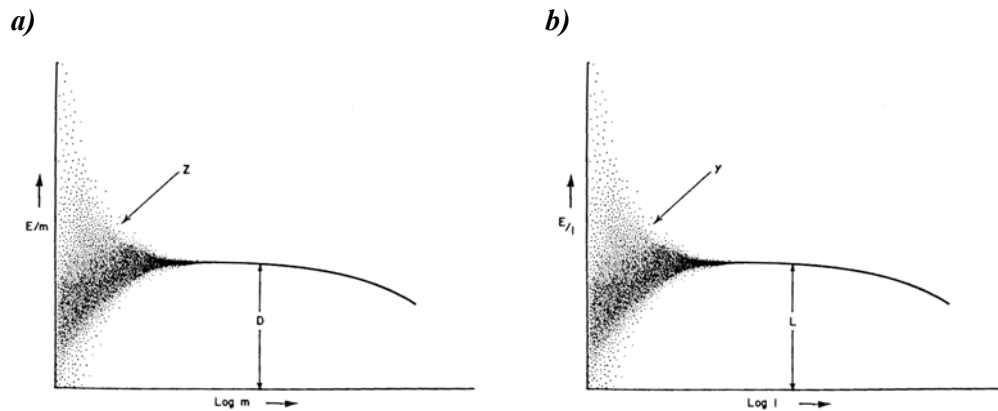


Figure 4.1: Plots showing the random nature of dose (figure a) or LET (figure b) at microscopic dimensions.

Figure 4.1a shows how the *local energy density* (z) deposited in a mass m of a limited volume of the irradiated material (sampling volume) fluctuates as the sampling volume becomes smaller. These fluctuations are of course due to the fact that the energy is deposited by charged particles in discrete steps; hence the local energy density in some small mass depends on how many charged particles, if any, happen to traverse the mass and on how much energy they happen to lose in their traversal. As mass m is increased, the number of particles traversing the sampling volume increases and the distribution of energy exchanged in the collisions between particles and matter becomes sufficiently uniform so that the quotient E/m becomes constant. It is this particular value of the ratio E/m that represents the absorbed dose (D). Therefore, the absorbed dose represents an average measurement of statistical fluctuations observed at microscopic level. These fluctuations, of course, occur no matter how large the sampling mass is, but commonly their magnitude is so small for large sizes of volume (volumes $> 0.1ml$) that D may be evaluated with any necessary precision.

The situation in Figure 4.1b is similar to that described in Figure 4.1a but in this case the sampling object is a segment of the track traversing a limited volume. When the segment of the track is very small, there might be no interaction between the particle and the material irradiated in that particular segment of the track; or there might be a limited number of interactions where the amount of energy exchanged in each one of them is different. For each individual exchange then there will be a different value of

local energy density, called in this case ‘ y ’ to differentiate it from its homologous ‘ z ’ based on mass sampling. As we increase the length of the sampling segment, more interactions occur between the particle along its track and matter, until the point where the distribution of energies deposited becomes homogenous and the quotient E/l (y) becomes constant. This constant is the linear energy transfer L of that particle which, similarly to the absorbed dose, it is an average magnitude subjected to fluctuations.

From this discussion it is possible to infer the macroscopic nature of quantities such as *absorbed dose* (D) and *LET* (L), realising also their microscopic origin and the differences with their microscopic counterparts, the *specific energy* (z) and the *linear energy* (y) respectively. Due to the practicality and simplicity of the macroscopic description of radiation, one may wonder what is the point in considering its microscopic description. However, extensive experimental work carried out on different biological systems has shown differences in the effectiveness of various types radiations, that is, differences in response to equal absorbed doses. These differences must certainly be due to differences in the microscopic distribution of energy in the irradiated material. In the following, different ways of describing this microscopic distribution of energy will be presented using concepts commonly used in *Microdosimetry*. The fact that the microscopic patterns of energy deposition differ so widely with different types of radiation and on different level of spatial resolution usually means that even the most detailed description or simulation of events will contribute little towards the recognition of those features and parameters that are critical for the biological effect. The purpose of Microdosimetry is therefore not the unlimited generation of data, but their deliberate reduction in order to identify the most essential parameters.

4.1. Quantitative and qualitative parameters at a macroscopic scale: Absorbed Dose (D) and Linear Energy Transfer (L)

At the macroscopic level of description, radiation quantity is measured in terms of the ‘absorbed dose’, which is defined by the ICRU 59 (ICRU, 1998) as ‘the quotient of $\bar{d\epsilon}$ by dm , where $\bar{d\epsilon}$ is the energy imparted by ionising radiation to the matter in a volume element, dm is the mass of the matter in that volume element’, i.e.

$$D = \frac{d\bar{\varepsilon}}{dm} \quad (4.1)$$

Radiation quality is more difficult to determine and even to define macroscopically. As it is established that quality is related to differences in the pattern of energy deposition on a microscopic scale and since one is dealing with a pattern rather than a single number, the situation is quite complex, and it has been commonly dealt with by approximations that are used not only to specify radiation quality but also its biological consequences. One of these approximations is the use of Linear Energy Transfer. This concept, introduced for the first time by Zirkle *et al.* (1952), is defined by ICRU (1998) as:

‘The *linear energy transfer* or *restricted linear collision stopping power* (L_{Δ}) of charged particles in a medium is the quotient of $d\bar{\varepsilon}$ by dl , where $d\bar{\varepsilon}$ is the average energy locally imparted to the medium by a charged particle of specified energy in traversing a distance of dl . That is,

$$L_{\Delta} = \left. \frac{d\bar{\varepsilon}}{dl} \right|_{\Delta} \quad (4.2)$$

The subscript Δ refers to the word ‘locally’ in the definition and indicates the cut-off limit of energy transfer. Any particle with energy greater than this cut-off limit will not be considered local and therefore not taken into account in the calculation of *LET*. L_{∞} indicates that all the possible energy transfers have been included and this ‘unrestricted’ *LET* is synonymous with collisional stopping power. Common units are kilo-electron-volts per micrometer (keV/ μm) in water of unit density for *LET* or linear stopping power and mega-electron-volts centimetres squared per gram for mass stopping power. An approximate geometrical interpretation of this cut-off energy is given in the following figure.

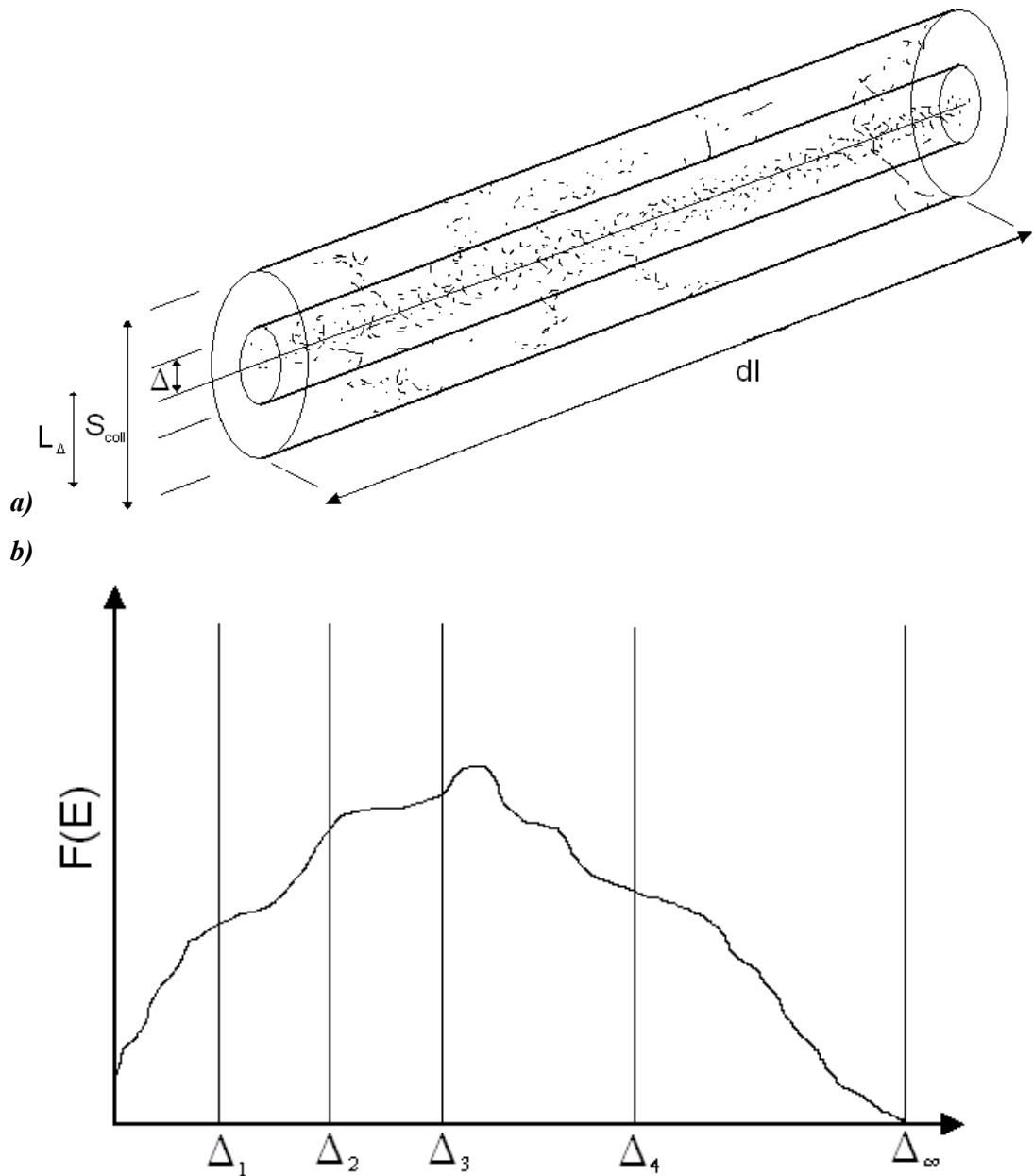


Figure 4.2: Geometrical interpretation of LET. Top: Concentric cylinders representing the cut-off energies of the delta-rays considered in the calculation of LET; bottom: Energy spectrum measured within the inner cylinder in figure (a), considering different cut-off (i.e. radius) energies.

On Figure 4.2a, the two concentric cylinders represent energetic boundaries for the delta-rays produced along the primary track. Particles with ejection energies larger than Δ will traverse the inner cylinder and be considered as primary particles themselves. The outer cylinder represents the case in which there is no cut-off limit and therefore,

every δ -ray is considered in the calculation of L (i.e. $L_{\Delta=\infty}$)². In this case, the definition of L coincides with that of the unrestricted linear stopping power, S . As mentioned before, the LET of a single primary track is expressed in terms of the arithmetic mean energy deposited in each individual interaction taking place within the inner cylinder in Figure 4.2a. Therefore, LET does not describe random fluctuations of energy deposition in interactions of a given primary particle or fluctuations among identical primary particles. This lack of microscopic descriptiveness of LET makes it suffer from the following limitations to describe patterns of energy deposition (Rossi, 1959; Goodhead, 1987):

- *Statistical fluctuations*: as discussed before, *LET* represents an average magnitude that does not take into account the random nature of energy loss along the track (i.e. *energy loss straggling*), which can result in wide variations in energy deposition by identical particles passing through small volumes.

- *Change in LET along the Track*: Any given dose delivered on a section of the track of fixed length can be deposited along a few long track sections or along many short ones. If the length of these sections is of the order of the dimensions of sensitive biological structures the consequences may be important, since incomplete passage through the structure may not result in inactivation. For instance, protons of energies of 1 MeV and 30 keV and electrons of 2 keV energy all have approximately the same *LET* of about 30 keV/ μm . These particles have not only markedly different penetration, but, more importantly, they maintain a *LET* which is, say, 10% of the above value, over distances which vary from several microns in the case of the more energetic proton down to magnitudes of the order of atomic diameters for the electron. For this reason, the validity of LET as a microscopic description for a given application depends on the distances of interest in that application and on the nature of the charged particles (charge, velocity and mass).

² When $\Delta=\infty$ is considered, it does not mean that the radius of the inner cylinder in Fig2a is infinite. It simply means that there is not restriction imposed on the energy of the delta-rays considered in the calculation of LET. Thus, ∞ has the meaning of 'all' in this formulation.

- *Lateral Extension and curvature of Track*: as has also been discussed before, this refers to the restriction in the definition of *LET* to energy ‘locally’ imparted. The δ -rays produced within the inner cylinder in Figure 4.2a are ejected from the primary track with different energies, and the representation of the δ -rays energy spectra is shown in Figure 4.2b. If different cut-off values are selected ($\Delta_1, \Delta_2, \Delta_3\dots$) the energy spectra changes together with its mean. This in turn changes the value of *LET* for that particular value of Δ .

Implications of these limitations have been discussed by Kellerer and Chmelevsky (1975) and Berger (1985). The former have considered the particular cases of energy deposition by electrons, protons, α -particles and oxygen ions in 0.1-10 μm diameter spherical volumes of unit density with specific quantitative criteria for the acceptability of the *LET*-based description. Leuthold and Burger (1984) have extended these criteria to energy deposition by protons and α -particles in spheres of diameter down to 1nm. Based on these criteria, *LET* can give an adequate description of protons, α -particles and oxygen ions, but only in particular regions of particle energy and site diameter. Electron tracks are unable to meet these criteria for any combination of electron energy and site diameter, emphasizing that *LET* descriptions of electrons should be used only with extreme caution.

4.1.1. LET distributions

Since the *LET* parameter inherently describes an average value, it may be calculated in two different ways:

1. Track Average *LET* ($\overline{L_{\Delta,T}}$), which is obtained by dividing the track into equal lengths, calculating the energy deposited in each length, and finding the mean. Mathematically, it is described as:

$$\overline{L_{\Delta,T}} = \frac{\int_0^{\infty} Lt(L)dL}{\int_0^{\infty} t(L)dL} \Bigg|_{\Delta} \quad (4.3)$$

In other words, this method assumes that each unit of track length has equal statistical weight and the average represents the expectation value of L .

2. Absorbed Dose Average LET ($\overline{L_{\Delta,D}}$), which is obtained by dividing the track into equal energy increments and averaging the lengths of track over which this energy increments are deposited. Its mathematical description is given by:

$$\overline{L_{\Delta,D}} = \frac{\int_0^{\infty} L^2 t(L)dL}{\int_0^{\infty} Lt(L)dL} \Bigg|_{\Delta} \quad (4.4)$$

In this case, the calculation is done such that $\overline{L_{\Delta,D}}$ weights each unit of track length in proportion to the energy transferred as the particle traverses it. $\overline{L_{\Delta,D}}$ is the expectation value of L^2 multiplied by a number ($1/\overline{L_{\Delta,T}}$) which is proportional to the mean number of unit track lengths per unit absorbed dose.

These two distributions have different properties and relate with one another in different ways (Goodhead, 1987). In the case of either X-rays or mono-energetic charged particles, the two methods of averaging yield similar results. In the case of 14MeV neutrons, by contrast, the track average LET is about 12 keV/ μm and the energy average LET is about 75 keV/ μm . The biologic properties of the neutrons tend to correlate with the energy average (Hall, 2000). In general, it happens that, for the same cut-off energy (Δ):

$$\overline{L_D} \geq \overline{L_T} \quad (4.5)$$

and this can be proven as follows:

$$\overline{L_D} = \int_0^{\infty} L^2 t(L)dL / \int_0^{\infty} Lt(L)dL \Rightarrow \overline{L_D} = \int_0^{\infty} L^2 t(L)dL / \overline{L_T} \int_0^{\infty} t(L)dL = \frac{\overline{L_T^2}}{\overline{L_T}}$$

The variance of any distribution is:

$$\sigma_T^2(L) = \overline{L_T^2} - \overline{L_T}^2 \Rightarrow \overline{L_T^2} = \sigma_T^2(L) + \overline{L_T}^2$$

Therefore,

$$\overline{L_D} = \frac{\overline{L_T^2}}{\overline{L_T}} = \frac{\sigma_T^2(L)}{\overline{L_T}} + \overline{L_T}.$$

$$\text{As } \sigma_T^2(L) > 0 \text{ and } \overline{L_T} > 0 \Rightarrow \overline{L_D} > \overline{L_T} \quad (4.6)$$

When the distribution of LET within the volume of interest ($E < \Delta$) has only one value of L, then

$$\overline{L_T^2} = \overline{L_T}^2 \Rightarrow \sigma_T(L) = 0 \Rightarrow \overline{L_D} = \overline{L_T} \quad (4.7)$$

Both, the track average and the absorbed dose average are sensitive to the cut-off energy selected to calculate the LET of the track, but it is observed that the latter is more sensitive than the former (ICRU, 1970). Thus for ^{60}Co γ -rays the following values are reported:

$$\begin{aligned} \overline{L_{\infty,T}} &= 0.24 \text{ keV}/\mu\text{m} & \overline{L_{\infty,D}} &= 0.31 \text{ keV}/\mu\text{m}, \\ \overline{L_{100,T}} &= 0.23 \text{ keV}/\mu\text{m} & \overline{L_{100,D}} &= 6.9 \text{ keV}/\mu\text{m}. \end{aligned}$$

One possible reason for this difference in the dependence of the cut-off energy is that, in the case of the absorbed dose average, the higher the cut-off, the smaller would be the track length required to achieve the same amount of absorbed dose and, therefore, the smaller $\overline{L_{\Delta,D}}$ would be. In general:

$$\overline{L_{\infty,T}} \geq \overline{L_{\Delta,T}} \quad (4.8)$$

but $\overline{L_{\infty,D}}$ maybe less than, equal to or greater than $\overline{L_{\Delta,D}}$ depending on how the values of unrestricted LET compare with those of the separate δ -rays and on the consequence of preferentially weighting the components of greater L .

4.2. Quantitative and qualitative parameters at a microscopic scale: Classical Microdosimetry

The lack of microscopic descriptiveness of LET has made necessary the definition of alternative quantities (Kellerer *et al.*, 1972; ICRU, 1980 and 1983; Kellerer, 1985) capable of providing the required microscopic description of energy deposition along particle tracks. All physical descriptions of the microscopic patterns of energy deposition along particle tracks constitute the field of *microdosimetry* in its broadest sense.

One of these quantities is the *linear energy*, y , defined as the energy ε imparted to the matter in a volume (typically that of a spherical Rossi Tissue Equivalent Proportional Counter (Rossi *et al.*, 1955), which can range between 10cm to 0.3 μ m in diameter) by a single energy-deposition event, divided by the mean chord length l through that volume, i.e.:

$$y = \varepsilon / \bar{l} \quad (4.9)$$

This quantity is very similar to the one provided for LET (Equation (4.2)), and indeed they coincide in value for idealised straight tracks passing through the volume with constant rate of energy loss (Goodhead, 1987). Similarly there is an equivalent microscopic quantity to absorbed dose, the *specific energy*, which is defined for each energy deposition event as the ratio between energy deposited ε and the mass of the volume where the deposition event takes place m , i.e.

$$z_1 = \varepsilon / m \quad (4.10)$$

When in the volume of interest more than one event takes place, the specific energy should incorporate the energy deposited in each of the deposition events:

$$z = \sum \varepsilon / m \quad (4.11)$$

Linear energy³ (y) and the single event specific energy (z_1) differ only by a numerical factor that depends on the magnitude, shape, and density of the volume (Kellerer, 1985).

For a sphere of diameter d and density ρ

$$z_1 = y / \rho d^2 \quad (4.12)$$

If y is given in units of kilo-electron-volts per micrometer, ρ in grams per cubic centimetre, d in micrometers, and z_1 in grams Equation (4.12) becomes

$$z_1(\text{Gy}) = 0.204 \frac{y(\text{keV}/\mu\text{m})}{[d(\mu\text{m})]^2} \quad (4.13)$$

The two quantities introduced above, y and z_1 , describe the energy imparted by single event depositions taking place in a microscopic volume. When a given dose D is imparted to that volume, more than one event will occur within it, each of them with different energies. Therefore, within the volume of interest a distribution of single events can be established as

$$F_1(z) = P(\underline{z} < z | \nu = 1) \quad (4.14)$$

$$F(y) = P(\underline{y} < y | \nu = 1)$$

i.e. the distribution function of single events is equal to the probability that the random variable \underline{z} does not exceed z when exactly one event has taken place in the volume. It must be noted that these distributions do not contain a discrete component at $z = 0$. By definition, an event requires energy deposition; the mere passage of a charged particle

³ The index 1 is not required with the distribution of y , because y relates by definition only to a single event.

without energy transfer to the volume is therefore not counted as an event. Equally, the differential distributions corresponding to the distributions above are:

$$\begin{aligned} f_1(z) &= dF_1(z)/dz \\ f(y) &= dF(y)/dy \end{aligned} \quad (4.15)$$

The density functions correspond to the probability that the specific energy assumes a value between z and $z+dz$ in each individual event. Some important relationships between frequency distributions and differential distributions are:

1. $F(y) = F_1(z)$, i.e. single-event distributions of lineal energy are largely equivalent to the single-event distribution of specific energy.
2. $f(y) = (V/\bar{l})f_1(z) = (S/4)f_1(z)$ for a volume of density $\rho=1\text{g/cm}^3$ with volume V and surface area S .

In order to establish the relationship between microdosimetric variables and their macroscopic counterparts, the average values of the former have to be calculated. As with the case of LET, these averages can be calculated for two different distributions: *frequency distributions* and *weighted distributions* of lineal energy or specific energy. In the case of the frequency distributions, the average specific energy produced by an event in the volume is:

$$\overline{z}_F = \int_0^{\infty} z f_1(z) dz = \int_0^{\infty} (1 - F_1(z)) dz \quad (4.16)$$

and the average linear energy is:

$$\overline{y}_F = \int_0^{\infty} y f(y) dy / \int_0^{\infty} f(y) dy \quad (4.17)$$

The weighted distributions are also called *dose distributions*. They determine the fractions of absorbed dose, or of energy imparted, that are associated with certain values of y and z and they are therefore relevant to all considerations of the effectiveness of

radiation as a function of local energy deposition in microscopic volumes. To calculate the average of the dose distributions we require the differential dose distribution of the specific and the linear energy, given by:

$$d(y) = \frac{y}{y_F} f(y) \quad d_1(z) = \frac{z}{z_F} f_1(z) \quad (4.18)$$

Their mean values are:

$$\begin{aligned} \overline{y_D} &= \int y d(y) dy = \frac{1}{y_F} \int y^2 f(y) dy = \frac{\overline{y_F^2}}{y_F} \\ \overline{z_D} &= \int z d_1(z) dz = \frac{1}{z_F} \int z^2 f_1(z) dz = \frac{\overline{z_F^2}}{z_F} \end{aligned} \quad (4.19)$$

As the variance of any distribution is equal to the second moment of the distribution minus its mean, i.e.:

$$\sigma_F^2(y) = \overline{y_F^2} - \overline{y_F}^2 \quad (4.20)$$

then an inequality similar to that obtained in Equation (4.8) can be found for the specific and the linear energies also:

$$\therefore \overline{y_F^2} = \sigma_F^2(y) + \overline{y_F}^2 \Rightarrow \overline{y_D} = \frac{\sigma_F^2(y)}{y_F} + \overline{y_F}$$

As $\sigma_F^2(y) > 0$ and $\overline{y_F} > 0$, then $\overline{y_D} > \overline{y_F}$. From this and the analogous relation for z one concludes that the dose averages $\overline{y_D}$ and $\overline{z_D}$ are always larger than the frequency averages $\overline{y_F}$ and $\overline{z_F}$.

It is clear that the average values of the dose distributions are given in terms of the first and second moments of the frequency distributions (Equation (4.19)). To discover the relation between the microdosimetric and the macrodosimetric variables, it is necessary

to study the relationship of the latter with the moments of the frequency distributions. At the beginning of this chapter it was said that absorbed dose D is the mean magnitude of the specific energy deposited in ν events within a volume. Therefore, the average specific energy at the absorbed dose D is the product of the mean event size \bar{z}_F and the mean number $\bar{\nu}$ of events,

$$\bar{z}(D) = \bar{z}_F \bar{\nu} \quad (4.21)$$

but it is also equal to D , i.e.:

$$\bar{z}(D) = D \quad (4.22)$$

Hence,

$$\boxed{\bar{z}_F \bar{\nu} = D} \quad (4.23)$$

It follows that the mean number of events $\bar{\nu}$ within the volume of interest is equal to D/\bar{z}_F . In particular, one concludes that the event frequency per unit absorbed dose is:

$$\phi = \frac{\bar{\nu}}{D} = \frac{1}{\bar{z}_F} \quad (4.24)$$

4.3. Brief introduction to mechanistic models based on microdosimetric magnitudes.

There have been numerous interpretations to the LQ model that have been developed from first principles on how radiation should interact with DNA to produce the final effect in irradiated cells. One of the firsts was proposed by Leenhouts and Chadwick (1974), who were able to derive expressions of the α and β parameters of the LQ model based on statistical interpretations different to those presented in this chapter. In this section we are going to introduce mechanistic interpretations of the LQ model based on microdosimetric interpretations. Therefore, three different models based on microdosimetry are going to be briefly discussed:

- The dual radiation action model
- The kinetic-microdosimetric model
- The Local Effect Model

4.3.1. The theory of dual radiation action (TDRA)

The Theory of Dual Radiation Action (Kellerer *et al.*, 1972) was originally developed to explain the form of the observed RBE values as a function of dose per fraction for high-LET radiations, especially neutrons.

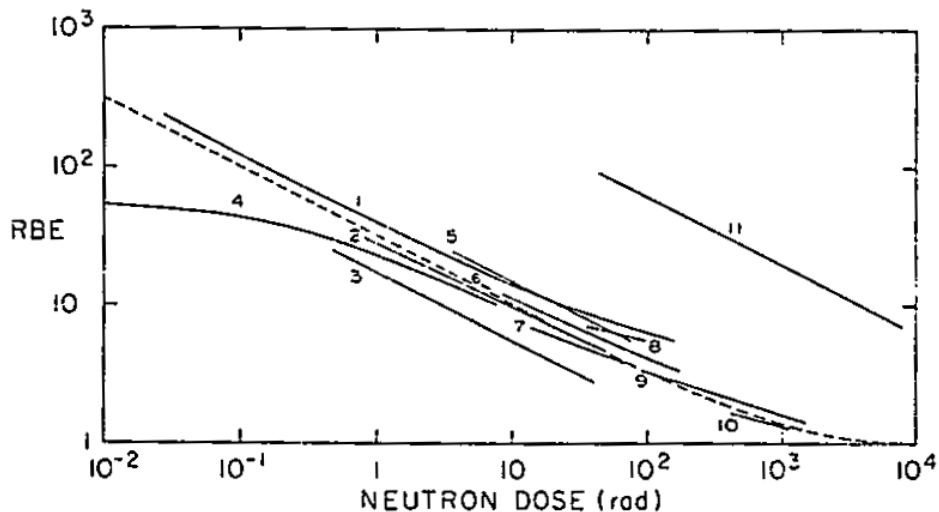


*Figure 4.3: Relative biological effectiveness of neutrons as a function of absorbed of neutrons for various biological endpoints (Kellerer *et al.*, 1972).*

The entire theory is based on the analysis and quantification of the fluctuating energy deposited along the track of the particles, together with the relation of this deposition events with the macroscopic biological effects observed, which ultimately will determine the RBE of that effect.

As indicated in the previous section, the relationship between microdosimetric and macrodosimetric variables is obtained from the moments of the frequency distributions, and these are defined in terms of the means of the frequency distributions (Equation (4.19)). The appropriate choice of mean value is determined by the postulation of how energy is imparted at the microscopic level. In the case of the TDRA, Kellerer and Rossi (1972) assumed that the biological effect (mutation or inactivation) occurs *only* by the accumulation and interaction of sub-lethal events, which can be produced in pairs by a single energy deposition event (one-track or intra-track effect) or separately from two different events in the same site (two-tracks or inter-track effect). Only pairs of sub-lesions within a ‘sensitive site’ are assumed to interact with one another to produce a lesion that leads directly to the observed biological effect; the precursor sub-lesions, by themselves, are not considered to be sufficient to produce observable damage.

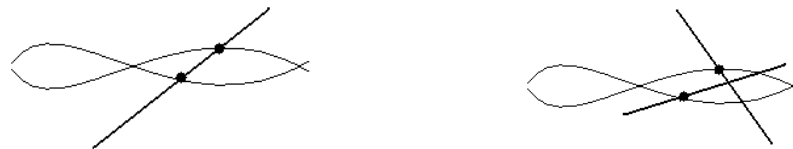


Figure 4.4: Lethal damage is produced ONLY by the interaction in ‘pairs’ of sub-lethal events produced in two different ways: one-track events (left) or two-track events (right).

Based on this assumption, Kellerer and Rossi (1972) postulated that the biological effect ε is proportional to the square of the specific energy z deposited in the volume of a sensitive site; i.e.

$$\varepsilon(z) = kz^2 \tag{4.25}$$

Where k represents the probability of any two lesions interacting, and it will be a constant different than zero if the two lesions are within the same site, and it will be

zero if they are further apart. As the probability is a constant value within the site diameter, it means that the probability is assumed to be independent of the distance between the sublethal lesions. This is the so-called *site interpretation*.

The biological effect as a function of dose can be obtained from Equation (4.25) as:

$$\varepsilon(D) = \int_0^{\infty} \varepsilon(z) f(z; D) dz = \int_0^{\infty} k z^2 f(z; D) dz = k \overline{z^2} \quad (4.26)$$

where $\overline{z^2}$ is the mean or expectation value of z^2 for dose D , and it can be shown that (see Appendix A):

$$\overline{z^2} = \frac{\overline{z^2}}{\overline{z_1}} D + D^2 = \frac{\int_0^{\infty} z^2 f_1(z) dz}{\int_0^{\infty} z f_1(z) dz} D + D^2 = \overline{z_D} D + D^2 \quad (4.27)$$

This equation is normally written as:

$$\overline{z^2} = \zeta D + D^2 \quad (4.28)$$

where ζ is the dose-weighted mean of the increments in specific energy z produced in the sensitive volume by single events (i.e. $\zeta = \overline{z_D}$), an event being the passage of a single track and all its secondaries. ζ is a constant characteristic of the site size of the biological system and of the type of radiation (constant 'c' in Appendix A). Consequently, Equation (4.26) becomes:

$$\varepsilon(D) = k(\zeta D + D^2) \quad (4.29)$$

where $k\zeta D$ represents the contribution to the biological effect resulting from 'intra-track' action and kD^2 represents the contribution due to 'inter-track' action. The quantity ζ can be evaluated experimentally in gases for different sensitive volumes

down to $\sim 0.3 \mu\text{m}$ by microdosimetric techniques and these measurements are often given in terms of the lineal energy density (y) distributions, whose dose-weighted mean $\overline{y_D}$ is related to ζ by expressions similar to Equations (4.12) and (4.13):

$$\zeta = \overline{z_D} = \frac{30.60}{d^2} \overline{y_D} \quad (4.30)$$

where d represents the site diameter. In Equation (4.30) two conceptually different parameters are related: $\overline{y_D}$, which is of *physical* nature and can be obtained using, for example, a Rossi (or any other) proportional counter (Rossi *et al.*, 1955; Booz, 1976); and ζ , which is of *biological* nature and is obtained from the non-linearity of the biological dose response (Equation (4.29)). The site diameter d of the biological system under study can then be deduced from Equation (4.30) and, for the case of mammalian cells, Kellerer and Rossi (1972) observed that the sensitive sites must be of diameter $\sim 1 \mu\text{m}$ (as a difference to the 2nm in diameter of the DNA molecule) to explain the observed curvature of the dose-effect relationship obtained for them. If the sites were much smaller there would be insufficient probability of coincidence of tracks in a site at conventional doses.

However, investigations with ultra-soft X-rays show that the assumptions on which the model is based are not valid in the case of mammalian cells. Experiments with ultra-soft X-rays producing electron track lengths much shorter than the dimensions of the assumed sensitive sites, showed greatly *enhanced* effectiveness per unit absorbed dose rather than a *reduced* effectiveness as predicted by the model (Goodhead, 1977; 1982; 1983; *et al.* 1979; Virsik *et al.*, 1980; Raju *et al.*, 1984; Wilkinson *et al.*, 1985; Thacker *et al.* 1985; Frankenberg *et al.* 1980). These experimental data indicate that the biological effectiveness of radiation is determined largely by the microscopic patterns of energy deposition over much smaller distances, probably of the order of nanometers or tens of nanometer. Therefore, total energy deposition in simulated volumes of *micrometric* dimensions does not provide a wholly adequate microscopic description of these observations.

As a consequence of the findings from the ultra-soft X-rays experiments Kellerer and Rossi extended the TDRA to the generalised formulation of dual radiation action (GTDRA) – also known as the *distance interpretation* of the TDRA – where the probability of interaction between sublethal lesions within the site is considered to be dependent on the distance between the lesions instead of being constant. In this case, the GTDRA incorporates an ‘effective interaction distance’ that replaces the distance d in the TDRA:

$$\Delta = 3 \left(\frac{\int_0^{\infty} x \rho(x) dx}{\int_0^{\infty} \rho(x) dx} \right)^{1/2} \quad (4.31)$$

where $\rho(x)$ is the probability for a sub-lesion to interact with another sub-lesion at a distance x (Kellerer *et al.*, 1972). Therefore, the probability of interaction in the entire site can be formulated as:

$$k \propto \int_0^{\infty} x^2 \rho(x) dx \quad (4.32)$$

This formulation should support the findings by Goodhead (1977) of large values of k for aluminium ultra-soft X-rays, small k for helium ion track intersections and intermediate k for γ -rays for inactivation and mutation of V79 hamster cells. According to this formulation, Equations (4.25) and (4.29) should be then modified to a more general formulation such as,

$$\varepsilon(z) = k(x)z^2 \quad (4.33)$$

$$\varepsilon(D) = \int_0^{\infty} \int_0^{\infty} k(x)z^2 f(z; D; x) dx dz \quad (4.34)$$

There are also difficulties understanding how a model can, from purely microdosimetric (physical) considerations, lead to the linear-quadratic dose-effect relationship. This is because, as is well known, the final expression of biological effect takes place, not immediately after the dose deposition (physical stage), but after the relevant repair

enzyme process (bio-molecular stage) finalises, at which point any un-repaired DNA damage will determine the course of evolution for the cell at the end its mitotic cycle. For this reason there have been efforts to combine microdosimetric-based models with repair kinetic models in order to combine the key features of each. This is the case of the Microdosimetric-Kinetic (MK) model studied in the following subsection.

4.3.2. The kinetic-microdosimetric model

Hawkins (1994; 1996; 1998; 2003; 2006) proposed a model which expanded the fundamental assumption of the TDRA (Equation 4.25) without requiring proximity functions (i.e. $\rho(x)$), as well as allowing for the final expression of survival (the linear quadratic equation) to be obtained from repair kinetic principles similar to those proposed in the lethal-potentially lethal (LPL) (Curtis, 1986) and the repair miss-repair (RMR) (Tobias *et al.*, 1980) models.

Microdosimetric considerations

The MK model extends the fundamental assumption of the TDRA by considering that lethal (non-repairable) lesions are due not only to the association of two sub-lethal lesions, but also due to some of a sub-lethal lesions not being repaired after a certain amount of time (e.g. a number of completed mitotic cycles). As pairs of sublethal lesions is represented by the TDRA by a quadratic dependency with z , the MK model proposes the following mathematical expression for the average number of lethal lesions after z sub-lethal lesions are created in a domain d :

$$\varepsilon(z) = Az + Bz^2 \tag{4.35}$$



Figure 4.5: Interaction types considered in the ballistic version of the MK model. One extra pathway is considered as a difference to the TDRA model, where the new (left hand) diagram represents the non-repairable sub-lethal lesion which produces a further amount of lethality which is proportional to dose.

As the effect produced by a single track should be proportional to dose D while two-track action should be proportional to the square of the dose, Figure 4.5 implies that the dose-effect relationship for this model should be similar to,

$$\varepsilon(D) = aD + bD + cD^2 = (a + b)D + cD^2 \quad (4.36)$$

where a , b and c correspond to the probabilities of occurrence of a non-repairable 1 track-ssb, 1 track-dsb and 2 track-dsb respectively. It can be shown (Hawkins, 1998) that the corresponding dose-effect relationship obtained from Equation (4.35) is:

$$\varepsilon(D) = (\alpha_0 + \gamma\beta)D + \beta D^2 \quad (4.37)$$

where α_0 represents the probability associated with 1 track-dsb damage, $\gamma\beta$ the probability associated with 1 track-ssb damage and β the probability for 2 tracks-dsb damage. The MK model is based on a ‘hybrid’ theory and the parameters of the Linear-Quadratic expression are linked to the repair kinetics of the system under study for the known conditions of irradiation. Therefore, α_0 and β can be expressed as a function of kinetic parameters, as will be demonstrated in the following subsection. γ however, has the same role as ξ in the TDRA model and is related to the dimensions of the domains within the cell nucleus that contains the critical targets and also to the LET of the radiation used to irradiate them. This relationship is established through the following expression:

$$\gamma = \frac{0.229}{d^2} L \quad (4.38)$$

where d is the dimension of the domain in microns, and L represents the LET of the radiation used, expressed in keV/ μm .

Repair Kinetic considerations

The kinetic interpretation of the MK model is presented by Hawkins as a reformulation of the breakage-reunion model of chromosome aberration formation (Revell, 1974). The

model stands half-way between the Repair-Misrepair model (RMR) (Tobias *et al.*, 1980) and the Lethal Potentially-Lethal model (LPL) (Curtis, 1986). Hawkins recognised a number of weaknesses in these two models, i.e.:

1. Both, the RMR and the LPL models do not account for the 1 track-1 SSB lesion type in Figure 4.6 (MK diagram, mitotic misrepair, *a*), which can contribute significantly to cell lethality under some circumstances. In particular, the LPL model does not account for lethal lesions produced by un-repaired sublethal lesions, and the RMR does not account for production of primary lethal lesions (i.e. lesions not produced by sublethal accumulation).

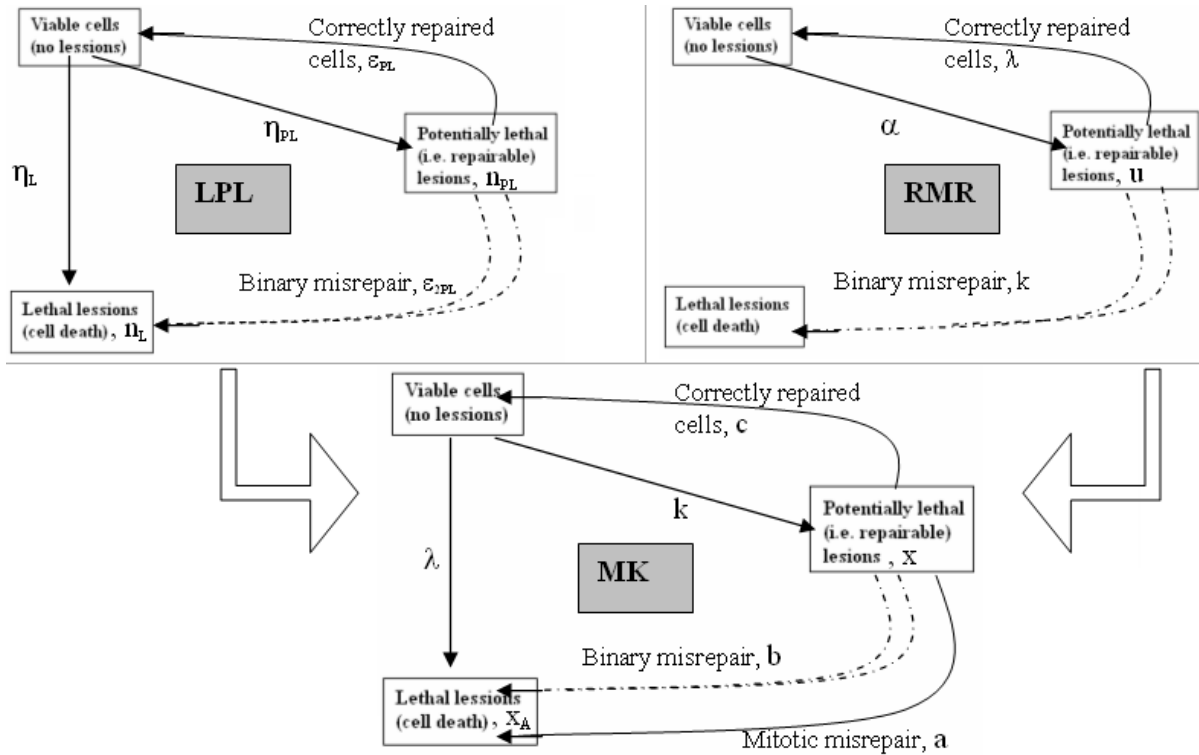


Figure 4.6: Differences between the LPL, RMR and MK models

LPL	n_{PL}	n_L	ϵ_{PL}	1	ϵ_{2PL}	ϵ	η_{PL}	η_L	t_r	0
RMR	u	...	λ	ϕ	k	ϵ	α	0	T	0
MK	x_d	x_{Ad}	(a_d+c_d)	$c_d/(a_d+c_d)$	b_d	$(a_d+c_d)/b_d$	k_d	λ_d	t_r	γ

Table 4.1: Correspondence between the kinetic and microdosimetric parameters of the MK, LPL and RMR models. Observe that the MK model can be reduced to the RMR if $\lambda = 0$, and to the LPL if $a = 0$ for radiation possessing effectively zero LET (Hawkins, 1996). Subscript ‘d’ stands for ‘domain’.

2. The equations that are fitted to important types of cell survival data and which allow quantitative estimation of the contribution of various pathways to cell death or recovery have been incompletely developed.
3. The effect on survival of the microscopic inhomogeneity of dose deposition inherent in the use of radiation with significantly non-zero LET is not dealt with in either the LPL and RMR models.

As can be seen in Figure 4.6, there are two types of lesions: Type I (TI), characterised by the parameter x_{Ad} , which represents the 1 track-2 SSB case; and Type II (TII), represented by x_d , which includes all those lethal lesions originated from 1 track-1SSB or 2 track-2 SSB in the same figure. The ratio of production by these two processes will be proportional to the dose absorbed by the domain, represented by z_d . Thus, the average number of TI and TII lesions developed in the domain after having absorbed exactly z_d Gy is λ_d and k_d respectively.

From the k_d TII lesions produced, a_d will become lethal through the mitotic misrepair process while b_d will become lethal by binary misrepair. The former only requires *one* sublethal lesion to form a lethal lesion (first order process), whereas the later needs *two* sublethal lesions to combine to produce a lethal event (second order process). The rest of the k_d TII lesions not converted into TI lesions will either be repaired or will remain unrepaired for a period of time t_r , after which, if they are still present, they become lethal and unreparable. The number of repaired TII lesion is denoted by the parameter c . Therefore, a and c represent first order processes and for this reason they are proportional to x_d , whereas b_d is related to second order processes and will be proportional to x_d^2 . The rate equations describing these processes are:

$$\left. \begin{aligned} \dot{x}_d &= k_d \dot{z}_d - (a + c)x_d - 2b_d x_d^2 \\ \dot{x}_{Ad} &= \lambda_d \dot{z}_d + a x_d + b_d x_d^2 \end{aligned} \right\} \quad (4.39)$$

$$\left. \begin{aligned} \dot{x}_d &= k_d \dot{z}_d - (a + c)x_d - 2b_d x_d^2 \\ \dot{x}_{Ad} &= \lambda_d \dot{z}_d + a x_d + b_d x_d^2 \end{aligned} \right\} \quad (4.40)$$

In these two equations it is important to realise that the factor $2b_d$ in Equation (4.39) symbolises the fact that, for each line entering into the x_{Ad} box in Figure 4.6, two lines coming out from the x_d box will be required. This is not to be confused with the squared exponent which indicated the type of lesion the parameter b_d refers to.

It can be proved (see Appendix B) that the solution of the system of differential equations constituted by Equations (4.39) and (4.40) provides expressions for α_0 and β as a function of the repair kinetic parameters:

$$\alpha_0 = \lambda + \frac{ak}{(a+c)} + \frac{kc}{(a+c)} e^{-(a+c)t_r} \quad (4.41)$$

$$\beta = \frac{bk^2}{2(a+c)} (1 - e^{-2(a+c)t_r}) \quad (4.42)$$

Although the MK model represent an elegant and much more powerful option than the TDRA due to the extra kinetic information that can be extracted from it relevant to the biological system under study, it still possesses a number of weaknesses inherited from its predecessors, the TDRA, RMR and LPL models.

For instance, the inclusion of a linear power of z into the initial assumption of the TDRA model was already discussed qualitatively in relation to biological data by Kellerer and Rossi (1973). Similarly, Goodhead (1977) studied this inclusion of a linear power into the TDRA hypothesis in order to study a possible better prediction of the TDRA for the ultra-soft X-rays. However, Goodhead had already concluded that the addition of the linear term increased the conflict between model and data as it would require an increase of the site diameter d for the γ -ray results.

Also, the MK model proposes a linear relationship between the RBE at very low doses (i.e. RBE_{\max}) and LET, given by

$$RBE_{\max} = \frac{\alpha_0 + \gamma\beta}{\alpha_R} = \frac{\alpha_0}{\alpha_R} + \frac{\beta}{\alpha_R} \frac{0.229}{d^2} L \quad (4.43)$$

where α_R corresponds the initial slope of the reference irradiation. This is however in contradiction with all data on the RBE dependence with LET, which always shows that RBE increases with LET until it reaches a turnover point from where RBE decreases. Hawkins has recently resolved this shortcoming in the theory by considering a non-Poisson distribution of radiation events (Hawkins, 2003). In this case, there is a problem in deciding which non-Poisson distribution is more convenient for each biological system, but this can be circumvented if the dependence with LET is introduced throughout the repair kinetic parameters instead of through the parameter γ (Equation (4.38)) in the MK theory or the ξ (Equation (4.30)) in the TDRA. This probably would make much more sense as a dependency of $a = a(L)$, $b = b(L)$, $c = c(L)$, $\lambda = \lambda(L)$ and $k = k(L)$ would imply an intrinsic dependency of α_0 and β of LET, which is what it is observed from the survival curves of biological systems exposed to different radiation qualities. The way the TDRA model (in its ‘site’ interpretation) and the MK model are formulated, implies that β (which appears in the quadratic term of the LQ model) is constant with LET (which is an argument dealt with later on in Chapter 5) and that α (linear term of LQ model) is only linearly dependent on LET through Equations (4.30) or (4.38), which as it has been said, contradicts experimental findings.

The dependency of repair parameters with LET can be readily observed from experimental work performed on multiple biological systems exposed to different radiation qualities such as, for instance, V79 cells irradiated with ions of different LET by Belli *et al.* (2000) (Figure 4.7a) and Goodwin *et al.* (1994) (Figure 4.7b).

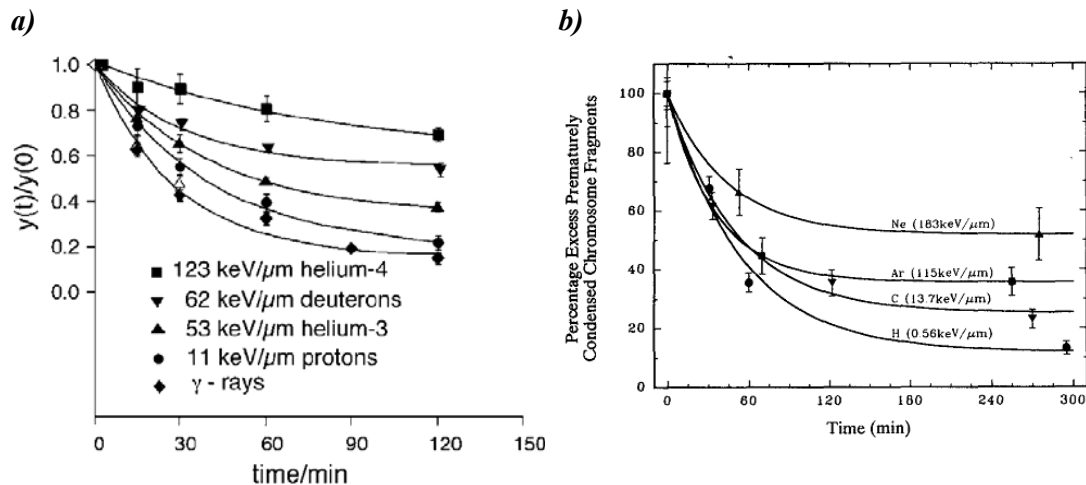


Figure 4.7: Variation of DNA repair rate for V79 cells exposed to radiations of different LET.

This alternative of introducing the LET dependence of the effect through the repair kinetics has been tried out by Russian teams (Kozubek *et al.*, 1982a,b,c,d,e; 1983a,b,c,d,e; 1984a; 1984b), who have arrived to some conclusions that warrant serious consideration. However, as is the case with Equation (B.7) in Appendix B, the final expressions of α and β derived by these teams are extremely complex with far too many parameters to allow them to be easily applied to radiobiological experiments and, ultimately, to clinical practice.

For this reason a much more simplistic, but perhaps more clinically relevant repair kinetic model incorporating changes of the kinetic parameters with LET, is proposed in Chapter 8. The model is proposed from the perspective of analysing what type of repair kinetics might be of more relevance to high-LET radiations and as an effective approach to the ideas discussed in the paragraphs above.

4.3.3. The Local Effect Model (LEM)

Scholz and Kraft (1994; 1996; 2004) proposed the LEM model in order to be able to include RBE values in the treatment planning process for patients undergoing ion therapy at GSI. Due to its clinical relevance, it is worthwhile to summarise the model in this section.

The most fundamental assumption on which the LEM model is constructed upon is that cell inactivation is due to the production of lethal events, regardless of the radiation type that produced them, their biochemical nature or the precise molecular structure of these lethal events; only their number is relevant. Also, it is assumed in the model that no long distance interaction between sublethal damage occurs, and for this reason it is called the *local effect* model.

The mathematical structure of the model starts by quantifying the frequency of lethal events locally deposited within the nucleus of the cell for a given dose D , i.e. average number of lethal event per unit of critical volume (nucleus volume):

$$v(D) = \frac{\overline{N_{lethal}(D)}}{V_{nucleus}} \quad (4.44)$$

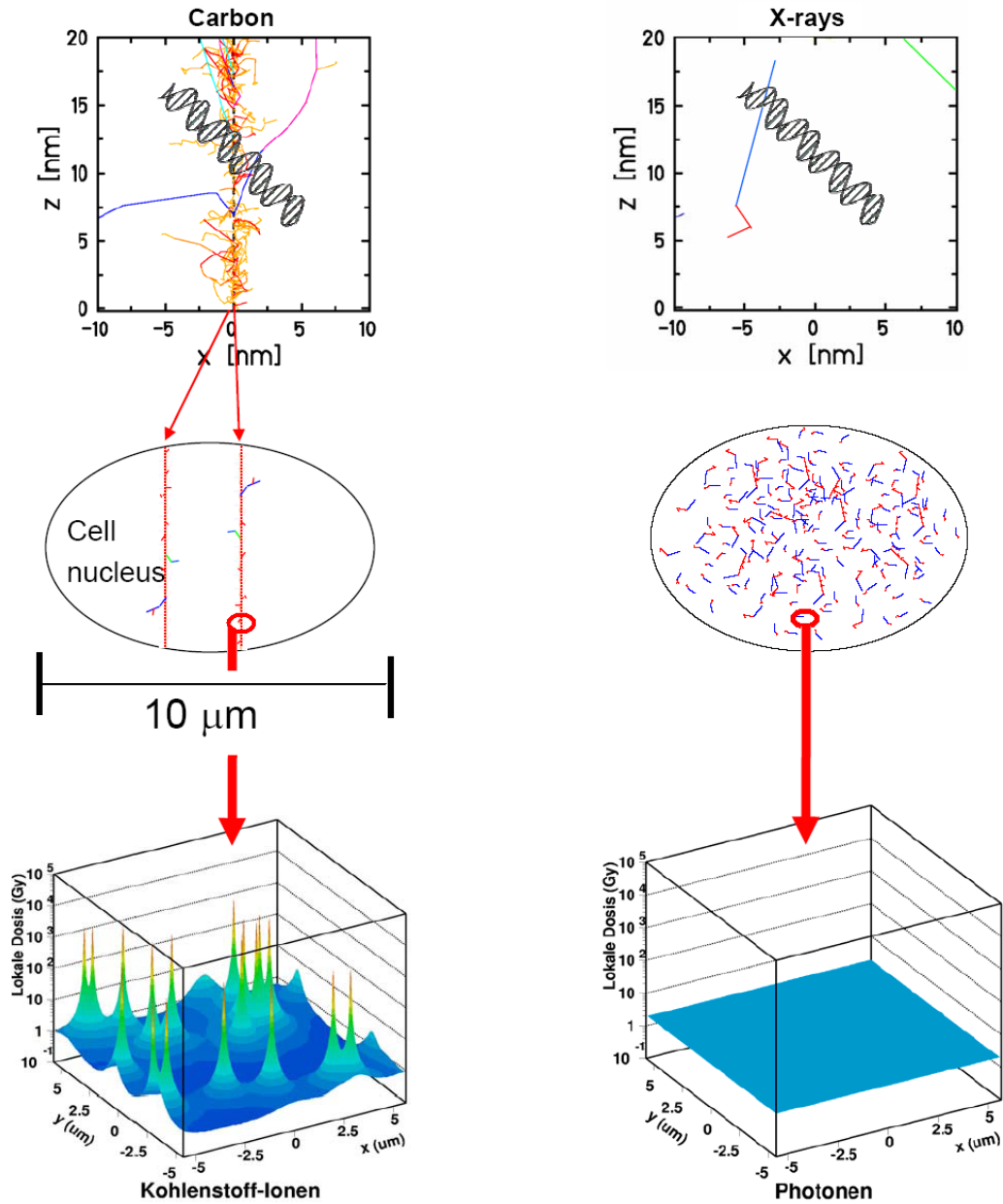


Figure 4.8: Difference on the pattern of energy deposition between carbon ions and X-rays.

For X-rays, as we can see in Figure 4.8 (right) the dose D is delivered homogeneously among the cells of a population. Therefore the lethal events are randomly distributed and the number of survival cells (i.e. fraction of cells carrying no lethal events) can be described using Poisson statistics:

$$S_X = e^{-\overline{N_{lethal,X}}} \Rightarrow \overline{N_{lethal,X}} = -\log S_X \quad (4.45)$$

Hence, the frequency number of lethal events within the critical target (nucleus) for X-rays is obtained from Equation (4.44),

$$v_X(D) = \frac{\overline{N_{lethal,X}(D)}}{V_{nucleus}} = \frac{-\log S_X(D)}{V_{nucleus}} \quad (4.46)$$

In the case of a cell population exposed to ion beams, the dose is not distributed homogeneously (see Figure 4.8 left) and its distribution has to be specified in every point of the cell nucleus, i.e. $d=d(x,y,z)$. In this case, the frequency of lethal events is obtained from the sum of the frequency of lethal events produced in every infinitesimal volume constituting the critical volume,

$$v_{ion}(D(x,y,z)) = \frac{d \overline{N_{lethal,ion}^{local}}}{dV^{Nucleus}} = \frac{d \overline{N_{lethal,ion}^{local}}}{dxdydz} \Rightarrow \overline{N_{lethal,ion}^{nucleus}} = \int_x \int_y \int_z v_{ion}(D(x,y,z)) dx dy dz \quad (4.47)$$

If the average number of lethal events produced by photons and ions is the same at any differential volume of the nucleus (i.e. $\overline{N_{lethal,ion}^{local}} = \overline{N_{lethal,X}^{local}}$) where the dose is $D(x,y,z)$ (so called, *local dose* – see Figure 4.8), it follows that:

$$v_X(D(x,y,z)) = v_{ions}(D(x,y,z)) \quad (4.48)$$

Hence, Equation (4.47) can be reformulated as

$$\overline{N_{lethal,ion}^{nucleus}} = \int_x \int_y \int_z v_X(D(x,y,z)) dx dy dz \quad (4.49)$$

and, from Equation (4.46), we obtain:

$$\overline{N_{lethal,ion}^{nucleus}} = \int_x \int_y \int_z \frac{-\log S_X(D(x,y,z))}{V_{nucleus}} dx dy dz \quad (4.50)$$

Three components are required to solve this integral: the nucleus volume ($V_{nucleus}$), the local dose distribution ($D(x,y,z)$) and the X-ray survival curve (S_X).

The nucleus volume, which in the theory is assumed to be given by a cylinder with geometrical cross section A_{Nucl} and height H_{Nucl} , can be obtained from the experimental data. An important assumption made here is that a unique radiosensitivity and nucleus size is maintained in the cell population throughout their cell cycle. This assumption implies the adoption of an average nucleus size, which is necessary as the nucleus size increases in moving through the cell cycle and this in turn increases the radiosensitivity of the cell (Scholz *et al.*, 1996).

The local dose distribution can be obtained from measurement of the radial dose distributions obtained from experiments using gas chambers (Varma *et al.*, 1977; Metting *et al.*, 1988), Monte Carlo calculations (Krämer *et al.*, 1994) or numerical calculations (Butts *et al.*, 1967; Chatterjee *et al.*, 1981; Kiefer *et al.*, 1986). These calculations suggest a $1/r^2$ dependence for the radial dose distribution (see Figure 4.9), which is defined in the model as:

$$D(r) = \begin{cases} \lambda LET/r_{min}^2 & : & r < r_{min} \\ \lambda LET/r^2 & : & r_{min} \leq r \leq r_{max} \\ 0 & : & r > r_{max} \end{cases} \quad (4.51)$$

where λ is a normalization constant, r_{min} is the minimum radius of the track (and has to be assumed) and r_{max} is the maximum radius of the track determined by the range of the highest energetic electrons produced by the primary particle.

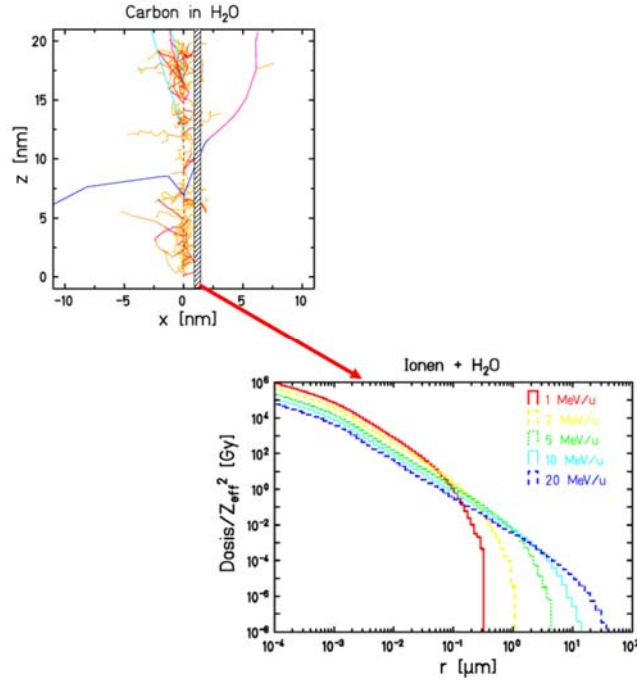


Figure 4.9: Radial dose distribution for a carbon ion traversing water.

Finally, the x-ray survival curves, which are assumed to be comprised of two sections: a shouldered section at low doses and a purely exponential section at higher doses. For this reason, the model assumes a parameterisation of these survival curves, which is linear-quadratic for low doses, and linear for high doses. The dose threshold D_t marks the transition from the shouldered to the exponential part of the survival curve. The slope of the survival curve at $D = D_t$ is given according to the linear quadratic term:

$$s = \left. \frac{dS(D)}{dD} \right|_{D=D_t} = \alpha + 2\beta D_t \quad (4.52)$$

And the proposed parameterisation of the x-ray survival curve is:

$$S(D) = \begin{cases} e^{-\alpha D - \beta D^2} & ; \quad D \leq D_t \\ S_t e^{-s(D-D_t)} & ; \quad D > D_t \end{cases} \quad (4.53)$$

where S_t is the survival at the threshold dose D_t .

The LEM model has been heavily criticised by the Track Structure community (Katz, 2003), the principal objection being the very fundamental assumption of the model, i.e. that equal numbers of local deposition events implies that a low-LET survival curve can be used to obtain the effect produced by high-LET radiations. This proposition may be true within the cell nucleus at the nano-scale, but when considering the entire nucleus volume, and therefore a higher value of the hit cross section, the probability of successful hits are entirely different for X-rays and ions and, subsequently, for their effect too. To assume that the high-LET effect can be predicted from the X-ray survival curve is equivalent to saying that the ion beam survival curve is a surrogate of the X-ray survival curve despite it being well-known that there are huge difference in the intrinsic nature of low- and high-LET radiations and, consequently, in their biological effectiveness.

4.4. Summary

This chapter shows the complexities involved in using a mechanistic approach to derive the linear quadratic expression presented in Chapter 3. Each of the mechanistic models discussed in this chapter introduce different numbers of parameters and which, in general, are not easily accessible from the experimental (in-vitro) data available. This should not be considered as a criticism to these models, but as an indication of the enormous complexity of the problem in hand. For this reason, a number of compromises have to be made when modelling a specific problem and which will depend on the application being considered.

In the case of clinical radiobiology, the models need to be easy to handle, with high definition and with a limited number of degrees of freedom to predict the intended effect. Perhaps for this reason, the LEM model has a clear advantage over the TDRA and MK models, although, as it has been seen, the assimilation of the LEM model requires a number of compromises to be assumed (a difficult task for some, not so difficult for others). Another way to finding a practical way forward is sometimes to use semi-empirical models, where a minimum number of mechanistic assumptions are made in order to maintain the simplicity of the model, while a number of dummy parameters are introduced to provide enough freedom for the model to adapt to the majority of

clinical situations for which it is to be used. This is the position adopted in Chapter 8, where a semi-empirical model is proposed with which to introduce microdosimetric considerations to a generalised formulation of the reciprocal repair kinetic model originally proposed by Fowler (1999; 2002).

4.5. Bibliography

- Belli M., Cherubini R., Dalla Vecchia M., Dini V., Moschini G., Signoretti C., Simone G., Tabocchini M. A., Tiveron P. *International Journal of Radiation Biology* 76(8):1095-1104 (2000).
- Berger M.J. *Radiation Protection Dosimetry* 13(1):87-90 (1985).
- Booz J. *In: Proceedings of the Fifth Symposium on Microdosimetry.* Booz, J., Ebert, H. G., Smith, B. G. R. (eds.), pp. 311-344. EUR 5452 (1976).
- Butts J.J., Katz R. *Radiation Research* 30(4):855-879 (1967).
- Chatterjee A., Magee J.L. *In: Biological and Medical Research with Accelerated Heavy Ions at the BEVALAC 1977-1980,* Eds. MC Pirucello and CA Tobias, LBL-report 11220 (University of California, Berkeley), pp.55-61 (1981).
- Curtis S.B. *Radiation Research* 106(2):252-270 (1986).
- Frankenberg D., Goodhead D.T., Frankenberg-Schwager M., Harbich R., Bance D.A., Wilkinson R.E. *International Journal of Radiation Biology* 50(4):727-741 (1980).
- Fowler J.F. *Radiation Research* 152(2):124-136 (1999).
— *Radiation Research* 158(2):141–151 (2002).
- Goodhead D. T., Thacker J., Cox R., Wilkinson R. E. *International Journal of Radiation Biology* 36(2):101-114 (1979).
- Goodhead D.T. *International Journal of Radiation Biology* 32(1):43-70 (1977).
— *Radiation Research* 91(1):45-76 (1982).
— *In: The Biological Basis of Radiotherapy.* Steel G. G., Adams G. E. and Peckham M. J. (eds.), pp.81-92. Amsterdam: Elsevier Biomedical Press (1983).
- Goodhead D. T. *In: The Dosimetry of Ionizing Radiation (Vol. 2).* Kase K.R., Bjarngard B.E. and Attix F.H. (eds.), pp.1–89. Academic Press, San Diego (1987).
- Goodwin E.H., Blakely E.A., Tobias C.A. *Radiation Research* 138(3):343-51 (1994).
- Hall E.J. *In: Radiobiology for the radiologist (5th Ed),* Lippincott Williams and Wilkins (eds.), pp.112-123 (2000).
- Hawkins R.B. *Radiation Research* 140(3):366-74 (1994);
— *International Journal of Radiation Biology* 69(6):739-55 (1996);

- *Medical Physics* 25(7):1157-1170 (1998);
- *Radiation Research* 160(1):61-69 (2003);
- *Radiation Research* 166(2):431-442 (2006).

International Commission on Radiation Units and Measurements (ICRU), *Report 17*.

International Commission on Radiation Units and Measurements, Bethesda, MD (1970).

International Commission on Radiation Units and Measurements (ICRU), *Report 36*.

International Commission on Radiation Units and Measurements, Bethesda, MD (1983).

International Commission on Radiation Units and Measurements (ICRU), *Report 59*.

International Commission on Radiation Units and Measurements, Bethesda, MD (1998).

Katz R. *Radiation Research* 160(6):724-728 (2003).

Kellerer A.M., Chmelevsky D. *Radiation Research* 63(2):226-234 (1975).

Kellerer A.M., Rossi H.H. *Current Topics in Radiation Research Quarterly* 8(2):85-158 (1972).

Kellerer A.M., Rossi H.H. *Annual Report on Research Project, COO-3243-2* (E.R.D.A.) pp.264 (1973).

Kellerer A.M. *In: The Dosimetry of Ionizing Radiation* (Vol. 1). Kase K.R., Bjarngard B.E. and Attix F.H. (eds.), pp.77–162. Academic Press, Orlando (1985).

Kiefer J., Straaten H. *Physics in Medicine and Biology* 31(11):1201-1209 (1986).

Kozubek S., Krasavin E.A. *Joint Institute for Nuclear Research (JINR)*. Report 19-82-882. Dubna (1982a).

— *JINR*. Report 19-82-883. Dubna (1982b).

— *JINR*. Report 19-82-884. Dubna (1982c).

— *JINR*. Report 19-82-928. Dubna (1982d).

— *JINR*. Report 19-82-929. Dubna (1982e).

— *JINR*. Report 19-83-685. Dubna (1983a).

— *JINR*. Report 19-83-715. Dubna (1983b).

— *JINR*. Report 19-83-743. Dubna (1983c).

— *JINR*. Report 19-83-744. Dubna (1983d).

— *JINR*. Report 19-83-788. Dubna (1983e).

Kozubek S., Krasavin E.A. *Neoplasma* 31(6), 675-683 (1984a).

- Kozubek S., Krasavin E.A. *Neoplasma* 31(6), 685-695 (1984b).
- Krämer M., Kraft G. *Radiation and Environmental Biophysics* 33(2):91-109 (1994).
- Leenhouts H.P., Chadwick K.H. *Theoretical and Applied Genetics* 44:167-172 (1974).
- Leuthold G., Berger M.J. *Radiation Protection Proceedings. Symposium on Neutron Dosimetry 5th*, Munich-Neuherberg, pp.245-253 (1984).
- Metting N.F., Rossi H.H., Braby L.A., Kliauga P.J., Howard J., Zaider M., Schimmerling W., Wong M., Rapkin M. *Radiation Research* 116(2):183-195 (1988).
- Raju M.R., Brenner D., Carpenter S., Chmielewsky J., Freyer J.P., Hoshi M., Schillaci M., Wilder M.E., Goodhead D.T. *Abstract Proceedings of the Annual Meeting of the Radiation Research Society 32nd*, Orlando, Fla. Pp.99, Radiation Research Society, Philadelphia, Pennsylvania (1984).
- Revell G.H. *Advances in Radiation Biology* 4: 367-416 (1974).
- Rossi H.H., Rosenzweig W. *Radiation Research* 2(5):417-425 (1955).
- Rossi H.H., Rosenzweig W. *Radiology* 64(3):404-411 (1955).
- Rossi H.H. *Radiation Research* 10(5):522-531 (1959).
- Scholz M., Kraft G. *Radiation Protection Dosimetry* 52(1-4):29-33 (1994).
— *Advances in Space Research* 18(1-2):5-14 (1996).
— *Radiation Research* 161(5), 612-629 (2004).
- Thacker J., Wilkinson R. E., Goodhead D. T. *International Journal of Radiation Biology* 49(4):645-656 (1985).
- Tobias C.A., Blakely E.A., Noo F.Q.H., Jang T.C.H. *In: Radiation Biology in Cancer Research*, Meyn and Withers (Raven, New York) (eds.), pp.195-230 (1980).
- Varma M.N., Baum J.W., Kuehner A.V. *Radiation Research* 70(3):511-518 (1977).
- Virsik R. P., Schäfer Ch., Harder D., Goodhead D. T., Cox R., Thacker J. *International Journal of Radiation Biology* 38(5):545-557 (1980).
- Wilkinson R.E., Goodhead D.T., Thacker J. *Radiation Protection Dosimetry* 13(1):161-165 (1985).
- Zirkle R.E., Marchbank D.F., Kuck K.D. *Journal of Cellular Physiology. Supplement.* 39(Suppl. 1):78-85 (1952).

Time and dose fractionation effects in non-conventional Radiotherapy

In the previous four introductory chapters the main features of the LQ model have been discussed along with the basis of the formulation presently used in clinical Radiobiology. The purpose of this thesis is to extend this formulation to non-conventional Radiotherapy (specifically, that involving high-LET radiations), which is dealt with in this chapter to account for some of the effects observed in high-LET Radiotherapy. In Chapter 6, the validity of the new formulation proposed in this chapter is then assessed by comparing the predictions obtained from the present theory with the published data.

5.1. Revision of time-dose relationships in non-standard radiotherapy

Contemporary methods of radiotherapy are in continuous evolution in order to improve the outcomes of the treatments. The use of conformal techniques to deliver radiation has allowed the prospect of substantial improvement in tissue sparing. Among these techniques is Intensity Modulated Radiation Therapy (IMRT) which, aided by imaging systems such as PET/CT or MR/CT scanners and amorphous-crystal-based portal imagers, allows precise demarcation and treatment of the planning treatment volume (PTV).

Another method to increase the physical selectivity of the treatment, at the same time increasing the effect of radiation on the tumour, is by using non-standard radiation

types, e.g. high-LET (high-linear energy transfer) radiation. The use of this type of radiation in radiotherapy (RT) requires that careful attention be given to the associated radiobiological issues. The general rationale for using high-LET RT is the higher impact this type of radiation has on certain radioresistant tumours, as cell killing is less affected by the position of the cells in the cell cycle or their oxygen status, and also because cells have less ability to repair high-LET radiation injury (Withers *et al.*, 1982; Wambersie *et al.*, 2004). These three aspects lead to the conclusion that fractionation effects are of diminished importance when using high-LET radiations, as illustrated in Figure 5.1. It will be noted that, for the high-LET cases, increasing of number of fractions (n) has little effect on the total dose required to achieve a given effect, except perhaps when n is quite small.

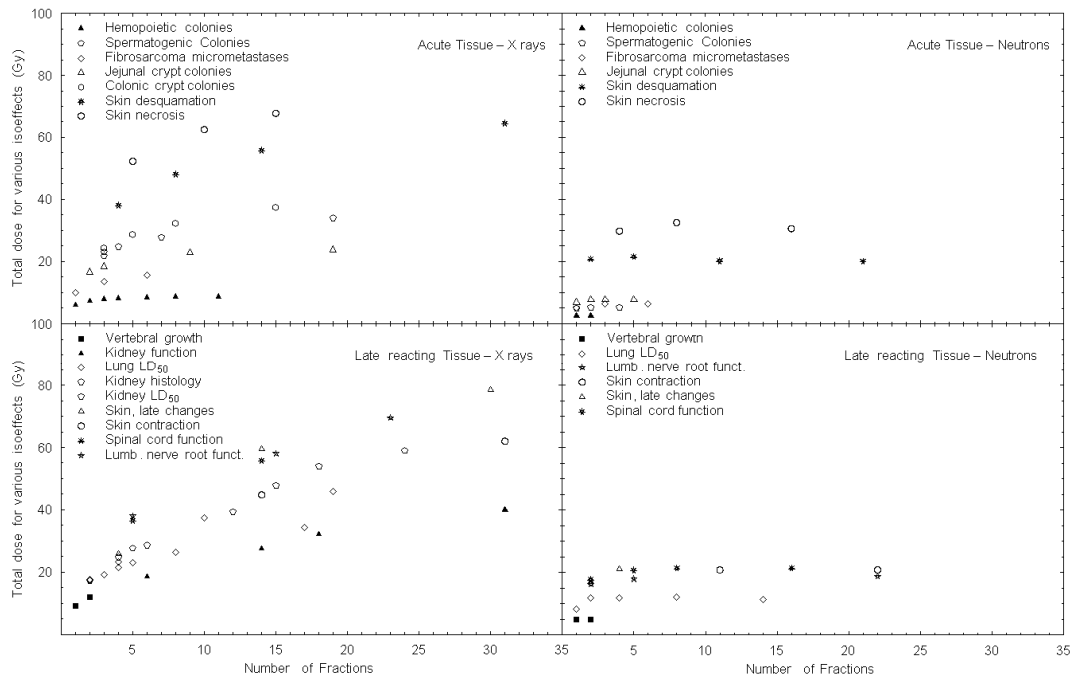


Figure 5.1: Total Isoeffective Doses versus number of fractions for different early (top) and late (bottom) reacting tissues using low- (X rays, left) and high-LET (neutrons, right) radiations.

Figure 5.1 demonstrates that high-LET radiations are more effective than low-LET to produce a given effect as, at any given number of fractions, the total dose required to produce the same effect is always lower (Kramer *et al.*, 2003). This is a consequence of the higher ionization density within the charged particle tracks, which ultimately produce more un-repairable damage to the DNA structure. This increased effectiveness

is usually expressed in terms of the relative biological effectiveness (RBE), which as shown in Equation (2.1) was defined as the ratio of photon dose (usually 250 kV X-rays as reference radiation) and the dose of the high-LET (or test radiation) radiation required to produce the same biological effect:

$$RBE = \frac{Dose_{photon}}{Dose_{Ion}} \Bigg|_{Isoeffective} \quad (5.1)$$

It is also important to notice in Figure 5.1 the continuous increase of the low-LET total dose with number of fractions while the high-LET total dose remains relatively insensitive to the changes of the fraction size. This implies that the ratio of the total dose of low-and high-LET radiation required to produce the same effect increases with increasing the number of fractions, or equivalently, with decreasing the dose per fraction (Withers et al., 1982).

Two conclusions can immediately be drawn from Figure 5.1, that is: (i) little sensitivity observed on the high-LET time-dose relationship to changes in fractionation, which in turn is related to the near-exponential shape of the survival curves produced by this type of radiation (see Figure 3.5); and (ii) the increased dose effectiveness at high-LET, related to the fact that, relative to low-LET, lower total doses are required to produce the same effects. *Fractionation effects* and *fraction effectiveness* should not be confused in the present context.

Different interpretations have been proposed to explain the drastic reduction of total dose required at low number of fractions (i.e. big doses per fraction) for low-LET radiations. Some authors (e.g. Fowler – see Chapter 3) suggest that, as the dose per fraction increases, there is an extra amount of lethal damage produced by the accumulation of sublethal damage and therefore a lower total dose is required to achieve the same effect. In the case of high-LET radiations, the contribution to the overall effect from sublethal damage accumulation is traditionally considered to be small compared to that produced by directly lethal events due to the higher density energy deposition characteristic of this type of radiations. As it was indicated in Chapter 4, in the framework of the LQ model, α is considered as an indicator of the lethality produced by

directly ionising events while β is related to the lethality produced by the accumulation of sublethal damage. Therefore, according to this interpretation, the contribution to cell killing by the β component when using high-LET radiations is almost negligible compared to the α component, hence the survival curves obtained from this kind of radiations are usually quasi-exponential.

As mentioned before, the fact that the total isoeffective dose is less sensitive to the increase of the number fraction for high-LET radiations compared to the continuous increase observed for low-LET radiations, implies an increase of RBE with the number of fractions¹. As the increase of number of fractions can be translated into a decrease of the dose per fraction, we should expect an increase of RBE when the dose per fraction decreases. Thus, in the limiting case where *dose per fraction approaches zero*, RBE should reach a maximum. The existence of this limit has been proven to exist not only in the case of neutrons (Field, 1976) but also for and protons and heavier ions (e.g. ¹²C, He, Ar, etc...) (Paganetti *et al.*, 2000; Chapman *et al.*, 1977). However, in the *in-vivo* case of protons of all energies, it has been shown that RBE has a near-constant value of 1.1 for all doses and tissue types (Paganetti *et al.*, 2002; Gerweck *et al.*, 1999; Urano *et al.*, 1980, 1984; Gueulette *et al.* 1997), although it has recently been proposed that a dose dependent function would be found if the sample population used to study this case were more extensive (Jones *et al.*, 2000).

To characterise the variation of RBE with dose per fraction, we need to select an end point which has to be the same for low- and high-LET radiations. If, for instance, the selected end point is the production of a given number (N) of lethal events at both high- and low-LET, then:

$$N|_{low-LET} = N|_{high-LET} \Rightarrow \alpha_L d_L + \beta_L d_L^2 = \alpha_H d_H + \beta_H d_H^2 \quad (5.2)$$

At very low doses the quadratic terms of Equation (5.2) are negligible compared to the linear components, hence Equation (5.2) can be reduced to,

¹ Where RBE would be defined in this case as the ratio of the low-LET to the high-LET total doses.

$$\alpha_L d_L = \alpha_H d_H \Rightarrow RBE|_{d \approx 0 \text{Gy}} = \frac{d_L}{d_H} = \frac{\alpha_H}{\alpha_L} \quad (5.3)$$

Thus, the maximum value of RBE (RBE_{\max}) is obtained from the ratio of the limiting slopes of the LQ survival curves at very low doses. In Figure 5.1, RBE_{\max} can be interpreted as being the ratio of the total doses delivered in an infinite number of fractions (which correspond to an infinitely small dose per fraction). If one considers that at this limit of infinite number of fractions, the total dose necessary to produce a given effect corresponds to the BED for that specific effect, it is easy to realise that RBE_{\max} is also given by the ratio of isoeffective BEDs produced by two different radiation qualities, i.e.

$$\left. \begin{aligned} BED_L &= \frac{-\log SF}{\alpha_L} \\ BED_H &= \frac{-\log SF}{\alpha_H} \end{aligned} \right\} \longrightarrow RBE_{\max} = \frac{BED_L}{BED_H} = \frac{\alpha_H}{\alpha_L} \quad (5.3.a)$$

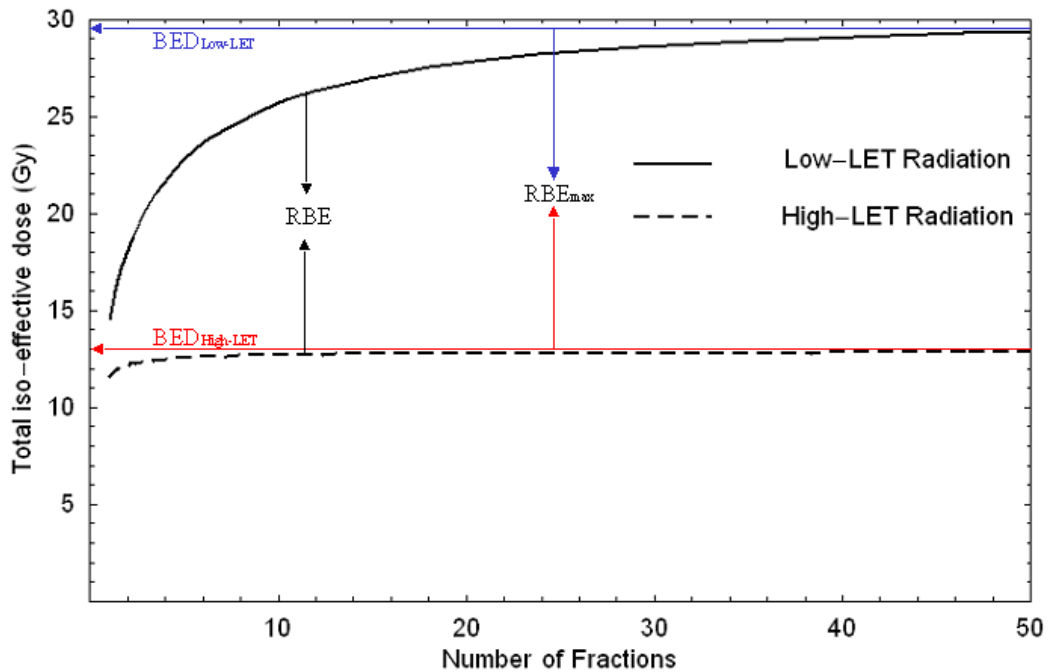


Figure 5.2: Characterisation of RBE values at different number of fractions

The existence of a maximum RBE at very low dose per fraction sparks questions on the possible existence of another limiting value of RBE corresponding to the case where *dose per fraction approaches infinity*. For a given end point, as the dose per fraction is increased the number of fractions decreases and, as it is observed from Figure 5.1, the ratio of total isoeffective doses decreases, i.e. RBE decreases as the number of fraction decreases or the dose per fraction increases. The relevant question here would be whether or not in the limiting case of $d=\infty$, the RBE reaches a minimum value, RBE_{\min} . This minimum value could not be obtained from Figure 5.1 though, as n can only be equal or greater than 1.

This minimum value could be obtained from Equation (5.2) by taking into account that at $d=\infty$ Gy the linear terms are negligible compared to the quadratic terms and Equation (5.2) can be approximated to

$$\beta_L d_L^2 = \beta_H d_H^2 \Rightarrow RBE|_{d \rightarrow \infty Gy} = \frac{d_L}{d_H} = \sqrt{\frac{\beta_H}{\beta_L}} \quad (5.4)$$

According to Equation (5.4), the limiting value of RBE at $d=\infty$ Gy is unity if β is considered independent of radiation quality, but, is this really the case always? And if not, what are the possible radio-therapeutic implications?

Several authors have investigated the dependency of the parameters used in the LQ model (α and β) with LET. Chapman *et al.* (1977, 1979) carried out a series of experiments using Chinese hamster cells V79-379A irradiated with heavy ions (230 MeV/n He, 400 MeV/n C, 400MeV/n Ne and 500 MeV/n Ar) at different points of the Bragg peak curve to study the variation of these parameters with radiation quality.

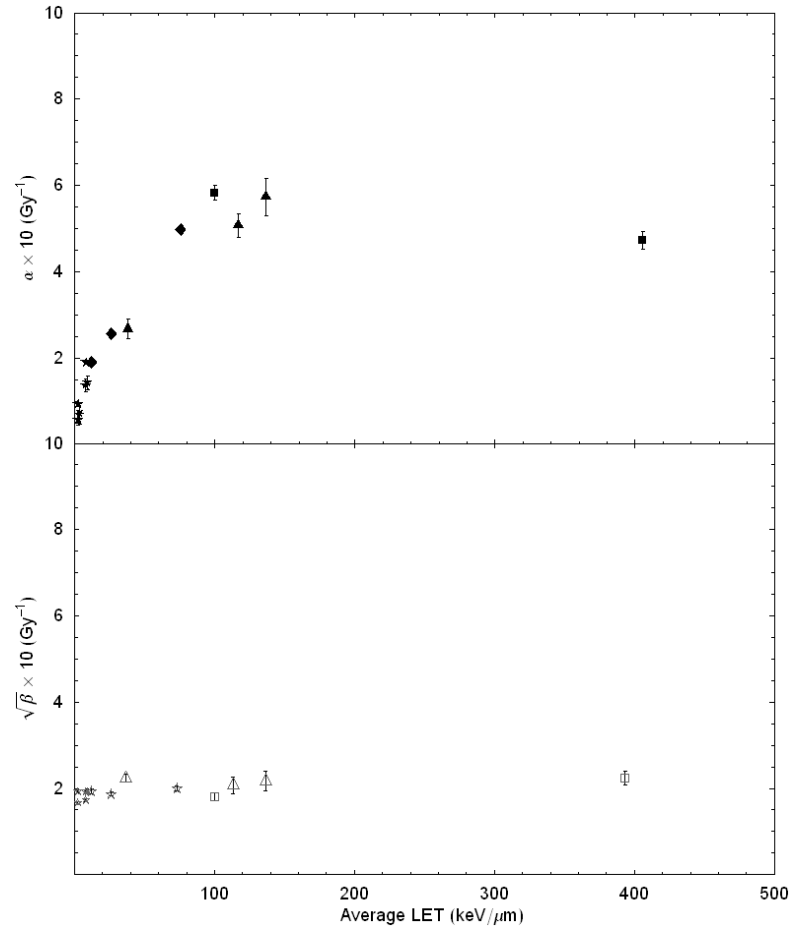


Figure 5.3: Changes of α (top) and $\sqrt{\beta}$ (bottom) with LET. The data was produced using Chinese hamster cells (V79-379A) cultured in stationary phase and irradiated at different points of the SOBPs to achieve different values of LET. Different radiation qualities were used: 220 kVp X-rays (★, ☆), 230 MeV/n Helium (◆, ◇), 400 MeV/n Carbon (▲, △), 400 MeV/n Neon (▲, △) and 500 MeV/n Argon (■, □) (Chapman et al., 1977).

His results, shown in Figure 5.3, indicated that the increase in RBE observed at high-LET is predominantly the result of an increase in cell killing by the single hit mechanism (α), but also that at every LET there is a (non-negligible) double-hit component of cell inactivation ($\sqrt{\beta}$) present which must be factored into any calculation made to predict the RBE of a particle beam. The variation of $\sqrt{\beta}$ with LET in Figure 5.3 is 10-15% going up to a top RBE value of 2.23 which coincides with the predicted limit of increase of sub-lethal damage to an RBE of at most 2-3 between 10 and 100 keV/μm as proposed by Barendsen (1997).

Similar small variations of $\sqrt{\beta}$ have been reported by other authors using neutrons. Joiner *et al.* (1983) reported that 3MeV fast neutrons increased the α and $\sqrt{\beta}$ terms of mouse foot skin reaction by a factor of 7.2 and 0.83 respectively. The same authors irradiated mouse foot with beams of 3 MeV fast neutrons with different percentages of γ -contamination (Joiner *et al.*, 1984) which altered the average LET of the total beam (lower average LET as the γ -component increases (Zaider *et al.*, 1980)), showing an increase in α by a factor of 4.8 without affecting the $\sqrt{\beta}$ term when reducing the percentage of γ -contamination from 100% to 11%. Joiner observed that, when plotting α and $\sqrt{\beta}$ versus percentage of γ -contamination in the neutron beam, the least square fit could be extrapolated back to 0% of γ -contamination, from which they could derive the α/β ratio corresponding to 100% neutron irradiation. The resulting value of α/β found was $85 \pm 21.8\text{Gy}$, hence a finite, though small, contribution of quadratic events would be predicted even in a pure 3MeV neutron beam. This is thought to correspond to a low-LET contribution from the neutrons themselves rather than to the γ -contamination of the beam. This conclusion coincides with the suggestion made by Barendsen (1997) on the ‘flooring’ of double-hit component of cell inactivation ($\sqrt{\beta}$) present at any LET which must be factored in when calculating RBE.

However, there is also published data reporting the change of $\sqrt{\beta}$ with LET. In particular, Higgins *et al.* (1983) showed that $\sqrt{\beta}$ varied by a factor of 8.7 when comparing survival curves of V79 Chinese hamster cells exposed to ^{60}Co γ -ray and neutrons of 14.8 MeV.

Leith *et al.* (1981) reported similar changes in α and β for the average skin response of hamsters to 225 kVp X-ray and 400 MeV/amu carbon ions. Skin was situated on the proximal portion of a 4cm wide spread Bragg peak. The values of α and β were derived from Fe-plots and α was found to change from 0.023 to 0.530 Gy^{-1} when irradiating with X-rays and carbon ions respectively, while β changed from 0.0018 to 0.0197 Gy^{-2} . In both cases, α and β increased more than 90% when using carbon ions, however, this result cannot be considered definitive as only three dose schedules were used and therefore the sample is too small to consider the results as being definitive.

More recently, Koike *et al.* (2002) and Ando *et al.* (2005) have studied fractionation effects on time-dose curves using carbon ions in both tumour (NFSa fibrosarcoma) and normal tissue (skin) of C3H/HeMsNrsf mice. The advantage of using carbon ions rather than neutrons to study fractionation effects (and the subsequent dependencies of sensitivity with radiation quality) is due to the characteristic depth dose curves of this type of radiation, i.e. the presence of a Bragg peak. In the case of the 290 MeV/u ions, the LETs in the plateau section of the depth-dose curve are in the range of 14-20 keV/ μm , while in the spread-out Bragg peak (SOBP) section the range is of the order of 40-100 keV/ μm . The low-LET (and low-dose) characteristic of the plateau section contrasts with the high-LET (and high dose) characteristic typical of the SOBP section and which provides with a high therapeutic index when using this type of radiation. Ando calculated the dose-response curves produced by one to six fractions for both, tumour growth delay and skin reaction and observed that, overall, the isoeffective total dose was smaller for carbon ions than for ^{137}Cs γ -ray. He also observed the effect illustrated earlier in Figure 5.1, i.e. that the increase in isoeffective dose is LET-dependent and the higher the LET the smaller the total isoeffective dose.

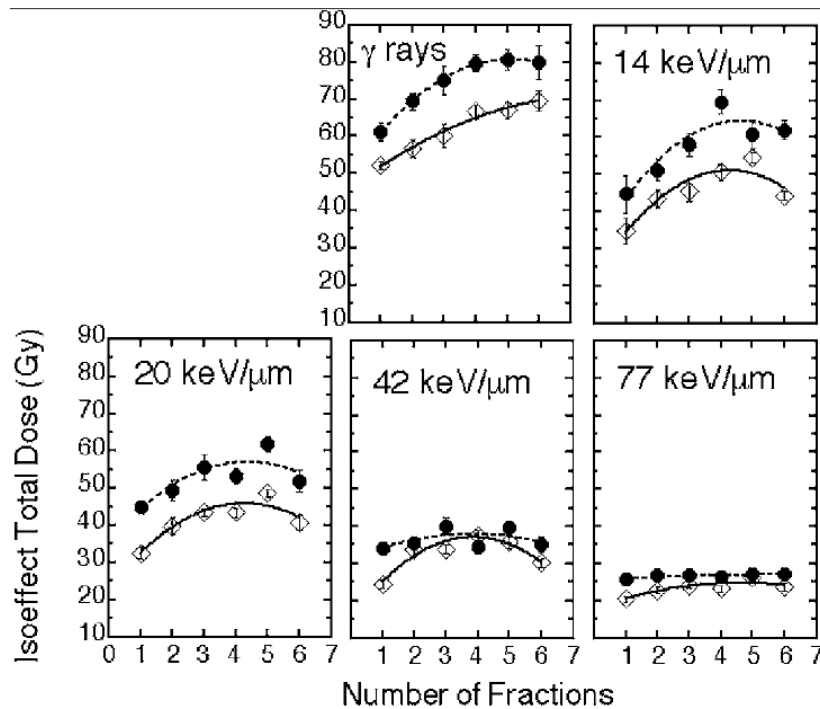


Figure 5.4: Isoeffect doses versus number of fractions to produce a NFSa tumour growth delay time of 15 days (black symbols) and skin reaction score of 3.0 (white symbols) (Ando *et al.* 2005).

Figure 5.4 shows how the isoeffect dose progressively increased with an increase in the number of fractions for both the skin reaction and tumour growth delay until it became much less prominent for number of fraction (n) higher than 4. This was true for γ rays as well as low-LET carbon ions (14-20 keV/ μ m). For high-LET carbon ions (42-77 keV/ μ m) not only the isoeffect dose further reduced, but the difference between the skin reaction and of the tumour growth delay also diminished. No fractionation effects were observed for 77 keV/ μ m carbon ions. Ando *et al.* (2005) used these results and their representation in terms of Fe plots to obtain the corresponding values of α and β at different LETs. These results are presented in Figure 5.5.

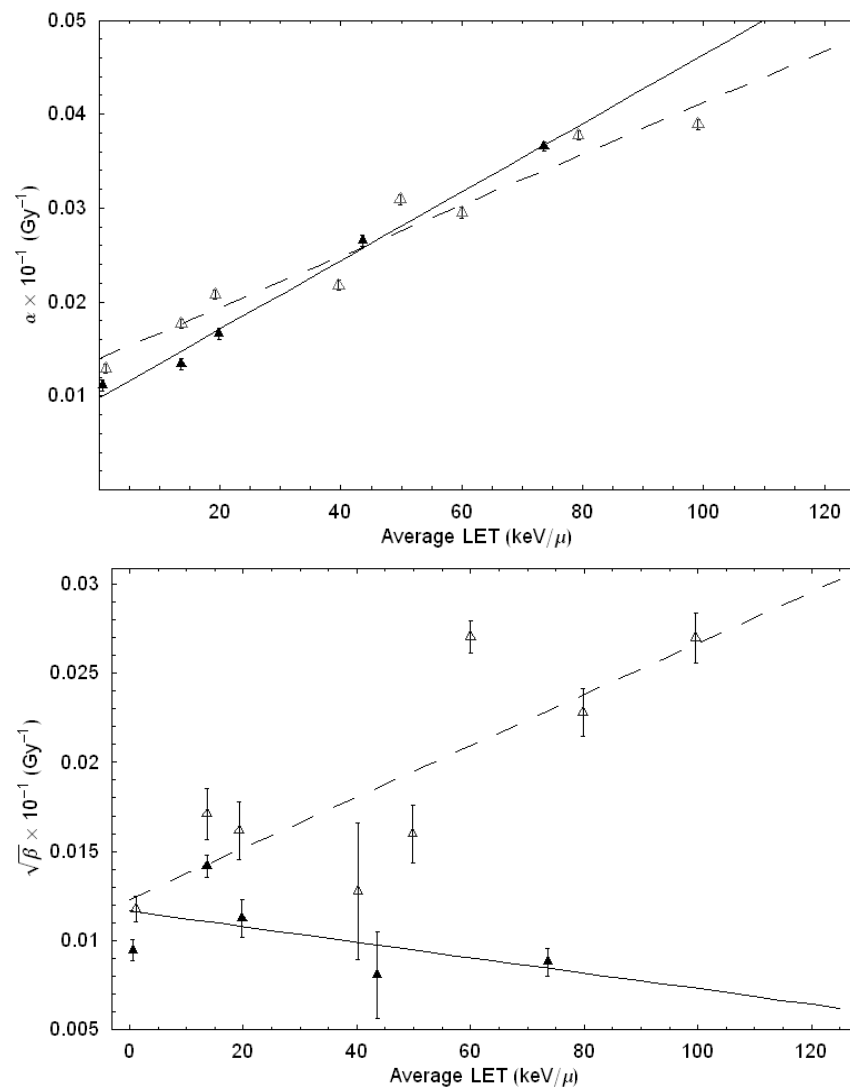


Figure 5.5: Fraction effect plots for tumour growth delay time of 15 days (black triangles) of NFSa tumour and skin reaction score of 3.0 (white triangles). Top: values of α versus LET. Bottom: values of $\sqrt{\beta}$ versus LET (Ando *et al.* 2005).

The calculated α showed a dependency of LET similar to those found previously in other works. Although a slightly larger increase is observed on the tumour growth delay than for the skin reactions, no statistical difference was detectable between the two tissues. On the other hand, the LET-dependence of the β component appeared to be markedly different for the two tissues; in particular, the β term of the skin reaction (early reaction) significantly increases with LET, while that of the tumour growth delay (late reaction) was largely independent of LET. If this is correct, this result would imply that the well known increase of RBE towards the end track, where the LET is higher, does involve a large contribution from β . This change in β could introduce complications when calculating the RBE because, if we consider β constant, calculations would predict a value probably much lower than the true value.

This result, together with those mentioned above, raises an important question: how plausible is it to consider that β is always independent of LET? It is clear that fractionation studies can yield important information on the change of the different sensitivity parameters with changing LET and Fowler was one of the first to recognise this (Fowler *et al.*, 1963) via the different degree of bending of the dose-time relationships shown in Figure 5.1. This degree of bendiness can be taken as proof of the different amounts of sublethal damage produced by low- and high-LET radiations. Fowler explained the increase of the isoeffective total dose with the number of fractions in two different ways:

- (i) It can be interpreted as a result of tissue repair (where the term ‘repair’ here may include cellular ‘repopulation’ effects) and which will diminish the effect of the earliest fractions by the time the later fractions are given. Thus, in extended fractionation, a higher total dose must be given to produce the same effect as with the equivalent single dose.
- (ii) It could be that biological effect is not simply proportional to dose, but increases supra-linearly with increasing fraction size. Thus, a fractional dose of $2x$ Gy produces more than twice the effect of a fraction of x Gy. The result of giving a greater number of smaller fractions is therefore to diminish the effect of each more than proportionally, so that a larger total

dose would be required. This second explanation requires that complete repairs occur between fractions.

These two possibilities are not mutually exclusive and a certain degree of repair plus non-linear effects will dictate the final shape of the dose-time relationship. It is important to notice however how explanation (i) relates the shape of the dose-time relationship to the overall time of the treatment or experiment, while (ii) emphasizes the influence of the number of fractions and the size of each fraction. According to this second interpretation, the quantitative relationship between total dose and number of fractions would depend upon the relative effectiveness of fractions of various sizes, i.e. upon the shape of the appropriate dose-effect curve. Fowler and Stern (1963) designed an experiment on skin that helped to distinguish the relative magnitude of the two explanations. The design of that experiment is summarised in the following table:

1 fraction	1 day	20 Gy
5 fractions	5 days	30 Gy
		30 Gy?
5 fractions	28 days	or
		50 Gy?
20 fractions	28 days	50 Gy

The fractionation regimes outside of the inner rectangle (i.e. 1 fraction/1 day, 5 fractions/5 days, and 20 fractions/28 days) were found to produce approximately equal effects on skin. Thus, the experiment was designed to find whether the dose required to produce the same effect in five fractions distributed over 28 days was closer to that for five fractions over five days, or to that for 20 fractions over 28 days. The results showed that five fractions over 28 days gave the same skin effect with doses of about 35Gy. This result clearly showed that the overall time could be considered relatively unimportant, at least between five and 28 days where the slow tissue repair component is small, and that the *size* and the *number* of the individual fractions were the principal parameters determining the increase of dose with extended fractionation.

Assuming that number and size of fractions are the relevant parameters determining the shape of curves of the type shown in Figure 5.1, Fowler and Stern (1961, 1960) then speculated over what would be the shape of the dose-effect curves required to explain the increase of the total isoeffective dose with number of fractions. To answer this question, they drew a 'mean dose-time curve' through different datasets obtained from human skin and tumour reaction experiments. The resultant curve was linear-quadratic in form and in the light of this result, they concluded that 'the increase of dose with overall time in extended fractionation can be explained mainly by the disproportionate decrease in effectiveness of smaller fractions as the number of fractions increases. This requires that the interval between successive fractions should exceed six to nine hours in order to allow full recovery from sub-lethal damage'. Today we know: (i) that different tissues have different proliferation onset times and for those tissues with short onset times (early reacting tissues) the overall treatment time is an important factor to consider (Fowler, 1983); and (ii), from different mechanistic interpretations of the LQ model (Chadwick *et al.*, 1973; Kellerer *et al.*, 1972; Hawkins, 1994), we also know that this disproportional effect as the number of fractions increase is due to the increase of lethality due to accumulation of sublethal damage, which is represented by the βd^2 component of the LQ model. The model predicts that only in the range of very high doses per fractions is where the quadratic term is dominant over the linear term and only at the theoretical value of $d = \infty$ Gy is when the survival fraction is entirely determined by the quadratic term. Thinking in terms of number of fractions (i.e. time-dose curves, like the ones shown in Figure 5.1), we could equivalently say that at very low number of fractions the total dose required to produce a given iso-effect will be mainly determined by the quadratic term of the LQ model, so any effect on the β term produced by the change of radiation quality used should be reflected on this part of the time-dose curve. Thus, the following hypothesis can be proposed:

Hypothesis: If fractionation effects are a consequence of the accumulation of sublethal damage (represented by the β -component), those theories assuming that β is independent of the radiation quality should not be able to predict the correct shape of dose-time relationships at small numbers of fractions for high-LET radiations.

5.2. Development of the theory supporting the evidences to prove the working hypothesis

To probe the hypothesis presented in the previous section, it is necessary to examine how the shape of time-dose relationships varies with radiation quality and how much this change is related to a change of β with LET. The LQ model predicts that two different fractionation regimes (using identical radiation types in each case) are characterised by total doses and number of fractions given by $[TD_1, n_1]$ and $[TD_2, n_2]$ and are isoeffective only if,

$$n_1(\alpha d_1 + \beta d_1^2) = n_2(\alpha d_2 + \beta d_2^2) \quad (5.5)$$

Re-arranging:

$$\begin{aligned} n_1 d_1 (\alpha + \beta d_1) &= n_2 d_2 (\alpha + \beta d_2) \\ n_1 d_1 \left(1 + \frac{d_1}{(\alpha/\beta)} \right) &= n_2 d_2 \left(1 + \frac{d_2}{(\alpha/\beta)} \right) \end{aligned} \quad (5.6)$$

But, remembering the total dose (TD) is related to the dose per fraction (d) by $TD = nd$, the above equation can be reformulated to,

$$TD_1 \left(1 + \frac{TD_1}{n_1(\alpha/\beta)} \right) = TD_2 \left(1 + \frac{TD_2}{n_2(\alpha/\beta)} \right) \quad (5.7)$$

Thus, the isoeffective condition can be expressed as,

$$TD + \frac{1}{n(\alpha/\beta)} TD^2 = const \quad (5.8)$$

Similarly,

$$Effect, E = n(\alpha d + \beta d^2)$$

$$\therefore \frac{E}{\alpha} = nd \left(1 + \frac{d}{(\alpha/\beta)} \right) = TD \left(1 + \frac{TD}{n(\alpha/\beta)} \right) \quad (5.9)$$

So, Equation (5.8) becomes,

$$TD + \frac{1}{n(\alpha/\beta)}TD^2 = \frac{E}{\alpha} = \text{const} \quad (5.10)$$

Therefore, isoeffective fractionation regimes are those preserving the quotient E/α as constant, once the biological system under study is fixed ($\alpha = \text{constant}$) and the desired end-point has been selected ($E = \text{constant}$). The quotient E/α is also known as the Biologically Effective Dose (BED), which is a measure of the effect of a course of fractionated or continuous irradiation (see Chapter 3, Section 2). BED has the units of dose and is expressed in terms of Gy_x , where x is the value of α/β used in its derivation. Equation (5.10) then means that two fractionated regimes are isoeffective as long as the BED is preserved in both of them. Therefore,

$$TD + \frac{1}{n(\alpha/\beta)}TD^2 = BED \quad (5.11)$$

is the time-dose relationship predicted from the LQ model which should fit data obtained from fractionation experiments. To obtain the functional relationship between TD and n , Equation (5.11) can be reformulated and solved for TD as follows,

$$TD^2 + n(\alpha/\beta)TD - n(\alpha/\beta)BED = 0 \quad (5.12)$$

$$TD = \frac{-n(\alpha/\beta) + \sqrt{n(\alpha/\beta)(4BED + n(\alpha/\beta))}}{2} \quad (5.13)$$

The question now would be: is Equation (5.11) valid for high-LET fractionation regimes and, if not, what new considerations do we need to introduce in the LQ formulation in order to predict a time-dose relationship capable of fitting existing high-LET fractionated data?

Firstly, it is clear that the constant value of E/α determined by Equation (5.9) must be maintained in the high-LET case, i.e.:

$$BED_{low-LET} = BED_{high-LET} \quad (5.14)$$

In general, two fractionation regimes carried out with different radiation qualities will produce the same biological effect only if:

$$n_L(\alpha_L d_L + \beta_L d_L^2) = n_H(\alpha_H d_H + \beta_H d_H^2) \quad (5.15)$$

As it has been shown in Equation (5.3), α_L and α_H are related to each other via the maximum RBE (RBE_{max}) observed for very small doses per fraction. On the other hand, the hypothesis enunciated before requires considering β dependent of the radiation quality, and in this case, β_L and β_H will be related as shown in Equation (5.4). In anticipation of the fact that β_L and β_H may not always be identical, we re-write Equation (5.4) as:

$$\sqrt{\frac{\beta_H}{\beta_L}} = RBE_{min}$$

In this case, dividing both sides of Equation (5.15) by α_L and substituting α_H and β_H by their low-LET analogues, we can derive an expression for BED_H as follows,

$$\begin{aligned} n_L d_L \left(1 + \frac{d_L}{(\alpha/\beta)_L} \right) &= n_H \left(RBE_{max} d_H + \left(\frac{\beta_H}{\alpha_L} \right) d_H^2 \right) = n_H \left(RBE_{max} d_H + \left(\frac{\beta_L RBE_{min}^2}{\alpha_L} \right) d_H^2 \right) \\ &= n_H d_H \left(RBE_{max} + RBE_{min}^2 \frac{d_H}{(\alpha/\beta)_L} \right) \end{aligned} \quad (5.16)$$

This identity indicates we can define BED for high-LET radiations as follows,

$$BED_H = \frac{E_H}{\alpha_H} = n_H d_H \left(RBE_{max} + RBE_{min}^2 \frac{d_H}{(\alpha/\beta)_L} \right) \quad (5.17)$$

For low-LET radiation $RBE_{\max} = RBE_{\min} = 1$, and Equation (5.17) reverts to the familiar low-LET form given in Equation (5.9). Equation (5.17) provides us with a tool to compare treatments carried out using radiations of different quality. It is important to realise from Equations (5.9) and (5.17) that treatments using different radiation qualities with the same number of fractions ($n_L = n_H$) and the same physical doses ($d_L = d_H$) will produce different biological doses at the end of the treatment ($BED_L \neq BED_H$). This is expected due to their difference on LET, which is reflected by the difference between their respective (α/β) values: in the case of the low-LET radiation $(\alpha/\beta)_L$, and in the case of high-LET radiation $(\alpha/\beta)_H = \left(\frac{RBE_{\max}}{RBE_{\min}^2} \right) \cdot (\alpha/\beta)_L$. The fact that Equation (5.17) has been formulated in terms of $(\alpha/\beta)_L$ is especially important as this means the low- and high-LET BED are being expressed in the same biological dose units and may therefore be directly compared, one with another (Dale *et al.*, 1999).

Thus, the condition expressed in Equation (5.10) can now be formulated for high-LET radiations as follows:

$$n_{H,1} d_{H,1} \left(RBE_{\max} + RBE_{\min}^2 \frac{d_{H,1}}{(\alpha/\beta)_L} \right) = n_{H,2} d_{H,2} \left(RBE_{\max} + RBE_{\min}^2 \frac{d_{H,2}}{(\alpha/\beta)_L} \right)$$

$$TD_{H,1} \left(RBE_{\max} + RBE_{\min}^2 \frac{TD_{H,1}}{n_{H,1}(\alpha/\beta)_L} \right) = TD_{H,2} \left(RBE_{\max} + RBE_{\min}^2 \frac{TD_{H,2}}{n_{H,2}(\alpha/\beta)_L} \right)$$

$$\therefore n_H d_H \left(RBE_{\max} + RBE_{\min}^2 \frac{d_H}{(\alpha/\beta)_L} \right) = BED \quad (5.18)$$

$$\therefore TD_H RBE_{\max} + RBE_{\min}^2 \frac{TD_H^2}{n_H(\alpha/\beta)_L} = BED$$

$$\therefore TD_H^2 + \frac{RBE_{\max}}{RBE_{\min}^2} \cdot n_H(\alpha/\beta)_L TD_H - \frac{RBE_{\max}}{RBE_{\min}^2} \cdot n_H(\alpha/\beta)_L BED = 0 \quad (5.19)$$

$$TD_H = \frac{-n_H RBE_{\max} (\alpha/\beta)_L + \sqrt{n_H (\alpha/\beta)_L (4BED \cdot RBE_{\min}^2 + n_H (\alpha/\beta)_L RBE_{\max}^2)}}{2RBE_{\min}^2} \quad (5.20)$$

Therefore, Equations (5.13) and (5.20) should fit dose fractionation data respectively determined at low- and high-LET. To study the effects of sublethal damage accumulation on the shape of the high-LET time dose relationship, Equation (5.20) could be compared with an equivalent equation derived when β is assumed to be independent of the radiation quality (i.e. $RBE_{\min} = 1$). In this case Equation (5.20) would be reduced to,

$$TD_H = \frac{-n_H RBE_{\max} (\alpha/\beta)_L + \sqrt{n_H (\alpha/\beta)_L (4BED + n_H (\alpha/\beta)_L RBE_{\max}^2)}}{2} \quad (5.21)$$

By comparing the goodness of fit of Equations (5.20) and (5.21) to high-LET fractionation data, we should be able to assess the validity of the hypothesis under test.

The evaluation of Equations (5.13), (5.20) and (5.21) depend on the specific values of $(\alpha/\beta)_L$, BED , RBE_{\max} and RBE_{\min} corresponding to the data sets used. Similar to the method proposed by Douglas *et al.* (1976) based on Fe plots to calculate values of $(\alpha/\beta)_L$ and BED for low-LET fractionation data, we will calculate the limiting values of RBE (RBE_{\max} and RBE_{\min}) by using an equivalent expression of Fe plots for high-LET radiations. Thus, from the BED formulas given in Equations (3.9) and (5.18):

$$BED = nd_L \left(1 + \frac{d_L}{(\alpha/\beta)_L} \right) \Rightarrow \frac{1}{TD_L} = \frac{1}{BED} + \frac{1}{(\alpha/\beta)_L BED} d_L \quad (5.22)$$

$$BED = nd_H \left(RBE_{\max} + \frac{RBE_{\min}^2 d_H}{(\alpha/\beta)_L} \right) \Rightarrow \frac{1}{TD_H} = \frac{RBE_{\max}}{BED} + \frac{RBE_{\min}^2}{(\alpha/\beta)_L BED} d_H \quad (5.23)$$

Since RBE_{\max} and RBE_{\min} are assumed to be fixed (but as yet unknown) values, Equation (5.23) defines a straight line when the reciprocal of TD_H is plotted against d_H .

Therefore, from the intersection of the low-LET Fe-plot on the vertical axis we obtain the reciprocal of the BED associated with the given end-point. Knowing the slope of the line, the BED is then used to derive the $(\alpha/\beta)_L$ ratio of the tissue. Using Equation (5.23) the corresponding Fe-plot is derived from the high-LET doses required to achieve the same biological end point. The intersection value and the slope, used in conjunction with the values for BED and $(\alpha/\beta)_L$ derived from the low-LET data, allow RBE_{max} and RBE_{min} to be derived.

5.3. Example of the derivation of RBE_{max} and RBE_{min} from fractionated data on mouse oesophagus exposed to neutrons.

The method presented above to calculate RBE_{max} and RBE_{min} will now be used to derive the RBEs for the mouse oesophageal endpoint of LD_{50} in 10-40 days (animals which survive this period may die later from radiation pneumonitis) after irradiation of the thorax with 250 kVp X-rays and d(16)Be neutrons. Endpoint doses are available for single doses, 2 fractions in 24h, 5 fractions in 4 days and 10 fractions in 11 days Hornsey *et al.* (1979). Figure 5.6 shows the resultant Fe plots.

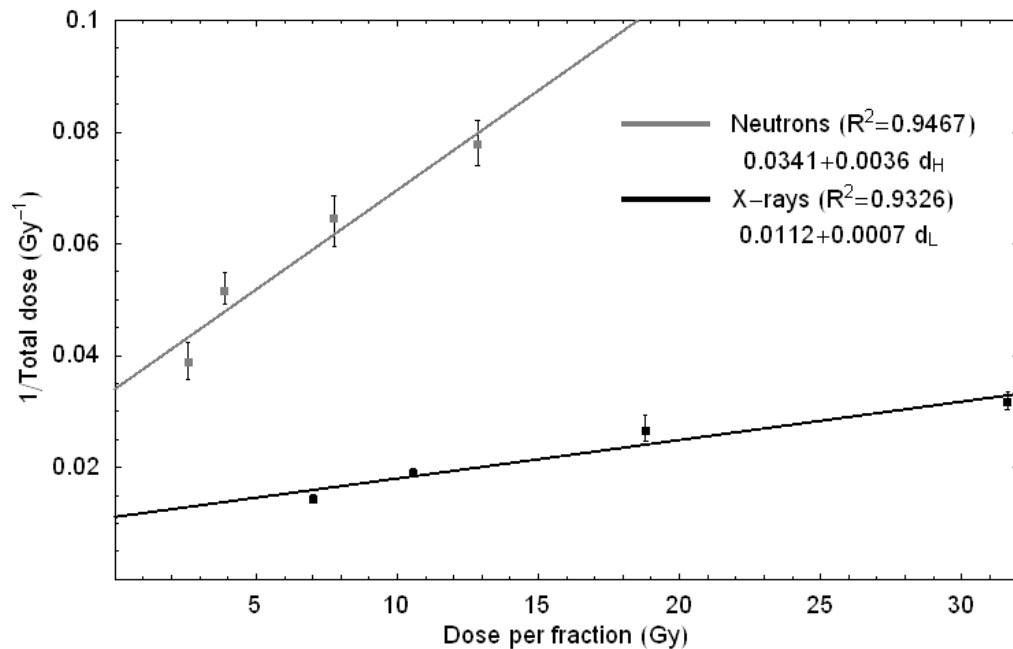


Figure 5.6: Fe-plots for LD_{50} due to Oesophagus injury in TO mice after irradiations with X-rays and fast neutrons (Hornsey *et al.*, 1979).

From the x-ray slope and intersection point the derived BED and $(\alpha/\beta)_L$ are:

$$BED = \frac{1}{0.0112} = 89.54\text{Gy} \Rightarrow (\alpha/\beta)_L = \frac{1}{BED \cdot 0.0007} = \frac{0.0112}{0.0007} = 16.25 \quad (5.24)$$

Therefore, from the Fe-plot corresponding to the fast neutrons, the subsequently derived RBE_{\max} and RBE_{\min} are:

$$RBE_{\max} = 89.54 \times 0.0341 = 3.05 \Rightarrow RBE_{\min} = \sqrt{BED \times (\alpha/\beta)_L \times 0.0036} = 2.28 \quad (5.25)$$

Substituting the results obtained from Equations (5.24) and (5.25) into Equations (5.13), (5.20) and (5.21), the resultant time-dose relationships are shown in Figure 5.7,

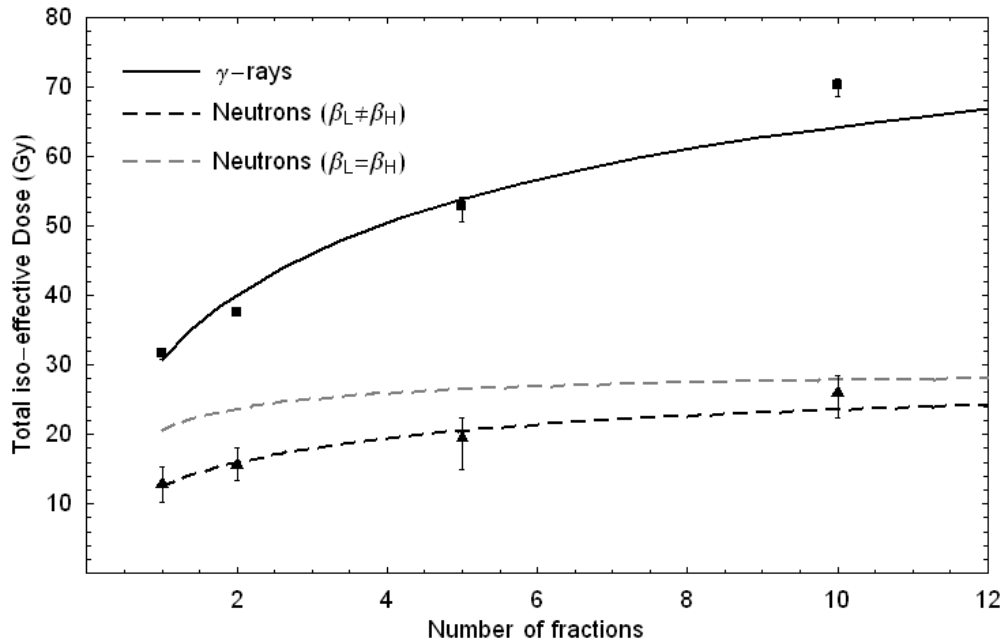


Figure 5.7: Time-dose relationships for LD50 due to Oesophagus injury in TO mice after irradiations with X-rays and fast neutrons (Hornsey et al., 1979). The black solid line is obtained from Equation (5.13); and the grey dashed line is obtained from Equation (5.20); the black dashed line is obtained from Equation (5.21). The same colour criteria apply to the rest of the time-dose results.

Similar indications of disagreement between dose-time relationships obtained from the LQ model assuming β independent of radiation quality and high-LET dose fractionation

data have been found. These results are included in Chapter 6, where further examples of this disagreement for data obtained for different normal tissues exposed to different radiation qualities (i.e. neutrons, as well as carbon, helium, neon and argon ions) are presented.

5.4. Repercussions of the present theory on RBE calculations at clinically relevant fraction sizes in non-conventional radiotherapy

In this section we will review the impact of the working hypothesis (β dependent on LET) on the calculation of clinically relevant values of RBE. In Equation (5.15) it was proposed that a given high-LET fraction dose (d_H) will produce the same effect as a given low-LET dose (d_L) only if:

$$\alpha_L d_L + \beta_L d_L^2 = \alpha_H d_H + \beta_H d_H^2 \quad (5.26)$$

But, taking into account that $\alpha_H = \alpha_L RBE_{\max}$ and $\beta_H = \beta_L RBE_{\min}^2$, and dividing both sides of the equation by β_L , we arrive at:

$$(\alpha/\beta)_L d_L + d_L^2 = (\alpha/\beta)_L RBE_{\max} d_H + RBE_{\min}^2 d_H^2 \quad (5.27)$$

Dividing both sides of Equation (5.27) by d_H , and noting that $d_H = \frac{d_L}{RBE}$, Equation (5.27) can be re-written purely in terms of low-LET parameters, as follows:

$$(\alpha/\beta)_L RBE + RBE d_L = (\alpha/\beta)_L RBE_{\max} + RBE_{\min}^2 \frac{d_L}{RBE} \quad (5.28)$$

Solving Equation (5.28) for positive values of RBE:

$$RBE = 0.5 \cdot \frac{(\alpha/\beta)_L RBE_{\max} + \sqrt{(\alpha/\beta)_L^2 RBE_{\max}^2 + 4d_L RBE_{\min}^2 ((\alpha/\beta)_L + d_L)}}{(\alpha/\beta)_L + d_L} \quad (5.29)$$

Equation (5.29) describes RBE as a function of changing low-LET dose per fraction and is similar in form to an earlier equation (Dale and Jones 1999) but which did not allow for non-constancy of β with changing LET and therefore did not include the RBE_{\min} factor, i.e.

$$RBE = 0.5 \cdot \frac{(\alpha/\beta)_L RBE_{\max} + \sqrt{(\alpha/\beta)_L^2 RBE_{\max}^2 + 4d_L((\alpha/\beta)_L + d_L)}}{(\alpha/\beta)_L + d_L} \quad (5.30)$$

One relevant point of Equation (5.29) is that RBE is entirely determined by low-LET parameters, $(\alpha/\beta)_L$ and d_L the former of which, for a range of tissues, are more extensively tabulated. In Equation (5.28), as $d_L \rightarrow 0\text{Gy}$, $RBE \rightarrow RBE_{\max}$, which is also the case for the earlier formulation. However, when $d_L \rightarrow \infty\text{Gy}$ then $RBE \rightarrow RBE_{\min}$ rather than unity.

The principle of introducing a limiting factor at very high doses per fraction might seem unnecessary as this range of doses is never used in clinical radiotherapy. However, as RBE is defined as a continuous function, position of the asymptotic tail of the RBE curve will directly influence the rate at which RBE changes over the whole range of doses. In particular, if β increases with LET as shown in Figure 5.5, RBE_{\min} will be greater than 1 and this will increase the value of RBE at 2Gy/fraction compared to the case in which β is considered independent of LET, where RBE_{\min} will then be 1. This effect is explained in Figure 5.8 and Figure 5.9, where in the later the case of the oesophagus RBE data is compared with the predicted RBE values obtained from Equations (5.29) and (5.30). Both figures demonstrate the influence of a variation of RBE_{\min} over values of RBE at 2Gy per fraction of X-ray dose, which corresponds to a typical value of dose per fraction in the treatment of oesophagus and tracheal malignancies. In particular, Figure 5.9 shows a 5.2% difference in RBE predicted by Equations (5.29) and (5.30) at 2Gy per fraction (Carabe-Fernandez *et al.*, 2007).

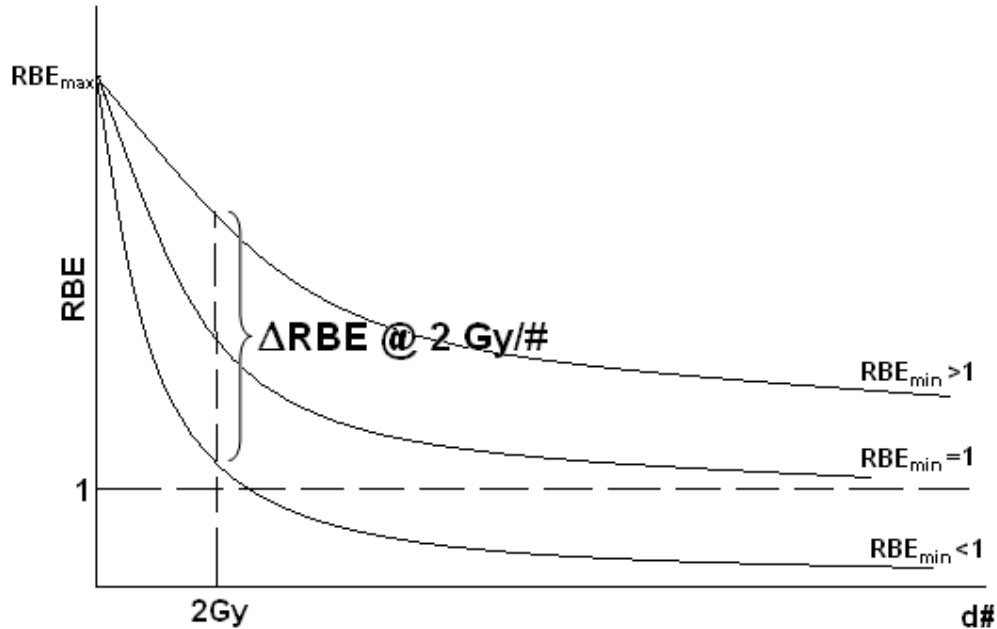


Figure 5.8: Potential over or under estimation of the RBE when β is considered independent of radiation quality. The 2Gy per fraction is selected as a representative fraction dose used in conventional radiotherapy.

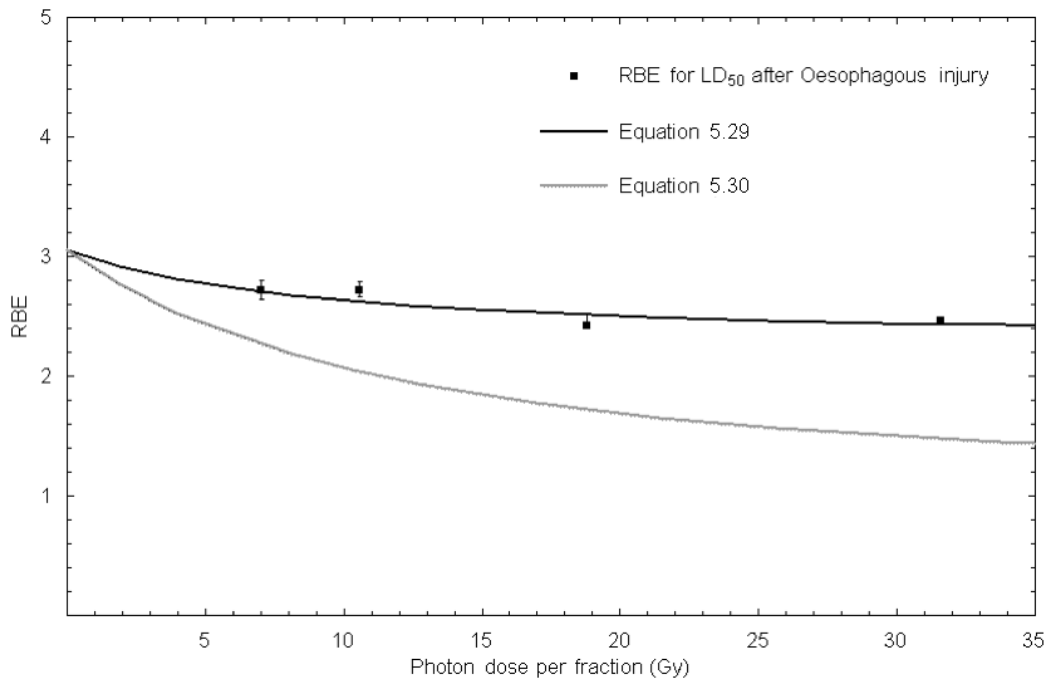


Figure 5.9: Data points show the RBE variation with dose derived from the data plotted in Figure 5.6. The black line is derived from Equation (5.29) and incorporates a fitted value of RBE_{min} whilst the grey line assumes that the RBE_{min} is unity. The observed difference between the RBE values predicted by the black and the grey lines is of 5.2%.

Thus, on the basis of these results and those shown in Chapter 6, it is possible to conclude that the assumption that β is independent of LET can lead to an under- or over- estimation of the RBE at the doses per fraction relevant to clinical practice. This could have an impact when using Equation (5.17) for BED calculations in non-conventional radiotherapy: the dose per fraction (d) used in the calculation is affected by the value of RBE_{min} so, if $RBE_{min} < 1$, RBE will decrease faster at low doses per fractions and a lower RBE factor will be expected than in the case where β is independent of LET ($RBE_{min}=1$). Consequently, the dose per fraction used to produce the same effect with high-LET radiations as with low-LET radiations will be lower than in the case of assuming $RBE_{min}=1$.

5.5. Potential problems that may rise from the proposed method of analysis

There is an issue related to the statistical significance of the raw data. Although Fe-plots have been used for many years to estimate the (α/β) parameter, several authors have commented on the statistical shortcomings of this method (Tucker, 1984; de Boer, 1988; Taylor *et al.*, 1989). Some of these criticisms are: (i) the method derives the (α/β) parameter via a two-stage (indirect) analysis (Fischer *et al.*, 1977; Herring, 1980); and (ii) the method tends to be biased in its estimation of (α/β) as a consequence of the uncertainty in both, the independent and the dependent variables (d and $1/TD$ respectively). This double uncertainty precludes the use of linear regression analysis (which may be applied only if the experimental uncertainty is restricted to the values of the ordinate (de Boer, 1988)) and forces the use of non-linear analysis (Tucker, 1984). However, Fe-plots do use clinically relevant data (dose per fraction and iso-effective total doses) and link it with BED, a parameter of widely recognised value and which is very helpful when comparing isoeffective treatments. de Boer (1988) proposed a method based again on a linear least-square fit of data presented as a TD vs $d \cdot TD$ plot, which provided values of E/α and (α/β) very similar to those derived from non-linear statistical methods. Carabe-Fernandez *et al.* (2007) compared the values of BED and (α/β) obtained from both methods (i.e. Fe plots and de Boer method), arriving at very similar values for both parameters.

When examining Figure 5.7, it is interesting to notice that the predicted total doses at 10 fractions for both X-rays and neutrons is always lower than the actual total dose, suggesting that RBE_{max} may be higher than that predicted by the theory. One of the main features of the oesophagus data when fitting an RBE curve to it is its slow rate of decrease, which forces the introduction of the RBE_{min} concept in order to explain the data. However, if the RBE_{max} was higher than the one calculated in this analysis, it is still possible to find a fit to the data with a RBE curve tending to 1 at very high doses per fractions, as can be seen in Figure 5.10 (Hopewell – personal communication. E-mail), with the consequential conclusion that β might yet be independent of LET. In order to clarify this argument, it would be necessary to have data produced with

fractionation regimes using very high number of fractions, which would provide more data points at very low dose per fractions and which in turn would improve the reliability of the Fe-plot fit.

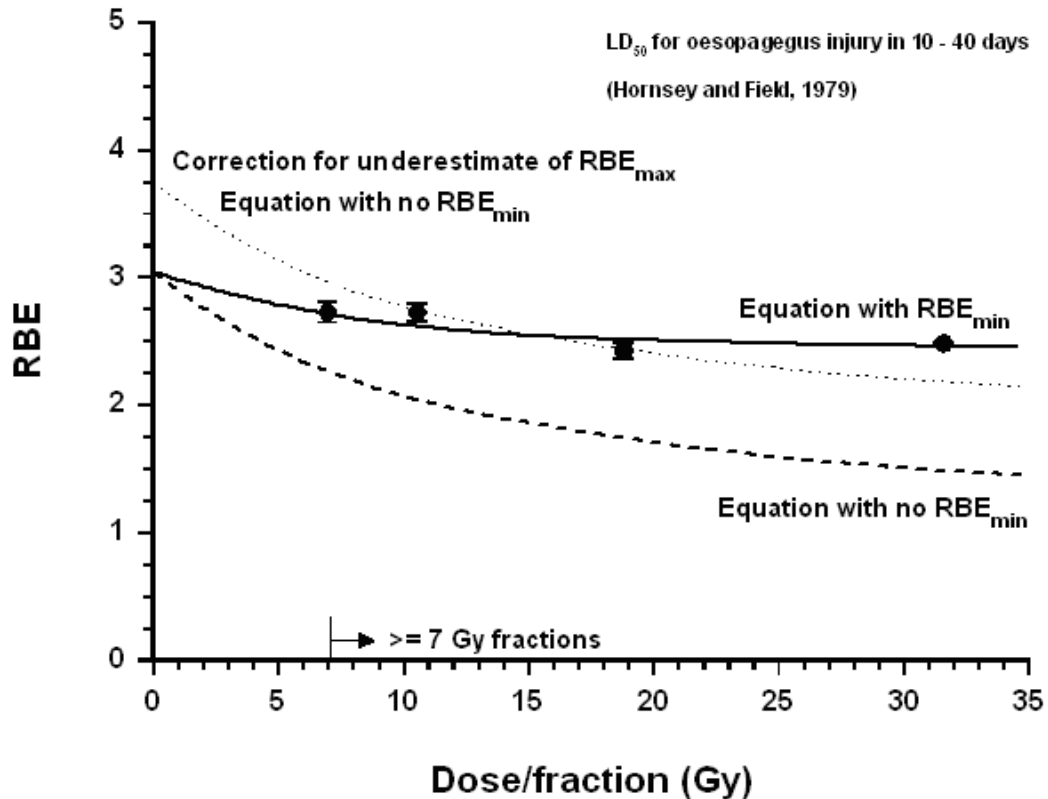


Figure 5.10: Alternative fits to the Oesophagus data produced by Hornsey and Field with neutrons. This figure was kindly provided by Professor Hopewell in a personal communication.

In order to see if the use of a higher RBE_{max} could avoid the use of an RBE_{min} the oesophagus data was reanalysed using a different procedure. Instead of using the Fe plot data to apply a linear regression from which the values of $(\alpha/\beta)_L$, BED, RBE_{max} and RBE_{min} could be derived, we applied a non-linear regression to the total dose versus number of fractions. In this way, the RBE_{max} calculated from this method should increase in order for the non-linear regression curve to fit the total dose at $N = 10$. According to this alternative method, we obtain the following fit to the X-ray and neutron total dose versus number of fractions data:

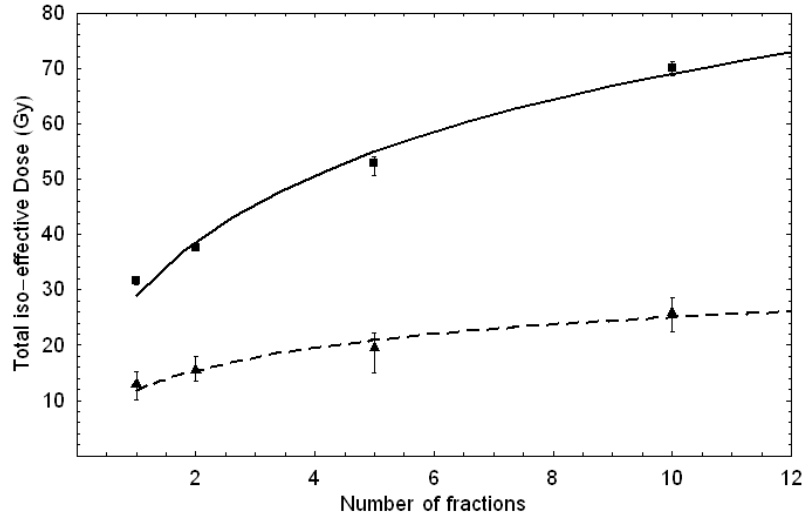


Figure 5.11: Non-linear fit to the total dose versus number of fractions keeping $(\alpha/\beta)_L$, BED , RBE_{max} and RBE_{min} as independent variables.

This improves the fit at high numbers of fractions at the cost of worse prediction at lower numbers of fractions. The equations corresponding to these curves are:

For the X-ray TD versus N data:

$$TD = \frac{1}{2} \left(-8.85709n + 2.99284 \sqrt{n(488.734) + 8.95709n} \right)$$

For the neutron TD versus N data:

$$TD = 0.0969383 \left(-30.7796n + 2.99284 \sqrt{n(2520) + 105.769n} \right)$$

Taking into account that the TD versus N equation for X-rays is given by:

$$TD = \frac{-n(\alpha/\beta) + \sqrt{n(\alpha/\beta)(4BED + n(\alpha/\beta))}}{2}$$

and for neutrons is

$$TD_H = \frac{-n_H RBE_{\max} (\alpha/\beta)_L + \sqrt{n_H (\alpha/\beta)_L (4BED \cdot RBE_{\min}^2 + n_H (\alpha/\beta)_L RBE_{\max}^2)}}{2RBE_{\min}^2}$$

we can infer that the values for BED, (α/β) , RBE_{\max} and RBE_{\min} are:

BED = 122.18 Gy (instead of the 89.54 predicted from Figure 5.6)

(α/β) = 8.96 Gy (instead of the 16.25 predicted from Figure 5.6)

RBE_{\max} = 3.44 (instead of the 3.05 predicted from Figure 5.6)

RBE_{\min} = 2.27 (instead of the 2.28 predicted from Figure 5.6)

So the new Fe plots would be:

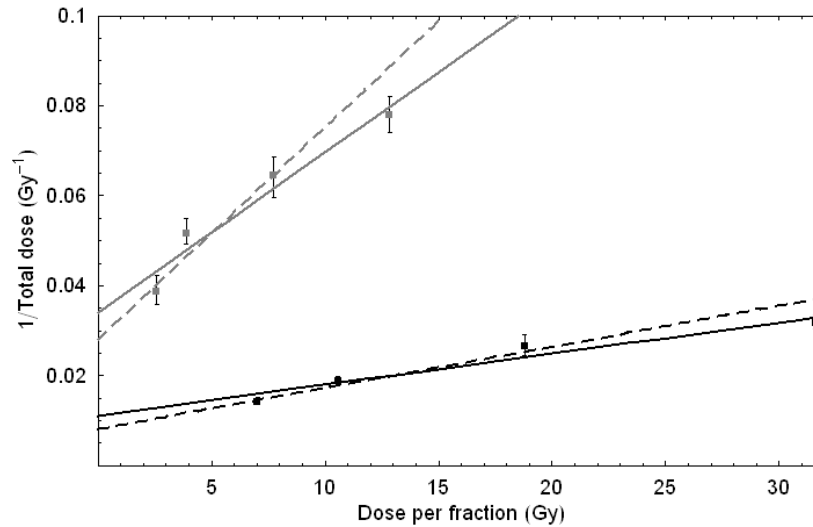


Figure 5.12: the solid lines correspond to the Fe plots presented in Figure 5.6, while the dashed lines are obtained using the values of BED, (α/β) , RBE_{\max} and RBE_{\min} indicated above.

Substituting the new values of (α/β) , RBE_{max} and RBE_{min} , the resultant RBE curve is

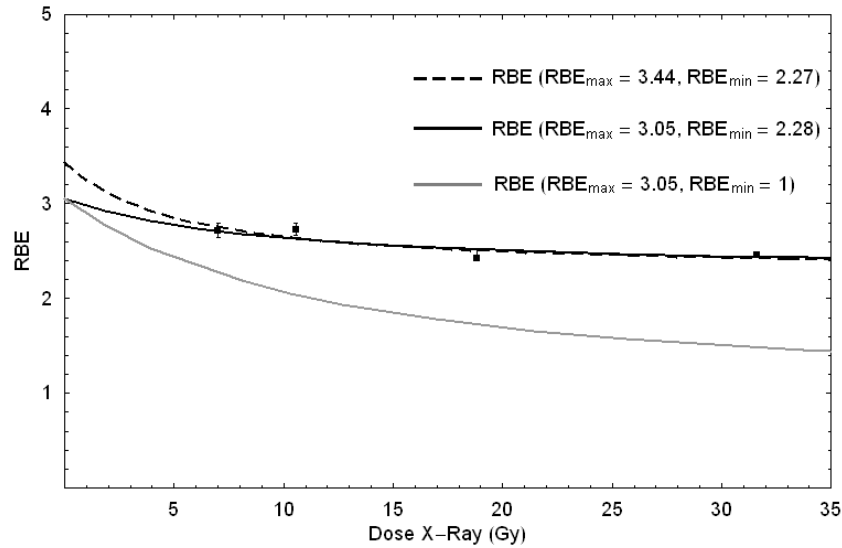


Figure 5.13: New RBE curve (dashed line) obtained with the values of BED , (α/β) , RBE_{max} and RBE_{min} .

In the previous fit to the TD vs N data, BED , (α/β) , RBE_{max} and RBE_{min} were kept as fitting parameters. If we make $RBE_{min} = 1$ and repeat the non-linear fit to the total dose per fraction versus number of fractions we obtain:

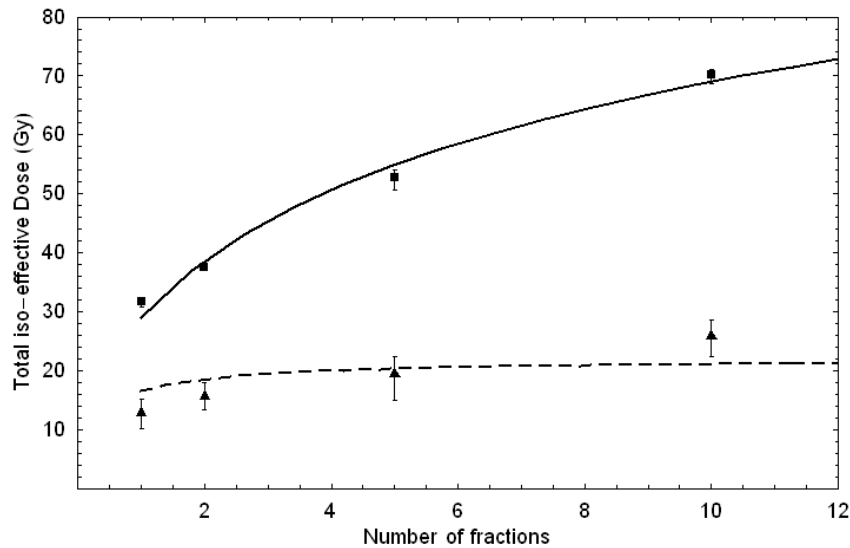


Figure 5.14: Non-linear fit to the TD versus N data assuming $RBE_{min}=1$.

From which we obtain the following results:

$$BED = 122.184 \text{ Gy}; (\alpha/\beta) = 8.96 \text{ Gy}; RBE_{max} = 5.57; RBE_{min} = 1.$$

The relevant Fe plots for these values are

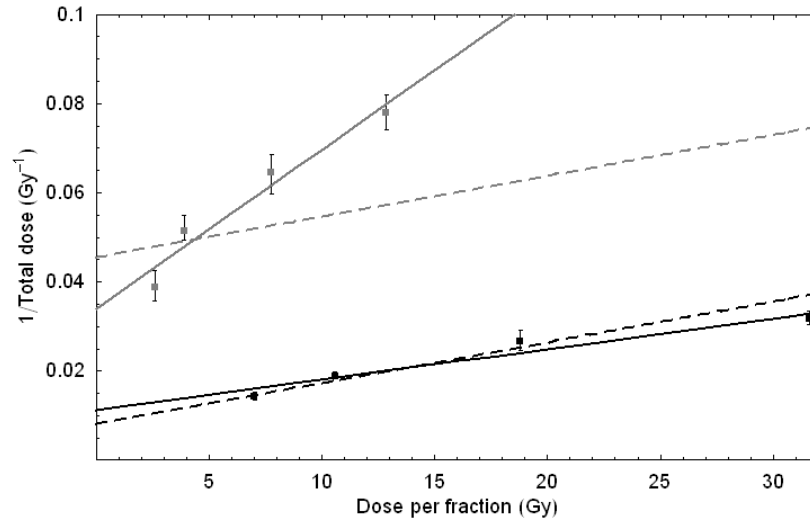


Figure 5.15: New Fe-plots obtained when assuming $RBE_{min}=1$. Observe how this assumption makes the slopes of the low and high-LET fit to be the same.

This last figure shows how bad the predicted Fe plot for neutrons fits the data when RBE_{min} is assumed to be 1. The RBE plots obtained from the above values of BED, (α/β) , RBE_{max} , RBE_{min} are:

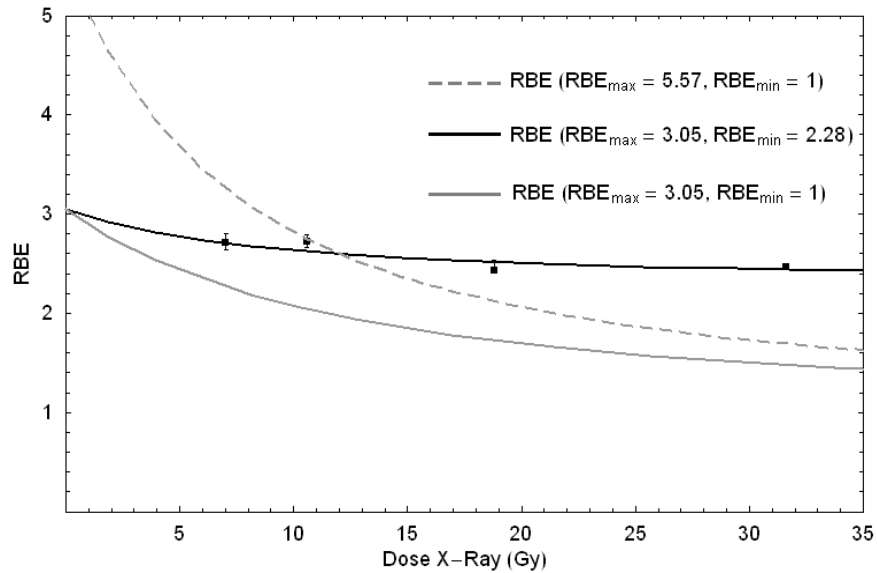


Figure 5.16: New RBE plots obtained when assuming $RBE_{min}=1$.

According to these results, and particularly to those shown in Figure 5.13, the use of a higher RBE_{max} in order to improve the fit to the isoeffective total dose at high number of

fractions ($N = 10$) does not help the argument for fixing RBE_{\min} at unity. Figure 5.15 and 5.16 show how this introduces great conflicts between the model and the data and indicates that, in this case, a better fit is only achieved only if β_H is considered bigger than β_L , so $RBE_{\min} > 1$.

It is worth mentioning also that the analysis included in this thesis does not take into account repopulation effects and it may be possible that, if repopulation has occurred during the treatment time, then the dose required to compensate for repopulation could be subtracted from the TD. This could help the point at $N = 10$ to be better predicted by Equation (5.20).

5.6. Bibliography

- Ando K, Koike S., Uzawa A., Takai N., Fukawa T., Furusawa Y., Aoki V., Miyato Y. *Journal of Radiation Research* 46(1), 51-57 (2005).
- Barendsen G.W. *International Journal of Radiation Biology* 71(6):649-655 (1997).
- Carabe-Fernandez A., Dale R.G., Jones B. *International Journal of Radiation Biology* 83(1):27-39 (2007).
- Chapman J.D., Blakely E.A., Smith K.C., Urtasun R.C. *International Journal of Radiation Oncology Biology Physics* 3:97-102 (1977).
- Chapman J.D., Doern S.D., Reuvers A.P., Gillespie C.J., Chatterjee A., Blakely E.A., Smith K.C., Tobias C.A. *Radiation and Environmental Biophysics* 16(1):29-41 (1979).
- Chadwick K.H., Leenhouts H.P. *Physics in Medicine and Biology* 18(1):78-87 (1973).
- Dale R.G., Jones B. *International Journal of Radiation Oncology Biology Physics* 43(3):639-645 (1999).
- De Boer R.W. *Radiation Oncology* 11(4):361-367 (1988).
- Douglas B.G., Fowler J.F. *Radiation Research* 66(2):401-426 (1976).
- Field S.B. *Current Topics in Radiation Research Quarterly* 11(1):1-86 (1976).
- Fischer D.B., Fischer J.J. *International Journal of Radiation Oncology Biology Physics* 2(7 – 8):773 – 781 (1977).
- Fowler J.F., Stern B.E. *British Journal of Radiology* 31:316 (1958).
- Fowler J.F., Stern B.E. *British Journal of Radiology* 33:389-395(1960).
- Fowler J.F., Stern B.E. *British Journal of Radiology* 36(423):163-173 (1963).
- Fowler J.F. *Radiotherapy and Oncology* 1(1): 1-22 (1983).
- Gerweck L.E., Kozin S.V. *Radiotherapy and Oncology* 50(2):135-142 (1999).
- Gueulette J., Böhm L., De Coster B.M, Vynckier S., Octave-Prignot M., Schreuder A.N., Symons J.E., Jones D.T., Wambersie A., Scalliet P. *Radiotherapy and Oncology* 42(3):303-309 (1997).
- Hawkins R.B. *Radiation Research* 140(3):366-74 (1994).
- Higgins P.D., De Luca P.M. Jr., Pearson D.W., Gould M.N. *Radiation Research* 95(1):45-56 (1983).
- Herring D.F. *International Journal Radiation Oncology Biology Physics* 6(2):225 – 232 (1980).

- Hornsey S., Field S.B. *European Journal of Cancer* 15(4):491-498 (1979).
- Joiner M.C., Maughan R.L., Fowler J.F., Denekamp J. *Radiation Research* 95(1):130-141 (1983).
- Joiner M. C., Bremner J. C., Denekamp J., Maughan R. L. *International Journal of Radiation Biology* 46(5):625-638 (1984).
- Jones B., Dale R.G. *International Journal of Radiation Oncology Biology Physics* 48(5):1549-1557 (2000).
- Kellerer A.M., Rossi H.H. *Current Topics in Radiation Research Quarterly* 8(2):85-158 (1972).
- Kramer M., Weyrather W. K., Scholz M. *Technology in Cancer Research and Treatment* 2(5):427-436 (2003).
- Koike S., Ando K, Oohira C., Fukawa T., Lee R., Takai N., Monobe M., Furusawa Y., Aoki M., Yamada S., Shimizu W., Nojima K., Majima H. *Journal of Radiation Research* 43(3), 247-255 (2002).
- Leith J.T., Powers-Risius P., Woodruff K.H., McDonald M., Howard J. *Radiation Research* 88(3):565-576 (1981).
- Paganetti H, Goitein M. *Medical Physics* 27(5):1119-1126 (2000).
- Paganetti H., Niemierko A., Ancukiewicz M., Gerweck L.E., Goitein M., Loeffler J.S., Suit H.D. *International Journal of Radiation Oncology Biology Physics* 53(2):407-21 (2002).
- Urano M., Goitein M., Verhey L.J., Mendiondo O., Suit H.D., Koehler A. *International Journal of Radiation Oncology Biology Physics* 6(9):1187-1193 (1980).
- Urano M., Verhey L.J., Goitein M., Tepper J.E., Suit H.D., Mendiondo O., Gragoudas E.S., Koehler A. *International Journal of Radiation Oncology Biology Physics* 10(4):509-514 (1984).
- Taylor J.M.G., Kim D.K. *International Journal of Radiation Biology* 56(2):61-167 (1989).
- Tucker S.L. *International Journal of Radiation Oncology Biology Physics* 10(10):1933-1939 (1984).
- Wambersie A., Hendry J., Gueulette J., Gahbauer R., Pötter R., Grégoire V. *Radiotherapy and Oncology* 73 (Supl 2):S1-14 (2004).
- Withers H.R., Thames H.D.Jr, Peters L.J. *International Journal of Radiation Oncology Biology Physics* 8(12):2071-6 (1982).

Zaider M., Rossi H.H. *Radiation Research* 83(3):732-739 (1980).

Results and conclusions relevant to Chapter 5

The results presented in this chapter were obtained from data dating back from the early 60's to the present. No new laboratory work has been involved in this work, however the original data from the experiment has been included. For each data set presented, the system used, the laboratory conditions in which they were prepared as well as the radiobiological end point used are briefly described. Three plots are given for each data set:

1. The Fe plot for low- and high-LET (Equations (5.22) and (5.23) respectively), from which the values of α/β , BED , RBE_{max} and RBE_{min} were derived
2. The total dose (TD) versus number of fractions (N)
 - a. For low-LET data (Equation (5.13))
 - b. For high-LET data assuming $\beta_L \neq \beta_H$ (Equation (5.20)) and $\beta_L = \beta_H$ (Equation (5.21))
3. The RBE plots assuming $\beta_L \neq \beta_H$ (Equation (5.29)) and $\beta_L = \beta_H$ (Equation (5.30))

Error bars have been included in each of these plots when such were provided in the original data. From the comparison between the fits assuming $\beta_L = \beta_H$ and those assuming $\beta_L \neq \beta_H$ it has been possible to evaluate the rigidity of the working hypothesis

presented in the previous chapter. Also, the particular values of RBE_{max} and RBE_{min} are plotted versus LET for the heavy ion results, this being used as a method to compare the variation of α_H versus α_L as well as β_H versus β_L . In the case of RBE_{max} , as α increases with LET, it is expected to increase with LET for any given biological system. In the case of β however, if the proposed hypothesis is correct, RBE_{min} will either increase or decrease with LET. The question then will be, in which cases does it decrease with LET and when does it increase?

6.1. Neutron data

6.1.1. Early reactions on pig skin from exposure to neutrons

- *System used:* Pigs of the English Middle White variety (40 to 60 kg at age 4 to 6 months) (Fowler *et al.*, 1963; 1965; Bewley *et al.*, 1967).
- *Laboratory conditions and Methodology of experiments:* Pigs were lightly anaesthetised with halothane, nitrous oxide and oxygen. While under the anaesthetic the colour of the pig's skin always remained pink. Twelve rectangular radiation fields (5cm × 4cm) were applied to different parts of the pig's body and spaced 3 to 4 cm apart. Single and fractionated X-rays doses from the M.R.C. 8 MV linear accelerator were used, with a sheet of Perspex fixed just clear of the skin to provide electron build-up. The M.R.C. cyclotron was used to produce fast neutrons with average energy of 6MeV. Skin reactions were observed by different observers individually and daily for the first 110 days after treatment, and skin reaction scores averaged for all observers were derived.
- *Radiobiological end point:* mid term skin reaction (30-70 days) with average score reaction 2, assuming that no repopulation occurs before 28 days. The X-ray data was obtained from Fowler *et al.* (1963 and 1965), while the neutron data was obtained from Bewley *et al.* (1967).

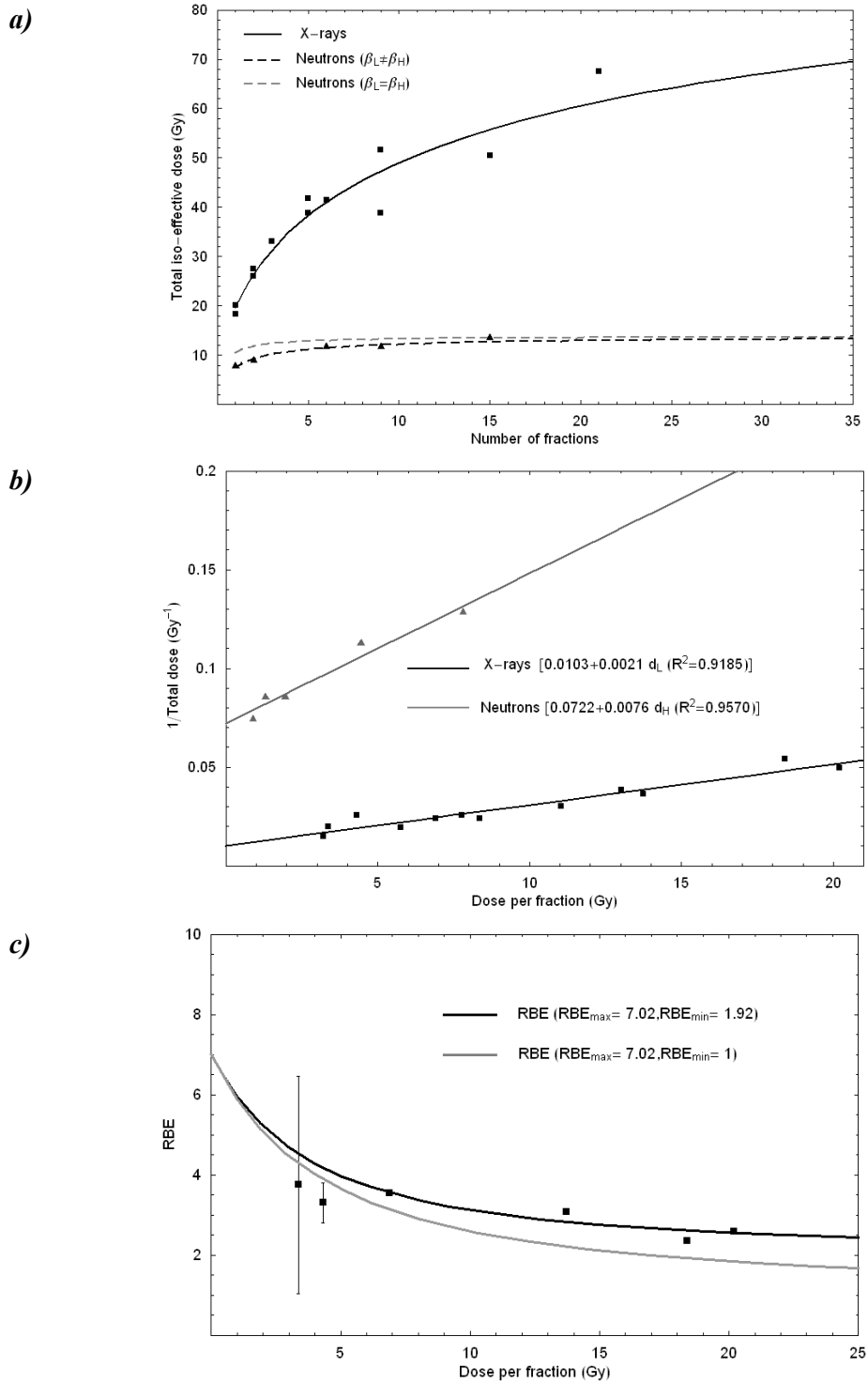


Figure 6.1: (a) Total dose required with different fractionation regimes to produce the same average skin reaction 2; (b) Fe plot; (c) RBE curve for pig skin exposed to X-rays and neutrons.

- Data points:

X-rays	Average Total Dose (Gy)	Aver. Ratios of Total Dose
1F/1d	20.20	1
2F/2d	26.058	1.29
2F/5d	27.472	1.36
3F/3d	33.128	1.64
5F/5d	38.784	1.92
5F/28d	41.814	2.07
9F/17d	51.712	2.56
21F/28d	67.468	3.34

Table 6.1: Data obtained from Fowler et al. (1963).

X-rays	Average Total Dose (Gy)	Aver. Ratios of Total Dose
1F/1d	18.40	1
6F/17d	41.40	2.25
9F/17d	38.824	2.11
15F/18d	48.76	2.65
15F/18d	47.84	2.6
15F/18d	54.832	2.98

Table 6.2: Data obtained from Fowler et al. (1965).

Neutrons	Average Total Dose (Gy)	Aver. Ratios of Total Dose	RBE
1F/1d	7.80	1	2.59 (20.20)
			2.36 (18.40)
2F/5d	8.892	1.14	3.09
6F/17d	11.70	1.5	3.54
9F/17d	11.856	1.52	3.31 (± 0.54)
9F/17d	11.622	1.49	
15F/18d	13.884	1.78	3.76 (± 5.43)
15F/18d	12.636	1.62	
15F/18d	13.806	1.77	

Table 6.3: Data obtained from Bewley et al. (1967) (the brackets in the RBEs for 1F/1d specify the dose/fraction considered to calculate the RBE)

6.1.2. Early skin reaction on the feet of mice

- *System used:* Young adult albino male mice (WHT/GyfbSVS) of 10-12 weeks old (Joiner *et al.*, 1983).

- *Laboratory conditions and Methodology of experiments:* All mice were anaesthetised with 100% oxygen to avoid hypoxia and to achieve uniform radiosensitivity. X-irradiations were carried out using a 240-kVp X-ray source generated by a Pantak machine (filtration= 0.25mmCu + 1mm Al, HVL=1.3 mmCu), giving a dose rate of 2.7 Gy/min. The circular field size used with X-rays was of 10cm in diameter exposing the left foot of the mouse. In the case of the neutron irradiation, a 4-MV Van de Graaff accelerator was used to produce 3 MeV neutrons by the reaction of 4-MeV deuterons with a thick beryllium target. The beam direction for the neutrons was vertically downward, a difference to the horizontal arrangement used in the case of X-rays. Four individual 25mm diameter circular fields were used providing a dose uniformity across each field of $\pm 3.5\%$ with a variation from one field to another of $< 1.5\%$. The average neutron dose rate was approximately 0.3Gy/min, and the γ contamination of the neutron beam was estimated to be 10.7% on the incident dose.

Skin reactions were scored three times a week between 5 and 35 days after treatment using the system described in Denekamp (1973). The average skin reaction over the period 10-32 days (or equivalent) after 1,2,5 and 9 fractions of either X-rays or neutrons was calculated for each mouse in a dose group and the group average and standard error were calculated from these values.

- *Radiobiological end point:* Average skin reaction with score 1.5

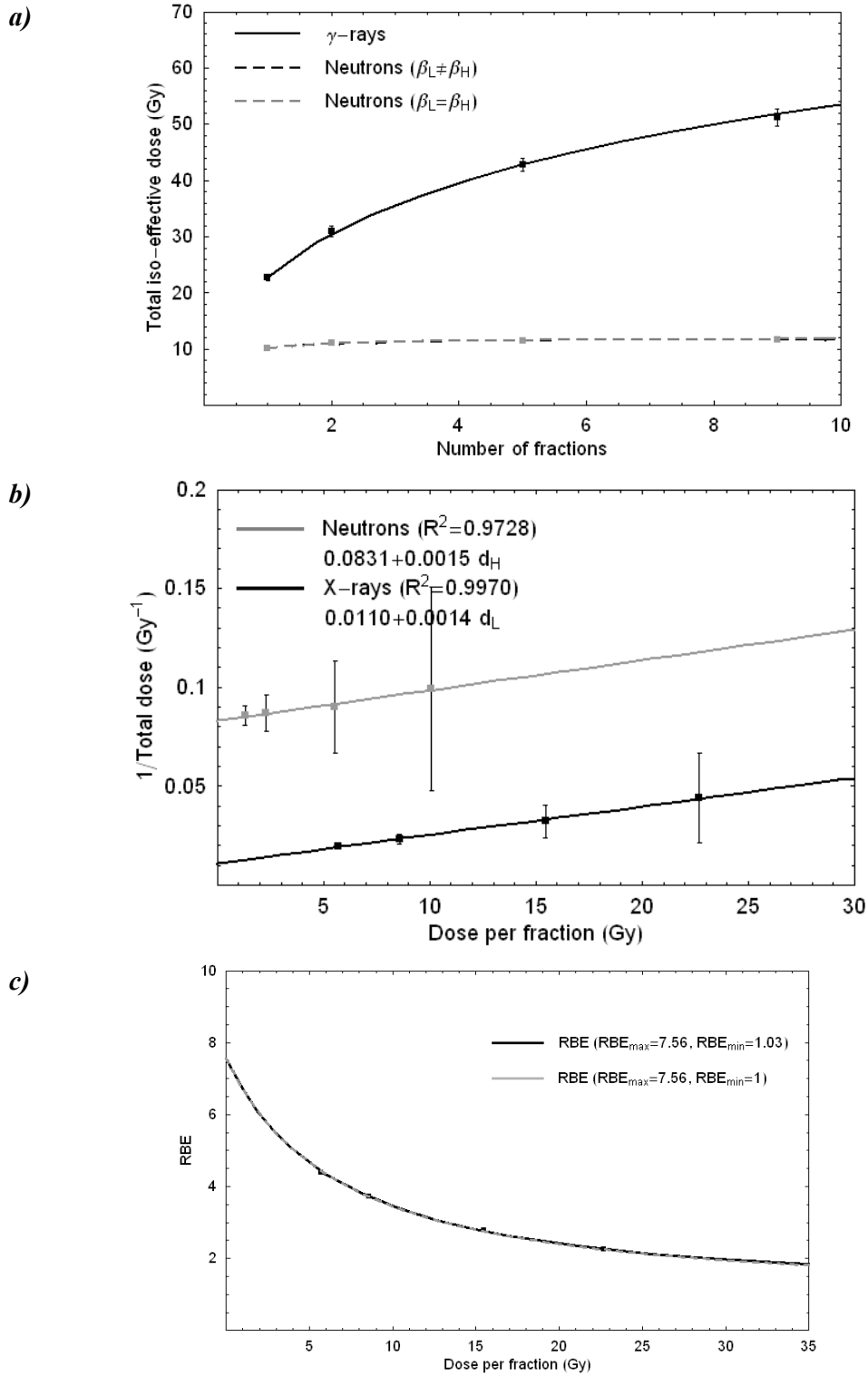


Figure 6.2: (a) Total dose required with different fractionation regimes to produce the same average skin reaction 1.5; (b) Fe plot; (c) RBE curve for mice leg skin exposed to X-rays and neutrons.

- *Data points:*

Fractions	Average Total Dose X-rays (Gy) (range)	Average Total Dose neutrons (Gy) (range)	RBE
SD	22.68 (23.02-22.49)	10.08 (10.22-9.83)	4.38
2F	30.91 (31.25-30.27)	11.10 (11.34-10.95)	3.73
5F	42.82 (43.32-42.20)	11.49 (11.68-11.25)	2.79
9F	51.23 (52.21-50.65)	11.69 (11.79-11.49)	2.25

Table 6.4: Average total dose data obtained from Joiner et al. (1983).

6.1.3. Mouse small intestine

- *System used:* Female CD-1 mice (25-30g) (Geraci *et al.*, 1977).

- *Laboratory conditions and Methodology of experiments:* Anaesthetised mice (sodium pentobarbital) were restrained in Plexiglass and exposed to graded doses of X-rays and neutrons in groups of 8. X rays were generated by a General Electric Maxitron therapy unit (250kVp, SSD = 50cm, HVL= 0.5mm Cu plus 1mm of added filtration and dose rate of 1Gy/min), while the neutrons were produced at the university of Washington cyclotron by 22MeV deuteron bombardment of a beryllium (Be) target which absorbed 70% of the incident deuterons. The animals were irradiated 125cm from the Be target, the γ -contamination of the neutron beam was of ~5% and the dose rate was 0.35Gy/min. 4cm segments of the ileum were exteriorised and exposed to fractionated doses of X-rays and neutrons. The field size used was $15 \times 15 \text{ cm}^2$ keeping the animal shielded and exposing the intestine through an aperture in the shielding. The dose to the shielded portion of the animal was less than 2% of the primary field dose for X-irradiation and 5% for neutron irradiation.

- *Radiobiological end point:* doses required with X-rays and neutrons to kill 50% of the population after 5 days (acute intestinal death) and 90 days (late damage to intestine) after the start of the treatment.

Figures corresponding to LD/50 5 days after irradiation with X-rays and neutrons (early damage):

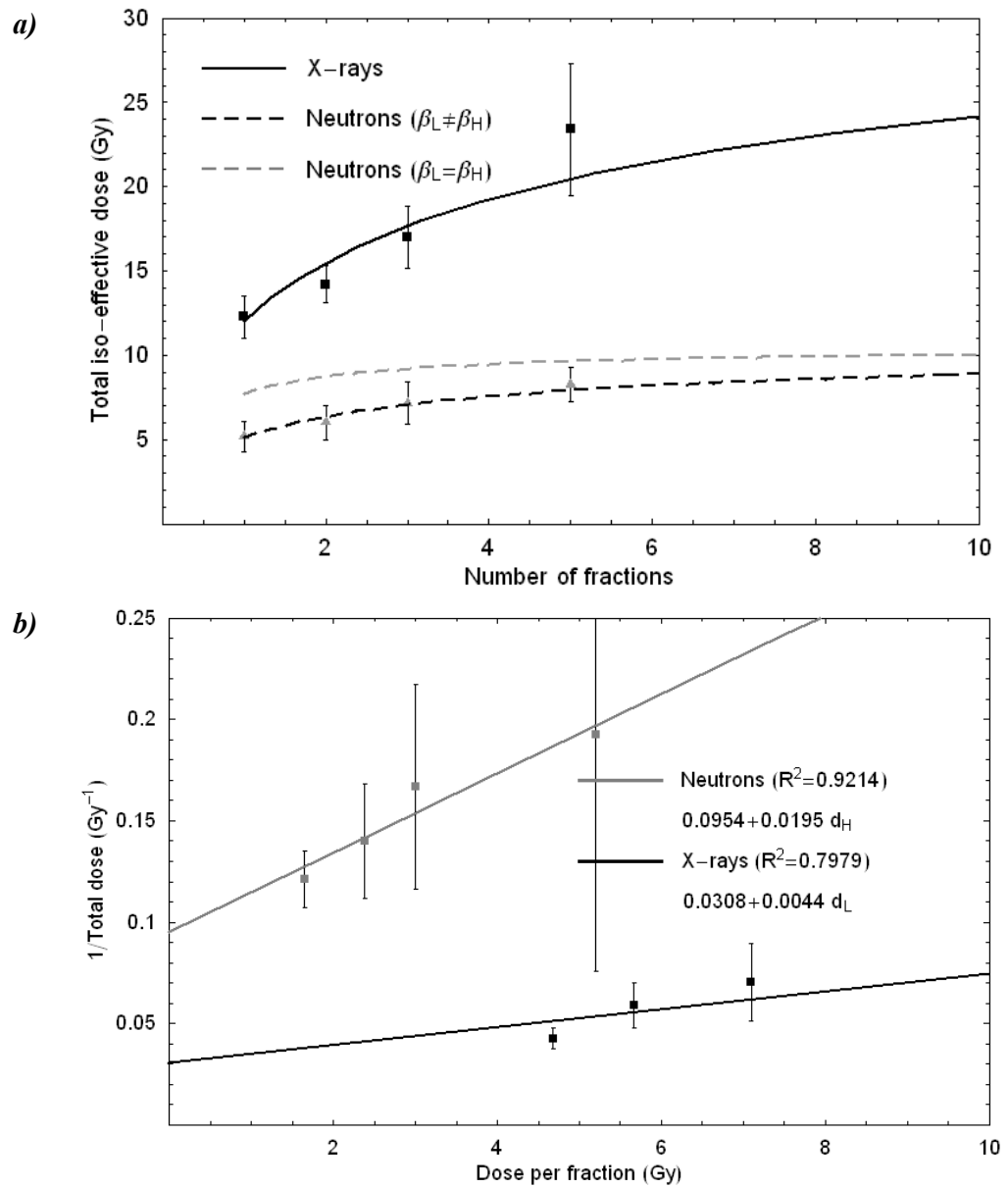


Figure 6.3: (a) Total dose required with different fractionation regimes to kill 50% of the mice population after 5 days; (b) Fe plot.

Figures corresponding to LD/50 at 90 days after irradiation with X-rays and neutrons (late damage):

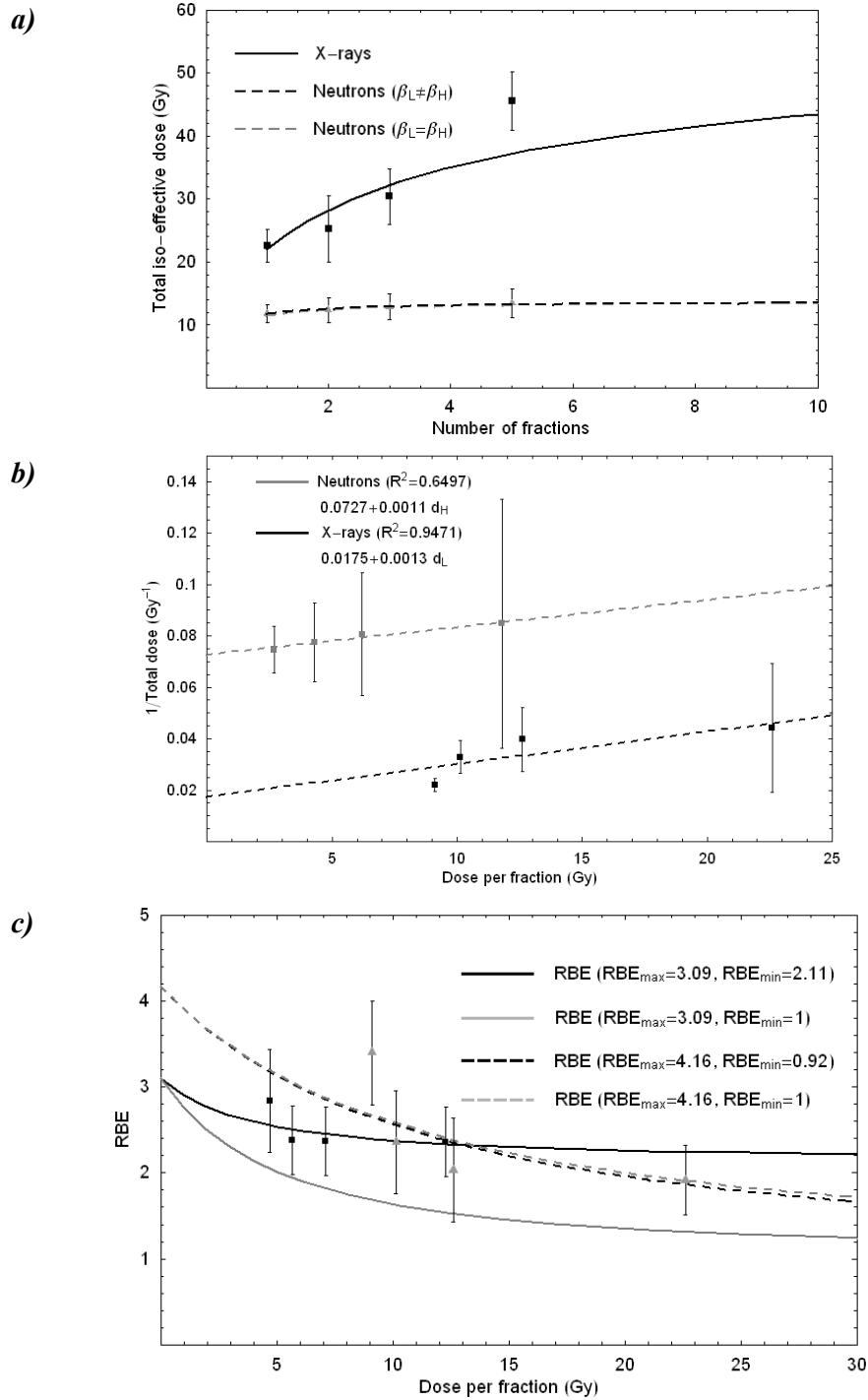


Figure 6.4: (a) Total dose required with different fractionation regimes to kill 50% of the mice population after 90 days; (b) Fe plot; (c) RBE curve for mice small intestine damage produced after exposure to X-rays and neutrons, where squares correspond to early reaction data and triangles to late reaction data.

Data points:

Total iso-effect doses (Gy) and RBE LD/50 at 5 days after X-rays and neutron			
Fraction	X-rays (range)	Neutrons (range)	RBE (range)
1F	12.28 (11.67-12.92)	5.20 (4.77-5.67)	2.4 (2.2-2.6)
2F	14.20 (13.67-14.75)	6.00 (5.50-6.55)	2.4 (2.2-2.6)
3F	17.00 (16.09-17.96)	7.15 (6.55-7.80)	2.4 (2.2-2.6)
5F	23.40 (21.53-25.43)	8.25 (7.75-8.78)	2.8 (2.5-3.1)
Total iso-effect doses (Gy) and RBE (\pm SE) for LD/50 at 90 days after X-rays and neutron			
Fraction	X-rays (range)	Neutrons (range)	RBE (range)
1F	22.60 (21.32-23.95)	11.80 (11.09-12.55)	1.9 (1.7-2.1)
2F	25.20 (22.70-27.98)	12.40 (11.45-13.42)	2.0 (1.7-2.3)
3F	30.40 (28.28-32.67)	12.90 (11.92-13.96)	2.4 (2.1-2.7)
5F	45.50 (43.22-47.90)	13.40 (12.30-14.60)	3.4 (3.1-3.7)

Table 6.5: Total iso-effect doses (Gy) and RBE for early and late damage after X-rays and neutron of small intestine in mice (Geraci et al., 1977).

6.1.4. Mice jejunal mucosa

- *System used:* Jejunal crypt stem cells extracted from pathogen free female C₃Hf/Bu mice aged between 8-12 weeks (Withers *et al.*, 1974).

- *Laboratory conditions and Methodology of experiments:* 2-3 days after whole body irradiation using single or multiple fractions of radiation, the animal was sacrificed and the number of repopulating crypts in the jejunal circumference was counted (Withers *et al.*, 1970). The crypts were irradiated using the 88-inch cyclotron at Texas A & M University by bombarding a beryllium target with a beam of 50MeV deuterons or 16MeV deuterons. The gamma contribution to the total dose was about 5%. Neutron doses were delivered at 0.80 to 0.90 Gy/min for 50MeV neutrons and at about 0.25 Gy/min for the 16MeV neutrons. The γ radiation was delivered at ~100rads/min using a ⁶⁰Co unit. It was assumed that inter-fractionation repair of sublethal lesion occurred within 3 hours after irradiation. Cells were synchronised to the same cycle stage by using hydroxyurea to kill all those cells in any other stage of the cell cycle other than those at the G₁-S boundary.

- *Radiobiological end point:* The radiobiological point of interest was reduction of crypt cells to 10 per jejunal circumference. The following results were obtained.

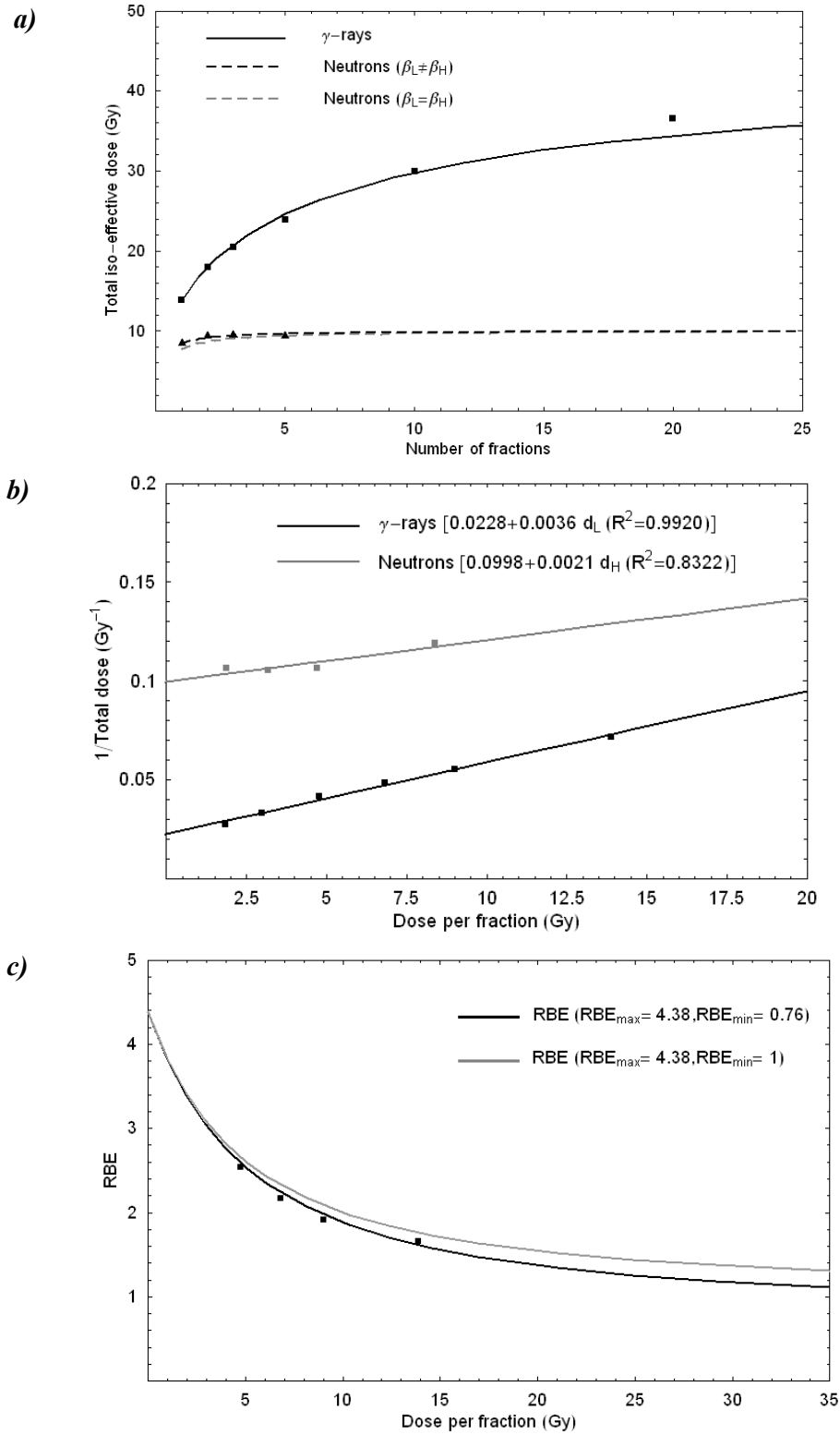


Figure 6.5: (a) Total dose required with different fractionation regimes to produce a 10% survival level of jejunal crypts; (b) Fe plot; (c) RBE curve for 10% survival level of jejunal crypts.

- Data points:

X-rays	Total isoeffective dose (Gy)
1F	1.39
2F	26.058
3F	33.128
5F	38.784
10F	41.814
20F	67.468

Table 6.6: Data obtained from (Withers et al., 1974).

Neutrons	Total isoeffective dose (Gy) for the 50MeV (Be) cyclotron
1F	8.4
2F	4.70
3F	3.16
5F	1.88

Table 6.7: Data obtained from (Withers et al., 1974).

6.1.5. Mice central nervous system.

- *System used:* Three month old male CFHB rats (Hornsey *et al.*, 1980; 1991).

- *Laboratory conditions and Methodology of experiments:* Irradiation of 2.5 cm of the lumbar cord (vertebrae L2-L5) was carried out using X-rays of 250 kVp (filtration 0.3mm Cu + 1mm Al, HVL=1.35mm Cu, dose rate = 2 Gy/min) and neutrons of 7MeV (average) energy (Be bombardment with 16MeV deuterons, dose rate = 0.7Gy/min). The description of the radiation sources and dosimetry is described in detail in subsection 6.1.6. For these experiments, all X-ray data has been converted into Co- γ -ray doses by multiplying each dose by a factor 1.11 (Hornsey, 1991). Multiple fractions were used for the lumbar experiments, with an overall treatment time of 6 weeks.

- *Radiobiological end point:* Total doses required to produce ataxia in 50% of the animals exposed to X-rays or neutrons (50% effective dose, ED/50).

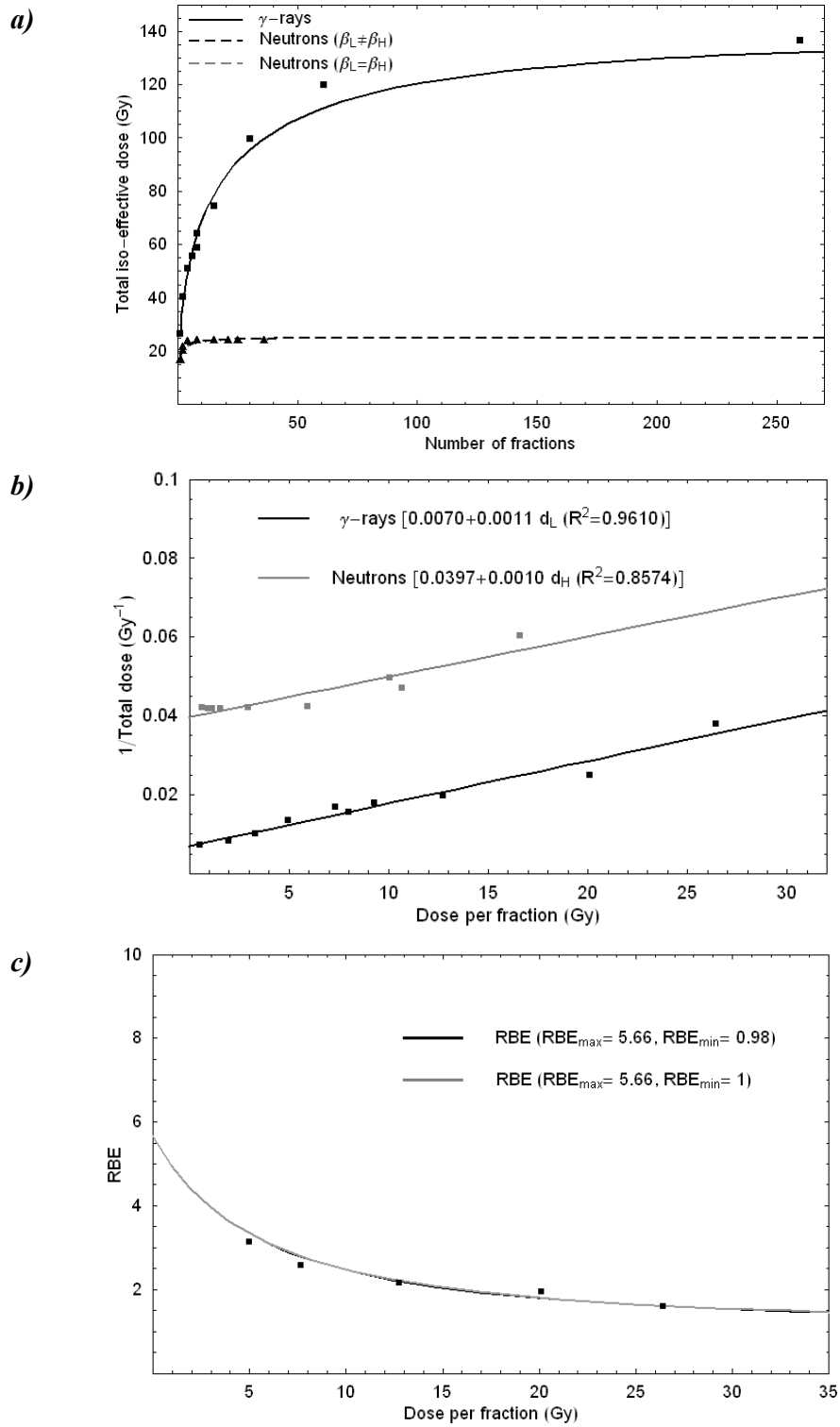


Figure 6.6: (a) Total dose to produce ataxia in 50% of animals plotted against the number of fractions used for γ -rays and $d[16]\text{Be}$ neutrons; (b) Fe plot; (c) RBE curve for ataxia-ED50% after γ -rays and neutrons.

- Data points:

γ -rays	Total isoeffective dose (Gy)
1F	26.41
2F	40.23
4F	50.92
6F	55.77
8F	58.9
8F	64.17
15F	74.56
30F	99.63
61F	120.02
260F	136.55

Table 6.8: Data obtained from (Hornsey, 1991).

Neutrons	Total isoeffective dose (Gy) From the d[16]Be cyclotron
1F	16.6
2F	20.09
2F	21.3
4F	23.66
8F	23.8
15F	23.83
21F	23.85
25F	23.96
36F	23.76

Table 6.9: Data obtained from (Hornsey, 1991).

6.1.6. Radiation pneumonitis Mice lung

- *System used:* Female TO mice, 12-15 weeks old (Field *et al.*, 1974; 1976; Hornsey *et al.*, 1975).

- *Laboratory conditions and Methodology of experiments:* Before each irradiation, mice were anesthetized with sodium pentobarbitone (Nembutal). They were irradiated at room temperature while breathing air. Each radiation beam was collimated to give fields of 2.5×3.0 cm to the mouse thorax, with the head and abdomen shielded. Mice were exposed either to a 250 kVp beam of X-rays filtered by a 0.25mm Cu and 1 mm Al, with an HVL=1.3mm Cu; or to a 8MV X-ray beam produced by a linear accelerator, collimated by blocks of 7cm of lead to produce the field size of interest; or to 7.5MeV neutrons produced with a 16MeV deuterons bombarding a beryllium target (3% gamma contamination (Bewley *et al.*, 1969)) and imparted through a thin layer of tissue equivalent plastic stuck over the tails to avoid skin sparing by allowing full build up. The dose rate of the X-rays and neutrons beams were, 1.7Gy/min (250kVp X-rays), 1.0Gy/min (8MV X-rays) and 0.7Gy/min (neutrons) respectively. The whole-body dose calculated for the 8MV X-rays experiments was 5% of that given to the thorax, while in the case of the 7.5MeV neutron beam it was 10%.

- *Radiobiological end point:* Single or fractionated total dose required to kill 50% of the animals from radiation pneumonitis within 180 days after irradiation. The variability of the total dose required was associated to changes in environment and bacterial flora.

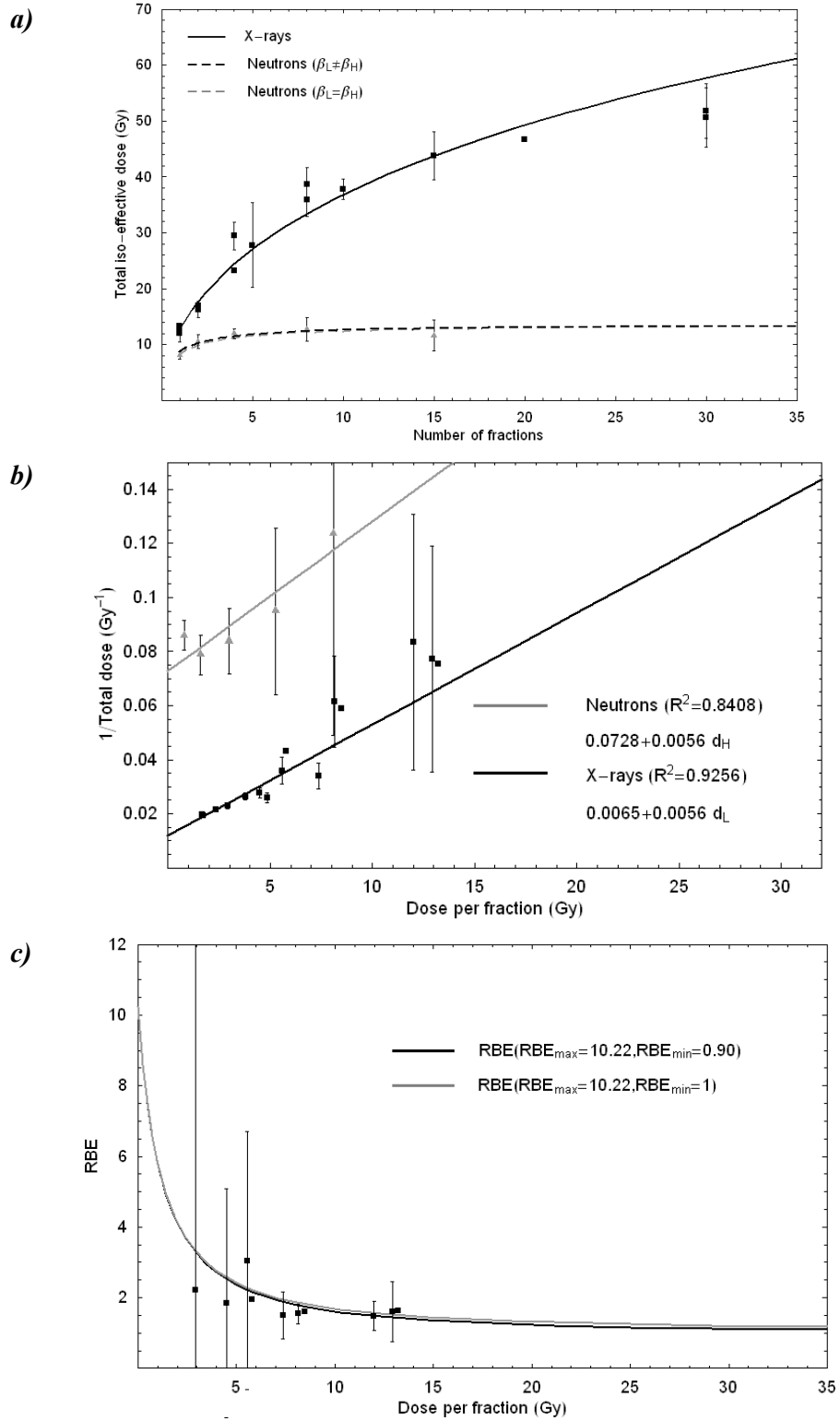


Figure 6.7: (a) Total dose required with different fractionation regimes to produce LD/50 due to pneumonitis; (b) Fe plot; (c) RBE curve for mice exposed to X-rays and neutrons on the thorax.

- Data points:

250 kVp X-rays			
Fraction	LD/50 (cGy)	Range of LD/50 (cGy)	Mean
1F	1317	(1254-1419)	1199 (1150.3-1295)
	1078	(1025-1131)	
	1234	(1172-1335)	
	1167	-	
2F	1454	(1386-1520)	1629.25 (1560.5-1705)
	1690	(1618-1762)	
	1834	(1739-1931)	
	1539	(1499-1607)	
5F	2466	-	2781.4 (3221-2466)
	2685	-	
	2846	-	
	2689	-	
	3221	-	
8F	3872	(3730-4021)	-
30F	5063	(4806-5332)	-

Table 6.10: LD/50, 40-180 days (95% CI) as function of number of fractions. Data for 250 kVp obtained from (Field et al., 1976).

300 kVp X-rays			
Fraction	LD/50 (cGy)	Range of LD/50 (cGy)	Mean
1F	1324	-	-
2F	1698	-	-
4F	2318	-	-
10F	3694	-	3783.5 (3694-3873)
	3873	-	
20F	4668	-	-

Table 6.11: LD/50, 40-180 days (95% CI) as function of number of fractions. Data for 300 kVp obtained from (Field et al., 1976).

7.5 MV X-rays			
Fraction	LD/50 (cGy)	Range of LD/50 (cGy)	Mean
1F	1293	(1252-1338)	-
4F	2944	(2821-3064)	-
8F	3597	(3444-3750)	-
15F	4376	(4161-4588)	-
30F	5180	(4938-5432)	-

Table 6.12: LD/50, 40-180 days (95% CI) as function of number of fractions. Data for 7.5MV obtained from (Field et al., 1976).

8MeV neutrons			
Fraction	LD/50 (cGy)	Range of LD/50 (cGy)	Mean
1F	808	(738-876)	-
2F	911	(610-1036)	1053
	1195	(1167-1225)	(888.5-1130.5)
4F	1193	(1117-1280)	-
8F	1269	(1116-1538)	-
15F	1163	(849-1409)	-

Table 6.13: LD/50, 40-180 days (95% CI) as function of number of fractions. Data for 8MeV fast neutrons obtained from (Field et al., 1976; Hornsey et al., 1975).

RBE values for each energy			
250 kVp X-ray			
Fraction	D/# (cGy)	RBE	Range
1F	1199	1.484	(1.478-1.559)
2F	814.63	1.363	(1.337-1.392)
8F	484	3.051	(2.614-3.342)
300 kVp X-rays			
1F	1324	1.639	-
2F	849	1.613	-
4F	579.5	1.943	-

(Continue from previous page...)

7.5 MV X-rays			
1F	1293	1.600	(1.527-1.696)
4F	736	2.468	(2.394-2.536)
8F	449.63	2.835	(2.4380-3.086)
15F	291.73	3.763	(3.106-5.154)

Table 6.14: Corresponding RBE values for the different energy data sets.

6.1.7. Lung damage in mice as measured from increased breathing rate and lethality

- *System used:* CBA/Ht GyfBSVS male mice aged 8 to 10 weeks (22-30g) (Parkins *et al.*, 1985).

- *Laboratory conditions and Methodology of experiments:* Mice were exposed to 240kVp (HVL 1.3mm Cu, dose rate 1.8 Gy/min at 25 cm from the target) using a 2 × 2 cm field size on the thorax, with the remainder of the body being shielded. The 3 MeV (average energy) neutron beam was produced by a Van de Graaff accelerator using a 4 MeV deuteron beam incident on a thick beryllium target. The dose rate of the neutron beam remained between 0.2 and 0.3 Gy/min and was reported to have a less than 10% gamma-ray contamination. Mice were exposed to various fractionation schemes; when two fractions/day were used the interval between fractions was 6 ± 0.5 hours as in (Field *et al.*, 1974).

- *Radiobiological end point:* Two different radiobiological end points were used to assess the damage to lungs by the different types of radiation:
 - *increase in breathing rate* (by a factor of 1.1 with respect the normal rate), measured at 4 weeks intervals from 20 to 72 weeks. In order to assess the predicted gain on the therapeutic ratio by using the ideas proposed in Chapter 5 (i.e. the differences between early and late effects), the increase of breathing rate by a 1.1 factor (BR×1.1) at 28 and 68 weeks have been reported here.
 - *lethality (LD/50)*, corresponding to those mice which died due to breathing difficulties. Similar to the case before, LD/50 at 28 and 68 weeks after irradiation have been considered.

Figures corresponding to $BRI \times 1.1$ at 28 weeks after irradiation:

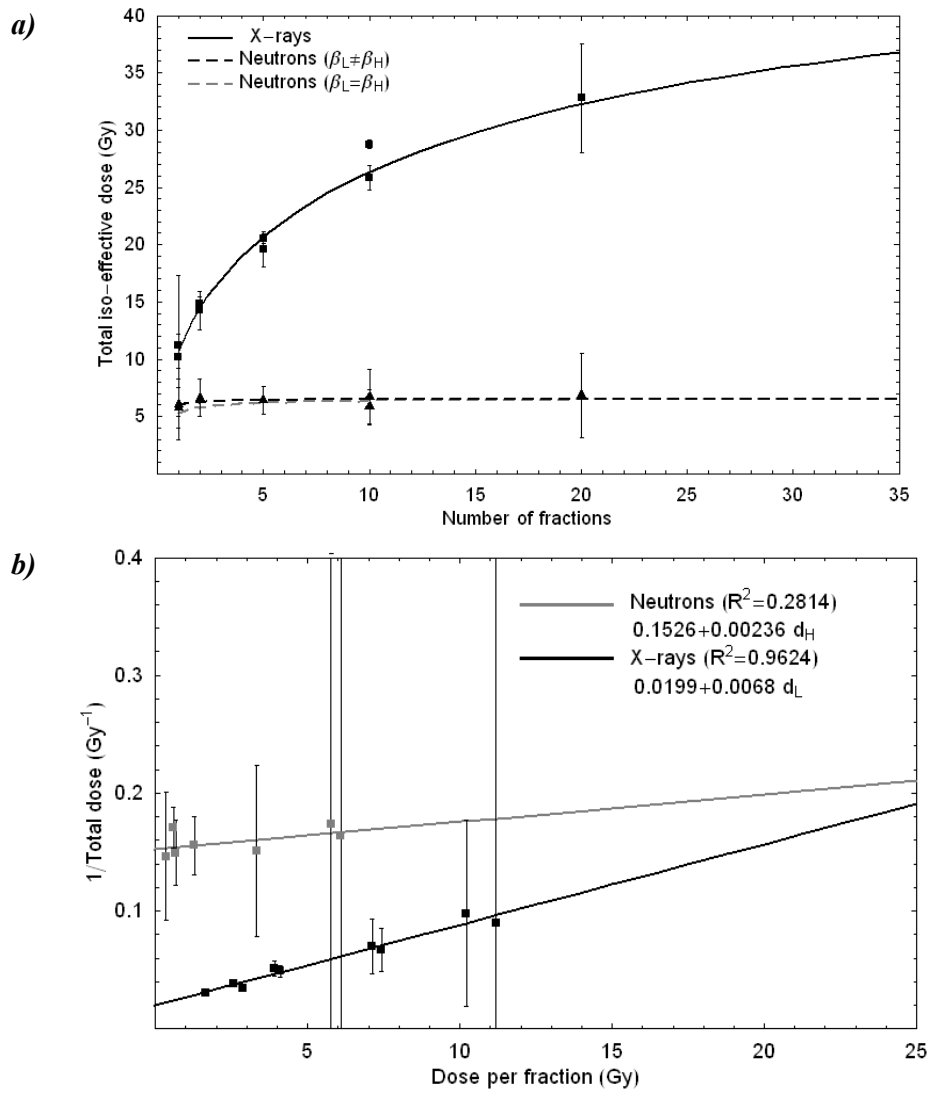


Figure 6.8: (a) Total dose required with different fractionation regimes to produce an increase of the breath rate by a factor 1.1 compared to the normal rate after 28 week of radiation (early effects); (b) Corresponding Fe-plot.

Figures corresponding to $BRI \times 1.1$ at 68 weeks after irradiation:

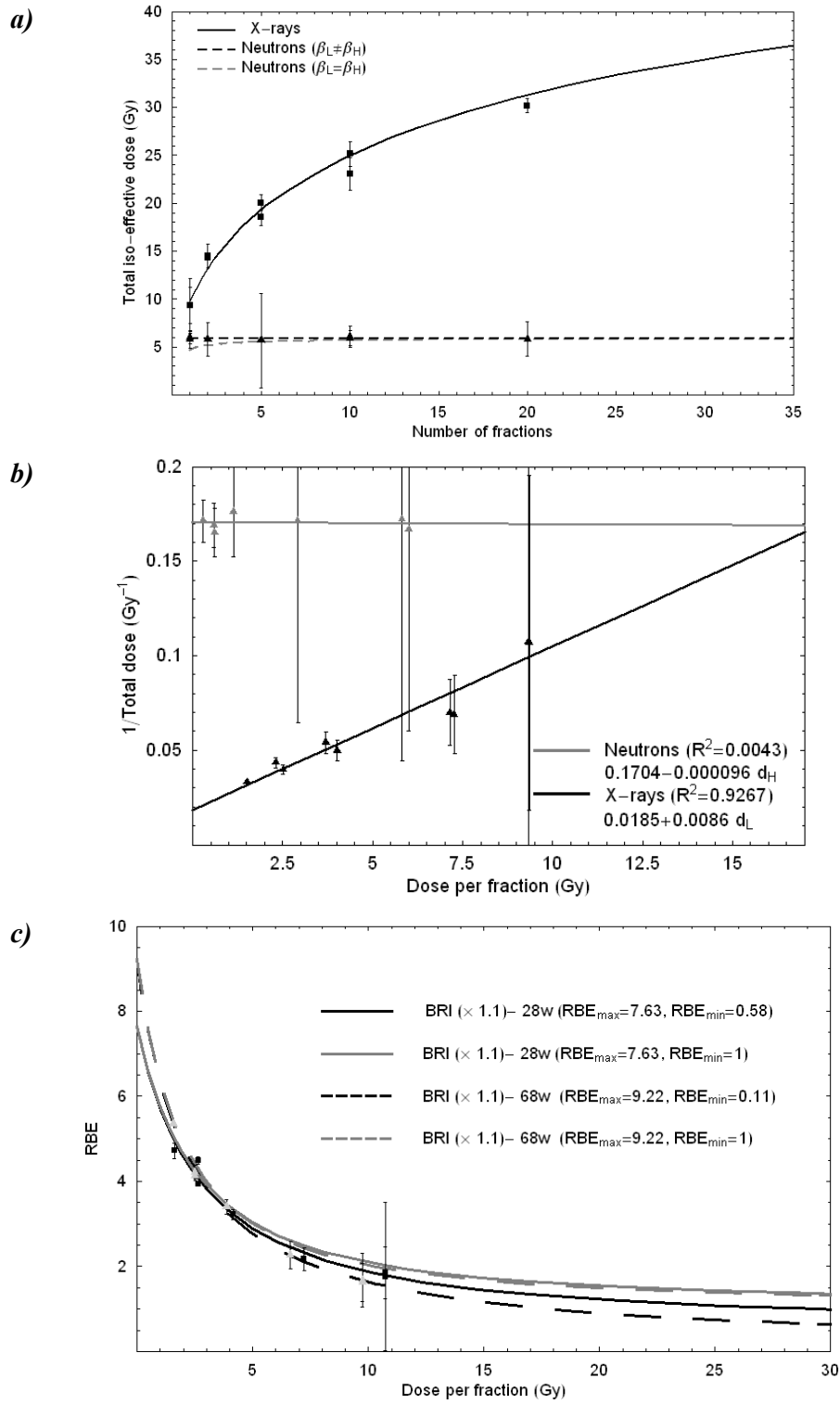


Figure 6.9: (a) Total dose required to produce an increase of the breath rate by a factor 1.1 compared to the normal rate after 68 week of radiation (late effects); (b) Corresponding Fe-plot; (c) RBE curves for early and late effect, where squares correspond to early reaction data and triangles to late reaction data.

Figures corresponding to LD/50 at 28 weeks after irradiation:

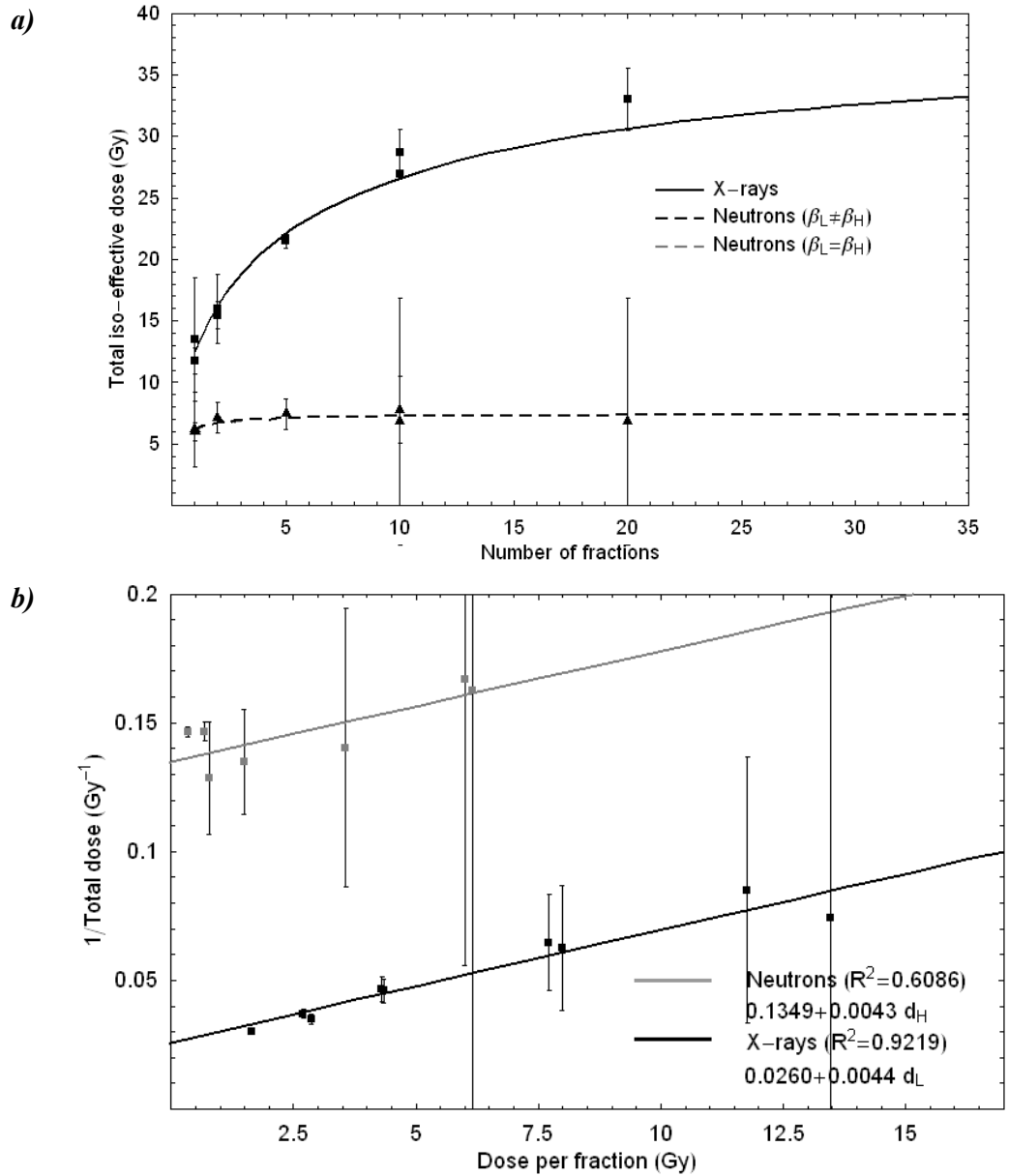


Figure 6.10: (a) Total dose required with different fractionation regimes to kill 50% of the population from breathing deficiency after 28 week of radiation (early effects); (b) Corresponding Fe-plot.

Figures corresponding to LD/50 at 68 weeks after irradiation:

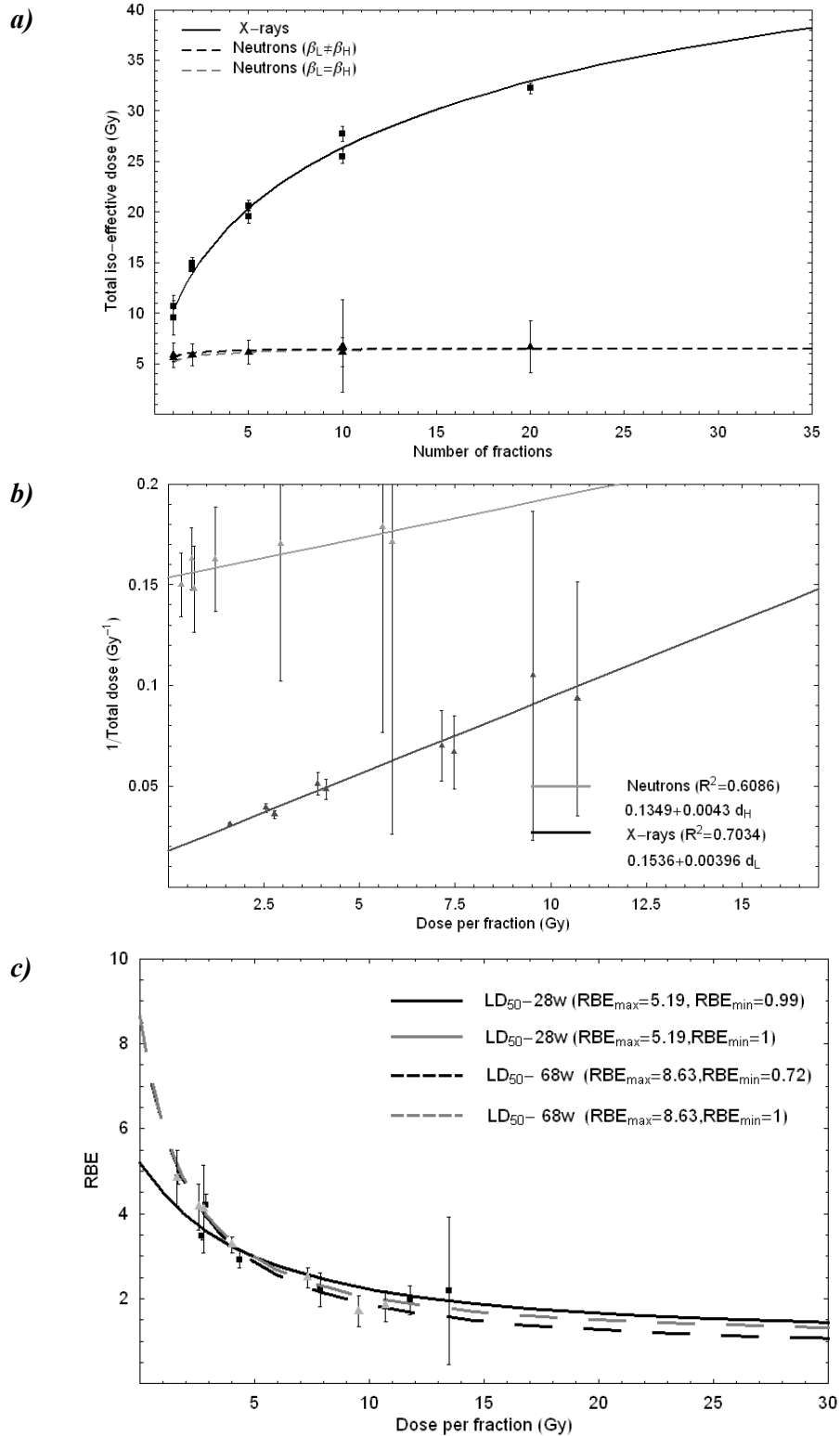


Figure 6.11: (a) Total dose required to kill 50% of the population from breathing deficiency after 68 week of radiation (late effects); (b) Corresponding Fe-plot; (c) RBE curves for early and late effect, where squares correspond to early reaction data and triangles to late reaction data.

- Data points:

240 kVp X-rays – BRI×1.1 after 28 weeks			Neutrons rays – BRI×1.1 after 28 weeks		RBE ±1 SE
Fraction	BRI×1.1 (Gy)	±1 SE	BRI×1.1 (Gy)	±1 SEM	
1F	10.21	3.9	5.77	3.6	1.86 (0.61)
	11.18	12.3	6.09	6.3	1.76 (1.75)
2F	14.26	3.4	6.64	3.2	2.17 (0.27)
	14.85	1.2			
5F	19.57	3.1	6.43	2.4	3.22 (0.12)
	20.52	0.9			
10F	25.86	2.2	5.86	3.0	4.49 (0.09)
	28.77	0.8	6.70	4.9	3.93 (0.04)
20F	32.79	9.5	6.84	7.3	4.72 (0.18)
240 kVp X-rays – BRI×1.1 after 68 weeks			Neutrons rays – BRI×1.1 after 68 weeks		RBE ±1 SE
Fraction	BRI×1.1 (Gy)	±1 SE	BRI×1.1 (Gy)	±1 SE	
1F	9.32	5.7	5.81	1.9	1.68 (0.64)
	9.35	3.7	6.00	1.3	1.62 (0.44)
2F	14.3	0	5.84	3.5	2.27 (0.31)
	14.54	2.5			
5F	18.52	1.6	5.68	9.9	3.40 (0.17)
	20.06	1.6			
10F	23.03	3.4	6.06	2.2	4.12 (0.09)
	25.14	2.5	5.92	1.6	4.22 (0.16)
20F	30.19	1.4	5.84	3.6	5.35 (0.03)

Table 6.15: Total doses required to increase the breathing rate by a 1.1 factor after different fractionation schemes 28 and 68 weeks after irradiation with X-rays and neutrons. Data obtained from (Parkins et al., 1985).

240 kVp X-rays – LD/50 after 28 weeks			Neutrons rays LD/50 after 28 weeks		
Fraction	LD/50 (Gy)	±1 SE	LD/50 (Gy)	±1 SEM	RBE ±1 SE
1F	11.76	2.1	6.0	1.5	1.96 (0.34)
	13.47	10	6.15	6.1	2.19 (1.73)
2F	15.44	2.2	7.13	2.5	2.20 (0.40)
	15.96	5.6			
5F	21.54	1.2	7.42	2.5	2.91 (0.20)
	21.70	-			
10F	26.95	-	7.78	5.5	3.46 (0.09)
	28.69	3.8	6.82	20.1	4.21 (0.25)
20F	33.01	5.1	6.82	20.1	4.84 (0.15)
240 kVp X-rays – LD/50 after 68 weeks			Neutrons rays – LD/50 after 68 weeks		
Fraction	LD/50 (Gy)	±1 SE	LD/50 (Gy)	±1 SE	
1F	9.53	3.4	5.6	0.7	1.70 (0.36)
	10.70	2.1	5.85	2.4	1.83 (0.36)
2F	14.3	-	5.88	2.2	2.49 (0.23)
	14.94	1.2			
5F	19.54	1.3	6.15	2.3	3.27 (0.19)
	20.63	1.1			
10F	25.49	1.4	6.14	2.9	4.15 (0.54)
	27.76	1.5	6.76	9.1	4.11 (1.03)
20F	32.23	1.0	6.67	5.1	4.83 (0.66)

Table 6.16: Total doses required to kill 50% of the mice population after different fractionation schemes 28 and 68 weeks after irradiation with X-rays and neutrons. Data obtained from (Parkins et al., 1985).

6.1.8. *Reaction from different normal tissues of pig to neutrons: skin, kidney and lung.*

6.1.8.1. *Effects on epidermis and dermal vascular/connective tissues.*

- *System used:* Female pigs of the of the Large White strain (Hopewell *et al.*, 1988).

- *Laboratory conditions and Methodology of experiments:* All procedures were carried out under anaesthesia using a standard 2% halothane, ~70% oxygen and ~30% nitrous oxide gas mixture. Prior to fractionated irradiation several 16cm × 4cm fields were tattooed on the right and the left flanks of each pig. The radiation sources used were a X-ray beam (250kVp; HVL 1.4mm Cu; FSD 50cm; dose rate ~69 cGy/min (Hopewell *et al.*, 1979)) and a neutron beam (Variable Energy Cyclotron at the Atomic Energy Research Establishment at Harwell; bombardment of 2mm thick gold-backed beryllium target with 42MeV deuterons; FSD 150cm, dose rate ~54 cGy/min). In the case of the neutron irradiation, skin build up was provided by 10mm of tissue-equivalent gelatine taped on the skin surface. A 4mm lead shield was used on the adjacent fields of exposure to avoid proton contamination. Fractionated doses of X-rays were given as 6, 12 or 14 fractions over 18 days and 6, 14, 18 and 30 fractions over 39 days. Neutron doses were given as 6 or 12 fractions over 18 days and 6, 12 or 30 fractions over 39 days. The analysis here assumes no proliferation occurring during the 39 days fractionation period. After fractionation, the skin was examined at weekly intervals by a minimum of 4 observers for 16 weeks after X-rays and 20 weeks after neutrons.

- *Radiobiological end point:* Dose-effect curves were fitted by probit analysis and from these the dose required to produce a 50% incidence (ED/50) of severity of erythema and presence or absence of moist desquamation and dermal necrosis was assessed.

Figures corresponding to $ED/50$ for epithelial reaction of skin after irradiation:

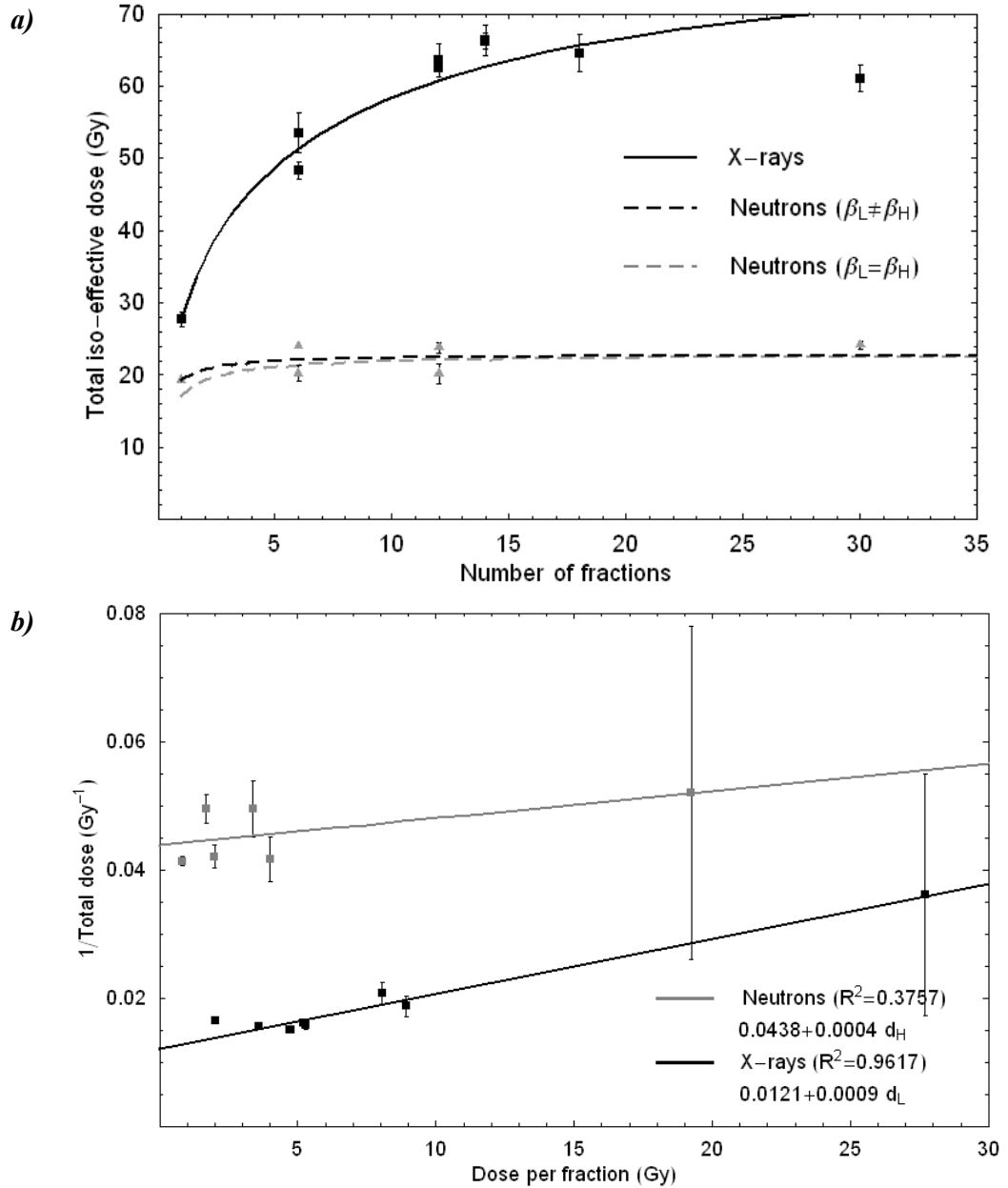


Figure 6.12: (a) Total dose ($ED/50$) required with different fractionation regimes to produce epithelial reaction on pig skin; (b) Corresponding Fe-plot.

Figures corresponding to ED/50 for late dermal necrosis of skin after irradiation:

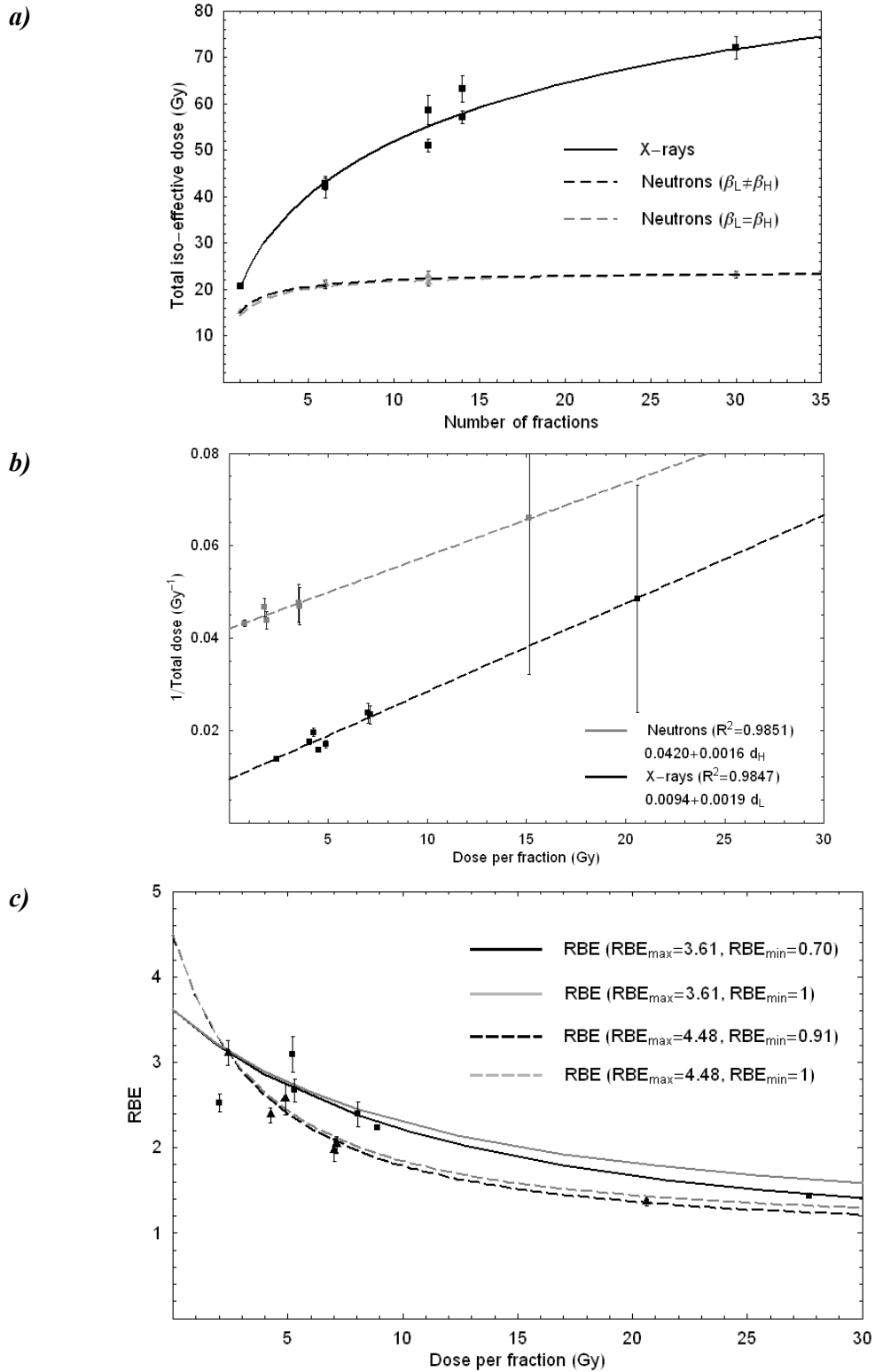


Figure 6.13: (a) Total dose (ED/50) required with different fractionation regimes to produce dermal necrosis on pig skin; (b) Corresponding Fe-plot; (c) RBE curves for early and late reactions, where squares correspond to early reaction data and triangles to late reaction data.

Data points:

Iso-effect ED/50 doses (Gy) and RBE (\pm SE) for early epithelial reactions in pig skin after X-rays and neutron			
Fraction	X-rays	Neutrons	RBE
1F	27.70 \pm 1.1	>19.25	<1.4
6F/18d	48.31 \pm 1.16	20.2 \pm 1.12	2.39 \pm 0.15
12F/18d	62.44 \pm 1.13	20.2 \pm 1.35	3.09 \pm 0.21
14F/18d	66.18 \pm 1.08	-	-
6F/39d	53.51 \pm 2.76	>24	<2.23
12F/39d	63.57 \pm 2.3	23.8 \pm 0.74	2.67 \pm 0.13
14F/39d	66.38 \pm 2.11	-	-
18F/39d	64.56 \pm 2.55	-	-
30F/39d	61.08 \pm 1.88	24.2 \pm 0.55	2.52 \pm 0.1

Table 6.17: ED/50 doses (Gy) and RBE values as function of number of fractions for early epithelial reactions in pig skin. Data obtained from (Hopewell et al., 1988).

Iso-effect ED/50 doses (Gy) and RBE (\pm SE) for late dermal necrosis in pig skin after X-rays and neutron			
Fraction	X-rays	Neutrons	RBE
1F	20.60 \pm 0.28	15.15 \pm 0.4	1.36 \pm 0.04
6F/18d	42.69 \pm 1.27	21.01 \pm 0.79	2.03 \pm 0.1
12F/18d	50.98 \pm 1.31	21.42 \pm 0.58	2.38 \pm 0.09
14F/18d	57.04 \pm 1.39	-	-
6F/39d	42.09 \pm 2.3	21.33 \pm 0.75	1.97 \pm 0.13
12F/39d	58.63 \pm 3.22	22.81 \pm 1.12	2.57 \pm 0.19
14F/39d	63.12 \pm 2.89	-	-
30F/39d	71.96 \pm 2.38	23.14 \pm 0.69	3.11 \pm 0.14

Table 6.18: ED/50 doses (Gy) and RBE values as function of number of fractions for late dermal necrosis in pig skin. Data obtained from (Hopewell et al., 1988).

6.1.8.2. Effects on cutaneous and subcutaneous tissues

- *System used:* Female pigs of the Large White strain (Hopewell *et al.*, 1990).

- *Laboratory conditions and Methodology of experiments:* Laboratory conditions, radiation sources and fractionation schemes used are described in 1.7.1. For the particular case relevant to this subsection, the degree of late radiation-induced damage to the cutaneous and subcutaneous tissues was assessed by measuring the length of the long axis of each of the irradiated skin fields and comparing this with the length of the matching field on the opposite flank of the same pig. For each field, measurements were taken of the field edges and that of the central axis and the mean of these measurements was calculated. After X irradiation, the comparison was always with the matching site on the opposite flank. However, after fast neutron irradiation only, comparison was made with a single ‘control’ site length per pig. The ratio of the lengths of the irradiated to the control sites was referred to as the ‘relative field length’. At each dose level for each fractionation schedule of X-rays or fast neutrons, the proportion of skin fields showing a relative field length of <0.9, <0.875, <0.85 or <0.825 was assessed at two different periods, 26-52 weeks after treatment (considered early reactions) and 65-104 weeks after treatment (considered late reactions).

- *Radiobiological end point:* Using the data described above, the doses associated with a 50% incidence (ED/50±SE) of these four increasing levels of effect were determined by probit analysis. The ED/50 doses presented in this thesis have been obtained as an average of the ED/50 doses of the four relative field lengths (i.e. ED/50 iso-effective dose to produce a relative field length of 0.863)

Figures corresponding to measurements at 26-52 weeks after irradiation with X-rays and neutrons:

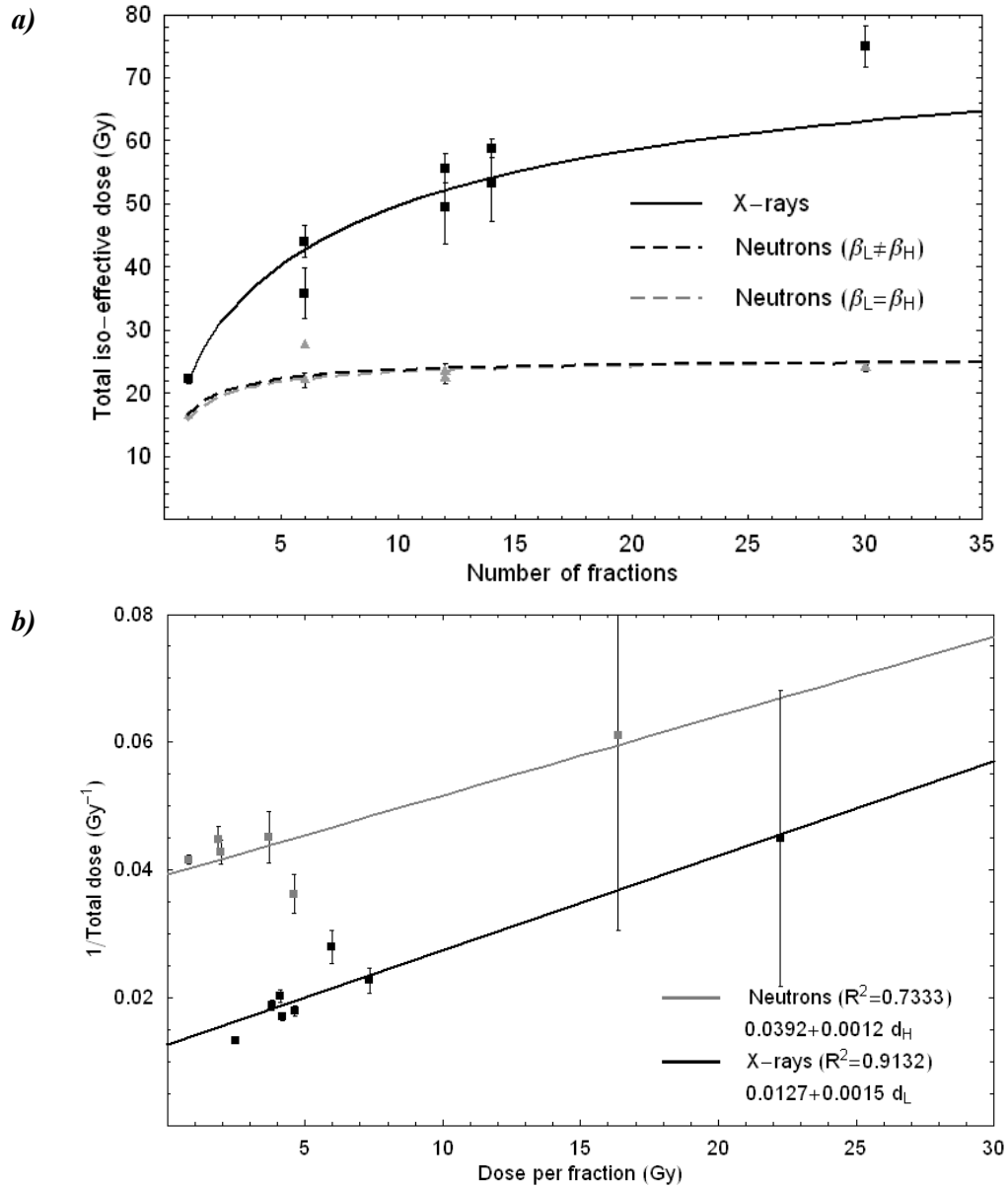


Figure 6.14: (a) ED/50 iso-effective dose to produce a relative field length of 0.863 at 26-52 weeks after irradiation with X-rays and neutrons; (b) Corresponding Fe-plot.

Figures corresponding to measurements at 65-104 weeks after irradiation with X-rays and neutrons:

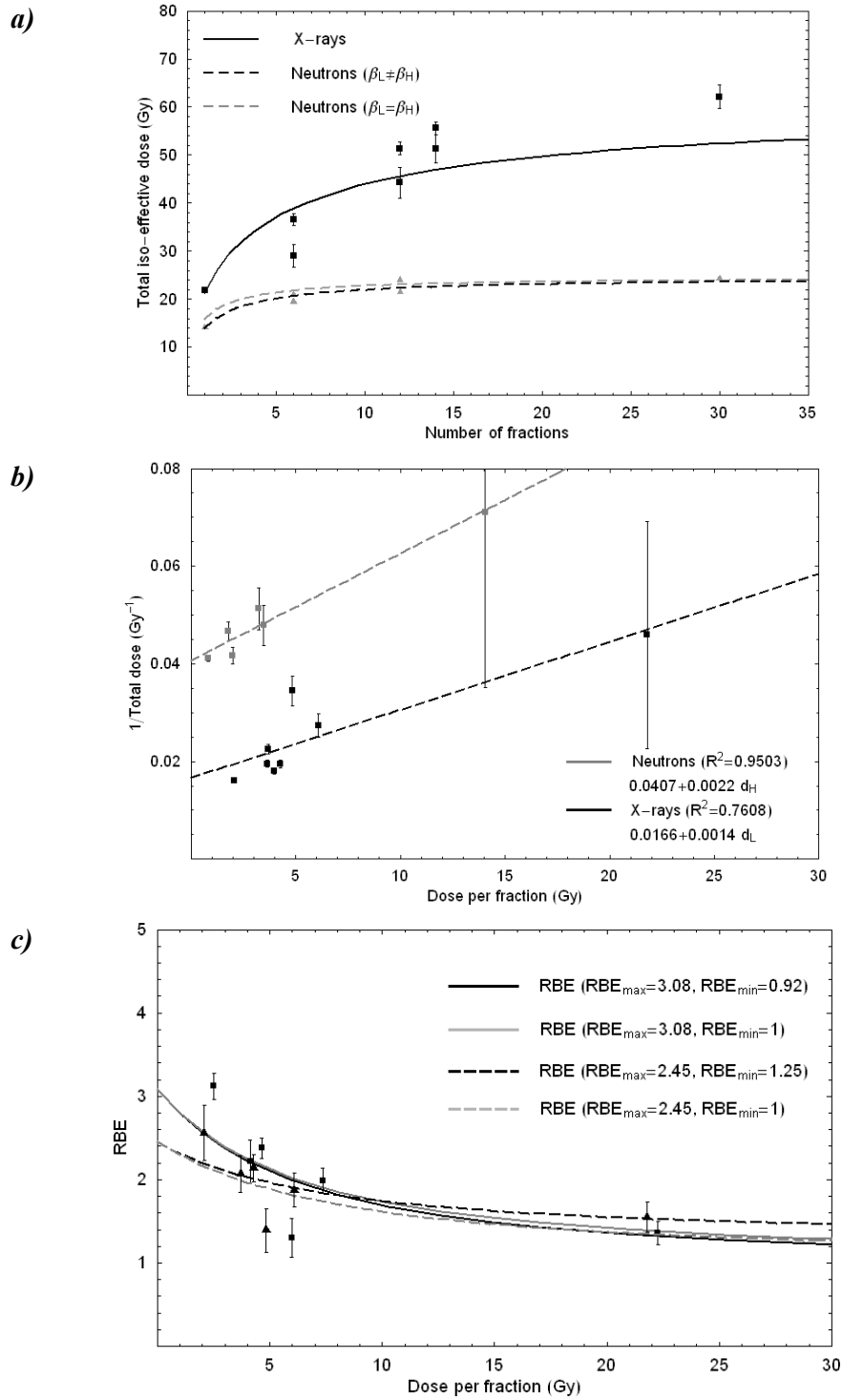


Figure 6.15: (a) ED/50 iso-effective dose to produce a relative field length of 0.863 at 65-104 weeks after irradiation with X-rays and neutrons; (b) Corresponding Fe-plot; (c) RBE curves for early and late reactions, where squares correspond to early reaction data and triangles to late reaction data.

- Data points:

Iso-effect ED/50 doses (Gy) and RBE (\pm SE) for an average relative field size of 0.863 at 26-52 weeks in pig skin after X-rays and neutron			
Fraction	X-rays	Neutrons	RBE
1F	22.26 \pm 0.74	16.36 \pm 1.65	1.37 \pm 0.14
6F/18d	44.09 \pm 2.54	22.15 \pm 0.96	1.97 \pm 0.15
12F/18d	55.63 \pm 2.36	23.39 \pm 0.51	2.37 \pm 0.12
14F/18d	58.82 \pm 1.46	-	-
6F/39d	35.87 \pm 4.00	27.60 \pm 3.53	1.28 \pm 0.23
12F/39d	49.38 \pm 5.66	22.30 \pm 0.68	2.20 \pm 0.26
14F/39d	53.18 \pm 5.92	-	-
30F/39d	75.02 \pm 3.27	24.04 \pm 0.67	3.11 \pm 0.16

Table 6.19: ED/50 doses (Gy) and RBE values as function of number of fractions for early cutaneous and subcutaneous reactions in pig skin. Data obtained from (Hopewell et al., 1990).

Iso-effect ED/50 doses (Gy) and RBE (\pm SE) for an average relative field size of 0.863 at 65-104 weeks in pig skin after X-rays and neutron			
Fraction	X-rays	Neutrons	RBE
1F	21.79 \pm 2.07	14.06 \pm 1.15	1.46 \pm 0.18
6F/18d	36.54 \pm 2.62	19.49 \pm 1.42	1.85 \pm 0.20
12F/18d	51.38 \pm 2.13	24.01 \pm 1.39	2.14 \pm 0.16
14F/18d	55.57 \pm 1.50		
6F/39d	29.03 \pm 4.70	20.89 \pm 1.62	1.31 \pm 0.26
12F/39d	44.31 \pm 4.63	21.42 \pm 0.46	2.05 \pm 0.22
14F/39d	51.26 \pm 4.42		
30F/39d	62.15 \pm 5.29	24.30 \pm 2.19	2.75 \pm 0.33

Table 6.20: ED/50 doses (Gy) and RBE values as function of number of fractions for late cutaneous and subcutaneous reactions in pig skin. Data obtained from (Hopewell et al., 1990).

6.1.8.3. Effects on lung function

- *System used*: Female pig of the Large White strain (Rezvani *et al.*, 1990).

- *Laboratory conditions and Methodology of experiments*: Laboratory conditions, radiation sources and fractionation schemes used are described in 1.7.1. For the particular case of this subsection, the quoted doses refer to those at the centre of the fully ventilated lobe of the irradiated lung without a correction for changes in tissue density. The irregular shape of the irradiated lung tissue resulted in a maximum dose variation across the ventilated lung of $\pm 14\%$. However, the average dimensions of the lung suggested that a $\pm 9.5\%$ variation in total dose across the lung was more representative. Lung function tests were performed prior to irradiation and then at 13-weekly intervals until 104 weeks after irradiation. Each animal was tested twice on each occasion using a standard ^{133}Xe washout technique (Rezvani *et al.*, 1986) where accumulation and clearance of the ^{133}Xe from comparable areas of the irradiated and unirradiated lung in the same animal was recorded using a gamma camera. Activity counts, collected for a total period of 160s, plotted against time were integrated over intervals of 0.4s using a multichannel analyser. From each time-activity curve the exchange capacity of the irradiated lung, monitored via the rate of ^{133}Xe clearance, was obtained. A 'functional index' (FI) of the irradiated lungs was calculated from the comparison of the rate-constant obtained for the irradiated lung with respect to that of the contralateral unirradiated lung in the same animal. A change of the FI by more than 15% was considered a change of the lung function; thus any lung with $\text{FI} \leq 85\%$ was considered to be affected.

- *Radiobiological end point*: Tests were performed in two phases: *pneumonitic* phase, where the tests were done 13-26 weeks after irradiation (early damage); and *fibrotic* phase, where the tests were done 39-104 weeks after irradiation (late damage).

Figures corresponding to measurements at 13-26 weeks after irradiation with X-rays and neutrons:

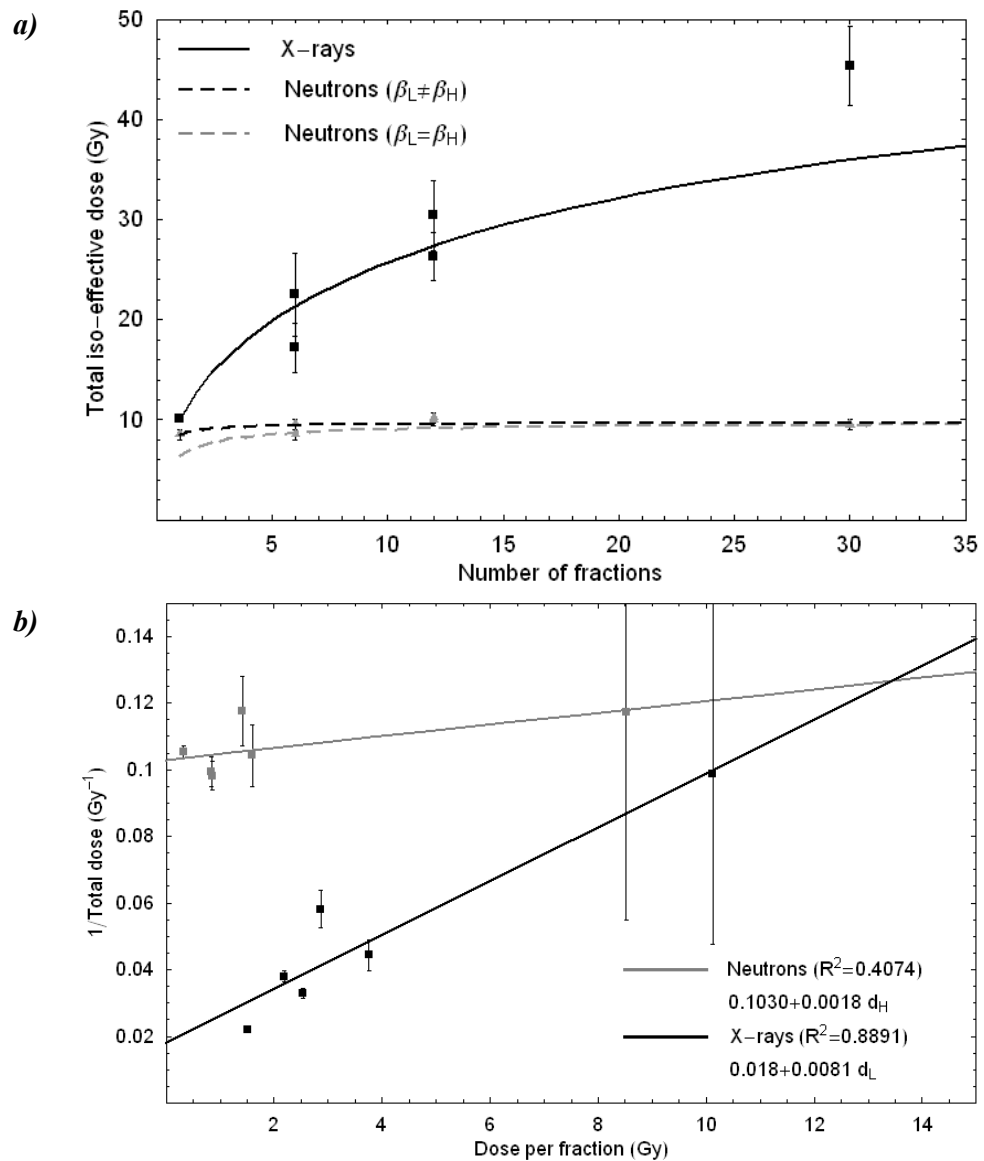


Figure 6.16: (a) Iso-effective ED/50 values for a $\geq 15\%$ reduction in lung function after irradiation with single and fractionated doses of either photons or fast neutrons assessed at 13-26 weeks after irradiation (early damage); (b) Corresponding Fe-plot.

Figures corresponding to measurements at 39-104 weeks after irradiation with X-rays and neutrons:

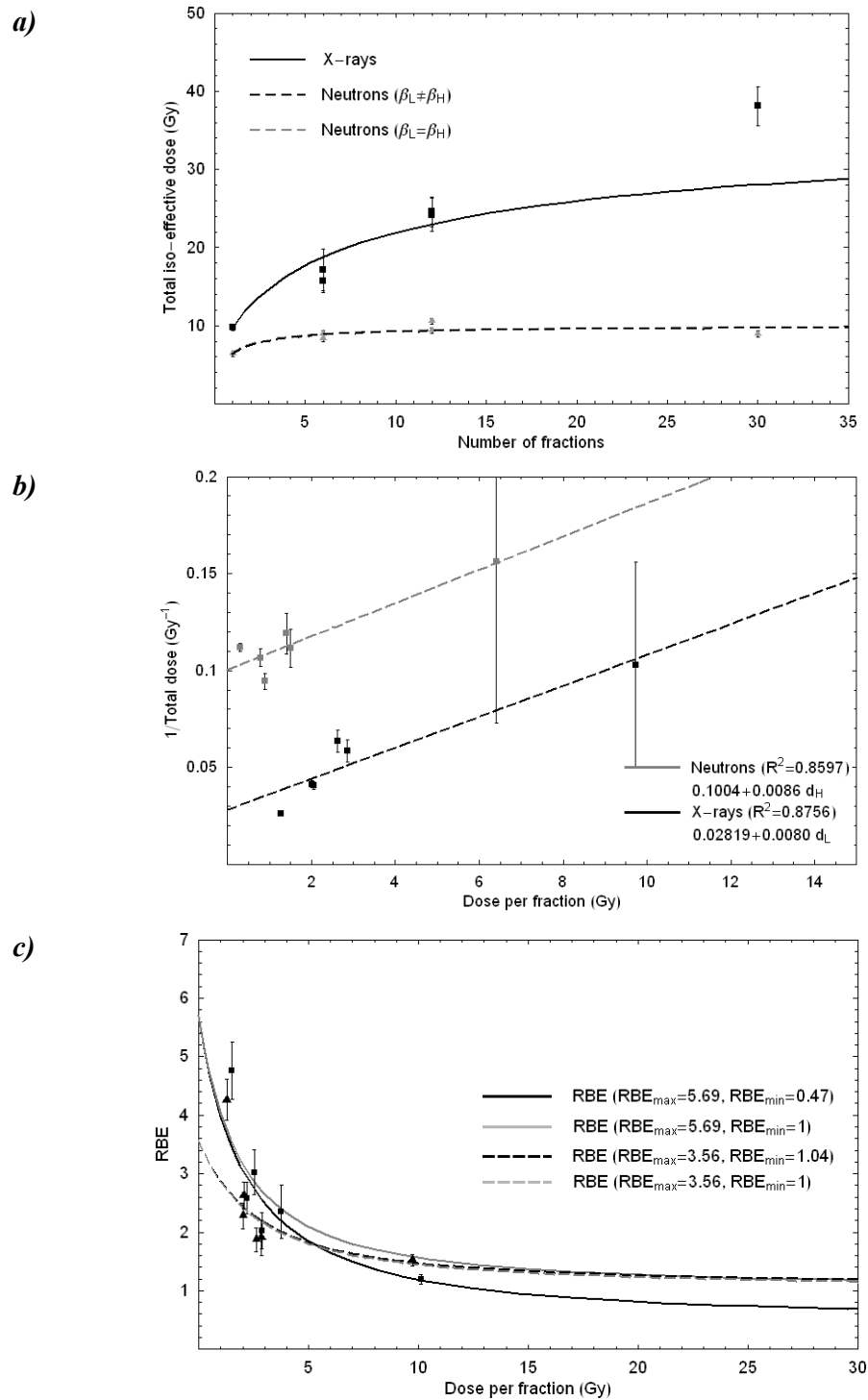


Figure 6.17: (a) Iso-effective ED/50 values for a $\geq 15\%$ reduction in lung function after irradiation with single and fractionated doses of either photons or fast neutrons assessed at 39-104 weeks after irradiation (late damage); (b) Corresponding Fe-plot; (c) RBE curves for early and late reactions, where squares correspond to early reaction data and triangles to late reaction data.

Data points:

Iso-effect ED/50 doses (Gy) and RBE (\pm SE) for a reduction in lung function $\geq 15\%$ at 13-26 weeks after X-rays and neutron			
Fraction	X-rays	Neutrons	RBE
1F	10.12 \pm 0.33	8.52 \pm 0.50	1.19 \pm 0.08
6F/18d	17.19 \pm 2.46	8.51 \pm 0.53	2.02 \pm 0.31
12F/18d	26.30 \pm 2.40	10.19 \pm 0.52	2.58 \pm 0.27
6F/39d	22.53 \pm 4.13	9.59 \pm 0.52	2.35 \pm 0.45
12F/39d	30.44 \pm 3.50	10.06 \pm 0.60	3.03 \pm 0.39
30F/39d	45.29 \pm 3.95	9.50 \pm 0.51	4.77 \pm 0.49

Table 6.21: ED/50 doses (Gy) and corresponding RBE values for a reduction in lung function $\geq 15\%$ at 13-26 weeks (early damage) after X-rays and neutron (Rezvani et al., 1990).

Iso-effect ED/50 doses (Gy) and RBE (\pm SE) for a reduction in lung function $\geq 15\%$ at 39-104 weeks after X-rays and neutron			
Fraction	X-rays	Neutrons	RBE
1F	9.73 \pm 0.34	6.41 \pm 0.38	1.52 \pm 0.10
6F/18d	15.71 \pm 1.43	8.40 \pm 0.50	1.87 \pm 0.20
12F/18d	24.59 \pm 1.88	9.38 \pm 0.37	2.62 \pm 0.23
6F/39d	17.13 \pm 2.64	8.98 \pm 0.39	1.91 \pm 0.30
12F/39d	24.17 \pm 2.13	10.58 \pm 0.38	2.28 \pm 0.22
30F/39d	38.11 \pm 2.50	8.94 \pm 0.43	4.26 \pm 0.35

Table 6.22: ED/50 doses (Gy) and corresponding RBE values for a reduction in lung function $\geq 15\%$ at 39-104 weeks (late damage) after X-rays and neutron (Rezvani et al., 1990).

6.1.8.4. *Effects on renal function*

- *System used*: Female pig of the Large White strain (Robbins *et al.*, 1991).
- *Laboratory conditions and Methodology of experiments*: Laboratory conditions, the radiation sources and fractionation schemes used are described in 1.7.1. In this particular study, renal function was assessed by renography prior to irradiation and 4-104 weeks after irradiation using effective renal plasma flow (ERPF) and glomerular filtration rate (GFR) techniques. Function in the irradiated kidney was compared with that in the contralateral unirradiated kidney to establish a functional index (FI). The FI was estimated from the ratio of the uptake function of ¹³¹I-hippuran (measured using a gamma camera) in the irradiated kidney compared with that obtained from the unirradiated kidney in the same animal. Three different levels of function were defined from the values of the FI:

FI (%)	Classification
72-138	Normal Function (F)
30-72	Reduced Function (RF)
<30	No significant function (NF)

- *Radiobiological end point*: RBE values were obtained from the maximum doses that maintain the functionality of the kidney and the minimum dose at which no functionality was appreciated. As a larger time interval was always required to produce a NF response from the kidney than a RF, any result with FI>72% was considered early damage, while FI<30% was considered late damage.

Figures corresponding to total doses producing $FI > 72\%$ after irradiation with X-rays and neutrons:

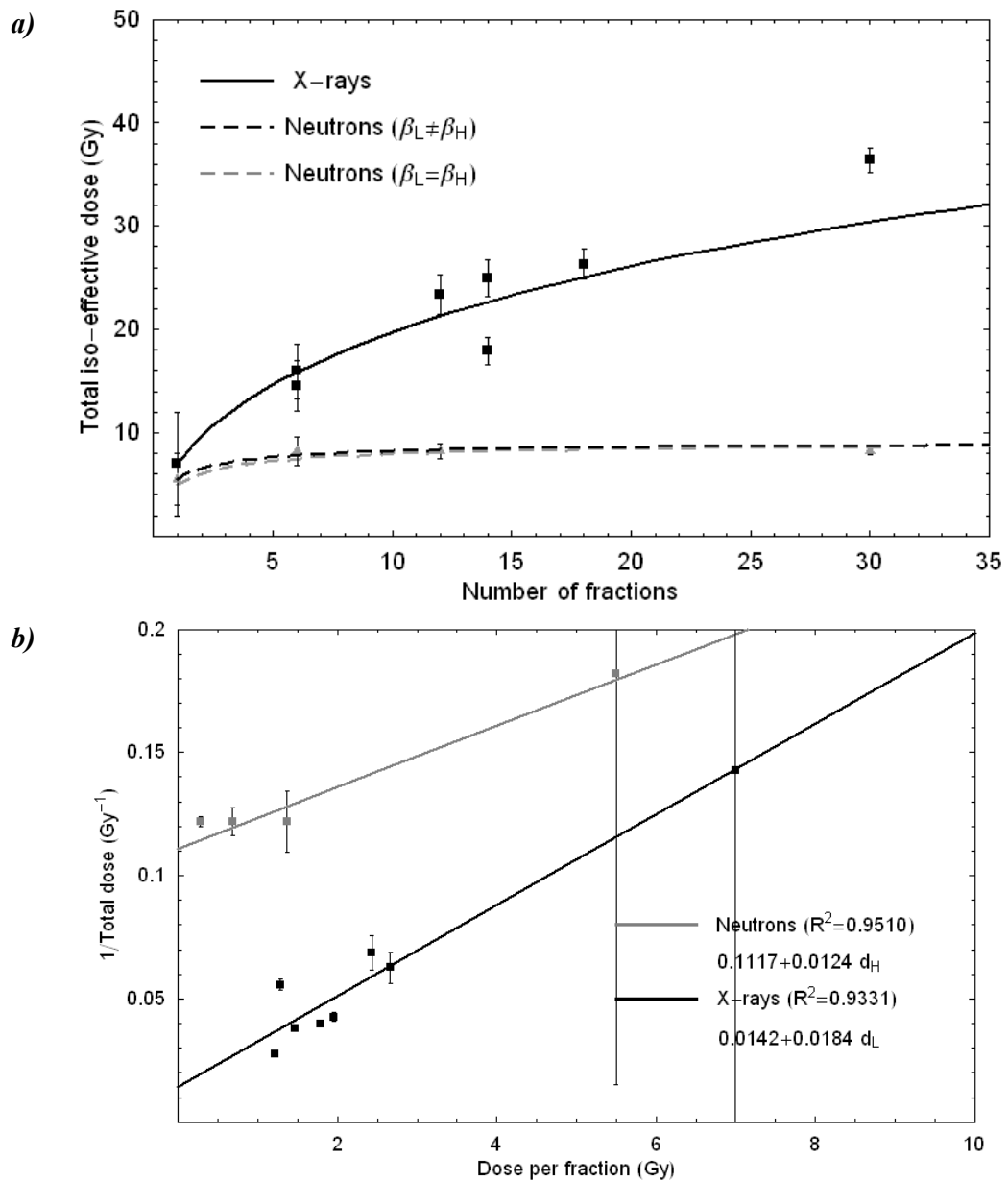


Figure 6.18: (a) Maximum total iso-effective doses that preserve the kidney function (early damage); (b) Corresponding Fe plot.

Figures corresponding to total doses producing $FI < 30\%$ after irradiation with X-rays and neutrons:

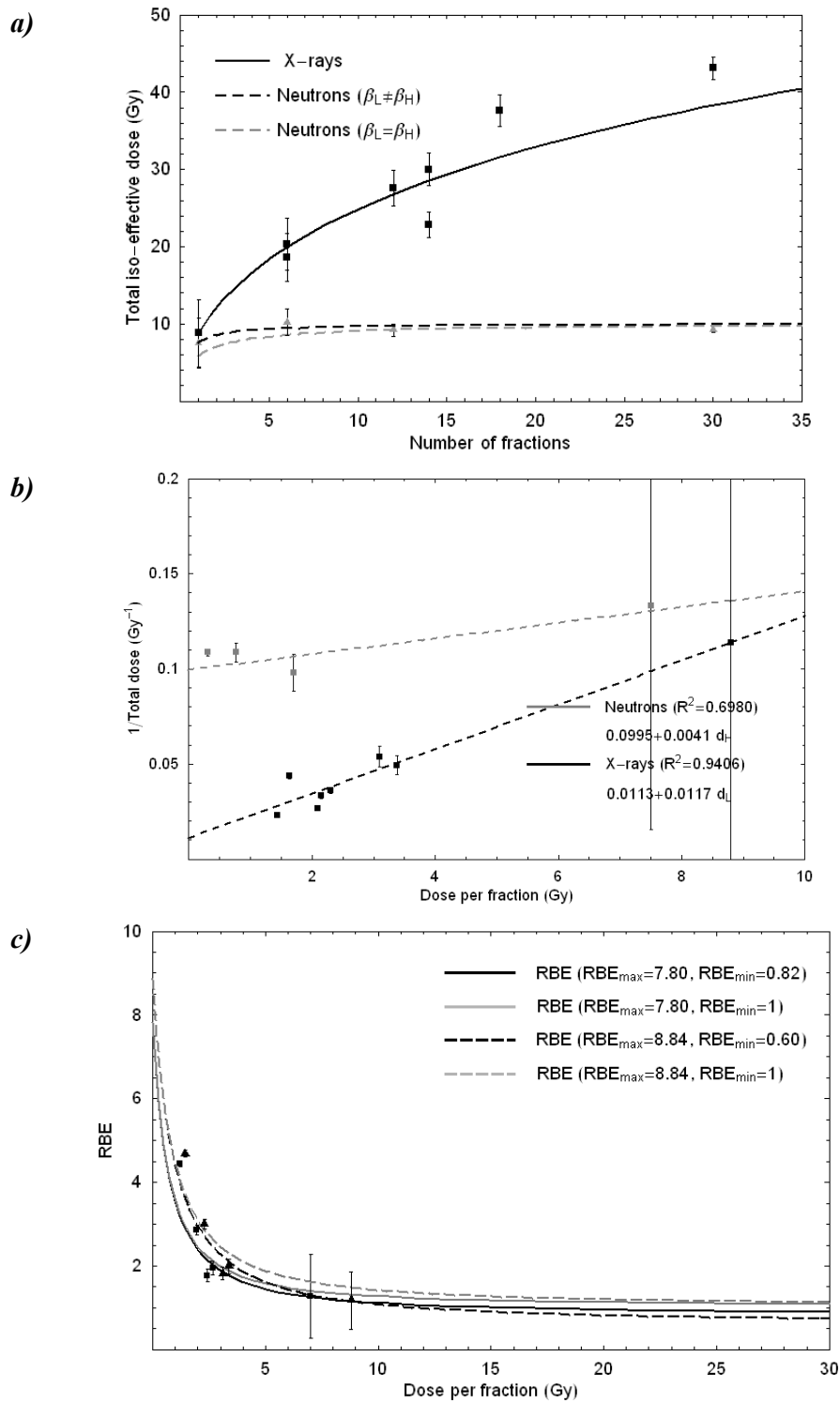


Figure 6.19: (a) Minimum total iso-effective doses at which the kidney stops functioning (late damage); (b) Corresponding Fe-plot; (c) RBE for early and late damages, where squares correspond to early reaction data and triangles to late reaction data.

Data points:

Iso-effect ED/50 doses (Gy) and RBE (\pm SE) for a FI>72% (effect level F) in kidney function after X-rays and neutron			
Fraction	X-rays	Neutrons	RBE
1F	7.0 \pm 7.0	5.50 \pm 5.50	1.27
6F/39d	15.95 \pm 2.66	8.20 \pm 1.37	1.95
12F/39d	23.40 \pm 1.95	8.20 \pm 0.68	2.85
14F/39d	25.00 \pm 1.79	-	-
18F/39d	26.30 \pm 1.46	-	-
30F/39d	36.40 \pm 1.21	8.20 \pm 0.27	4.44
6F/18d	14.56 \pm 2.43	8.20 \pm 1.37	1.78
14F/18d	17.93 \pm 1.28	-	-

Table 6.23: Iso-effect ED/50 doses (Gy) and RBE for a FI>72% (effect level F – early damage) in kidney function after X-rays and neutron (Robins et al., 1991).

Iso-effect ED/50 doses (Gy) and RBE (\pm SE) for a FI<30% (effect level NF) in kidney function after X-rays and neutron			
Fraction	X-rays	Neutrons	RBE
1F	8.8 \pm 8.8	7.50 \pm 7.50	1.17
6F/39d	20.29 \pm 3.38	10.20 \pm 1.70	1.99
12F/39d	27.60 \pm 2.30	9.20 \pm 0.77	3.00
14F/39d	30.00 \pm 2.14	-	-
18F/39d	37.60 \pm 2.09	-	-
30F/39d	43.10 \pm 1.44	9.20 \pm 0.31	4.69
6F/18d	18.57 \pm 3.10	10.20 \pm 1.70	1.82
14F/18d	17.93 \pm 1.28	10.20 \pm 0.85	-

Table 6.24: Iso-effect ED/50 doses (Gy) and RBE for a FI<30% (effect level NF – late damage) in kidney function after X-rays and neutron (Robins et al., 1991).

6.1.8.5. RBE comparisons for early and late reacting tissues as predicted when considering $RBE_{min}=1$ and $RBE_{min}\neq 1$

In Sections 6.1.8.1 to 6.1.8.4, we have compared the actual and the predicted RBEs for tissue-specific early and late reactions. In this section, the comparison will be made between the different predicted RBE curves for early and late reacting normal tissues. In particular, skin, which is usually considered an early reacting normal tissue with (α/β) between 9-12 Gy (Joiner *et al.*, 2002), and lung and kidney, both considered late reacting tissues with (α/β) between 1-5 Gy. The impact of the introduction of the RBE_{min} concept into the RBE formulation and the consequence it has in calculating limiting doses beyond which the therapeutic potential of neutrons becomes adverse (i.e. $RBE_{late} > RBE_{early}$) to the treatment will be quantified and commented in Section 6.4.

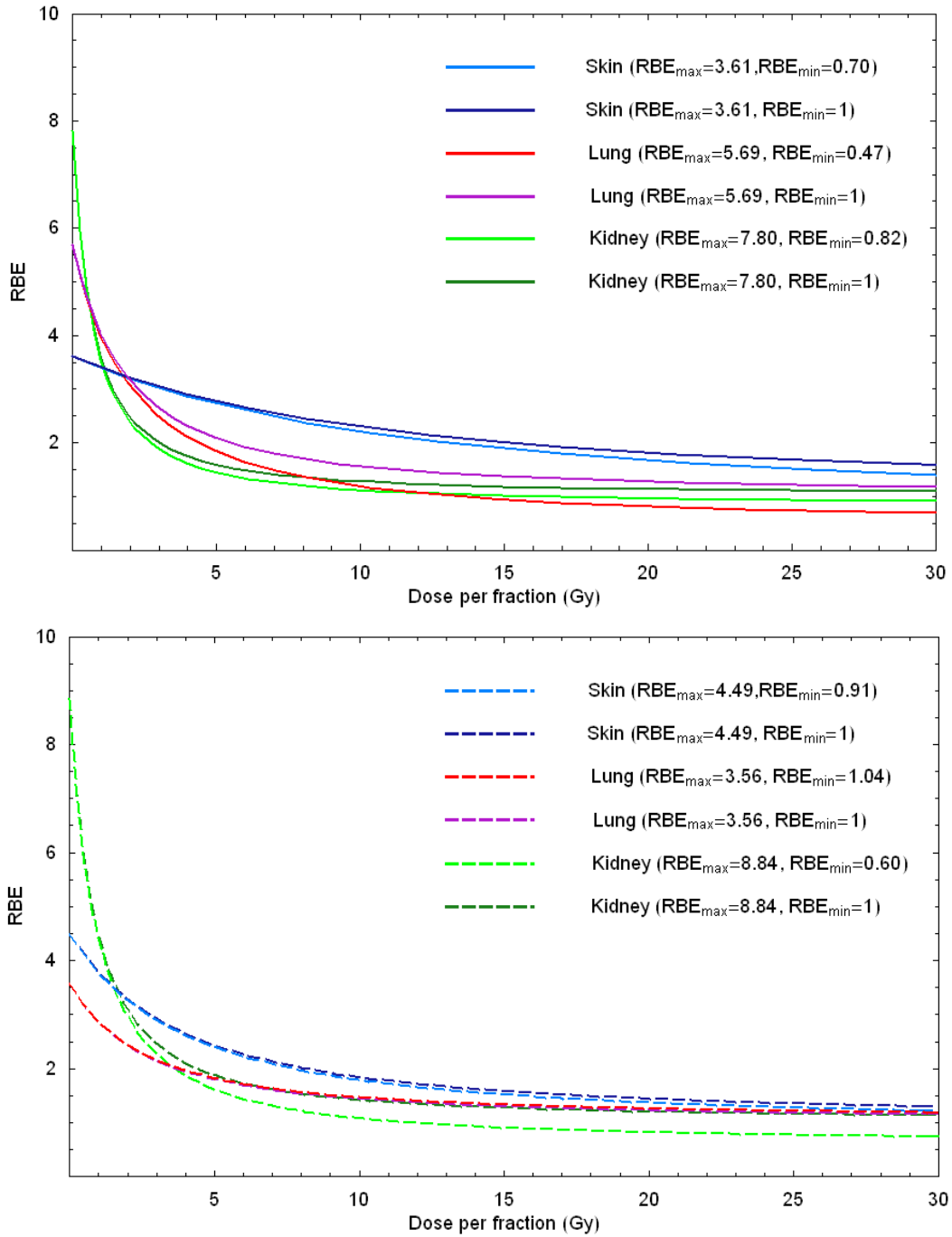


Figure 6.20: Top: comparison of the early reactions of skin, lung and kidneys when considering $RBE_{min}=1$ and $RBE_{min}\neq 1$. Bottom: comparison of the late reactions of skin, lung and kidneys when considering $RBE_{min}=1$ and $RBE_{min}\neq 1$.

6.1.9. Renal damage in mice

- *System used:* Kidneys of female CBA/Ht GyfBSVS mice (Stewart *et al.*, 1984).

- *Laboratory conditions and Methodology of experiments:* Kidneys were irradiated with either 240 kVp X-rays or 3MeV neutrons via a 17×13 mm field which included both kidneys. The characteristics of the X-ray beam was: dose rate of 1.7 Gy/min with a target to skin distance of 20 cm and the HVL was 1.3 mm Cu. The neutron beam, with average energy was 3MeV (maximum of 8.4 MeV), were produced from the Gray Laboratory Van der Graaft accelerator by bombarding a thick beryllium target with 4MeV deuterons. The field size used with neutrons was of 20×12 mm and the source to skin distance was 42.7 cm with a dose rate of 0.35 Gy/min. The gamma contamination of the beam was found to be 12.2%. The irradiations with both beams were performed with the mice being unanaesthetized and on fractionated schedules of 1, 2, 4 and 8 fractions delivered over 18±1 days.

- *Radiobiological end point:*
 - *Hematocrit assay:* The level of hematocrit observed in normal unirradiated mice was of 49±0.5%. Damage to the kidney resulted in a reduced haematocrit in the first 22 weeks after irradiation, which presumably reflects loss of the juxtaglomerular cells which are responsible for production of erythropoietin. The total doses required to produce a 40% reduction in hematocrit in each of the fractionation schemes was used to calculate RBE values of early kidney damage.
 - *Isotope clearance:* The clearance of Ethylene-diamide-tetra-acetate (EDTA) is a measure of the efficiency of glomerular filtration. The dose required to produce a 3% retention of 10μCi ⁵¹Cr EDTA from blood 28 weeks after irradiation was used to measure RBE values of late kidney damage

Figures corresponding to a haematocrit reduction to 40% in kidney at 22 weeks after irradiation with X-rays and neutrons (early damage):

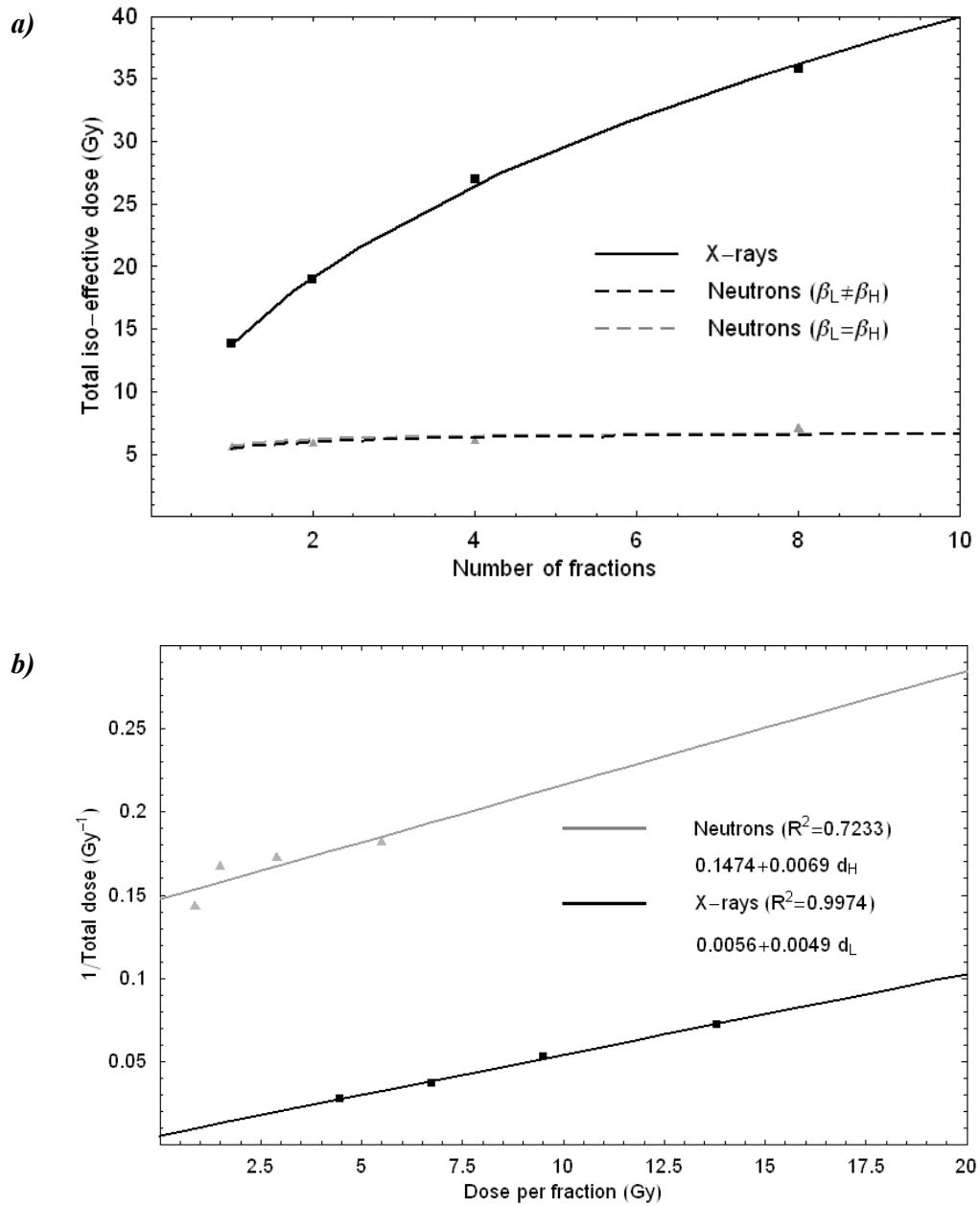


Figure 6.21: (a) Total iso-effective dose required to produce a haematocrit reduction to 40% in kidney after 22 weeks using different fractionation schemes of X-rays and neutrons; (b) corresponding Fe plot.

Figures corresponding to EDTA clearance of 3% retention in kidney at 28 weeks after irradiation with X-rays and neutrons (late damage):

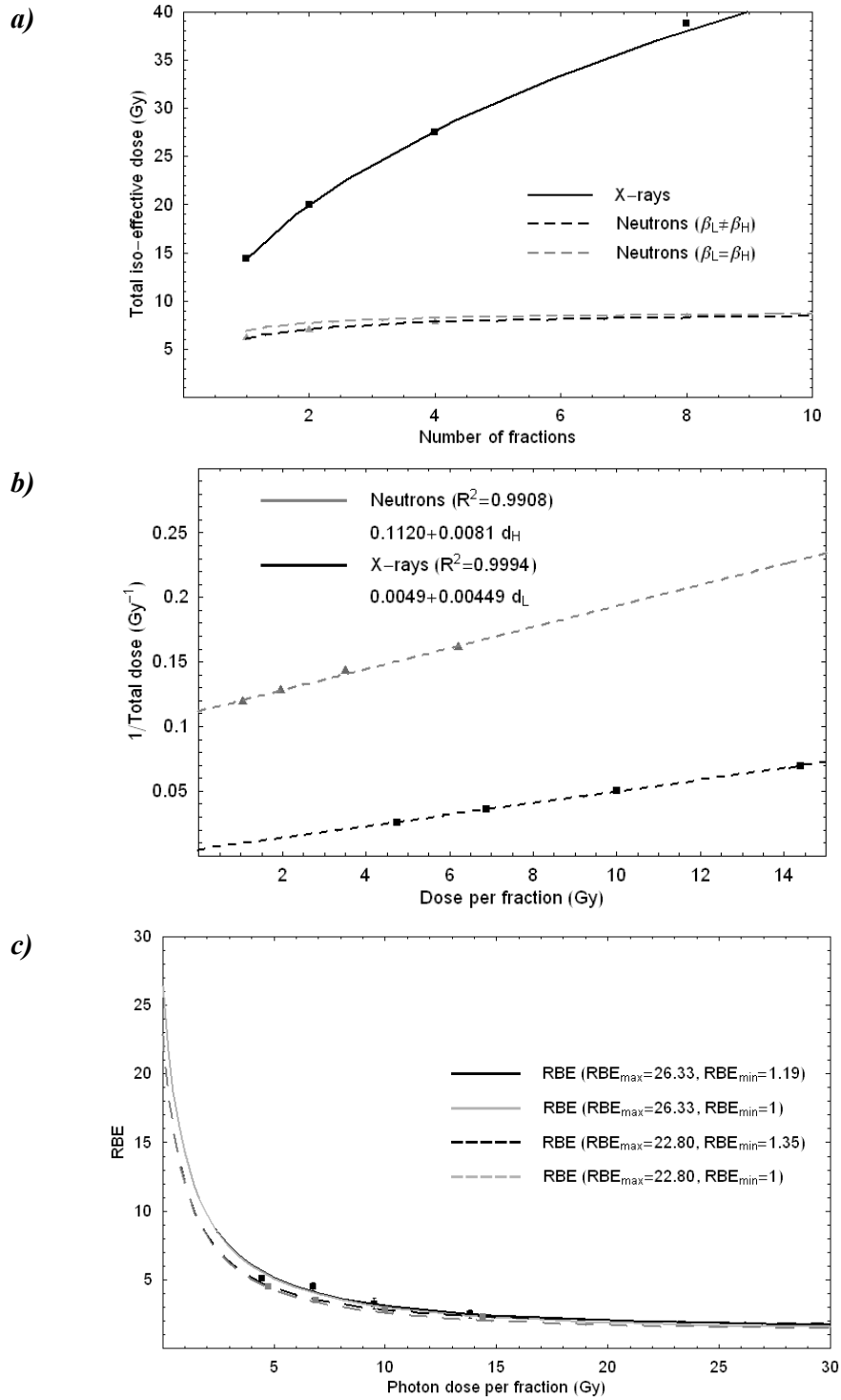


Figure 6.22: (a) Total iso-effective dose corresponding to EDTA clearance of 3% retention in kidney after 28 weeks using different fractionation schemes of X-rays and neutrons; (b) Corresponding Fe-plot; (c) RBE for early and late damages, where squares correspond to early reaction data and triangles to late reaction data.

Data points:

Total iso-effect doses (Gy) and RBE (\pm SE) for haematocrit reduction to a 40% in kidney at 22 weeks after X-rays and neutron			
Fraction	X-rays	Neutrons	RBE
1F	13.8	5.5	2.5 \pm 0.3
2F	19.0	5.8	2.3 \pm 0.1
4F	27.0	6.0	3.3 \pm 0.4
8F	35.8	7.0	5.1 \pm 0.2
Total iso-effect doses (Gy) and RBE (\pm SE) for EDTA clearance of 3% retention in kidney at 28 weeks after X-rays and neutron			
Fraction	X-rays	Neutrons	RBE
1F	14.4	6.2	2.3 \pm 0.4
2F	20.0	7.0	2.9 \pm 0.1
4F	27.5	7.8	3.5 \pm 0.1
8F	38.0	8.4	4.5 \pm 0.1

Table 6.25: Total iso-effect doses (Gy) and RBE for early and late damage in kidney function after X-rays and neutron (Stewart et al., 1984).

6.1.10. Colo-rectal injury in mice

- *System used:* Male CBA/HtGyfBSVS mice (Terry *et al.*, 1984).

- *Laboratory conditions and Methodology of experiments:* 8 to 14 unanesthetized mice per dose group were irradiated with ^{137}Cs γ -rays or 3MeV neutrons to obtain dose-response curves. Doses were administered in 1, 2, 5 or 10 fractions in intervals of 8-24h from irradiation to produce the same end point with γ -rays and neutrons. The ^{137}Cs γ -rays were generated by a double headed ^{137}Cs unit with a dose rate of 3.8Gy/min. The neutron beam was generated with a Van der Graaff accelerator by the reaction of 4MeV deuteron colliding into a thick beryllium target, at a dose rate of 0.41 Gy/min. The mean energy of the neutron beam spectrum was 3MeV with a maximum energy of 8.4MeV. For both types of radiations, mice were restrained using a jig located 8.5cm to the ^{137}Cs source and 51.5cm to the neutron source. In the case of the neutron, the mice were positioned vertically with their heads down in order to allow the small intestine to fall out of the beam. The γ contamination of the beam was 9.3-9.4%. 22 \pm 1mm of descending colon, rectum and anus were included within the 50% isodose region for both γ rays and neutrons.

- *Radiobiological end point:*
 - o *Faecal deformity.* The quality and quantity of faeces produced several months after pelvic irradiation varied with radiation dose. The proportion of pellets \leq 4.5mm long for each individual mouse showed to have the strongest dependence on dose. Pellets were collected after 24h periods and the means and standard deviations of the collected proportions were calculated for each dose group.
 - o *Body weight.* The mean weight of animals in each dose group was 33 \pm 1g (1 SEM). The weight lost shortly after irradiation and the maximum body weight attained were both studied as a function of radiation dose.
 - o *Lethality.* The proportion of surviving animals was assessed sequentially at monthly intervals up to 16 months after irradiation. LD/50 values and confidence limits were calculated by logit analysis.

Figures corresponding to nadir of body weight (5g level) after irradiation with γ -rays and neutrons (early end point):

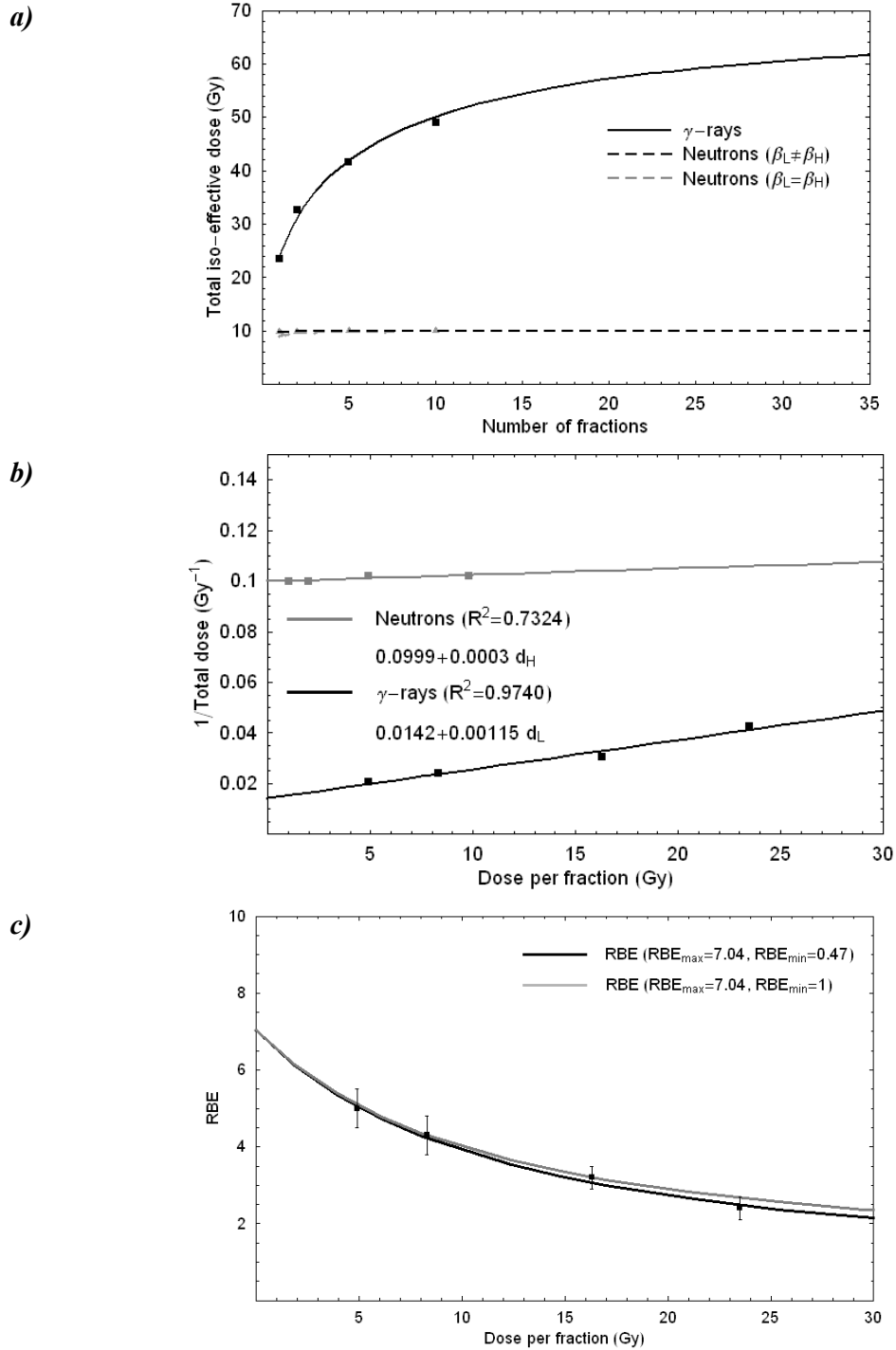


Figure 6.23: (a) Total iso-effective dose required to produce a loss of 5g (nadir of body weight at 11 to 17 days after start of treatment) using different fractionation schemes; (b) corresponding Fe plot to nadir weight level; (c) corresponding RBE curve.

Figures corresponding to peak of body weight (35g) after irradiation with γ -rays and neutrons (early damage):

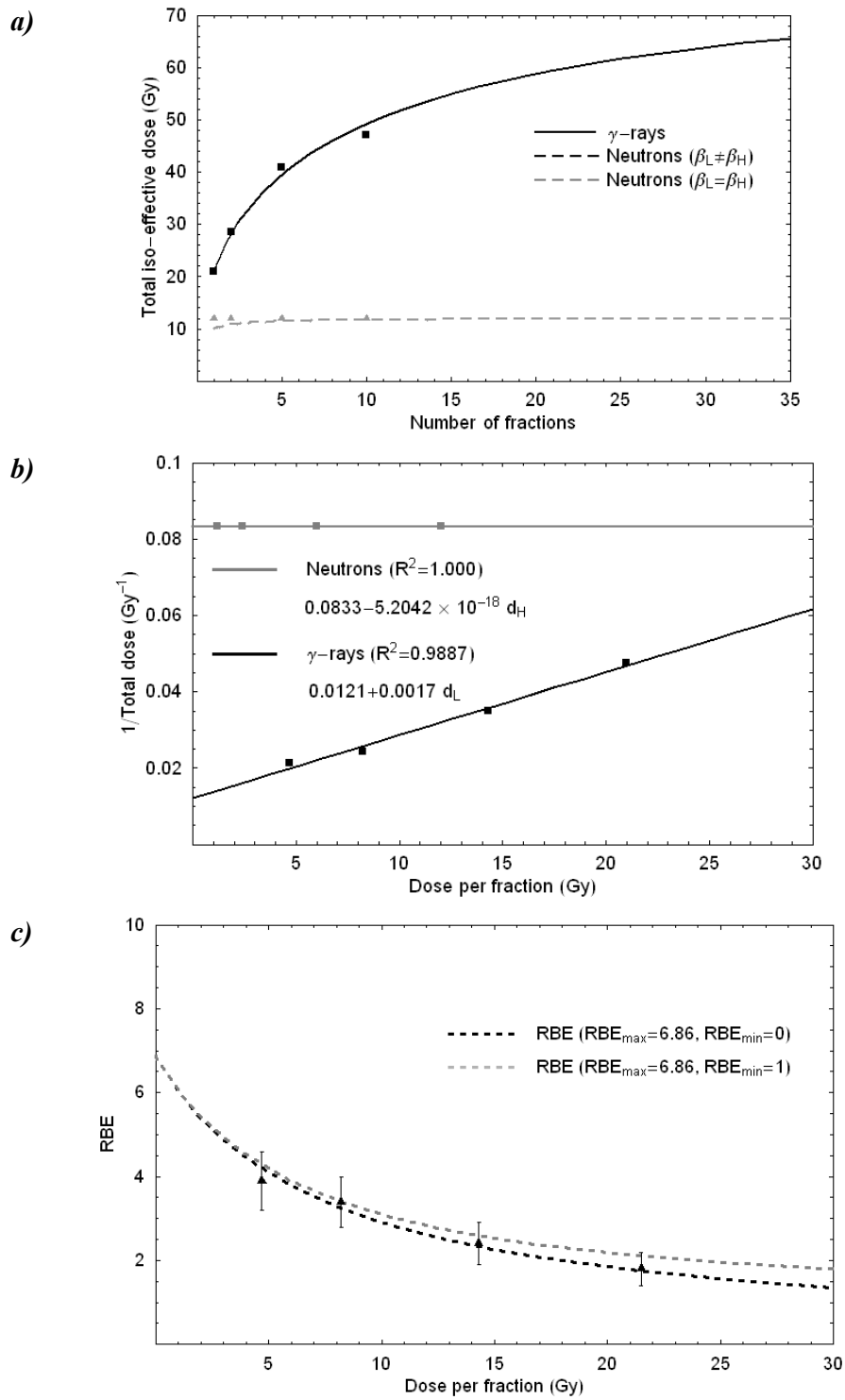


Figure 6.24: (a) Total iso-effective dose required to produce a maximum of 35g (peak of body weight at 4-7 months after start treatment) using different fractionation schemes; (b) corresponding Fe plot to peak of body weight; (c) corresponding RBE curves.

Figures corresponding to the proportion of short faeces ($\leq 4.5\text{mm}$ long) excreted after irradiation with γ -rays and neutrons (early damage):

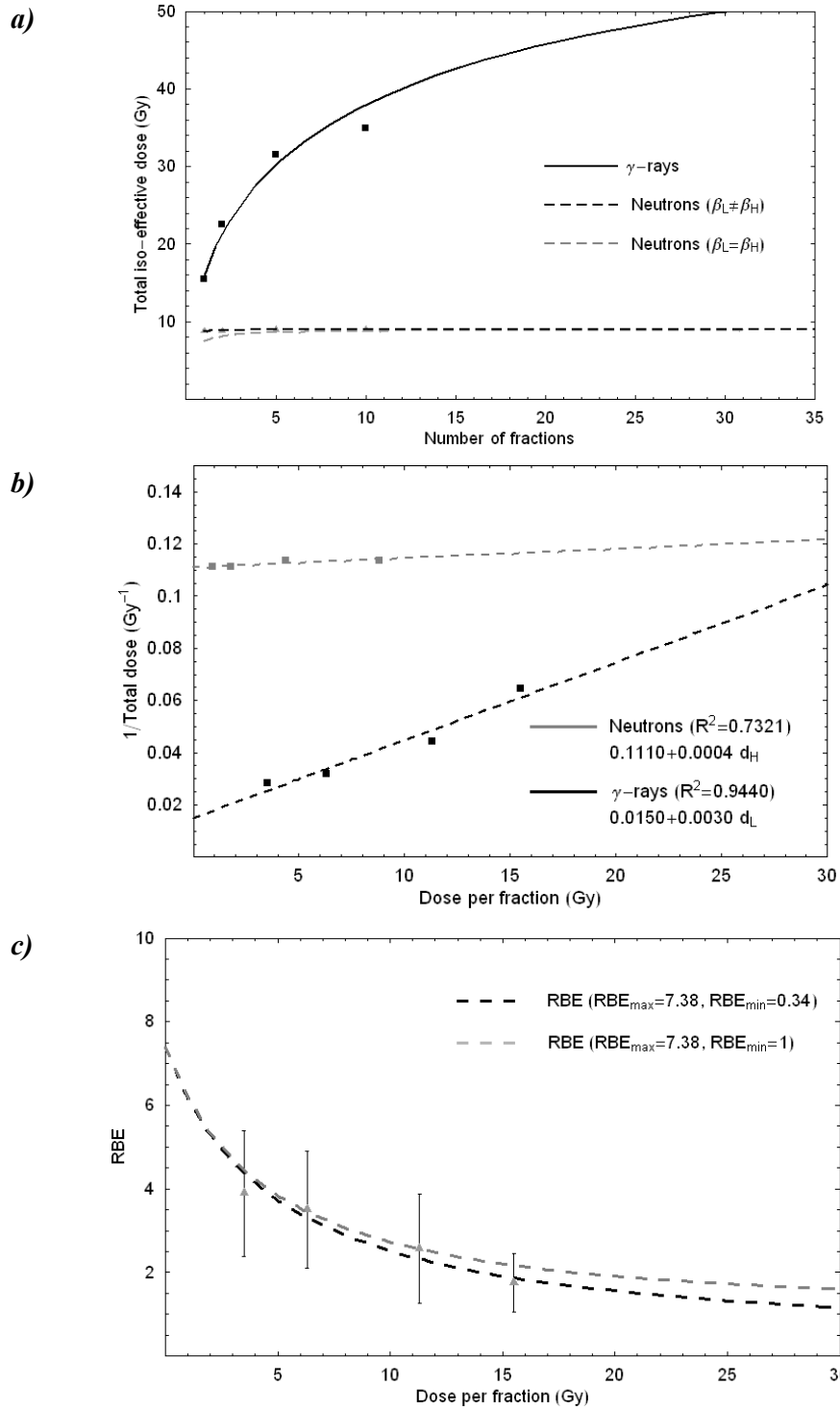


Figure 6.25: (a) Total iso-effective dose corresponding to the proportion of short faeces ($\leq 4.5\text{mm}$ long) excreted over a 24h period, measured at 4 times using different fractionation schemes; (b) corresponding Fe plot to proportion of short faeces; (c) RBE curves for short faeces.

Data points:

Total iso-effect doses (Gy) and RBE (\pm SE) for nadir body weight after γ -rays and neutron (11-17 days after start treatment)			
Fraction	X-rays	Neutrons	RBE
1F	23.5	9.8	2.4 (0.3)
2F	16.3	4.9	3.2 (0.3)
5F	8.3	2.0	4.3 (0.5)
10F	4.9	1.0	5.0 (0.5)
Total iso-effect doses (Gy) and RBE (\pm SE) for peak body weight after γ -rays and neutron (4-7 months after start treatment)			
Fraction	X-rays	Neutrons	RBE
1F	21.0	12.0	1.8 (0.4)
2F	14.3	6.0	2.4 (0.5)
5F	8.2	2.4	3.4 (0.6)
10F	4.7	1.2	3.9 (0.7)
Total iso-effect doses (Gy) and RBE (\pm SE) short faeces after γ -rays and neutron (12 months after start treatment)			
Fraction	X-rays	Neutrons	RBE
1F	15.5	8.8	1.8 (0.7)
2F	11.3	4.4	2.6 (1.3)
5F	6.3	1.8	3.6 (1.4)
10F	3.5	0.9	4.0 (1.5)

Table 6.26: Total iso-effect doses (Gy) and RBE for different early and late damages related to colorectal damage after γ -rays and neutron (Terry et al., 1984).

Figures corresponding to LD/50 at 2 months after irradiation with γ -rays and neutrons (early end point):

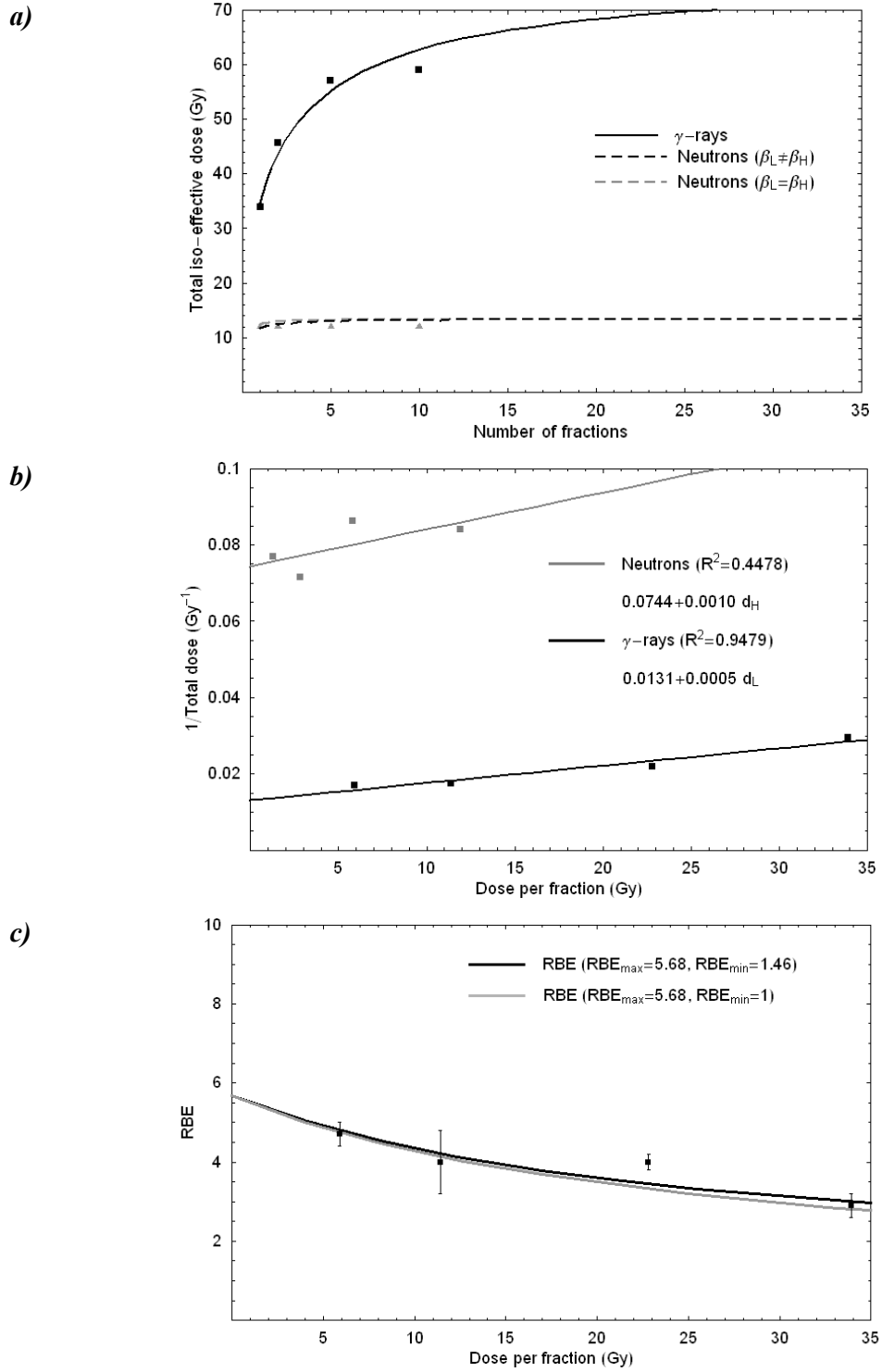


Figure 6.26: (a) Total iso-effective dose required to produce LD/50 at 2 months after the start of treatment using different fractionation schemes; (b) corresponding Fe plot to nadir weight level; (c) RBE curves for LD/50.

Figures corresponding to produce LD/50 at 12 months after irradiation with γ -rays and neutrons (late damage):

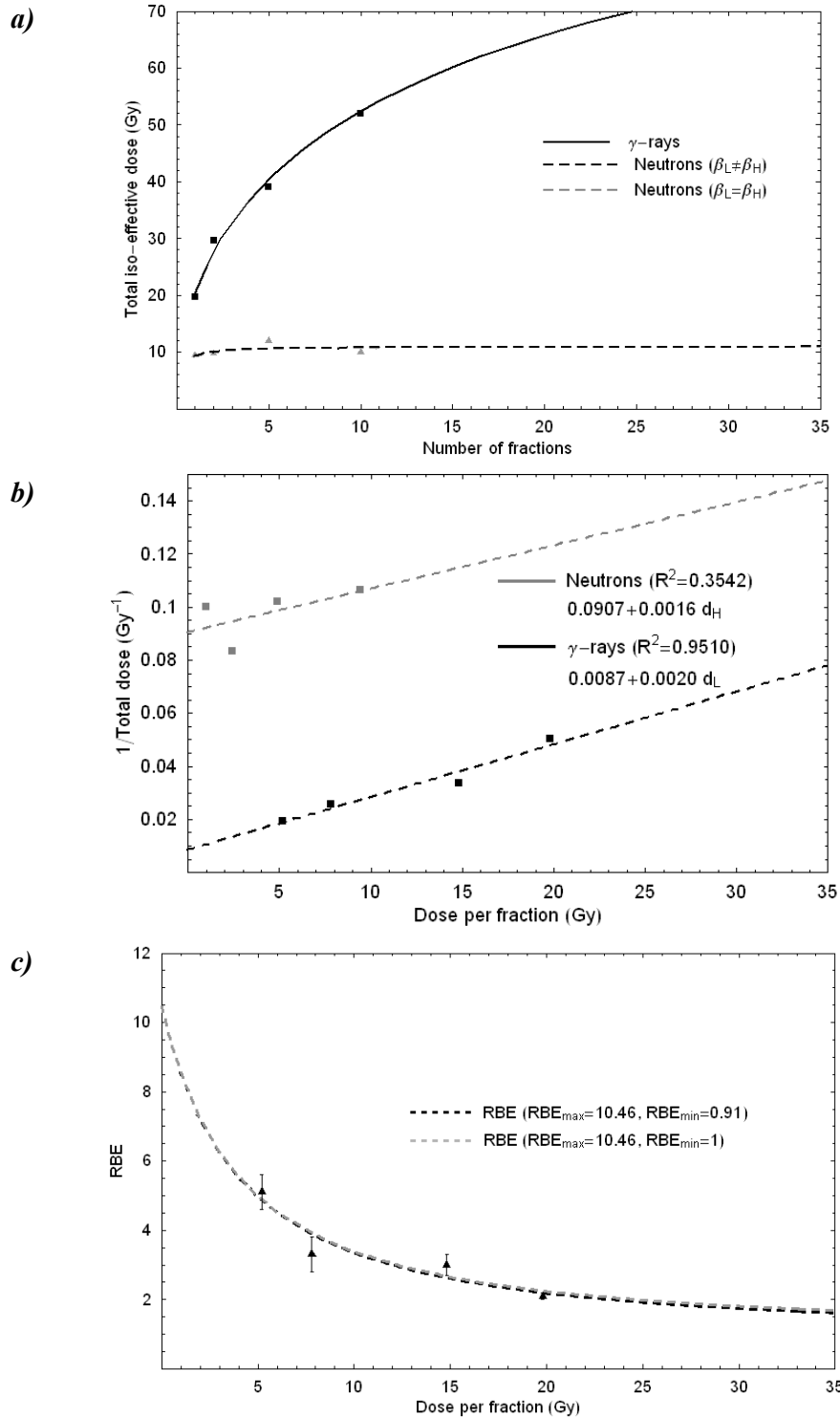


Figure 6.27: (a) Total iso-effective dose required to LD/50 after 12 months after treatment using different fractionation schemes; (b) corresponding Fe plot to peak of body weight; (c) RBE curves for LD/50 after 12 months after treatment.

Figures corresponding LD/50 at 15 months after irradiation with γ -rays and neutrons (late damage):

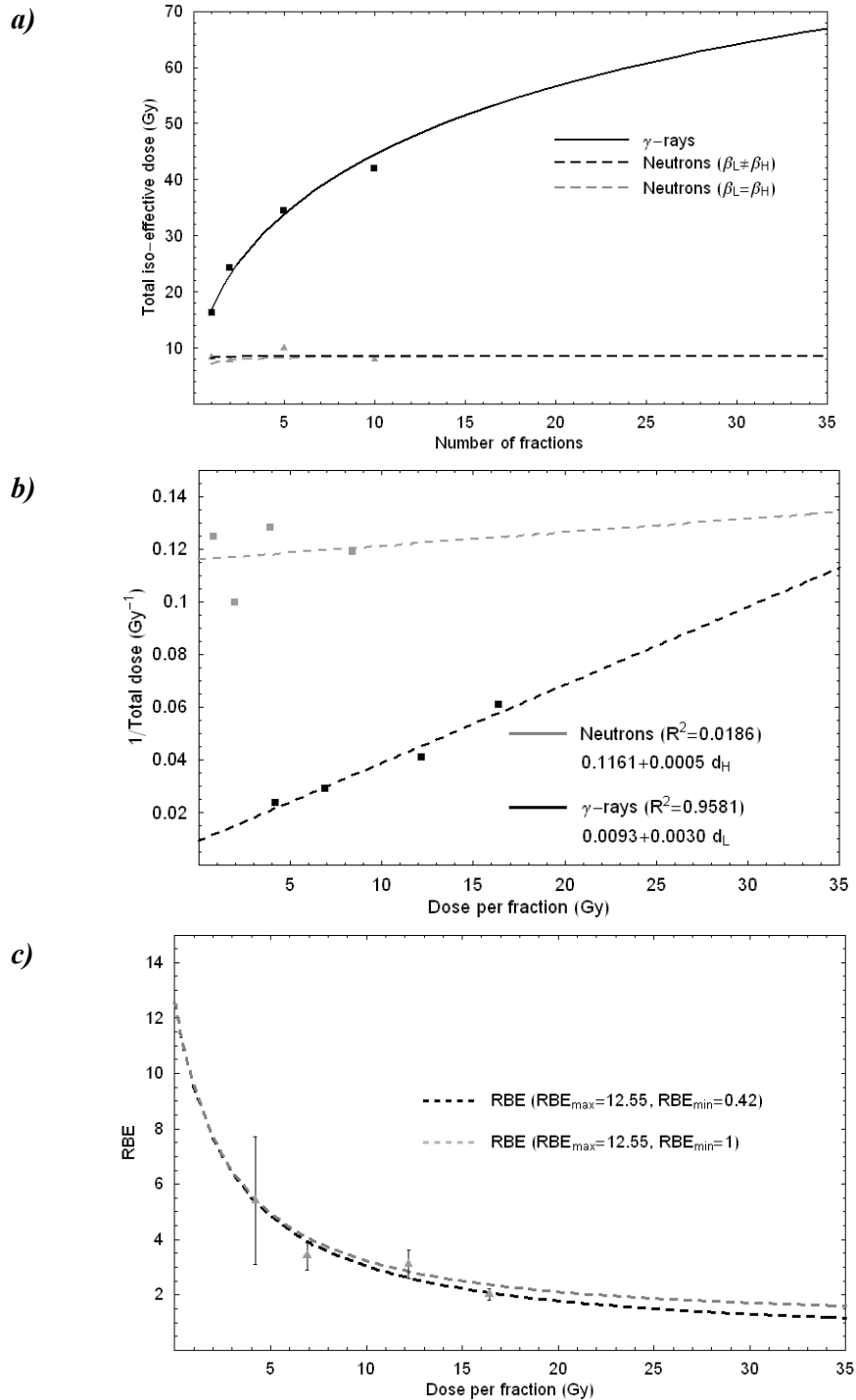


Figure 6.28: (a) Total iso-effective dose corresponding to the proportion of short faeces ($\leq 4.5\text{mm}$ long) excreted over a 24h period, measured at 4 times using different fractionation schemes; (b) corresponding Fe plot to proportion of short faeces; (c) RBE curves for LD/50 after 15 months after start of treatment.

Data points:

Total iso-effect doses (Gy) and RBE (\pm SE) for LD/50 at 2 months after γ -rays and neutron (early reaction effect)			
Fraction	X-rays	Neutrons	RBE
1F	33.9	11.9	2.9 (0.3)
2F	22.8	5.8	4.0 (0.2)
5F	11.4	2.8	4.0 (0.8)
10F	5.9	1.3	4.7 (0.3)
Total iso-effect doses (Gy) and RBE (\pm SE) for LD/50 at 12 months after γ -rays and neutron (late reaction effect)			
Fraction	X-rays	Neutrons	RBE
1F	19.8	9.4	2.1 (0.1)
2F	14.8	4.9	3.0 (0.3)
5F	7.8	2.4	3.3 (0.5)
10F	5.2	1.0	5.1 (0.5)
Total iso-effect doses (Gy) and RBE (\pm SE) for LD/50 at 15 months after γ -rays and neutron (late reaction effect)			
Fraction	X-rays	Neutrons	RBE
1F	16.4	8.4	2.0 (0.2)
2F	12.2	3.9	3.1 (0.5)
5F	6.9	2.0	3.4 (0.5)
10F	4.2	0.8	5.4 (2.3)

Table 6.27: Total iso-effect doses (Gy) and RBE for different early and late damages related to colorectal damage after γ -rays and neutron (Terry et al., 1984).

6.1.10.1. RBE curve comparisons between early and late effects for each type of end points

In this section we are comparing the different predicted RBE curves for early and late reaction effects. In particular, the comparison is made between early changes in body weight (early reaction effects) and proportion of faeces pellets produced 12 months after the start of treatment (late reaction effect). Similarly, the comparison is made between the RBE curves obtained for early lethal effects (2 months) and late lethal effects (12 and 15 months). The impact of the introduction of the RBE_{\min} concept into the RBE formulation and the consequence it has in calculating limiting doses beyond which the therapeutic value of neutrons become adverse (i.e. $RBE_{\text{late}} > RBE_{\text{early}}$) to the treatment will be quantified and commented in Section 6.4.

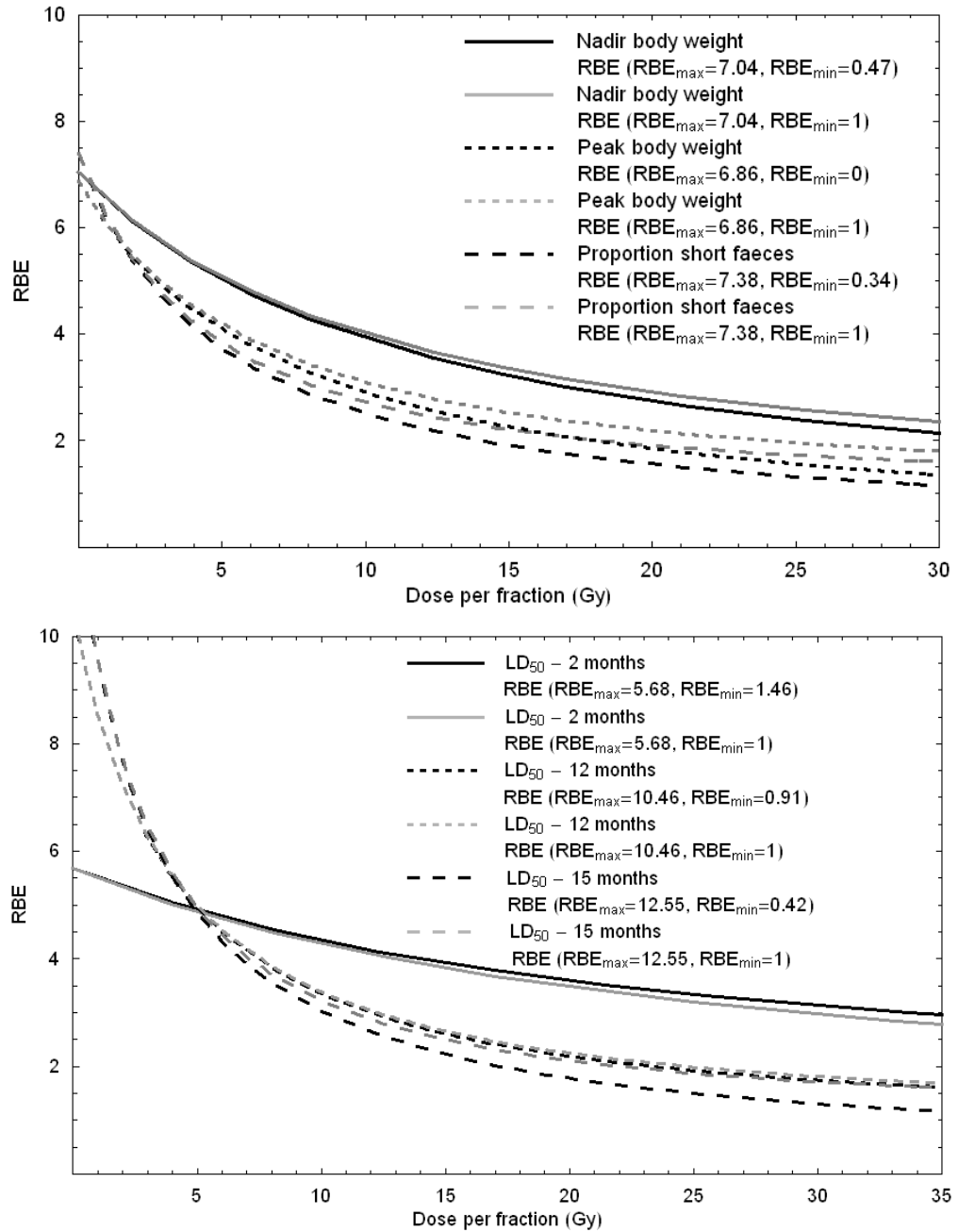


Figure 6.29: Comparison of RBE curves for early and late reaction levels. Top - nadir and peak body weight (early reaction points) are plotted with RBE for short faeces. Bottom - LD/50 at 2 months after treatment is compared with LD/50 at 12 and 15 months after the start of treatment.

6.2. Heavier Ion data

6.2.1. Skin reactions on mouse legs

- *System used:* C3H/HeMsNrsf female mice aged 12-18 week-old (Ando *et al.*, 1998).
- *Laboratory conditions and Methodology of experiments:* Hairs on the mouse right hind leg were removed by applying a depilatory agent 7-8 days before the first irradiation. Animals were anaesthetised with 50mg per kg of pentobarbital and then exposed to a 28×100mm field size of Cs-137 γ -rays or carbon-ions. The reference beam consisted of Cs-137 γ -rays with a dose rate of 1.6 Gy/min at an FSD of 21 cm. The interfractional interval used was 24±1h and the LET of the Cs beam was considered 1 keV/ μ m. In the case of the carbon-12 ions, they were produced in the HIMAC facility using a synchrotron of 290 MeV/u. The dose rate used was 3Gy/min, and the LET of the carbon ion beam was calculated at different depths, as shown in the following figure:

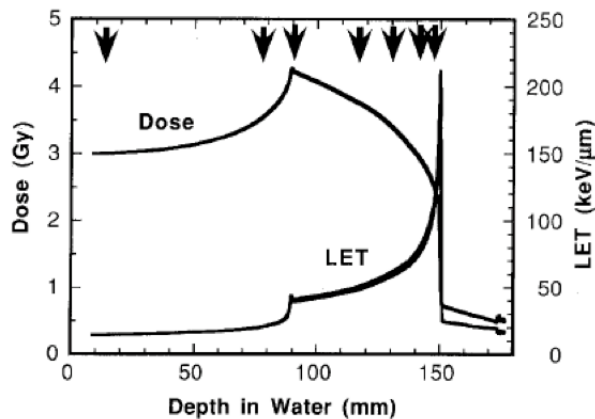


Figure 6.30: positions at which measurements of doses were carried out

As shown in Figure 6.30, the LET at each of these positions was different, with values of 14keV/ μ m at the shallowest position and 100keV/ μ m at the deepest.

- *Radiobiological end point:* Skin reaction data was collected from day 7 after irradiation and up to day 35. The data was fitted with a polynomial function using least square method and the doses producing a peak reaction of 3.0 were calculated.

- Figures corresponding to $LET=14\text{ keV}/\mu\text{m}$ at 1.5cm deep:

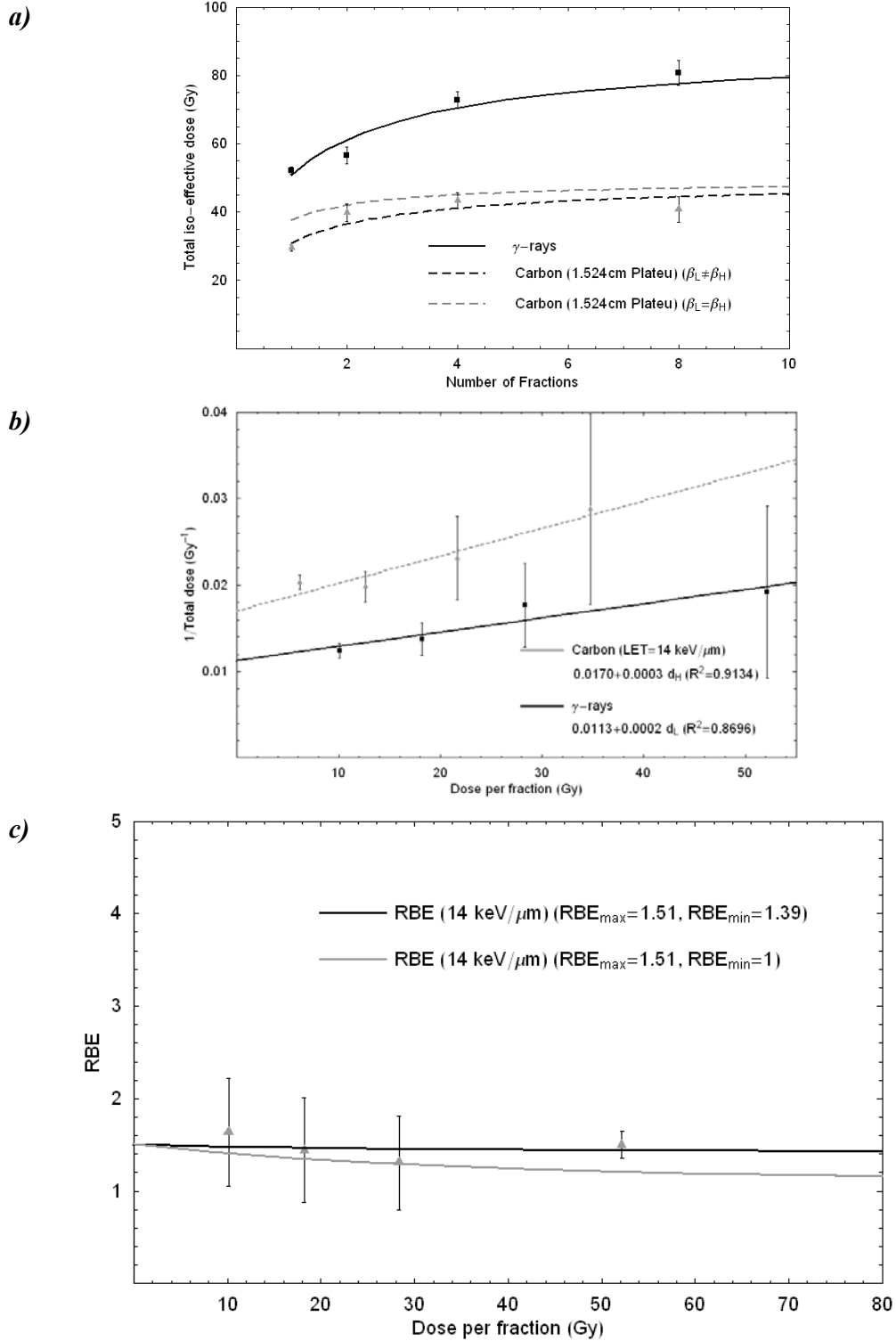


Figure 6.31: (a) Total dose required with different fractionation regimes to produce the same average skin reaction 3.0 with γ -rays and 14 keV/ μm ions; (b) Fe plot; (c) RBE curve for mice skin exposed to X-rays and carbon ions.

- Figures corresponding to $LET=20\text{ keV}/\mu\text{m}$ at 8cm deep:

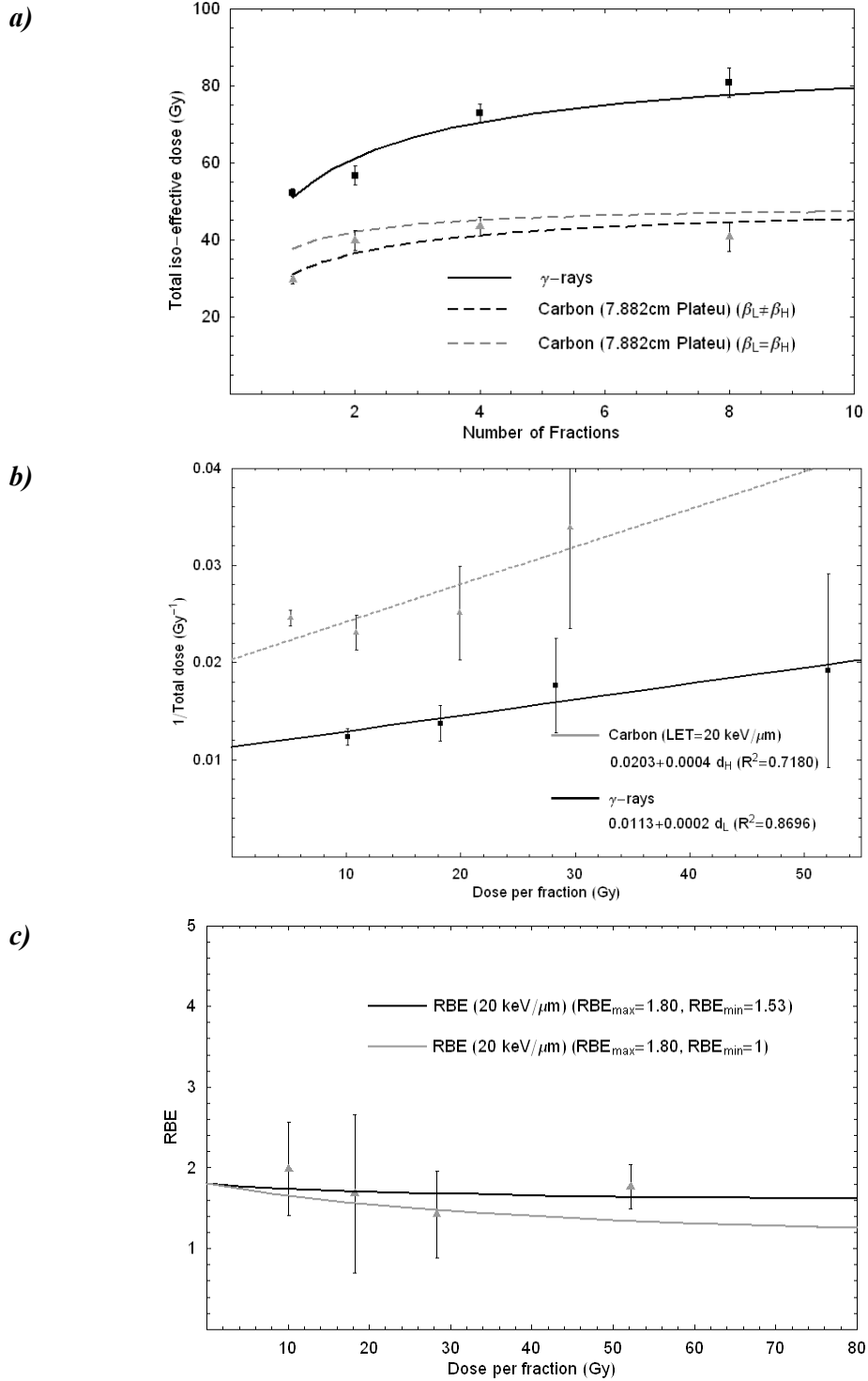
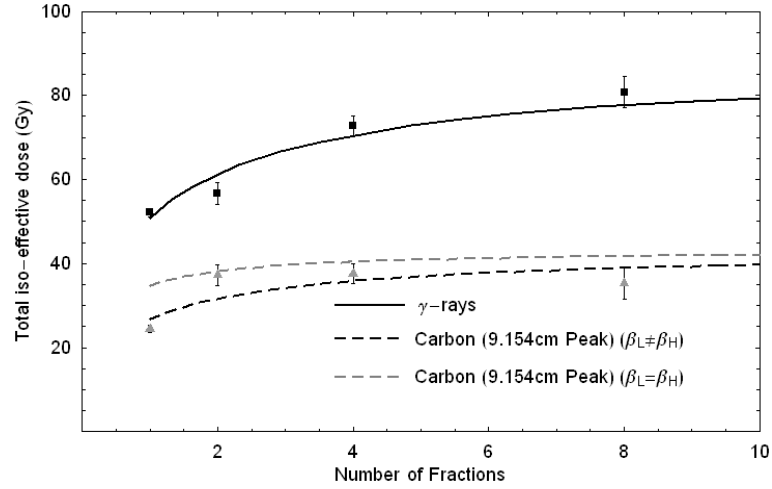


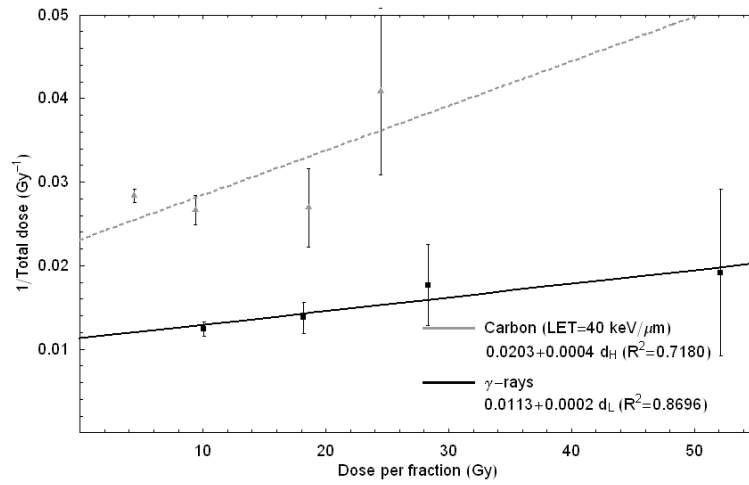
Figure 6.32: (a) Total dose required with different fractionation regimes to produce the same average skin reaction 3.0 with γ -rays and 20 keV/ μm ions; (b) Fe plot; (c) RBE curve for mice skin exposed to X-rays and carbon ions.

- Figures corresponding to $LET=40\text{ keV}/\mu\text{m}$ at 9cm deep:

a)



b)



c)

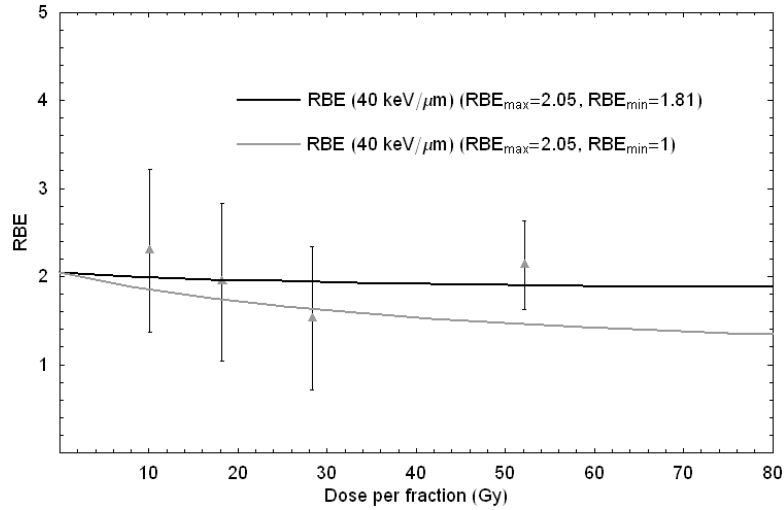


Figure 6.33: (a) Total dose required with different fractionation regimes to produce the same average skin reaction 3.0 with γ -rays and 40 keV/ μm ions; (b) Fe plot; (c) RBE curve for mice skin exposed to X-rays and carbon ions.

- Figures corresponding to $LET=50\text{ keV}/\mu\text{m}$ at 12cm deep:

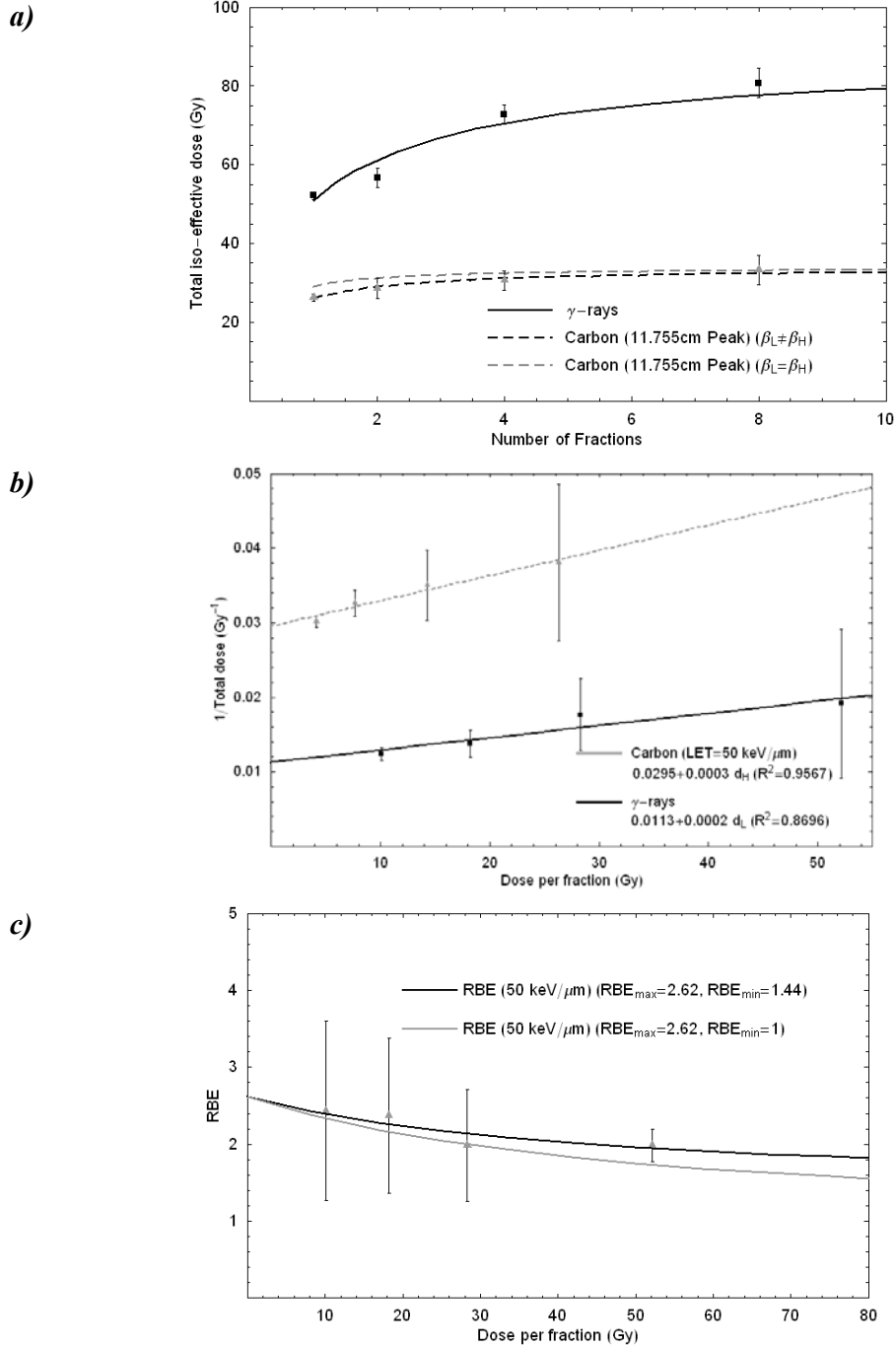
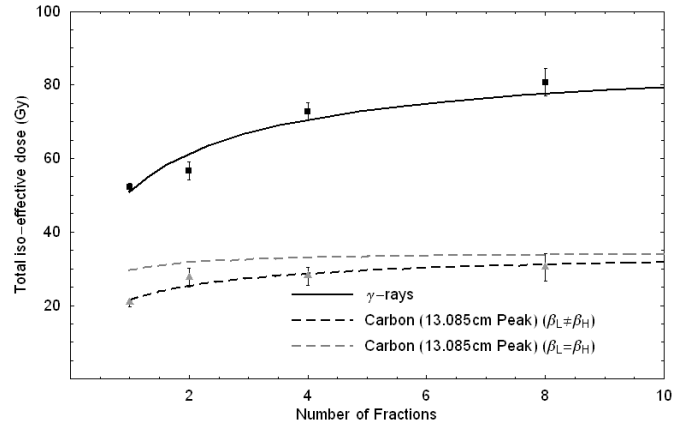


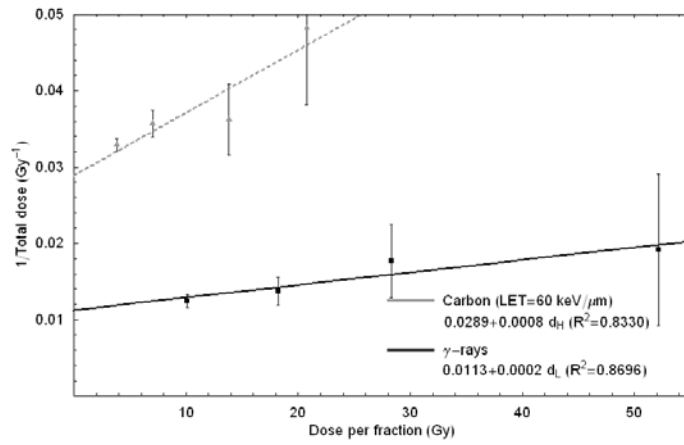
Figure 6.34: (a) Total dose required with different fractionation regimes to produce the same average skin reaction 3.0 with γ -rays and 50 keV/ μm ions; (b) Fe plot; (c) RBE curve for mice skin exposed to X-rays and carbon ions.

- Figures corresponding to LET=60 keV/ μ m at 13cm deep:

a)



b)



c)

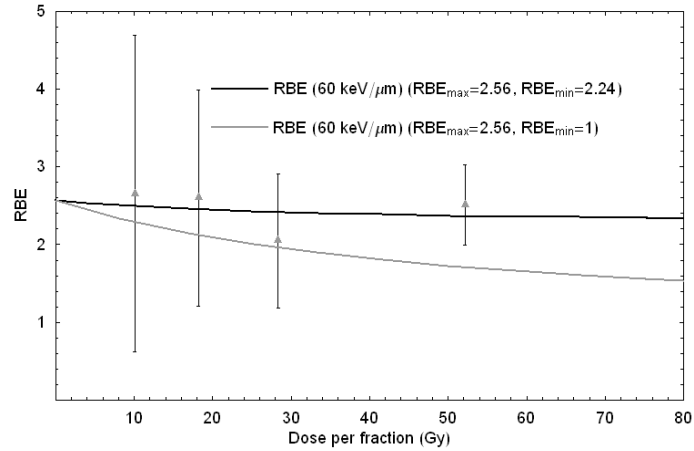


Figure 6.35: (a) Total dose required with different fractionation regimes to produce the same average skin reaction 3.0 with γ -rays and 60 keV/ μ m ions; (b) Fe plot; (c) RBE curve for mice skin exposed to X-rays and carbon ions.

- Figures corresponding to $LET=80\text{ keV}/\mu\text{m}$ at 14cm deep:

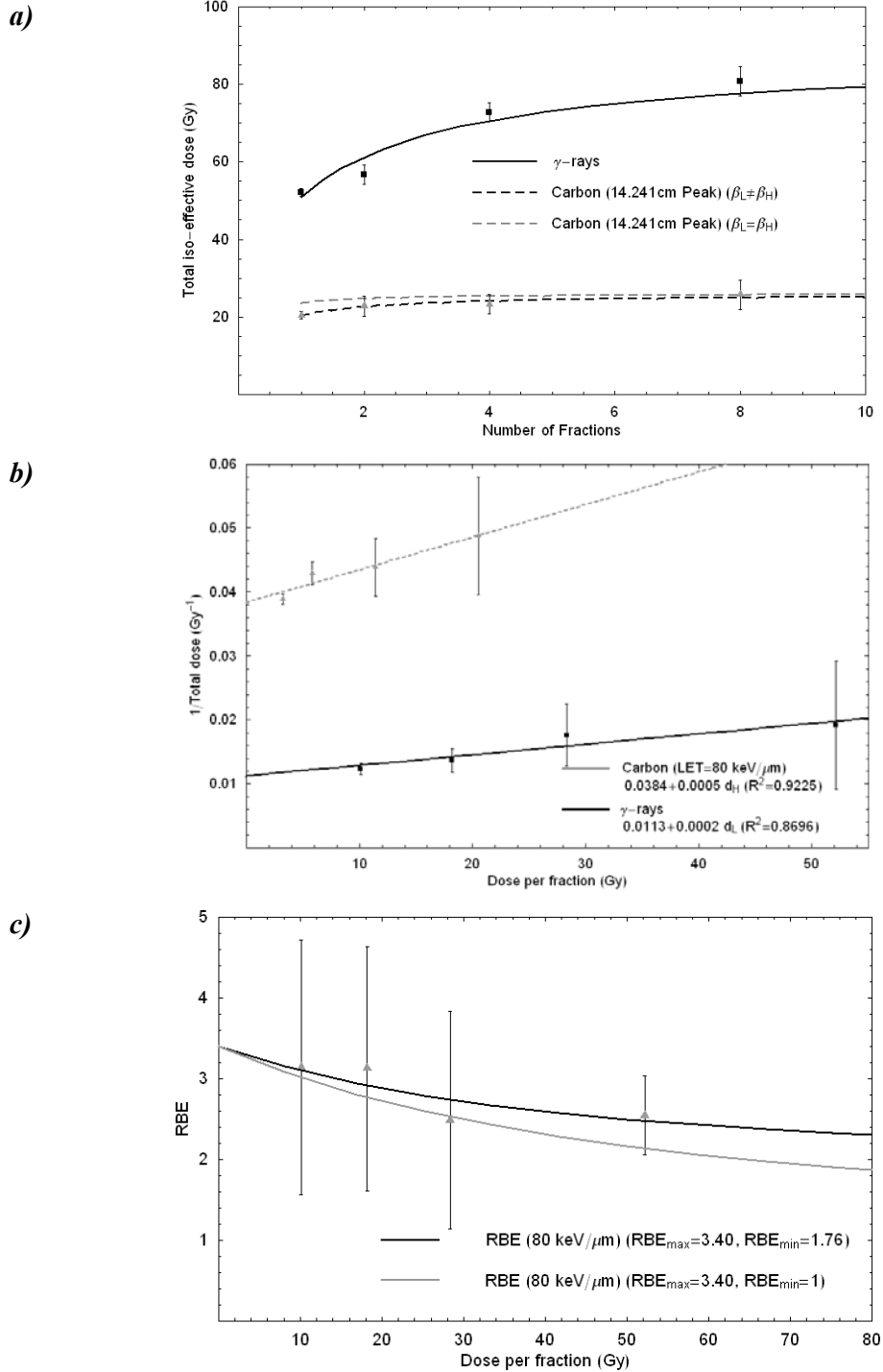


Figure 6.36: (a) Total dose required with different fractionation regimes to produce the same average skin reaction 3.0 with γ -rays and $80\text{ keV}/\mu\text{m}$ ions; (b) Fe plot; (c) RBE curve for mice skin exposed to X-rays and carbon ions.

- Figures corresponding to $LET=100\text{ keV}/\mu\text{m}$ at 15cm deep:

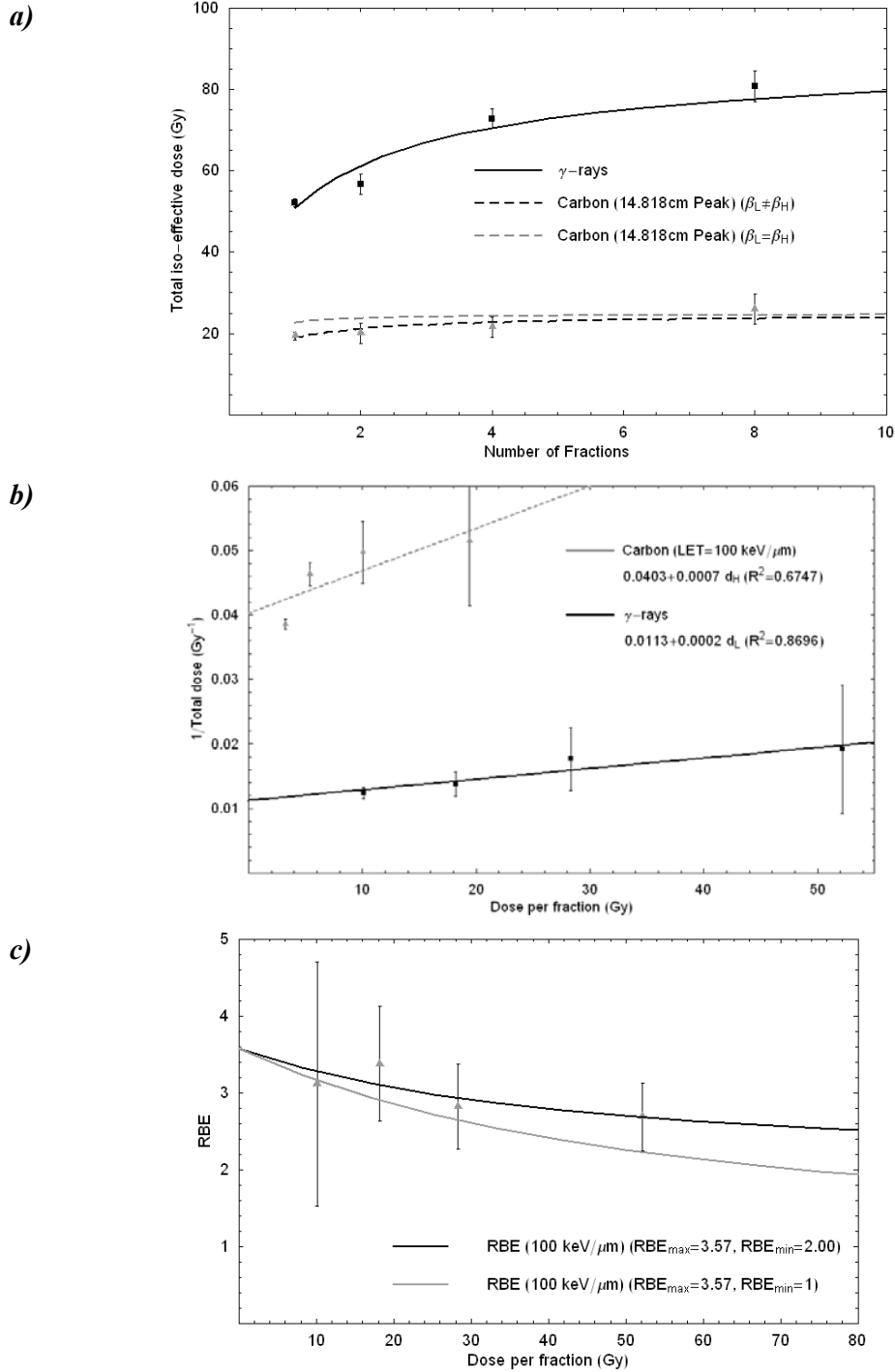


Figure 6.37: (a) Total dose required with different fractionation regimes to produce the same average skin reaction 3.0 with γ -rays and $100\text{ keV}/\mu\text{m}$ ions; (b) Fe plot; (c) RBE curve for mice skin exposed to X-rays and carbon ions.

Data points:

Fractions	γ -rays	Carbon	RBE	LET
1F	52.15 (53.18-51.21)	34.76 (38.25-31.38)	1.50±0.14	14keV/ μ m
2F	56.64 (59.16-54.11)	43.33 (45.87-40.90)	1.31±0.51	
4F	72.8 (75.23-70.37)	50.53 (52.70-48.41)	1.44±0.57	
8F	80.75 (84.39-76.92)	49.31 (52.54-46.14)	1.64±0.58	
1F	-	29.55 (31.34-27.77)	1.76±0.55	20keV/ μ m
2F	-	39.8 (42.08-37.38)	1.42±0.54	
4F	-	43.37 (44.55-42.08)	1.68±0.99	
8F	-	40.69 (43.96-37.48)	1.98±0.58	
1F	-	24.47(25.42-23.45)	2.13±0.5	40keV/ μ m
2F	-	37.16 (38.66-35.55)	1.52±0.81	
4F	-	37.57 (38.86-36.14)	1.94±0.90	
8F	-	35.23 (37.24-33.18)	2.29±0.92	
1F	-	26.29 (28.68-23.94)	1.98±0.21	50keV/ μ m
2F	-	28.53(30.27- 26.78)	1.99±0.72	
4F	-	30.67 (31.86-29.44)	2.37±1.00	
8F	-	33.17 (34.76-31.55)	2.43±1.16	
1F	-	20.76 (21.72-19.82)	2.51±0.52	60keV/ μ m
2F	-	27.62 (29.12-26.19)	2.05±0.88	
4F	-	28.02 (28.86-27.11)	2.60±1.39	
8F	-	30.41 (31.34-29.50)	2.66±2.03	
1F	-	20.51 (21,52-19.49)	2.54±0.49	80keV/ μ m
2F	-	22.81 (23.76-21.88)	2.48±1.34	
4F	-	23.31 (24.11-22.50)	3.12±1.51	
8F	-	25.72 (26.92-24.55)	3.14±1.58	
1F	-	19.42 (20.51-18.29)	2.69±0.44	100keV/ μ m
2F	-	20.09 (22.37-17.84)	2.82±0.56	
4F	-	21.57 (23.17-19.93)	3.38±0.75	
8F	-	25.95 (27.12-24.77)	3.11±1.59	

Table 6.28: Data obtained from (Ando et al., 1998).

6.2.2. Tumour growth delay (TGD) versus skin reactions (ASR) on mouse legs

- *System used:* C3H/HeMsNrsf female mice aged 12-18 week-old (Ando *et al.*, 1998).
- *Laboratory conditions and Methodology of experiments:* Hairs on the mouse right hind leg were removed by applying a depilatory agent 7-8 days before the first irradiation. Animals were anaesthetised with 50mg per kg of pentobarbital and their legs exposed to a 28×100mm field of Cs-137 γ -rays or carbon-ions. The tumour was a syngeneic NFSa fibrosarcoma, in its 16 - 18th generation and was transplanted intramuscularly into the right hind legs of mice 7 days before the first irradiation. Tumour growth delay (TGD) for each dose group was determined by measuring the time (from the first day of irradiation) required for each tumour to become 5-times as large as the initial volume.

The reference beam consisted of Cs-137 γ -rays with a dose rate of 1.6 Gy/min at an FSD of 21 cm. The interfractional interval used was 24±1h and the LET of the Cs beam was considered 1 keV/ μ m.

In the case of the carbon-12 ions, they were produced in the HIMAC facility using a synchrotron of 290 MeV/u. The dose rate used was 3Gy/min, and the LET of the carbon ion beam was calculated at different depths, as shown in the following figure:

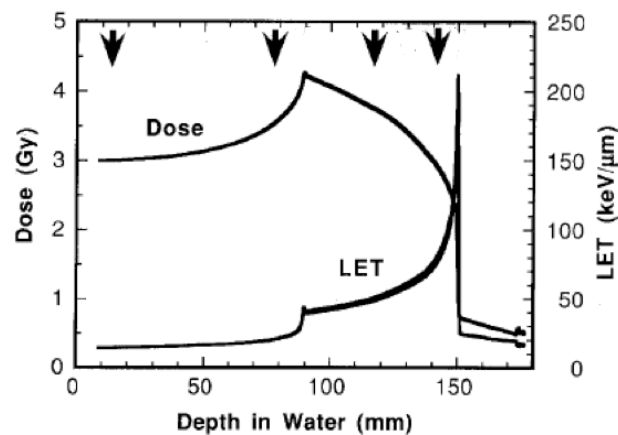


Figure 6.38: positions at which measurements of doses were carried out

As shown in Figure 6.30, the LET at each of these positions was different, with values of $14\text{keV}/\mu\text{m}$ at the shallowest position and $77\text{keV}/\mu\text{m}$ at the deepest.

- *Radiobiological end point:* Dose response curves were constructed by plotting either TGD time or the averaged peak reaction as a function of the irradiation dose for each scheme. Then, the doses required in each fractionation scheme to produce either a TGD time of 15 days or an average skin reaction (ASR) score of 3.0 were computed.

- Figures corresponding to $LET=14\text{ keV}/\mu\text{m}$ at 1.5cm deep for $ASR=3.0$:

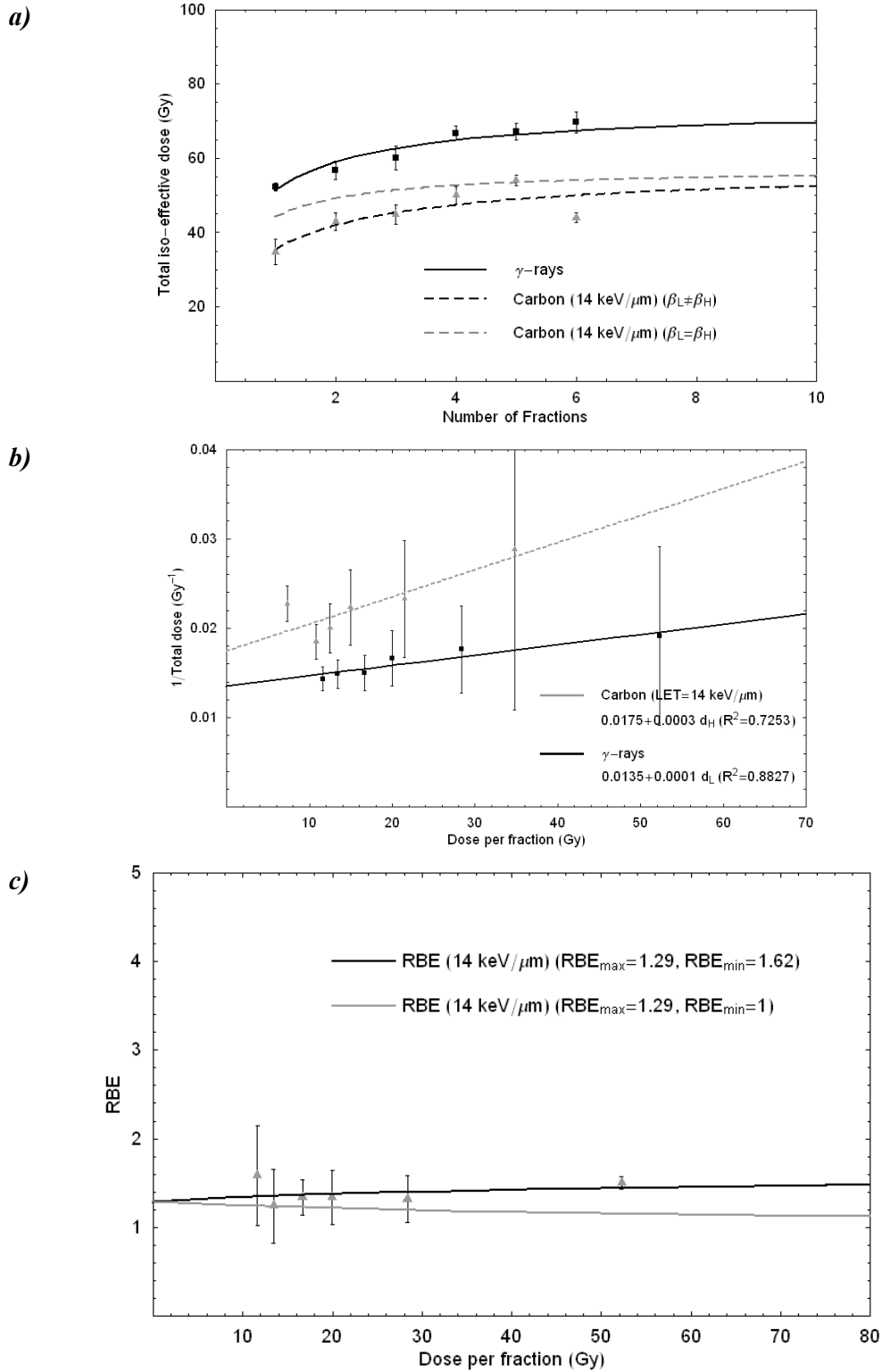
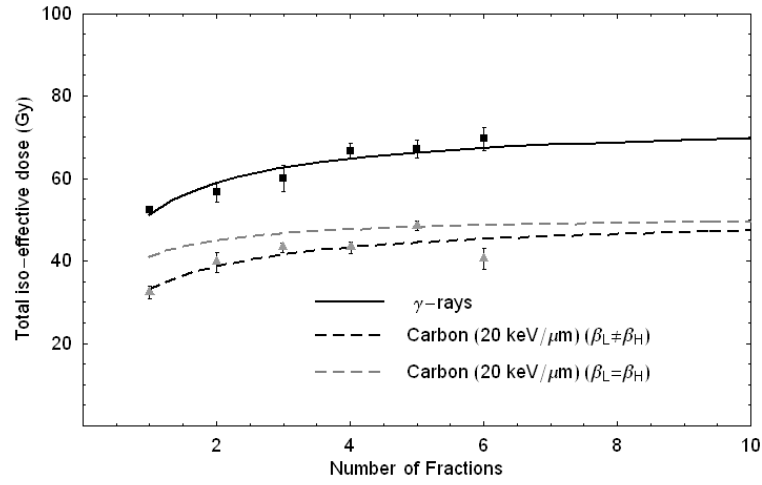


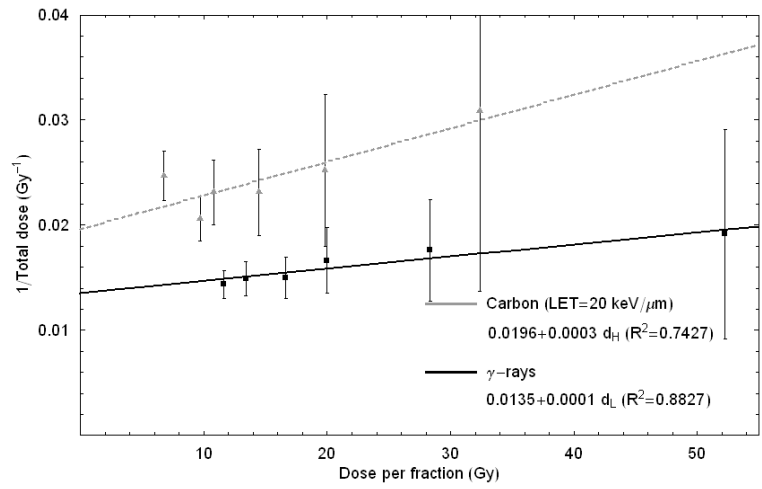
Figure 6.39: (a) Total dose required with different fractionation regimes to produce the same average skin reaction 3.0 with γ -rays and $14\text{ keV}/\mu\text{m}$ ions; (b) Fe plot; (c) RBE curve for mice skin exposed to X-rays and carbon ions.

- Figures corresponding to $LET=20\text{ keV}/\mu\text{m}$ at 8cm deep for $ASR=3.0$:

a)



b)



c)

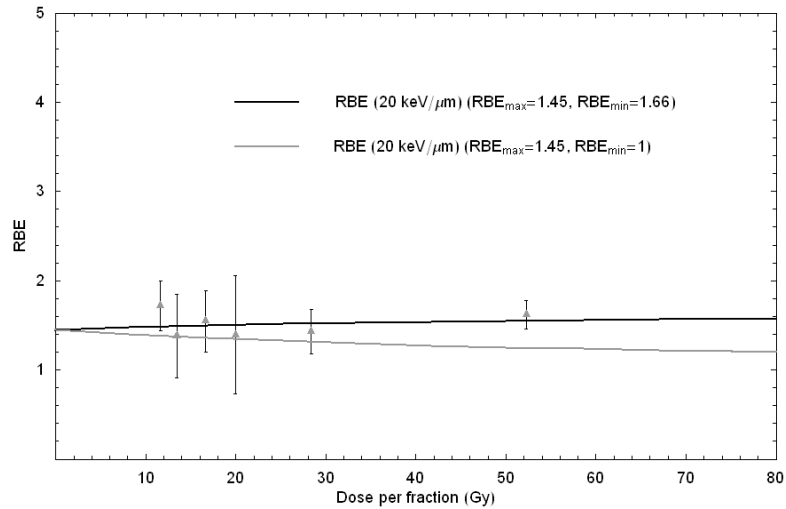
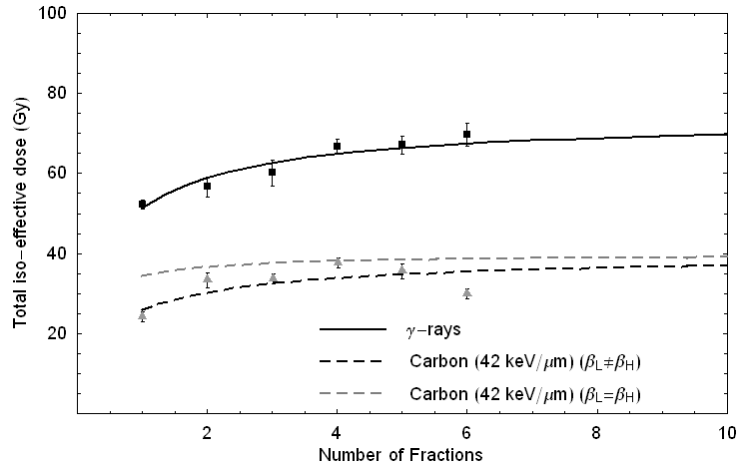


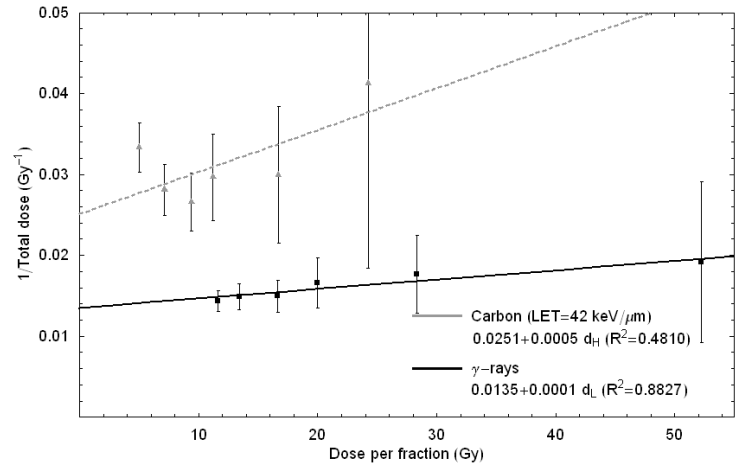
Figure 6.40: (a) Total dose required with different fractionation regimes to produce the same average skin reaction 3.0 with γ -rays and 20 keV/ μm ions; (b) Fe plot; (c) RBE curve for mice skin exposed to X-rays and carbon ions.

- Figures corresponding to $LET=42\text{ keV}/\mu\text{m}$ at 9cm deep for $ASR=3.0$:

a)



b)



c)

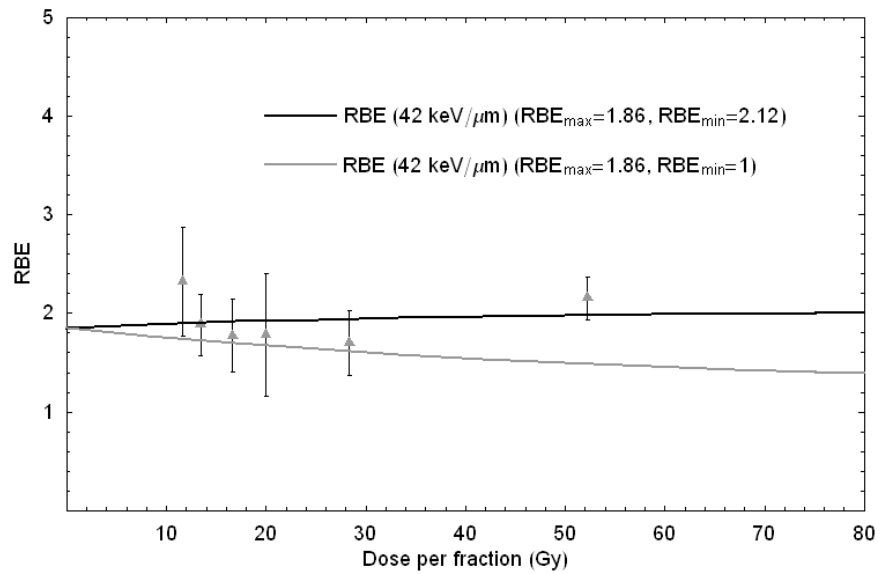
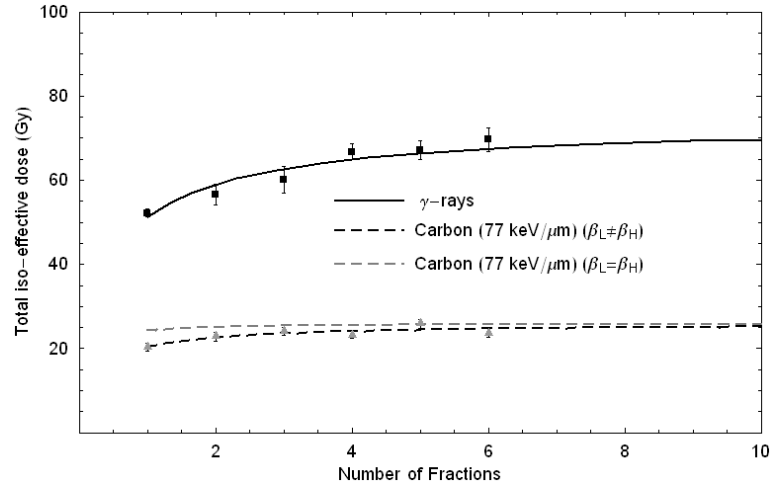


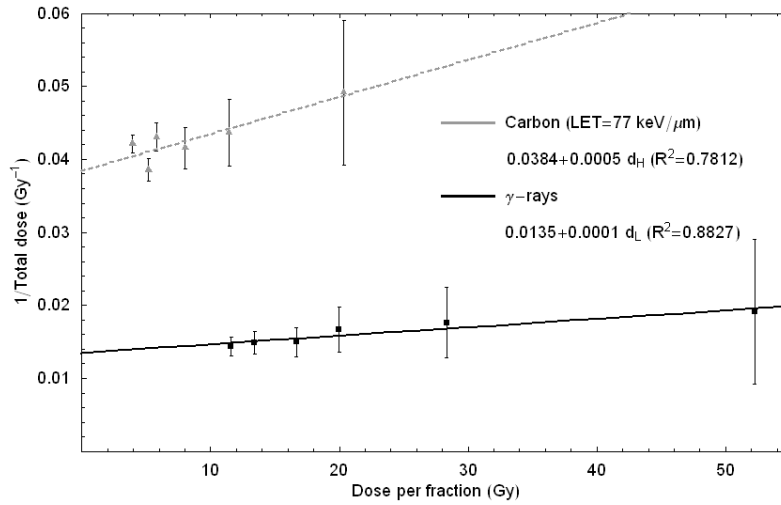
Figure 6.41: (a) Total dose required with different fractionation regimes to produce the same average skin reaction 3.0 with γ -rays and 40 keV/ μm ions; (b) Fe plot; (c) RBE curve for mice skin exposed to X-rays and carbon ions.

- Figures corresponding to $LET=77\text{ keV}/\mu\text{m}$ at 14cm deep for $ASR=3.0$:

a)



b)



c)

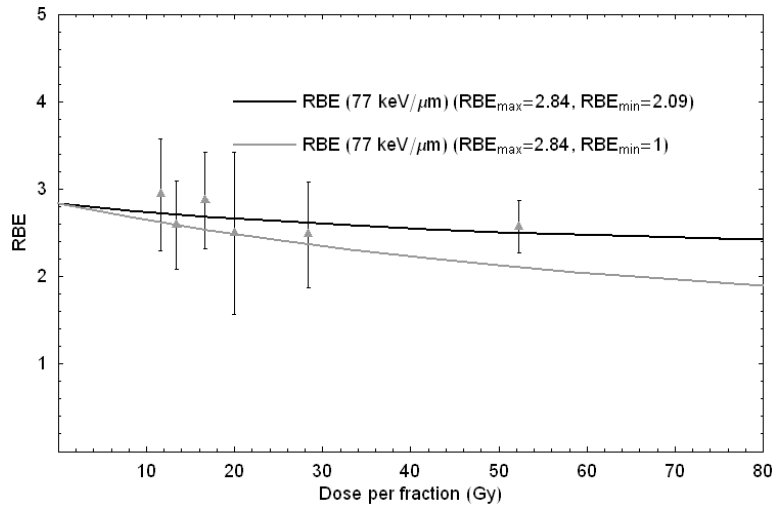


Figure 6.42: (a) Total dose required with different fractionation regimes to produce the same average skin reaction (of 3.0) with γ -rays and 80 keV/ μm ions; (b) Fe plot; (c) RBE curve for mice skin exposed to X-rays and carbon ions.

- Figures corresponding to $LET=14\text{ keV}/\mu\text{m}$ at 1.5cm deep for TGD time= 15days :

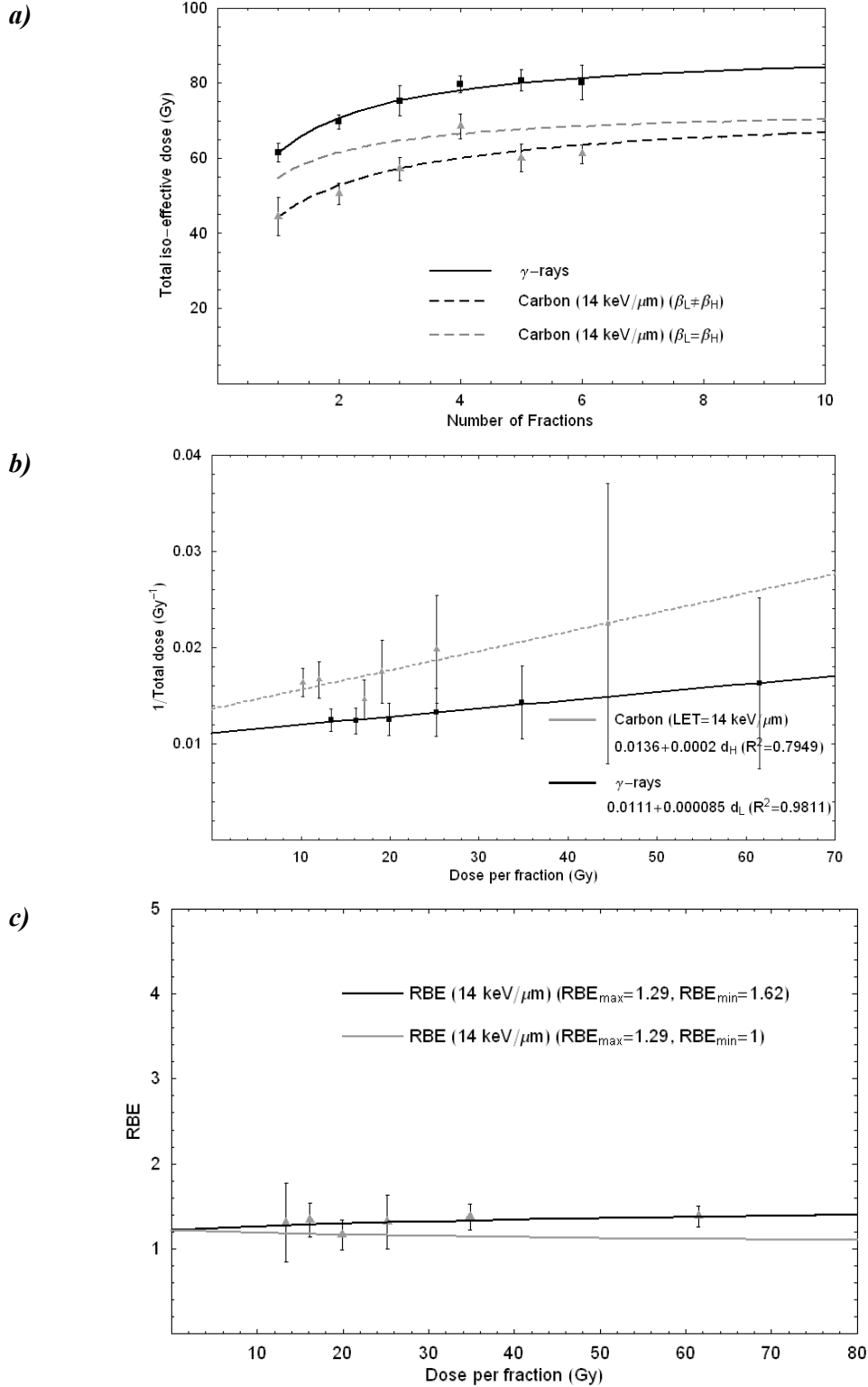


Figure 6.43: (a) Total dose required with different fractionation regimes to produce the same TGD time of 15 days with γ -rays and $14\text{ keV}/\mu\text{m}$ ions; (b) Fe plot; (c) RBE curve for TGD time =15 days after exposure to X-rays and carbon ions.

- Figures corresponding to $LET=20\text{ keV}/\mu\text{m}$ at 8cm deep for TGD time=15days:

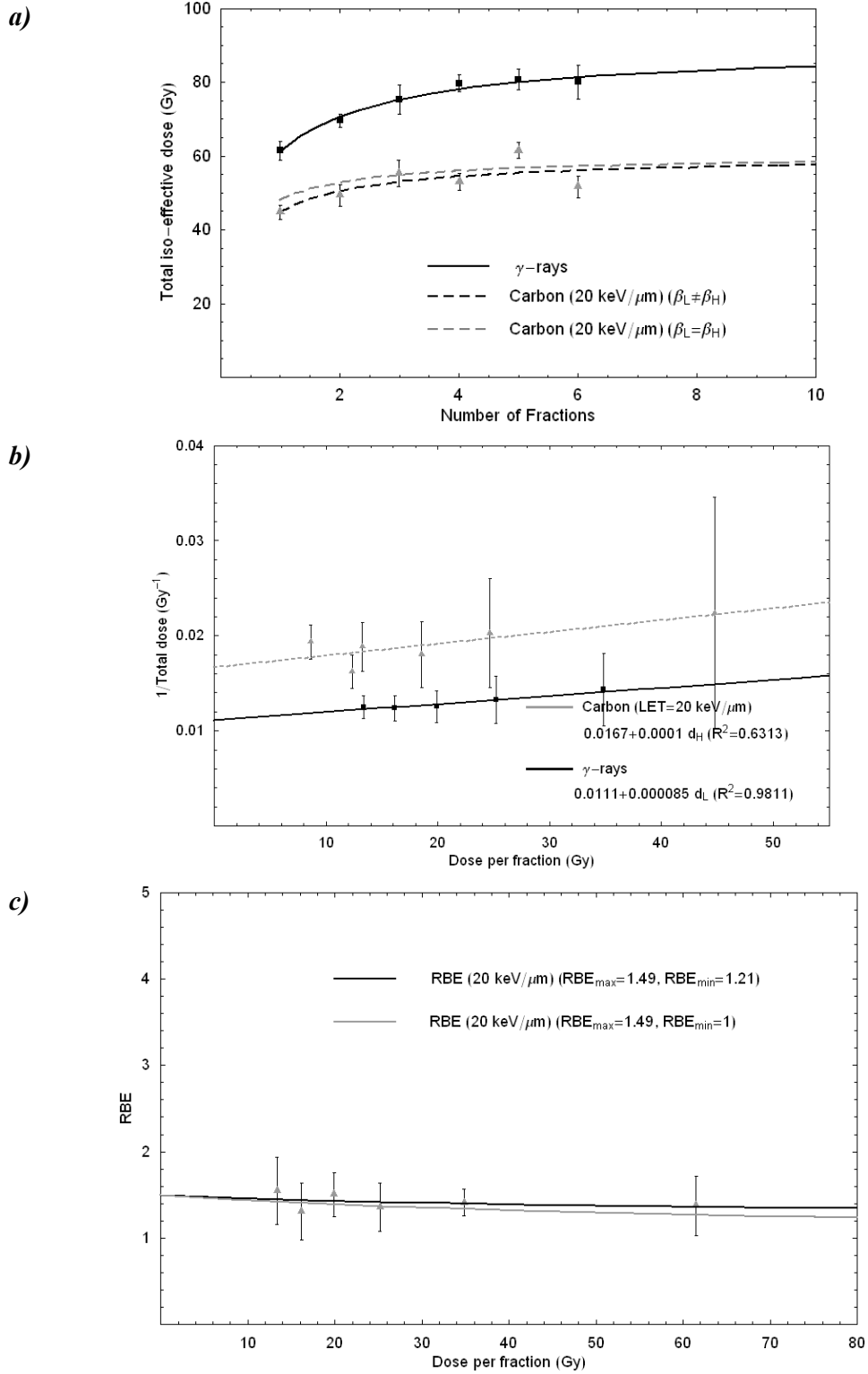


Figure 6.44: (a) Total dose required with different fractionation regimes to produce the same TGD time of 15 days with γ -rays and 20 keV/ μm ions; (b) Fe plot; (c) RBE curve for TGD time =15 days after exposure to X-rays and carbon ions.

- Figures corresponding to LET=42 keV/ μm at 9cm deep for TGD time=15days:

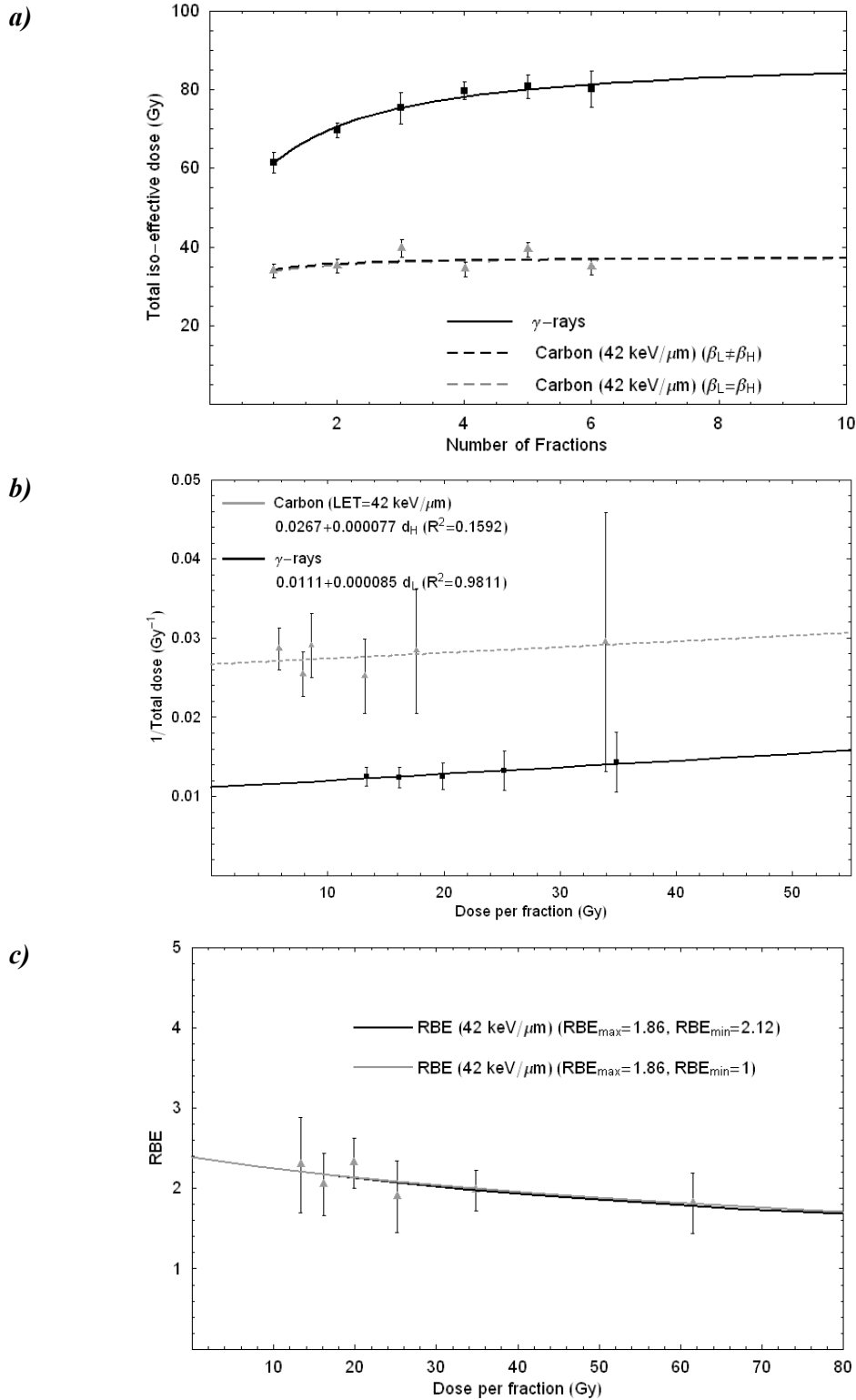


Figure 6.45: (a) Total dose required with different fractionation regimes to produce the same TGD time of 15 days with γ -rays and 42 keV/ μm ions; (b) Fe plot; (c) RBE curve for TGD time =15 days after exposure to X-rays and carbon ions.

- Figures corresponding to $LET=77\text{ keV}/\mu\text{m}$ at 14cm deep for TGD time=15days:

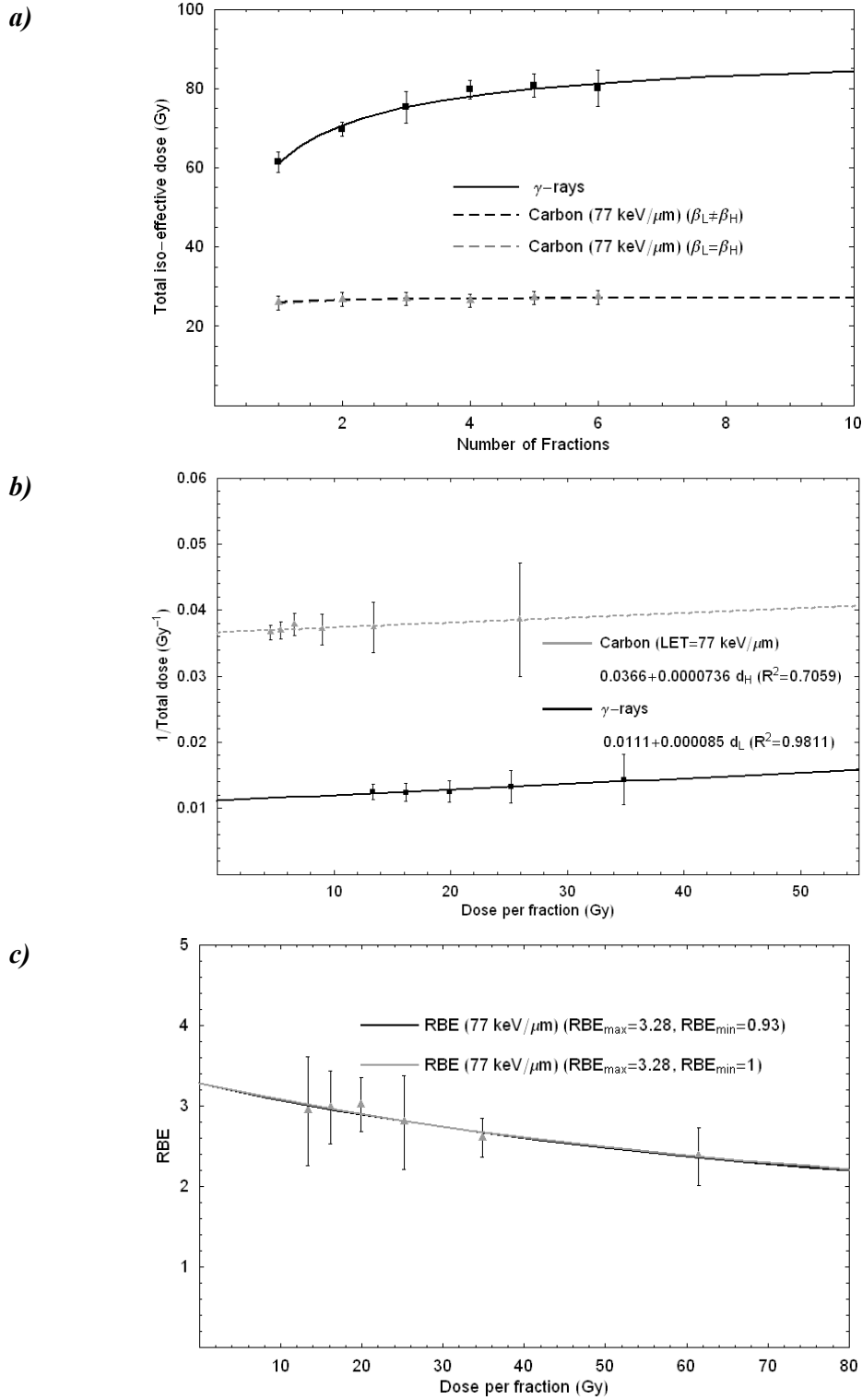


Figure 6.46: (a) Total dose required with different fractionation regimes to produce the same TGD time of 15 days with γ -rays and $77\text{ keV}/\mu\text{m}$ ions; (b) Fe plot; (c) RBE curve for TGD time =15 days after exposure to X-rays and carbon ions.

- Data points:

Fractions	γ -rays	Carbon	RBE	LET
1F	52.25 (53.28-51.23)	34.75 (37.93-31.06)	1.50±0.07	14keV/ μ m
2F	56.69 (59.25-54.30)	42.96 (45.31-40.61)	1.32±0.26	
3F	60.10 (63.34-57.03)	44.80 (47.32-42.12)	1.34±0.30	
4F	66.76 (68.63-64.88)	50.00 (52.51-47.82)	1.34±0.20	
5F	67.71 (69.32-64.88)	54.02 (55.20-52.51)	1.24±0.41	
6F	69.66 (72.56-66.93)	43.97 (45.14-42.63)	1.58±0.56	
1F	-	32.37 (34.07-30.85)	1.61±0.16	20keV/ μ m
2F	-	39.66 (41.86-36.95)	1.43±0.25	
3F	-	43.22 (44.41-42.03)	1.39±0.66	
4F	-	43.22 (44.58-41.86)	1.54±0.34	
5F	-	48.47 (49.66-47.29)	1.38±0.47	
6F	-	40.51 (43.05-37.97)	1.72±0.28	
1F	-	24.24 (25.42-23.05)	2.16±0.22	42keV/ μ m
2F	-	33.39 (35.08-31.36)	1.70±0.33	
3F	-	33.73 (34.92-32.37)	1.78±0.61	
4F	-	37.63 (38.64-36.10)	1.77±0.37	
5F	-	35.59 (37.46-33.90)	1.89±0.31	
6F	-	30.00 (31.19-28.64)	2.32±0.55	
1F	-	20.34 (21.19-19.49)	2.57±0.30	77keV/ μ m
2F	-	22.88 (23.90-21.86)	2.48±0.61	
3F	-	24.07 (24.92-23.22)	2.50±0.93	
4F	-	23.22 (24.07-22.37)	2.88±0.55	
5F	-	25.93 (26.95-24.75)	2.59±0.50	
6F	-	23.73 (24.75-22.54)	2.94±0.64	

Table 6.29: Data for skin reaction obtained from (Ando et al., 2005) for ASR=3.0.

Fractions	γ -rays	Carbon	RBE	LET
1F	61.47 (63.86-58.74)	44.47 (49.16-39.11)	1.38±0.13	14keV/ μ m
2F	69.66 (71.54-67.95)	50.50 (53.52-47.65)	1.38±0.15	
3F	75.29 (79.04-71.19)	57.21 (60.39-54.19)	1.32±0.32	
4F	79.73 (82.12-77.51)	68.44 (71.96-65.42)	1.16±0.18	
5F	80.75 (83.65-77.85)	60.06 (63.41-56.20)	1.34±0.20	
6F	80.07 (84.51-75.29)	61.06 (63.74-58.72)	1.31±0.46	
1F	-	44.75 (46.61-42.88)	1.37±0.34	20keV/ μ m
2F	-	49.32 (52.20-46.27)	1.41±0.15	
3F	-	55.42 (58.98-51.86)	1.36±0.28	
4F	-	53.05 (55.25-50.68)	1.50±0.25	
5F	-	61.53 (63.73-59.32)	1.31±0.33	
6F	-	51.69 (54.75-48.81)	1.55±0.39	
1F	-	33.90 (35.59-32.20)	1.81±0.38	42keV/ μ m
2F	-	35.25 (36.95-33.39)	1.98±0.25	
3F	-	39.66 (42.20-37.80)	1.90±0.45	
4F	-	34.41 (36.10-32.37)	2.32±0.31	
5F	-	39.32 (41.36-37.63)	2.05±0.39	
6F	-	34.92 (36.95-33.05)	2.29±0.59	
1F	-	25.93 (27.63-24.07)	2.37±0.36	77keV/ μ m
2F	-	26.78 (28.64-24.92)	2.60±0.24	
3F	-	26.95 (28.64-25.25)	2.79±0.58	
4F	-	26.44 (28,31-24.92)	3.02±0.34	
5F	-	27.12 (28.81-25.59)	2.98±0.45	
6F	-	27.29 (28.81-25.42)	2.93±0.68	

Table 6.30: Data for tumour growth delay obtained from (Ando et al., 2005) for TGD time of 15 days.

6.2.2.1. RBE curve comparisons between early (ASR) and late effects (TGD) for each LET value

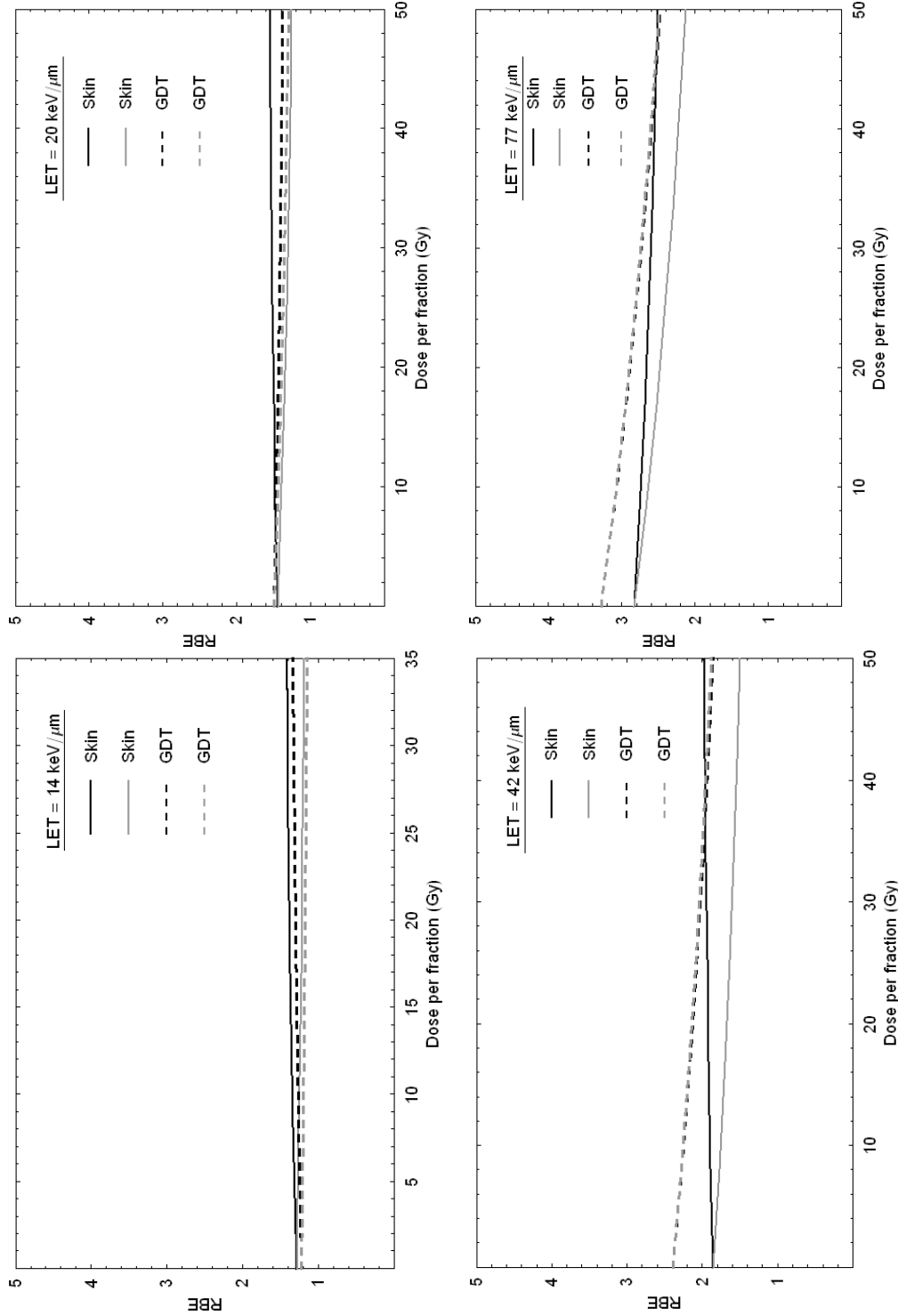


Figure 6.47: RBE comparison between average skin reaction = 3.0 and tumour growth delay time = 15 days. The black traces correspond to the calculated RBE with $RBE_{min} \neq 1$ while the grey curves correspond to RBE with $RBE_{min} = 1$.

6.2.3. Survival of intestinal crypt cells

- *System used*: Male LAF₁ mice 8-12 weeks old (Goldstein *et al.*, 1981).
- *Laboratory conditions and Methodology of experiments*: The immobilised mice were positioned vertically and the abdomen exposed to the charged-particle beam. 3.5 days after irradiation, animals were sacrificed and 8-10 sections 5- μ m thick of jejunum tissue were prepared for histology. The surviving crypts were counted as discussed in (Withers *et al.*, 1970).

Carbon ions were produced at the 184-in synchro-cyclotron of the Lawrence Berkley Laboratory (LBL) of the University of California, Berkeley. The energy of the beam was 400 MeV/amu and the Bragg peak of the beam was spread to 4 or 10cm. 3 \times 5 cm fields were used with a beam homogeneity of not less than 85% from the centre to the periphery of the field. Scattering of the beam was by Pb foils of 0.5 to 5 mm thick. Dose rates were set between 1-2 Gy/min although higher dose rates resulted in some occasions. Mice were irradiated at different locations within the beam path, which was achieved by changing the attenuation of the beam by removing (plateau) or inserting (SOBP) a water column in the absorber of the beam. Mice were irradiated in 1,2,5 or 10 fractions separated by a 3hr interval except when the beam availability made it impossible.

The reference radiation was γ -rays produced by the 2000-Ci ¹³⁷Cs irradiator with a dose rate of 2.17 Gy/min.

- *Radiobiological end point*: 10% survival of the population of intestinal crypt cells.

- Figures corresponding to the plateau region of the 4cm SOBP beam:

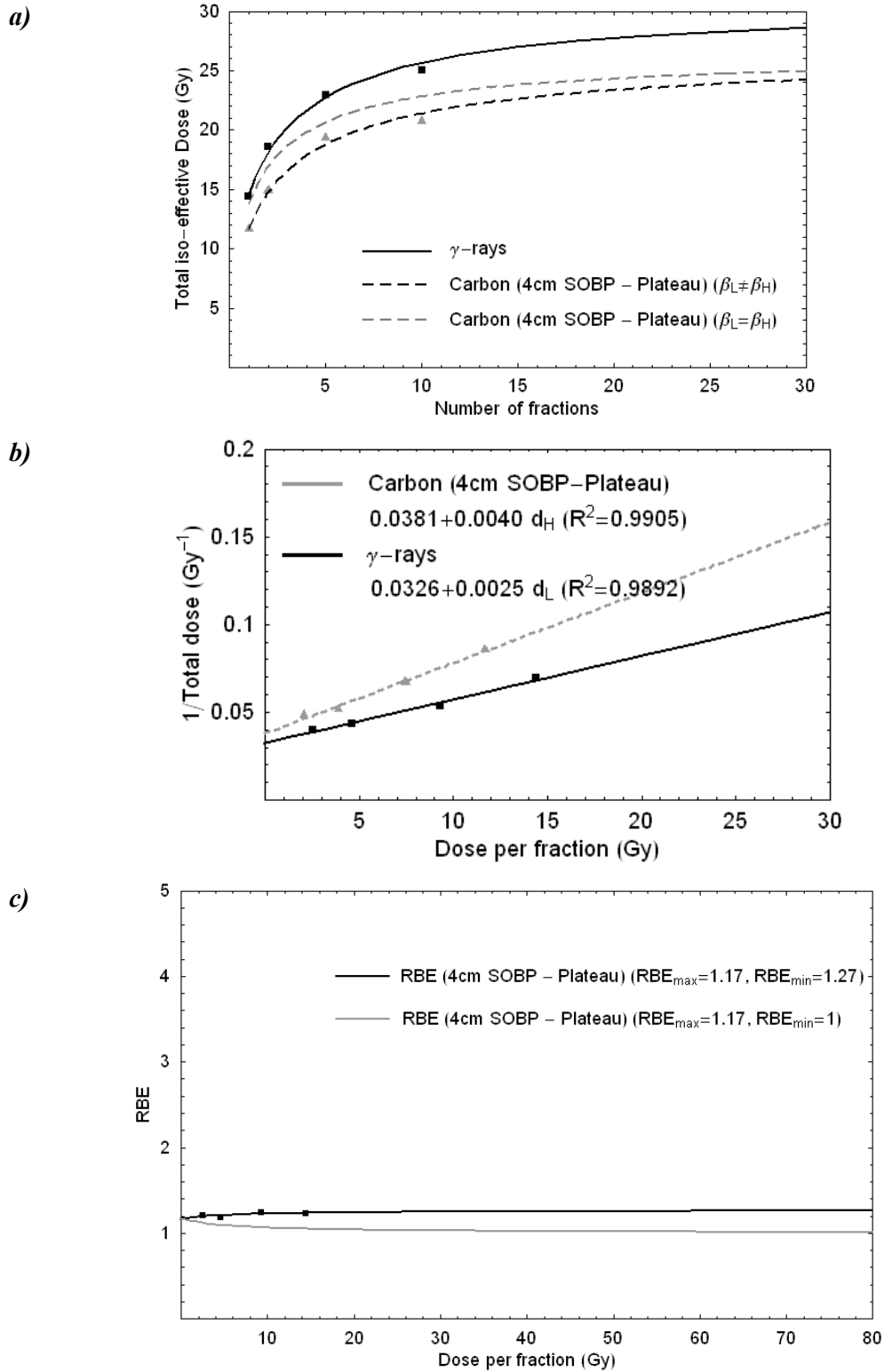


Figure 6.48: (a) Total dose required with different fractionation regimes to produce 10% survival level with γ -rays and 400 MeV/amu carbon ions with 4cm SOBP at the plateau region; (b) Fe plot; (c) RBE curve for mice skin exposed to X-rays and carbon ions.

- Figures corresponding to the peak region of the 4cm SOBP beam:

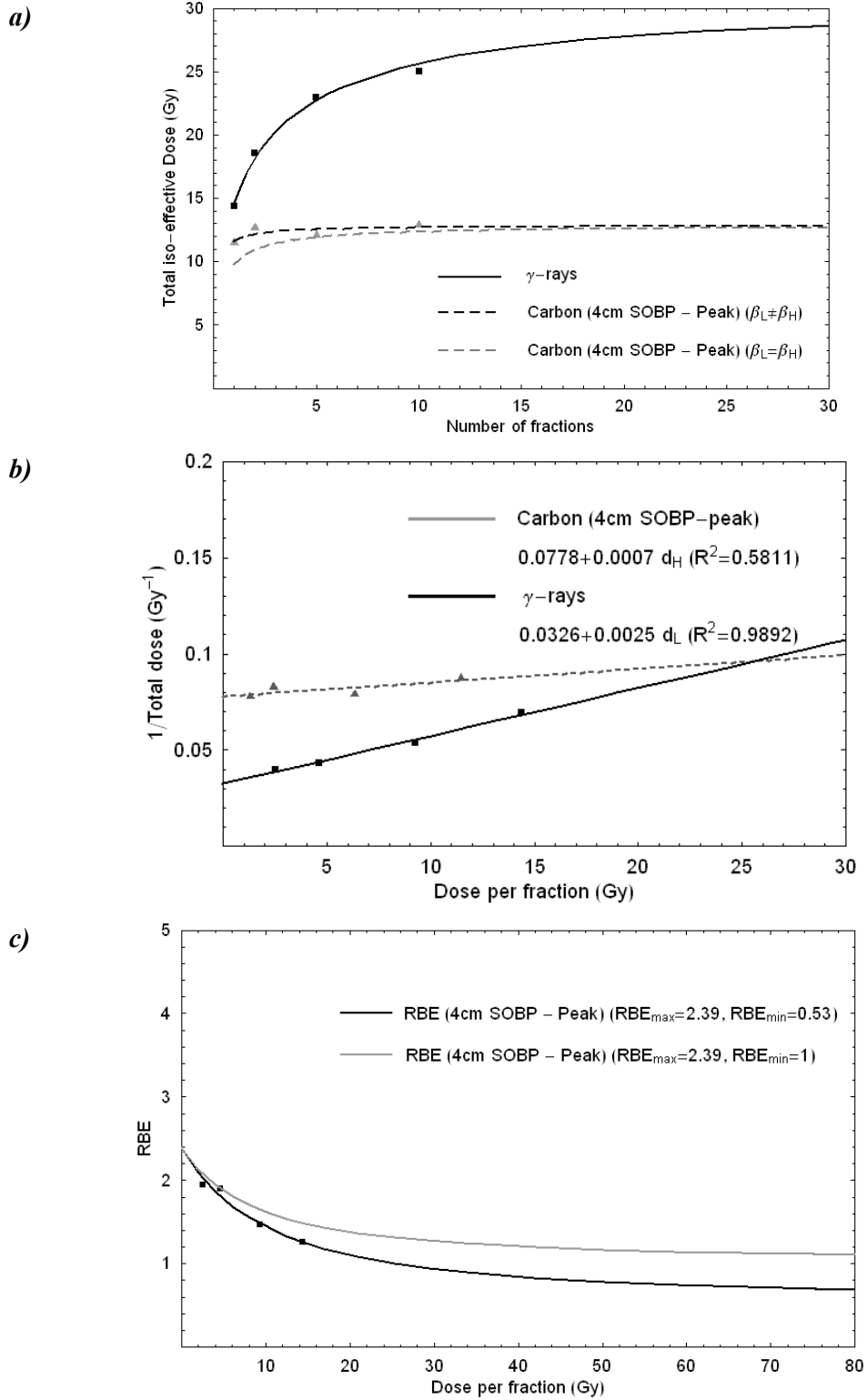


Figure 6.49: (a) Total dose required with different fractionation regimes to produce 10% survival level with γ -rays and 400 MeV/amu carbon ions with 4cm SOBP at the peak region; (b) Fe plot; (c) RBE curve for mice skin exposed to X-rays and carbon ions.

- Figures corresponding to the plateau region of the 10cm SOBP beam:

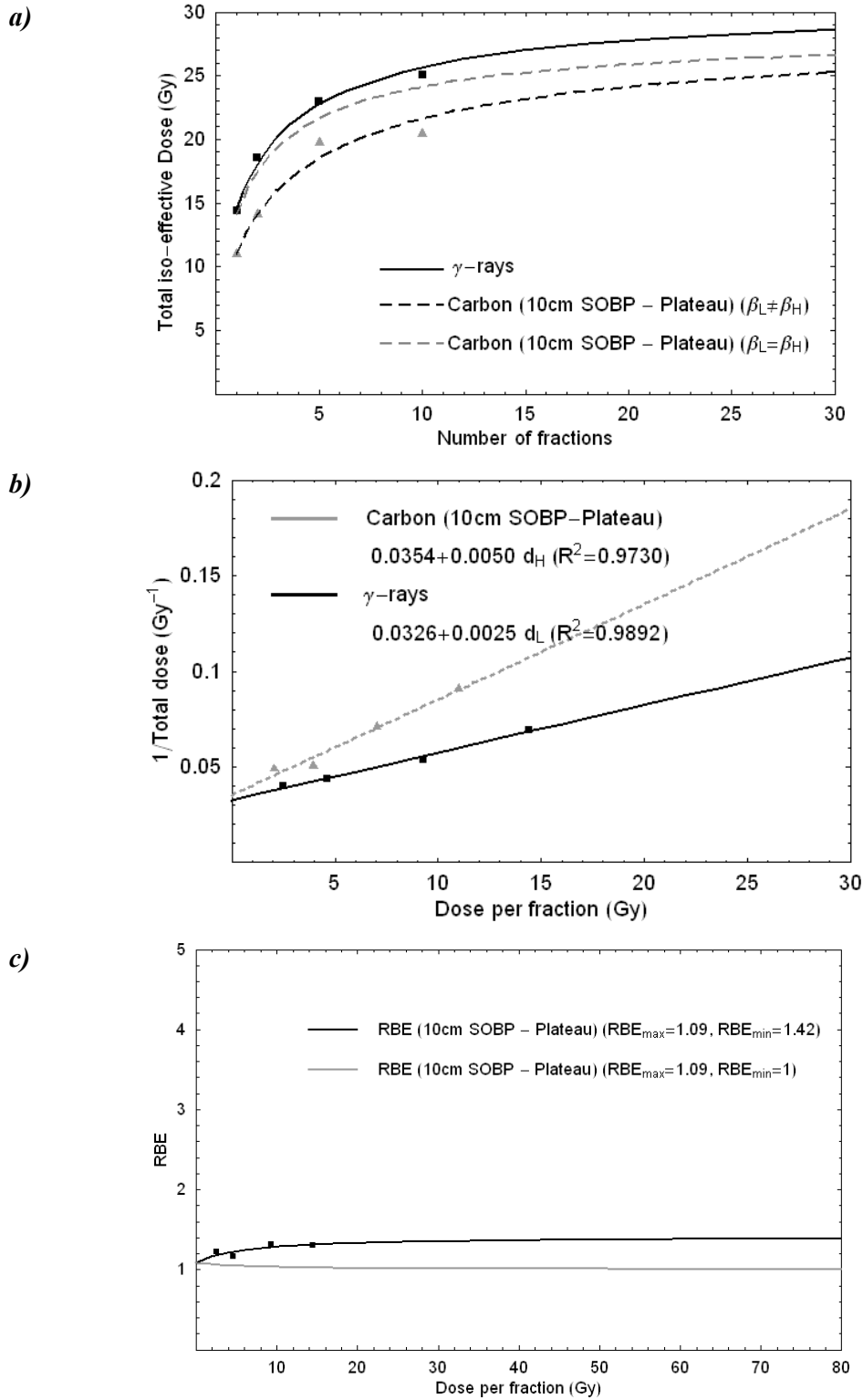


Figure 6.50: (a) Total dose required with different fractionation regimes to produce 10% survival level with γ -rays and 400 MeV/amu carbon ions with 10cm SOBP at the plateau region; (b) Fe plot; (c) RBE curve for mice skin exposed to X-rays and carbon ions.

- Figures corresponding to the peak region of the 10cm SOBP beam:

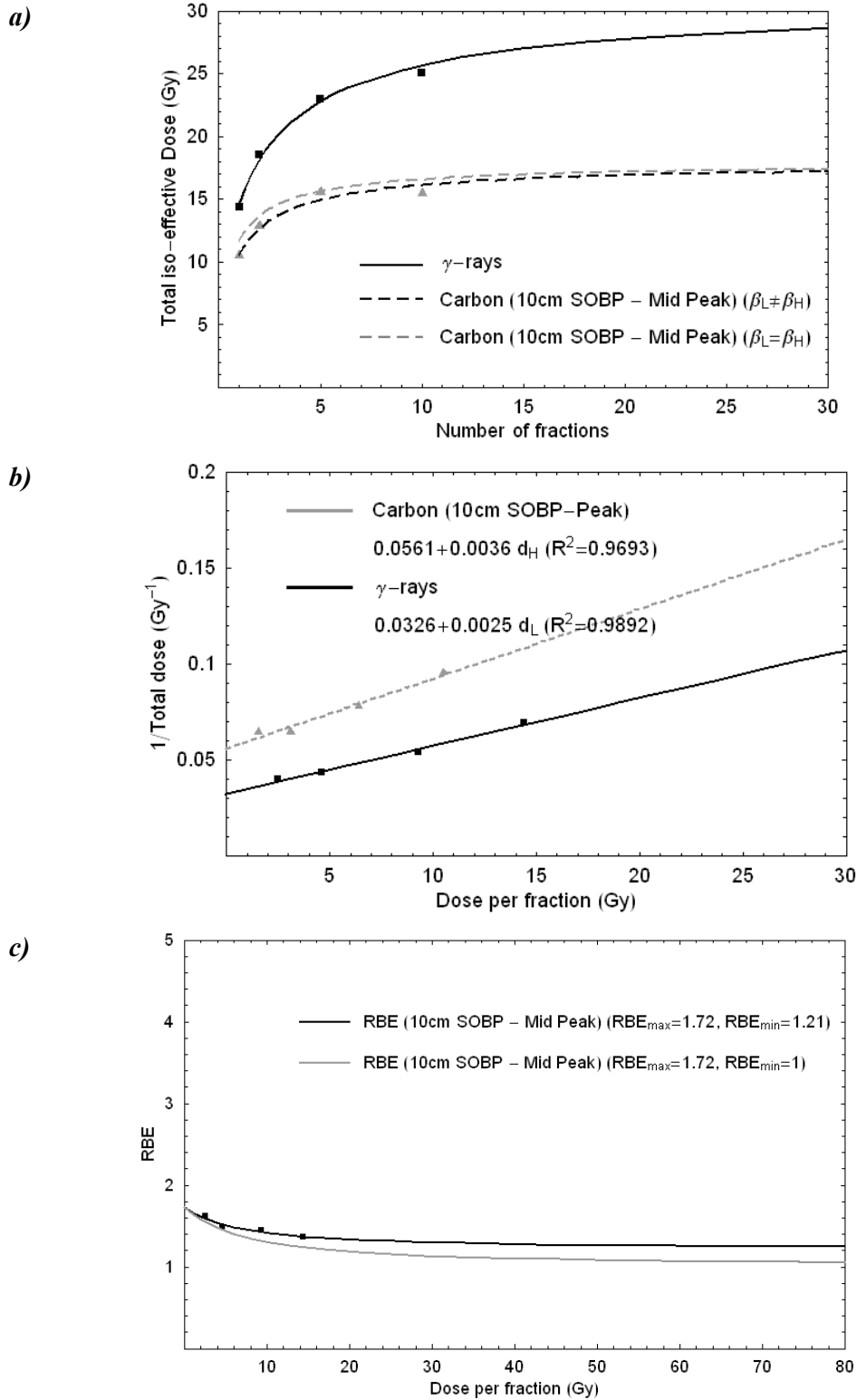


Figure 6.51: (a) Total dose required with different fractionation regimes to produce 10% survival level with γ -rays and 400 MeV/amu carbon ions with 10cm SOBP at the peak region; (b) Fe plot; (c) RBE curve for mice skin exposed to X-rays and carbon ions.

- Data points:

Fractions	γ -rays	Carbon	RBE	LET
1F	14.4	11.68	1.23	4cm SOBP Plateau
2F	18.55	14.89	1.25	
5F	22.99	19.36	1.19	
10F	25.04	20.73	1.21	
1F	-	11.46	1.26	4cm SOBP Peak
2F	-	12.66	1.47	
5F	-	12.11	1.90	
10F	-	12.87	1.95	
1F	-	11.00	1.31	10cm SOBP Plateau
2F	-	14.10	1.32	
5F	-	19.76	1.16	
10F	-	20.45	1.22	
1F	-	10.50	1.37	10cm SOBP Peak
2F	-	12.81	1.45	
5F	-	15.52	1.48	
10F	-	15.48	1.62	

Table 6.31: Data for 10% survival level of intestinal crypt obtained from (Goldstein et al., 1981).

6.3. Tabulated data of calculated (α/β) ratios, BED , RBE_{max} , RBE_{min} and ΔRBE_{2Gy}

6.3.1. Neutrons

	EARLY EFFECTS				LATE EFFECTS			
	(α/β) [Gy]	BED [Gy]	RBE_{max}	RBE_{min}	(α/β) [Gy]	BED [Gy]	RBE_{max}	RBE_{min}
Skin (erythema)	5.00	97.15	7.02	1.92				
Pig normal tissues	Epithelial reaction	14.20	3.61 (2.75)	0.70	4.91	106.72	4.49 (4.32)	0.91
	Relative field length	8.61	3.08	0.92	11.91	60.15	2.45	1.25
	Lung func.	2.24	5.69	0.47	3.53	35.48	3.56	1.04
	Renal func.	0.77	70.22	7.80	0.82	88.86	8.84	0.60
Mice Lung					1.16	153.76	10.21	0.90
Mice Lung	LD_{50}	5.95 (4.5)	5.20	0.99	2.33 (2.15)	56.19	8.63	0.72
	Breath rate $\times 1.1$	2.93 (2.9)	50.04	7.63	2.14 (2.11)	54.11	9.22	0.11
Mice renal damage	1.15	178.65	26.34	1.19	1.09	203.57	22.80	1.35
Mice jejunum	6.30	43.91	4.38	0.76				
Mice CNS					6.53	142.5	5.66	0.98
Small intestine	7.05	32.42	3.09	2.11	13.84	57.15	4.16	0.92
Oesophagus					16.25	89.54	3.05	2.28
Mice skin	7.65	90.89	7.56 (7.02)	1.03				
Colorectal injury	Nadir weight	12.33 (13.07)	70.50 (67.11)	7.04 (8.50)	0.47			
	Peak weight	7.35 (9.21)	82.34 (85.47)	6.86 (5.70)	0	5.06	66.48	7.38
	LD_{50}	28.94 (28.63)	76.31 (76.92)	5.68 (5.70)	1.46	4.37	115.30	10.46
					3.11 (3.12)	108.11 (107.87)	12.55 (12.70)	0.42

Table 6.32: Resultant values of (α/β) , BED , RBE_{max} and RBE_{min} obtained for neutrons.

	EARLY EFFECTS			LATE EFFECTS		
	RBE _{2Gy} (RBE _{max} , RBE _{min})	RBE _{2Gy} (RBE _{max} , 1)	ΔRBE _{2Gy} (%)	RBE _{2Gy} (RBE _{max} , RBE _{min})	RBE _{2Gy} (RBE _{max} , 1)	ΔRBE _{2Gy} (%)
Skin (erythema)	5.216	5.070	2.79			
Pig normal tissues	Epithelial reaction	3.183	3.202	3.261	3.276	0.46
	Relative field length	2.563	2.575	2.198	2.162	1.65
	Lung func.	3.041	3.156	2.434	2.424	0.43
	Renal func.	2.379	2.467	2.959	3.096	4.63
Mice Lung				4.123	4.150	0.63
Mice Lung	LD ₅₀	3.951	3.952	4.691	4.738	1.00
	Breath rate × 1.1	4.565	4.623	4.769	4.867	2.06
Mice renal damage	9.720	9.693	0.28	8.200	8.136	0.77
Mice jejunum	3.367	3.397	0.03			
Mice CNS				4.381	4.384	0.06
Small intestine	2.765	2.498	9.68	3.662	3.667	0.15
Oesophagus				2.912	2.757	5.33
Mice skin	6.028	6.025	0.04			
Colorectal injury	Nadir weight	6.064	6.081	5.292	5.339	0.88
	Peak weight	5.394	5.433	7.212	7.220	0.11
	LD ₅₀	5.336	5.322	7.657	7.699	0.55

Table 6.33: Percentage difference of RBE at 2Gy per fraction when RBE_{min} is considered =1 and ≠1 for neutrons.

6.3.1.1. Analysis of the variation of RBE_{max} and RBE_{min} with $(\alpha/\beta)_L$

As was indicated in Chapter 2, tissue type is one of the main factors affecting RBE, and as $(\alpha/\beta)_L$ is the main parameter used to characterise the fractionation sensitivity of a particular tissue and is used in Equations (5.29) and (5.30) to calculate RBE, it would be interesting to study how RBE for neutrons is affected by the difference in fractionation sensitivity of the tissues included in Table 6.32. As all results are produced with neutrons (all of them were produced with particles of very similar value of LET), it is assumed that the change in RBE_{max} and RBE_{min} does not come from the change of α_H and β_H but from the change in their low-LET counterparts, α_L and β_L . When analysing these results, it is very important to remember that they were produced for different end points and with beams of different energy and spectrum, three factors that affect the RBE strongly.

6.3.1.1.1. Early reactions

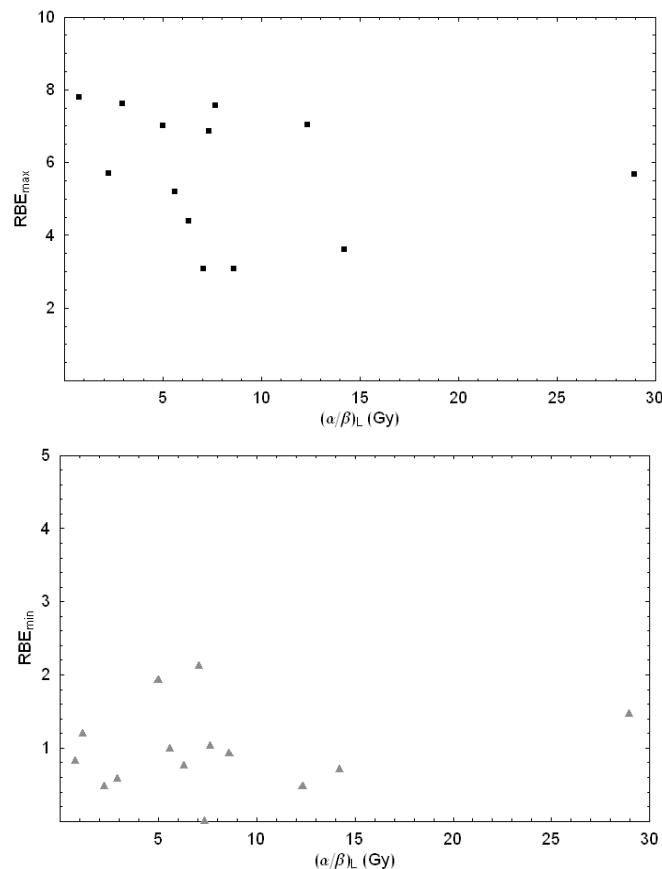


Figure 6.52: Plots of RBE_{max} (top) and RBE_{min} (bottom) versus $(\alpha/\beta)_L$ for early reactions.

6.3.1.1.2. Late reactions

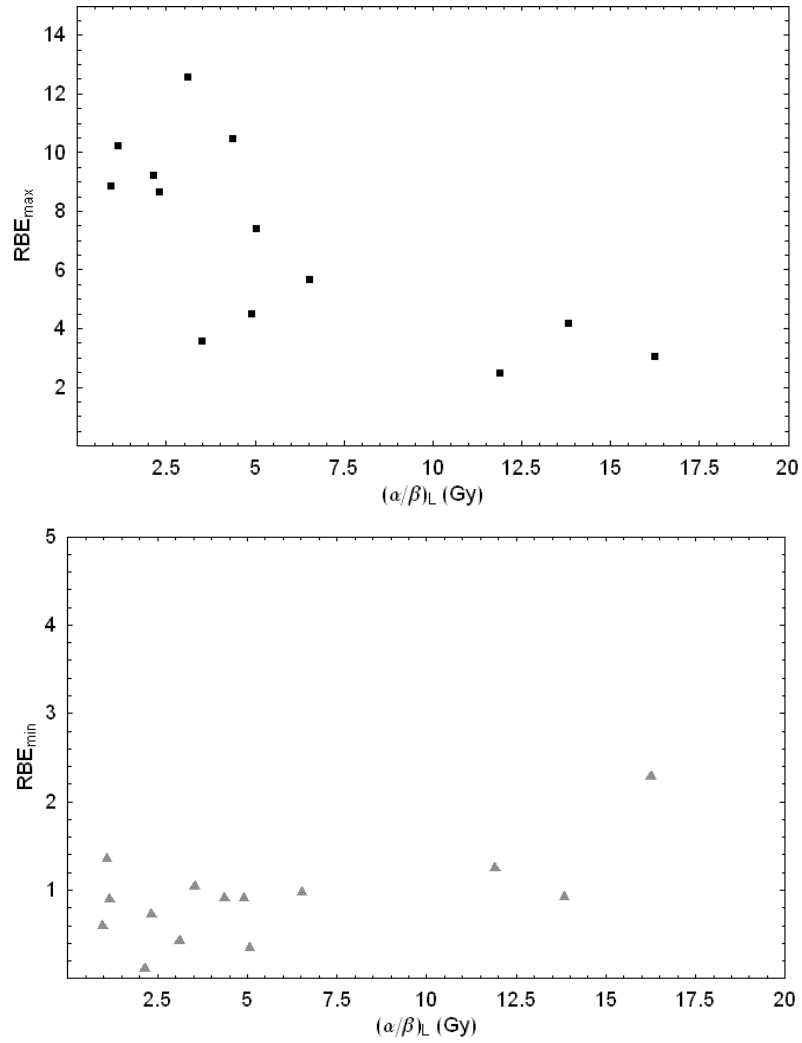


Figure 6.53: Plots of RBE_{max} (top) and RBE_{min} (bottom) versus $(\alpha/\beta)_L$ for late reactions.

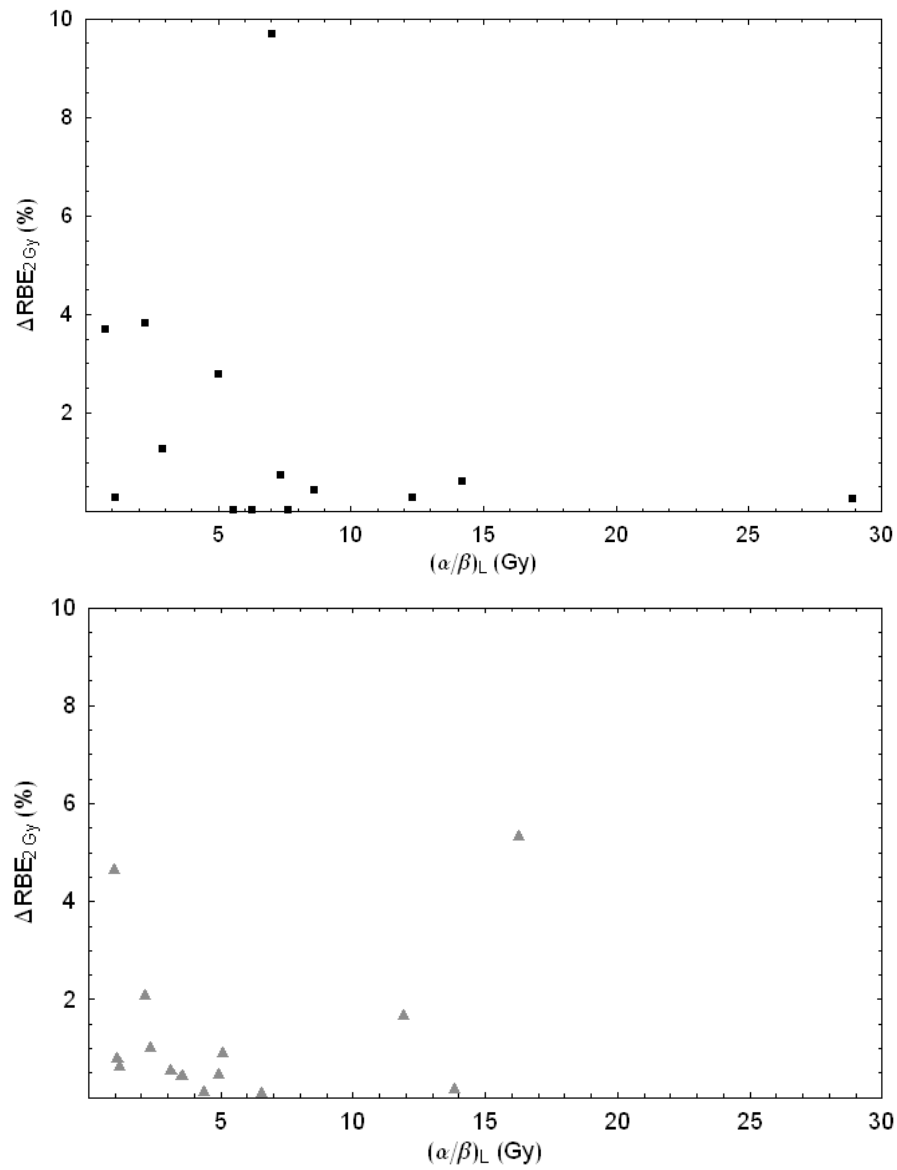
6.3.1.2. Analysis of the variation of ΔRBE_{2Gy} with (α/β) 

Figure 6.54: Study of the difference in calculated RBE when considering $RBE_{min} \neq 1$ and $RBE_{min} = 1$ for early and late reactions produced by neutrons on different types of tissues.

LET [keV/ μ m]	EARLY EFFECTS				LATE EFFECTS			
	RBE _{2Gy} (RBE _{max} , RBE _{min})	RBE _{2Gy} (RBE _{max} , 1)	Δ RBE _{2Gy} (%)	RBE _{2Gy} (RBE _{max} , RBE _{min})	RBE _{2Gy} (RBE _{max} , 1)	Δ RBE _{2Gy} (%)	RBE _{2Gy} (RBE _{max} , RBE _{min})	RBE _{2Gy} (RBE _{max} , 1)
14	1.500	1.483	1.17					
20	1.789	1.768	1.18					
40	2.035	2.004	1.53					
50	2.565	2.553	0.46					
60	2.546	2.502	1.74					
80	3.328	3.310	0.55					
100	3.500	3.477	0.69					
Mouse skin reaction = 3.0								
14	1.303	1.282	1.59	1.233	1.217	1.33		
20	1.457	1.437	1.38	1.487	1.482	0.31		
42	1.865	1.834	1.67	2.361	2.362	0.04		
77	2.816	2.796	0.72	2.238	2.239	0.02		
Mouse skin reaction = 3.0								
Tumour growth delay time (15 days)								
10% Survival of jejunum crypt cells								
4cm PK (58 keV/ μ m)	2.091	2.135	2.10					
4cm PL (11 keV/ μ m)	1.193	1.131	5.18					
10cm PK (58 keV/ μ m)	1.614	1.578	2.20					
10cm PL (11 keV/ μ m)	1.170	1.067	8.79					

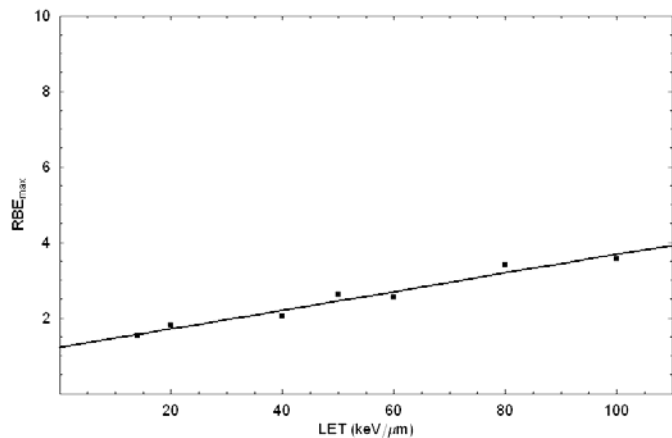
Table 6.35: Percentage difference of RBE at 2Gy per fraction when RBE_{min} is considered =1 and \neq 1.

6.3.2.1. Analysis of variation of RBE_{max} and RBE_{min} with LET

As RBE_{max} and RBE_{min} are ratios between a figure which varies with LET (α_H and β_H) and a fixed figure (α_L and β_L), the variation of each of them should resemble the change of α and β with LET. For this reason, RBE_{max} and RBE_{min} have been plotted versus LET in order to study the possible dependence (or independence) of α and β with LET for both, normal and tumour tissues. In order to establish the true variation of β with LET, we have plotted RBE_{min}^2 versus LET, so a fair comparison can be made between the rates of change of α and β with LET.

6.3.2.1.1. Normal Tissues

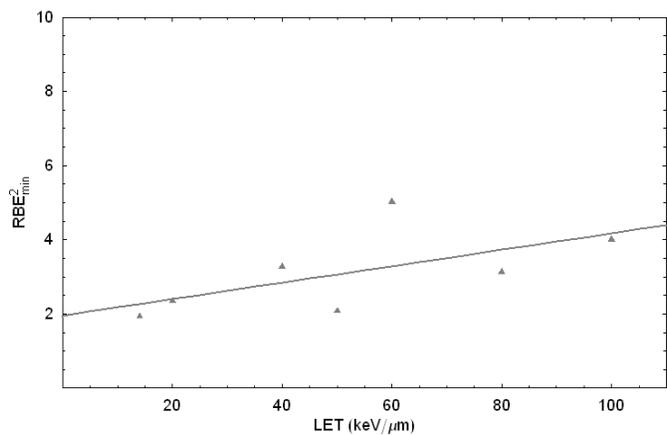
- Results for skin reaction = 3.0 obtained from (Ando *et al.*, 1998):



Regression line:

$$1.2193 + 0.0247 L$$

$$R^2 = 0.9619$$



Regression line:

$$1.9559 + 0.0222 L$$

$$R^2 = 0.3785$$

Figure 6.55: Plots of RBE_{max} (top) and RBE_{min} (bottom) versus LET for skin reaction = 3.0.

- Results for skin reaction = 3.0 obtained from (Ando *et al.*, 2005):

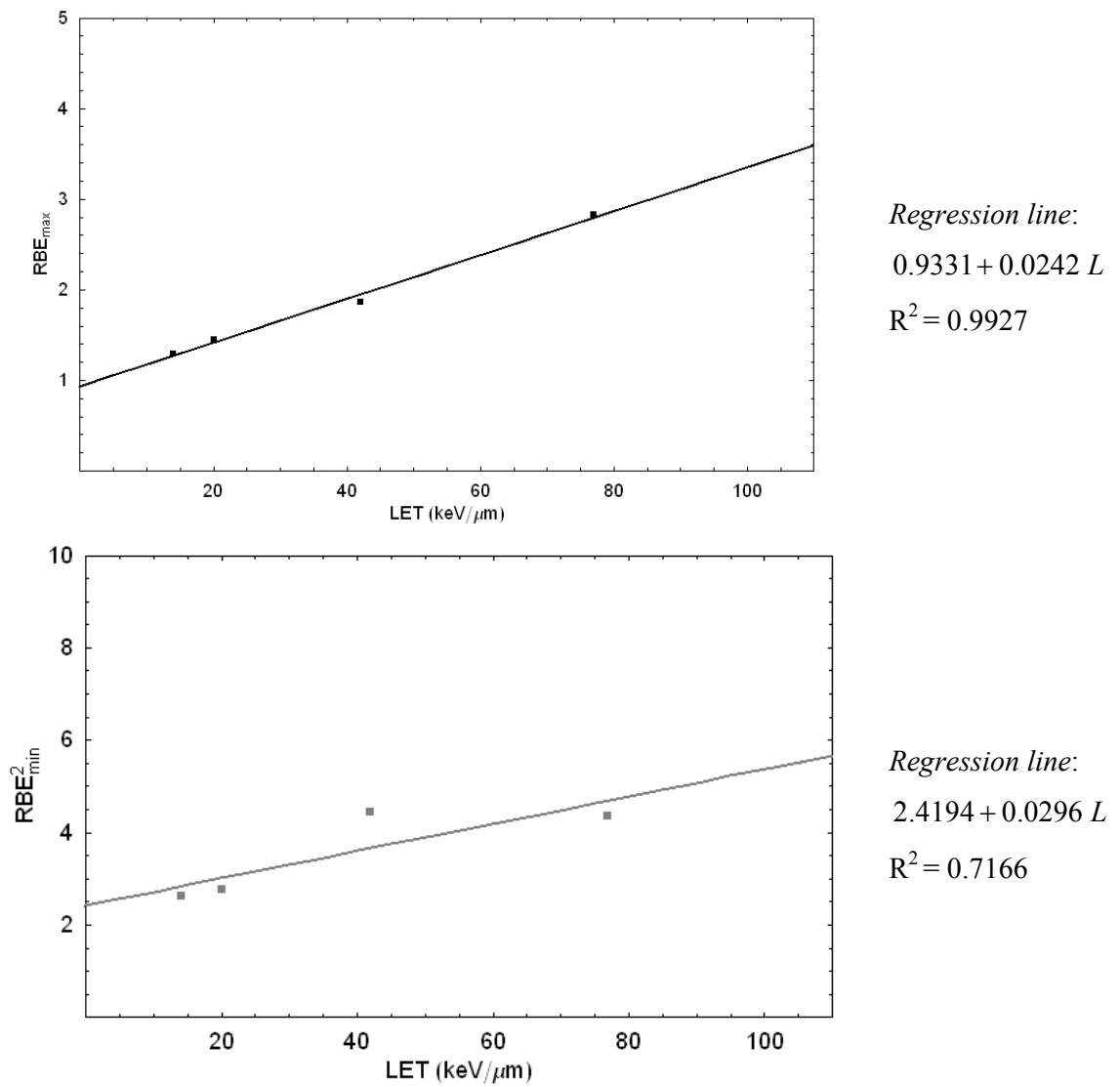
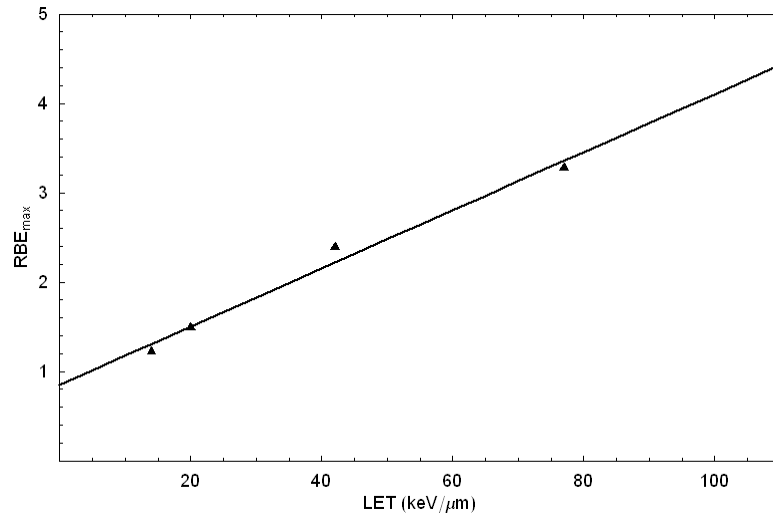


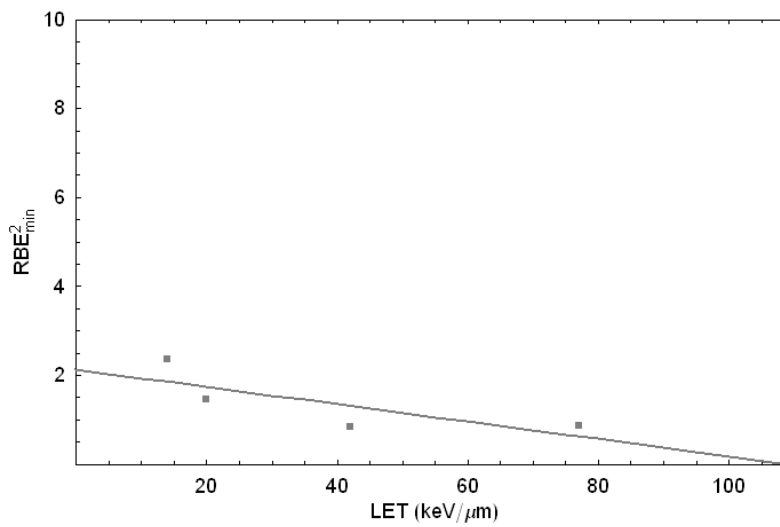
Figure 6.56: Plots of RBE_{max} (top) and RBE_{min} (bottom) versus LET for skin reaction = 3.0.

6.3.2.1.2. Tumour tissues

- Results for TGD = 15 days obtained from (Ando *et al.*, 2005):



Regression line:
 $0.8505 + 0.0325 L$
 $R^2 = 0.9835$



Regression line:
 $2.133 - 0.0195 L$
 $R^2 = 0.6022$

Figure 6.57: Plots of RBE_{max} (top) and RBE_{min} (bottom) versus LET for tumour growth delay time = 15 days.

6.3.2.2. Analysis of variation of ΔRBE_{2Gy} with LET

At different depths of the SOBP there is a different value of LET and, due to the dependency of RBE on LET, there will be varying values of RBE along the depth dose curves associated with carbon ions. As the proposed hypothesis in this thesis predicts differences of the calculated RBE when the accumulation of sublethal damage is incorporated into the RBE analysis, it would be interesting to determine if there is a specific region of the SOBP in which there is a consistent difference between the predicted RBE without the contribution of sublethal damage and that predicted with the contribution of sublethal damage.

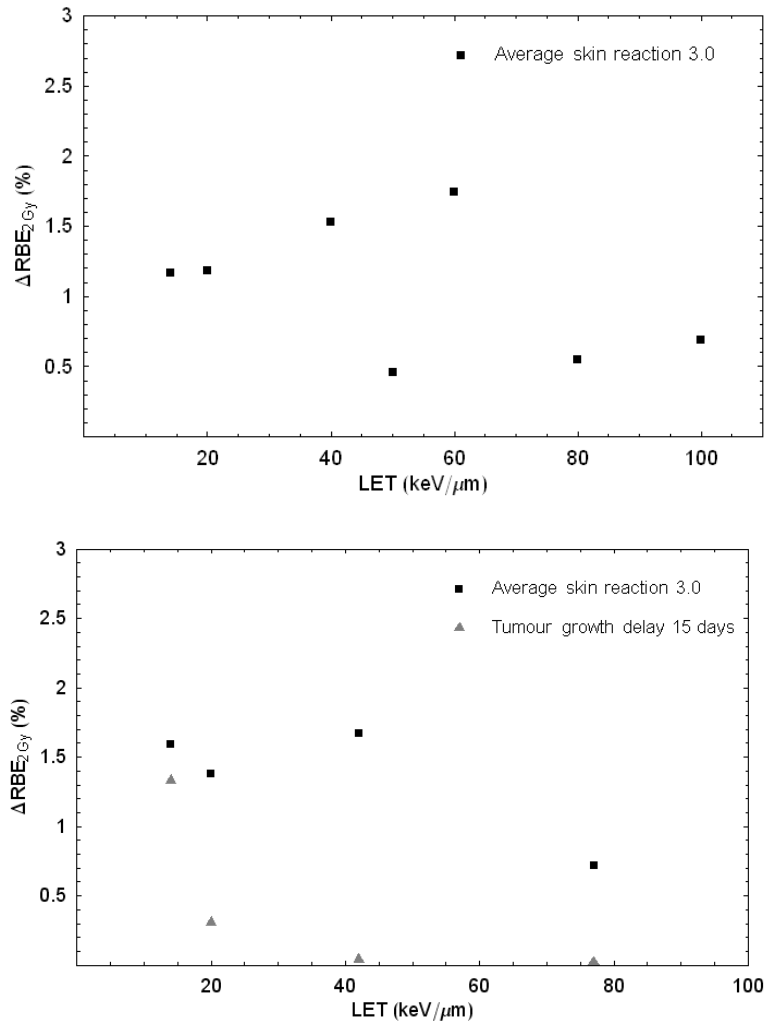


Figure 6.58: Study of the difference in calculated RBE when considering $RBE_{min} \neq 1$ and $RBE_{min} = 1$ at different positions of the SOBP. Top, results for ASR=3.0 from (Ando et al., 1998); bottom, results for ASR=3.0 and TGD=15 days from (Ando et al., 2005).

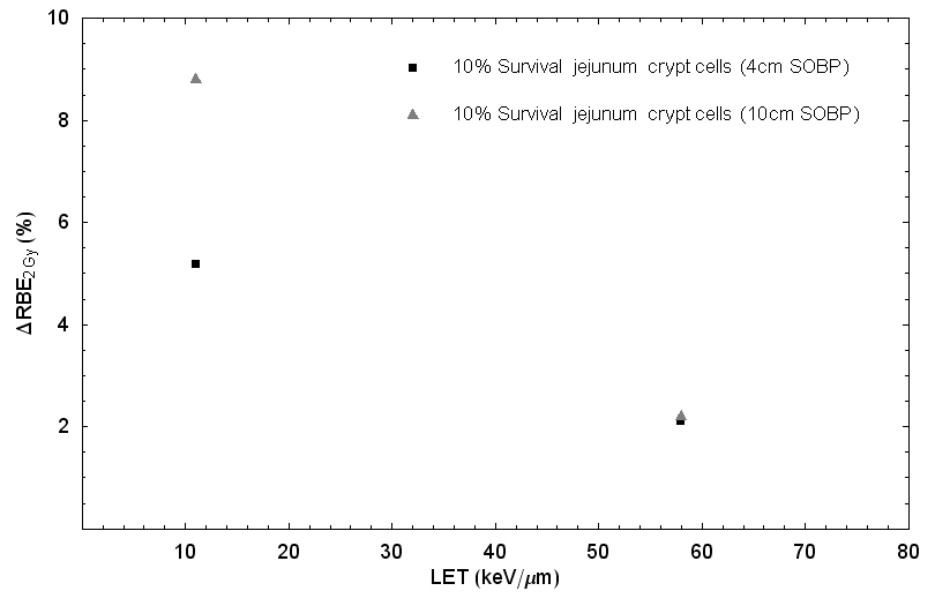


Figure 6.59: Study of the difference in calculated RBE when considering $RBE_{min} \neq 1$ and $RBE_{min} = 1$ at different positions of the SOBP for 10% survival crypt from (Goldstein et al., 1981).

6.4. Analysis of threshold doses where the therapeutic index changes when considering $RBE_{min}=1$ and $RBE_{min}\neq 1$.

6.4.1. Neutrons

	Effect		$RBE_{min}=1$	$RBE_{min}\neq 1$	ΔD (%)
	Early	Late			
Colorectal Injury	Nadir body weight	Short faeces	0.432	0.423	2.13
	Peak body weight	Short faeces	1.505	1.479	1.76
	LD/50 2 months	LD/50 12 months	5.332	5.171	3.11
	LD/50 2 months	LD/50 15 months	5.180	4.871	6.34
Colorectal injury vs skin erythema	Skin erythema	Short faeces	∞	∞	-
	Skin erythema	LD/50 12 months	8.650	7.960	8.67
	Skin erythema	LD/50 15 months	6.780	5.864	15.62
Lung Injury	BR \times 1.1 28 wks	BR \times 1.1 68 wks	4.215	3.236	30.25
	LD/50 28 wks	LD/50 68 wks	4.938	4.235	16.60
Pig normal tissues	skin erythema	skin necrosis	2.327	2.351	1.02
	Skin field length<0.863 (26-52 wks)	Skin field length<0.863 (65-104 wks)	∞	8.243	-
	Lung function (13-26 wks)	Lung function (39-104 wks)	∞	5.205	-
	Kidney FI=F	Kidney FI=NF	∞	8.396	-
Renal damage	Haematocrit reduction<40%	EDTA clearance	∞	25.260	-
Small intestine	LD/50 – 5 days	LD/50 – 90 days	∞	12.836	-

Table 6.36: Calculated doses where the therapeutic index of neutrons changes when considering $RBE_{min}=1$ and $RBE_{min}\neq 1$. Observe how the threshold dose is lower in 86.7% of the cases when $RBE_{min}\neq 1$.

6.4.2. Carbon ions

LET	Effect		RBE _{min} =1	RBE _{min} ≠1	ΔD (%)
14	Average Skin Reaction = 3.0	Tumour Growth Delay = 15 days	∞	∞	-
20			∞	6.407	-
42			∞	37.351	-
77			∞	45.573	-

Table 6.37: Calculated doses where the therapeutic index of carbon ion changes.

6.5. Statistical analysis

In order to prove the validity of the hypothesis formulated in Chapter 5, a t-test has been performed to compare the actual values of RBE with the expected values of RBE calculated with RBE_{min}=1 and those calculated with RBE_{min}≠1. The hypothesis formulated in Chapter 5 was formulated in terms of the comparison between dose-time (Total Dose versus number of fractions) relationships. The analysis presented here is done in terms of the comparison between RBE curves but this is justified on the basis that, as shown in Section 5.4, if β is considered dependent of LET an RBE_{min}≠1 would need to be introduced within the LQ formula to predict the correct RBE at any given dose per fraction. Thus, the following Null Hypotheses (NH) can be formulated:

$$\text{NH-A: } \beta = f(L) \Rightarrow \overline{RBE(RBE_{\max}, RBE_{\min} \neq 1)} - \overline{RBE(\text{actual})} = 0$$

$$\text{NH-B: } \beta \neq f(L) \Rightarrow \overline{RBE(RBE_{\max}, RBE_{\min} = 1)} - \overline{RBE(\text{actual})} = 0$$

In words, NH-A means that, if β is considered dependent on LET, there is no difference between the mean of the RBE values obtained from Equation (5.29) (with RBE_{min}≠1) and the mean of the published values of RBE (where the values of RBE from Equation (5.29) have been calculated for the same doses per fraction as those for the published RBE data). Alternatively, NH-B would mean that, if β is considered independent of LET, there is no difference between the mean of the RBE values obtained from Equation (5.30) (with RBE_{min}=1) and the mean of the published values of RBE. The calculated two-tailed p values are shown in Table 6.38 (significance level = 0.05). The

larger the value of p , the weaker is considered the evidence to reject the corresponding Null Hypothesis.

6.5.1. Neutrons

		Calculated $p_{\text{two-tailed}}$ values				
		Early Reactions		Late reactions		
		NH-A	NH-B	NH-A	NH-B	
Pig normal tissues [refs]	Effects					
	Skin (erythema)[ref]	0.2122	0.4166	-	-	
	Epithelial react.	0.7096	0.3795	0.6041	0.2143	
	Relative field length <0.863	0.7458	0.8742	0.9342	0.5710	
	Lung funct.	0.5749	0.9425	0.5988	0.5672	
	Renal funct.	0.4082	0.6147	0.5210	0.9419	
	Mice Lung [ref]	-	-	0.3674	0.2041	
Mice Lung [ref]	LD ₅₀	0.5019	0.5109	0.7444	0.0991	
	Breath rate × 1.1	0.9945	0.1619	0.7435	0.0053	
	Mice renal damage [ref]	0.8825	0.7392	0.4189	0.0276	
	Mice jejunum [ref]	0.2684	0.0043	-	-	
	Mice CNS [ref]	-	-	0.4064	0.3141	
	Small intestine [ref]	0.8239	0.0061	0.7620	0.8526	
	Oesophagus[ref]	-	-	0.8389	0.0075	
	Mice skin [ref]	0.7269	0.7835	-	-	
Colorectal injury [refs]	Nadir weight	0.7656	0.2280	0.8552*	0.2416*	
	Peak weight	0.9923	0.0797			
	LD ₅₀		0.8452	0.4866	0.9284**	0.7998**
					0.9217***	0.3804***

Table 6.38: T-test values for comparison between actual neutron data and models with $RBE_{\text{min}}=1$ and $RBE_{\text{min}}\neq 1$. Values corresponding to * are for short faeces measured 12 months after irradiation; ** correspond to LD/50 after 12 months of irradiation; and, *** LD/50 after 15 months of irradiation.

6.5.2. Carbon ions

		Calculated $p_{\text{two-tailed}}$ values				
		Early Reactions		Late reactions		
		Effects	NH-A	NH-B	NH-A	
Mouse skin reaction = 3.0	14	0.8833	0.0872			
	20	0.8919	0.1501			
	40	0.9090	0.1688			
	50	0.8695	0.1065			
	60	0.8930	0.0617			
	80	0.8913	0.1303			
	100	0.9619	0.1190			
Mouse skin reaction = 3.0	14	0.9497	0.0296	0.9802	0.0109	Tumour growth delay time (15 days)
	20	0.9354	0.0341	0.9951	0.2157	
	42	0.9453	0.0521	0.9971	0.8385	
	77	0.9313	0.0448	0.9733	0.8174	
10% Survival of jejunum crypt cells	4cm PK (58 keV/ μm)	0.9549	0.0631			
	4cm PL (11 keV/ μm)	0.9974	0.0159			
	10cm PK (58 keV/ μm)	0.9781	0.0369			
	10cm PL (11 keV/ μm)	0.9853	0.0165			

Table 6.39: T-test values for comparison between actual carbon ion data and models with $RBEmin=1$ and $RBEmin \neq 1$.

6.6. Conclusions

The conclusions that can be drawn from Sections 6.3 to 6.5 can be summarised as follows:

- Section 6.3:
 - The values of (α/β) , BED , RBE_{max} and RBE_{min} obtained in this study are very similar to those reported by the original authors of the data (values in brackets in Tables 6.32 and 6.34), which supports the validity of the method followed in this thesis to obtain the values of these parameters and which therefore allows the conclusions extracted in this thesis to be applied to the reported data from which they were obtained.
 - Due to the dispersion of the points in Figures 6.52 and 6.53, it is not possible to recognise any strong dependency between RBE_{max} and RBE_{min} with $(\alpha/\beta)_L$ for neutrons. However, these data have been produced with neutron beams of different average energy and spectrum, and for experiments with different end points.
 - Figures 6.55, 6.56 and 6.57 show a strong relationship between RBE_{max} and RBE_{min}^2 with LET, although the dispersion of the data in the case of RBE_{min}^2 versus LET is larger than in the case of RBE_{max} versus LET and Figures 6.56 and 6.57 present only four points for the statistical analysis. It is interesting to notice how, for normal tissues, the slope of the RBE_{min}^2 versus LET regression line is positive while for tumour tissues the slope is negative. There are similarities between the implied changes on α and β shown in Figures 6.55, 6.56 and 6.57 and those presented in Figure 5 of Chapter 5.
 - From Figure 6.54, there is no strong indication of a change of RBE at 2Gy per fraction (ΔRBE_{2Gy}) when RBE_{min} is considered $\neq 1$ from the case in which it is considered equal to 1 for tissues of different $(\alpha/\beta)_L$ exposed to neutrons. However, Figure 6.59 shows how ΔRBE_{2Gy} changes with LET in the case of carbon ions, with values ranging from 0.46 – 8.79% in the case of early reactions and 0.02-1.33% in the case of late reactions and with the

largest differences always found at around 40 keV/ μm corresponding to the distal portion of the plateau region of the SOBP.

- Section 6.4:

- Tables 6.36 and 6.37 show a consistent change of the dose per fraction at which the RBE for late reactions become larger than that for early reactions or vice versa. In some cases, where the RBE curve for early reactions and that for late reactions would not cross when considering $\text{RBE}_{\min}=1$ (corresponding to the value ∞ in the table), there is a drastic reduction of dose per fraction down to the level of therapeutic doses used in different centres using neutrons. This implies that the consideration of an $\text{RBE}_{\min}\neq 1$ could introduce new dose limits at the therapeutic ratio of neutrons or carbon ions change.
- Table 6.47 shows how the limit dose at which therapeutic ratio may change depends on LET with the biggest change at low LET (20 keV/ μm approximately, which corresponds to the plateau region of the SOBP).

- Section 6.5:

- When comparing the averages of the RBE values obtained from Equations (5.29) and (5.30) with that of the published RBE data using the t-test, 57% of the resultant p values for early reactions and 86% of the p values for late reactions produced after neutrons (Table 6.38) are larger for the data produced when considering $\text{RBE}_{\min}\neq 1$, meaning that in a larger number of cases for both early and late reactions, there is weaker evidence against NH-A than against NH-B.
- The statistical analysis in the case of carbon ion results are even more convincing than the one for neutrons as in this case, in 100% of the cases for both, early and late reactions produced after carbon ion radiation, the p value corresponding to the NH-A is much bigger than that for the NH-B. However the amount of data in hand is so limited (only three end points are considered) that it is not possible to assume this as a definitive conclusion.

6.7. Bibliography

- Alpen E.L., Powers-Risius P., McDonald M. *Radiation Research* 83(3):677-687 (1980).
- Ando K., Koike S., Nojima K., Chen Y-J., Ohira C., Ando S., Kobayashi N., Ohbuchi T., Shimizu W., Kanai T. *International Journal of Radiation Biology* 74(1):129-138 (1998).
- Ando K., Koike S., Uzawa A., Takai N., Fukawa T., Furusawa Y., Aoki M., Miyato Y. *Journal of Radiation Research* 46(1):51-57 (2005).
- Bewley D.K., Field S.B., Morgan R.L., Page B.C., Parnell C.J. *British Journal of Radiology* 40(478):765-770 (1967).
- Bewley D.K., Parnell C.J. *British Journal of Radiology* 42(496):281-288 (1969).
- Denekamp J. *British Journal of Radiology* 46(545):381-387 (1973).
- Field S.B., Hornsey S. *European Journal of Cancer* 10:621-627 (1974).
- Field S.B., Hornsey S., Kutsutani Y. *British Journal of Radiology* 49:700-707 (1976).
- Fowler J.F., Morgan R.L., Silvester J.A., Bewley D.K., Turner B.A. *British Journal of Radiology* 36(423):188-196 (1963).
- Fowler J.F., Bewley D.K., Morgan R.L., Silvester J.A. *British Journal of Radiology* 38:278-284 (1965).
- Geraci J.P., Jackson K.L., Christensen G.M., Thrower P.D., Weyer B.J. *International Journal of Radiation Oncology Biology Physics* 2(7-8):693-696 (1977).
- Goldstein L.S., Phillips T.L., Ross G.Y. *Radiation Research* 86(3):542-558 (1981).
- Hopewell J.W., Foster J.L., Young C.M., Wiernik G. *Radiology* 130(3):783-788 (1979).
- Hopewell J.W., Barnes D.W., Robbins M.E., Sansom J.M., Knowles J.F., van den Aardweg G.J. *British Journal of Radiology* 61(730):928-938 (1988).
- Hopewell J.W., Barnes D.W., Robbins M.E., Corp M., Sansom J.M., Young C.M., Wiernik G. *British Journal of Radiology* 63(754):760-70 (1990).
- Hornsey S., Kutsutani Y., Field S.B. *Radiology* 116(1):171-174 (1975)
- Hornsey S., Morris C.C., Myers R., White A. *International Journal of Radiation Oncology Biology Physics* 7:185-189 (1980).
- Hornsey S. *In: Radiation Injury to the Nervous System*. Gutin P.H., Leibel S.A., Sheline G.E. (eds.). Raven Press Ltd., New York (1991).
- Joiner M.C., Maughan R.L., Fowler J.F., Denekamp J. *Radiation Research* 95(1):130-141 (1983).

- Joiner M.C., Bentzen S.M. *In: Basic Clinical Radiobiology*. Steel G.G. (ed.), pp.124 (2002) 3rd Edition.
- Parkins C.S., Fowler J.F., Maughan R.L., Roper M.J. *British Journal of Radiology* 58(687):225-241 (1985).
- Rezvani M., Hopewell J.W. *Nuclear Medicine and Biology* 13:245-251 (1986).
- Rezvani M., Barnes D.W., Hopewell J.W., Robbins M.E., Sansom J.M., Adams P.J., Hamlet R. *British Journal of Radiology* 63(755):875-81 (1990).
- Robbins M.E., Barnes D.W., Campling D., Hopewell J.W., Knowles J.F., Sansom J.M., Simmonds R.H. *British Journal of Radiology* 64(765):823-30 (1991).
- Stewart F.A., Soranson J., Maughan R., Alpen E.L., Denekamp J. *British Journal of Radiology* 57(683):1009-1021 (1984).
- Terry N.H., Denekamp J. *British Journal of Radiology* 57(679):617-629 (1984).
- Withers H.R., Elkind M.M. *International Journal of Radiation Biology* 17(3):261-267 (1970).
- Withers H.R., Mason K., Reid B.O., Dubravsky N., Barkley H.T. Jr, Brown B.W., Smathers J.B. *Cancer* 34(1):39-47 (1974).

High-LET repair kinetics: predictions from standard repair models

The most relevant factors affecting the calculation of RBE were introduced in Chapter 2, where in section 2.1 it was indicated that dose fractionation and cell cycling are two of the factors with greatest impact on the final value of the RBE for any prescribed treatment outcome. These two factors are inherently related to the specific response of the biological system exposed to the radiation and how it repairs the damage caused by this radiation. It is therefore important to review how repair can be accounted for, not only in conventional radiotherapy, but also in high-LET radiotherapy. Some of the more traditional repair models on repair kinetics are revised in this chapter, with a special focus on the so called ‘Reciprocal Repair’ model, which will be extended in Chapter 8 to high-LET radiotherapy. Then, in Chapter 9, some results of the analysis of repair kinetic data produced after exposure to high-LET radiations will be contrasted with the new model to assess its validity as a viable alternative to those currently used.

7.1. General revision of standard repair models

The kinetics of repair has been a subject of major interest since the realization that such processes occur in all living tissues following irradiation (Lea, 1938). The determination of the repair kinetics associated with different tissues is of extreme importance in radiotherapy due, for example, to its impact on the inter-fractional time required to allow total recovery of normal tissue. A multitude of studies have been carried out to examine the influence of changing inter-fraction times for different tissues exposed to

low-LET radiations and various repair models (also called ‘reaction-rate models’) have been used to analyse the data. In particular, many authors have used repair models incorporating first- or second-order repair kinetics in their fundamental equations, some of them have already been mentioned before (Chapter 4), such as the Repair Miss-Repair (RMR) model (Tobias *et al.*, 1980) and the Lethal-Potentially Lethal (LPL) model (Curtis, 1986), along with models of biphasic repair kinetics, which assume the existence of a slow and a fast component in the repair process. Additionally there are repair saturation models (Goodhead, 1985), which predict cell survival curves on the basis of a competing processes between production of DNA strand breaks and their repair by a limited pool of repair enzymes, and more recently, the reciprocal time model (Fowler, 1999).

A number of cases have been found where the RMR and the LPL models do not correctly predict surviving fraction for different cellular systems. In particular, Sachs *et al.* (1990) found that these models tend to overestimate the surviving fraction of cells at low doses per fraction and underestimate it at large fractional doses. Stewart (2001) indicated that, although these models are based on some form of mechanistic interpretation of the repair kinetics (e.g. the assumption of mono-molecular (first-order) or bi-molecular (second-order) repair mechanisms), they do not take into account the changing structure of chromatin during or after exposure. This influences the initial yield of radiation-induced DNA damage as well as the subsequent rate of damage repair (Stewart *et al.*, 2000).

Other mechanistic models, both stochastic (Albright, 1989; Brenner, 1990; Dikomey, 1990; Hawkins, 1998; Kellerer *et al.*, 1972; Kruglikov, 1992; Sachs *et al.*, 1990) and non-stochastic (Curtis, 1986, 1989; Goodhead, 1985; Nilsson *et al.*, 1990; Ostashevsky, 1993; Ward, 1985), have been proposed that are able to incorporate many of the effects related to chromatin structure and cell cycling after irradiation by using a large amount of adjustable parameters.

The usefulness of mechanistic models is based on their ability to postulate the existence of specific repair pathways characterised by assumed patterns of repair rates. One of the simplest examples among the non-stochastic mechanistic models is the RMR model

(Tobias, 1980), which starts from a general differential equation embedding first- and second-order kinetic principles, i.e.

$$\frac{dU(t)}{dt} = -\lambda U(t) - \kappa U(t)^2 \quad (7.1)$$

Where $U(t)$ represents the number of uncommitted lesions that can either be repaired or misrepaired, the latter possibility leading to mutation, chromosome abnormalities or cell death. No specific lesion is pre-assumed to follow any of these two paths as all lesions are treated equally. Also, λ represents the linear self-repair coefficient and κ is the coefficient for cooperative repair involving the interaction of pairs of U lesions. Equation (7.1) assumes that any repair process in the cell will follow either a first-order repair process ($\lambda U(t)$) or a second-order repair process ($\kappa U(t)^2$). Other processes may occur simultaneously and will require the incorporation of new terms into Equation (7.1). However, Equation (7.1) can be considered a generalised expression of repair kinetics. Curtis' LPL model uses this same interpretation but, while the RMR model did not pre-established pathways for each type of damage, the LPL model assumed there are two types of damage (lethal and potentially lethal), which commit damaged cells to follow different repair paths. This differentiation between damage types and repair paths is reflected in the introduction of an extra reaction-rate parameter, which reflects the rate at which potentially lethal damage is converted into lethal damage, i.e.:

$$\frac{dn_{PL}(t)}{dt} = \eta_{PL} \dot{D} - \varepsilon_{PL} n_{PL}(t) - \varepsilon_{2PL} n_{PL}^2(t) \quad (7.2)$$

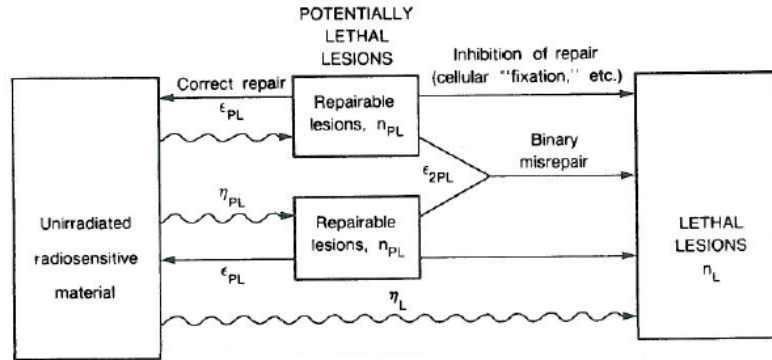
$$\frac{dn_L(t)}{dt} = \eta_L \dot{D} + \varepsilon_{2PL} n_{PL}^2(t) \quad (7.3)$$

In Equations (7.2) and (7.3), $n_{PL}(t)$ and $n_L(t)$ respectively correspond to the number of potentially lethal lesions and lethal lesions at a time t , η_{PL} and η_L correspond to the formation rate of lethal and potentially lethal lesions respectively; and ε_{PL} and ε_{2PL} are the respective rates per unit of time of correct repair and binary misrepair. Thus, compared to the RMR model, which involves only two parameters, five parameters are

needed in order to allow for an extra repair path¹. It is therefore possible to see how rapidly the number of parameters increases when more repair paths are considered. Other models of similar characteristics to the RMR and the LPL have been presented with the common characteristic that all of them lead to the standard LQ formalism at low acute/protracted doses. In the case of the LPL model, the survival equation obtained for the approximation of low doses delivered at high rates is:

$$-\ln S = (\eta_L + \eta_{PL} e^{-\epsilon_{PL} t}) D + \frac{\eta_{PL}^2}{2 \epsilon_{PL} / \epsilon_{2PL}} (1 - e^{-\epsilon_{PL} t})^2 D^2 \quad (7.4)$$

¹ As a matter of fact, the reaction-rate equation of the LPL model for the lethal damages (Equation (7.3)) seem to be incomplete as it does not include the contribution from inhibition of repair pathways (cellular “fixation”, etc.) which is, however, included in the diagram on pg. 255 of (Curtis, 1986):



If *correct repair* rate and the *fixation repair* rate are assumed to be different, an independent factor should have been added to the reaction rate equations to account for damage fixation. This fixation pathway has been however included in the reaction-rate equations of the Microdosimetric-Kinetic model produced by Hawkins (1998).

$$\frac{dn_{PL}(t)}{dt} = k_d \dot{D} - (a + c) n_{PL}(t) - 2b_d n_{PL}^2(t)$$

$$\frac{dn_L(t)}{dt} = \lambda_d \dot{D} + a n_{PL}(t) + b_d n_{PL}^2(t)$$

Where k_d and λ_d are equivalent to η_{PL} and η_L respectively, c is equivalent to ϵ_{PL} , b_d is equivalent to $\epsilon_{2PL}/2$, and a is the new factor accounting for the fixation pathway. This model arrives, after the low dose approximation, to the LQ equation with α and β defined in similar terms of those in the LPL model. Hawkins’ model has however the advantage of including microdosimetric quantities that have been measured previously by other authors (Kellerer *et al.*, 1972; Rossi *et al.*, 1996; etc...) and that allow the model different radiation conditions such as the change in radiation quality, low-LET contamination on high-LET beams, etc... It is also capable of incorporating chromatine structure and cell cycle effects reaching a total number of 9 parameters (Hawkins, 2005).

Once the survival LQ equation has been derived, it is common practice to fit these models to survival data and, from the resultant values of α and β , to reach conclusions on the role of each pathway in each laboratory condition in which the data has been extracted. However, when the number of parameters is large, as it is the case shown for the LPL model, it is difficult to arrive at any conclusion without hypothesising on the individual values of the parameters contributing to α and β , a step which can compromise the reality represented by the model. It is for this reason that various authors (Stewart, 2000; Sachs *et al.*, 1997) have recognised that the validity of such models should not rest only on results of goodness-of-fit tests to survival data for acute or protracted irradiation. Rather, in the case of models using large number of parameters, it is probably best to prove the existence of the relative importance of the different repair pathways via repair kinetic data, where the number of different types of DNA damage (SSB, DSB of different complexities, chromatine aberrations, etc...) are plotted against repair time (i.e. time elapsed from the end of the exposure to radiation). Isolation of the different types of damage in order to study the repair pathways involved with them can only be achieved by irradiating *in-vitro* systems under very controlled laboratory conditions. But even under strictly controlled experimental conditions, Fowler (1999) has noted “... *if data on SSB repair were contaminated with even a small proportion of DSBs, the slower repair for DSBs would dominate the repair curves as time increased, and would demonstrate second-order kinetics over a major part of the recorded repair time. Since there are uncertainties about exactly what is being measured by various methods, it is probably unwise to be too dogmatic about the purity of the data on SSB repair...*”; and then he follows by saying: “...*Even 10 % of a slow component of repair can dominate...(the data)...if the other components are much faster...*”. According to this, experimental conditions would be more difficult to force on *in-vivo* systems (animal and clinical) where SSBs and DSBs will not be isolated and where the reaction to radiation is dictated, not only by the intra-cellular kinetics, but also by extra-cellular processes (e.g. low-dose hyper-sensitivity (Joiner *et al.*, 1996), bystander effect (Prise *et al.*, 2003), etc...). From these considerations we could suggest that different models should be applied to different data sets because, in particular, the more controllable the conditions in which the data is produced the lower the number of assumptions needed to be made and the larger the number of parameters that can be used. *In-vivo* tissue repair kinetic data (which is the closest case to clinical studies)

should therefore be better described by models with the lesser number of parameters where fewer assumptions are required. Sachs *et al* (1997) suggest that given the fact that most repair pathways lead to the same dependence of response on dose and/or dose-protraction as given by the standard LQ formalism, it is feasible to recognise which pathways are dominant for the biologically important endpoints and then study their relevant kinetics in order to use these as being the representatives of the system under study. Obviously, the kinetics of the dominant repair pathway will be the dominant repair kinetic; hence, we could establish the following working hypothesis: *if there is a dominant repair process, the use of its kinetic equations alone to describe the overall repair of our system is a good approximation*. The real problem is how to identify the dominant repair pathway among the possibly many intervening processes.

Fowler (1999) has proposed a method to recognise those cases in which second-order kinetics dominates the repair process. This approach has the advantage of not relying on survival curves of acute irradiation to test the validity of the model; instead, the model relies on evidence of linearity in the decrease of the proportion of un-repaired lesions with time to justify its validity. This may be advantageous for two different reasons, (i) linear regression on repair data is always more reliable than non-linear (exponential and polynomial) regression to survival data; (ii) regression on survival data cannot separate out the contribution from the different repair processes to the final biological end-point.

Also, if one assumes that the repair kinetics of the DNA damage produced by different radiation qualities involve different repair paths, it follows that each model will fit (with differing degrees of fidelity) the data produced from the same biological system exposed to different radiation qualities. Therefore, a good fit to this data will only be achieved by using complex mechanistic models. However, is it still possible to fit repair data produced by different radiation qualities assuming that a single², dominant, repair process can describe them all for the biologically relevant endpoint? In the following chapter we will show how this is possible using a modified version of the reciprocal repair model proposed by Fowler (1999; 2002).

² As we will see later in this chapter, as high-LET radiations produce a much higher percentage of a particular type of DNA damage (i.e. DSB), it is more likely that the repair process after high-LET irradiation is mostly dominated by those repair pathways related to that type of damage.

7.2. The reciprocal repair (RR) model: model revision and preliminary analysis

As it has been indicated above, there are four main categories in which repair models tend to fall into:

- i) Mono-exponential models (repair process follows first order kinetics only, where the main assumption is that there is an unlimited number of repair entities to deal with radiation assaults on DNA).
- ii) Bi-exponential models (two different repair processes – with fast and slow rates each – each following first order kinetics).
- iii) Reciprocal repair (also called reciprocal-time) models (repair process follows second order kinetics only, where, in contrast to first-order repair models, it is assumed that there is only a limited pool of repair entities to deal with the DNA assaults).
- iv) Repair saturation models (which assume second-order repair kinetics with the additional assumption that repair rate is dose-rate dependant – i.e. the rate of repair per lesion is dependent on the number of lesions present assuming a linear relationship between dose and number of lesions).

The advantages and disadvantages of each of these types of models have been briefly mentioned before and different references can be found where the fitting of these models to the data is compared (Fertil *et al.*, 1988; Thames, 1989; Bradford *et al.*, 1994).

We will be concerned with the use of reciprocal repair models, which were used for repair kinetics analysis for the first time by Bradford *et al.* in 1994 and then reintroduced independently by Fowler in 1999. Fowler proposed that, whenever first-order (repair) and second-order (misrepair) processes occur together and in competition (as they do when considering biphasic repair) then, if the half-time of the later is much longer than that of the former, the repair process will be dominated by the second-order

repair kinetics. Under these circumstances, the biphasic and the second-order repair models should be very similar to each other. It is in this case, when the working hypothesis of describing the whole repair process on the basis of it being only second-order repair should be a good approximation, that the reciprocal of the proportion of damage should be seen to increase linearly with increasing time allowed for repair.

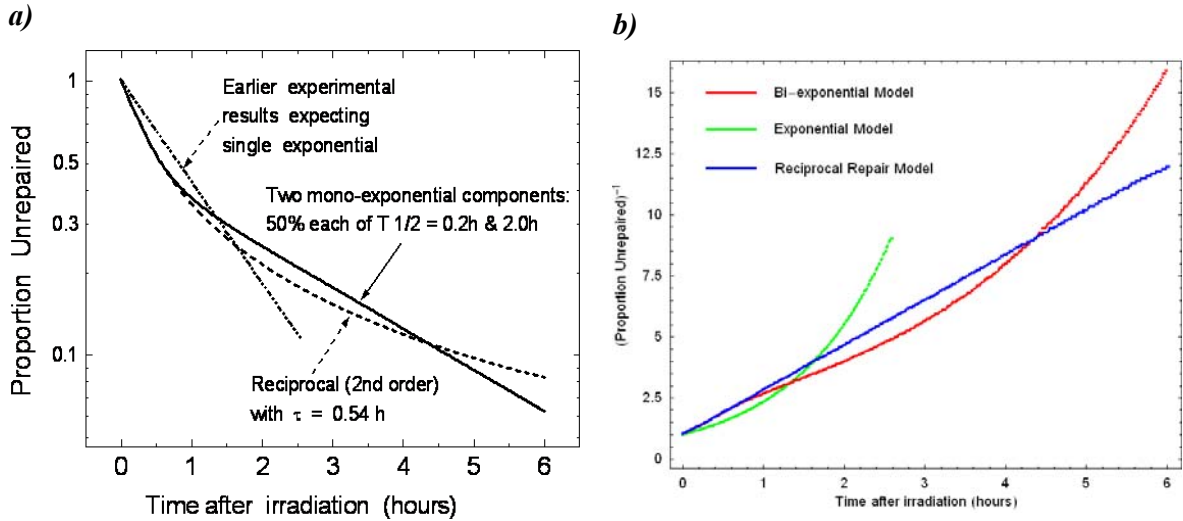


Figure 7.1: Left - graphical comparison between the mono-exponential, bi-exponential and reciprocal repair models, showing their differences in a log-linear coordinate system. Right – the same models are compared for the reciprocal of the proportion of unrepaired damage.

The excellence of the fit of straight reciprocal-repair lines found by Fowler in many different DNA experiments can be considered sufficient justification to think that the role of second-order repair kinetics has been underestimated and needs to be reviewed.

There is however a critical point that needs to be clarified before explaining the theoretical basis of the reciprocal model and which could be considered as a weakness of it. Unlike other purely mechanistic models, the reciprocal repair model assumes as a starting point that the relationship between dose and effect is given by the standard LQ formalism, rather than arriving at it by working out the average rate of lethal lesions per-cell and then obtaining the surviving fraction of cells assuming that lethal lesions are distributed between cells according to a Poisson distribution. This, however, should not be considered a weakness of the model, as other models only assuming first-order

kinetics, such as the widely used Incomplete Repair model (Thames, 1985) are proposed under the same assumption of validity of the LQ model.

7.2.1. Theoretical considerations relating to the Reciprocal Repair model.

Second order repair models assume that, for each number of lesions on a DNA strand there has to be the same number of opposite strand ends to produce repair. Thus, allowing the same probability of rejoining for each possible combination of DNA strand ends, we arrive at the conclusion that the instantaneous rate of repair is given by,

$$\frac{dn}{dt} = -Cn^2 \tag{7.5}$$

Where C is the appropriate rate constant. Figure (7.2) explains this equation in more detail:

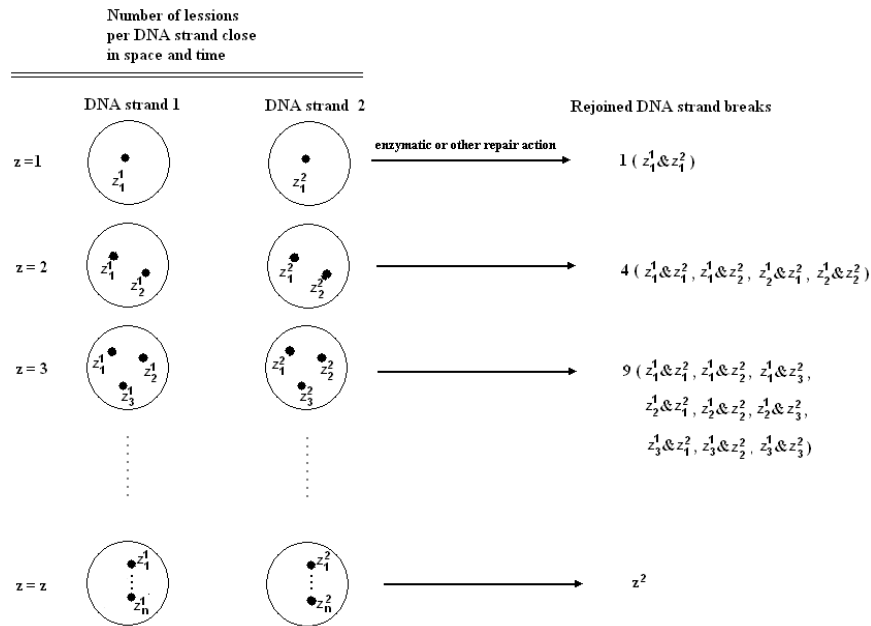


Figure 7.2: Repair dynamics relevant to Equation (7.5). Each dot inside the circle represents a ‘loose end’ of one strand. For repair to exist there has to be a complementary end to ‘tie up with’. When there are multiple ends, any combination of end-rejoining is equally probable.

The solution of Equation (7.5) once the differential equation has been integrated for an initial value of ‘loose ends’, n_o , given as:

$$p = \frac{n_t}{n_0} = \frac{1}{1 + n_0 C \cdot t} = \frac{1}{1 + zt} \quad (7.6)$$

Where n_t is the number remaining at time t and where $z (= n_0 C = 1/\tau)$ is a repair constant, with units of h^{-1} . τ represents the *first-half* time of repair of the system under study. An important remark about this model made by Fowler (1999; 2002), and Dale (1999) is the fact that it seems to predict that the first half-time decreases (i.e. the repair rate increases) as the initial damage (n_0) increases, which is equivalent to saying that *repair rate increases with dose*. But experimental evidence has consistently proven otherwise, suggesting the independence of repair rate and dose, which means the rate C must decrease in direct proportion to the increase of n_0 , and this is consistent with the condition of enzyme saturation (see Dale (1999) for a more in-depth discussion).

This model has been applied by Fowler (1999; 2002) to an extended number of experimental DNA repair data existing in the literature for both, cellular and animal tissue. Fowler analysed the goodness of fit of the RR model by means of Pearson's correlation coefficient (r) value of the weighted regression line used to fit the reciprocal repair data, but no reference was given to the goodness of fit achieved with any other model other than the mono-exponential repair model. However, if after analysing the goodness of fit of different models most of the 'best-fit' τ are obtained from the same model, this could be considered as a strong indication that the model is describing repair kinetics generally better than any other.

The models used in this work to compare with the reciprocal repair (RR) model are the mono-exponential model, due to its extended use in clinical radiobiology, and the bi-exponential model, which is potentially assumed (because it has more variable parameters) to be always more precise than either of the other two. Hence, it is predicted that the goodness of fit produced by the RR model will be better than the mono-exponential model but worse than the bi-exponential model.

Table 7.2 shows the resultant first-half time obtained from the reciprocal repair, the mono- and bi-exponential models (Column 3, 'Recalculated τ using different models')

and compares the results with the half-life proposed by the original authors of the data (Column 2, 'Reported τ by original author'). In order to ensure that the statistical analysis is based on good and reliable data (manually digitised from Fowler's papers) the first-half life values, the 95% CI and the Pearson's regression coefficient (r) calculated in this work were compared with those obtained by Fowler using the reciprocal repair model. For this purpose, each row of the reciprocal repair column was split in two, with Fowler's results on the top and the present results at the bottom of each table cell.

Similarly to Fowler (1999; 2002), all the results shown in column 3 of Table 7.2 have been obtained applying weighted linear regression (in the case of the mono-exponential and the reciprocal repair analysis), and weighted non-linear regression (in the case of the bi-exponential analysis). The weight applied to each point corresponded to the inverse proportion of the standard error (σ^2) associated with the data point. This means that a small error on the original data would produce a large error on the reciprocal data. Therefore, according to Fowler (1999; 2002), a fair fit to the reciprocal data requires to provide a higher weight to those data points with less standard error than those with larger standard error, and for that reason each reciprocal repair data point is weighted in inverse proportion to its standard error. The following table shows the transformations applied to the data in order to use linear regression on it, as well as the weighting scheme applied on the transformed data:

	Original Data	Transformed Data	Weighting scheme on transformed data	Regression function applied to transformed data
Reciprocal Repair	(x, y)	$\left(x, \frac{1}{y}\right)$	$\frac{1000y^4}{\sigma^2}$	$1 + ax$
Mono-exponential Repair	(x, y)	$(x, \log[y])$	$\frac{1000y^2}{\sigma^2}$	$\log[100] + ax$
Bi-exponential Repair	(x, y)	(x, y)	$\frac{1000}{\sigma^2}$	$me^{ax} + ne^{bx}$

Table 7.1: Regression functions and weighting schemes used in analysis with σ representing the standard error of each measurement.

The functions fitted to the original data for the reciprocal repair and the mono-exponential repair analyses were then $\frac{100}{1 + ax}$ and $100e^{ax}$ respectively. As shown in

Table 7.2, the non-linear regression analysis performed with the bi-exponential function would not always converge to sensible values of a and b . In such cases ‘??’ has been entered in the appropriate box.

Biological System		Reported τ by original auth.		Recalculated τ using different models			Original data Ref.		
				Reciprocal Repair		Mono-Exp		Bi-Exp	
CELLULAR				τ	95% CI	r			
SSB	V79	Fast: 6-8''		8.7''	(8.2-9.1)''	0.996	76.22''	Fast: 9.93'' Slow: 216.28''	Dikomey <i>et al.</i> 1995
		Slow: 200±30''		8.84''	(8.04-9.83)''	0.994			
	EAT	Fast: 6-8''		7.5''	(6.8-8.4)''	0.984	75.03''	Fast: 8.78'' Slow: 219.47''	"
		Slow: 190±30''		8.33''	(7.54-9.30)''	0.993			
	CHO	Fast: 6-8''		5.85''	(5.63-6.10)''	0.992	60.18''	Fast: 10.62'' Slow: 231.84''	"
		Slow: 220±30''		5.40''	(4.86-6.09)''	0.994			
DSB	LY-R	Total < 90''		26.1''	(24.1-28.1)''	0.981	62.72''	Fast: ?? Slow: ??	Wlodek <i>et al.</i> , 1988
				34.1''	(27.4-45.0)''	0.987			
	CHO-Exp.	Fast: 7.5'' (6.9-8.2)		13.0''	(11.5-14.9)''	0.980	51.37''	Fast: ?? Slow: ??	Metzger <i>et al.</i> , 1991
		Slow: 67'' (60-76)		13.8''	(11.9-16.3)''	0.980			
	GM38	Total < 2'		0.67'	(0.54-0.82)'	0.890	2.12'	Fast: 1.07' Slow: 5.78'	Schlesing <i>et al.</i> , 1984.
				0.85'	(0.70-1.09)'	0.972			
ANIMAL									
Spinal Cord	Mono-exp: 1.5' (1.3-1.8)'		2.7'	(2.4-3.1)'	0.983	9.26'	Fast: 3.30' Slow: 62.12'	Ruifrok <i>et al.</i> , 1993	
			2.68'	(2.31-3.19)'	0.902				
	Fast: 0.7' Slow: 3.8'		2.8'	(2.6-3.0)'	0.994	4.41'	Fast: 0.50' Slow: 17.57'	Ang <i>et al.</i> , 1992	
			2.53'	(1.52-7.56)'	0.867				
Mouse Lung	Mono-exp: 0.83' (0.76'-0.92')		0.9'	(0.73-1.08)'	0.948	2.01'	Fast: 0.17' Slow: 2.85'	Travis <i>et al.</i> 1993	
	Bi-exp:	F: 0.4' S: 4.01'	0.92'	(0.78- 1.15)	0.659			Van Rongen <i>et al.</i> , 1993	
	Mono-exp (>2Gy): 0.83' (0.76'-0.92')		0.9'	(0.6-1.2)'	0.867	2.19'	Fast: ?? Slow: ??	Parkins <i>et al.</i> , 1988	
	Bi-exp (<1.1Gy):	F < 0.4' S $\approx \infty$	1.12'	(0.70-2.72)'	0.842			"	
Skin	Rat			4.2'	(3.9-4.6)'	0.997	8.56'	Fast: ?? Slow: ??	
				4.26'	(3.81-4.83)'	0.997			
	Mouse			2.6'	(1.9-3.3)'	0.876	5.12'	Fast: 1.73' Slow: 5.47'	
				3.54'	(2.79-4.84)'	0.968			
	Pig			0.62'	(0.45-0.82)'	0.901	1.60'	Fast: ?? Slow: ??	
				0.86	(0.51-2.89)	0.959			

Table 7.2: (From previous page) Results of the analysis of repair kinetics assuming a mono-exponential, a bi-exponential and a reciprocal repair process. The original first-half life calculated by the original authors has been included for comparison purposes. The values calculated by Fowler (1999; 2002) are displayed and compared to those calculated in this work in order to calibrate the quality of the data used for the mono- and bi-exponential models. (’ – hours; ” – minutes)

The average difference between the τ values calculated by Fowler and those calculated here is 12.3% (0.75-27.91), which was considered sufficiently small to assume the method of data extraction from Fowler’s paper was accurate enough. Once the goodness of the data was calibrated, the three models were fitted to it. The analysis of the goodness of fitness of each model was based on:

- Pearson’s correlation coefficient, as an absolute measure of goodness of fitness in the case of the lineal models.
- the Akaike’s Information Criteria (AIC) (Burnham *et al.*, 2002), which is used in information theory to determine which model is more likely to be correct and quantify how much more likely it is. The AIC factor can be computed using the following equation, when the scatter points around the model curve is assumed to follow a Gaussian distribution:

$$AIC = N \cdot \ln\left(\frac{SS}{N}\right) + 2K + 2K \frac{K+1}{N-K-1} \tag{7.7}$$

Where N is the number of data points, K is the number of parameters fit by the regression plus one, and SS is the sum of the square of the vertical distances of the point from the curve. The model with lower AIC value is more likely to be correct.

Table 7.3 summarises the models’ equation, the Pearson’s correlation coefficient and the AIC values corresponding to the data in Table 7.2.

Biological System		Mono-Exponential		Bi-Exponential		Reciprocal Repair	
CELLULAR		AIC	r	AIC		AIC	r
SSB	CHO	$100 e^{-0.0167 x}$		$87.81 e^{-0.094 x} + 6.57 e^{-0.0043 x}$		$100 (1 + 0.185 x)^{-1}$	
		203.76	0.864	113.83		118.81	0.987
	V79	$100 e^{-0.0131 x}$		$96.20 e^{-0.1007 x} + 11.64 e^{-0.0046 x}$		$100 (1 + 0.113 x)^{-1}$	
		197.59	0.881	104.64		126.56	0.994
	EAT	$100 e^{-0.0133 x}$		$93.60 e^{-0.114 x} + 11.23 e^{-0.0046 x}$		$100 (1 + 0.120 x)^{-1}$	
		181.13	0.862	106.03		112.61	0.993
DSB	LY-R	$100 e^{-0.0159 x}$		OVERFLOW		$100 (1 + 0.029 x)^{-1}$	
		93.69	0.968			79.81	0.986
	CHO	$100 e^{-0.0195 x}$		OVERFLOW		$100 (1 + 0.073 x)^{-1}$	
		120.9	0.972			100.22	0.980
	GM38	$100 e^{-0.471 x}$		$74.54 e^{-1.937 x} + 27.16 e^{-0.173 x}$		$100 (1 + 1.171 x)^{-1}$	
		80.54	0.969	71.32		74.31	0.972
ANIMAL							
Spinal Cord	$100 e^{-0.108 x}$		$77.56 e^{-0.303 x} + 16.14 e^{-0.016 x}$		$100 (1 + 0.323 x)^{-1}$		
	97.61	0.848	70.53		66.35	0.902	
	$100 e^{-0.108 x}$		$52.94 e^{-2.001 x} + 47.30 e^{-0.057 x}$		$100 (1 + 0.395 x)^{-1}$		
	55.72	0.810	53.30		49.62	0.867	
Mouse Lung	$100 e^{-0.497 x}$		$42.35 e^{-5.654 x} + 60.22 e^{-0.351 x}$		$100 (1 + 1.078 x)^{-1}$		
	130.55	0.810	115.63		119.77	0.659	
	$100 e^{-0.458 x}$		$27.52 e^{-0.5205 x} + 73.10 e^{-0.520 x}$		$100 (1 + 0.893 x)^{-1}$		
	55.80	0.914	58.33		61.51	0.841	
Skin	Rat foot	$100 e^{-0.117 x}$		OVERFLOW		$100 (1 + 0.235 x)^{-1}$	
		49.07	0.974			33.21	0.997
	Mouse	$100 e^{-0.195 x}$		$11.08 e^{-0.571 x} + 89.50 e^{-0.179 x}$		$100 (1 + 0.282 x)^{-1}$	
		60.27	0.995	69.99		76.23	0.968
	Pig	$100 e^{-0.010 x}$		OVERFLOW		$100 (1 + 0.0194 x)^{-1}$	
		54.74	0.894			48.78	0.959

Table 7.3: (From previous page) Corresponding model equations used to fit the repair kinetic data presented in Fowler (1999; 2002) and their associated AIC value. The r and AIC values suggest a better fit of the RR or biexponential models to the data than the mono-exponential model.

According to Table 7.3, the lower AIC values usually correspond, as predicted, to the bi-exponential model in the case of cellular studies, with the overall second best model being the RR model and the mono-exponential model third. The correspondence between the AIC factor and the Pearson's correlation factor is also very good for the cellular data. In some cases, the fit to the data using non-linear weighted regression made the calculation software³ overflowed during the computation.

The results are similar in the case of the animal studies, where in most of the datasets the worst predicting model is the mono-exponential model, except for the mouse lungs and mouse skin data where the worst predicting model is the RR model. However, as Fowler (2002) explains in his analysis, both of these two data sets present a bi-exponential behaviour with extremely large slow components (“...indeterminately very long for small doses per fraction” in the case of Parkins (1988)). It is therefore possible that an experiment capable of resolving a larger number of elapsed half-times would have revealed a better fit by the reciprocal repair model, probably because a larger amount of strand breaks would have been scored and which would have improved the statistics of second-order terms. Similarly, in the case of mouse skin, Fowler proposes, as a possible reason for the poor RR fit, the dependence of repair rate with temperature, which would manifest itself more severely in skin due to large ambient changes in temperature.

³ Mathematica® v4.1

These results indicate the practical feasibility of using second order kinetics to describe repair processes, both in cellular and animal tissues. One can conclude that, according to these results, it is over simplistic to assume that half-time values derived from models assuming first repair kinetic processes (e.g. Incomplete Repair model) will always be correct⁴. *These models do not distinguish between the different features of initial breaks formed by radiation as they assume that all such breaks are identically restituted by the repair mechanisms.* Conversely, bi- or multiphasic models assume the existence of slower and faster components of rejoining due to the varying action times of enzymes in the biomolecular reactions which repair DNA damage of various complexities. It is for this reason that any model based on repair enzyme-DNA complex and competition between rejoining pathways should reflect naturally the slowing down on the repair curve characteristic of multiphasic processes (Cucinotta *et al.*, 2000).

⁴ It is common practice in clinical situations for radiobiologist to use the IR model to calculate repopulation factors to compensate for unplanned treatment gaps, i.e.

$$h(\theta) = \frac{2}{n} \left(\frac{\theta}{1-\theta} \right) \left(n - \frac{1-\theta^n}{1-\theta} \right)$$

Where $\theta = e^{-\frac{0.693}{T_{1/2}}f}$, where $T_{1/2}$ is the half-time of repair and f is the inter-fraction interval.

7.3. Bibliography

- Albright N., *Radiation Research* 118(1):1-20 (1989).
- Ang K.K., Jiang G.L., Guttenberger R., Thames H.D., Stephens L.C., Smith C.D., Feng Y. *Radiotherapy Oncology* 25:287–297 (1992).
- Bradford D.L., Geard C.R. *Radiation Research* 138(3):352-360 (1994).
- Brenner J. *Radiation Research Supplement* 124, S29-S37 (1990).
- Burnham K.P., Anderson D.R. *In: Model Selection and Multimodel Inference – A practical Information-theory approach*, Second Edition, Springer, pp.59-96 (2002).
- Cucinotta F.A., Nikjoo H., O'Neill P., Goodhead D.T., *International Journal of Radiation Biology* 76(11):1463-1474 (2000).
- Curtis S.B. *Radiation Research* 106(2):252-270 (1986). See also Curtis S.B., Erratum, *Radiation Research* 119(3):584 (1989).
- Curtis S.B. *Radiation Research* 106(2):252-270 (1986).
- Dale R.G. *Acta Onologica* 38(7):919-929 (1999).
- Dikomey E. *International Journal of Radiation Biology* 57(6):1169-82 (1990).
- Dikomey E., Flentje M., Dahm-Daphi J. *International Journal of Radiation Biology* 67:269-275 (1995).
- Fertil B., Deschavanne P.J., Debieu D., Malaise E.P. *Radiation Research* 116(1):74-88 (1988).
- Fowler J.F. *Radiation Research* 152(2):124-136 (1999).
- Fowler J.F. *Radiation Research* 158(2):141-151 (2002).
- Goodhead D.T. *Radiation Research Supplement*, Vol. 8, Heavy Charged Particles in Research and Medicine. Proceedings of a Symposium Held at the Lawrence Berkeley Laboratory, University of California, Berkeley, California, May 1-3, pp. S58-S67 (1985).
- Hawkins R.B. *Medical Physics* 25(7):1157-1170 (1998);
- Hawkins R.B. *International Journal of Radiation Oncology Biology Physics* 63(2):529-535 (2005).
- Joiner M.C., Lambin P., Malaise E.P., Robson T., Arrand J.E., Skov K.A., Marples B. *Mutat Res* 358:171–183 (1996).

- Kellerer A.M., Rossi H.H. *Current Topics in Radiation Research Quarterly* 8(2):85-158 (1972).
- Kruglikov I.L. *Radiation Research* 130(1):26-30 (1992).
- Lea, D. E. *British Journal of Radiology* 11: 489-497 (1938).
- Metzger L., Iliakis G. *International Journal of Radiation Biology* 59(6):1325-1339 (1991).
- Nilsson P., Thames H.D., Joiner M.C. *International Journal of Radiation Biology* 57(1):127-142 (1990).
- Ostashevsky J.Y. *International Journal of Radiation Biology* 63(1):47-58 (1993).
- Parkins C.S., Whitsed C.A., Fowler J.F. *International Journal of Radiation Biology* 54:429-443 (1988).
- Prise K.M., Folkard M., Michael B. D. *Radiation Protection Dosimetry* 104(4):347-355 (2003).
- Rossi H. H., M. Zaider, *Microdosimetry and its Applications* (Springer, Berlin, 1996).
- Ruifrok A.C.C., Kleiboer B.J., van der Kogel A. J. *International Journal Radiation Biology* 63:501-508 (1993).
- Sachs R.K., Hlatky L., Hahnfeldt P., Chen P. *Radiation Research* 124(2):216-226 (1990).
- Sachs R.K., Hahnfeld P., Brenner D. J. *International Journal of Radiation Biology* 72(4):351-374 (1997).
- Schlesinger M. F., Montroll E. W. *Proceedings of the Natural Academy of Sciences USA* 81:1280-1283 (1984).
- Stewart R.D. *Radiation Research* 156(4):365-378 (2001).
- Stewart R.D., Shultis J.K., Montelone B.A. Pacific Northwest National Laboratory Report PNNL-13258. Richland, WA 99352, May 30 (2000).
- Thames H.D. *International Journal of Radiation Biology* 47(3):319-339 (1985).
- Thames H.D. *Radiation and Oncology* 14(4):321-327 (1989).
- Tobias C.A., Blakely E.A., Noo F.Q.H., Jang T.C.H. *In: Radiation biology and Cancer Research*. Meyn R. E., Withers H. R. (eds.). New York: Raven Press, p.195-230 (1980).
- Travis E.L., Thames H.D., Watkins T.L., I. Kiss. *International Journal of Radiation Biology* 52:903-919 (1987).
- Ward J.F. *Radiation Research* 104(Suppl.): S103-S111 (1985).

Wlodek D., Hittelman W.N. *Radiation Research*. 115(3):566-575 (1988).

Extension of the Reciprocal Repair Model to high-LET radiations

8.1. General Considerations

8.1.1. Single Strand Breaks production and repair for high-LET radiations

The increasing complexity of DNA damage with increasing LET has been extensively documented by different authors. Two of the first studies on strand breakage by different radiation qualities were those of Christensen (1971) and Neary *et al.* (1972). These authors arrived at opposite conclusions on the efficiency of production of SSB: Christensen found that SSB *decreased* with increasing LET, while Neary found the opposite effect. However, different experimental setup as well as the use of different restricted definitions of LET to calculate the number of relevant events contributing to each type of strand breakage (electron ranges up to 100eV in the case of Neary's work) could have been the reason for the observed differences (Neary *et al.* 1972).

Similarly, Kampf *et al* (1977a; 1977b) found that the rates of SSB production decreased by about 50% over the region of $LET_{\infty} = 1$ to 1000 keV/ μm . In their repair studies they also showed that SSB repair rates remained the same after increasing doses of X-rays and neutrons (up to 40Gy of each), which contradicted some previous analyses made by Ahnström *et al* (1974) as well as that by Tuschl *et al.* (1975) who found a reduced or non-existent repair rate of SSB after neutron doses of 30Gy. Painter *et al.* (1974) found that only 50% of the SSB produced by a 0.03 Gy/decay source of ^{125}I are repaired as compared with the 70-100% repaired ratio for a 300-kV peak X-ray beam delivered at

15 Gy/min. However, for all these studies, different cell lines, incubation conditions and techniques of DNA damage analysis were used.

Along with the line of Ahnström *et al.* (1974), Tuschl *et al.* (1975) and Painter *et al.* (1974), Körner *et al.* (1978) concluded that SSB repair rate is also affected by radiation quality, slowing down as LET increases, up to a point where no SSB repair takes place. An increased yield of unrejoined SSB after high-LET irradiation is also reported for CHO cells, where 20% of the SSB induced by α -particles remained unrejoined after 6 hours compared to only 10% after low-LET irradiation (Cole *et al.*, 1980). Peak *et al.* (1989) showed that the fraction of unrepaired SSB after exposure to different neutron energies and γ -rays, and after long periods of incubation (60-180 min) is slightly higher than those produced by X-rays (see Table 8.1). A comprehensive review of how LET affects the initial yield of base damage, chromosome crosslink and SSB and their repair kinetics has been provided by Gunter *et al.* (1983) and Frankenberg-Schawger (1990).

Cell	Radiation	Dose (Gy)	Repair time (min)	Percentage remaining (%)	Assay Technique	Ref
Human P3 epithelioid	0.85MeV neutrons	6	120	10	Alkaline elution profiles	Peak <i>et al.</i> 1989
Chinese hamster V79	0.85MeV neutrons	6	120	10	Alkaline elution profiles	Peak <i>et al.</i> 1989
Human Fibroblast	14.6MeV neutrons	7	60	10	Alkaline elution profiles	van der Schans <i>et al.</i> 1983
Maurine Leukemia	13MeV neutrons	500	180	25	Alkaline Sucrose gradient	Furuno <i>et al.</i> 1979
Human lymphocytes	14.6MeV neutrons	2	80	< 10	Alkaline Sucrose gradient	McWilliams <i>et al.</i> 1983
Maurine Leukemia	7MeV neutrons	300	30	11	Alkaline Sucrose gradient	Hesslewood 1978
HeLa	Thermal Neutrons	5.3	60	5	Alkaline/Neutral Sucrose gradient	Maki <i>et al.</i> 1986
Maurine Leukemia	gamma	500	180	10	Alkaline Sucrose gradient	Furuno <i>et al.</i> 1979
Human lymphocytes	gamma	2	80	<10	Alkaline Sucrose gradient	McWilliams <i>et al.</i> 1983
Chinese Hamster	X-rays	8	60	0	Neutral filter elution	Radford 1985
Chinese Hamster	X-rays	540	200	3	Alkaline/Neutral Sucrose gradient	Dugle <i>et al.</i> 1976
Maurine Leukemia	X-rays	4	90	0	Alkaline/Neutral Sucrose gradient	Sinclair <i>et al.</i> 1987
Human P3 epithelioid	X-rays	3	90	0	Alkaline elution profiles	Hill 1988

Table 8.1: SSB remaining after repair following different radiations in normal cells and measured using different assay methods (Peak *et al.* 1989).

It is interesting to notice in Table 8.1 how different methods of DNA damage analysis produce similar estimates of the unrepaired fraction of SSB. It is known (Peak *et al.*, 1989; Ahnström *et al.*, 1988) that sedimentation techniques are not accurate in differentiating between true SSB and DSB that express themselves as SSB during the damage analysis. If this is the case, it is possible to think that both techniques (i.e.: *velocity sedimentation techniques* and *filter elution techniques*) arrive at the same or similar numbers because both are equally imprecise when measuring levels of unrejoined SSB. Peak *et al.* (1989) and Chadwick *et al.* (1981) accept this possibility as an explanation of the unexpected experimental findings in some studies on the positive contribution by SSB to cell lethality. This coincides with the fact that many other authors (Barendsen 1979, 1990, 1993, 1994, 1997; Frankenberg-Schawger, 1990; Ward *et al.* 1985; Hesslewood 1978) have found little correlation between RBE for SSB production and chromosome aberration/mutation and cell killing. These end points have been attributed to DSB (Kraft, 1987), so for this reason it can be argued that, *even if we accept that the repair efficiency of SSB is affected by radiation quality, the contribution of SSB to chromosome aberration, mutation and cell lethality is negligible in comparison to that produced by DSB; especially at high-LETs, where the number of DSB is comparable to that of SSB and with different levels of complexity* (Prise, 1994). Frankenberg-Schawger (1990) summarised some of the evidence found in the literature defending and contradicting the involvement of SSB in cell killing as follows:

“ ...

- a) With increasing LET, efficiency for cell killing increases (Fowler 1981), yet the efficiency for SSB induction decreases (Roots *et al.*, 1979; Van der Schans *et al.*, 1983; Sakai *et al.*, 1987)
- b) The rate of rejoining of the majority of SSB is about the same after high- and low-LET radiation (Van der Schans *et al.*, 1983; Sakai *et al.*, 1987) and not related to cellular radiosensitivity (Szumiel, 1981).
- c) The number of SSB induced by hydrogen peroxide via HO radicals and corresponding to those expected from 10Gy of radiation does not result in cell killing of Chinese hamster cells and does not affect cell inactivation by γ -rays (Ward *et al.* 1985).

However, a correlation between unrejoined SSB and cell killing is observed for radiation-resistant and radio-sensitive cell lines (Sakai *et al.*, 1984), for the cell cycle dependency (Sakai *et al.*, 1984), for the LET dependency (Cole *et al.*, 1980) and for pre-irradiation hyperthermia (Clark *et al.*, 1976; Bowden *et al.*, 1981; Lunec *et al.*, 1981; Mills *et al.*, 1981). It remains to be seen to what extent DNA double-strand breaks contribute to the amount of unrejoined SSB (see Ritter *et al.*, 1977; Dikomey *et al.*, 1986; Radford, 1986; Sakai *et al.*, 1987)".

Gunter *et al.* (1983) also defended the hypothesis that, although un-rejoined SSB are not of the same nature as un-repaired DSB they could, with justification, be considered as those which underlie inactivation of mammalian cells. However, Gunter and Schulz present this hypothesis as an unlikely alternative to the hypothesis of DSB being the critical lethal lesion, mainly because of the small correlation between observed cell survival RBE data and induction/un-repairable efficiency of SSB data. Figure 8.1 shows a graphical interpretation of the above remarks:

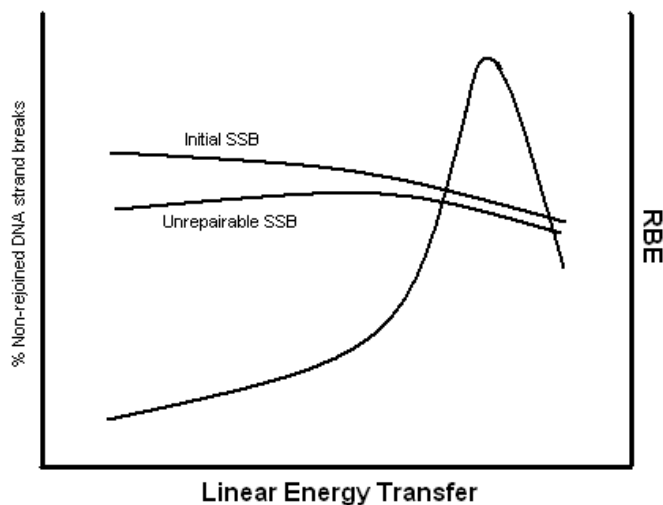


Figure 8.1: Relationship of the rate of induction and repair of SSB with LET and RBE: (i) the rate of induction decreases with increasing LET; (ii) the rate of repair decreases with increasing LET, i.e. the fraction of unrejoined SSB increases with increasing LET; (iii) The correlation between the RBE for unrejoined SSB and the RBE for cell lethality is very small.

8.1.2. Double Strand Breaks production and repair for high-LET radiations

Evidence for the increase on the efficiency of high-LET radiations to produce DSB has been extensively documented (Christensen, 1971; Neary *et al.*, 1972; Lett, 1992; Root *et al.*, 1979). The scope of this section is however to analyse the efficiency of different radiation qualities to produce *unrejoinable* DSB and to investigate the possible correlation between unrejoined DSB and cell killing.

In the previous subsection there have been references to different types of SSB, broadly classified as repairable and unreparable. According to Sakai *et al.* (1987) and Nuñez *et al.* (1996), the same classification can be applied to DSB. The latter author mentions three types of DSB:

- (1) *type I*, those rejoined by the fast component of the kinetic process;
- (2) *type II*, those rejoined by the slow component; and
- (3) *type III*, breaks that are not rejoined at the end of the incubation time (residual damage).

A more detailed classification of DNA strand breaks was introduced by Charlton *et al* (1989), who then used Monte Carlo track simulation to calculate the exact number of each type of strand break. Charlton classified SSB and DSB in three subgroups each: SSB, SSB⁺, 2SSB, DSB, DSB⁺, DSB⁺⁺, where each one of them is defined as indicated in Figure 8.2.

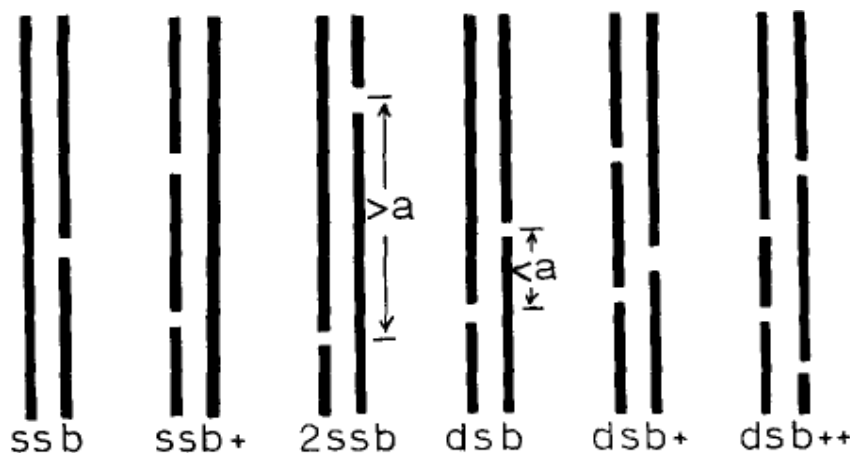


*Figure 8.2: Definition of different types of SSB and DSB (Charlton *et al.*, 1989).*

This classification was extended by Nikjoo *et al.* (1999) who introduced different complexity (or clustering) levels of SSB and DSB, i.e.: $SSB_c = SSB^+ + 2SSB$; $SSB_{cb} =$ sum of SSB containing at least one base damage in the hit region of the DNA; $DSB_c = DSB^+ + DSB^{++}$; and, $DSB_{cb} = DSB_c + DSB_{bd}$, where DSB_{bd} are those DSB with at least one base damage not included in DSB_c . There appears to be no information in the literature on the repair kinetics of each of these individual types of DNA strand breaks, nor about their individual correspondence with cell lethality. Barendsen (1994) studied the correspondence between the RBE-LET relationships for different types of DNA damage (single-track lethal damage, sub-lethal damage and potentially lethal damage (PLD)) with the RBE-LET for reproductive death of cells. These three types of damages were defined by Barendsen as:

- *Single Track-Lethal Damage (STLD)*: damage produced by 10 ionizations (approximately 300eV) in volumes with dimension of about 10nm giving place to two DSBs produced close together. Barendsen hypothesised two types of STLD, i.e.:
 - i. Unrepairable STLD ($STLD_U$), which has a very strong dependence on LET and which is associated with somewhat higher energy depositions locally in small volumes than 300eV in 10-nm-diameter volume.
 - ii. Potentially repairable STLD ($STLD_{PR}$), also called *Potentially Lethal Damage (PLD)*, with a lower dependence on LET (similar to that for SLD and DSB) and associated with energy depositions of the order of 60-150eV in 2-4nm-diameter volumes. Barendsen hypothesised that this component of the STLD could be associated with DSB which remain unrepaired because they are induced at specific locations in the genome or at locations associated with intracellular membranes.
- *Sublethal Damage (SLD)*: Barendsen compared the RBE-LET relationships for sublethal damage and DSBs obtained from Helium ions of different LET on T-1 and V-79 cells at different stages of their cell cycle and concluded that the RBE for DSB is similar to the dependence of the RBE for SLD on

LET (Barendsen, 1990; 1993; 1994). From this similarity of the LET dependence of SLD and DSB, Barendsen hypothesised that lethal damage due to accumulation of sublethal lesions could result from two DSBs induced by two independent ionizing particles, whereby these DSBs initially are induced much further than 10nm apart.

Barendsen (1990) postulated that possible candidates for the biological target involved in cell reproductive death induced by single particles corresponding to STLD were the nucleosome of 11nm diameter or the chromatin fibre of packed nucleosomes of 30nm diameter.

The following figure shows the results obtained by Barendsen and the hypotheses he assumed to identify the different types of damage listed above. The conclusion from this figure is that there is a good correspondence between the RBE-LET relationship for unreparable STLD (STLD_{unr}) and the RBE-LET for reproductive death of cells.

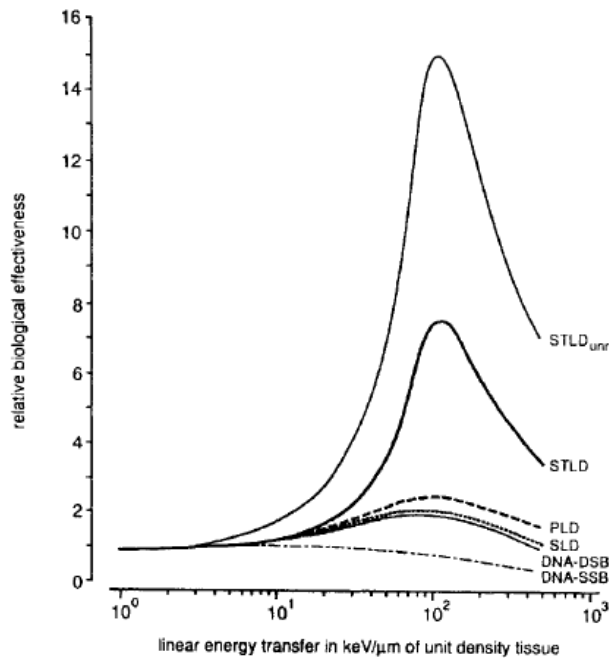


Figure 8.3: RBE versus LET relationships for the different types of damage in mammalian cells which contribute to cell reproductive death: STLD = single track lethal damage caused by individual ionizing particles and their associated secondaries, STLD(unr) = STLD that remains effective after the component of PLD is repaired, PLD = potentially lethal damage, that contributes to the linear as well as to the quadratic term in the dose-response relationship, SLD = sublethal damage that determines the quadratic term in the dose response relationship, DNA-dsb = DNA double-strand breaks, DNA-ssb = DNA single-strand breaks (Barendsen, 1976).

Goodhead (1989) and Goodhead *et al.* (1993) also studied the origin and efficiency to produce lethality of different types of damage that they then classified into four groups, as shown in the following table:

Class	Initial physical damage	Typical energy and target dimensions	Possible target	Frequency* of occurrence (cell ⁻¹ Gy ⁻¹)	Comment
1	Sparse	Few tens of eV within ~2 nm (~1 ionization)	DNA segment	~10 ³	Little biological relevance?
2	Moderate cluster	~100 eV within ~2 nm (~4 ionizations)	DNA segment	~20–100	Characteristic of low-LET; ~repairable
3	Large cluster	~400 eV within 5–10 nm (~15 ionizations)	Nucleosome	~4–100	Characteristic of high-LET; ~unrepairable
4	Very large cluster	~800 eV within 5–10 nm (~30 ionizations)	(Nucleosome)	~0–30	Unique to high-LET; unrepairable; special relevance?

*The range of values is for different radiations, from low-LET X- and γ -rays to high-LET slow α -particles.

Table 8.2: Suggested classes of initial subcellular damage (Goodhead et al., 1993).

It can be concluded from these classifications of initial damage mentioned by Barendsen and Goodhead that unrepairable damage corresponds to clusters of energy deposition formed of DSB pairs separated by 10nm approximately and with energy depositions ranging from 100eV to 400eV (10 to 15 ionizations). This type of damage could correspond to the DSB++, SSB_c, SSB_{cb}, DSB_c, and DSB_{cb} of Charlton and Nikjoo classification.

Similarly to the data presented by Barendsen, other authors have found a correspondence between unrepaired DNA strand breaks and cell lethality. Such is the case of Ritter *et al.* (1977), Goodhead *et al.* (1978) and more recently Eguchi-Kasai *et al.* (1996), but none of the three groups provided information on the specific nature of the unrepaired DNA strand breaks.

Ritter *et al.* (1977) provided the first evidence of a good correlation between the efficiency of exponential (*lethal single hit*) cell killing in T-1 human kidney Todd (1975) and the induction of non-rejoining DNA strand breaks in Chinese hamster V79 S171 cells exposed to the same range of LETs (1-1953keV/um) and measured using alkaline sucrose gradients. In the current framework of the LQ model, lethal single hits are represented by DSB produced by single-track action (termed Type A damage by

Dale (1985)) which are accounted for in the linear term of the LQ model (αd), and it is precisely this component that predominates in the survival curves obtained by Todd (1975). Ritter *et al.* (1977) also found an excellent correlation of non-rejoining DNA strand breaks for Chinese hamster V79 S171 cells with single-hit killing of Chang human liver cells (Todd, 1975) and Chinese hamster CH2B2 cells Skarsgard *et al.* (1967).

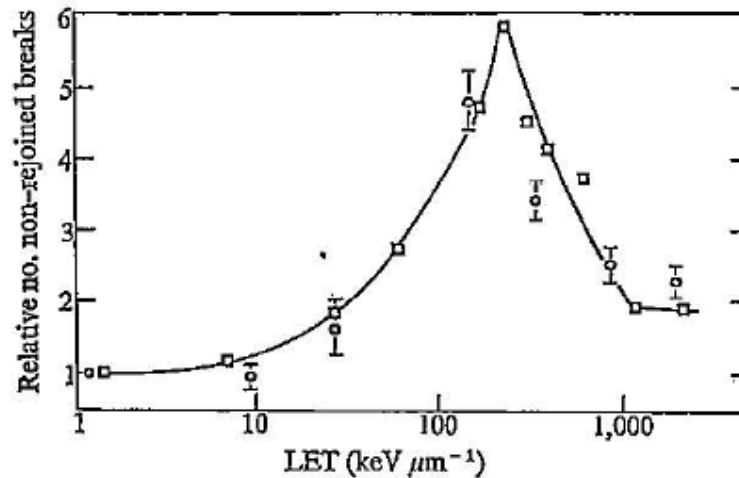


Figure 8.4: Correlation between non-rejoining strand breaks and cell killing efficiency. The data included here is T1-kidney (Todd, 1975) and V79 S171 (Ritter *et al.*, 1977).

Goodhead *et al.* (1978) criticised Ritter's data on the basis that it corresponded to non-rejoining DNA strand breaks (NRB) at high doses (30 - 45Gy) as compared to those responsible for the initial slopes of survival curves (very low doses). They suggested this comparison should be made between the efficiency of NRB production and survival curves at as high a dose as possible, taking into account that cell inactivation measurements underestimate the number of lethal events because one or more lethal events per cell is detected as only one inactivation. At high doses and after correcting for the underestimation of lethal events incurred by survival data, Goodhead *et al.* (1978) found a good agreement between relative efficiencies of NRB production and mammalian (V79) cell inactivation at different LET, except at very high LET, where the correction for the underestimation of lethal events for survival data is very sensitive to small alterations in projected nuclear area and the presence of δ -rays (see Figure 8.5). However, Hawkins (2003) has proposed recently that this observed difference at high-LET could be resolved by considering both, the distribution of lethal events produced

by a single track passing through the sensitive nuclear volume and the distribution of number of tracks passing through this volume, to be both non-Poissonian distributions.

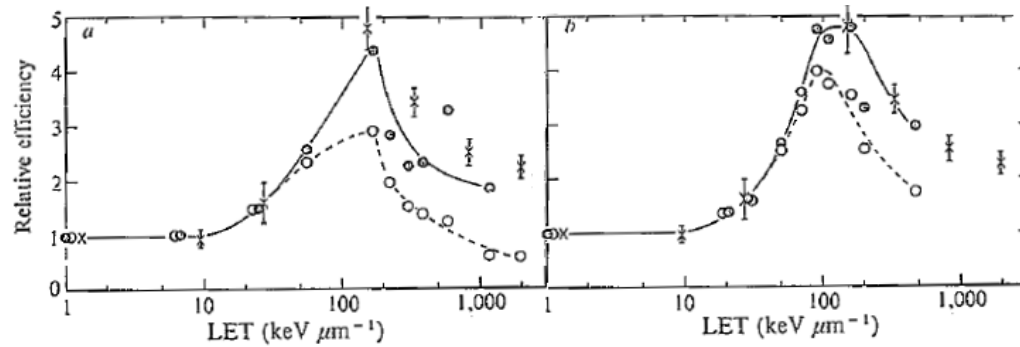


Figure 8.5: Relative efficiencies of non-rejoinable DNA break production (x) and of mammalian cell inactivation (•, o) by radiations of different LET (Goodhead *et al.*, 1978).

Neither Ritter *et al.* (1977) nor Goodhead *et al.* (1978) provided information on the initial yield of DNA strand breaks so it is difficult to assess the effect of repair on the efficiency curves shown by them. Similarly, Monte Carlo simulation studies provide the initial yield of SSB and DSB of different complexities but do not follow their repair kinetics. Barendsen (1990) showed that the initial number of different types of strand breaks, as well as the final number of un-rejoined strand breaks, would ultimately be determined by the radiosensitivity and repair capability of the system under study and he mentioned three main factors affecting radiosensitivity and repair, i.e.

- (i) Radiation quality (LET) effects
- (ii) Oxygen effects
- (iii) Cell cycle effects

(i) *Intrinsic cellular radiosensitivity effects produced by changes on LET*

Different cell lines have different responses to radiation. This difference in response to radiation is called *intrinsic radiosensitivity* as a difference to the more general term of *radiosensitivity* which also agglomerates differences in response to radiation due to time factors (i.e. cell cycle) or external agents of the cell environment (i.e. oxygen, misonidazole, etc...) and it is easily demonstrated by comparing the survival curves produced when different cell lines are exposed to the same type of radiation - the more

radiosensitive the cell, the steeper and more exponential its survival curve becomes¹. This means, in terms of absolute sensitivity parameters, that the linear component of the survival curve becomes more predominant than the quadratic term at all doses. Conversely, radioresistance is usually associated with a relatively weaker influence from the linear component of the LQ model. Several authors have compared the radiosensitivity of mammalian cells with those from simpler micro-organisms such as yeast or bacteria, finding that mammalian cells are always more sensitive than any other cell type (Ritter *et al.*, 1977; Goodhead *et al.* 1978). Different factors have been associated with the change of intrinsic radiosensitivity among cell types (Barendsen, 1990; Hall, 2000), i.e.:

- Mammalian cells are found to be more radiosensitive because they have a larger DNA content, which will increase the chances to produce lethal damage.
- Cells with similar content of DNA are also found to have different radiosensitivity based on the different efficiency of their respective repair mechanisms.
- In higher organisms the alternative modes of cell death (apoptotic versus mitotic) also affect radiosensitivity.

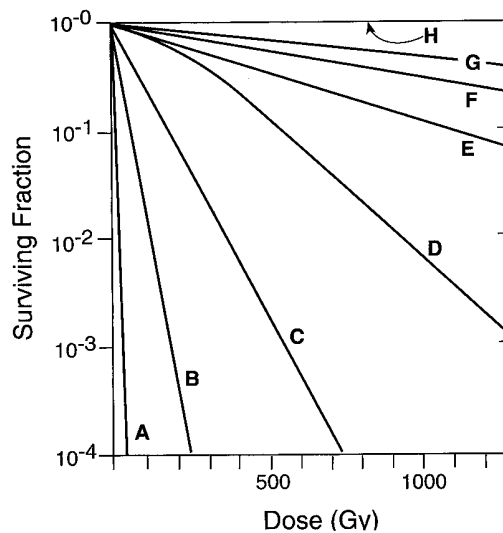


Figure 8.6: Survival curves for mammalian cells and for a variety of micro-organisms: A, mammalian cells; B, *E. Coli*; C, *E. Coli B/r*; D, yeast; E, phage staph E; F, *B. megatherium*; G, potato virus; H, *Micrococcus radiodurans* (Hall, 2000; pp.47).

¹ The word *radiosensitivity* in subsection (i) refers to *intrinsic radiosensitivity*.

The use of different radiation qualities will have an impact on each of these factors as the higher the ionisation density the greater the chance to inflict lethal damage, particularly on cell lines with larger DNA content. Therefore, the intrinsic radiosensitivity for one particular cell line will change when the cell is exposed to different radiation qualities. This is normally explained in terms of inactivation cross sections (σ) (Katz, 1990; Barendsen 1964; Tood, 1967; Goodhead *et al.* 1980; Butts *et al.* 1967), which is defined as

$$\sigma_{in} = AP = 16L\alpha \quad (8.1)$$

where A is the total projected area of the cell nucleus and P is the probability of a single track through this area being lethal, L is the average LET of the radiation used to expose the cell and α is the sensitivity parameter of the linear component of the LQ model.

According to this definition, if the projected area of the cell nucleus for higher organisms is larger than that for simpler micro-organisms, the inactivation cross section for higher organisms will be larger than that for simpler organisms at any given LET. This phenomenon can be observed in Figure 8.7, which also shows the saturation effect of the inactivation cross-section as the particle track cross-section approaches to the size of the nuclear target cross section. After the saturation region, the inactivation cross-section decreases again as a result of the decrease of the diameter of the particle track ('thin down region'). For a more detailed explanation of the different features of these curves, see (Kiefer, 1985; Kraft *et al.*, 1992; Kraft, 1987).

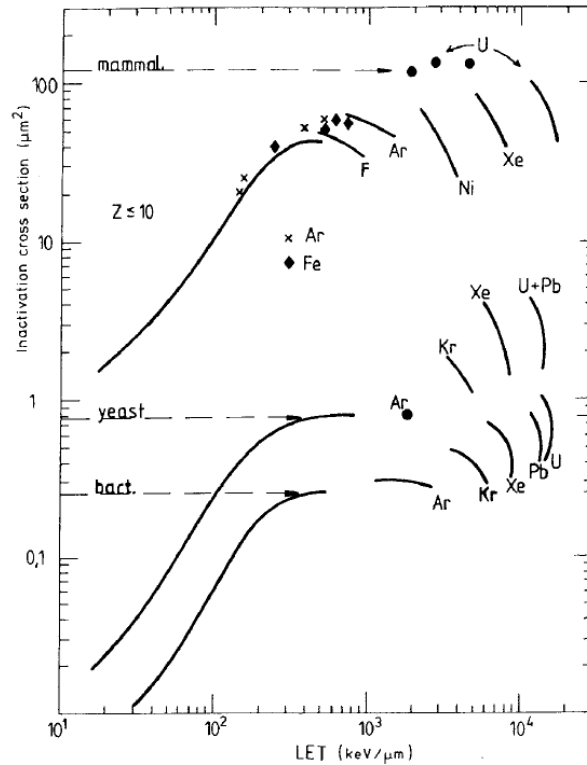


Figure 8.7: *Inactivation cross sections of bacteria (bottom), yeast (middle) and mammalian cells (top) as function of the linear energy transfer (LET) (Kraft et al., 1992).*

Similar studies of sensitivity effects due to changes of radiation quality have been done based on the analysis of the initial number of DSB produced by different types of radiation qualities on cells of similar DNA content and cells of different DNA content. The following figures show the different initial number of DSBs produced by different LETs on different mammalian cells (left) as well as yeast (right).

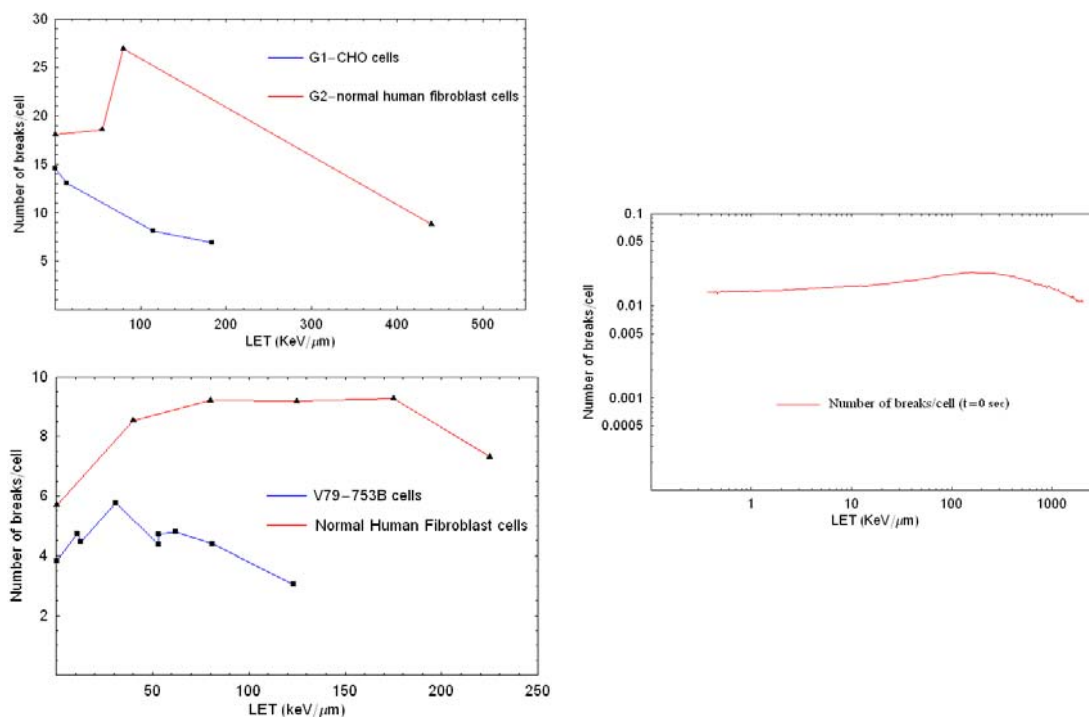


Figure 8.8: Left. Initial number of DSB produced on mammalian cells measured with PCC (top) (CHO - Kawata *et al.*, 2004; Fibroblasts – Goodwin *et al.*, 1994) and FGE (bottom) (Belli *et al.*, 2000; Stenerlow *et al.*, 2000). Right. Number of DSB produced on *E. Coli* (Kozubek *et al.*, 1984).

As we can see in the plots on the left side, the resultant number of DSB is sensitive to the method used to measure them (Premature Chromosome Condensation – PCC, Constant Field Gel Electrophoresis – CFGE, or Pulsed Field Gel Electrophoresis – PFGE), but for the same method applied to cells of similar DNA content the number of DSB of the same order of magnitude. On the right, a plot of the number of DSB using the same measurement method for biological systems of different complexity shows the same differential response as in Figure (8.7) but with a lower magnitude of DSB produced.

As indicated above, cells with similar DNA content irradiated with the same type of radiation may express different radiosensitivity due to their different repair capabilities. A good example of this is demonstrated when comparing the repair kinetics of healthy tissues and tumours. A whole discipline has been created around this topic, with fundamental contributions from authors like Elkind *et al.* (1960), Ellis (1969), Denekamp *et al.* (1974; 1976; 1979), Denekamp (1986; 1989), Barendsen (1982),

Fowler *et al.*(1984), Fowler (1989) and Dale (1985). This difference in the repair of healthy and tumour tissue constitutes the cornerstone which explains the success of fractionation in conventional radiotherapy as has been discussed in Chapters 3 and 5.

The previous paragraphs concern differences of repair kinetics observed for different types of tissues or cell lines. This thesis is however more concerned with studying the different repair kinetics observed, in a particular tissue type or cell line, for different types of radiation. Several authors have studied the dependence of radiation repair processes with LET. Horneck *et al.* (1989) studied the impact of radiation quality on the repair system of bacterial spores by comparing survival of repair deficient strains with that of wild type strains. From the survival curves they derived the correspondent inactivation cross-sections and, from the ratio of the inactivation cross-section of the repair deficient strain to that of the wild type, defined a ‘repair factor’. They then studied the dependence of this repair factor with LET, arriving at the following conclusions:

<i>Phenomenon studied</i>	<i>Biological effects of heavy ions at LET intervals [keV/μm]</i>		
	Low LET (≤ 200)	Intermediate LET (200 < LET < 1000)	High LET (≥ 1000)
Inactivation Cross-section	Dependent on LET	‘Saturation Cross-Section’	Dependent on Z and E (thin down region)
Repair Factor	Decreases with increasing LET	No repair factor	Dependent on Z and E, no repair for E < 10 ⁶ eV/u

Table 8.3: LET dependence of the inactivation cross section and the repair factor associate with particles of different LET ranges (Horneck et al., 1989).

Although these results correspond to bacterial spores, similar results have been found for yeast and mammalian cells (Weber *et al.*, 1993; Taucher-Scholz *et al.*, 1996; Heilmann *et al.*, 1993). In general it is observed that:

- (i) Different types of cell have different repair capability, this being greater for mammalian cells at any given LET than for yeast or spore cells.

- (ii) For all of the three systems studied, the repair capability is severely diminished at high-LET.

The second point means that, for high-LET, the amount of unrepaired DSB remaining at very long times after their creation (unrepairable damage) should be of the same order than the initial amount of DSB. This can be observed in the following figures.

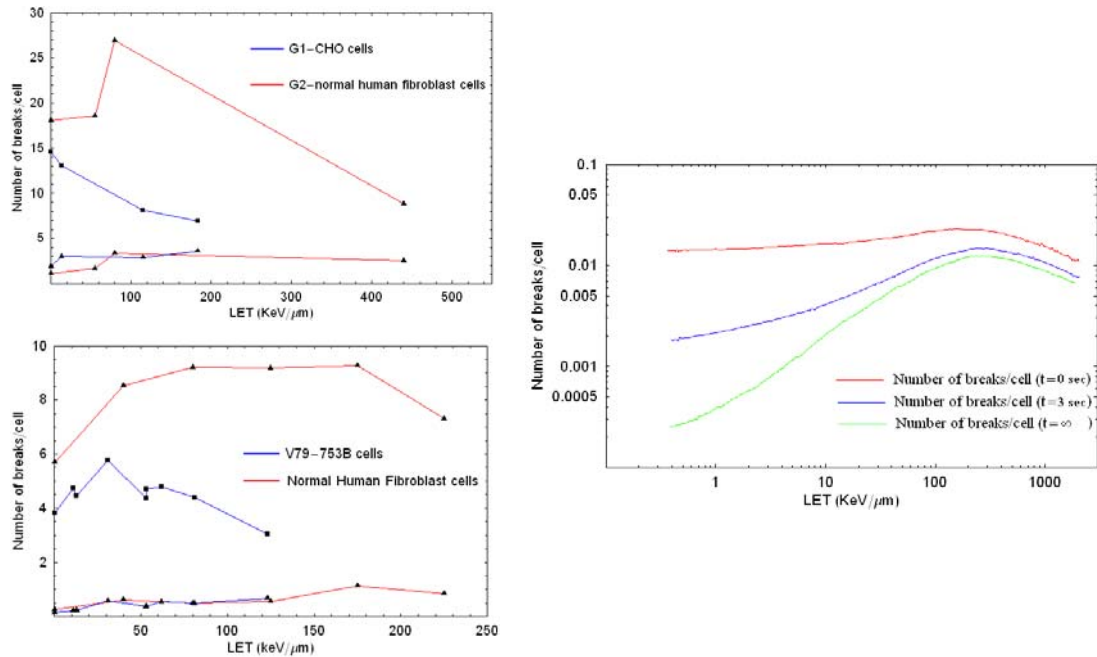


Figure 8.9: Plots showing the initial (top curves in each figure) and the final number (bottom curves in each figure) DSB produced on mammalian cells measured with PCC (top) (CHO - Kawata et al., 2004; Fibroblasts – Goodwin et al., 1994) and FGE (bottom) (Belli et al., 2000; Stenerlow et al., 2000). Right. Number of DSB produced on E. Coli (Kozubek et al., 1984).

It is obvious that the final amount of unrejoined DSB will depend heavily on: (i) the number of DSB created at $t = 0$ sec; and (ii), the repair capability of the cell line considered. It is also clear that the initial number of DSB curves and the final number of DSB curves tend to approach as LET increases. The following table of plots provide with more evidences found in the literature of this behaviour.

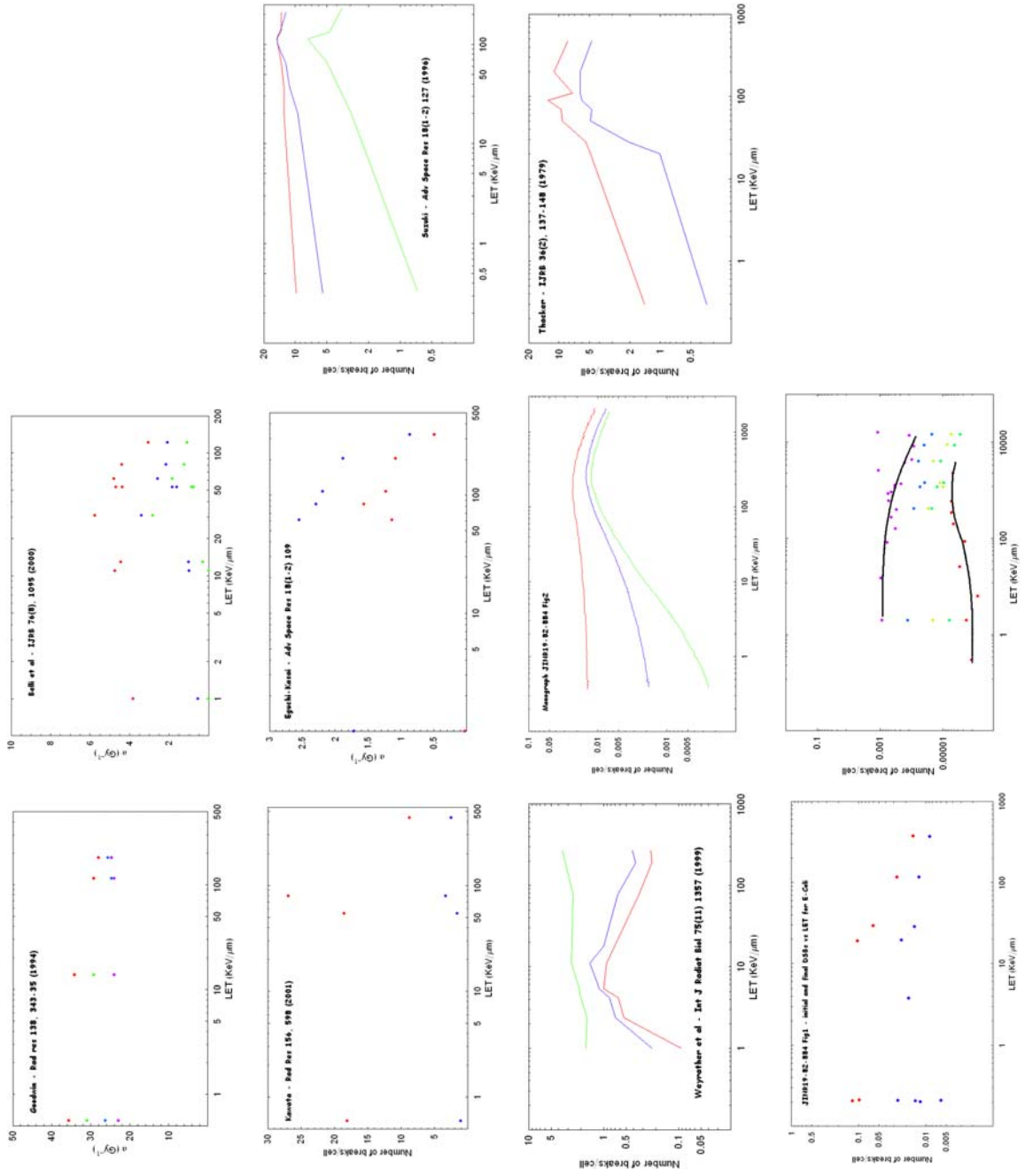


Figure 8.10: Initial and final number of DSB for human, yeast and viral cells exposed to radiations of different LET.

(ii) *Oxygen effects*

From all the known chemical and pharmacologic agents that modify the biological effect of ionising radiations, none is simpler than oxygen, none produces such a dramatic effect and none has such obvious practical implications. One of the main theories explaining how oxygen may alter the radiosensitivity state of a particular biological system is the ‘*oxygen fixation hypothesis*’ (OFH). This theory establishes that, in the presence of oxygen, DNA strands broken by either fast travelling charged particles (direct action of radiation) or ion pairs (indirect action of radiation), may become unreparable (i.e. *fixed*) as oxygen will react with the free radicals present on the broken DNA strands to produce organic peroxide that is a non-restorable form of the target material (see 8.12a). If oxygen was not present at the time of radiation exposure, most of the ionised target molecules could repair themselves and recover the ability to function normally. However, if the oxygen concentration is $\geq 30\text{mmHg}$, the radiosensitivity of the biological system is found to be approximately three times greater than that in hypoxic conditions (see 8.12b).

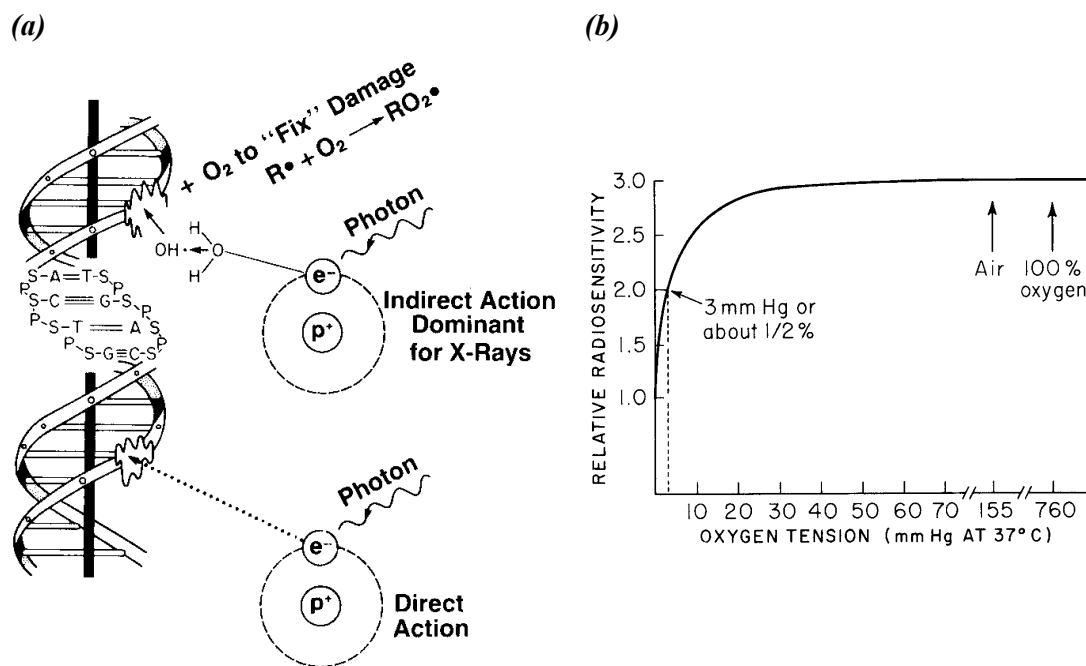


Figure 8.11: (a) *The Oxygen Fixation Hypothesis*; (b) *The dependence of radiosensitivity on oxygen concentration.* (Hall, 2000).

The parameter representing the effectiveness of oxygen is the Oxygen Enhancement Ratio (OER). The OER is defined as the ratio of hypoxic to aerated doses needed to achieve the same biological effect, and will vary with radiation quality and position in the cell cycle as well. Hall *et al.* (1968) has shown that OER values range from 2.3-2.4 during the G₂ phase up to 2.8-2.9 during the S phase, with intermediate values during the G₁ phase.

The following figure shows the relationship between LET and OER for radiation-induced lethal damage to human kidney-derived T-1 cells *in-vitro* (Barendsen *et al.* 1966) and to murine leukaemia P-388 cells assayed *in-vivo* (Berry, 1970; 1971). Although the data for the two cell types are qualitatively similar, there are important differences in detail between them. The OER for tumour cells at low-LET is lower than that for normal cells but tends to the same OER value at high-LET values. This means that, at low-LET, hypoxic tumour cells will be more protected than normal cells, whereas such a protection does not exist in the high-LET range. Also, there is a more rapid decay of OER at high-LET for tumour cells and for normal cells. This means that, at high-LET, hypoxic cells present in the tumour will be damaged more readily than by low-LET radiation, but the degree of injury to well-oxygenated normal tissues will be similar in both cases (Fowler, 1972; Gray, 1961).

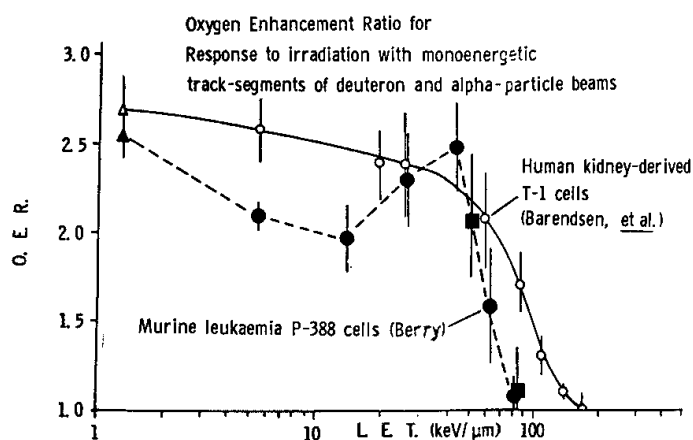


Figure 8.12: OER for irradiation with monoenergetic charged particles as a function of their ionization density. The open symbols represent data for human kidney-derived T-1 cells, while solid symbols represent data for P-388 murine leukaemia cells. Vertical bars represent $\pm 1SE$. (Berry, 1972).

Different hypotheses have been formulated to explain the reduction of OER as LET increases. Alper *et al.* (1974) tested two different hypotheses initially suggested by Neary (1965):

- (i) It has been previously discussed that as LET increases, the complexity of the DNA damage increases. The fixation of the damage will occur in this case due to the interaction between SSB and DSB rather than the interaction of these types of damage with oxygen. At very high LET values, the killing effect of radiation is entirely dependent on the type of damage inflicted on the DNA structure and not on the presence of oxygen in its microenvironment. For this reason, at very high LET, the difference between the oxic and hypoxic survival curves is indistinguishable, i.e. OER = 1.
- (ii) An alternative to this theory is the ‘oxygen-in-the-track’ hypothesis, where molecular oxygen is engendered in the track of a densely ionising particle as it traverses biological material: the denser the track, the greater the effective concentration of oxygen (Shekhtman, 1960).

Critics of the ‘oxygen-in-the-track’ hypothesis (Howard *et al.*, 1974; Frankenberg-Schwager *et al.*, 1994) hold that oxygen will only make a difference on radiosensitivity at low-LET values, while radiosensitivity at high-LET will mainly depend on the track structure of radiation. Therefore, *if the same biological system is exposed to different LET radiations at different oxygen concentrations, the number of unrepaired DSBs will differ most at low-LET values but will become more similar at high-LET.* This is the case shown next for V79 and HSG cells exposed to different radiation qualities, where the initial slope of the survival curve represents number of unrepaired DSB (Furusawa *et al.*, 2000).

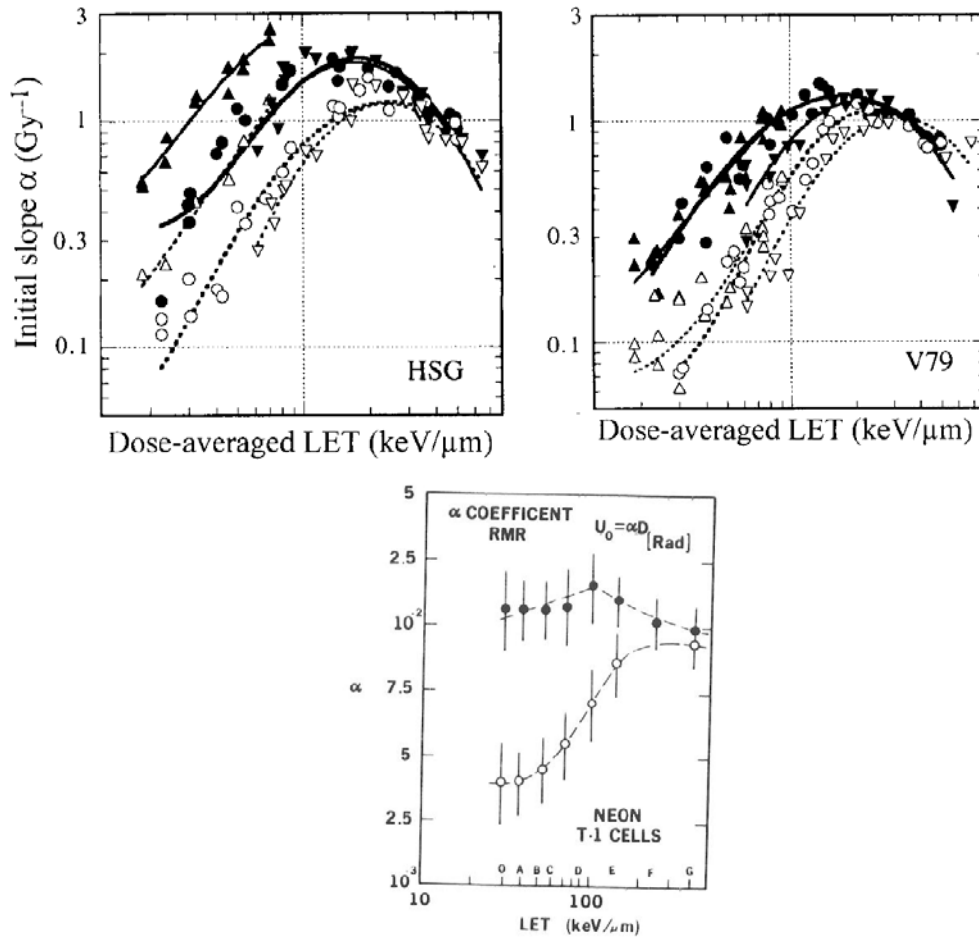


Figure 8.13: (Top) Distribution of the initial slope (α) of the linear-quadratic equation under aerobic (solid line, closed symbols) and hypoxic (dotted lines, open symbols) conditions for V79, HSG and T1 cells exposed to Helium (^3He : \blacktriangle , \triangle), carbon (^{12}C : \bullet , \circ), or neon (^{20}Ne : \blacktriangledown , \triangledown) ion as a function of the dose-averaged LET (Furusawa *et al.*, 2000). (Bottom) Values of α obtained from survival curves of T-1 kidney cells in air (closed symbol) and nitrogen (open symbol) exposed to different types of radiation (Tobias *et al.*, 1980).

(iii) Cell Cycle effects

In the previous section it was stated that radiosensitivity during the different stages of the cell cycle could be affected by the oxygen effect. Radiation quality can also affect the radiosensitivity at different stages of the cell cycle and this was proven by Wambersie *et al.* (2004) who performed a systematic study of the variation of radiosensitivity of Chinese hamster cells exposed to helium, carbon, neon and argon ions at different stages of the cell cycle. The result of this analysis showed that the large differences in radiosensitivity observed after low-LET irradiation between cells in

mitosis, G₁ and in stationary phase diminished with increasing LET and disappear above 100 keV/μm.

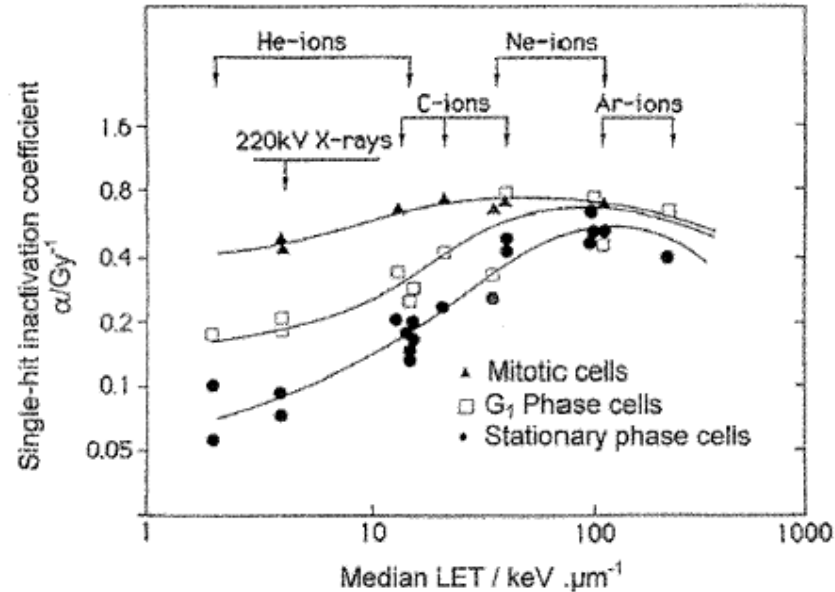


Figure 8.14: Differences in radiosensitivity related to the position of the cells in the mitotic cycle for homogeneous populations of Chinese hamster cells in mitotic, G₁, and stationary phase. (Wambersie et al., 2004).

8.2. Assumptions and working hypotheses of the proposed repair model for high-LET radiations

The evidences found in the previous section can be summarised as follows:

- The number of SSB reduces with increasing LET while the number of DSB++ increases with LET. If the repair efficiency remains the same at any given value of LET, this would mean that the contribution of fast repair components tend to diminish with increasing high-LET, so the repair process tends to be more dominated by the increasing presence of slow repair components which are better described by second order kinetics.

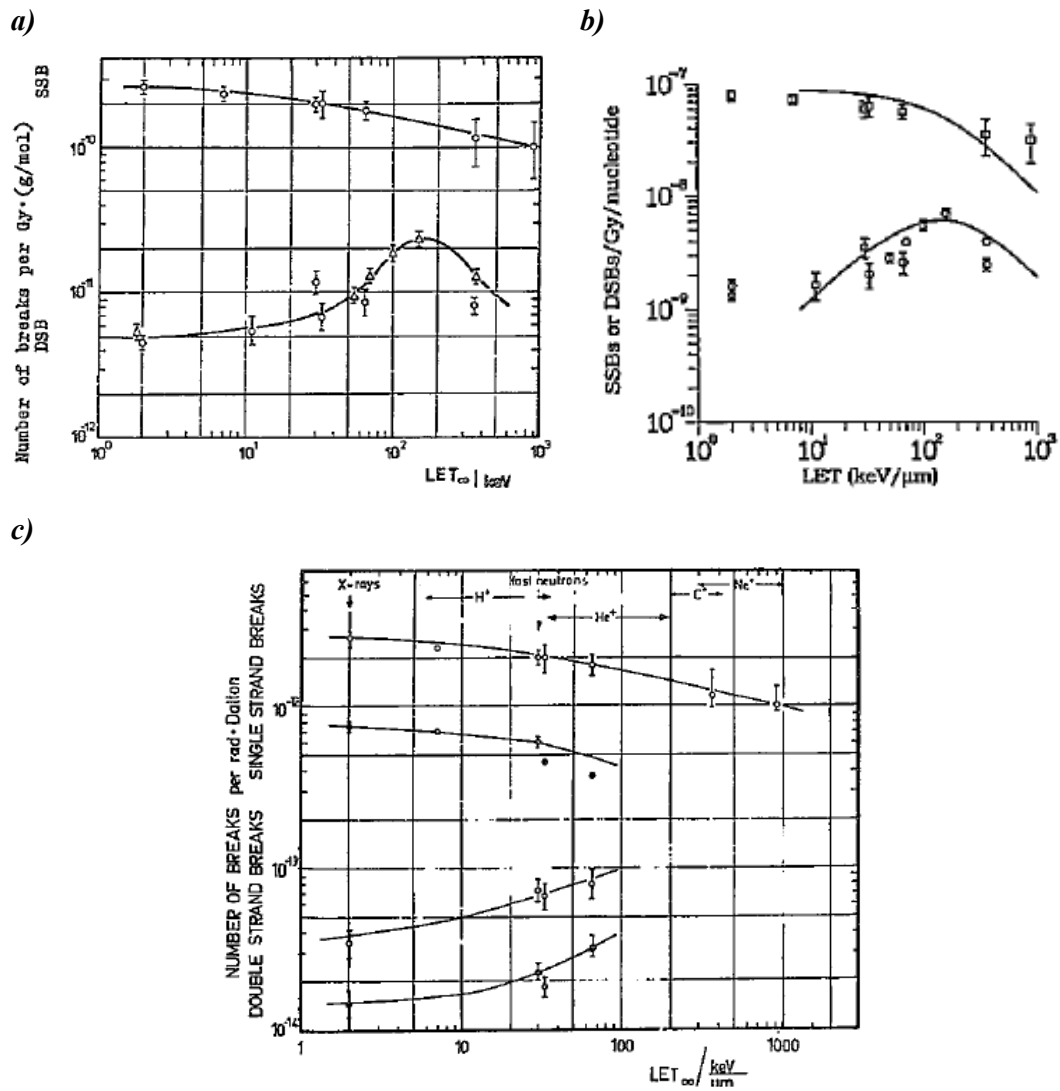


Figure 8.15: (a) Induction rates of SSB (top line) and DSB (bottom line) as a function of LET for CHO cells (Kampf et al., 1983); (b) Yield of DNA SSB (top) and DSB (bottom) in Chinese hamster V79 cells by low-LET (^{60}Co , X-rays) and high-LET (4He , ^{12}C , ^{22}Ne) (Zaider, 1993); (c) DNA strand break rates (SSB –top; DSB – bottom) from V79 cells as a function of LET and oxygen tension. ● – irradiation in nitrogen; ○ – irradiation in air. (Kampf et al., 1977a)

- When cell lines of different repair capability are exposed to radiations of different LET, the biggest difference between the initial number of DSB produced during irradiation and the final number of DSB remaining after a given repair time is observed at low LET for those lines with the highest capability of repair. As LET is increased, the difference between the initial yield and the unrepaired fraction of DSB becomes very small (negligible in some cases) regardless the repair capability of the cells.

- The repair capacity of a cell is modified during its mitotic cycle or by adding oxygen-based-compounds to its microenvironment, and in both cases, the same reduction of the difference between the initial yield and the final unrepaired fraction of DSB is observed as LET increases.
- The average difference found between the initial yield and final fraction (unrepairable) of DSB in Figures 8.10, 8.11, 8.14 and 8.15 at 10 keV/um and 100 keV/um is 75.74% and 54.28% respectively. In some cases where the data extends further than 100 keV/um, this difference becomes even smaller.
- It is assumed that a minimum number of DSB (δ) will never repair.

On the bases of the above, the following hypothesis can be formulated:

As LET increases the fraction of unrepaired strand breaks and the fraction of complex DSB (slow repair components) increase while the amount of SSB and simple DSB (fast repair component) decreases. Therefore, *once the unreparable fraction of complex DSB is subtracted from the total amount of DSB produced at high LET, the repair process in cells exposed to high-LET radiation is mainly driven by second order repair kinetics.* The unreparable fraction of DSB will be a fraction of the initial yield of DSB, and as LET increases these two will be of the same order.

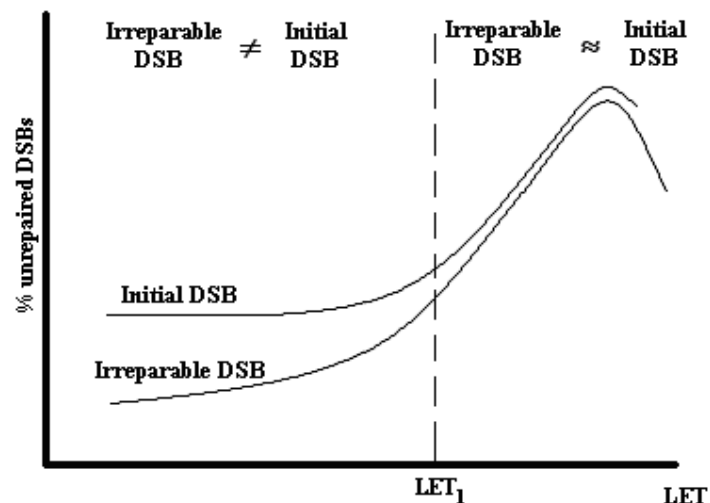


Figure 8.16: The number of unrepaired DSBs is always lower than the initial number of DSBs, but the difference between them is much smaller at high-LET than at low-LET. LET_1 represents the limit at which the fraction of unrepaired DSBs after repair can be considered equal to the initial yield of DSB due to the lack of repairability after high-LET exposure.

According to the idea expressed in Figure 8.16, we can use the Physics laws on radiation transport to predict the radiobiological outcome of exposure to high-LET radiations on the basis that, at low-LET, the initial amount of DSB can be calculated via Monte Carlo simulation while the calculation of the unrepaired fraction of DSB requires assumptions relating to repair paths that are very difficult to model. However, at high-LET, as the irreparable amount of DSB is very similar to the initial amount of DSB, the calculation of the initial number of DSB based on radiation transport Physics alone can explain biochemical and radiobiological effects.

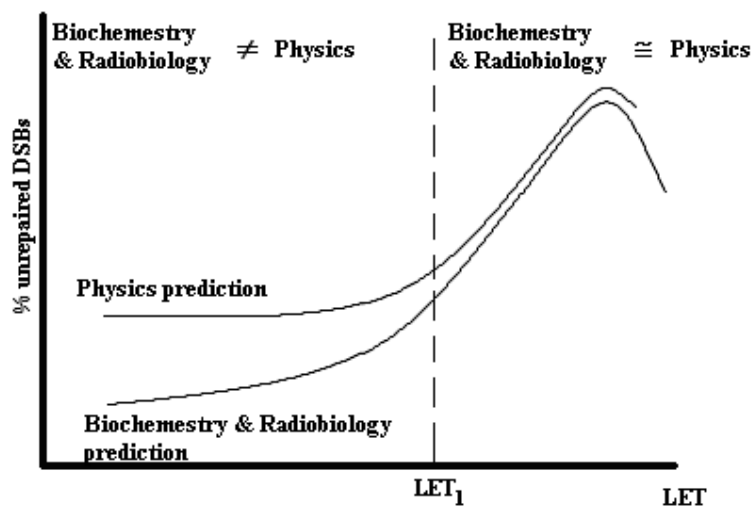
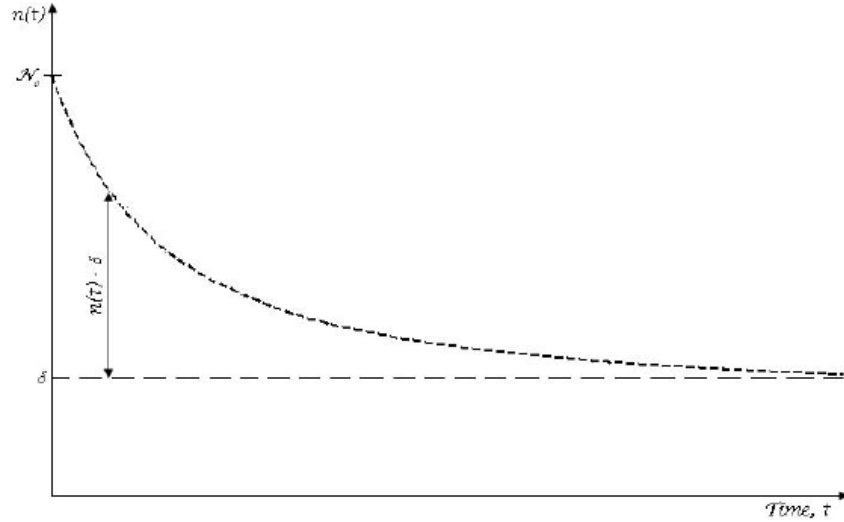


Figure 8.17: Ranges of LET where radiobiological predictions can be made based using Physics principles alone.

8.3. Generalisation of the Reciprocal Repair Model to all LET

According to the assumption established in the previous section, if there is a minimum number of breaks (δ) that never repair, the repairable damage (i.e. $n(t)-\delta$) will be removed at a rate described by:



$$\frac{d[n(t) - \delta]}{dt} = -C[n(t) - \delta]^2 \tag{8.2}$$

where C corresponds to the repair rate factor and $n(t)$ corresponds to the number of unrepaired DSB at any given time. Considering δ as an intrinsic constant, the number of unrepaired DNA breaks at any given time will be found rearranging Equation (8.2) as:

$$\frac{dn(t)}{dt} = -Cn(t)^2 - 2\delta Cn(t) + (\delta - C\delta^2) \tag{8.3}$$

With initial value: $n(t=0) = N_0$.

This is a Riccati equation, which has to be solved using analytical functions; but using a simple transformation as follows can also solve it. Let $n(t) - \delta = X$, then Equation (8.2) becomes:

$$\frac{dX}{dt} = -CX^2 \Rightarrow \frac{1}{X^2} \frac{dX}{dt} = -C \Rightarrow -\frac{1}{X} = -Ct + B \Rightarrow n(t) - \delta = \frac{1}{Ct - B} \Rightarrow n(t) = \delta + \frac{1}{Ct - B} \tag{8.4}$$

The value of the integral constant B is found at $t = 0$: $\delta - \frac{1}{B} = N_0 \Rightarrow B = \frac{-1}{N_0 - \delta}$

$$\therefore n(t) = \delta + \frac{1}{Ct + \frac{1}{N_0 - \delta}} = \delta + \frac{N_0 - \delta}{(N_0 - \delta)Ct + 1} \quad (8.5)$$

In most cases, repair kinetic data is reported in terms of fractions of the total initial amount of unrepaired DNA breaks, i.e. in terms of the fraction of repairable breaks ($\frac{n(t)}{N_0}$) and the fraction of unreparable DNA breaks ($\frac{\delta}{N_0}$), which requires to transform

Equation (8.5) as follows:

$$\frac{n(t)}{N_0} - \frac{\delta}{N_0} = \frac{1 - \frac{\delta}{N_0}}{zt + 1} \quad (8.6)$$

where, $z = (N_0 - \delta)C$ is the repair constant with units of h^{-1} . This equation is very similar to the equation reported by Dale *et al.* (1999) for low-LET radiations where it was assumed that all breaks were repairable:

$$\frac{n(t)}{N_0} = \frac{1}{zt + 1} \quad (8.7)$$

Comparing both equations, it is easy to conclude that in Equation (8.6) the remaining fraction of repairable breaks is not a fraction of the entire population of DNA breaks (represented by the number 1 on the right hand side of Equation (8.7)) but is a fraction of the entire population minus the unreparable fraction ($1 - \frac{\delta}{N_0}$). This is an important point to remember in the following section, where we discuss how to obtain values of δ from experimental data.

8.3.1. Experimental analysis of δ

Equation (8.7) can be rearranged as follows:

$$\frac{N_0}{n(t)} = 1 + zt \tag{8.8}$$

Fowler (1999; 2002) proposed the hypothesis that when plotting the reciprocal of the proportion of damage unrepaired (i.e. $\frac{N_0}{n(t)}$) as a function of t , the resulting plot would be a straight line only if purely second-repair order kinetics applies. Any departure from the straight line would indicate divergence from second-order kinetics, with first-order kinetics causing the plot to veer upwards (see Chapter 7).

A different hypothesis is proposed in this theory, explicitly indicated in Equation (8.6), where it is suggested that second-order kinetics applies, but any apparent departure from it will simply be due to there being a fraction of unreparable damage, measured by the factor $\frac{\delta}{N_0}$. Therefore, when plotting the reciprocal of the proportion of damage unrepaired as a function of t , if the resulting plot is straight it would mean that all the damage is repaired according to second-order repair kinetics, while in the case the plot veer upwards or downwards, it would mean that some fraction of the initial damage remains unrepaired and the subtraction of this fraction should correct the plot to a straight line. This is the rationale followed here, where a cyclic calculation has been made over the fraction of unrepaired damage at any time until maximising the correlation coefficient (r^2) of the least square fit to a straight line. The following example describes the general process applied to the results which are shown in the next chapter. This example comes from Stenerlow *et al.* (2000) produced by Nitrogen 80 keV/um on low passages of normal fibroblasts.

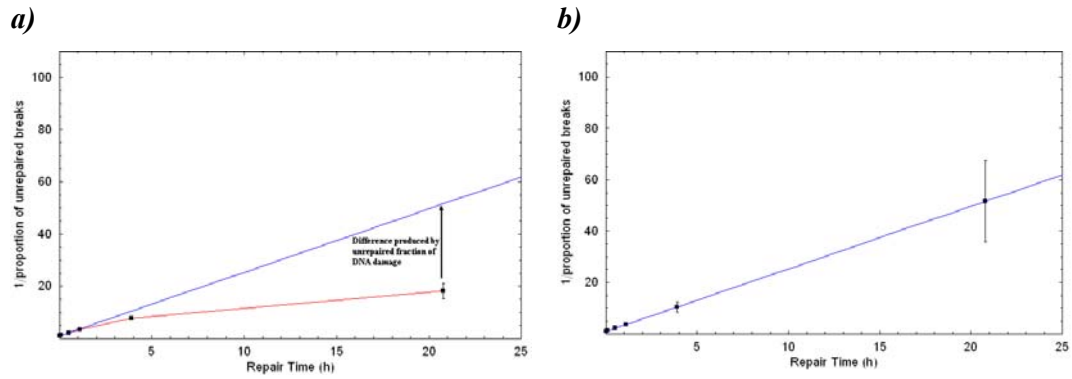


Figure 8.18: Corrected reciprocal repair data for unreparable DSB (b) after δ has been subtracted from the original data (a). The reason of the enlargement of the error bars of the data is explained in detail in section 9.1.1.

In Figure 8.18 left, the data is presented without correction for unrepaired damage (i.e. $\delta = 0$) while the right plot shows the straight fitting after the correction using $\delta = 33.66$ kbp representing a 3.7% of the initial population of unrepaired breaks (920.34 kbp) that represents the fraction of unreparable breaks. This value of δ corresponds to the maximum value of the correlation fraction coefficient (r^2), which in this particular case started from value 0.957 for $\delta = 0$ kbp and increased to 1.000 when used $\delta = 33.66$ kbp. The following plots show the difference in the fitting to the repair kinetic data by the reciprocal repair model proposed by Fowler (1999; 2002) in Equation (8.7) and the general reciprocal repair model proposed in this thesis in Equation (8.6).

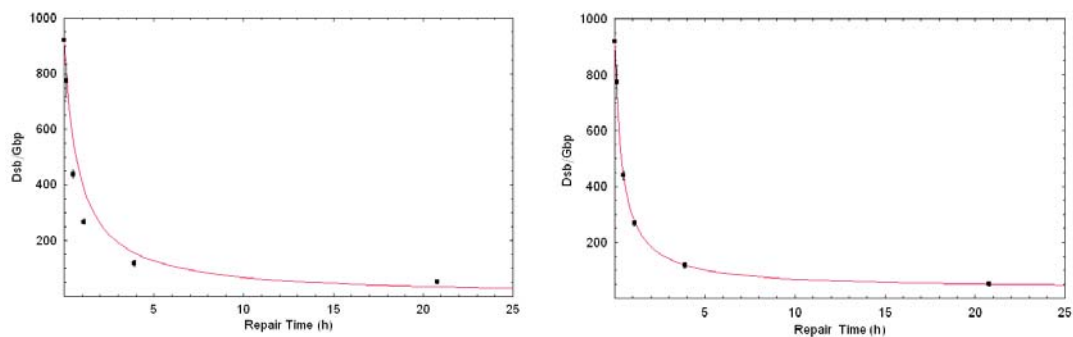


Figure 8.19: Fit to the repair kinetic curves using Equation (8.7) (left) and Equation (8.6) (right).

It is suggested that the better fit in the case of the general reciprocal repair model is due to the fact that very slow or unreparable components are taken into account into the calculation. Their presence is manifested at very long repair times, where the repair curve tends to flatten (see Figure 8.19 right) instead of continue to decay (see Figure

8.19 left). Obviously, the continuous decay predicted by Equation (8.7) will be reflected in the half time of the repair characteristic of the system under study and, from there, the mismatch between data and curve at long repair times. It is expected that the introduction of the unreparable fraction would modify this half-time value to a more realistic one, which in turn should improve the fitting at low repair times, as can be seen when comparing the right and left plots in Figure 8.19.

8.3.2. *Theoretical analysis of δ*

As it was explained in Figures 8.16, 8.17 and 8.18, values of δ can be predicted at high-LET based on the assumption that mostly, very slow repair components will exist. Therefore, the initial (N_0) and the final (δ) amounts of unrepaired damage will be of the same order (i.e. $\frac{\delta}{N_0} \approx 1$) at high-LET.

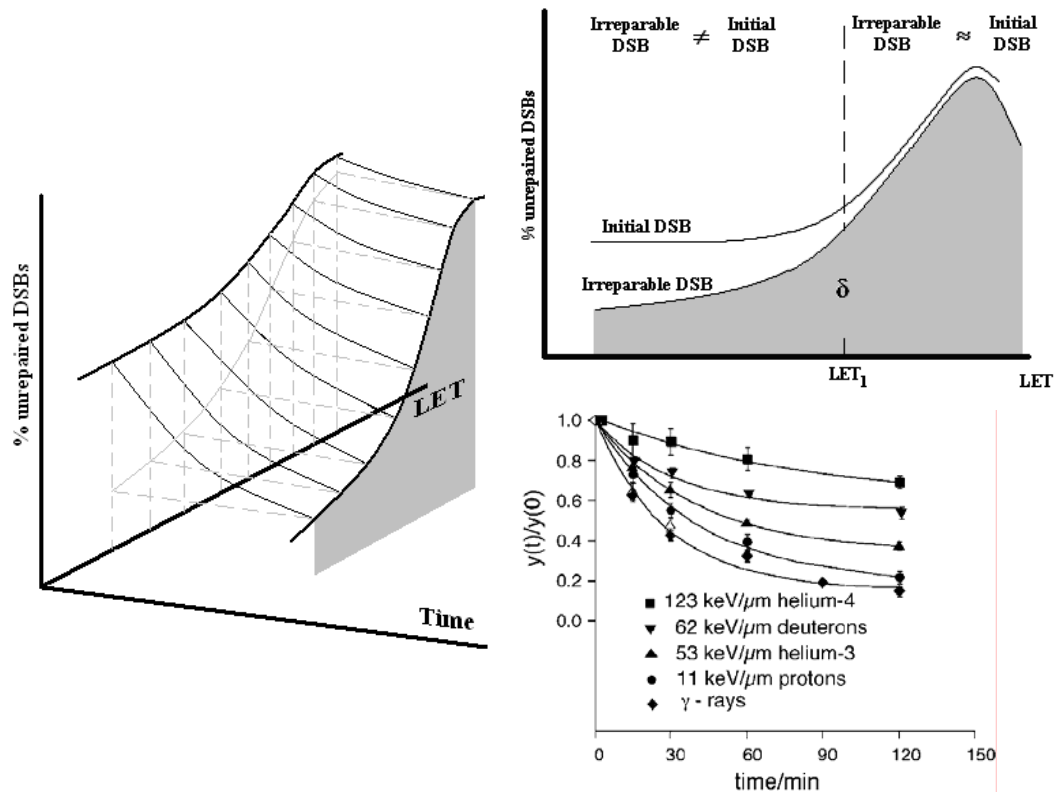


Figure 8.20: Left – predicted shape of the surface plot for unrepaired number of DSB as a function of time and LET according to the characteristics of the unrepaired DSB versus time and unrepaired DSB versus LET curves discussed in the text. Right – Front (time = 0) and lateral (LET=0) views of the surface plot on the left (the data on the right-bottom figure corresponds to Belli et al. 2000).

In this case, both sides of Equation (8.6) become:

$$\boxed{L \rightarrow \infty \Rightarrow \frac{\delta}{N_0} \rightarrow 1}: \lim_{\frac{\delta}{N_0} \rightarrow 1} \left(\frac{n(t)}{N_0} - \frac{\delta}{N_0} \right) = \lim_{\frac{\delta}{N_0} \rightarrow 1} \left(\frac{1 - \frac{\delta}{N_0}}{z t + 1} \right) \Rightarrow \frac{n(t)}{N_0} - 1 = 0 \Rightarrow n(t) = N_0 \quad (8.9)$$

Several authors have investigated stochastic and non-stochastic (or deterministic) methods to calculate the initial distribution of different types of DNA breaks. Stochastic methods are based on Monte Carlo simulations of track structure that provide a history of the different interactions taking place along the track of the particles and of the energy deposited in each of these interactions. The different amounts of energy deposited in each interaction, together with a scoring system to establish the energy required to produce a certain type of DNA damage, will generate a map of the initial amount of different types of DNA damage produced by different types of radiation (Charlton *et al.*, 1985; 1989; Nikjoo *et al.*, 1991). Although these methods tend to be very powerful when predicting the number of different types of DNA strand breaks, they also require powerful computational capabilities and long computation times in order to provide good statistics. Deterministic methods require very little calculation time but they are not as powerful as the stochastic methods in determining initial amounts of the different types of DNA breakage. However, they allow the use of an analytical expression that can be added to the mathematical body of the biophysical theory used to simulate biological end-points after irradiation. In the next two subsections two different semiempirical models are presented to calculate the initial fraction of DNA damage.

- *The Fast Monte Carlo Damage Simulation Algorithm (MCDS)*

Semenenko *et al.* (2004; 2005a; 2005b; 2006) produced a quasi-phenomenological model that used a fast Monte Carlo algorithm to calculate the spectrum of DNA damage yields formed by ionising irradiations of different qualities. The fast Monte Carlo Damage Simulation (MCDS) algorithm performs the simulation in two major steps: (1) it randomly distributes in a DNA segment the expected number of DNA lesions

produced in a cell per Gy of radiation, and (2) it subdivides the lesions in the segment into clusters. Four adjustable parameters are used in the algorithm:

1. Number of strand breaks, σ_{sb} ($\text{Gy}^{-1}\text{cell}^{-1}$).
2. Number of base damages σ_{Bd} ($\text{Gy}^{-1}\text{cell}^{-1}$). The yield of base damages may conveniently be specified in terms of the base damage to strand break ratio, i.e. $f \equiv \sigma_{Bd} / \sigma_{sb}$.
3. DNA segment length, n_{seg} , in base pairs ($\text{bp Gy}^{-1}\text{cell}^{-1}$). This DNA segment is an *ad hoc* parameter and should not be considered equivalent to the DNA content of a specific chromosome or cell.
4. Minimum length, N_{min} , of undamaged DNA (bp) between neighbouring elementary damage such that these elements of damage are said to belong to different lesions. Here, the term lesion means both isolated elementary damages and multiply damaged sites (MDS).

Semenenko *et al.* (2006) provided a method to calculate the best estimates of each parameter indicated above ($\sigma_{sb}, f, n_{seg}, N_{min}$), arriving at the following expression for the MCDS algorithm for the case of electron, proton and α -particles of different energy:

$$\begin{aligned} \sigma_{sb} &= 1300 \text{ Gy}^{-1}\text{cell}^{-1} \\ f &= 3 \\ n_{seg} &= 149200 - \frac{123600x}{x+267} \text{ bp Gy}^{-1}\text{cell}^{-1}, \quad x \equiv \frac{Z_{eff}^2}{\beta^2} \quad (8.10) \\ N_{min} &= 9 \text{ bp} \end{aligned}$$

The values of σ_{sb} (~ 1000 SSBs $\text{Gy}^{-1}\text{cell}^{-1}$ and $\sim 80 = 2 \times 40$ DSB according to Ward (1988), f ($2.0 \leq f \leq 2.4$ according to Nikjoo *et al.* (1999), $f = 2.7$ according to Ward (1985) and N_{min} (≤ 10 base pair separation between 2 SSB according to Charlton *et al.* (1988), Holley *et al.* (1990), Terrissol *et al.* (1994), Nikjoo *et al.* (1996) are in accordance with experimental results and it is only the parameter describing the clustering of damage at different LET (i.e. n_{seg}) that is modelled semi-empirically.

An important observation from Equation (8.10) is that three of the four parameters used in the MCDS algorithm are the same for electron, protons and α -particles. The fourth parameter (n_{seg}), which depends on the ratio Z_{eff}^2/β^2 , characterises the degree of damage clustering within one or two turns of the DNA molecule. This suggest that the absolute yield of strand breaks and base damage is approximately the same, per Gy per Gbp, for electron and energetic light ions but the degree of lesion clustering on a nanometre scale (10-20 bp) is quite different for low- and high-LET radiation. For this reason n_{seg} is the only parameter of the four that characterise the amount of initial number of SSB and DSB produced at any given LET. When this parameter is plotted versus LET using data on yield of SSB and DSB from different authors [Nikjoo *et al.*, 1999; 1997; 1994; 2001; Friedland *et al.* 2005; 2003) an excellent correlation is observed

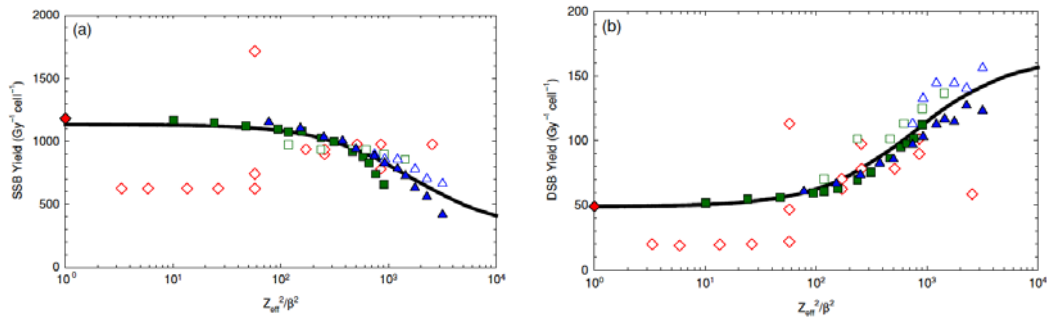


Figure 8.21: Dependence of SSB and DSB yields predicted by detailed Monte Carlo calculations of Nikjoo *et al.* (1994, 1997, 1999, 2001, 2002) (open symbols) and Friedland *et al.* (2003, 2005) on Z_{eff}^2/β^2 (Semenenko *et al.*, 2006).

A number of criticisms could be made to this model:

1. As it is observed in Figure 8.10 the yield of DSB has a maximum somewhere between 50–120 keV/um, and for higher LET values the yield decreases. However, in Figure 8.21 the predicted yield of DSB increases at any value of LET. The predicted maximum of n_{seg} can be obtained from the first derivative of its expression in Equation (8.10):

$$\frac{d}{dx} \left[149200 - \frac{123600x}{x + 267} \right] = -\frac{33001200}{(x + 267)^2} \Rightarrow \frac{df(x)}{dx} \neq 0 \forall x \in (0, \infty)$$

Therefore, there is no maximum n_{seg} and thus the function increase monotonically with x , as it can be seen in Figure 8.22. For this reason, at higher LETs, the model proposed by Semenenko will not correctly predict the closeness between initial and unreparable DSB at high-LET values, and consequently, this model will not predict the correct values of δ characterising the repair ratios at different LET. An alternative expression to the one proposed by Semenenko is required for n_{seg} that predicts a maximum at $80 \leq LET \leq 120$ and, from there, a decrease of the length of the DNA segment (i.e. increase of the DNA damage clustering) with increasing LET.

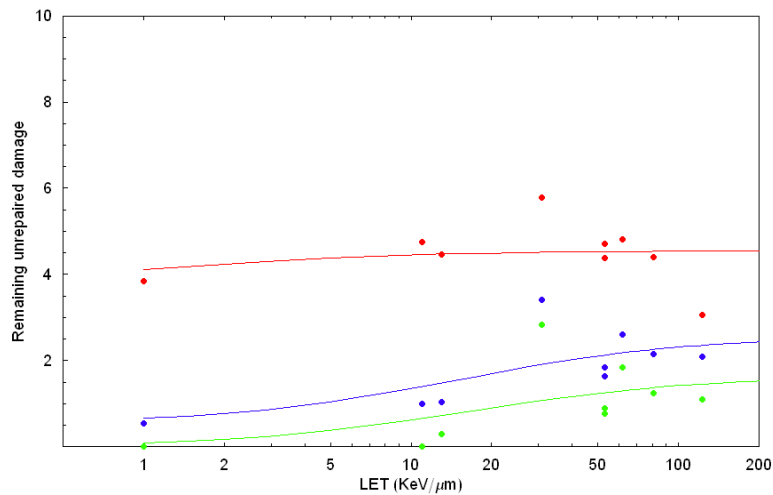


Figure 8.22: Fit of n_{seg} (Equation 8.10) to the data produced by Belli et al. (2000).

2. The parameters on which the MCDS model is based upon (i.e. $\sigma_{Sb}, f, n_{seg}, N_{min}$), are uncorrelated to the parameters of the LQ model which ultimately would determine the effect of a given number of SSB and DSB produced by a particle of a given LET. Only σ_{Sb} could be argued to maintain some radiobiological meaning through out Equation (8.1), but the values of this parameter have to be fed into the model instead of been attributed by the biological system exposed to the radiation of interest. This means that, in order to use realistic values of σ_{Sb} , one would have to experimentally obtain the survival curve for that particular system exposed to the radiation of interest and then convert the value of α into the relevant σ_{Sb} value using Equation (8.1).

- *Alternative model to predict initial number of DSB*

Jones *et al.* (in preparation) proposed an alternative model to the MCDS based on parameters readily available from radiobiological experiments. This semi-empirical model also incorporates the characteristic turnover point present when either the number of DSBs or, at a higher level, RBE, is plotted versus LET. The central idea of the model is that the probability P to produce a DSB due to an increase in LET in any critical DNA site is assumed to be linearly related to $LET (L)$, so that

$$P = kL \tag{8.11}$$

where k is a constant of proportionality that reflects all the processes involved in translating multiple strand breaks into a lethal DSB. Applying Poisson statistics for a small number of lethal DSBs (e.g. 0, 1 or 2 per cell) relative to the large numbers of strand breaks present per unit of dose per cell (i.e. $\text{cell}^{-1} \text{Gy}^{-1}$), the probability of a lethal event occurring in each cell will be given by

$$P_C = kL e^{-kL} \tag{8.12}$$

where e^{-kL} represents the correction probability function for extra hits with increasing LET. The features of the function described in Equation (8.12) are:

1. At $L=0 \text{ keV } \mu\text{m}^{-1}$, P_C is zero; at large values of L , P_C approaches again to zero.
2. When $\frac{dP_C}{dL} = 0$, the value of P_C is a maximum at $L=1/k$.
3. For a turnover point at approximately $L=100 \text{ keV}/\mu\text{m}$, as occurs in published data sets, the value of k is around 0.01.
4. The maximum value of P_C at the turnover point is $P_{\text{max}} = e^{-1} = 0.37$

In order to relate the probability P_C of lethal events with dose, Jones *et al.* also assume that the efficiency of cell kill with dose is described by the α parameter in the LQ model at low dose and that α is the radiosensitivity coefficient that changes the most with increasing LET. Several authors (Frankenberg *et al.*, 1981, 1984, 1999; Radford, 1985;

Prise *et al.*, 1987; Belli *et al.*, 1996) have provided evidence of *linear* correlation between number of lethal DSB and αd , so that α represents the coefficient of lethal DSB production and will vary with LET in a similar way to the variation of RBE. This is clearly seen in Figure 8.23, where a direct linear correlation is shown between lethal lesions and number of DSBs measured by Relative Log Elution (Prise *et al.*, 1989; 1990) as well as the increase of efficiency in producing lethal DSB with higher LETs. This means that, if α_H is the increment in α with increasing LET, α_H must be linearly proportional to the probability P_C :

$$\alpha_H = jP_C \tag{8.13}$$

where j is the parameter that determines the formation of lethal DSB per unit of dose per cell. This same assumption was also used by Hawkins in his Microdosimetric-Kinetic model (1994, 1996, 1998). Therefore, substituting Equation (8.12) in (8.13), we arrive at:

$$\alpha_H = jkLe^{-kL} \tag{8.14}$$

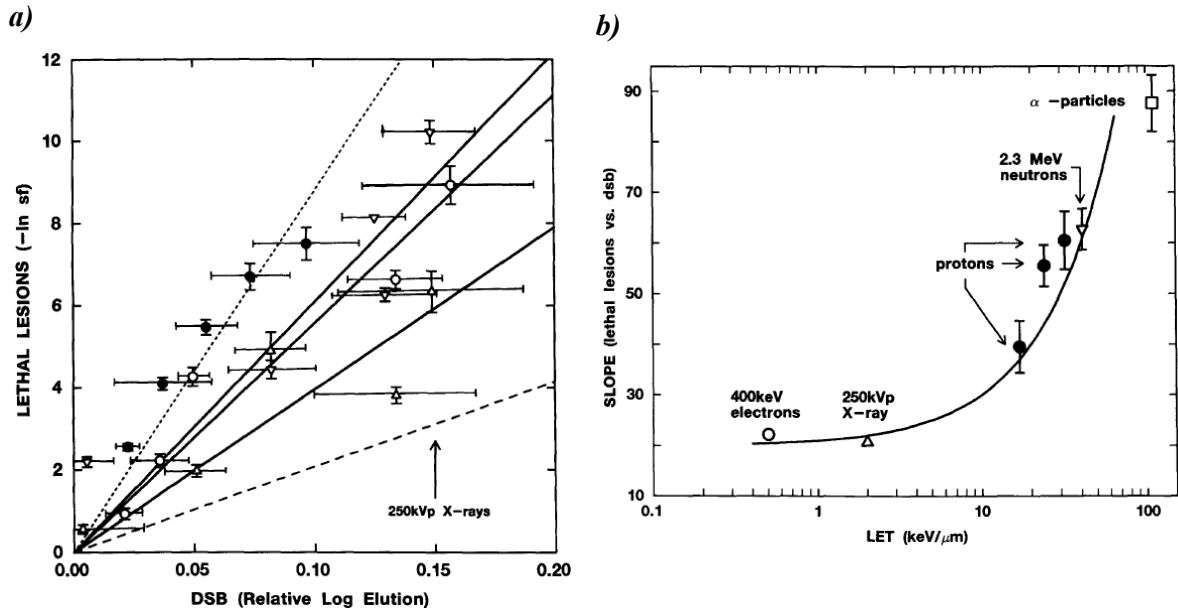


Figure 8.23: (a) Plot of lethal lesions (-ln(survival fraction)) against DSB (measured by relative log elution, Prise *et al.* 1989) for particles of different LET; (b) increase of efficiency in producing lethal DSB with higher LETs. (Prise *et al.* 1990)

According to Equation (8.14), the maximum value of α_H corresponds to the LET at which the probability of lethal DSB production is maximum, i.e.:

$$P_{\max} = \frac{1}{e} \Rightarrow \alpha_{H,\max} = \frac{j}{e} \quad (8.15)$$

hence,

$$j = e \alpha_{H,\max} \Rightarrow \alpha_H = e \alpha_{H,\max} kL e^{-kL}$$

which drives to the final expression proposed by Jones *et al.* for the linear sensitivity parameter at high-LET:

$$\alpha_H = \frac{\alpha_{H,\max}}{e^{-1}} kL e^{-kL} \quad (8.16)$$

This formulation will be extended in this section to derive the total number of DSBs present at any time on a cell nucleus that has been exposed to either low- or high-LET particles. In general, the total number of DSB produced by any given type of radiation can be expressed as:

$$\alpha_T = \alpha_L + \alpha_H \quad (8.17)$$

where for low-LET radiations, $\alpha_L \neq 0$ and $\alpha_H = 0$; and for high-LET, depending on the type of radiation, a combination of values for α_L and α_H will apply. For instance, for some of the neutrons studies analysed in Chapter 6, an estimated average gamma contamination of the neutron beam of 7% would imply that $\alpha_T = 0.07\alpha_L + 0.93\alpha_H$.

Substituting Equation (8.16) into (8.17) we arrive to:

$$\alpha_T = \alpha_L + \frac{\alpha_{H,\max}}{e^{-1}} kL e^{-kL} \quad (8.18)$$

According to Equation (8.16), the maximum of α_H ($\alpha_{H,\max}$) is obtained at $-\ln SF = 1$. However, experimental work shows that the maximum α_H changes with the survival level (see Figure 2.4). Therefore, it is assumed that Equation (8.18) can be generalised to any desired end point by substituting:

$$\alpha_T = \alpha_L + \frac{\alpha_{H,\max}}{e^{-m}} kL e^{-kL} \quad (8.19)$$

where, $m = -\ln SF$. According to Equation (8.19), for a specified biological system exposed to a radiation type of a know LET to produce a predetermined survival level m , the value of α_T should be fixed. Let us assume that this value of α_T determines the final number of DSBs expressed by the cell after repair has taken place, i.e. the remaining damage after $t = \infty$. In this case, and according to Equation (8.2), the value of α_T would correspond to δ , i.e.

$$\delta = \alpha_T^{final} = \alpha_L + \frac{\alpha_{H,\max}}{e^{-m}} kL e^{-kL} \quad (8.20)$$

The only factors that can be affected by time in this equation are α_L and $\alpha_{H,\max}$ due to the repair of the initial pool of DSB, thus the following expression is proposed to count for the initial number of DSB at $t=0$:

$$N_0 = \alpha_T^{initial} = (\alpha_L + X) + \frac{(\alpha_{H,\max} - X)}{e^{-m}} kL e^{-kL} \quad (8.21)$$

where X represents the viable pool of DSB susceptible to repair. From Equations (8.20) and (8.21), we can then compute what is going to be the difference between the initial and the final number of DSBs at any given time by:

$$\begin{aligned} N_0 - \delta &= \left[(\alpha_L + X) + \frac{(\alpha_{H,\max} - X)}{e^{-m}} kL e^{-kL} \right] - \left[\alpha_L + \frac{\alpha_{H,\max}}{e^{-m}} kL e^{-kL} \right] = \\ &= X + \frac{(\alpha_{H,\max} - X)}{e^{-m}} kL e^{-kL} - \frac{\alpha_{H,\max}}{e^{-m}} kL e^{-kL} = \\ &= X \left[1 - \frac{1}{e^{-m}} kL e^{-kL} \right] \end{aligned} \quad (8.22)$$

To calculate the exact number of DSBs ($n(t)$) at any given time, Equation (8.6) can be re-arranged as:

$$n(t) = \delta + (N_0 - \delta) \frac{1}{z t + 1} \quad (8.23)$$

Substituting the respective values of δ and $(N_0 - \delta)$ into Equation (8.23), we arrive to the final expression of $n(t)$:

$$n(t) = \alpha_L + \frac{\alpha_{H,max}}{e^{-m}} kL e^{-kL} + \left(1 - \frac{1}{e^{-m}} kL e^{-kL}\right) \frac{X}{zt + 1} \quad (8.24)$$

Remembering that α is measured now in terms of number of DSB per cell per Gy, we can plot Equation (8.24) using the following

$$\begin{aligned} \alpha_L &= 0.15 \frac{dsb}{cell \cdot Gy} & X &= 1.0 \frac{dsb}{cell \cdot Gy} \\ \alpha_{H,max} &= 1.0 \frac{dsb}{cell \cdot Gy} & k &= 0.01 \\ & & m &= 0.86 \text{ (i.e. SF = 0.42)} \\ & & z &= 0.05 \end{aligned}$$

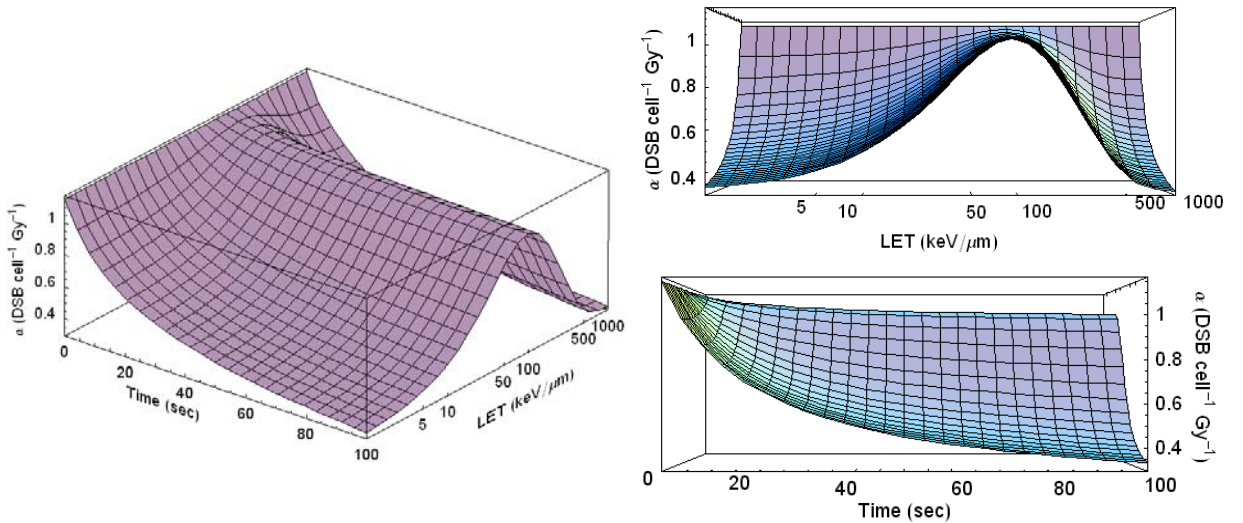


Figure 8.24: Resultant plots obtained from Equation (8.24). Observe the similarities with Figure (8.20)

The values used to produce the plots in Figure 8.24 do not correspond to any particular system, but they are all within reasonable limits. All these parameters can be obtained from the extensive literature on repair kinetics for low- and high-LET, but the z parameter needs some consideration. Equation (8.24) only uses one value of z , whereas each of the repair kinetics curves at each individual LET (Figure 8.25 right-bottom)

would have a different value of z associated. It is expected that, in order to fit the 3D plot to a set of data points, an average value of z would be required, which potentially might introduce errors in the predicted value of α at any given value of (t, LET) .

Both of the models presented in this section represent interesting ‘fast’ approaches to predict number of DSB produced for different types of radiations, with the extra advantage (in the case of the alternative model presented here) of incorporating repair effects which could improve the power of predictability of the modelling at any given time after irradiation.

However, both of these approaches are semi-empirical and potentially subject to errors in the measured data used to calculate their fitting parameters. This could be avoided by using a mechanistic approach, as in the case of the models presented in Chapter 4. Out of the three models presented, only the MK model introduces kinetic repair considerations, but the model fails to predict the correct shape of the RBE_{\max} (i.e. α_H/α_L at $d \sim 0Gy$) versus LET unless a non-Poisson distribution of lethal DSBs is assumed. A good alternative to this change of statistics in the models is to study how the parameters in Equations (4.39) and (4.40) depend on LET, i.e.

$$\dot{x}_d(t, L) = k_d(L)\dot{z}_d - [a(L) + c(L)]x_d - 2b_d(L)x_d^2$$

$$\dot{x}_{Ad}(t, L) = \lambda_d(L)\dot{z}_d + a(L)x_d + b_d(L)x_d^2$$

In this case, the dependency of α and β (Equations (4.41) and (4.42)) would be obtained not only from the microdosimetric part of the model but also from its characteristic repair kinetic since, according to Figure 8.24, this has been shown to be relevant.

8.4. Bibliography

- Ahnström G., Edvardsson K.A. *International Journal of Radiation Biology* 26(5), 493-497 (1974).
- Ahnström G. *International Journal of Radiation Biology* 54(5):695-707 (1988).
- Alper T., Bryant P.E. *International Journal of Radiation Biology* 26(3):203-18 (1974).
- Barendsen G.W. *International Journal of Radiation Biology* 8(5):453-466 (1964)
- *International Journal of Radiation Biology* 36(1):49-63 (1979).
- *International Journal of Radiation Biology* 57(4):885-896(1990).
- *International Journal of Radiation Biology* 63(3):325-330(1993).
- *International Journal of Radiation Biology* 66(5):433-436(1994).
- *International Journal of Radiation Biology* 71(6):649-55 (1997).
- Barendsen G.W. *Radiation Research* 139, 257-270 (1994).
- Barendsen G.W. *International Journal of Radiation Oncology Biology Physics* 8(11):1981-97 (1982).
- Barendsen G.W., Koot C.J., Van Kersen G.R., Bewley D.K., Field S.B., Parnell C.J. *International Journal of Radiation Biology* 10(4):317-27 (1966).
- Berry R.J. *Radiation Research* 44(1):237-47 (1970).
- *European Journal of Cancer* 7(2):145-52 (1971).
- *In: Conference on Particle Accelerators in Radiation Therapy. Report LA-5180-C. Los Alamos, New Mexico, October 2-5, pp.108 (1972).*
- Belli M., Ianzini F., Sapora O., Tabocchini M.A., Cera F., Cherubini R., Haque A.M., Moschini G., Tiveron P., Simone G. *Advances in Space Research* 18(1-2):73-82 (1996).
- Belli M., Cherubini R., Dalla Vecchia M., Dini V., Moschini G., Signoretti C., Simone G., Tabocchini M.A., Tiveron P. *International Journal Radiation Biology* 76(8):1095-104 (2000).
- Bowden G.T., Casunic M.D. *Radiation Research* 87:109-120 (1981).
- Butts J.J., Katz R. *Radiation Research* 30(4):855-871 (1967).
- Chapman J.D. *In: Radiation biology and Cancer Research. Meyn R. E., Withers H. R. (eds.). New York: Raven Press, pp.21-32 (1980).*
- Chadwick K.H., Leenhouts H.P. *In: The molecular theory of radiation biology. pp.20-21, Springer-Verlag, Berlin (1981).*

- Charlton D.E., Goodhead D.T., Wilson W.E., Paretzke H.G. *Radiation Protection Dosimetry* 13(1):123-125 (1985).
- Charlton D.E., Humm J.L. *International Journal of Radiation Biology* 53(3):353-365 (1988).
- Charlton D.E., Nikjoo H., Humm J.L. *International Journal of Radiation Biology* 56(1):1-19 (1989).
- Christensen R.C. *PhD Thesis, University of California, Report LBL-28* (1971).
- Clark E.P., Lett J.T. *Radiation Research* 67:519 (1976).
- Cole A., Meyn R.E., Chen R., Corry P.M., Hittelman W. *In: Radiation biology in cancer research*. Raven Press, New York, pp 33-58 (1980).
- Dale R.G. *British Journal of Radiology* 58(690):515-528 (1985).
- Dale R.G., Fowler J.F., Jones B. *Acta Oncologica* 38(7):919-929 (1999).
- Denekamp J., Field S.B. *European Journal of Cancer* 10(4):241-7 (1974).
- Denekamp J., Harris S.R. *International Journal of Radiation Oncology Biology Physics* 1(5-6):421-30 (1976).
- Denekamp J., Stewart F.A. *International Journal of Radiation Oncology Biology Physics* 5(11-12):2003-10 (1979).
- Denekamp J. *International Journal of Radiation Oncology Biology Physics* 49(2):357-380 (1986).
- Dikomey E., Franzke J. *Radiation Environmental Biophysics* 25:189-194 (1986).
- Dugle D.L., Gillespie C.J., Chapman J.D. *Proceedings of the National Academy of Sciences, U.S.A.*, 73:809-812 (1976).
- Eguchi-Kasai K., Murakami M., Itsukaichi H., Fukutsu K., Kanai T., Furusawa Y., Sato K., Ohara H., Yatagai F. *Advances in Space Research* 18(1-2):109-118 (1996).
- Elkind M.M., Sutton H. *Radiation Research* 13:556-593 (1960).
- Ellis F. *Clinical Radiology* 20(1):1-7 (1969).
- Fowler F.J. *In: Conference on Particle Accelerators in Radiation Therapy*. Report LA-5180-C. Los Alamos, New Mexico, October 2-5, pp.28 (1972).
- Fowler J.F. *In: Nuclear particles in cancer treatment*. Hilger, Bristol (1981).
- Fowler J.F., Denekamp J., Thames H.D., Travis E.L. *Radiotherapy and Oncology* 1(3):281-6 (1984).
- Fowler J.F. *British Journal of Radiology* 62(740):679-94 (1989).

- Fowler J.F. *Radiation Research* 152:124-136 (1999).
— *Radiation Research* 158:141-151 (2002).
- Frankenberg D., Frankenberg-Schwager M., Blocher D., Harbich R. *Radiation Research* 88:524-532 (1981).
- Frankenberg D., Brede H.J., Schrewe U.J., Steinmetz C., Frankenberg-Schwager M., Kasten G., Pralle E. *Radiation Research* 151:540-549 (1999).
- Frankenberg-Schwager M., Harbich R. *British Journal of Cancer (Suppl.)* 6:233-8 (1984).
- Frankenberg-Schwager M. *Radiation and Environmental Biophysics* 29(4):273-292 (1990).
- Frankenberg-Schwager M., Frankenberg D., Harbich R., Beckonert S. *Radiation Environmental Biophysics* 33:1-8 (1994).
- Friedland W., Jacob P., Bernhardt P., Paretzke H.G., Dingfelder M. *Radiation Research* 159(3):401-10 (2003).
- Friedland W., Dingfelder M., Jacob P., Paretzke H.G. *Radiation Physics and Chemistry* 72:279–286 (2005).
- Furuno I., Yada T., Matsudaira H., Maruyama T. *International Journal of Radiation Biology* 36(6):639-648 (1979).
- Furusawa Y., Fukutsu K., Aoki M., Itsukaichi H., Eguchi-Kasai K., Ohara H., Yatagai F., Kanai T., Ando K. *Radiation Research* 154:485-496 (2000).
- Gray L.H. *The American Journal of Roentgenology, radium therapy and nuclear medicine* 85:803-815 (1961).
- Goodhead D.T., Thacker J., Cox R. *Nature* 272, 379-380 (1978).
- Goodhead D.T., Munson R.J., Thacker J., Cox R. *International Journal of Radiation Biology* 37(2):135-167 (1980).
- Goodhead D.T. *International Journal of Radiation Biology* 56(5):623-634 (1989)
- Goodhead D.T., Thacker J., Cox R. *International Journal of Radiation Biology* 63(5):543-556 (1993).
- Goodwin E.H., Blakely E.A., Tobias C.A. *Radiation Research* 138(3):343-51 (1994).
- Günter K., Schulz W. *In: Biophysical theory of radiation action: A Treatise on Relative Biological Effectiveness*, pp 54, 55, 193-201, Akademie-Verlag, Berlin (1983).
- Hall E.J. *In: Radiobiology for the Radiobiologist*, pp.47, 5th Ed (2000).

- Hall E.J., Brown J.M., Cavanagh J. *Radiation Research* 35(3):622-34 (1968).
- Hawkins R.B. *Radiation Research* 140(3):366-74 (1994);
— *International Journal of Radiation Biology* 69(6):739-55 (1996);
— *Medical Physics* 25(7):1157-1170 (1998);
— *Radiation Research* 160(1):61-69 (2003);
- Heilmann J., Rink H., Taucher-Scholz G., Kraft G. *Radiation Research* 135(1):46-55 (1993).
- Hesslewood I.P. *International Journal of Radiation Biology* 34(5):461-469 (1978).
- Hill C.K., Holland J., Chang-Liu C.M., Buess E.M., Peak J.G., Peak M.J. *Radiation Research* 113:278-288 (1988).
- Holley W.R., Chatterjee A., Magee J.L. *Radiation Research* 121(2):161-8 (1990).
- Horneck G., Schafer M., Baltschukat K., Weisbrod U., Micke U., Facius R., Bucker H. *Advances in Space Research* 9(10):105-116 (1989).
- Howard A., Gilbert C.W., Greene D. *Radiation Botany* 14:101-107 (1974).
- Jones B., Carabe-Fernandez A., Dale R.G. *A simple model for high-LET radiation biological effects (in preparation)*.
- Kampf G., Regel K., Eichhorn K., Abel H. *Studia Biophysica* 61(1), 53-60 (1977a).
- Kampf G., Tolkendorf E., Regel K., Abel H. *Studia Biophysica* 62(1), 17-24 (1977b).
- Kampf G., Eichhorn K. *Studia Biophysica* 93(1), 17-26 (1983).
- Katz R. *Applied Radiation and Isotopes* 41:563-567 (1990).
- Kawata T., Ito H., Uno T., Saito M., Yamamoto S., Furusawa Y., Durante M., George K., Wu H., Cucinotta F.A. *Cytogenetic and Genome Research* 104(1-4):211-215 (2004).
- Kiefer J. *International Journal of Radiation Biology* 48(6):873-892 (1985).
- Kozubek S., Krasavin E.A. *Neoplasma* 31(6):685-695 (1984).
- Körner I.J., Günther K., Malz W. *Studia Biophysica* 70(3), 175-182 (1978).
- Kraft G. *Nuclear Science Applications* 3:1-28 (1987).
- Kraft G., Krämer M., Scholz M. *Radiation Environmental Biophysics* 31:161-180 (1992).
- Lunec J., Hesslewood I.P., Parker R., Leaper S. *Radiation Research* 85:116-125 (1981).
- Maki H., Saito M., Kobayashi T., Kawai K., Akaboshi M. *International Journal of Radiation Biology*, 50(5):795-810 (1986).

- McWilliams R.S., Gross W.G., Kaplan J.G., Birnboim H .C. *Radiation Research* 94:499-507 (1983).
- Mills M.D., Meyn R.E. *Radiation Research* 87:314-328 (1981).
- Neary G.J. *International Journal of Radiation Biology* 9(5):477-502 (1965).
- Neary G.J., Horgan V.J., Bance D.A., Stretch A. *International Journal of Radiation Biology* 22(6) 525-37 (1972).
- Nikjoo H., O'Neill P., Terrissol M., Goodhead D.T. *Radiation and Environmental Biophysics* 38(1):31-8 (1999).
- Nikjoo H., Goodhead D.T., Charlton D.E., Paretzke H.G. *International Journal of Radiation Biology* 60(5):739-756 (1991).
- Nikjoo H., O'Neill P., Terrissol M., Goodhead D.T. *Radiation Environmental Biophysics* 38:31–8 (1999).
- Nikjoo H., Martin R.F., Charlton D.E., Terrissol M., Kandaiya S., Lobachevsky P. *Acta Oncologica* 35(7):849-56 (1996).
- Nikjoo H., O'Neill P., Goodhead D.T., Terrissol M. *International Journal of Radiation Biology* 71(5):467-83 (1997).
- Nikjoo H., O'Neill P., Terrissol M., Goodhead D.T. *International Journal of Radiation Biology* 66(5):453-7 (1994).
- Nikjoo H., O'Neill P., Wilson W.E., Goodhead D.T. *Radiation Research* 156(5):577-83 (2001).
- Nikjoo H., Bolton C.E., Watanabe R., Terrissol M., O'Neill P. and Goodhead D.T. *Radiation Protection Dosimetry* 99:77–80 (2002).
- Nuñez M.I., McMillan T.J., Valenzuela M.T., Ruiz de Almodovar J.M., Pedraza V. *Radiotherapy and Oncology* 39:155-165 (1996).
- Painter R.B., Young B.R., Burk H.J. *Proceedings of the National Academy of Sciences of the USA*, 71(12) 4836-4838 (1974).
- Peak M.J., Peak J.G., Carnes B.A., Chang Liu C.M, Hill C.K. *International Journal of Radiation Biology* 55(5):761-772 (1989)
- Prise K.M., Davies S., Michael B.D. *International Journal of Radiation Biology* 52(6):893-902 (1987).
- Prise K.M., Davies S., Michael B.D. *International Journal of Radiation Biology* 55(3):323-330 (1989).

- Prise K.M., Folkard M., Davies S., Michael B.D. *International Journal of Radiation Biology* 58(2):261-277 (1990).
- Prise K.M. *International Journal of Radiation Biology* 65(1):43-48 (1994).
- Radford I.R. *International Journal of Radiation Biology* 48(1):45-54 (1985).
- Radford I.R. *International Journal of Radiation Biology* 49:621-637 (1986).
- Ritter M.A., Cleaver J.E., Tobias C.A. *Nature* 266, 653-655 (1977).
- Roots R., Yang T.C., Craise L., Blakely E.A. *Radiation Research* 78(1):38-49 (1979).
- Roots R., Yang T.C., Craise L., Blakely E.A. *Radiation Research* 78:38-49 (1979).
- Sakai K., Okada S. *Radiation Research* 98:479-490 (1984).
- Sakai K., Suzuki S., Nakamura N., Okada S. *Radiation Research* 110:311-320 (1987).
- Semenenko V.A., Stewart R.D. *Radiation Research* 161(4):451-457 (2004).
- Semenenko V.A., Stewart R.D., Ackerman E.J. *Radiation Research* 164(2):180-193 (2005a).
- Semenenko V.A., Stewart R.D. *Radiation Research* 164(2):194-201 (2005b).
- Semenenko V.A., Stewart R.D. *Physics in Medicine and Biology* 51(7):1693-1706 (2006).
- Sinclair W.K., Fry R.J.M. *Radiation Research* 112:407-417 (1987).
- Shekhtman Y.L. *Doklady Akademii Nauk USSR*. pp.116. Edited by AM Kuzin (1960).
- Skarsgard L.D., Kihman B.A., Parker L., Pujara C.M., Richardson S. *Radiation Research Supplement* 7:208-221 (1967).
- Stenerlow B., Hoglund E., Carlsson J., Blomquist E. *International Journal of Radiation Biology* 76(4):549-557 (2000).
- Szumiel I. *Advances in Radiation Biology* 9:281-321 (1981).
- Taucher-Scholz G., Heilmann J., Kraft G. *Advances in Space Research* 18(1-2):83-92 (1996).
- Terrissol M., Pomplun E. *Radiation Protection Dosimetry* 52:177-181 (1994).
- Tobias C.A., Blakely E.A., Noo F.Q.H., Jang T.C.H. *In: Radiation biology and Cancer Research*. Meyn R. E., Withers H. R. (eds.). New York: Raven Press, pp.195-230 (1980).
- Todd P.W. *Radiation Research* 61(2):288-297 (1975).
- Tuschl H., Klein W., Kocsis F., Kovac R., Altmann H. *Studia Biophysica* 50, 55-64 (1975).

- van der Schans G.P., Paterson M.C., Gross W.G. *International Journal of Radiation Biology* 44(1):75-85 (1983).
- Weber K.J.; Flentje M. *International Journal of Radiation Biology* 64(2):169-178 (1993).
- Wambersie A., Hendry J., Gueulette J., Gahbauer R., Pötter R., Gregoire V. *Radiotherapy and Oncology* 73 (Suppl 2): S1-S14 (2004)
- Ward J.F. *Radiation Research Supplement* 8:S103-11 (1985).
- Ward J.F., Blakely W.F., Joner E.I. *Radiation Research* 103, 383-392 (1985).
- Ward J.F. *Progress in Nucleic Acid Research and Molecular Biology* 35:95-125 (1988).
- Zaider M. *Radiation Research* 134(1):1-8 (1993).

Results and conclusions relevant to Chapter 8

The repair kinetic of different cell lines is analysed in this chapter using the three models discussed in Chapters 7 and 8, i.e. the mono-exponential, the bi-exponential and the reciprocal repair models. The analysis will be based on the same process used in Table 7.3, i.e. comparing the fit provided by each model to published data. Three parameters are assessed from the data:

1. Proportion of unrejoined DSB after exposure to radiations of different LET.
2. Repair half life predicted by each model for each radiation quality.
3. Regression coefficient (measured via r^2 or AIC) as an indication of the goodness-of-fit of each model to the experimental data.

According to the theory presented in the previous two chapters, it is predicted that:

- i. the repair half life and the proportion of unrepaired DSB, increases with LET.
- ii. the regression analysis will show that the reciprocal repair model fits the data better than the mono-exponential model but worst than the bi-exponential model.

For convenience, in all the figures and tables of sections 9.1 and 9.2, the *Reciprocal Repair* model is referred to by its original name: the *Hyperbolic* model (Fowler, 1998).

Whilst the analyses presented in Tables 7.2 and 7.3 were done using weighted regression as specified in Table 7.1 in order to make a fair comparison with the results obtained by Fowler (1999; 2002), the analyses presented here have been performed without applying any weighting to the original data as no such comparisons are required here. The main objective in this analysis is to compare the predictions obtained from the mono-exponential, bi-exponential and reciprocal repair models using raw data not subjected to any alteration.

9.1. Neutron data

9.1.1. Repair of mouse cells exposed to gamma rays and neutrons

- *System used:* Mouse lymphoma L5178Y cells (Sakai *et al.*, 1987).
- *Laboratory conditions and Methodology of experiments:*
 - *Neutrons:* A target of Beryllium was bombarded with deuterons of 14MeV to produce neutrons of an average energy of 6MeV (NIRS, Chiba). The dose rate was 1.43Gy/min with 8% of the dose produced from contaminating γ -rays.
 - *γ -rays:* A ^{60}Co source was used to produce a beam with a dose rate of 0.9Gy/min.
- *Radiobiological end point:* To examine the repair processes after irradiation, the cells were irradiated with 18Gy of γ -rays or with 58Gy of fast neutrons. The doses chosen were those which give almost the same number of initial breaks, i.e.: $(1.8 \pm 0.10) \times 10^3$ breaks/ 10^{12} Da DNA by γ -rays and $(2.1 \pm 0.20) \times 10^3$ breaks/ 10^{12} Da DNA by fast neutrons.
- *Original data points:*

Gamma rays (t, PUD \pm 1SE) [hr, %]	Fast Neutrons (t, PUD \pm 1SE) [hr, %]
(0, 99.90 \pm 0.42)	(0, 99.90 \pm 0.42)
(1, 1.54 \pm 0.64)	(0.1, 50.80 \pm 0.53)
(6, 0.74 \pm 0.32)	(0.5, 22.46 \pm 1.48)
	(1, 16.77 \pm 2.22)
	(2, 10.90 \pm 0.69)
	(2.5, 7.97 \pm 0.53)
	(3, 11.38 \pm 0.48)
	(4, 9.31 \pm 0.90)
	(5, 7.25 \pm 0.48)
	(6, 6.67 \pm 1.32)
	(7, 6.51 \pm 0.53)
	(8, 6.35 \pm 1.27)

Table 9.1: Repair kinetic data for mouse lymphoma L5178Y cells presented in Figure 9.1. (t= time; PUD = Proportion of unrepaired data; SE = Standard Error).

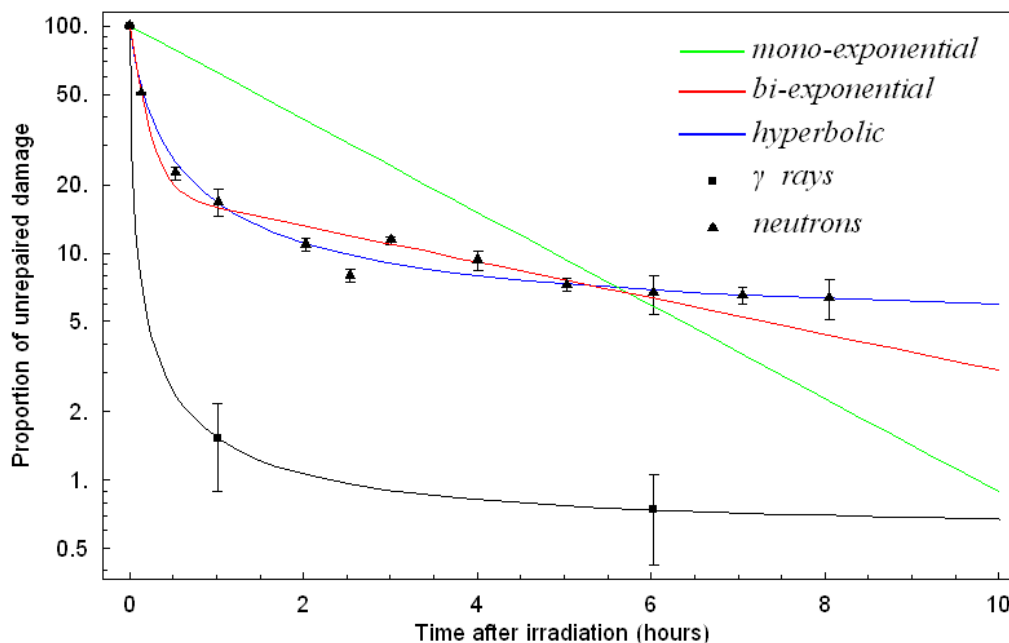


Figure 9.1: Repair kinetics of DNA breaks in mouse lymphoma L5178Y cells. The equations of each of the three models are:

Mono-exponential: $99.90 e^{-0.472 x}$
 Bi-exponential: $80.66 e^{-6.694 x} + 18.98 e^{-0.183 x}$
 Hyperbolic: $4.64 + 95.25 \times (1 + 6.93 x)^{-1}$

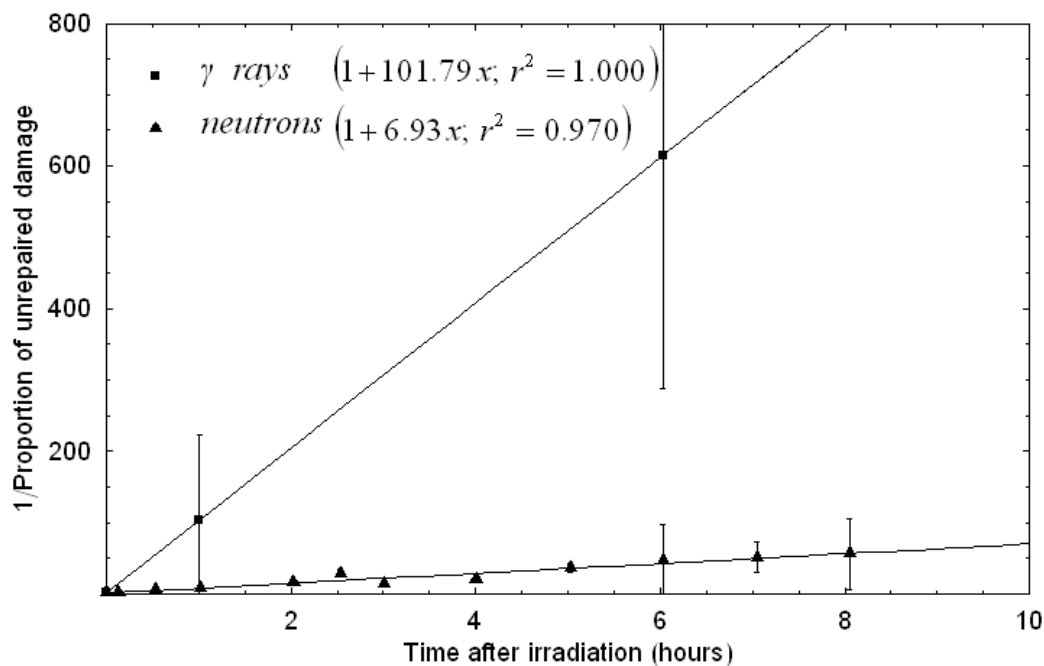


Figure 9.2: Reciprocal plot for 18Gy of γ -rays or with 58Gy of fast neutrons. The regression coefficients (r^2) reported here correspond to the linear regression on the data once the non-repairable proportion of damage is subtracted from the total initial proportion (i.e. $N_0 - \delta$) as indicated in subsection 8.3.1. and figure 8.18.

Figure 9.1 shows that γ -ray-induced DNA scissions are mostly repaired 6h post irradiation, while neutron-induced DNA scissions are also repaired but retain a fraction of non-repaired DNA breaks ($\sim 6\%$ of the initial amount). Sakai *et al.* (1987) repair kinetic analysis was based on the existence of three different repair components: a fast-repairable fraction of about 70% of the total initial breaks, with a repair half-time of 3-5min; a slow-repairable fraction of about 20% of the total initial breaks with a half-time of 70min; and a non-repairable fraction of about 6% at the neutron dose of 58Gy. This final proportion of unrepaired damage reported by Sakai *et al.* (1987) is of the same order of magnitude as the proportion reported in this thesis, i.e. 4.64%. Also, the unrepaired fraction of DNA damage for 18Gy of γ -rays found in this work to be 0.58%, which is not reported by Sakai *et al.* (1987). This figure for the proportion of unreparable damage is obtained from an iterative process of regression to correct the reciprocal of the original repair data to a straight line and, accordingly, to maximise the value of r^2 . For illustration, this process is here explained step-by-step for this particular data set:

1. The original repair data is firstly transformed into uncorrected reciprocal repair

$$\text{data: } (t, n(t) \pm SE) \rightarrow \left(t, \frac{N_o}{n(t)} \pm \frac{SE(t=0)}{SE(t)} \right).$$

2. Then, a regression line over the uncorrected reciprocal data is calculated to obtain the value of r^2 . If $r^2=1$ at this stage it means that we have reached the maximum value of r^2 without correcting the data and thus, $\delta=0$. If $r^2 \neq 1$, carry on to 3.

3. If $r^2 \neq 1$ (due to the tailing-off of the data), the uncorrected reciprocal data needs to be corrected to find the maximum value of r^2 . Therefore, a value of δ is selected and subtracted from the reciprocal of the proportion of unrepaired

$$\text{damage, i.e. } \left(t, \frac{N_o}{n(t)} \right) \rightarrow \left(t, \frac{N_o - \delta}{n(t) - \delta} \pm \frac{SE(t=0) - \delta}{SE(t) - \delta} \right).$$

4. A regression line is fitted again to the $\left(t, \frac{N_o - \delta}{n(t) - \delta} \pm \frac{SE(t=0) - \delta}{SE(t) - \delta} \right)$ data set in order to obtain a new value of r^2 . More values of δ are then tried iteratively in

order to find a maximum value of r^2 (i.e. best regression line to the resultant

$$\left(t, \frac{N_0 - \delta}{n(t) - \delta} \pm \frac{SE(t=0) - \delta}{SE(t) - \delta} \right) \text{ data set).}$$

- The value of δ that makes r^2 maximum is considered the non-repairable fraction of unrepaired DNA damage.

For the case of fast neutrons in Table 9.1, the application of this process results in the following data:

Time	$n(t)$	$SE(t)$	$N_0/n(t)$	$SE_0/SE(t)$	$\frac{N_0 - \delta}{n(t) - \delta}$	$\frac{SE_0 - \delta}{SE(t) - \delta}$
0	99.9	0.42	1.000	1.000	1.000	1.000
0.1	50.8	0.53	1.967	0.792	2.064	1.027
0.5	22.46	1.48	4.448	0.284	5.346	1.335
1	16.77	2.22	5.957	0.189	7.855	1.743
2	10.90	0.69	9.165	0.609	15.223	1.068
2.5	7.97	0.53	12.535	0.792	28.627	1.027
3	11.38	0.48	8.779	0.785	14.138	1.014
4	9.31	0.90	10.730	0.467	20.409	1.128
5	7.25	0.48	13.779	0.875	36.532	1.014
6	6.67	1.32	14.978	0.318	46.983	1.217
7	6.51	0.53	15.346	0.792	51.008	1.027
8	6.35	1.27	15.732	0.331	55.788	1.252

Table 9.2: Results from the iterative process explained above to calculate the fraction of unrepaired damage produced by 58Gy of fast neutrons. The value found for δ is 4.643, producing a maximum value of r^2 of 0.9408.

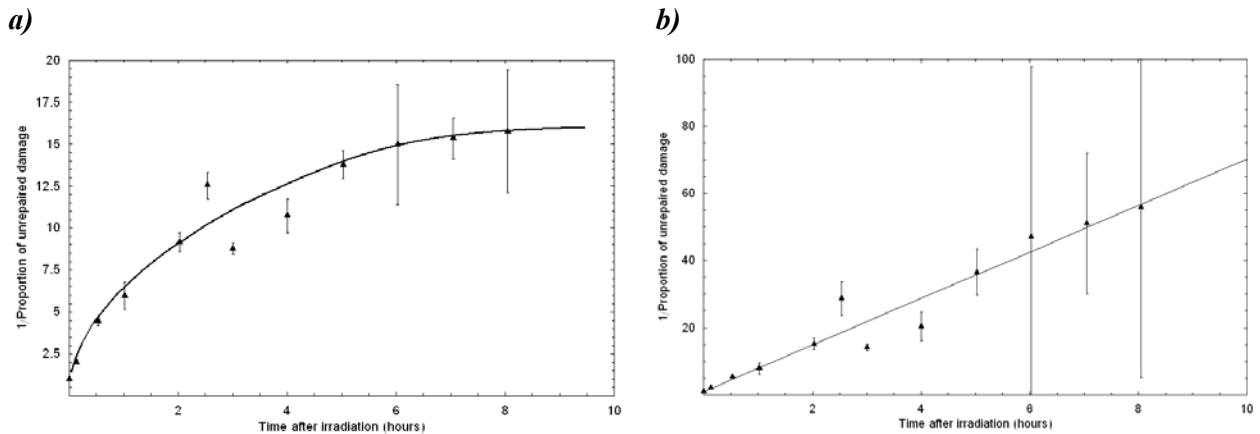


Figure 9.3: Reciprocal repair kinetics plots. (a) data uncorrected for unrepaired damage; (b) data corrected for unrepaired damage. Figure (a) shows the saturation effect (or slow-down effect) at large repair times due to the presence of the unrepaired damage. Once this unrepaired damage is subtracted from the data, the saturation effect disappears and the data can be fitted using second order repair kinetics.

The difference in the error bars between Figure 9.3a and Figure 9.3b is due to the fact that, while in column 5 of Table 9.2 the standard error of the reciprocal data is obtained by dividing the standard error at $t=0$ by the standard error at the corresponding time t , in column 7 we divide by a smaller amount (i.e. $SE(t)-\delta$).

To obtain the half-life of the damage produced by either gamma or fast neutrons, Equation (8.6) can be re-arranged as follows:

$$\frac{n(t)}{N_0} - \frac{\delta}{N_0} = \frac{1 - \frac{\delta}{N_0}}{zt + 1} \Rightarrow n(t) - \delta = \frac{N_0 - \delta}{zt + 1} \tag{9.1}$$

Thus, if we define $t = \tau$ when $[n(t) - \delta] = \frac{[N_0 - \delta]}{2}$, Equation (9.1) becomes:

$$\frac{N_0 - \delta}{2} = \frac{N_0 - \delta}{z\tau + 1} \Rightarrow 2 = z\tau + 1 \Rightarrow \tau = \frac{1}{z}$$

Therefore, the half-life of the corrected reciprocal data is obtained from the inverse of the slope of the regression line applied to it, which in this case is 0.144 ± 0.02 ($\pm 95\%$ CI) hours ($\frac{1}{6.93 \text{ hr}^{-1}}$). This value is within the range reported by Sakai *et al.* (1987):

Sakai <i>et al.</i> (1987)		Present Analysis			
Fast Comp.	Slow Comp.	Mono-exp.	Bi-exp.		Hyperbolic
			Fast	Slow	
3-5 min	70 min	127.12 min	8.96 min	327.87 min	8.66 min

Table 9.3: Repair half-lives reported by Sakai et al. (1987) and this report.

9.2. Heavier ion data

9.2.1. Induced chromosomal damage by X-rays and Neon ions

- *System used:* Human/hamster hybrid UV24C2-3 (Goodwin *et al.*, 1989) cells synchronised in stationary G₁ phase.
- *Laboratory conditions and Methodology of experiments:*
 - *X-rays:* A 220 kVp X-rays source filtered with 2.5mm Cu and 1mm Al was used. The dose rate was usually 270cGy/min.
 - *Neon ions:* 425MeV/amu neon beams produced at the Belavac heavy ion accelerator facility. Cells were irradiated near the Bragg peak where the LET was 183keV/μm
 - Premature chromosome condensation technique was used to determine the efficiency of X-ray and Neon ions to induce breakage in cellular chromatin. Neon ions were found to be 1.5 times more effective than X-rays to induce chromatin breakage (0.0754±0.0039 chromatin breaks/cell/cGy for 240cGy of X-rays compared to 0.1138±0.009 breaks/cell/cGy for 165cGy).
- *Radiobiological end point:* To examine the repair processes after irradiation, the cells were irradiated with 16Gy of X-rays or with 10.62Gy of Neons. The doses chosen were those which gave a comparable level of initial damage, i.e. 121 chromatin breaks.
- *Original data points:*

<i>X- rays</i>	<i>Neon ions</i>
<i>(t, PUD ± 1SE) [hr, %]</i>	<i>(t, PUD ± 1SE) [hr, %]</i>
(0.24, 66.54±1.51)	(0.24, 74.67±2.79)
(0.49, 32.68±1.08)	(0.58, 64.96±2.63)
(0.99, 18.37±0.79)	(6.01, 49.74±2.56)
(9.13, 11.68±0.49)	(7.58, 49.34±1.71)

Table 9.4: Repair kinetic data for UV24C2-3 cells presented in Figure 9.4. (*t*= time; *PUD* = Proportion of unrepaired data; *SE* = Standard Error).

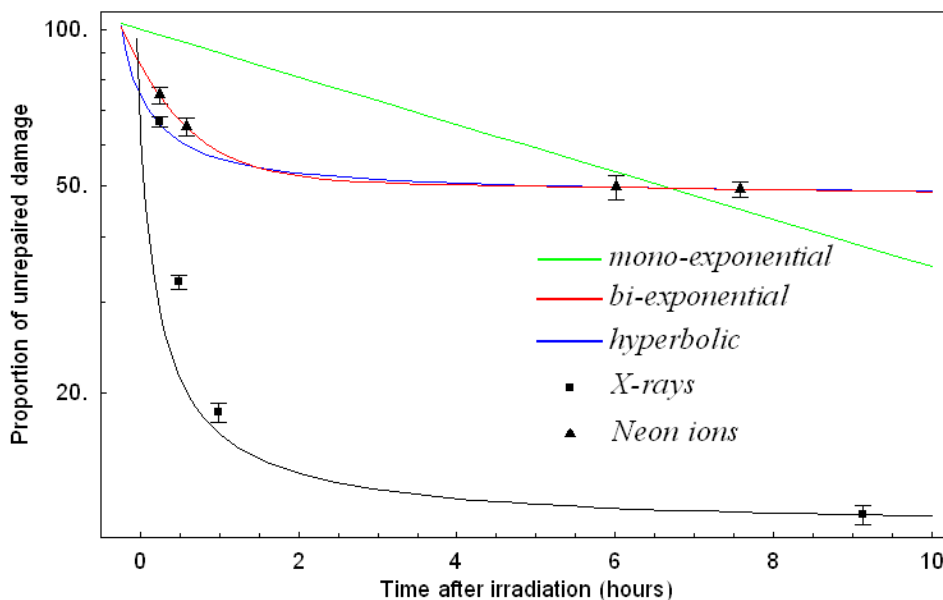


Figure 9.4: Repair kinetics of DNA breaks in UV24C2-3 cells. The equations of each of the three models are:

Mono-exponential: $100 e^{-0.105 x}$
Bi-exponential: $34.04 e^{-1.554 x} + 51.29 e^{-0.005 x}$
Hyperbolic: $10.99 + 55.55 \times (1 + 8.64 x)^{-1}$ (X-rays)
 $47.75 + 26.92 \times (1 + 2.09 x)^{-1}$ (neon ions)

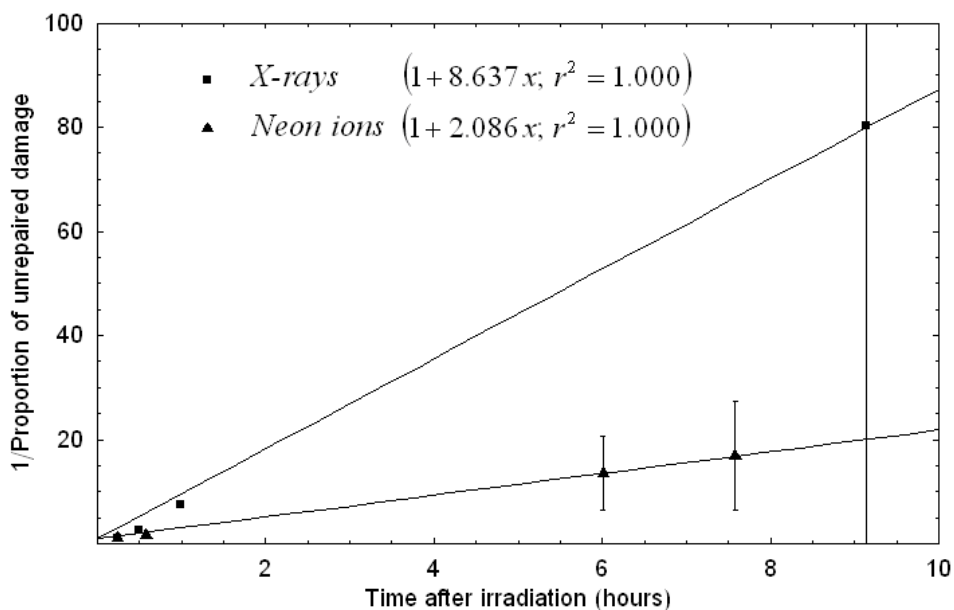


Figure 9.5: Reciprocal plot for 16Gy of X-rays or with 10.62Gy of Neon ions.

The following table shows the resultant half-lives obtained from each model and how these results compare with the original data.

	Goodwin <i>et al.</i> (1989)	Present Analysis				
	τ (min)	Mono-exp.	Bi-exponential		Hyperbolic	
			Fast	Slow	τ (min)	δ
X-rays	23.6	-	-	-	6.95±0.65	10.99
Neon	28.7	571.12 min	38.61 min	195.78 min	28.77±2.15	47.75

Table 9.5: Repair half-lives reported by (Goodwin et al., 1989) and this report.

Goodwin *et al.* (1989) used a mono-exponential model to obtain the values of τ included in Table 9.5. It is interesting to observe how for this data set there is a substantial difference between the final unreparable proportion produced by X-rays and neon ions, yet the half-lives of the damage produced by both types of radiation are of the same order. Similarly, the half-time predicted by the mono-exponential model in this thesis is extremely high, which has been related to the fact that no data is available at $t = 0$ hours which affects the non-linear regression applied to the data.

9.2.2. Induced chromatin damage in human cells irradiated with accelerated carbon ions.

- *System used*: Normal human embryo cells (Suzuki *et al.*, 1996).
- *Laboratory conditions and Methodology of experiments*:
 - *γ-rays*: cells were irradiated with *γ-rays* produced by a ¹³⁷Cs source at a dose rate of 1.2Gy/min.
 - *Carbon ions*: 135 MeV/u (produced at the Riken Ring Cyclotron, Japan) and 12 MeV/u (produced at the National Institute of Radiological Sciences, Japan) were used to produce chromatin damage at a dose rate of 2 Gy/min. Different LET values (39 and 124keV/μm) were produced by placing a Lucite absorber on the beam.
- *Radiobiological end point*: To examine the repair processes after irradiation, the cells were irradiated with 4Gy of ¹³⁷Cs gamma rays or 3Gy of 39 and 124 keV/μm. The doses chosen were those which gave a comparable level of initial damage (not specified by Suzuki *et al.* (1996)).
- *Original data points*:

<i>γ- rays</i> (<i>t, PUD ± 1SE</i>) [hr, %]	<i>Carbon ions (39keV/μm)</i> (<i>t, PUD ± 1SE</i>) [hr, %]	<i>Carbon ions (124keV/μm)</i> (<i>t, PUD ± 1SE</i>) [hr, %]
(0, 100±0.71)	(0, 100±0.71)	(0, 100±0.71)
(0.84, 49.97±0.71)	(0.37, 75.83±0.67)	(0.32, 81.48±0.60)
(1.90, 37.81±0.71)	(0.86, 59.86±0.64)	(0.84, 69.61±0.64)
(3.91, 9.26±0.74)	(1.89, 46.71±0.64)	(1.89, 61.41±0.67)
(7.91, 5.44±0.71)	(3.89, 31.87±0.67)	(3.86, 54.77±0.67)
(12.02, 5.58±0.71)	(7.91, 22.26±0.67)	(11.98, 52.93±0.64)
	(12.04, 19.29±0.67)	

Table 9.6: Repair kinetic data for normal human embryo cells presented in Figures 9.6 and 9.8. (*t*= time; *PUD* = Proportion of unrepaired data; *SE* = Standard Error).

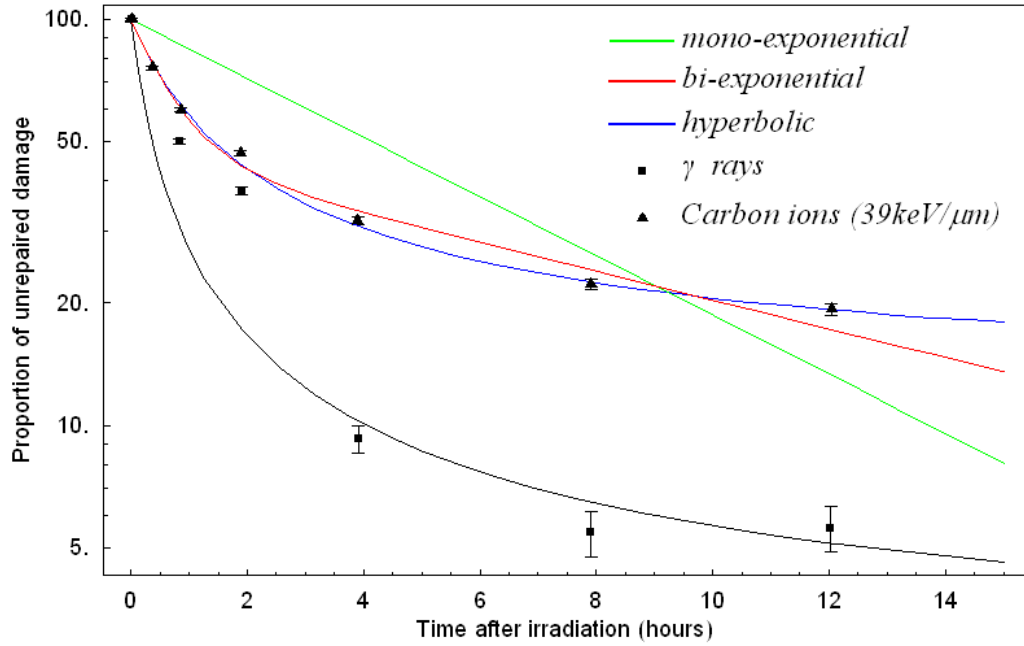


Figure 9.6: Repair kinetics of DNA breaks normal human embryo cells. The equations of each of the three models are:

Mono-exponential: $100 e^{-0.168 x}$
 Bi-exponential: $53.68 e^{-1.341 x} + 46.07 e^{-0.082 x}$
 Hyperbolic: $2.46 + 97.54 \times (1 + 2.96 x)^{-1}$ (γ -rays)
 $12.11 + 87.89 \times (1 + 0.94 x)^{-1}$ (^{12}C - 39keV/ μm)

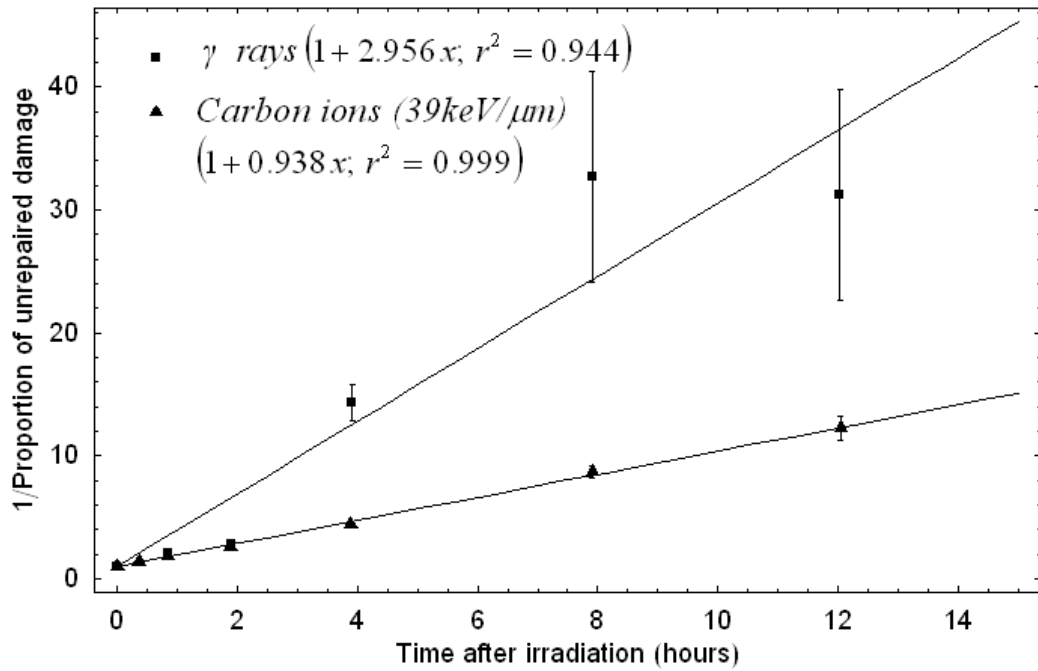


Figure 9.7: Reciprocal plot for 4Gy of ^{137}Cs gamma rays or 3Gy of ^{12}C -39keV/ μm .

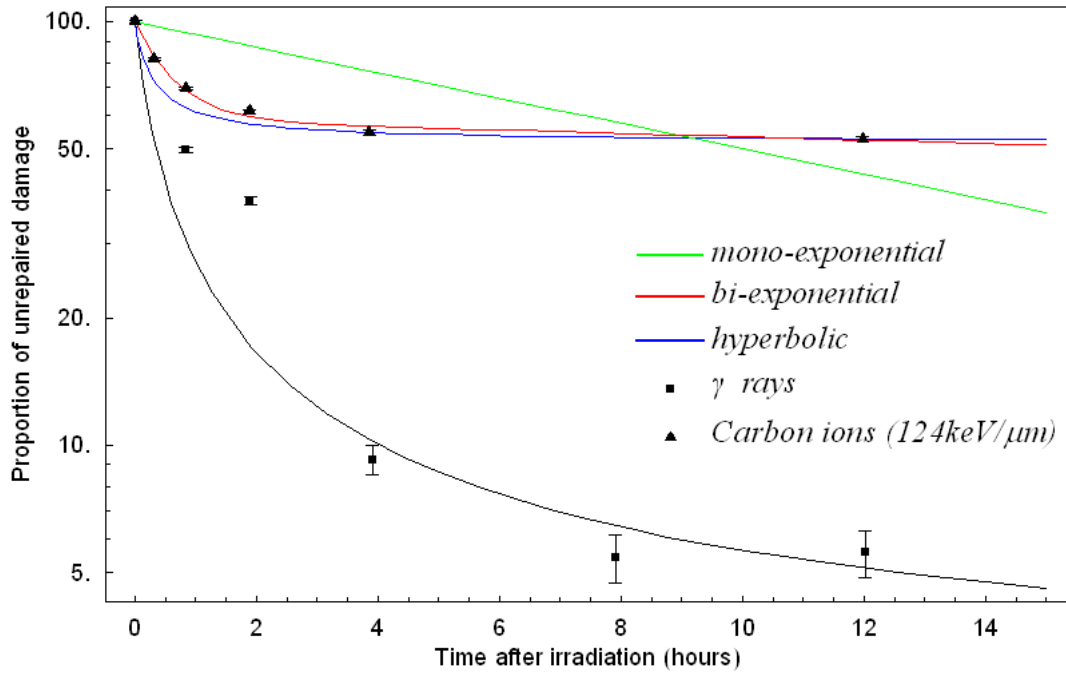


Figure 9.8: Repair kinetics of DNA breaks in normal human embryo cells. The equations of each of the three models are:

Mono-exponential: $100 e^{-0.069 x}$
Bi-exponential: $41.11 e^{-1.611 x} + 58.69 e^{-0.009 x}$
Hyperbolic: $2.46 + 97.54 \times (1 + 2.96 x)^{-1}$ (γ -rays)
 $52.01 + 47.99 \times (1 + 4.21 x)^{-1}$ (^{12}C - 124keV/ μm)

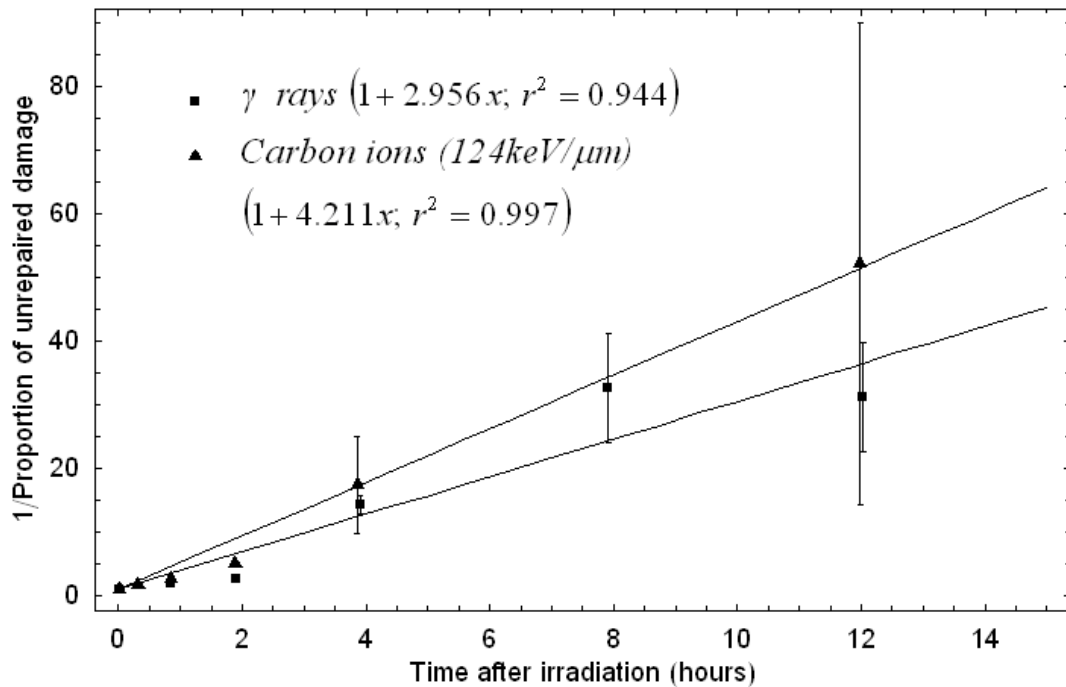


Figure 9.9: Reciprocal plot for 4Gy of ^{137}Cs gamma rays or 3Gy of ^{12}C -124keV/ μm .

	Suzuki <i>et al.</i> (1996)		Present Analysis				
	τ (min)		Mono- exp.	Bi-exponential		Hyperbolic	
	50%	95%		Fast	Slow	τ (min)	δ
γ -rays	60	480	-	-	-	20.30 \pm 6.17	2.46
^{12}C - 39keV/ μm	-	-	357.47 min	44.73min	724.76 min	63.98 \pm 1.80	12.11
^{12}C - 124keV/ μm	480	-	869.10 min	37.24 min	6523.7 min	14.25 \pm 1.34	52.01

Table 9.7: Repair half-lives reported by (Suzuki *et al.*, 1996) and this report.

9.2.3. Rejoining of DNA fragments produced by radiations of different linear energy transfer.

- *System used:* Low passages of normal human skin fibroblast (GM5758) cells (Stenerlow *et al.*, 2000).
- *Laboratory conditions and Methodology of experiments:* Petri dishes were kept at 4°C 30 min prior and after the irradiation to avoid DNA repair during irradiation.
 - *γ-rays:* cells were irradiated with *γ-rays* produced by a ⁶⁰Co source at a dose rate of 1-1.3 Gy/min.
 - *Ion irradiations:* the Gustaf Werner synchrocyclotron with nominal energy of 32MeV/u was used to produce Helium and Nitrogen ions of different LET.
- *Radiobiological end point:* Time-course rejoining kinetics of DSB was studied after irradiation with doses of ≈100Gy followed by incubation at 37°C for various periods of time up to 22h.
- *Original data points:*

<i>γ-rays</i> (<i>t, PUD ± 1SE</i>) [hr, N]	<i>Helium ions</i> (<i>40keV/μm</i>) (<i>t, PUD ± 1SE</i>) [hr, N]	<i>Nitrogen ions</i> (<i>t, PUD ± 1SE</i>) [hr, N]			
		<i>80keV/μm</i>	<i>125keV/μm</i>	<i>175keV/μm</i>	<i>225keV/μm</i>
(0, 568.9±0)	(0, 852.5±0)	(0, 920.3±0)	(0, 918.0±0)	(0, 927.4±0)	(0, 730.6±0)
(0.1, 511.5±9.0)	(0.4, 444.9±93.0)	(0.1, 774.6±59.7)	(0.55, 506.6±37)	(0.1, 827.4±51.6)	(0.1, 643.0±20.7)
(0.4, 332.8±23.0)	(0.7, 310.9±64.8)	(0.5, 439.0±14.0)	(1.1, 385.3±27.5)	(0.5, 459.7±8.5)	(0.6, 385.1±9.9)
(0.7, 222.9±41.0)	(1.0, 201.7±101.6)	(1.1, 267.8±9.3)	(3.0, 250.8±33.2)	(1.2, 350±8.9)	(1, 353.7±8.3)
(1.1, 182.0±18.9)	(4.0, 178.65±95.5)	(3.9, 118.6±10.2)	(5.8, 150.8±21.3)	(4.1, 182.3±6.5)	(4, 238.0±14.5)
(3.1, 54.1±12.3)	(20.3, 61.0±25.82)	(20.8, 50.9±7.6)	(22.3, 55.7±16.0)	(20.7, 112.9±15.3)	(20.3, 84.3±7)
(6.0, 41.0±5.7)					
(22.2, 26.2±9.0)					

Table 9.8: Repair kinetic data for normal human skin fibroblast cells presented in Figure 9.10, 9.12, 9.14 and 9.16. (*t* = time; *PUD* = Proportion of unrepaired data; *SE* = Standard Error; *N* = Number of DSB).

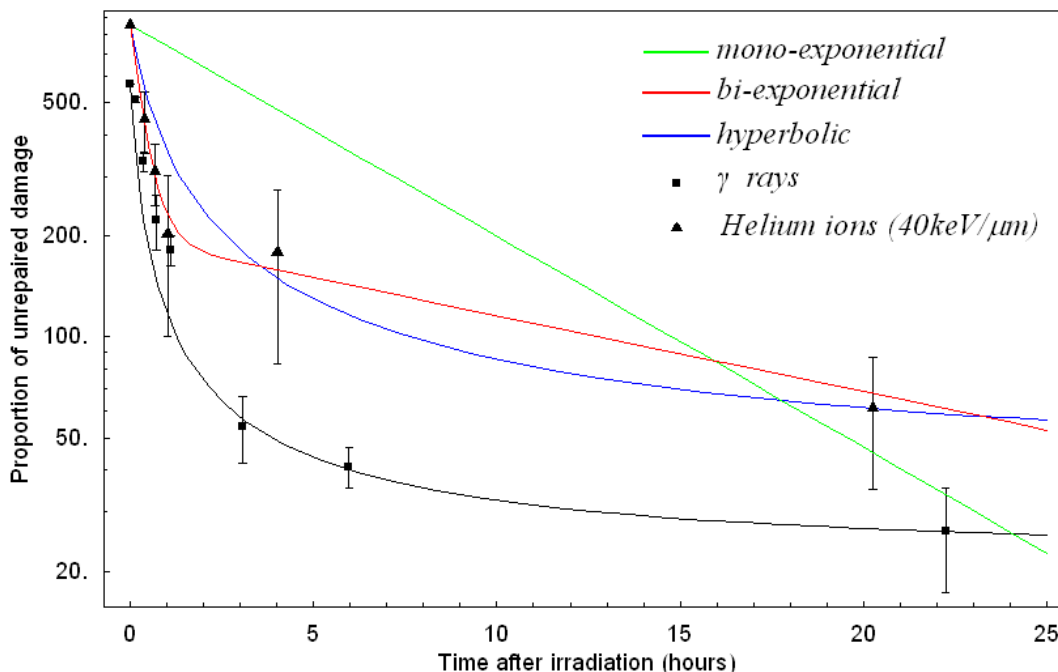


Figure 9.10: Repair kinetics of DNA breaks in normal human fibroblast cells. The equations of each of the three models are:

Mono-exponential:	$852.48 e^{-0.145 x}$
Bi-exponential:	$659.62 e^{-2.594 x} + 195.15 e^{-0.052 x}$
Hyperbolic:	$21 + 547.85 \times (1 + 4.65 x)^{-1}$ (γ -rays) $35.7 + 816.78 \times (1 + 1.54 x)^{-1}$ (He-40keV/ μ m)

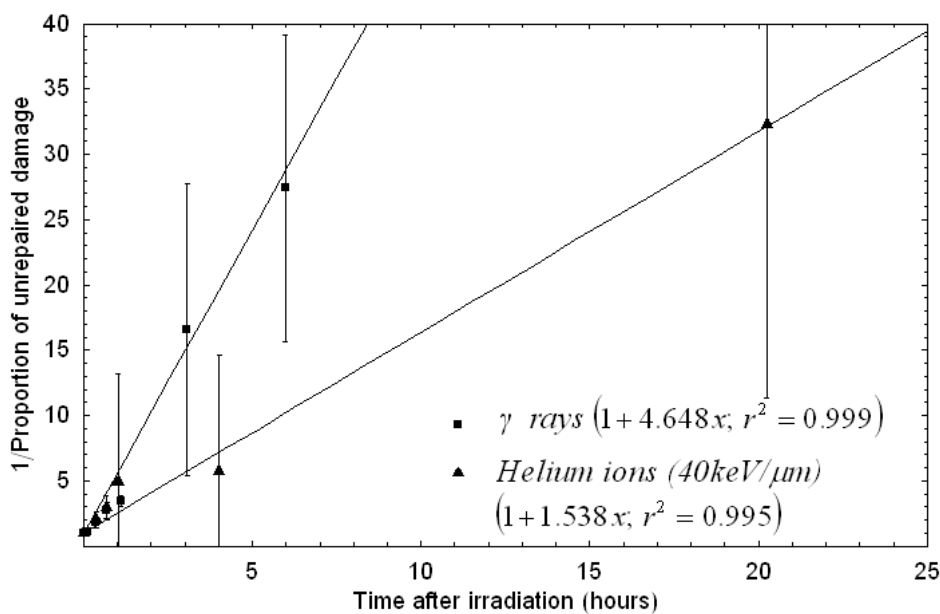


Figure 9.11: Reciprocal plot for 100Gy of ⁶⁰Co gamma rays or He-40keV/ μ m ions.

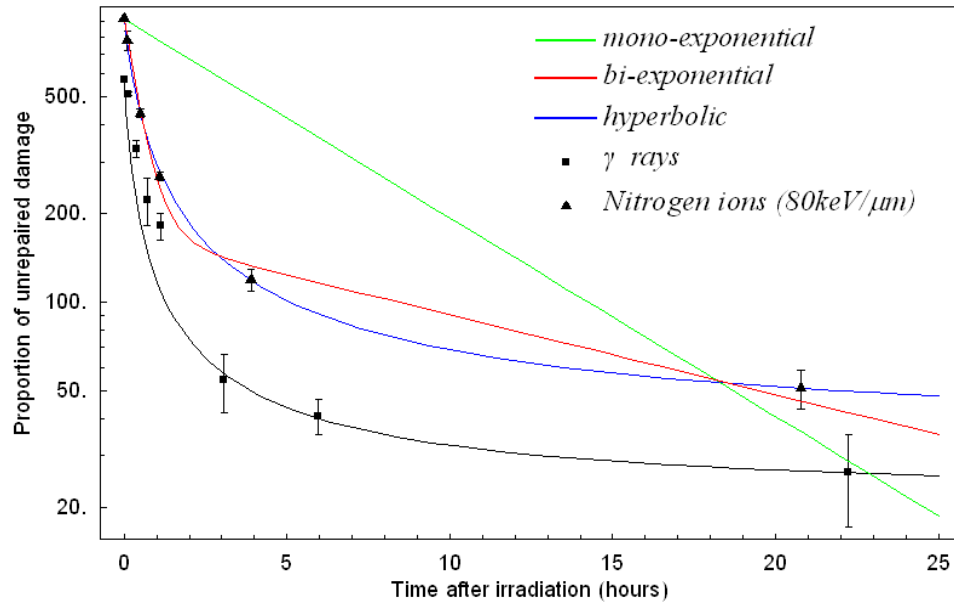


Figure 9.12: Repair kinetics of DNA breaks in normal human fibroblast cells. The equations of each of the three models are:

Mono-exponential: $920.34 e^{-0.156x}$
Bi-exponential: $744.17 e^{-1.941x} + 168.92 e^{-0.052x}$
Hyperbolic: $21 + 547.85 \times (1 + 4.65x)^{-1}$ (γ -rays)
 $33.66 + 886.68 \times (1 + 2.43x)^{-1}$ (N -80keV/ μ m)

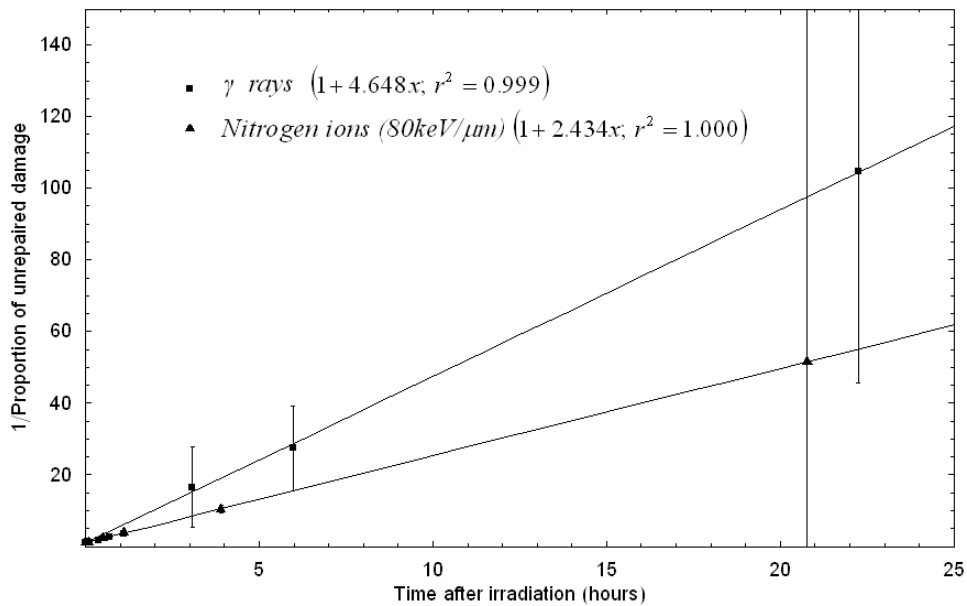


Figure 9.13: Reciprocal plot for 100Gy of ^{60}Co gamma rays or N -80keV/ μ m ions.

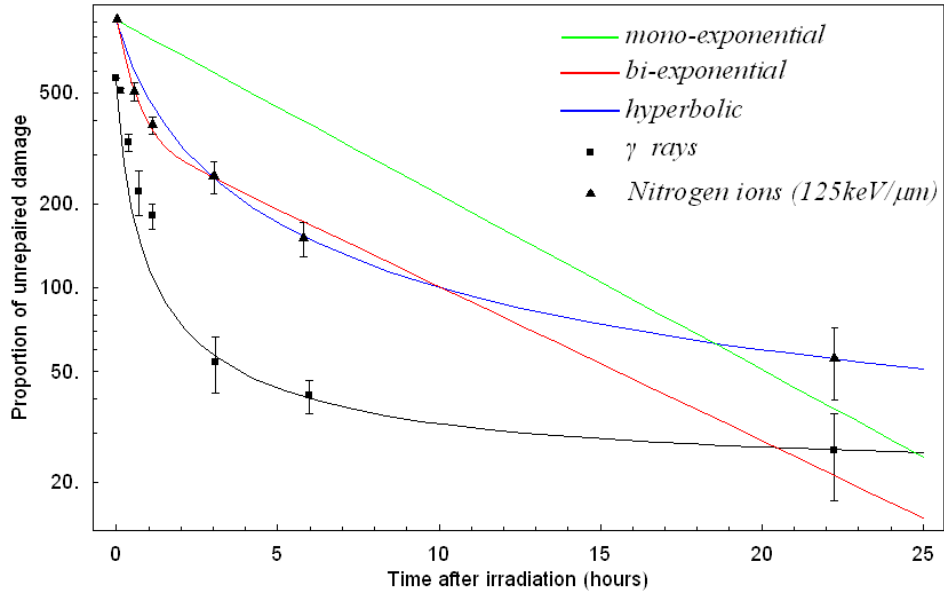


Figure 9.14: Repair kinetics of DNA breaks in normal human fibroblast cells. The equations of each of the three models are:

Mono-exponential: $918.03 e^{-0.145 x}$
Bi-exponential: $577.96 e^{-2.13 x} + 363.33 e^{-0.128 x}$
Hyperbolic: $21 + 547.85 \times (1 + 4.65 x)^{-1}$ (γ -rays)
 $15.1 + 902.93 \times (1 + 0.955 x)^{-1}$ (N-125keV/ μ m)

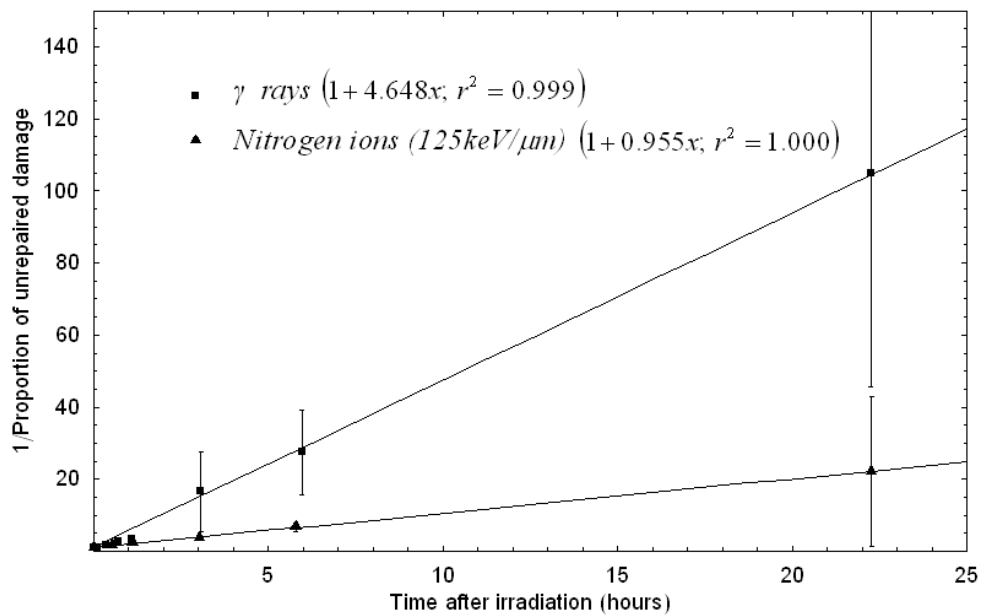


Figure 9.15: Reciprocal plot for 100Gy of ^{60}Co gamma rays or N-125keV/ μ m ions.

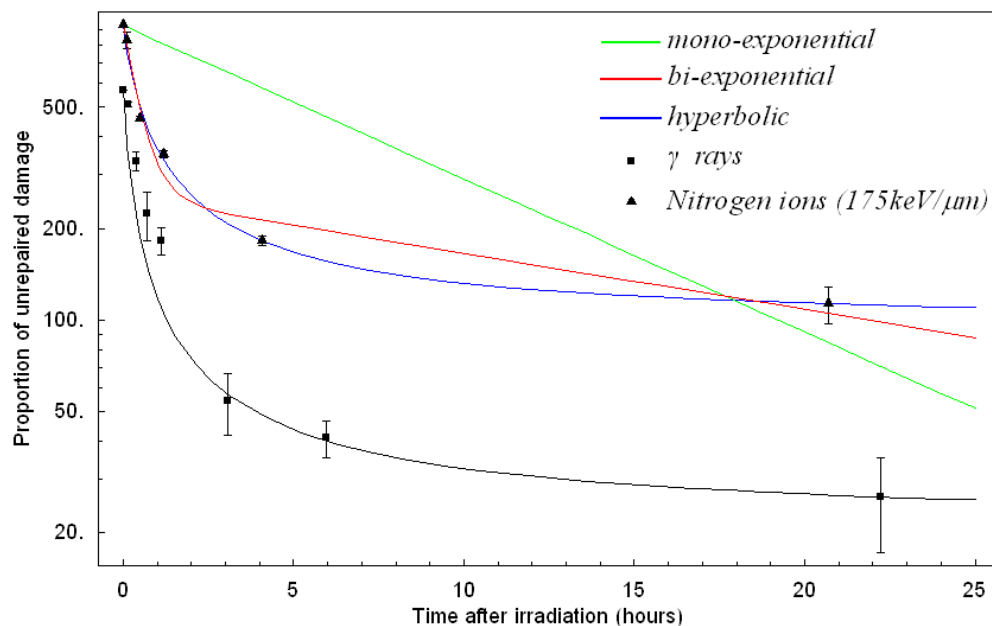


Figure 9.16: Repair kinetics of DNA breaks in normal human fibroblast cells. The equations of each of the three models are:

Mono-exponential: $927.42 e^{-0.116 x}$
Bi-exponential: $681.52 e^{-2.05 x} + 253.03 e^{-0.042 x}$
Hyperbolic: $21 + 547.85 \times (1 + 4.65 x)^{-1}$ (γ -rays)
 $93.96 + 833.46 \times (1 + 2.08 x)^{-1}$ (N-175keV/ μ m)

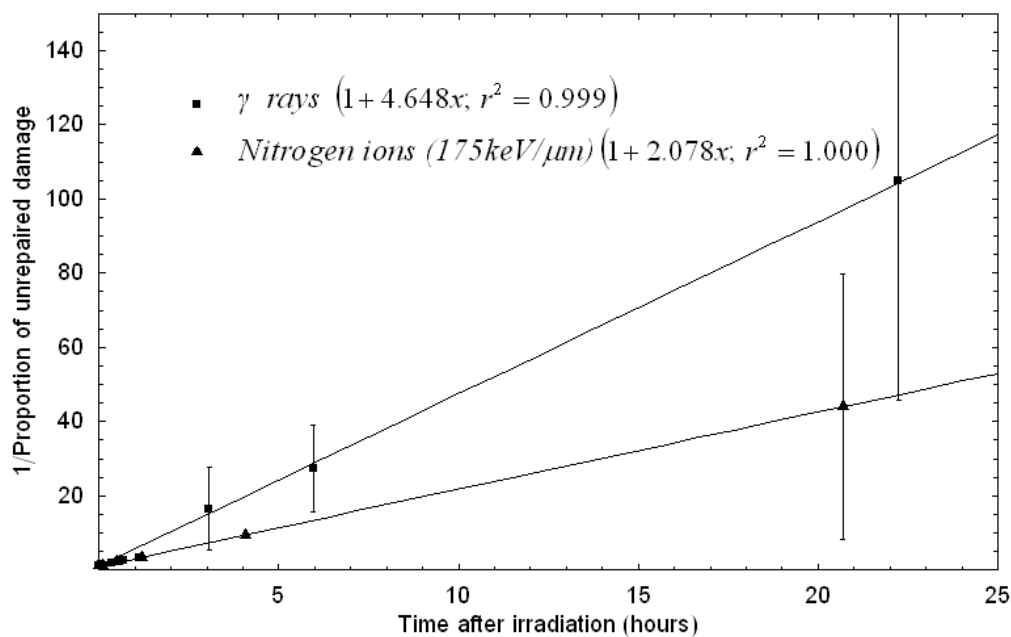


Figure 9.17: Reciprocal plot for 100Gy of ⁶⁰Co gamma rays or N-175keV/ μ m ions.

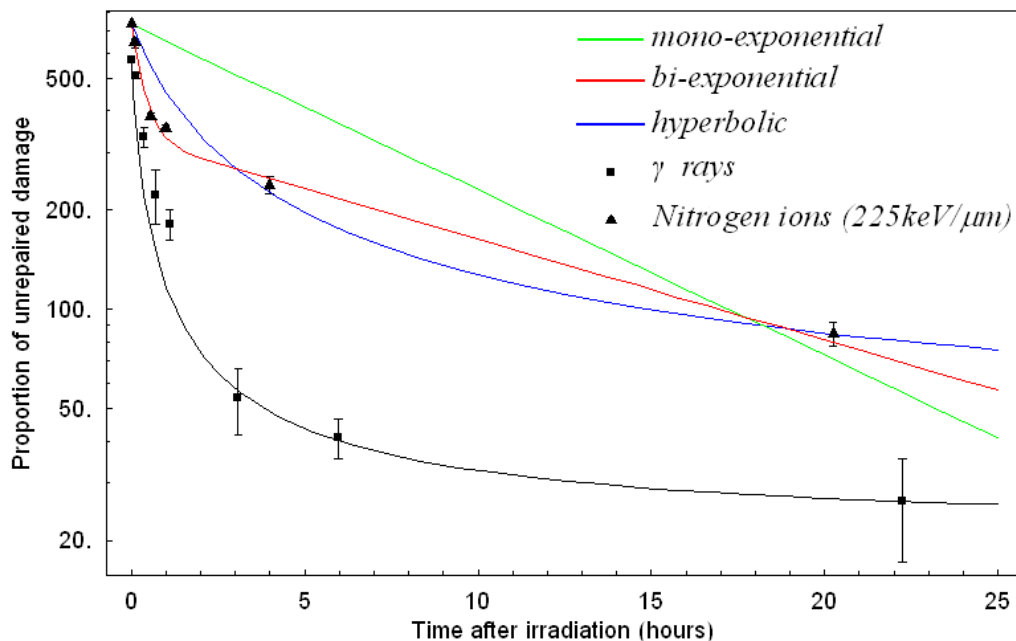


Figure 9.18: Repair kinetics of DNA breaks in normal human fibroblast cells. The equations of each of the three models are:

Mono-exponential: $730.58 e^{-0.115x}$
 Bi-exponential: $405.33 e^{-2.80x} + 329.83 e^{-0.070x}$
 Hyperbolic: $21 + 547.85 \times (1 + 4.65x)^{-1}$ (γ -rays)
 $35.95 + 694.64 \times (1 + 0.66x)^{-1}$ (N-225keV/ μm)

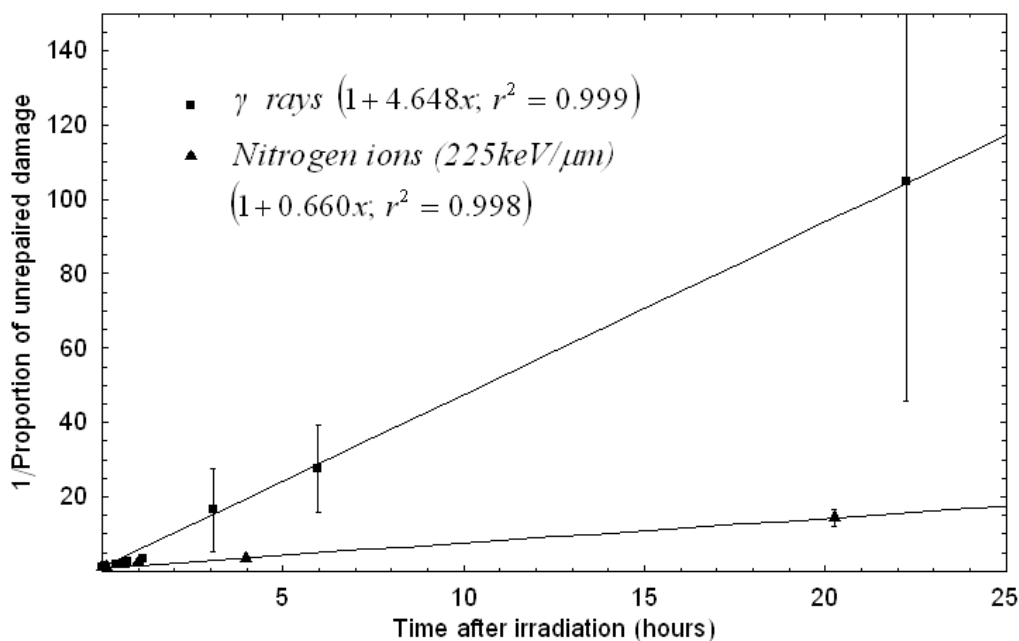


Figure 9.19: Reciprocal plot for 100Gy of ^{60}Co gamma rays or N-225keV/ μm ions.

The next table summarises the reported and the resultant repair kinetic parameters for each LET:

	Stenerlow <i>et al.</i> (2000)		Present Analysis				
	τ		Mono-exp.	Bi-exponential		Hyperbolic	
	Fast (min)	Slow (hr)		Fast	Slow	τ (min)	δ
γ -rays	19 \pm 8	1.3 \pm 1.0	-	-	-	12.91 \pm 0.41	21
He-40keV/ μ m	16 \pm 4	6.8 \pm 6.1	413.51 min	23.1min	19.10 hr	39.02 \pm 4.20	35.70
N-80keV/ μ m	17 \pm 2	2.7 \pm 0.5	384.94 min	30.9min	16.00 hr	24.6 \pm 0.1	33.66
N-125keV/ μ m	13 \pm 2	2.7 \pm 0.3	414.96 min	28.11min	7.83 hr	62.80 \pm 1.61	15.10
N-175keV/ μ m	15 \pm 7	2.1 \pm 1.5	517.95 min	29.25 min	23.56 hr	28.87 \pm 0.26	93.96
N-225keV/ μ m	12 \pm 4	4.1 \pm 1.4	520.12 min	21.47 min	14.23 hr	90.87 \pm 6.40	35.94

Table 9.9: Repair half-lives reported by (Stenerlow *et al.*, 2000) and this report.

9.2.4. DNA DSB induction and rejoining in V79 cells irradiated with light ions.

- System used: V79-753B cells (Belli *et al.*, 2000).
- Laboratory conditions and Methodology of experiments: Petri dishes were kept at 4°C to avoid DNA repair during irradiation.
 - o γ -rays: cells were irradiated with γ -rays produced by a ^{60}Co source at a dose rate of 20Gy/min.
 - o Ion irradiations: the 7MV Van de Graaff CN accelerator at the Istituto Nazionale di Fisica Nucleare (INFN) was used to produce ions of different energy and LETs. The dose rate used was 20Gy/min.
- Radiobiological end point: Time-course rejoining kinetics was studied after irradiation with doses of $\approx 45\text{Gy}$ ($\pm 10\%$) followed by incubation at 37°C for various periods of time up to 2h.
- Original data points:

γ - rays (t, PUD \pm 1SE) [min, %]	Protons 11keV/ μm (t, PUD \pm 1SE) [min, %]	Protons 31keV/ μm (t, PUD \pm 1SE) [min, %]	Deuterons 13keV/ μm (t, PUD \pm 1SE) [min, %]	Helium-3 53keV/ μm (t, PUD \pm 1SE) [min, %]	Helium-4 53keV/ μm (t, PUD \pm 1SE) [min, %]
(0, 1 \pm 0.01)	(0, 1 \pm 0.01)	(0, 1 \pm 0.01)	(0, 1 \pm 0.01)	(0, 1 \pm 0.01)	(0, 1 \pm 0.01)
(15, 0.63 \pm 0.02)	(15, 0.71 \pm 0.03)	(15, 0.87 \pm 0.03)	(15, 0.71 \pm 0.03)	(15, 0.77 \pm 0.02)	(15, 0.75 \pm 0.03)
(30, 0.43 \pm 0.01)	(30, 0.55 \pm 0.02)	(30, 0.74 \pm 0.02)	(30, 0.54 \pm 0.02)	(30, 0.65 \pm 0.02)	(30, 0.64 \pm 0.02)
(60, 0.33 \pm 0.01)	(60, 0.4 \pm 0.02)	(60, 0.66 \pm 0.02)	(60, 0.35 \pm 0.02)	(60, 0.49 \pm 0.02)	(60, 0.51 \pm 0.02)
(90, 0.19 \pm 0.01)					
(120, 0.15 \pm 0.01)	(120, 0.2 \pm 0.02)	(120, 0.59 \pm 0.02)	(120, 0.24 \pm 0.02)	(120, 0.37 \pm 0.02)	(120, 0.39 \pm 0.02)
			Deuterons 62keV/ μm (t, PUD \pm 1SE) [min, %]	Helium-3 81keV/ μm (t, PUD \pm 1SE) [min, %]	Helium-4 123keV/ μm (t, PUD \pm 1SE) [min, %]
			(0, 1 \pm 0.01)	(0, 1 \pm 0.01)	(0, 1 \pm 0.01)
			(15, 0.80 \pm 0.01)	(15, 0.79 \pm 0.02)	(15, 0.89 \pm 0.04)
			(30, 0.75 \pm 0.01)	(30, 0.71 \pm 0.01)	(30, 0.89 \pm 0.03)
			(60, 0.64 \pm 0.01)	(60, 0.60 \pm 0.01)	(60, 0.79 \pm 0.03)
			(120, 0.55 \pm 0.02)	(120, 0.49 \pm 0.01)	(120, 0.68 \pm 0.01)

Table 9.10: Repair kinetic data for V79-753B cells. (t = time; PUD = Proportion of unrepaired data; SE = Standard Error).

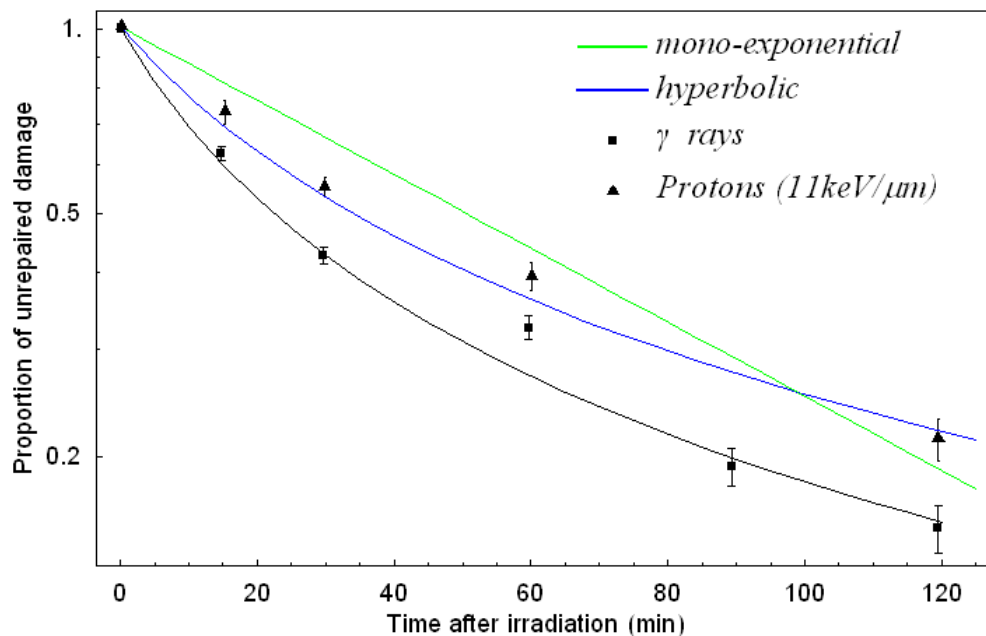


Figure 9.20: Repair kinetics of DNA breaks in V79-753B cells exposed to 11keV/μm protons. The equations of each of the three models are:

Mono-exponential: $1.008 e^{-0.014 x}$

Hyperbolic: $1.003 \times (1 + 0.045 x)^{-1}$ (γ -rays)
 $1.008 \times (1 + 0.030 x)^{-1}$ (Protons-11keV/μm)

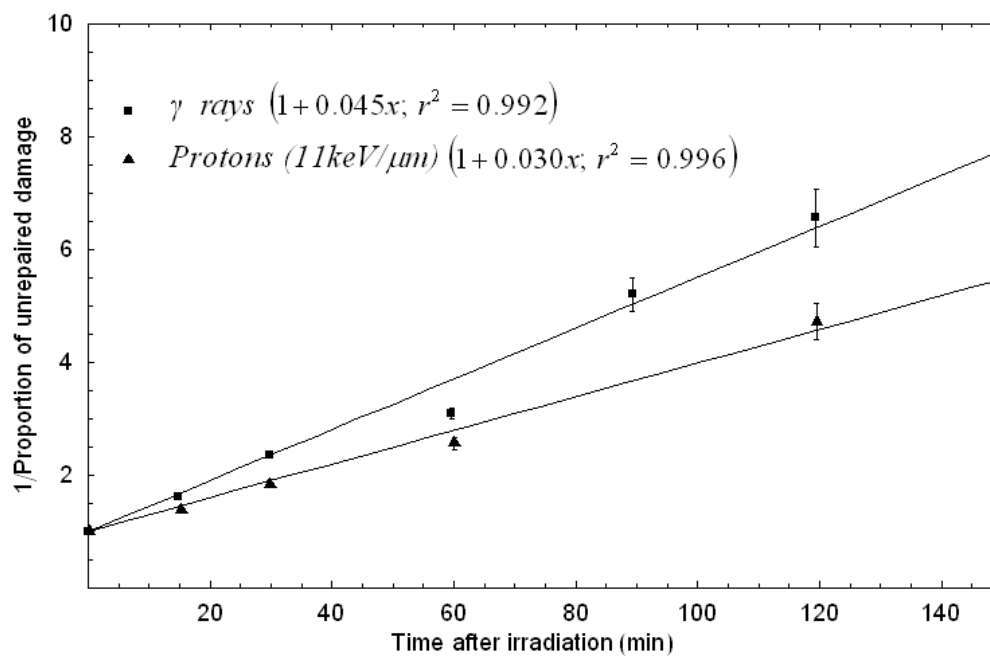


Figure 9.21: Reciprocal plot for V79-753B cells irradiated with 45Gy of ^{60}Co gamma rays or 11keV/μm protons.

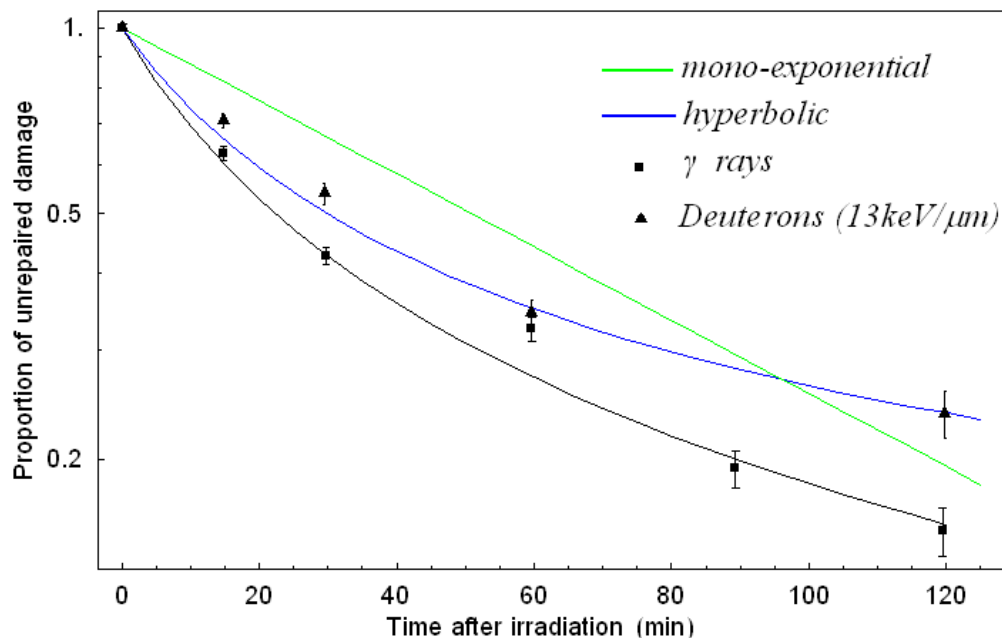


Figure 9.22: Repair kinetics of DNA breaks in V79-753B cells exposed to 13keV/μm deuterons. The equations of each of the three models are:

Mono-exponential: $1.003 e^{-0.014 x}$

Hyperbolic: $1.003 \times (1 + 0.045 x)^{-1}$ (γ -rays)
 $0.078 + .926 \times (1 + 0.040 x)^{-1}$ (Deut.-13keV/μm)

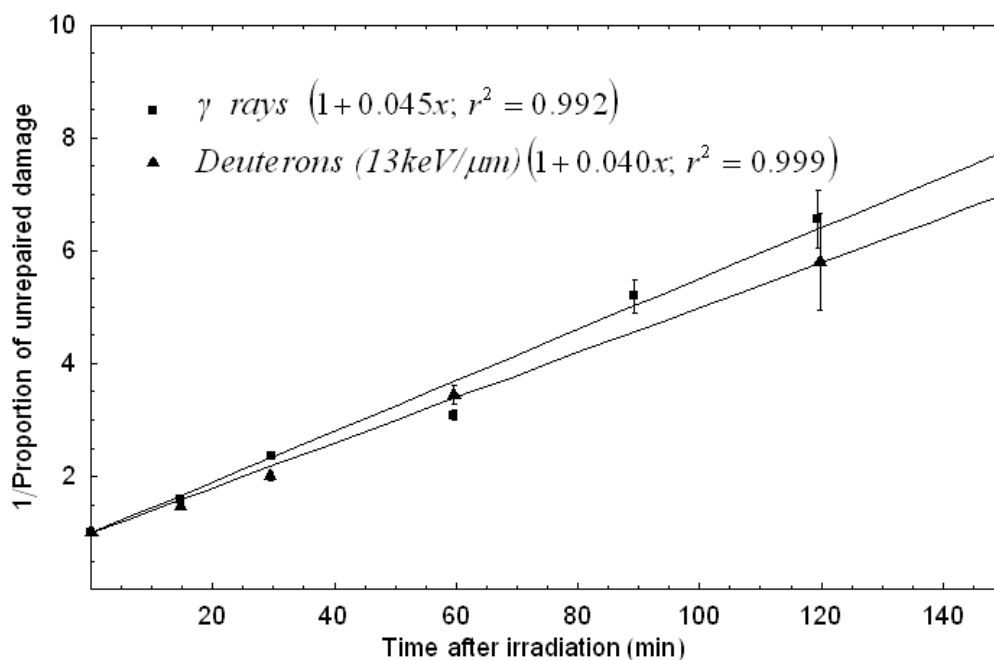


Figure 9.23: Reciprocal plot for V79-753B cells irradiated with 45Gy of ^{60}Co gamma rays or 13keV/μm protons.

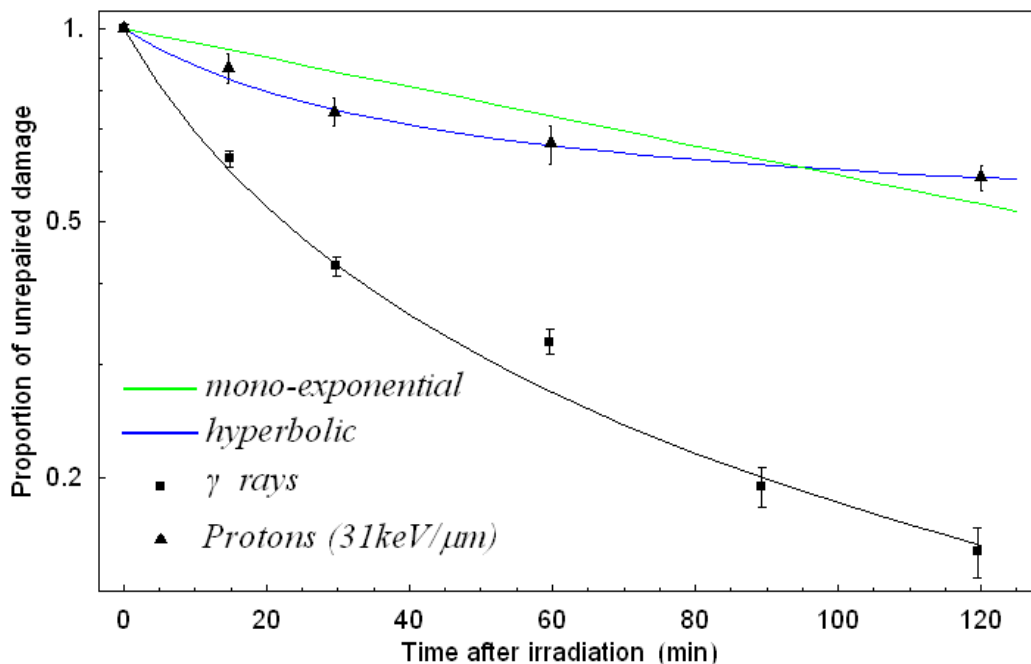


Figure 9.24: Repair kinetics of DNA breaks in V79-753B cells exposed to 31keV/μm protons. The equations of each of the three models are:

Mono-exponential: $1.003 e^{-0.0053 x}$

Hyperbolic: $1.003 \times (1 + 0.045 x)^{-1}$ (γ -rays)
 $0.048 + .526 \times (1 + 0.032 x)^{-1}$ (Protons-31keV/μm)

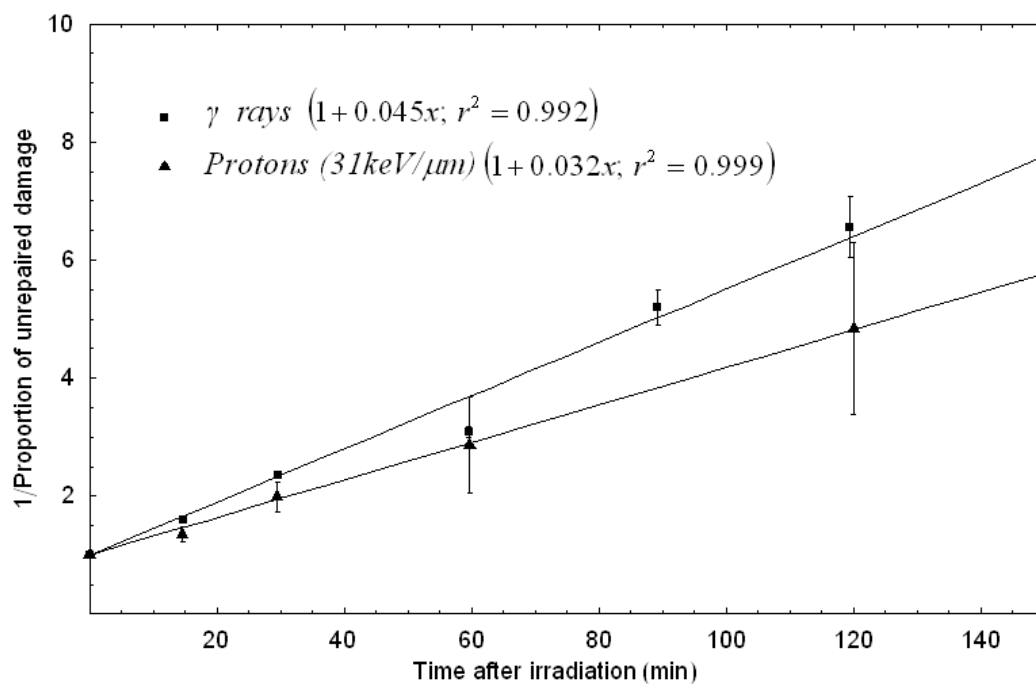


Figure 9.25: Reciprocal plot for V79-753B cells irradiated with 45Gy of ⁶⁰Co gamma rays or 31keV/μm protons.

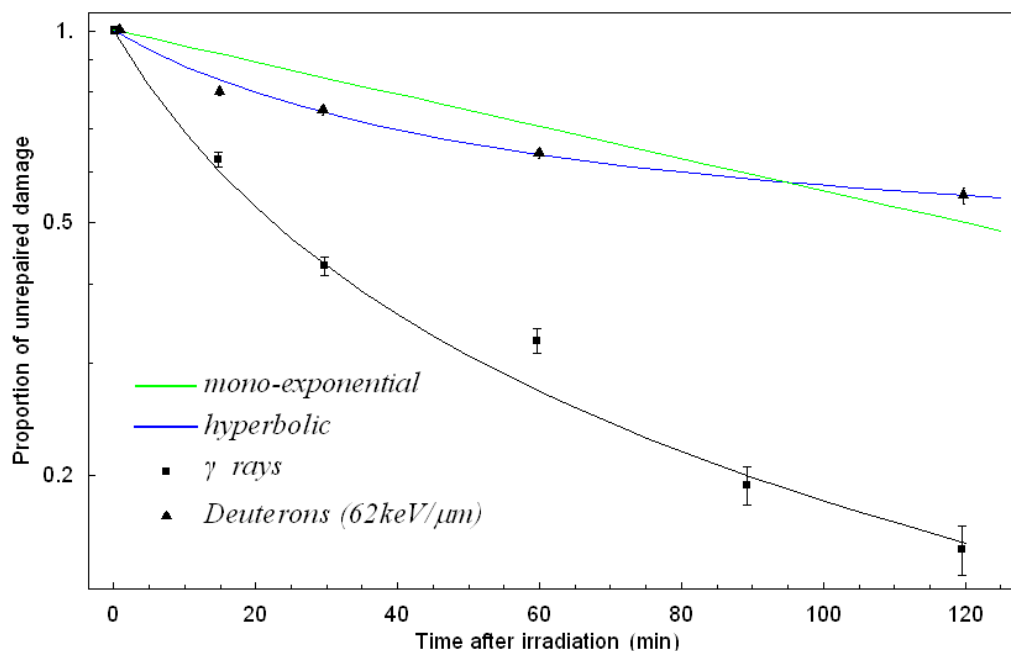


Figure 9.26: Repair kinetics of DNA breaks in V79-753B cells exposed to 62keV/μm deuterons. The equations of each of the three models are:

Mono-exponential: $1.003 e^{-0.0058 x}$

Hyperbolic: $1.003 \times (1 + 0.045 x)^{-1}$ (γ -rays)
 $0.403 + 0.60 \times (1 + 0.026 x)^{-1}$ (Deut.-62keV/μm)

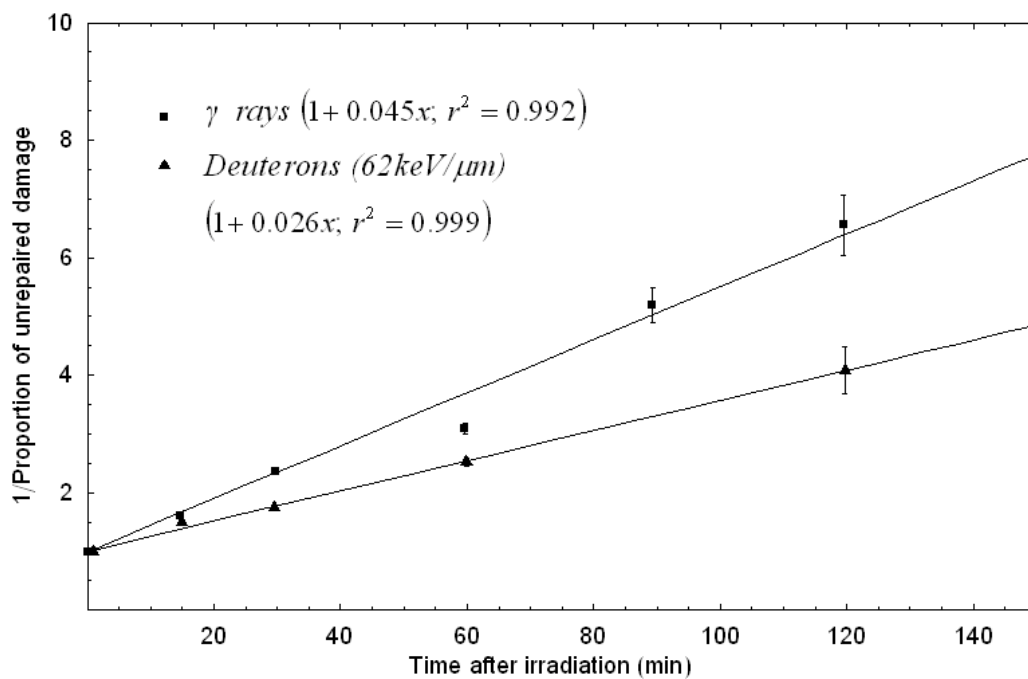


Figure 9.27: Reciprocal plot for V79-753B cells irradiated with 45Gy of ⁶⁰Co gamma rays or 62keV/μm deuterons.

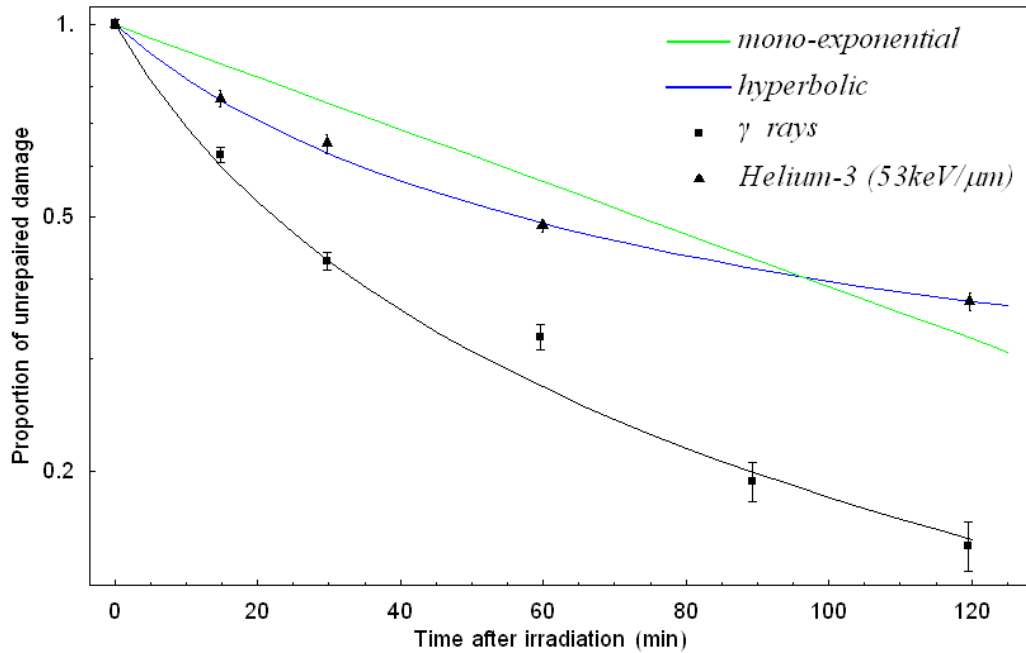


Figure 9.28: Repair kinetics of DNA breaks in V79-753B cells exposed to 53keV/μm helium-3 particles. The equations of each of the three models are:

Mono-exponential: $1.000 e^{-0.0043 x}$

Hyperbolic: $1.003 \times (1 + 0.045 x)^{-1}$ (γ -rays)
 $0.176 + 0.82 \times (1 + 0.027 x)^{-1}$ (He-3 53keV/μm)

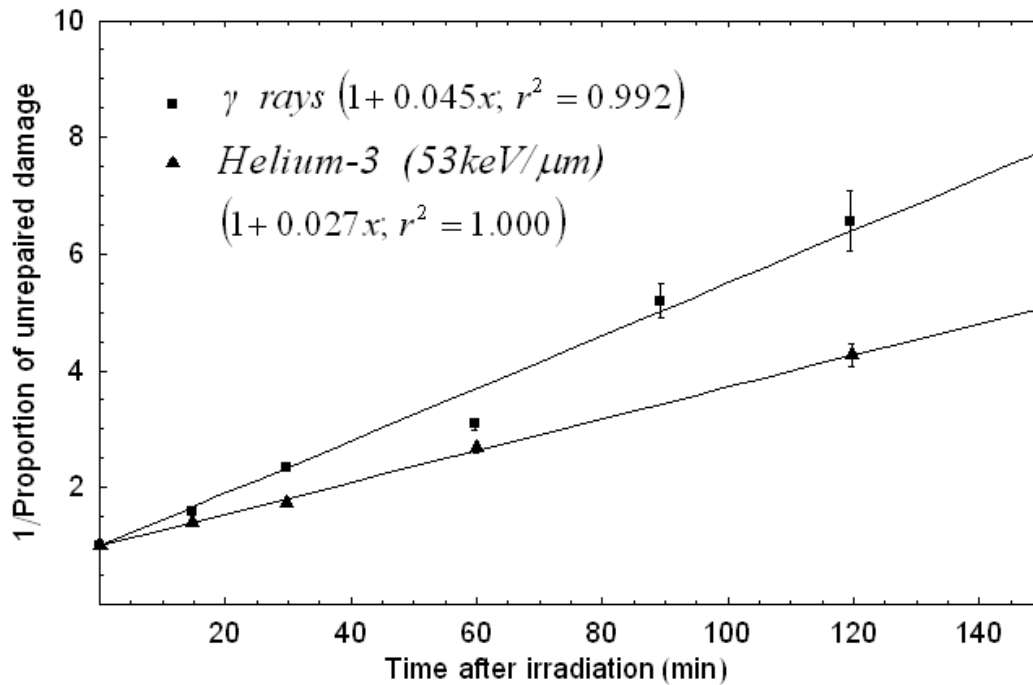


Figure 9.29: Reciprocal plot for V79-753B cells irradiated with 45Gy of ⁶⁰Co gamma rays or 53keV/μm helium-3 particles.

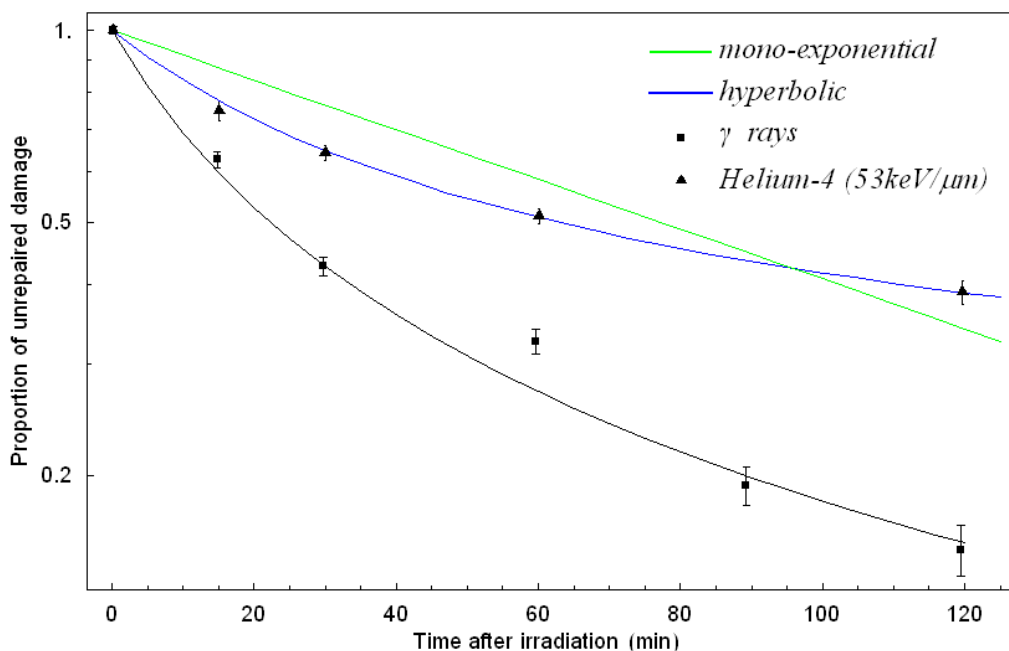


Figure 9.30: Repair kinetics of DNA breaks in V79-753B cells exposed to 53keV/μm helium-4 particles. The equations of each of the three models are:

Mono-exponential: $1.001 e^{-0.0090x}$

Hyperbolic: $1.003 \times (1 + 0.045x)^{-1}$ (γ -rays)
 $0.187 + 0.81 \times (1 + 0.025x)^{-1}$ (He-4 53keV/μm)

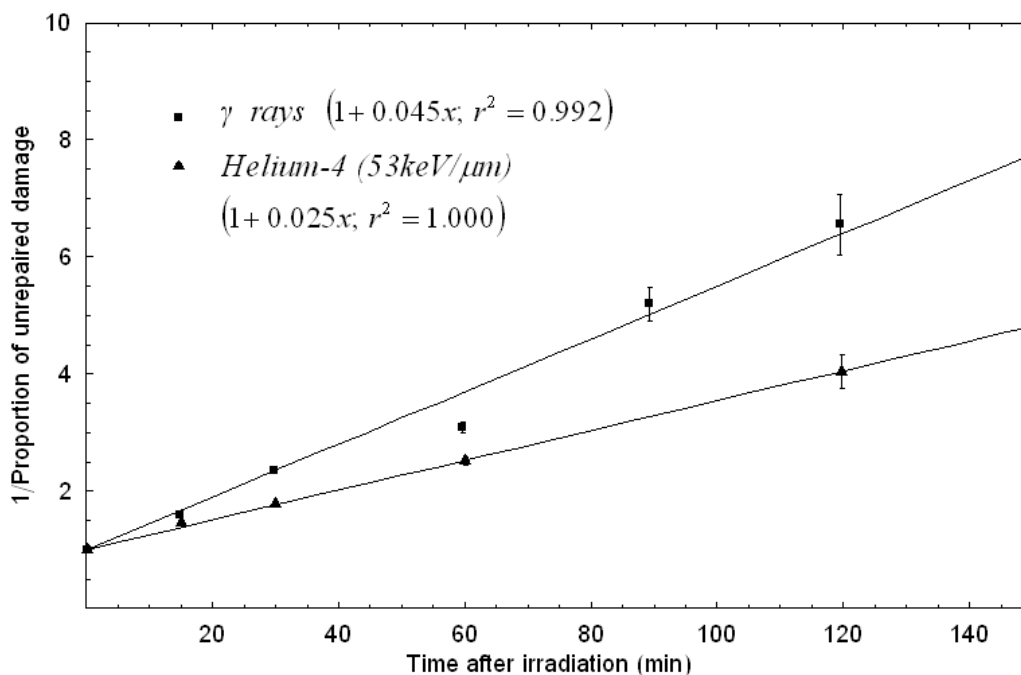


Figure 9.31: Reciprocal plot for V79-753B cells irradiated with 45Gy of ⁶⁰Co gamma rays or 53keV/μm helium-4 particles.

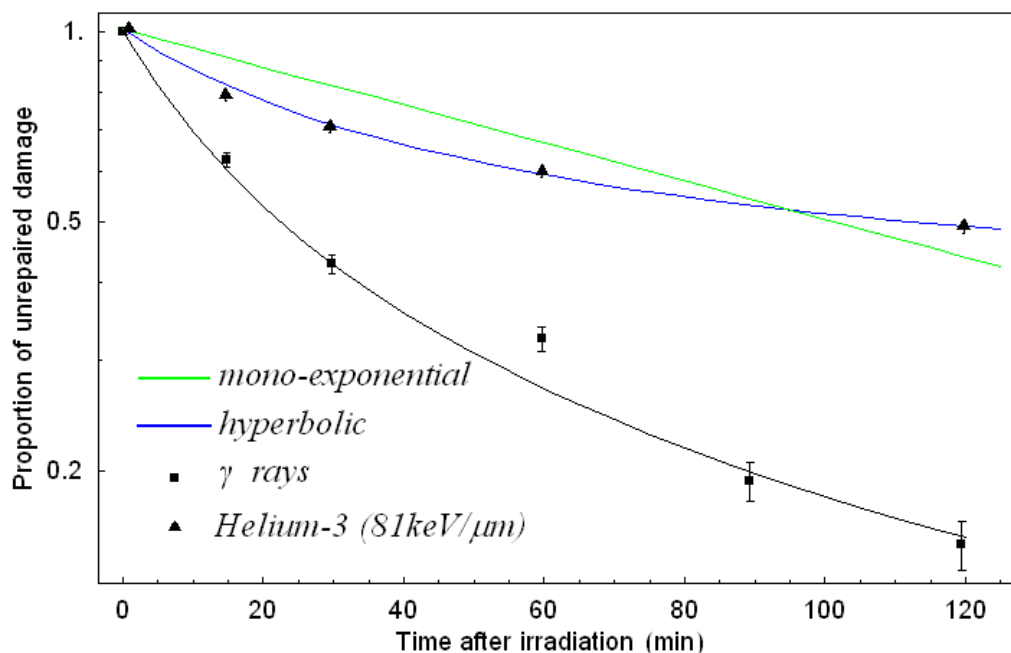


Figure 9.32: Repair kinetics of DNA breaks in V79-753B cells exposed to 81keV/μm helium-3 particles. The equations of each of the three models are:

Mono-exponential: $1.011 e^{-0.0070 x}$

Hyperbolic: $1.003 \times (1 + 0.045 x)^{-1}$ (γ -rays)
 $0.319 + 0.69 \times (1 + 0.025 x)^{-1}$ (He-3 81keV/μm)

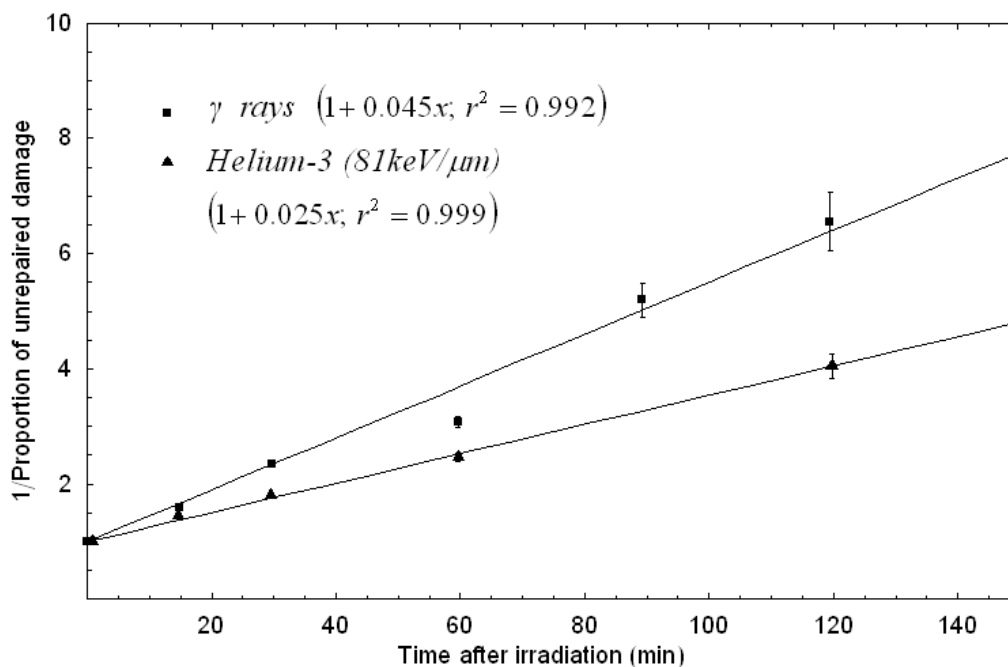


Figure 9.33: Reciprocal plot for V79-753B cells irradiated with 45Gy of ^{60}Co gamma rays or 81keV/μm helium-3 particles.

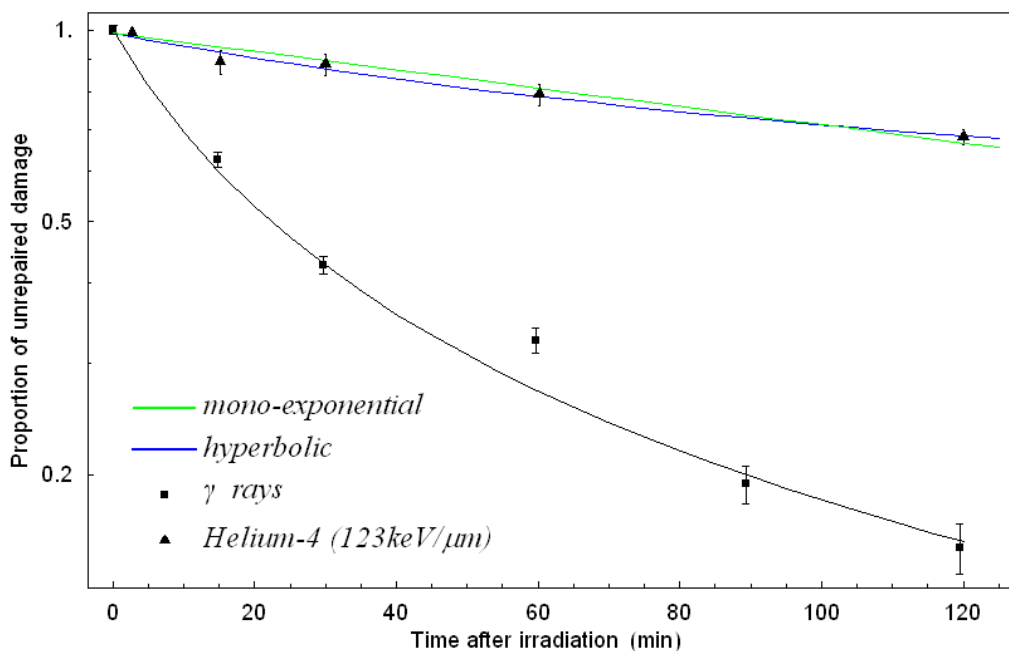


Figure 9.34: Repair kinetics of DNA breaks in V79-753B cells exposed to 123keV/μm helium-4 particles. The equations of each of the three models are:

Mono-exponential: $0.991 e^{-0.0033x}$

Hyperbolic: $1.003 \times (1 + 0.045x)^{-1}$ (γ -rays)
 $0.346 + 0.64 \times (1 + 0.008x)^{-1}$ (He-4 123keV/μm)

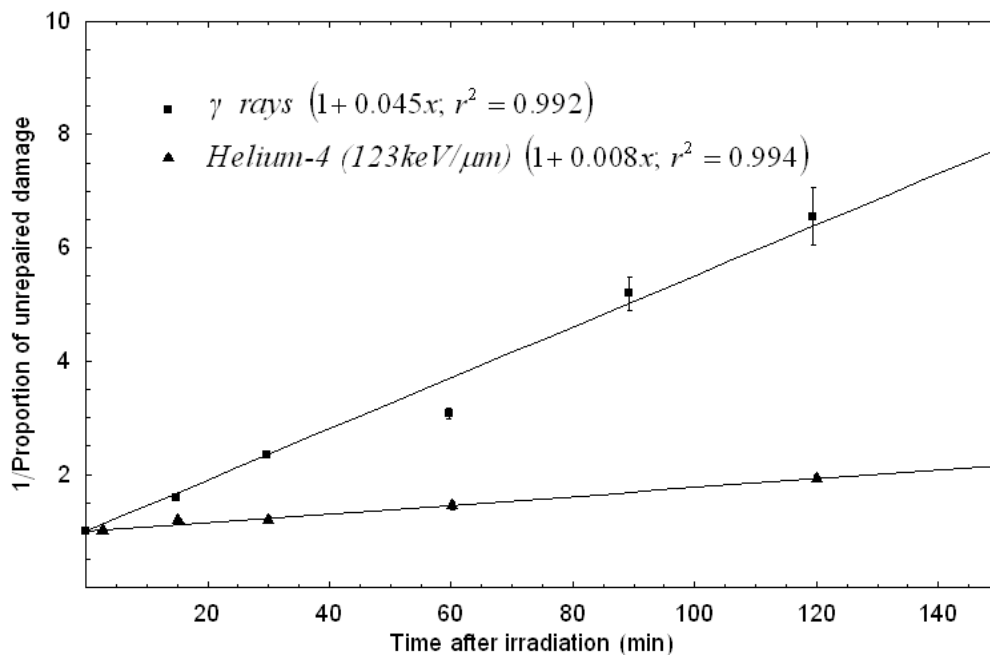


Figure 9.35: Reciprocal plot for V79-753B cells irradiated with 45Gy of ⁶⁰Co gamma rays or 123keV/μm helium-4 particles.

The next table summarises the reported and the resultant repair kinetic parameters for each LET:

	Belli <i>et al.</i> (2000)	Present Analysis			
	τ (min)	Mono-exp.	Bi-exponential	Hyperbolic	
				τ (min)	δ
γ -rays	28 ± 2	--	MATHEMATICA OVERFLOW ERROR	22.2 ± 3	0
Protons 11keV/ μm	40 ± 7	72.0 ± 23		33.5 ± 3	0
Protons 31keV/ μm	36 ± 19	189.9		31.4 ± 1.4	0.477
Deuterons 13keV/ μm	32 ± 5	73.1 ± 23		25.1 ± 1.5	0.078
Deuterons 62keV/ μm	31 ± 6	171.8		38.9 ± 2	0.403
Helium-3 53keV/ μm	40 ± 5	106.1 ± 25		36.7 ± 1.2	0.176
Helium-3 81keV/ μm	38 ± 4	143.6		39.3 ± 1.1	0.319
Helium-4 53keV/ μm	36 ± 6	111.2		39.3 ± 1.1	0.187
Helium-4 123keV/ μm	88 ± 80	301.2		130.4	0.346

Table 9.11: Repair half-lives reported by (Belli *et al.*, 2000) and this report.

MATHEMATICA[®] produced an error when a non-linear regression analysis was performed on the data using a bi-exponential model. Thus, neither regression lines nor information from the analysis was obtained for the bi-exponential model.

9.3. Analysis of the proportions of unrepaired DNA damage produced by each type of radiation

According to the discussion presented in chapters 7 and 8, there is an increase in the efficiency of producing unreparable DSB as LET increases. This was the case presented in Figures 8.9, 8.10 and 8.20. The extended version of the Reciprocal Repair model presented in section 8.3 allows us to calculate the final amount of unreparable damage (δ) which, when plotted against LET, should present similarities with Figure 8.20. The following plot shows the calculated proportion of unreparable damage versus LET for all those data sets analysed in the previous section where the LET information is available (Goodwin *et al.*, 1989; Suzuki *et al.*, 1996; Stenerlöw *et al.*, 2000; Belli *et al.*, 2000).

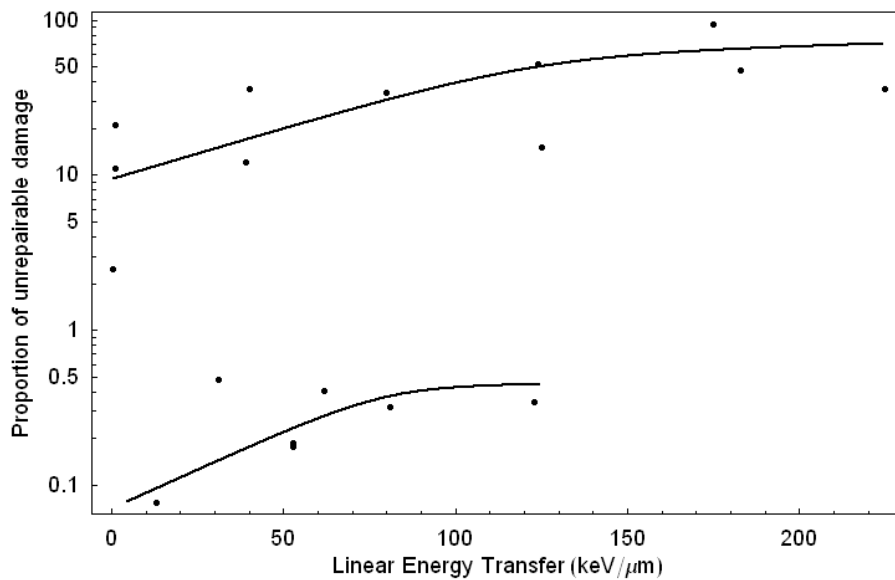


Figure 9.36: Plot showing the increase of the calculated proportion of unreparable damage with LET. Lines have been fitted by eye.

Although there is not enough data to extract any final conclusion on the shape of δ from Figure 9.36, it is observed that the data shows a tendency for an asymptotic increase of δ with LET.

9.4. Statistical analysis

Similarly to the analysis made in Table 7.3, the AIC and Pearson’s coefficient relevant to the data analysed in sections 9.1 and 9.2 are presented in Table 9.12.

	LET (keV/μm)	Mono-Exponential		Bi-Exponential	Reciprocal Repair	
		AIC	r ²	AIC	AIC	r ²
Godwin et al., 1989	183	31.4	0.959	-238.4	17.1	1.000
Suzuki et al., 1996	39	45.7	0.925	21.1	7.1	0.999
	124	41.3	0.719	17.6	22.2	0.997
Stenerlöw et al., 2000	40	76.2	0.846	47.2	57.2	0.995
	80	75.0	0.846	44.4	32.5	1.000
	125	73.4	0.903	49.3	49.8	0.999
	175	74.6	0.809	54.7	42.5	1.000
	225	69.5	0.921	44.4	55.4	0.998
Belli et al., 2000	11	-20.4	0.987	MATHEMATICA OVERFLOW ERROR	-33.2	0.996
	13	-17.2	0.963		-32.7	0.999
	31	-19.7	0.929		-38.9	0.999
	53 (³ He ⁺⁺)	-18.7	0.964		-43.6	1.000
	53 (⁴ He ⁺⁺)	-17.6	0.959		-40.8	1.000
	62	-18.8	0.939		-37.7	0.999
	81	-17.9	0.945		-38.0	0.999
	123	-29.8	0.984		-37.4	0.994

Table 9.12 : Goodness of fit of each individual model to the repair kinetic data analysed in section 9.2 (no LET information is available for the case of neutrons in section 9.1).

As explained in Table 7.1, the original data can be transformed in order to be analysed using linear regression analysis and, for this reason, the Pearson’s correlation coefficient is provided for the mono-exponential and reciprocal analysis but not for the bi-exponential. Therefore, for the results presented in Table 9.12, the following transformations have been applied:

	Original Data	Transformed Data	Regression function applied to transformed data
Reciprocal Repair	(x, y)	$\left(x, \frac{1}{y}\right)$	$1 + ax$
Mono-exponential Repair	(x, y)	$(x, \log[y])$	$\log[100] + ax$
Bi-exponential Repair	(x, y)	(x, y)	$me^{ax} + ne^{bx}$

Table 9.13: Same scheme of transformations applied to the data as per Table 7.1, with the only difference that the present analysis is free of any weighting applied to it.

9.5. Conclusions

Although the amount of data analysed is very limited, in 50% of the cases comparing the three models (data for Goodwin *et al.*, Suzuki *et al.* and Stenerlöw *et al.*) the extended version of the reciprocal repair model fits the data better than the other two (with the bi-exponential model better fitting the other 50%). Whereas, in the case of the data presented by Belli *et al.*, all the data sets are better predicted (lower AIC or bigger r^2 values) by the extended reciprocal repair model than the mono-exponential.

It is clear that an analysis based on mono-exponential models of repair tends to oversimplify the underlying kinetic processes taking place after irradiation, which in turn produces an over- or under-estimation of the characteristic repair half life of the system under study. Bearing in mind that the current practice in clinical Radiobiology to calculate incomplete repair factors for inclusion in BED assessments of fractionated treatments is often based on the Incomplete Repair (IR) model proposed by Thames (1985), which is purely based on mono-exponential repair, the current results suggest the necessity of reconsidering this practice and amend it with the use of an alternative model that retains the simplicity of the IR model but takes into account the existence of fast and slow repair components. The extended reciprocal repair model presented in Equation (8.5) not only takes into account the existence of fast and slow repair

components but also provides parallel information to that provided by the IR model, i.e. τ and δ instead of μ and h , where μ is the Thames mono-exponential repair constant and h the ‘incomplete-repair’ factor.

The extended reciprocal repair model suffers from a number of shortcomings however. In some of the figures shown in section 9.2 (e.g. Figures 9.4, 9.8, 9.10, etc...) it is possible to observe how the reciprocal repair (referred as hyperbolic) model fits the data very well at long repair times while the fit is not so good at short repair times. This is related to the fact that the regression line used to obtain τ and δ is forced to cut the y-axis at (proportion of unrepaired damage)⁻¹ = 1, as the reciprocal proportion of damage at any time is given from Equation (9.1) as,

$$zt + 1 = \frac{N_0 - \delta}{n(t) - \delta} \quad (9.2)$$

from which, once the iterative process explained in section 9.2 ($r^2 = \max$) is concluded, the value of z (and thus of τ) is obtained. If, however, the reciprocal of the repair kinetic data does not start from 1 at $t = 0$, the fit at low repair times will not be as accurate, and this will be reflected on the reciprocal (hyperbolic) repair kinetic curve. A good example of this is shown in Figures 9.4 and 9.5.

Also, it is interesting to observe how, in Figure 9.34, the mono-exponential and the hyperbolic models predict very similar half-time repair constants. This is due to the fact that, at high-LET, and more specifically, at the value of LET where α peaks in Figure 8.24, the amount of repair is very small and therefore the repair kinetic curve decays exponentially as the fast component of the repair process does no longer exist. Only at this range of LET values it is expected that the mono-exponential model will correctly predict the value of τ .

9.6. Bibliography

- Belli M., Cherubini R., Dalla Vecchia M., Dini V., Moschini G., Signoretti C., Simone G., Tabocchini M.A., Tiveron P. *International Journal of Radiation Biology* 76(8):1095-1104 (2000).
- Fowler J.F. *In: Progress in Radio-Oncology VI*. HD Kogelnik & F Sedlmayer. Munduzzi Editore S.p.A. (Eds.), Bologna, Italy. 471- 479 (1998).
- Fowler J.F. *Radiation Research* 152(2):124-136 (1999).
- Fowler J.F. *Radiation Research* 158(2):141-151 (2002).
- Goodwin E., Blakely E., Ivery G., Tobias C. *Advances in Space Research* 9(10):83-89 (1989).
- Rojas A., Joiner M.C. *Radiotherapy and Oncology* 14(4):329-336 (1989)
- Sakai K., Suzuki S., Nakamura N., Okada S. *Radiation Research* 110(3):311-20 (1987).
- Stenerlöv B., Höglund E., Carlsson J., Blomquist E. *International Journal of Radiation Biology*. 76(4):549-57 (2000).
- Suzuki M., Watanabe M., Kanai T., Kase Y., Yatagai F., Kato T., Matsubara S. *Advances in Space Research* 18(1-2):127-36 (1996).
- Thames H.D. *International Journal of Radiation Biology* 47(3):319-339 (1985).

General discussion and Conclusions

Two main conclusions have been established in this thesis:

- i. The neglect of the contribution of accumulation of sublethal damage to the observed biological end point resulting from a dose of high-LET radiation may under- or over-estimate the RBE at clinically relevant doses.
- ii. The assumption of a repair process based only on first-order kinetics may lead to an overestimation of the repair half-times of radiation damage by any type of radiation and to an underestimation of the proportion of unreparable DNA damage. The latter point arises because first repair kinetics assumes all damage is eventually repaired.

These two general conclusions are not unrelated as the cell-killing efficiency of a radiation has been shown to be intrinsically related to the proportion of unreparable damage it produces (see Figure 8.3).

The fundamental assumption made in this thesis, and which leads to conclusion (i), is that *both* radiosensitivity parameters describing the LQ model, α and β , are susceptible to change with changing LET. Figure 5.5 provides evidence that these changes can be substantial and even of the same order for α and β , which would imply that RBE_{\max} and RBE_{\min} are each important determinant parameters at very low and very high dose per fraction respectively. A very significant feature demonstrated in Figure 5.5 is that while α always increases, regardless of the type of tissue, with increasing LET, β increases

with increasing LET for normal tissue (skin) while decreasing for tumour tissues (NFSa fibrosarcoma tumour). Therefore, according to Figure 5.5, what makes the RBE for high-LET radiations different between normal and tumour tissues is not only due to a different rate of change in α with LET (which according to Figure 5.5 is very similar for both types of tissues) but also due to significant difference in the contribution of the LQ β term model towards the final effect, these being *positive* (i.e. *more* contribution towards the effectiveness of the radiation) for normal tissues, and *negative* (i.e. *less* contribution towards the effectiveness of the radiation) for tumour tissues. This idea contrasts with the common belief that the difference in RBE between normal and tumour tissues is due to the difference in the shapes of their low-LET dose-response curves (Withers *et al.*, 1982), which are curvier for normal tissues than for tumours. As the survival curve for high-LET particles is assumed to be virtually a perfect exponential, it is only the difference in the shape of the low-LET survival curves which determines the differences in RBE. There are fundamental differences between the approach suggested in this thesis and the more traditional approach: the former discusses an intrinsic difference between the survival curves of normal and tumour tissues for high-LET radiations; the later justifies the difference in RBE between normal and tumour tissues on the basis of their different low-LET survival curves. It is probably the case that both concepts play a concurrent role in the final expression of RBE for normal and tumour tissues.

On the other hand, Figures 6.55, 6.56 and 6.57 show that RBE_{\max} always increases with LET while RBE_{\min} increases for normal tissues and decreases for tumours. The parameters that make RBE_{\max} and RBE_{\min} change with LET are α_H and β_H respectively (as α_L and β_L are the reference parameters), so an increase in RBE_{\max} or RBE_{\min} must be strictly related to an increase in α_H or β_H respectively. Therefore, if β_H increases with LET for normal tissues, the RBE_{\min} of this type of tissue must increase with LET. Conversely, if β_H decreases with LET for tumours, the RBE_{\min} of this type of tissue must decrease with LET. This is in fact the case observed in Tables 6.34, where the RBE_{\min} for mouse skin reaction of 3.0 and 10% survival level of jejunum crypt cells increases with increasing LET while the RBE_{\min} for tumour growth delay time > 15 days decrease with increasing LET. According to the results shown in Tables 6.32 and 6.34, normal and tumour tissue can both have values of RBE_{\min} larger and smaller than

1, but according to this discussion, the greater the LET of the radiation used the more likely it is that RBE_{min} is larger than 1 for normal tissue and less than 1 for tumours. Whereas this is clearly seen in Table 6.34, it is more difficult to observe in Table 6.32 since the LET of neutrons is not specified and differences in the results could only be presented in terms of the difference in radiosensitivity expressed in terms of (α/β) ratios. In this case, it could be assumed that LET is similar for all the neutron results and therefore the variability of RBE_{min} must be related to some other factor, or factors, that remain to be investigated.

According to Figure 5.8, values of RBE_{min} larger or lower than 1 would have an impact on the values of RBE at clinically relevant doses. They will also impact on the threshold dose at which the use of high-LET radiations produce more damage (higher RBE) to tumours than to healthy tissues (i.e. positive therapeutic ratio). The following plot shows these two effects graphically.

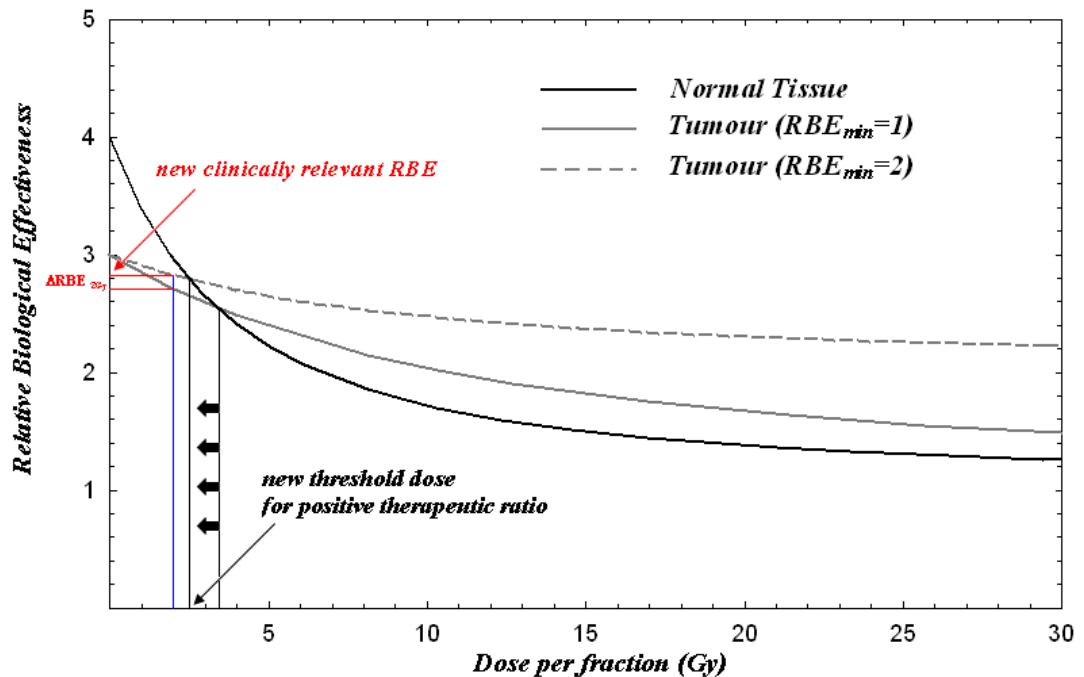


Figure 10.1: Effects of the change of RBE_{min} on RBE and threshold dose for positive therapeutic ratio. For clarity, only the RBE_{min} for tumour has been considered to change.

The likely pattern of changes in RBE at 2Gy fractions are shown in Table 6.33 and Figure 6.54 for neutrons and Table 6.35 and Figures 6.58 and 6.59 for carbon ions. The

changes in the threshold dose at which the therapeutic ratio becomes positive is summarised in Table 6.36 (for neutrons) and in Table 6.37 (for carbon ions).

The results obtained from Table 6.33 indicate there is a small change in RBE at 2Gy per fraction for both, early and late reacting tissues, when RBE_{\min} is considered different from 1. However, it is interesting to notice that, in 64.3% of the cases presented for early effects, the value of RBE_{2Gy} when $RBE_{\min} = 1$ is larger by $\sim 1.71\%$ (0.02% - 9.68%) than when $RBE_{\min} \neq 1$; similarly, in 71.4% of the cases presented for late effects, the value of RBE_{2Gy} when $RBE_{\min} = 1$ is larger by $\sim 1.33\%$ (0.06% - 5.33%) than when $RBE_{\min} \neq 1$. According to Figure 10.1, this would imply that in 67.9% (average[64.3%, 71.4%]) of the neutron data presented in this thesis, neutrons should had been considered $\sim 1.71\%$ less efficient for early reacting tissues, and $\sim 1.33\%$ less efficient for late reacting tissue at 2Gy per fraction, which can be expressed as an overall average decrease of efficiency of 1.52%.

On the other hand, when the RBE curves for early and late reactions are superimposed, in 86.7% of the cases shown in Table 6.36 the threshold dose corresponding to the case $RBE_{\min} \neq 1$ is lower than the one obtained for the case $RBE_{\min} = 1$.

Two findings are at hand, i.e.: the slightly lower efficiency than originally considered for neutrons at 2Gy per fraction (arising from the fact that $RBE_{\min} \neq 1$); and the decrease of the threshold dose for a change on the therapeutic ratio of neutrons. The question now is, how do these two findings correlate with the existing clinical data?

Various reports have been produced in the UK describing the technical aspects of the neutron treatments that took place at Hammersmith during the early 70's and at Edinburgh during the late 70's and early 80's. In particular, the Medical Research Council Neutron Therapy Working Group (1985) reported that neutron treatments were given three times weekly at Hammersmith and five times weekly at Edinburgh over a 4-week period in both centres. The contribution of the gamma rays, 5%-9% of the total dose, was ignored in the prescription at both centres. The typical dose per fraction was 1.3Gy at Hammersmith and 0.80Gy at Edinburgh, which corresponded to an average

RBE value of about 3 (2.7-3.8) to transform photon into neutron doses. According to the finding proposed above, where at 2Gy the RBE was found to be 1.52% lower when $RBE_{\min} \neq 1$ than the traditionally case considered of $RBE_{\min} = 1$, it is conceivable that at 1.1Gy (average[1.3Gy, 0.80Gy]) the actual RBE was overestimated by about 0.76% giving an actual RBE value of 2.98. Although this is a very marginal reduction in the RBE value, one must remember that the analysis presented in this thesis takes into account a limited amount of available data and therefore, it is possible that a larger macro-study would discover larger differences in the RBE values used clinically. Therefore, the reduction on the RBE mentioned above should be seen as a *suggestion of a tendency* rather than an *actual and confirmed* reduction. There are reported results of similar effectiveness for photons and neutrons for specific treatment sites, such as the case of head and neck patients, where the overall treatment failure (defined as death, never being locally well, recurrence of local disease or late radiation mortality) occurred in 28 out of 60 (47%) photon-treated patients and 28 out of 60 (47%) neutron treated patients in the Edinburgh trial. In the Hammersmith trial treatment failed overall in 35 out of 44 (80%) photon-treated patients and in 28 out of 51 (55%) neutron-treated patients (Medical Research Council Neutron Therapy Working Group, 1985). It is observed that neutrons appeared to be more efficient for treatment than photons in the case of the Hammersmith trial than in the Edinburgh trial, but 60% of the Hammersmith trial patients had Severity 3 disease (maximum Severity level) compared with only 22% of the Edinburgh patients, which perhaps reduced the chances of survival for the photon-treated patients at Hammersmith. According to this, poor prognosis of survival (or level of disease severity) may be considered a differential effect for neutron therapy.

The lower effectiveness of the neutron beam to treat certain diseases would not explain the severe reaction incidence of radiation-related morbidity (skin and subcutaneous tissue) and mortality (larynx and mucous membrane) that showed in neutron-treated patients compared to the photon-treated patients. However, the reasons for this higher morbidity/mortality rates could be found on the physical characterisation of the neutron beam more than on its radiobiological characterisation. At both of the centres of the UK neutron trial, the neutron beams had poorer penetration and skin sparing in comparison with the linear accelerators and cobalt units used to treat the photon patients (see Figure 10.2). This lack of skin sparing and the differential absorption of neutron dose in fat

contributed to the increased radiation morbidity in skin and subcutaneous tissues. Furthermore, the larynx is recognised as a sensitive tissue to neutron radiation (see Figure 5.9), for which a reduced dose is necessary.

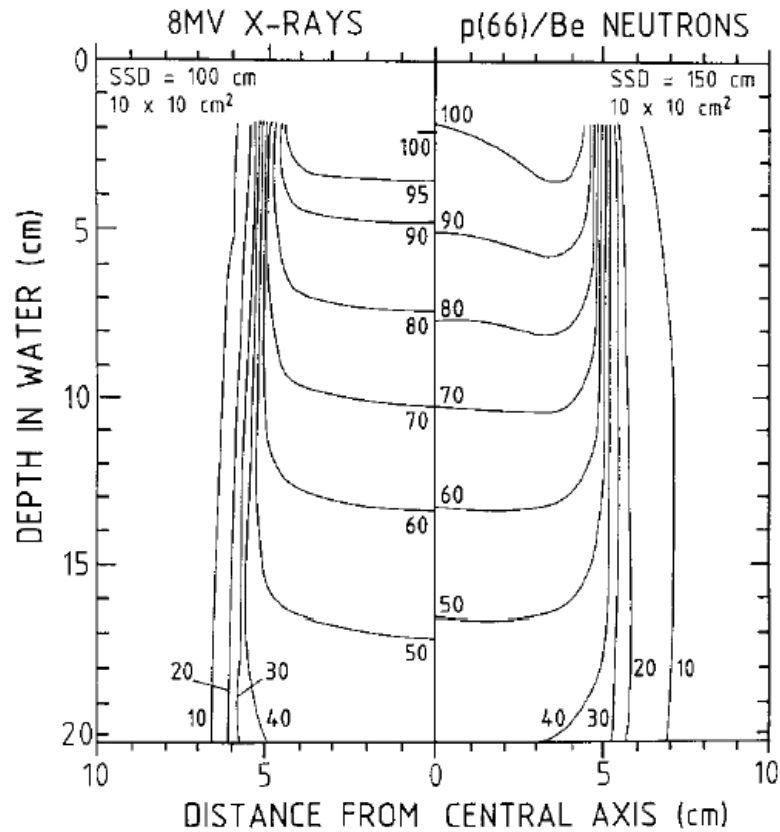


Figure 10.2: Isodose curves for a p(66)/Be neutron therapy beam (right) compared with a typical 8MV X-ray beam (left) (Jones, 2001)

Also, the higher neutron doses which were used predominantly at Hammersmith were associated with a significant increase in radiation-related mortality. More sophisticated prospective modelling of the type derived in this thesis, had it been available at the time, might well have avoided that particular problem.

In general, the reduced recurrence rate and improved life expectancy and tumour regression following neutron therapy was not confirmed by either of the studies carried out at Hammersmith and Edinburgh. On the other hand, the two trials agree in finding greater morbidity and more inter-current death in those patients whose tumours were controlled by neutrons.

According to the second finding mentioned above, a lower threshold dose has been found when $RBE_{\min} \neq 1$. If this is the case, a lower dose per fraction could have been applied which would have increased the effectiveness of radiation as well as decreased the skin sparing and subcutaneous tissues morbidity.

Studies of the variation of the RBE of carbon ions have also been included in chapter 6. Advances in technology are making such particles an attractive alternative mode of radiation therapy and, therefore, an accurate description of RBE values is required for different types of tissues when ion beams are to be used. Although the data analysed is very limited, it is interesting to observe the agreement among them in predicting an increase of RBE with increasing dose per fraction always in the same area of the SOBP, the entrance plateau. This is a very unusual effect, only observed once before by Chamberlain *et al.* (1980) on RBE values for cultured human lymphocytes which was interpreted by the authors as a consequence of T lymphocytes consisting of two subpopulations with different radiosensitivity, for which they suggested RBE values of 15MeV neutrons of 1.7 for the sensitive cells and 7.7 for the resistant subpopulation. In the cases studied in this thesis, the most likely interpretation is not in terms of the existence of different radiosensitivity subpopulations in the cell culture, but in terms of a comparable contribution of the β component with respect to the α component to the total log cell kill at LET values less than 70 keV/ μm , which are those in the plateau region of the SOBP. This is demonstrated in Figures 6.55, 6.56 for skin reaction of 3.0 (late reaction) and Figure 6.57 for tumour growth delay time of 15 days (early reaction). In Figures 6.55 and 6.56, the ratio of the β_H values with β_L (i.e. RBE_{\min}^2) is of the same order as the ratio of the α_H values with α_L (i.e. RBE_{\max}) at all LET values. This can only mean that β_H must vary with LET in the same proportionate manner as does α_H (but at a different order of magnitude, since $\beta_H < \alpha_H$). The fact that the slopes of the plots in Figure 6.55 are of the same order (0.0247 and 0.0222) for RBE_{\max} and RBE_{\min}^2 supports this statement. The amount of data however is far too small to assume this statement as a definitive conclusion, but it is interesting to observe that the same behaviour is observed in a completely different system such as jejunum crypts. Also, this same increase in β with LET was observed by Ando *et al.* (1998, 2005) and Koike *et al.*

(2002), who verified this finding by plotting Fe-plots of the fractionated data presented in section 6.2 as well as quasi-survival curves for skin cells irradiated with different LET radiations.

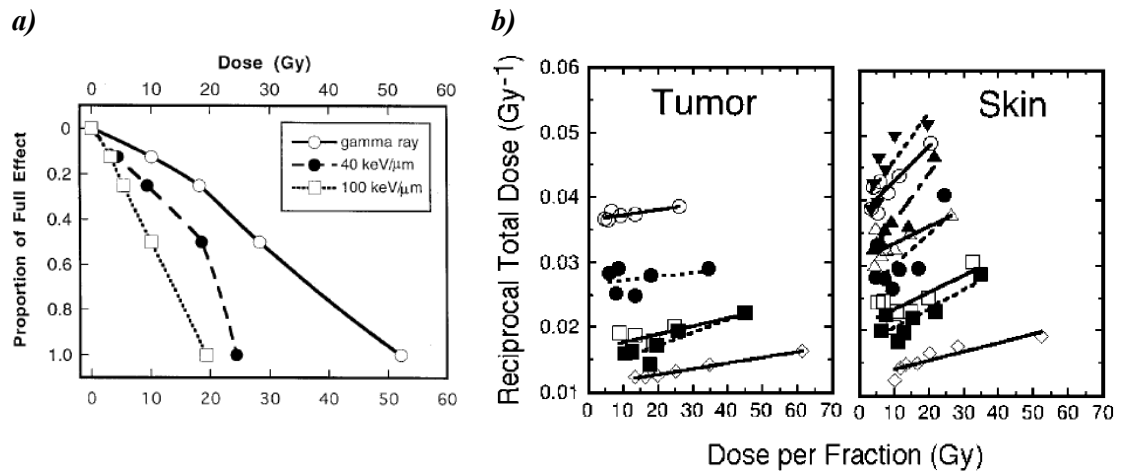


Figure 10.3: (a) *Quasi-survival curves measured for isoeffects doses to induce a skin reaction score 3.0. Observe how the curve for 40 keV/μm presents a significant shoulder while the response curve for 100 keV/μm is almost linear. This implies that the β value for skin cells irradiated with carbon ions of 40 keV/μm is significant enough to make the curve bend downwards (Ando et al, 1998).* (b) *Fe-plots for skin and tumour cells. Observe that the regression lines present different slopes (Ando et al., 2005).*

In Figure 6.47, it is shown that consideration of the influence of accumulation of sublethal damage in calculating the RBE for tumours and normal tissues situated at different positions within the SOBP (where the LET will differ from place to place) might have implications on the therapeutic gain from using carbon ions for treatment due to the change of the threshold dose, where the gain changes from positive to negative. These threshold doses are tabulated in Table 6.37. At the same time, in section 2.4 it was noted that the average number of fractions normally used in carbon ion radiotherapy at NIRS is 12, with large fraction sizes. In particular, for peripheral type early-stage NSCLC, fraction sizes of 42 GyE are used (see Table 10.1), which according to Table 6.37, is of the same order of dose per fraction as for 77 keV/μm and is bigger than any of the other threshold doses found at any other depth (different position of SOBP). This could imply that the hypofractionation regimes followed at the NIRS could infer greater damage to the normal tissues placed on the plateau of the beam than at the SOBP. This is a good reason for suggesting the institution of properly randomised clinical trials using carbon-ion therapy as the theoretical radiobiological predictions

made here, if shown to be substantially correct, could help guide the design of more appropriate fractionation schedules.

Site		Dose-Fractionation (GyE/fr/week)	Gy/fr	BED ($\alpha/\beta = 10$)	BED ($\alpha/\beta = 2.5$)
H&N:	ACC,MM etc	57.6/16/4	3.6	78.3	140.5
	Sarcoma	70.4/16/4	4.4	101.4	194.3
CNS		58.0/20/5	2.9	74.8	125.3
Skull Base		57.6/16/4	3.6	78.3	140.5
NSCLC: (Stage I)	Peripheral type	90.0/18/5	5.0	135.0	270.0
		72.0/9/3	8.0	129.6	302.4
		60.0/4/1	15.0	150.0	420.0
		42.0/1/1day	42.0	–	–
	Hilar type	57.6/9/3	6.4	94.5	205.1
Liver:	HCC	79.5/15/5	5.3	121.6	248.0
		69.6/12/3	5.8	110.0	231.1
		58.0/8/2	7.2	100.1	226.2
		52.8/4/2	13.2	122.5	331.6
		33.6/2/2days	16.8	90.0	259.4
Bone/Soft tissue		70.4/16/4	4.4	101.4	194.3
Prostate		66.0/20/5	3.3	87.8	153.1
Pancreas:	Pre-ope.	30.0/8/2	3.2	41.3	75.0
	Radical	38.4/12/3	3.8	50.7	87.6
Rectum		73.6/16/4	4.6	107.5	209.0

Table 10.1: Dose-fractionation employed in carbon ion RT at NIRS (Tsuji et al., 2007).

Nothing has been said in this discussion about what might be the mechanism for the radiation producing an increase in inter-track damage up to levels comparable with the intra-track damage produced by high-LET radiations. In the case of carbon ions, low-LET components exist in the tail of the SOBP as a consequence of the fragmentation of the projectile ions after their interaction with the nuclei of the atoms of the target material. In particular, if a 90mm thickness poly-methyl methacrylate phantom is exposed to a 290MeV/u carbon beam, 20% of the total dose is produced by light ions such as hydrogen and helium, which are particles known to have RBE values near 1.0. In the case of neutrons it is perhaps even easier to recognise the low-LET component,

which would be the γ -component of the beam and which, interestingly, was ignored when the RBE for fast neutron radiotherapy was being deduced.

It is difficult to justify the lower effectiveness (when $RBE_{\min} \neq 1$) of neutrons at a cellular level, but the idea of a lower efficiency when effects of accumulation of sublethal damage are included in the RBE formulation marries very well with the expected decrease in the effectiveness of a radiation after the repair of DNA damage. However, in chapters 7 to 9, it was shown that repair is not always complete after high-LET radiations and therefore radiation effectiveness should increase as LET increases, but the LET of a fast neutron beam is typically $75 \text{ keV}/\mu\text{m}$ (Jones, 2001) and at this level of LET it was shown in Chapter 9 that only a moderate percentage of damage remains unrepaired.

One of the main concerns that should be addressed in high-LET radiotherapy when designing clinical protocols and fractionation schemes is the inter-fractional repair which, as has been demonstrated, will decrease as the LET of the clinical beam increases. The use of mono-exponential repair models in radiotherapy was, perhaps, justified for low-LET radiations because the proportion of un-repaired damage is assumed to be zero. However, this model clearly introduces an over-estimation of the repair half life of damage, this being the main parameter to use in order to assess the minimum time required to separate two fractions of dose. More complex models are required in order to predict this time more accurately, but models with a higher complexity become increasingly impractical due to the difficulties in finding the correct values of the parameters involved. The model proposed in chapter 8 has the advantage of retaining the simplicity requested as well as providing an efficient method for calculating the fractions of unrepairable damage required for treatment design. This model, therefore, provides two important pieces of information using one formula and also has the advantage of providing a more accurate estimate of the repair half-time at any given LET.

If similar fractionation schemes to those already used in low-LET radiotherapy are intended also to be applied with high-LET sources, then it is mandatory to study the excess of unrepaired damage present at each fraction to correct the total treatment dose

and overall time of the treatment. This is especially as the treatment of slow proliferating tissues (normal or tumour) using daily fractions of high-LET radiations could potentially exceed the tolerance dose of these tissues or cause unexpected effects.

Currently there are treatment centres (eg at GSI in Germany) providing carbon ion therapy that use RBE models (e.g. Local Effective Model discussed in chapter 4) in their treatment planning software in order to account for the increase of the RBE of the radiation at different depths due to the reduction of dose. Within the LEM model these RBE values are maintained throughout the treatment without taking into account repair kinetic effects and the accumulation of unrepaired damage, both of which potentially may increase the overall treatment RBE value. A time factor should be included in these models, in the same way as has been shown in chapter 8, in order to account for unreparable damage and repair kinetic effects which have been shown to have an effect on the final RBE of radiations, instead of basing RBE values for radiotherapy treatment exclusively on physics principles (i.e. radial dose distribution around particle tracks to calculate survival levels).

It is in areas such as these in which it is suggested that the work of this thesis might contribute pertinent discussion and re-evaluation, with a view to providing an improved understanding of the complex radiobiology associated with high-LET radiotherapy.

10.1. Bibliography

- Ando K., Koike S., Nojima K., Chen Y-J., Ohira C., Ando S., Kobayashi N., Ohbuchi T., Shimizu W., Kanai T. *International Journal of Radiation Biology* 74(1):129-138 (1998).
- Ando K., Koike S., Uzawa A., Takai N., Fukawa T., Furusawa Y., Aoki M., Miyato Y. *Journal of Radiation Research* 46(1):51-57 (2005).
- Chamberlain S.M., Kirk J., Nias A.H. *International Journal of Radiation Oncology Biology Physics* 6(3):341-4 (1980).
- Jones D.T.L. *Radiochimica Acta* 89, 235-244 (2001).
- Koike S., Ando K., Uzawa A., Takai N., Fukawa T., Furusawa Y., Oohira C., Aoki M., Monobe M., Lee R., Suzuki M., Nojima K. *Radiation Protection Dosimetry*. 99(1-4):405-8 (2002).
- Medical Research Council. *British Journal of Radiology* 59(701):429-440 (1986).
- Tsujii H., Mizoe J., Kamada T., Baba M., Tsuji H., Kato H., Kato S., Yamada S., Yasuda S., Ohno T., Yanagi T., Imai R., Kagei K., Kato H., Hara R., Hasegawa A., Nakajima M., Sugane N., Tamaki N., Takagi R., Kandatsu S., Yoshikawa K., Kishimoto R., Miyamoto T. *Journal of Radiation Research (Tokyo)* 48(Suppl A):A1-A13 (2007).
- Withers H.R., Flow B.L., Huchton J.I., Hussey D.H., Jardine J.H., Mason K.A., Raulston G.L., Smathers J.B. *International Journal of Radiation Oncology Biology Physics* 3:227-33 (1977).
- Withers H.R., Thames H.D. Jr, Peters L.J. *International Journal of Radiation Oncology Biology Physics* 8(12):2071-6 (1982a).
- Withers, H.R., Thames, H.D. and Peters, L.J. *In: Progress in Radio- Oncology, Vol II*, K.H. Karcher, H.D. Kogelnik and G. Reinartz Ed. Raven Press, New York, pp. 287-296. (1982b).

The way forward

According to the results shown in chapters 6 and 9, there is still room for improvement in the current formulation of the RBE and repair models which are applied to high-LET radiations. An adequate validation of these models cannot be based on small subsets of data, but rather on macro studies with datasets from multiple types of tissues characterised by parameters such as tissue fractionation sensitivities, repopulation factors, hypoxic fractions, re-oxygenation rates, repair capability, growth rate, etc... The inclusion of RBE_{min} into the BED formulation for high-LET radiations, or the consideration of unrepairable damage in repair kinetic models applied to high-LET radiotherapy, are therefore only the first of a number of considerations that will need to be introduced to account for these effects.

The future objectives can be viewed as being short term or long term:

Short Term Objectives

The main short term objectives are to extend the data included in chapters 6 and 9 to:

- Improve the statistical analysis on the RBE values obtained for *in vitro* and *in vivo* cellular and tissue samples, with special attention to tumour cell lines and tissues.
- Increase the number of points in Figures 6.55, 6.56 and 6.57 to see if it is possible to verify that, while RBE_{max} always increase with LET, RBE_{min}

increases with LET for normal tissue and decreases for tumour. Is this always the case or are there both, positive and negative slopes for the regression line to RBE_{min} data for normal and tumour tissues? What are the implications in terms of the threshold dose where the therapeutic gain changes?

- Classify the neutron data, in particular, into different classes, i.e. by:
 - o centre of origin (as different beams, even with the same energy, would have different spectrum and microdosimetry)
 - o energy
 - o type of cell
 - o end point

in order to obtain information of the optimal combination of these factors to produce a positive therapeutic gain when using neutrons as an alternative to photons. This initial stratification will involve only *in vitro* data, which then will be extended to *in vivo* as part of the long term objectives.

- Increase the number of points for all carbon ion data to observe if, for each individual beam produced at different centres, the $RBE_{min} > RBE_{max}$ at the plateau region of the SOBP for different types of tissue. If this is the case, in what types of tissue is this true and at what values of LET is this effect reversed? According to Figure 6.58 (bottom), this effect introduces a differential between normal and tumour tissues. Is this still the case for a larger data set? What are the implications for the dose fractionation used in carbon ion therapy?
- Increase the information relating to repair kinetics following neutron exposure to study if the interfractional time used for neutron therapy during the UK fast neutron trial was adequate.
- The repair data presented in chapter 9 has encompassed studies carried out with different particle beams applied to one biological system in each study. To establish the correct minimum inter-fractional time to allow maximum repair in carbon ion radiotherapy, the analysis should be made on normal and tumour cellular systems exposed to the same beam at different points of the SOBP where different LET values apply and observe what are the repair kinetic characteristics at each depth. This would help to recognise the instances where carbon ion radiotherapy is more beneficial as a function of depth and tissue type. For example, if the longest repair time corresponds to tumour tissues

situated on the distal point of the SOBP while the repair is faster for normal tissue cell situated at shallower depths of the beam it would imply a beneficial situation for clinical applications. The data to assess this possibility should be obtained from *in-vitro* and *in-vivo* experiments.

- The model proposed in Equation (8.24) has not been fitted to any dataset. In order to do so, high-LET data needs to be searched to find cases where the parameters required are provided by the authors in order to study the modelling fit to the data. Once the model is validated, two different random distributions of values for the parameters of the model, one for normal tissue and one for tumours, can be used to investigate what combination of these parameters at a given LET will produce positive radiotherapeutic gains. This LET value will provide stronger clues as to the radiation type likely to produce the best therapeutic ratio.
- Study if the same effects observed for carbon ions also apply to other particles such as Helium, Hydrogen, Oxygen, Neon, Argon, etc... in order to establish if the hypotheses formulated in this thesis are applicable to all high-LET particles.

Long Term Objectives

None of the ‘high-LET’ models presented in this thesis include factors to predict effects such as those produced by changes in dose rate, gamma or low-LET ion contamination on neutron and high-LET ion beams, repopulation factors, hypoxia, etc. The introduction of neutron and other forms of high-LET radiotherapy was originally based on the premise that such radiation were likely to be of particular clinical benefit in treating larger tumours with a significant hypoxic (and hence more radioresistant) cell content. Evolving scientific experience suggests that the RBE is inversely related to tumour growth rate (Battermann *et al.*, 1981) which means that for higher LET lower repopulation factors are expected. Because of the quasi-exponential survival curves associated with high-LET radiations, it has always been assumed that changes in dose rate will have little impact for treatment with this type of radiations. The existence of low-LET components in high-LET beams has been mentioned in this thesis as a plausible possibility to explain the presence of a range of β values at different LETs and

which might introduce the possibility of fractionation and dose-rate effects with high-LET radiations. By extension, it would be worthwhile to study the synergistic properties of radiations of different LET imparted simultaneously in order to produce an ‘average’ beam with the best characteristics of low-LET (normal tissue sparing) and high-LET (higher effectiveness) radiations. Some of the relevant factors, such as repopulation factors, have been already incorporated into the BED equation (Dale *et al.*, 1998; Jones *et al.*, 2000; 2006), and novel fractionation schemes can be modelled using the new formulation in order to further optimise radiation effects.

Once the BED equation can be made to encompass some or all of the factors mentioned above, random values of the associated parameters considered will be tried to find those treatment schedules that will be expected to produce a positive therapeutic gain in a population of patients. Once the most appropriate treatment schedules have been identified, a further objective will be to conduct cost-benefit analyses (Dale *et al.*, 1996; Jones *et al.*, 1998) of high- versus low-LET treatment techniques using the optimally-determined treatment schedules models in association with known cost parameters. The analysis can include comparative assessment with the increasingly-fashionable low-LET intensity modulated radiotherapy (IMRT) used to treat tumours types for which high-LET radiations can also be used with success (Chao *et al.*, 2001; Rowbottom *et al.*, 2001). Modern radiotherapy (both low-and high-LET) is often perceived (perhaps wrongly) as being an expensive treatment modality and it is anticipated that the results of the cost-benefit analysis might help guide the debate over future resource allocation.

11.1. Bibliography

- Battermann J.J., Breur K., Hart G.A.M., van Peperzeel H.A. *European Journal of Cancer* 17:539-548 (1981).
- Chao K.S., Deasy J.O., Markman J., Haynie J., Perez C.A., Purdy J.A., Low D.A. *International Journal of Radiation Oncology Biology Physics* 49:907-916 (2001).
- Dale R.G., Jones B. *International Journal of Radiation Oncology Biology Physics* 36(3):739-746 (1996).
- Dale R.G., Jones B. *International Journal of Radiation Oncology Biology Physics* 43:639-645 (1998).
- Jones B., Dale R.G. *International Journal of Radiation Oncology Biology Physics* 41(5):1139-1148 (1998).
- Jones B., Dale R.G. *International Journal of Radiation Oncology Biology Physics* 48:1549-1557 (2000).
- Jones B., Carabe-Fernandez A., Dale R.G. *British Journal of Radiology* 79(939):254-7 (2006).
- Rowbottom G.G., Nutting C.M., Webb S. *Radiotherapy and Oncology* 59:169-177 (2001).

Appendixes

Appendix A

Derivation of Equation 4.28

Equation (4.14) is the special case of a general distribution function of z for an absorbed dose D in a site S when the number of events in this site is one ($\nu=1$). The expression for this general probability distribution is:

$$F(z;D) = P(\underline{z} \leq z|D) \quad (\text{A.1})$$

i.e. the distribution function is equal to the probability that the random variable \underline{z} does not exceed z at an absorbed dose D . The probability density (or differential distribution) $f(z;D)$ of z is the derivative of $F(z;D)$:

$$f(z;D) = \frac{dF(z;D)}{dz} \quad (\text{A.2})$$

The function $f(z;D)$ determines the probability for a specified value z of the specific energy at the absorbed dose D , i.e., $f(z;D) dz$ is the probability that the specific energy assumes a value between z and $z+dz$.

The average (expectation value) specific energy in a site is therefore given by

$$\bar{z} = \int_0^{\infty} z f(z;D) dz \quad (\text{A.3})$$

This should be equal to the absorbed dose D when the site is uniform and is exposed to a uniform radiation field, i.e.

$$\bar{z} = \bar{\nu} \bar{z}_1 = D \quad (\text{A.4})$$

This expression also corresponds to the first moment of the microdosimetric distribution $f(z;D)$. From the single event spectrum, given by $f_1(z)$ in Equation (4.15), one can compute the spectra of z for any number of events, i.e. $f(z;D)$, bearing in mind that the spectrum for exactly ν events, $f_\nu(z)$, is the ν -fold convolution of $f_1(z)$, i.e.

$$f_\nu(z) = \int_0^z f_1(x) f_{\nu-1}(z-x) dx \quad \text{with } \nu = 2, 3, \dots \quad (\text{A.5})$$

At the same time, at dose D the expected number of events is given by Equation (4.23), $\bar{\nu} = D/\bar{z}_1$. Because events are statistically independent, their number follows the Poisson distribution, and the probability for exactly ν events is:

$$p_\nu = \frac{(\bar{\nu})^\nu}{\nu!} e^{-\bar{\nu}} \quad (\text{A.6})$$

The dose-dependent z distributions, $f(z;D)$, can be expressed in terms of these Poissonian probabilities and the convolution products of the single event spectrum:

$$f(z;D) = \sum_{\nu=0}^{\infty} p_\nu f_\nu(z) \quad (\text{A.7})$$

The variance of this distribution can be readily obtained by considering that, if the random variable z at the dose D_1+D_2 is the sum of the corresponding random variables at doses D_1 and D_2 , then the variance of z at dose D_1+D_2 is equal to the sum of the variances at doses D_1 and D_2 . It follows that the variance must, accordingly, be proportional to absorbed dose:

$$\sigma_z^2 = cD \quad (\text{A.8})$$

To derive the value of the constant c , one must remember that the variance of a random variable is equal to the second moment minus the square of the expectation value,

$$\sigma_z^2 = \overline{(z - \bar{z})^2} = \bar{z}^2 - \bar{z}^2 = \bar{z}^2 - D^2 \quad (\text{A.9})$$

In general, the N-th moment of z is the expectation value of the power z^N and in particular, the second moment can be expressed as

$$\bar{z}^2 = \int_0^\infty z^2 f(z; D) dz = \sum_{\nu=0}^\infty p_\nu \int_0^\infty z^2 f_\nu(z) dz = \sum_{\nu=0}^\infty \frac{(\bar{\nu})^\nu}{\nu!} e^{-\bar{\nu}} \int_0^\infty z^2 f_\nu(z) dz = e^{-\bar{\nu}} \sum_{\nu=1}^\infty \frac{(\bar{\nu})^\nu}{\nu!} \bar{z}_\nu^2 \quad (\text{A.10})$$

where \bar{z}_ν^2 is the second moment of the ν -event distribution $f_\nu(z)$; while \bar{z}^2 is related to D through Equation (A.4), \bar{z}_ν^2 is not related to dose, but to the number of events occurring in the site of interest.

The power expansion of Equation (A.10) is,

$$\begin{aligned} \bar{z}^2 &= \left(1 - \bar{\nu} + \frac{1}{2}\bar{\nu}^2 - \dots\right) \cdot \left(\bar{\nu}\bar{z}_1^2 + \frac{1}{2}\bar{\nu}^2\bar{z}_2^2 + \dots\right) \\ &= \bar{z}_1^2 \bar{\nu} + \left(\bar{z}_2^2 - \bar{z}_1^2\right) \bar{\nu}^2 + \dots \\ &= \left(\bar{z}_1^2 / \bar{z}_1\right) \cdot D + \left[\left(\bar{z}_2^2 - \bar{z}_1^2\right) / \bar{z}_1^2\right] \cdot D^2 + \dots \end{aligned} \quad (\text{A.11})$$

From Equations (A.8), (A.9) and (A.11), we arrive at:

$$c = \frac{\sigma_z^2}{D} = \frac{\bar{z}^2}{D} - D = \frac{\bar{z}_1^2}{\bar{z}_1} + \frac{\bar{z}_2^2 - \bar{z}_1^2}{\bar{z}_1^2} D + \dots - D \quad (\text{A.12})$$

Since c is a constant, one can obtain its value from the limit $D \rightarrow 0 \text{ Gy}$, i.e.:

$$c = \lim_{D \rightarrow 0} c = \frac{\overline{z_1^2}}{z_1} \quad (\text{A.13})$$

Which, according to Equation (4.19) and taking into account that frequency distributions (subscript F) correspond to single event distributions (subscript 1), represents the average dose distribution of z , i.e.:

$$c = \overline{z_D} \quad (\text{A.14})$$

Thus one obtains the two fundamental relationships:

$$\boxed{\sigma_z^2 = \left(\overline{z_1^2} / z_1 \right) \cdot D^2} \quad (\text{A.15})$$

and, from Equation (A.9):

$$\sigma_z^2 = \overline{z^2} - D^2 \Rightarrow \overline{z^2} = \sigma_z^2 + D^2 = cD + D^2 = \left(\frac{\overline{z_1^2}}{z_1} \right) D + D^2 \quad (\text{A.16})$$

Due to its radiobiological relevance, the term $\left(\overline{z_1^2} / z_1 \right)$ has been given a special symbol:

$$\zeta = \frac{\overline{z_1^2}}{z_1} = \overline{z_D} \quad (\text{A.17})$$

Thus, Equation (A.16) can be written in its classical way as

$$\boxed{\overline{z^2} = \zeta \cdot D + D^2} \quad (\text{A.18})$$

Appendix B

Solutions to Equation 4.39 and 4.40

Equations (4.39) and (4.40) constitute a system of differential equations which can be easily solved once the boundary conditions are defined. These boundary conditions will be related to the way the biological system under study is irradiated, i.e.: single instantaneous irradiation, split-dose irradiation, continuous irradiation, etc. These cases are fully described by Hawkins (1996), and here we will only give the solution of one case, the single instantaneous irradiation.

Hawkins assumes that, at the doses used in Radiobiology experiments and in clinical radiotherapy, most of the cell damage and repair kinetic processes are of first order. This means that the following approximation can be accepted at such doses:

$$2b_d x_d^2 < (a+c) x_d \quad (\text{B.1})$$

In this case, the rate equation for x_d can be reduced to:

$$\dot{x}_d = k_d \dot{z}_d - (a+c)x_d \quad (\text{B.2})$$

Let us consider the case of instantaneous radiation, at the end of which we set our repair time origin ($t=0$). From Figure 4.6 (lower diagram) the number of repairable lesions produced at $t=0$ is $k_d z_d$. The ratio of sublethal lesions being either repaired or converted into lethal damage via mitotic misrepair between the repair time origin and a given repair time t_r (i.e. $0 < t < t_r$), is given by the equation:

$$\dot{x}_d = -(a + c)x_d \quad (\text{B.3})$$

The solution of this equation is:

$$\int_{k_d z_d}^{x_d} \frac{dx_d}{x_d} = -(a + c) \int_0^{t_r} dt \rightarrow x_d(t) = k_d z_d e^{-(a+c)t} \quad (\text{B.4})$$

Therefore, the number of total lethal lesions x_{Ad} at the time t ($0 \leq t \leq t_r$) should be derived from Equation (4.39) for the following boundary conditions:

$$\left. \begin{array}{l} t=0: \quad x_{Ad}(0) = \lambda_d z_d \\ \quad \quad z_d(0) = 0 \\ t=t_r: \quad x_{Ad}(t_r) = x_{Ad} \\ \quad \quad z_d(t_r) = 0 \end{array} \right\| \int_{\lambda_d z_d}^{x_{Ad}} dx_{Ad} = \lambda_d \int_{z_d(0)=0}^{z_d(t_r)=0} dz_d + \int_0^{t_r} [ak_d z_d e^{-(a+c)t} + b_d k_d^2 z_d^2 e^{-2(a+c)t}] dt \quad (\text{B.5})$$

As indicated in the paragraph immediately above Equations (4.39) and (4.40), there is one more term to add to Equation (B.5), corresponding to the TII lesions not converted to TI lesions and not being repaired after a time t_r . The final equation once this term is included is:

$$\begin{array}{l} \text{Total Number} \\ \text{of} \\ \text{lethal lesions} \end{array} = \begin{array}{l} \text{Lethal lesions} \\ \text{@ } t = 0 \end{array} + \begin{array}{l} \text{Lethal lesions} \\ \text{@ } 0 < t < t_r \end{array} + \begin{array}{l} \text{Lethal lesions} \\ \text{@ } t \geq t_r \end{array}$$

$$\overbrace{x_{Ad}} = \overbrace{\lambda_d z_d} + \overbrace{\int_0^{t_r} [ak_d z_d e^{-(a+c)t} + b_d k_d^2 z_d^2 e^{-2(a+c)t}] dt} + \overbrace{x_d(t_r)} \quad (\text{B.6})$$

Solving Equation (B.6), we finally derive the number of lethal lesions (x_{Ad}) after any given repair time for a given absorbed dose z_d in a domain:

$$x_{Ad} = \left[\lambda_d + \frac{ak_d}{(a+c)} + \frac{k_dc}{(a+c)} e^{-(a+c)t_r} \right] z_d + \frac{b_d k_d^2}{2(a+c)} (1 - e^{-2(a+c)t_r}) z_d^2 \quad (\text{B.7})$$

The average number of lethal lesions in a domain that absorbs z_d is given by Equation (4.35):

$$\begin{aligned} \varepsilon(z_d) &= A z_d + B z_d^2 = \\ &= \left[\lambda_d + \frac{ak_d}{(a+c)} + \frac{k_dc}{(a+c)} e^{-(a+c)t_r} \right] z_d + \frac{b_d k_d^2}{2(a+c)} (1 - e^{-2(a+c)t_r}) z_d^2 \end{aligned} \quad (\text{B.8})$$

Therefore, assuming p domains per nucleus, the parameter α_0 and β can be expressed as:

$$A = \lambda_d + \frac{ak_d}{(a+c)} + \frac{k_dc}{(a+c)} e^{-(a+c)t_r} \xrightarrow[\substack{\alpha_0 = pA \\ \lambda = p\lambda_d \\ k = pk_d}]{\substack{\alpha_0 = pA \\ \lambda = p\lambda_d \\ k = pk_d}} \alpha_0 = \lambda + \frac{ak}{(a+c)} + \frac{kc}{(a+c)} e^{-(a+c)t_r}$$

$$B = \frac{b_d k_d^2}{2(a+c)} (1 - e^{-2(a+c)t_r}) \xrightarrow[\substack{\beta = pB \\ b = pb_d \\ k = pk_d}]{\substack{\beta = pB \\ b = pb_d \\ k = pk_d}} \beta = \frac{bk^2}{2(a+c)} (1 - e^{-2(a+c)t_r})$$

Hence, Equation (4.23) for the average number of lesions per nucleus (i.e. cell) is given by:

$$\varepsilon(D) = \left[\lambda + \frac{ak}{(a+c)} + \frac{kc}{(a+c)} e^{-(a+c)t_r} + \frac{\gamma bk^2}{2(a+c)} (1 - e^{-2(a+c)t_r}) \right] D + \frac{bk^2}{2(a+c)} (1 - e^{-2(a+c)t_r}) D^2 \quad (\text{B.9})$$

Scientific Papers

Some of the results of this thesis are included in the following publications, one of them included in this appendix:

1. The incorporation of the concept of minimum RBE (*RBE_{min}*) into the linear-quadratic model and the potential for improved radiobiological analysis of high-LET treatments. *Carabe Fernandez A, Dale RG and Jones B. Int J Radiat Biol 83(1):27-39 (2007).*
2. Calculation of high-LET radiotherapy dose required for compensation of overall treatment time extensions. *Jones B, Carabe-Fernandez A, Dale RG. Br J Radiol 79(939):254-7 (2006).*
3. Conventional wisdom and activities of the middle range. *Jones B, Dale RG, Carabe A. Br J Radiol 78(936):1119 (2005).*
4. The radiobiology of conventional radiotherapy and its application to radionuclide therapy. *Dale RG, Carabe-Fernandez A. Cancer Biother Radiopharm 20(1):47-51 (2005).*
5. The Oxygen effect. *Jones B, Carabe-Fernandez A, Dale RG. In: Radiobiological Modelling in Radiation Oncology. pp.138-157. Dale RG and Jones B (eds.). The British Institute of Radiology (2007).*
6. High-LET Radiotherapy. *Jones B, Dale RG, Carabe-Fernandez A. In: Radiobiological Modelling in Radiation Oncology. pp.265-275. Dale RG and Jones B (eds.). The British Institute of Radiology (2007).*

The incorporation of the concept of minimum RBE (RBE_{\min}) into the linear-quadratic model and the potential for improved radiobiological analysis of high-LET treatments

ALEJANDRO CARABE-FERNANDEZ¹, ROGER G. DALE¹ & BLEDDYN JONES²

¹Department of Radiation Physics and Radiobiology, Imperial College School of Medicine, Hammersmith Hospitals NHS Trust, Charing Cross Hospital, London, and ²Oncology Department, Queen Elizabeth University Hospital, Birmingham, UK

(Received 24 March 2006; revised 14 June 2006; accepted 11 July 2006)

Abstract

Purpose: The formulation of relative biological effectiveness (RBE) for high linear energy transfer (high-LET) radiation treatments is revisited. The effects of changed production of sub-lethal damage with varying LET is now considered via the RBE_{\min} concept, where RBE_{\min} represents the lower limit to which RBE tends at high doses per fraction.

Materials and methods: An existing linear-quadratic formulation for calculating RBE variations with fractional dose for high-LET radiations is modified to incorporate the twin concepts of RBE_{\max} (which represents the value of RBE at an effective dose-per-fraction of 0 Gy) and RBE_{\min} .

Results: Fits of the model to data showed RBE_{\min} values in the range of 0.1–2.27. In all cases the raw data was a better statistical fit to the model which included RBE_{\min} , although this was only very highly significant in one case. In the case of the mouse oesophagus it is shown that, if change in the β -radiosensitivity coefficient with LET is considered as trivial, an underestimation > 5% in RBE can be expected at X-ray doses of 2 Gy/fraction if RBE_{\min} is not considered. To ensure that the results were not biased by the statistical method used to obtain the parameter values relevant to this analysis (i.e., using fraction-size effect or Fe-plots), an alternative method was used which provided very similar correlation with the data.

Conclusions: If the production of sublethal damage is considered independent of LET, there will be a risk that non-corrected evaluation of RBE will lead to an over- or under-estimate of RBE at low doses per fractions (the clinically relevant region).

Keywords: High-LET radiotherapy, RBE, isoeffective fractionation schedules, acute and late reacting tissue, neutrons

Introduction

The theory of dual radiation action (TDRA) (Kellerer & Rossi 1972) predicts that high linear energy transfer (high-LET) radiation increases the linear (α) component of radiation damage, while the quadratic (β) component remains unchanged. As a consequence it is to be expected that, as fractional dose size decreases, the relative biological effectiveness (RBE) tends asymptotically to an intrinsic maximum value and which is the ratio of the initial slopes at zero dose of the associated cell-survival curves relating to the high-LET radiation in question and the reference (low-LET) radiation (Dale & Jones 1999). Similarly, the TDRA prediction of β being independent of radiation quality will mean that RBE tends to unity at very high doses.

However, this latter point has been found not to be the case for a number of systems and radiation qualities.

The analysis of experimental data (especially that relating to ultrasoft X-rays) using the TDRA model has shown that the assumption that β is constant can lead to very unsatisfactory prediction of biological effectiveness (Goodhead 1977). The conclusion is that the initial hypothesis of the TDRA is not valid and also that β should change as a function of LET, i.e., $\beta_H \neq \beta_L$. Alternative mechanistic models have been proposed which allow for the variability of β on the basis of a LET-dependant saturable sub-lethal damage repair process.

This article presents an extension of an earlier radiobiological model developed by this group (Dale & Jones 1999) and introduces a new concept

(RBE_{\min}) within the linear-quadratic (LQ) model, which is defined as:

$$RBE_{\min} = \sqrt{\frac{\beta_H}{\beta_L}} \quad (1)$$

An experimental method is also proposed to search for the existence of the RBE_{\min} parameter which, together with RBE_{\max} , should provide a better description of the overall shape of the curve of RBE versus dose.

Methods and materials

RBE and fractionated irradiation

Under the LQ formulation, a given high-LET fraction dose (d_H) will produce the same effect as a given low-LET dose (d_L) only if:

$$\alpha_L d_L + \beta_L d_L^2 = \alpha_H d_H + \beta_H d_H^2 \quad (2)$$

But, taking into account that $\alpha_H = \alpha_L RBE_{\max}$ and $\beta_H = \beta_L RBE_{\min}^2$ (the latter being the new assumption), and dividing both sides of the resultant equation by β_L , we arrive at:

$$\begin{aligned} (\alpha/\beta)_L d_L + d_L^2 \\ = (\alpha/\beta)_L RBE_{\max} d_H + RBE_{\min}^2 d_H^2 \end{aligned} \quad (3)$$

Dividing both sides of Equation 3 by d_H , and noting that $d_H = (d_L/RBE)$, Equation 3 can be re-written purely in terms of low-LET parameters, as follows:

$$\begin{aligned} (\alpha/\beta)_L RBE + RBE d_L \\ = (\alpha/\beta)_L RBE_{\max} + RBE_{\min}^2 \frac{d_L}{RBE} \end{aligned} \quad (4)$$

Solving Equation 4 for positive values of RBE:

$$\begin{aligned} RBE = \\ \frac{(\alpha/\beta)_L RBE_{\max} + \sqrt{(\alpha/\beta)_L^2 RBE_{\max}^2 + 4d_L RBE_{\min}^2 ((\alpha/\beta)_L + d_L)}}{2((\alpha/\beta)_L + d_L)} \end{aligned} \quad (5)$$

Equation 5 describes RBE as a function of changing low-LET dose per fraction and is similar in form to an earlier equation (Dale & Jones 1999) but which did not allow for non-constancy of β with changing LET and therefore did not include the RBE_{\min} factor in the final term, i.e.,

$$\begin{aligned} RBE = \\ \frac{(\alpha/\beta)_L RBE_{\max} + \sqrt{(\alpha/\beta)_L^2 RBE_{\max}^2 + 4d_L ((\alpha/\beta)_L + d_L)}}{2((\alpha/\beta)_L + d_L)} \end{aligned} \quad (6)$$

This previous version was conceived as being adequate for low doses per fraction (or high surviving fraction) since β mediated damage is then relatively small compared with α mediated damage. One relevant point of Equation 5 is that RBE is entirely determined by low-LET parameters, $(\alpha/\beta)_L$ and d_L which, for a range of tissues, are more extensively tabulated. In Equation 5, as $d_L \rightarrow 0$ Gy, $RBE \rightarrow RBE_{\max}$, which is also the case for the earlier formulation. However, as $d_L \rightarrow \infty$ Gy, $RBE \rightarrow RBE_{\min}$, rather than unity.

Modification of BED equations to allow for RBE effects and calculation of relevant parameters

RBE_{\max} and RBE_{\min} are respectively the ratios of α and $\sqrt{\beta}$ as normally measured directly from survival curves. The measurement of these parameters is relatively easier in *in-vitro* experiments but, even then, the determination of both parameters from simple regression analysis applied to survival data is error prone. The only parameters used when specifying a patient treatment are the total dose and the dose per fraction, generally chosen to achieve the highest tumour control probability (TCP) while keeping the normal tissue complication probability (NTCP) as low as possible. Generic values of (α/β) ratios for each individual tissue included in the treatment field can usually be assumed. The question then would be if there is any way of obtaining RBE_{\max} and RBE_{\min} values from the parameters commonly used clinically, i.e., number of fractions (n), total dose (TD) and (α/β) ratios for the irradiated tissues.

These three parameters are related together by the Biologically Effective Dose (BED) concept. BED is defined as the theoretical total physical dose required for a given biological effect with a fractionated regime consisting of an infinite number of fractions of infinitesimally small doses and in the absence of repopulation. For low-LET radiations, the BED is formulated as (Joiner & Bentzen 2002):

$$BED_L = \frac{E_L}{\alpha_L} = n_L d_L \left(1 + \frac{d_L}{(\alpha/\beta)_L} \right) \quad (7)$$

For high-LET radiations the “ $1 + \dots$ ” term is simply changed to “ $RBE_{\max} + \dots$ ” (Dale & Jones 1999), i.e.,

$$BED_H = n_H d_H \left(RBE_{\max} + \frac{d_H}{(\alpha/\beta)_L} \right) \quad (8)$$

Equations 7 and 8 may be derived from the respective equations which define “effect” (E) in a fractionated treatment. Taking that same methodology a

stage further and incorporating Equation 1 leads to the following sequence:

$$\begin{aligned}
 n_L(\alpha_L d_L + \beta_L d_L^2) &= n_H(\alpha_H d_H + \beta_H d_H^2) \\
 \Rightarrow n_L d_L \left(1 + \frac{d_L}{(\alpha/\beta)_L}\right) &= \\
 &= n_H \left(RBE_{max} d_H + \left(\frac{\beta_H}{\alpha_L}\right) d_H^2\right) \\
 &= n_H \left(RBE_{max} d_H + \left(\frac{\beta_L RBE_{min}^2}{\alpha_L}\right) d_H^2\right) \\
 &= n_H \left(RBE_{max} d_H + RBE_{min}^2 \frac{d_H^2}{(\alpha/\beta)_L}\right) \quad (9)
 \end{aligned}$$

This identity indicates that the BED for high-LET radiations [earlier written as Equation 8] should be more comprehensively defined as:

$$BED_H = n_H d_H \left(RBE_{max} + RBE_{min}^2 \frac{d_H}{(\alpha/\beta)_L} \right) \quad (10)$$

Equation 10 provides a tool with which to compare treatments carried out using radiations of different quality. The fact that Equation 10 has been formulated in terms of $(\alpha/\beta)_L$ is convenient as this means the low- and high-LET BEDs are each being expressed in the same biological dose units and may therefore be directly compared, one with another.

Isoeffective low- and high-LET treatments must therefore comply by definition with the condition,

$$BED_L = BED_H \quad (11)$$

Equations 7 and 10 as applied to fractionation schedules corresponding to isoeffective low- and high-LET treatments can be respectively rewritten as,

$$\begin{aligned}
 BED_L &= n_L d_L \left(1 + \frac{d_L}{(\alpha/\beta)_L}\right) \Rightarrow \\
 \frac{1}{D_L} &= \frac{1}{BED} + \frac{1}{(\alpha/\beta)_L BED} d_L \quad (12)
 \end{aligned}$$

$$\begin{aligned}
 BED_H &= n_H d_H \left(RBE_{max} + \frac{RBE_{min}^2 d_H}{(\alpha/\beta)_L} \right) \Rightarrow \\
 \frac{1}{D_H} &= \frac{RBE_{max}}{BED} + \frac{RBE_{min}^2}{(\alpha/\beta)_L BED} d_H \quad (13)
 \end{aligned}$$

where the notation has been simplified to $BED = BED_L = BED_H$.

Equation 12 is the formulation proposed by Fowler (1989) for use in deriving the (α/β) ratios of tissues treated with isoeffective low-LET fractionated regimes, via the so-called fraction-size effect or 'Fe-plots', which are plots of $Y =$ reciprocal

total dose against $X =$ dose-per-fraction. Reciprocal total dose is the same as reciprocal BED only when dose-per-fraction tends to zero, as defined by Barendsen (1982a) for Extrapolated Total Dose (ETD) before it was renamed BED by Fowler (1989). From the intersection of the low-LET Fe-plot on the vertical axis we obtain the reciprocal of the BED associated with the given end point. Knowing the slope of the line, the BED is then used to derive the (α/β) ratio of the tissue. Using Equation 13 the corresponding Fe-plot is derived from the high-LET doses required to achieve the same biological end point. The intersection value and the slope, used in conjunction with the values for BED and (α/β) derived from the low-LET data, allow RBE_{max} and RBE_{min} to be derived. Comparing Equations 12 and 13 it is clear that the high-LET slope differs from that for low-LET by a factor of RBE_{min}^2 . Thus, Fe-plots showing little or no change in slope indicate that $RBE_{min} \sim 1$, whereas high-LET slopes which are greater or less than the low-LET slopes respectively indicate $RBE_{min} > 1$ or < 1 .

Testing of the model against measured data

Mice LD₅₀ after oesophagus injury

To illustrate the operation of the above method to calculate RBE_{max} and RBE_{min} , it will first be used to derive the RBE for the mouse oesophageal endpoint of LD₅₀ in 10–40 days (animals which survive this period may die later from radiation pneumonitis) after irradiation of the thorax with 250 kVp X-rays and d(16)Be neutrons. Endpoint doses are available for single doses, two fractions in 24 h, five fractions in 4 days and 10 fractions in 11 days (Hornsey & Field 1979). Figure 1 shows the resultant Fe-plots.

From the X-ray slope and intersection point the derived BED and (α/β) are:

$$\begin{aligned}
 BED &= \frac{1}{0.0112} = 89.54 \text{ Gy} \Rightarrow \\
 (\alpha/\beta)_L &= \frac{1}{BED \cdot 0.007} = \frac{0.0112}{0.007} = 16.25 \text{ Gy}
 \end{aligned}$$

Therefore, from the Fe-plot corresponding to the fast neutrons, the subsequently derived RBE_{max} and RBE_{min} are:

$$\begin{aligned}
 RBE_{max} &= 89.54 \times 0.0341 = 3.05 \Rightarrow \\
 RBE_{min} &= \sqrt{BED \times (\alpha/\beta)_L \times 0.0036} = 2.28
 \end{aligned}$$

Substituting the values obtained for $(\alpha/\beta)_L$, RBE_{max} and RBE_{min} into Equation 5, the resultant

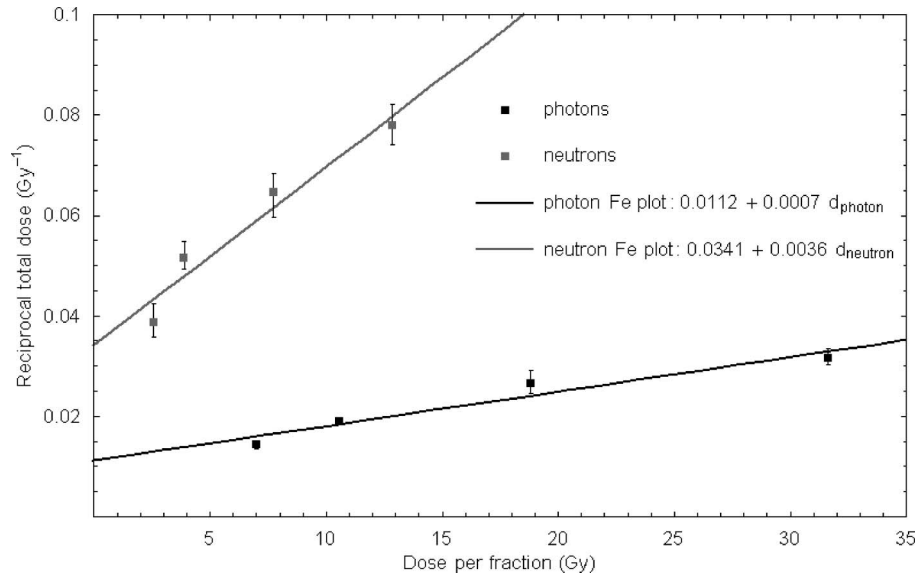


Figure 1. Fe-plots for LD₅₀ due to oesophagus injury in TO mice after irradiations with X-rays and fast neutrons. Data from Hornsey and Field (1979).

expression for RBE as a function of the X-ray dose per fraction is:

$$RBE = \frac{49.58 + \sqrt{2458.69 + 336.48d_L + 20.71d_L^2}}{32.49 + 2d_L} \quad (14)$$

The resultant RBE curve from Equation 14, along with the original data points, is shown in Figure 2.

The black trace corresponds to the RBE obtained when using RBE_{\max} and RBE_{\min} in Equation 5, while the grey line corresponds to the RBE obtained without using the concept of RBE_{\min} [i.e., that obtained via Equation 6). The RBE difference (ΔRBE) obtained between the two lines at 2 Gy per fraction is 5.2%. This difference is due to the large value of RBE_{\min} and which reflects the values of RBE at very large doses per fraction reported by Hornsey and Field (1979). The black squares in Figure 2 are the original data points and it is clear that the curve incorporating the RBE_{\min} concept provides an altogether better fit to the data.

Renal damage in mice after fast neutron irradiation

Stewart et al. (1984) reported RBE values for the renal damage of mice irradiated with 3 MeV neutrons based on early and late endpoints of reduction of haematocrit in the kidney to a 40% level (22 weeks) and ethylenediaminetetraacetic acid (EDTA) clearance of 3% retention (28 weeks), respectively. The resultant parameters from the Fe-plot analysis are summarized in Table I and the RBE curves obtained from Equation 5 for each endpoint are shown in Figure 3.

Very little difference was found between considering and not considering RBE_{\min} in the RBE equation (see Table I), primarily because the fitted RBE_{\min} value is ~ 1 . Figure 3 suggests that, up to around 25 Gy of X-ray dose, the RBE for early renal damage effects is higher than for late effects.

The data assessed in Figure 3 employed X-ray doses per fraction in the range 4.7–14.4 Gy. In a separate study, Joiner and Johns (1987) investigated the same range of fractional dose sizes for mouse renal damage, but used 1, 2, 5 and 10 fractions and also included 10 fractions plus a “top-up” dose of neutrons in order to measure RBE in the lower X-ray dose range of 0.75–3.0 Gy per fraction. This “top-up” data however has not been included in the present analysis in order to maintain the correspondence with the previous experiments and also to avoid including any low-dose hypersensitivity effects which might be produced by X-rays at very low doses per fraction. Also, RBE has been calculated at different levels of functional effect in order to reproduce the method used by Joiner and Johns. The resultant RBE_{\max} and RBE_{\min} calculated for these levels are shown in Table I. The value of RBE_{\max} and (α/β) calculated here are 15.85 and 2.23 Gy respectively, these values being in accordance with the values proposed by Joiner and Johns (see bracketed values in Table I). The fitted RBE versus dose-per-fraction curves are shown in Figure 4.

Colo-rectal injury in mice

Terry et al. (1983a, 1983b) studied the RBE of early- and late-effects in colo-rectal normal tissue after

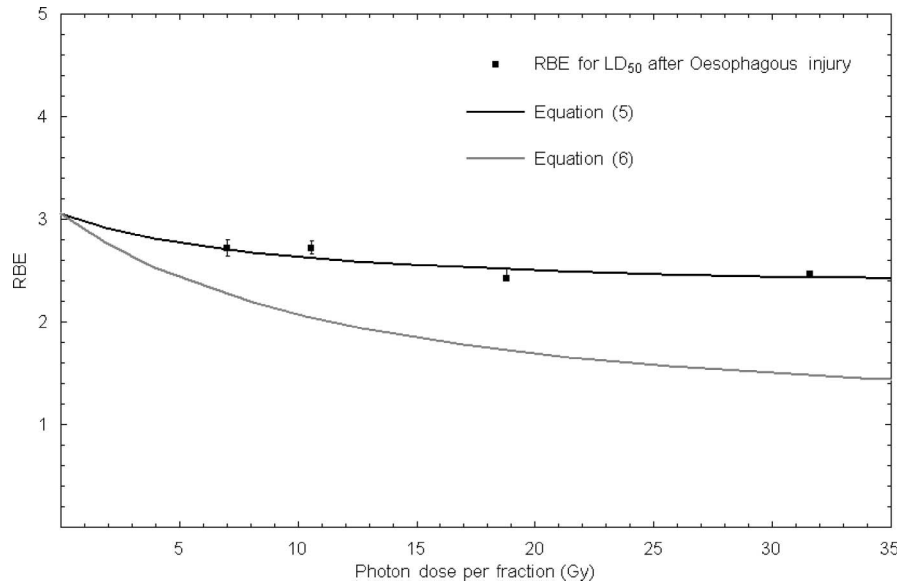


Figure 2. Data points show the RBE variation with dose derived from the data plotted in Figure 1. The black line is derived from Equation 5 and incorporates a fitted value of RBE_{min} whilst the grey line assumes that RBE_{min} is unity. The better match of the measured data to the former is apparent.

Table I. Relevant radiobiological parameters obtained from Equations 12 and 13 for the different end-points selected. The values in round brackets correspond to the published values. In the final two columns are listed the two-tailed t and (in square brackets) the associated p values of the fit of the data points to the two alternative models [Weatherbum (1962)]. For all of the data analysed the complex model (i.e., that including both RBE_{max} and RBE_{min}) provides the better statistical fit, although only in the case of oesophagus LD50 data is the fit very highly significant.

End point	$\left(\frac{\alpha}{\beta}\right)_L$ [Gy]	BED_L (d→0 Gy) [Gy]	RBE_{max}	RBE_{min}	t [$p_{two-tailed}$] (RBE_{min} , RBE_{max})	t [$p_{two-tailed}$] (RBE_{max})
LD ₅₀ – Oesophagus injury (Hornsey & Field 1979)	16.24	89.54	3.05	2.27	0.1348 [0.9013]	6.4745 [0.0075]
40% Residual Haematocrit (Stewart et al. 1984)	1.15	178.65	26.33	1.19	0.1678 [0.8774]	0.3223 [0.7684]
3% Residual EDTA (Stewart et al. 1984)	1.22	183.74	20.58	1.35	0.6348 [0.5706]	6.2033 [0.0084]
Mouse kidney (Joiner & Johns 1987)	2.23 (3.04 ± 0.35)	115.48	15.85 (11.65 ± 0.69)	0.73	0.4029 [0.6898]	0.9594 [0.3450]
Mouse skin injury (Joiner et al. 1983)	17.42 (43.6)	60.69	5.35 (7.2)	0.41	1.1813 [0.2486]	1.9109 [0.0675]
Colo-rectal injury (Nadir body weight) (Terry et al. 1983b)	12.33 (13.07)	70.50 (67.11)	7.04 (8.5)	0.47	0.7401 [0.4688]	3.4067 [0.0031]
Colo-rectal injury (Peak body weight) (Terry et al. 1983b)	7.38 (9.21)	82.10 (85.47)	6.84 (5.7)	0	1.0803 [0.3012]	2.2668 [0.0427]
LD ₅₀ – Colo-rectal injury (2 months) (Terry et al. 1983)	28.69 (28.63)	76.68 (76.92)	5.7 (5.7)	1.46	0.0925 [0.9321]	0.5223 [0.6376]
LD ₅₀ – Colo-rectal injury (15 months) (Terry et al. 1983)	3.11 (3.12)	108.24 (107.87)	12.56 (12.70)	0.41	0.2503 [0.8185]	1.2076 [0.3137]
BR × 1.1 – Lung injury (28 weeks) (Parkins et al. 1985)	2.93 (2.9)	50.04	7.63	0.58	0.5920 [0.5755]	1.0587 [0.3304]
BR × 1.1 – Lung injury (68 weeks) (Parkins et al. 1985)	2.14 (2.1)	54.11	9.22	0.10	0.8678 [0.4188]	2.9749 [0.0248]
LD ₅₀ – Lung injury (28 weeks) (Parkins et al. 1985)	5.95 (4.5)	38.51	5.19	0.99	0.7143 [0.5018]	0.6987 [0.5190]
LD ₅₀ – Lung injury (68 weeks) (Parkins et al. 1985)	2.32 (2.15)	56.18	8.62	0.72	0.5789 [0.5837]	1.9497 [0.0991]
Desquamation – Pig skin injury (Hopewell et al. 1988)	15.17	79.05	3.46 (2.75)	0.71	0.0227 [0.9827]	0.5692 [0.5938]
Necrosis – Pig skin injury (Hopewell et al. 1988)	5.25	101.27	4.26 (4.32 ± 0.39)	0.91	0.3146 [0.7657]	0.4138 [0.6962]

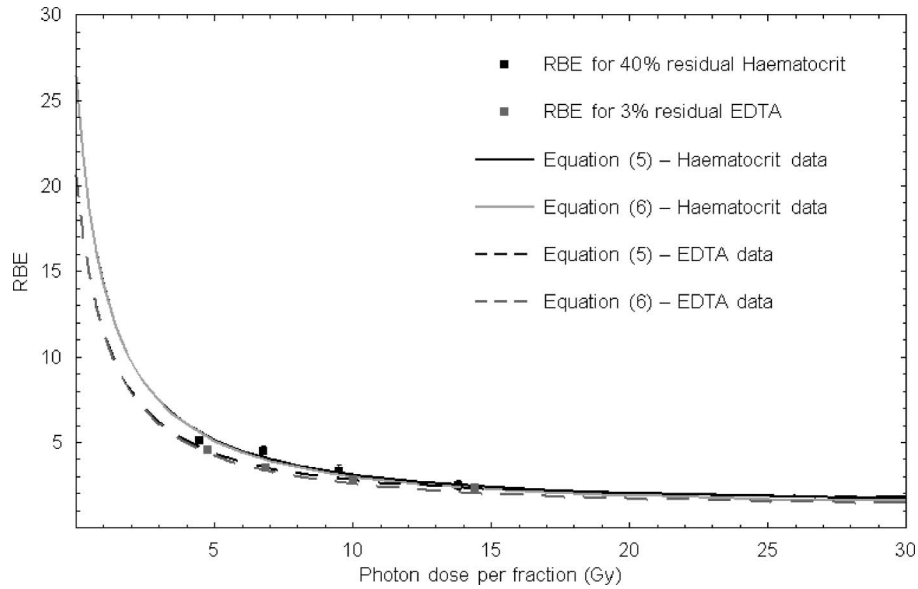


Figure 3. RBE versus dose curves for Haematocrit reduction to 40% level (early reaction – 22 weeks) and 3% ethylenediaminetetraacetic acid retention (late reaction – 28 weeks) for mice kidney after being irradiated with X-rays and fast neutrons. The fitted curves (respectively black and grey) are derived from Equation 5. Data from Stewart et al. (1984).

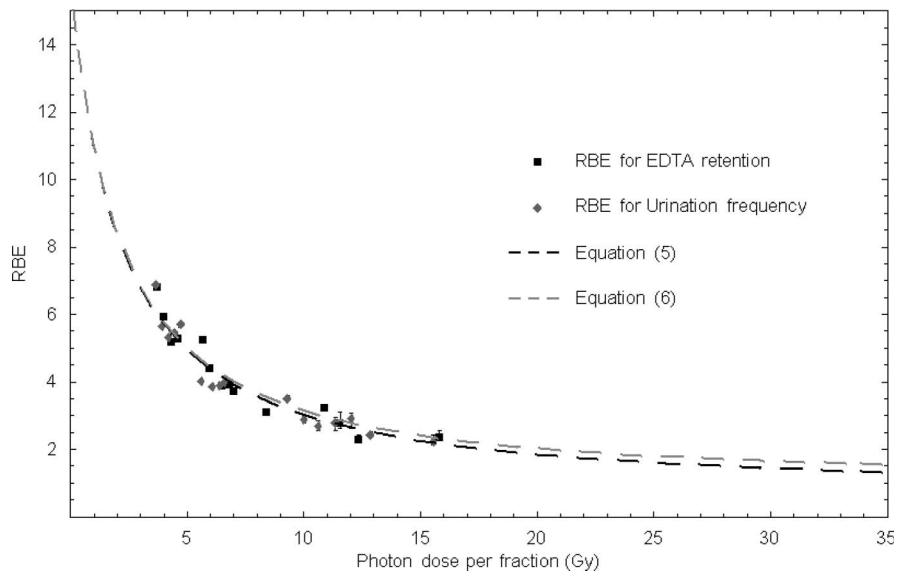


Figure 4. RBE versus dose curves corresponding to mouse kidney damage for X-rays and fast neutrons. The black squares are the data points obtained from the ethylenediaminetetraacetic acid clearance experiments, while the grey diamonds represent the data extracted from the urination frequency experiments. The black line corresponds to the RBE-fitted curve which includes RBE_{\min} , whilst the grey line corresponds to the calculation without taking RBE_{\min} into account. Data from Joiner and Johns (1987).

irradiation of mice with ^{137}Cs gamma-rays and fast neutrons. The end points used were:

- Body weight: The weight lost shortly after irradiation and the maximum body weight regained were both studied as a function of radiation dose. The nadir in weight occurred between 11 and 17 days (early effect), and the maximum body weight was achieved at 4–7 months after irradiation (late effect).
- Lethality: The proportion of surviving animals was assessed sequentially at monthly intervals up to 16 months after irradiation. The lethal total dose required to kill 50% of the mice population (LD_{50}) values were obtained at 15 days and 15 months after irradiation with both γ -rays and neutrons.

Table I summarizes the results obtained from the present analysis and the results determined by Terry et al. The associated RBE curves to the relevant end

point (with and without the RBE_{min} concept) are presented in Figures 5 and 6.

In both Figures major differences are only noted at doses-per-fraction larger than 10 Gy. A notable feature in Figure 6 however, is the existence of a certain threshold dose/fraction (≈ 5 Gy) above which the late-reacting RBE is lower than that for the acute response. As the fractionation response of most tumours is similar to that of acute-responding normal tissues then this divergence in RBE values might have important implications for therapy. To avoid more damage to the normal tissue than tumour, the doses/fraction required would have to be > 5 Gy, as lower doses would infer a higher RBE for normal tissues and higher toxicity. It is also interesting to notice how the difference between the early and late effects tend to increase for any given dose per fraction when RBE_{min} is included in Equation 5.

Damage to mouse lung

Parkins et al. (1985) measured lung damage after exposing the thorax of CBA/Ht male mice to 240 kVp X-rays and 3 MeV neutrons. The end points used were increase of breathing rate (by a factor 1.1 with respect the normal rate) and lethality (LD_{50}). The RBE curves for these are respectively presented in Figures 7 and 8.

In Figure 7, the RBE curves associated with increased breathing rates at early and late stages of the experiment shows a distinction between the cases

corresponding to inclusion or non-inclusion of RBE_{min} in Equation 5. The largest difference is observed in the late effects, but this difference is significant only at high doses per fractions. The implication is that treatment with neutrons would be beneficial only if the doses per fraction were larger than ~ 3 Gy. It is clear from the p values in Table I that a better fit to the RBE points is achieved when considering RBE_{min} in Equation 5. That can be seen from the points at higher doses per fractions and which lay well under the early- and late-RBE curves which do not include RBE_{min} .

In Figure 8 the same difference between considering and not considering RBE_{min} is observed in the case of late end points but it is not as great in the case of early end points, for which the associated RBE curves are almost perfectly coincident. Adverse therapeutic index is likely at fractional dose less than about 4 Gy.

Acute skin reactions in:

- *Pig skin.* Hopewell et al. (1988) exposed pig skin to different fractionated doses of 250 kV X-rays and $d(42)Be$ neutrons in order to investigate the respective early and late end-point RBE of pig skin desquamation and necrosis. The data from that study are presented in Figure 9, together with the RBE curves derived using the present analysis. Small differences between inclusion and non-inclusion of RBE_{min} are apparent at higher fractional doses. A positive therapeutic

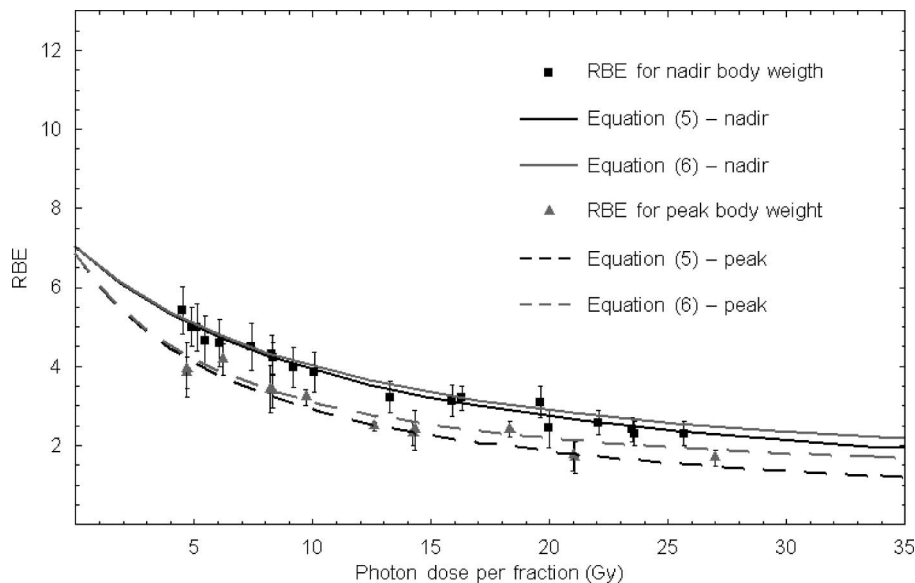


Figure 5. RBE versus dose curves for changes in body weight as a consequence of colo-rectal damage after pelvic irradiation. The black squares represent the data points for the lower limit of body weight attained, while the grey triangles are for the higher limit. The biggest differences between the predicted curves obtained from Equation 5 and 6 are noticeable at doses per fraction > 10 Gy. According to this figure, the use of neutron is contraindicated as the RBE for early effects is higher than for late effects at any given dose per fraction. Data from Terry et al. (1983a, 1983b).

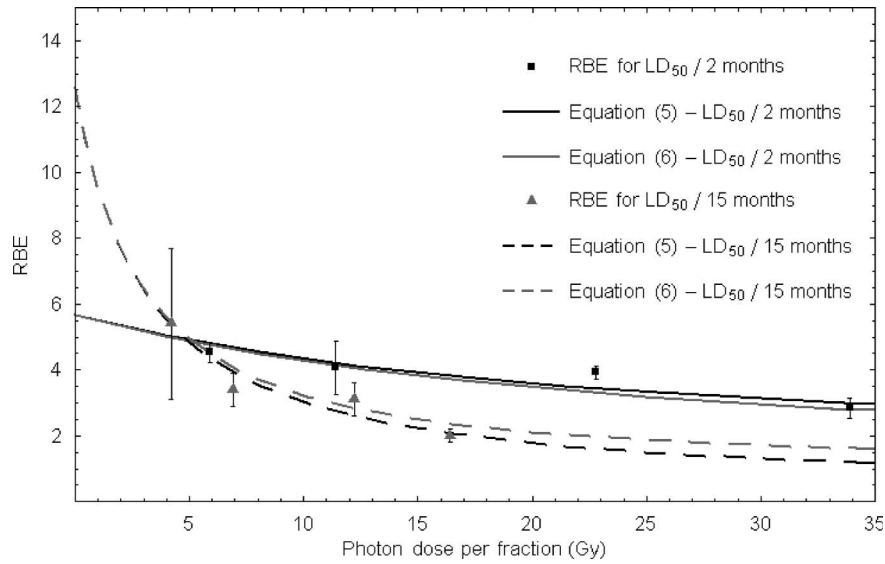


Figure 6. RBE versus dose for LD₅₀ following colo-rectal damage. Squares correspond to data for early effects while triangles correspond to late effects. The solid lines are fitted to the former data and the dotted lines to the latter. The data implies that favourable disposition of the RBE effect (assuming that tumours would behave similarly to the acute effects) is achievable only above 5 Gy. Data from Terry et al. (1983a, 1983b).

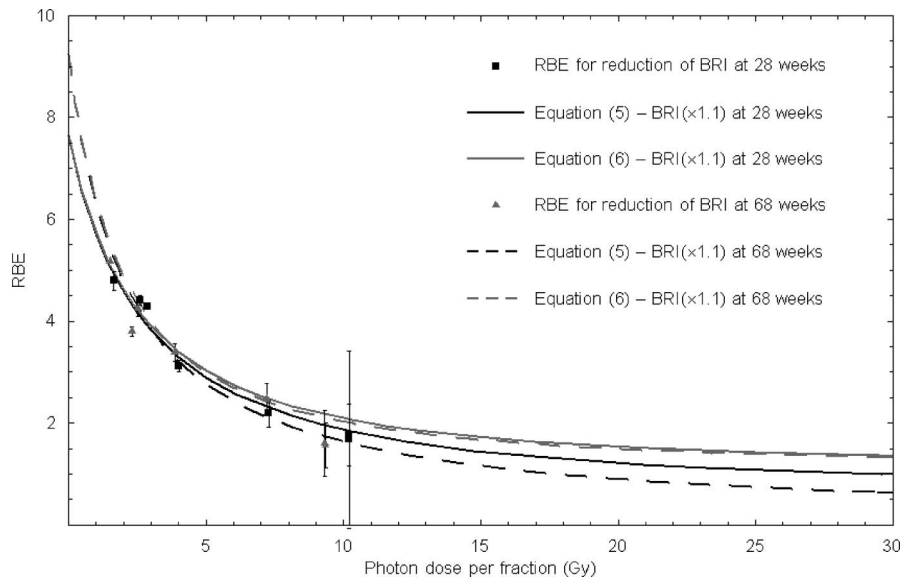


Figure 7. RBE versus dose for increased breath rate by a factor of 1.1 following exposure of whole mouse thorax to X-rays and neutrons. Squares correspond to early (28 weeks) data endpoint while triangles correspond to late (68 weeks) endpoint. Data from Parkins et al. (1985).

ratio will only be valid for doses greater than ~ 2 Gy.

- *Mouse skin.* Other useful data on normal tissue effects was produced by Joiner et al. (1983) using neutrons from the 4 MV van de Graaf accelerator at the Gray Laboratory. Two different experiments were performed, one where single, two or five equal fractions were delivered daily, and a repeat experiment that included 9 equal fractions, the dose being delivered twice per day with an inter-fraction interval of at least

6 h. The data analysis and curve fitting was performed slightly differently in this case in order to reproduce the method used by Joiner. The RBE were calculated for different skin reaction levels from 0.8–2.4, the resultant RBE_{\max} and RBE_{\min} values being as listed in Table I and the RBE curve fits being shown in Figure 10.

For comparison purposes, we have included the RBE curves for EDTA retention shown in Figure 4.

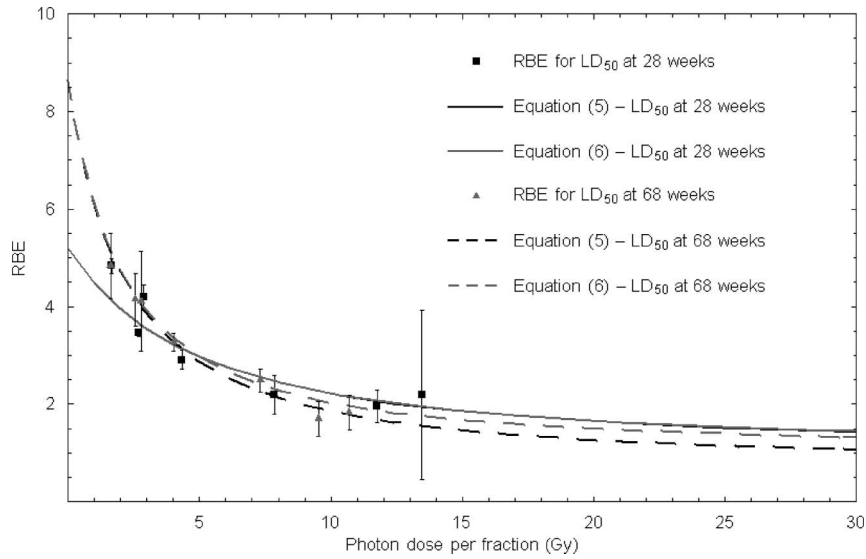


Figure 8. RBE versus dose for LD₅₀ determinations following exposure to X-rays and neutrons of whole mouse thorax. Squares correspond to early (28 weeks) end point while triangles correspond to late (68 weeks) end point. Data from Parkins et al. (1985).

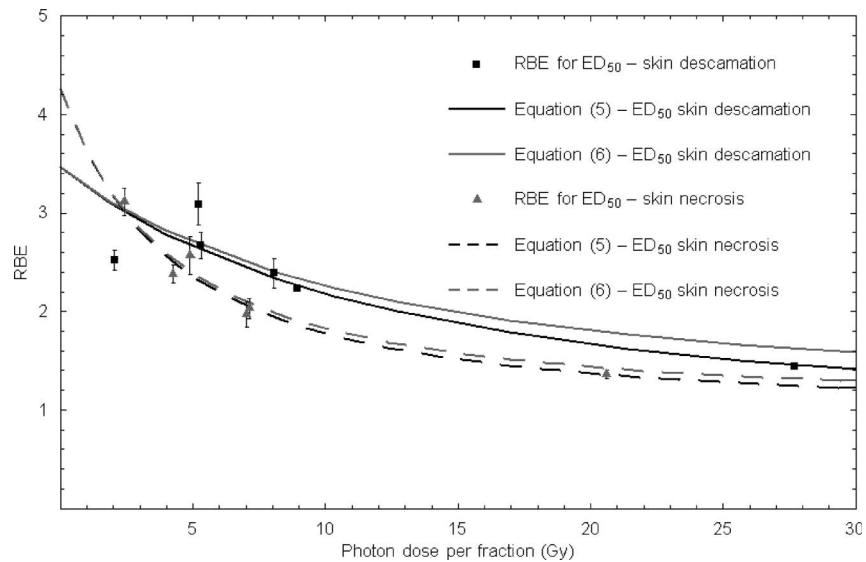


Figure 9. ED₅₀ after exposure to X-rays and neutrons of pig skin. Squares correspond to early end point (desquamation) while triangles correspond to late end point (necrosis). Data from Hopewell et al. (1988).

This shows that in these circumstances, a positive therapeutic ratio can only be achieved at doses higher than ~7 Gy.

Overall results and comparison with predicted values

Figures 6 to 10 show a general agreement of a higher RBE for late effects at the levels of dose per fraction conventionally used in clinical radiotherapy. Although these results are not conclusive, they corroborate earlier suggestions that the reason for adversity when using neutrons is a consequence of the greater impact they have on normal tissues

at lower fractional doses. The Hammersmith neutron trials in the 1970s (Catterall & Bewley 1979) are often considered to be disappointing because, although the tumour control in advanced head and neck cancer increased by a factor of four (from 12/62 to 54/71; Catterall 1989), so did the late complications (from 4–17%), the latter figure being considered unacceptably high and adding to the general impression that neutron therapy failed to match expectations. The Edinburgh neutron trials used lower fractional doses but failed to indicate an improved therapeutic ratio (Duncan 1994).

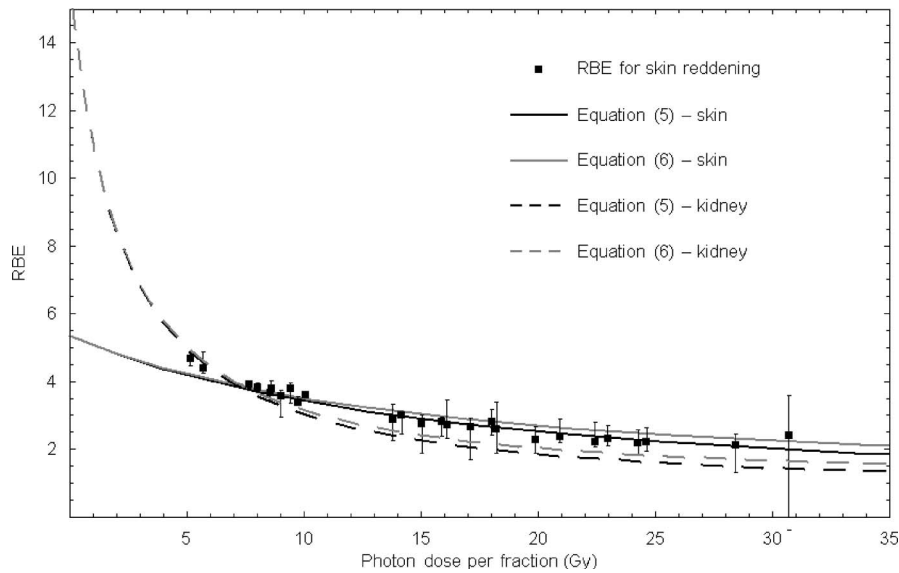


Figure 10. RBE versus dose corresponding to mice skin exposed to X-rays and fast neutrons. The back boxes represent the data obtained from the experiment using one, two or five daily fractions; the grey triangles represent the data extracted from the second experiment which included up to 9 fractions. The black solid line corresponds to the RBE fitted curve which includes RBE_{\min} , while the grey solid line corresponds to the calculation without taking RBE_{\min} into account. Data from Joiner et al. (1983).

Table I summarizes the results obtained from the present analysis and compares them with the measured data points. In the final two columns are listed the two-tailed t and (in square brackets) the associated p values of the fit of the data points to the two alternative models. For all of the data analysed the complex model (i.e., that including both RBE_{\max} and RBE_{\min}) provides the better statistical fit, although only in the case of oesophagus LD50 data is the fit very highly significant.

For this particular tissue, the difference in RBE at a dose per fraction of 2 Gy of X-rays between the two traces shown in Figure 2 is 5.15%. In the rest of the tissues analysed $\Delta RBE|_{2\text{Gy}}$ is minimal. However, it is interesting to notice how the presence of RBE_{\min} in Equation 5 makes a bigger change to the RBE of late effects than to those of the early effects. In all the cases analysed, the RBE late effect changes are smaller when RBE_{\min} is taken into account. This means that, if the RBE curves for early and late effects cross over at some point, the dose-per-fraction at which they cross could be shifted towards lower doses, which ultimately would affect the lower limiting dose required to achieve a positive therapeutic ratio. Conversely, had the RBE changes for late effects been larger when considering RBE_{\min} in Equation 5, the crossing point between early and late reaction curves would have shifted to higher doses-per-fraction. It is still not clear why, or in what cases, the RBE_{\min} correction increases the change in RBE in some cases and decreases it in others. The present authors are investigating this

effect using data produced with other tissues and radiation qualities.

Discussion

A method is proposed for calculating RBE values using the assumption that the main radiosensitivity parameters describing the LQ model, α and β , are *both* susceptible to change with changing LET. As indicated in a previous paper (Dale & Jones 1999), several authors have shown experimentally that the β -values for some cell lines appear to be LET-dependent (Kellerer & Rossi 1972, Goodhead 1988, Stenerlöv et al. 1995). As discussed here, a consequence of that is the requirement to consider two intrinsic RBE values (RBE_{\max} and RBE_{\min}) for every cell line and which, as demonstrated in Figure 2, could have an important impact in calculating the relative effectiveness of a given high-LET dose. In order to obtain a high TCP while keeping an NTCP as low as possible, it is essential in radiotherapy to keep the normal tissue dose well below its tolerance limit. This principle is valid whatever the radiation type is used and Figures 6–10 suggest that neutrons may produce more damage in normal tissue than in tumour for the doses per fraction normally used in radiotherapy. This might be an indication of the reasons why the UK neutron trial experience was disappointing although, perhaps, any radiobiological shortcomings may well have been exacerbated by a poorly-penetrating and heterogeneous neutron beam.

Several points arise from this analysis. Most of the cases reviewed do not show a tremendous difference between the plots produced with and without the RBE_{min} included in Equation 5 and, even then, the difference is noticed only at high fractional doses. However, the fact that, in the oesophagus case in particular, there is a significant difference suggests that the RBE_{min} might well be a parameter that must be more generally taken into account to avoid the risk of underestimating RBE at low fractional doses, particularly in critical organs. It follows then that the general consensus of considering β independent of LET might be inappropriate for some high-LET radiotherapy. One advantage of our revised model is that it does not require any additional clinical data from isoeffect or other studies and it therefore can serve to increase the clinical utility of BED/RBE iso-effect formulations, the potential usefulness of which were first identified by Barendsen (1982a). The overall variation of β with LET is in any case likely to be small and this *may* explain why derived RBE_{min} values, as seen from Table I, are both greater and less than unity (the majority being in the latter category). In addition to the possibility of a systematic dependence of β on LET there are a number of other influences which may affect the magnitude of the observed variations, e.g., measurement imprecision, variable radiosensitivity, breakdown of the LQ model at high doses, etc., and the

finding of β -values either side of unity does mean that experimental imprecision and/or modelling limitations cannot be ruled out.

There is also the issue of the statistical significance of the raw data. Although Fe-plots have been used for many years to estimate the (α/β) parameter (e.g., Douglas & Fowler 1976), several authors have commented on the statistical shortcomings of this method (Tucker 1984, de Boer 1988, Taylor & Kim 1989). Some of these criticisms are: (i) The method derives the (α/β) parameter via a two-stage (indirect) analysis, (Fischer & Fischer 1977, Herring 1980); and (ii) the method tends to be biased in its estimation of (α/β) as a consequence of the uncertainty in both, the independent and the dependent variables (d and $1/TD$ respectively). This double uncertainty precludes the use of linear regression analysis [which may be applied only if the experimental uncertainty is restricted to the values of the ordinate (de Boer 1988)] and forces the use of non-linear analysis (Tucker 1984). However, Fe-plots do use clinically relevant data (dose per fraction and iso-effective total doses) and link it with BED, a parameter of widely recognized value and which is very helpful when comparing isoeffective treatments. de Boer (1988) proposed a method based again on a linear least-square fit of data presented as a TD vs. $d \cdot TD$ plot, which provided values of E/α and (α/β) very similar to those derived from non-linear

Table II. Relevant radiobiological parameters obtained when applying de Boer's method.

End point	$(\alpha/\beta)_L$ [Gy]	BED_L ($d \rightarrow 0$ Gy) [Gy]	RBE_{max}	RBE_{min}	$t [p]$ (RBE_{min} , RBE_{max})	$t [p]$ (RBE_{max})
LD ₅₀ – Oesophagus injury (Hornsey & Field 1979)	14.87	94.38	3.10	2.28	0.0576 [0.9579]	6.5641 [0.0072]
40% Residual Haematocrit (Stewart et al. 1984)	1.47	145.07	21.23	1.02	0.6676 [0.5521]	0.7155 [0.5960]
3% Residual EDTA (Stewart et al. 1984)	1.17	190.84	21.30	1.25	3.4072 [0.0422]	5.7134 [0.0106]
Mouse skin injury (Joiner et al. 1983)	46.21	45.27	4.12	0.17	24.29 [0.8098]	0.0264 [0.9790]
Mouse kidney (Joiner & Johns 1987)	29.18	36.27	5.06	0.15	0.2429 [0.8098]	0.0264 [0.9791]
LD ₅₀ – Colo-rectal injury (2 months) (Terry et al. 1983)	34.39	72.04	5.35	1.52	0.0583 [0.9571]	0.8018 [0.4813]
LD ₅₀ – Colo-rectal injury (15 months) (Terry et al. 1983)	5.49	73.95	8.54	0.17	0.4031 [0.7139]	0.4677 [0.6719]
BR × 1.1 – Lung injury (28 weeks) (Parkins et al. 1985)	3.19	47.82	7.29	0.32	0.7726 [0.4691]	0.9916 [0.3697]
BR × 1.1 – Lung injury (68 weeks) (Parkins et al. 1985)	3.61	39.55	6.74	0.07	0.1283 [0.9021]	0.1771 [0.2837]
LD ₅₀ – Lung injury (28 weeks) (Parkins et al. 1985)	5.81	39.33	5.31	0.40	1.5105 [0.1817]	0.4634 [0.6594]
LD ₅₀ – Lung injury (68 weeks) (Parkins et al. 1985)	3.11	47.12	7.22	0.43	2.1008 [0.0804]	0.7342 [0.4905]
Desquamation – Pig skin injury (Hopewell et al. 1988)	17.72	75.54	3.29	0.17	0.7262 [0.5002]	0.3454 [0.7438]
Necrosis – Pig skin injury (Hopewell et al. 1988)	5.42	100.1	4.21	0.39	3.2473 [0.0228]	0.4723 [0.6566]

statistical methods. Table II shows the result of using the de Boer method to reassess the Fe-derived parameters listed in Table I. No significant variations are observed, suggesting that the use of Fe-plots is justified in this analysis.

A final comment needs to be made on the use of Equation 5 to obtain isoeffective fractionation schemes between high- and low-LET radiotherapy. The equation provides a first estimate of the RBE as a function of low-LET parameters, thus making it simpler to use clinically, but a number of adjustments might in future need to be made to this equation. Ideally, Equation 5 should be extended to consider the different RBE effects produced by the γ -contamination typically existing in a neutron beam since the equation is presently not designed for mixed-LET beams. It is highly likely that the neutron beams used in the experiments considered in this article possessed low-LET photon contamination. However, the applications discussed here, and the consequent clinical implications, do not require such resolution since, at this preliminary level, empirical correlations to “whole beams” are being assessed.

For those treatments where a mixture of radiation types is required it will be necessary to consider the dependency of RBE with LET. In a previous paper (Dale & Jones 1999), the Microdosimetric-Kinetic (MK) model (Hawkins 2003) was suggested as providing a good explanation of this dependency. However, the MK model itself leads to the implication that β is independent of LET. Thus, from what has been suggested in this paper, the philosophy embodied within the MK model itself may need to be reconsidered. In clinical practice, Equation 5 can be used as the first approach to finding the ‘clinical RBE’ (Barendsen [1982b], Wambersie [1999]) and then later readjusted as the result of clinical experience (e.g., dose escalation phase I studies) built up from treatments using that particular high-LET.

Acknowledgements

This work is supported by The Cyclotron Trust.

References

Barendsen GW. 1982a. Dose fractionation, dose-rate and iso-effect relationships for normal tissue responses. *International Journal of Radiation Oncology Biology Physics* 8:1981–1997.

Barendsen GW. 1982b. Radiobiology of neutrons. *International Journal of Radiation Oncology Biology Physics* 8:2103–2107.

de Boer RW. 1988. The use of the D versus dD plot to estimate the α/β ratio from isoeffect radiation damage data. *Radiation Oncology* 11:361–367.

Catterall M, Bewley DK. 1979. *Fast neutrons in the treatment of Cancer*. London: Academic Press.

Catterall M. 1989. Neutron therapy at Hammersmith Hospital 1970 to 1985. A re-examination of results. *Strahlentherapie und Onkologie* 165:298–301.

Dale RG, Jones B. 1999. The assessment of RBE effects using the concept of Biologically Effective Dose. *International Journal Radiation Oncology Biology Physics* 43(3):639–645.

Douglas BG, Fowler JF. 1976. The effect of multiple small doses of X rays on skin reactions in the mouse and a basic interpretation. *Radiation Research* 66:401–426.

Duncan W. 1994. An evaluation of the results of neutron therapy. *Acta Oncologica* 33:299–306.

Fischer DB, Fischer JJ. 1977. Dose response relationships in radiotherapy: Applications of a logistic regression model. *International Journal of Radiation Oncology Biology Physics* 2(7–8):773–781.

Fowler JF. 1989. The linear-quadratic formula and progress in fractionated radiotherapy. *British Journal of Radiology* 62: 679–694.

Goodhead DT. 1977. Inactivation and mutation of cultured mammalian cells by aluminium characteristic ultrasoft X-rays: III. Implications of the theory of dual radiation action. *International Journal of Radiation Biology* 32(1):43–70.

Goodhead DT. 1988. Inactivation and mutation of cultured mammalian cells by aluminium characteristic ultrasoft X-rays. III. Implications for theory of dual radiation action. *International Journal of Radiation Biology* 32(1):43–70.

Hawkins RB. 2003. A microdosimetric-kinetic model for the effect of non-Poisson distribution of lethal lesions on the variation of RBE with LET. *Radiation Research* 160:61–69.

Herring DF. 1980. Methods for extracting dose response curves from radiation therapy data. I. A unified method. *International Journal Radiation Oncology Biology Physics* 6(2):225–232.

Hornsey S, Field SB. 1979. The effects of single and fractionated doses of X-Rays and neutrons on the oesophagus. *European Journal of Cancer* 15:491–498.

Hopewell KW, Barnes DWH, Robbins MEC, Sansom JM, Knowles JF, van den Aardweg GJM. 1988. The relative biological effectiveness of fractionated doses of fast neutrons (42 MeV_{d→Be}) for normal tissues in the pig. I. Effects on the epidermis and dermal vascular/connective tissues. *British Journal of Radiology* 61:928–938.

Joiner MC, Mauhgan RL, Fowler JF, Denekamp J. 1983. The RBE for Mouse Skin irradiated with 3-MeV neutrons: Single and fractionated doses. *Radiation Research* 95:130–141.

Joiner MC, Johns H. 1987. Renal damage in the mouse: The effect of d(4)-Be neutrons. *Radiation Research* 109:456–468.

Joiner MC, Bentzen SM. 2002. Time-dose relationships: The linear-quadratic approach. In: GG Steel, editor. *Basic clinical radiobiology*. 3rd ed. London: Edward Arnold. pp 120–133.

Kellerer AM, Rossi HH. 1972. The theory of dual radiation action. *Current Topics in Radiation Research Quarterly* 8:85–158.

Parkins CS, Fowler JF, Maughan RL, Roper MJ. 1985. Repair in mouse lung for up to 20 fractions of X rays or neutrons. *British Journal of Radiology* 58:225–241.

Stenerlöw B, Petterson O-A, Essand M, Blomquist E, Carlson J. 1995. Irregular variations in radiation sensitivity when the linear energy transfer is increased. *Radiotherapy and Oncology* 36:133–142.

Stewart FA, Soranson J, Maughan R, Alpen EL, Denekamp J. 1984. The RBE for renal damage after irradiation with 3 MeV neutrons. *British Journal of Radiology* 57:1009–1021.

Taylor JMG, Kim DK. 1989. The poor statistical properties of the Fe-plot. *International Journal Radiation Biology* 56(2): 161–167.

Terry NHA, Denekamp J, Maughan RL. 1983a. RBE values for colo-rectal injury after caesium 137 gamma-ray and neutron irradiation. I. Single doses. *British Journal of Radiology* 56: 257–265.

- Terry NHA, Denekamp J, Maughan RL. 1983b. RBE values for colo-rectal injury after caesium 137 gamma-ray and neutron irradiation. II. Fractionation up to ten doses. *British Journal of Radiology* 57:617–629.
- Tucker SL. 1984. Tests for the fit of the Linear-Quadratic model to radiation isoeffect data. *International Journal of Radiation Oncology Biology Physics* 10(10):1933–1939.
- Wambersie A. 1999. RBE, reference RBE and clinical RBE: Applications of these concepts in Hadron therapy. *Strahlentherapie und Onkologie* 175(Suppl. II):39–43.
- Weatherburn CE. 1962. *A first course in mathematical statistics*. 2nd ed, reprinted. Cambridge, UK: Cambridge University Press.

Appendix D

Curriculum Vitae

CURRICULUM VITAE

ALEJANDRO CÁRABE-FERNÁNDEZ

ADDRESS

Department of Radiation Physics and Radiobiology
Charing Cross Hospital
Fulham Palace Road
London W6 8RF
Phone: +44 (0) 208 846 1724
Fax: +44 (0) 208 846 7640
Email: a.carabe@imperial.ac.uk

PERSONAL DETAILS

Gender: Male
Date of birth: September 12th, 1973
Place of birth: Seville, Spain

EDUCATION

- 11/2002–11/2005 PhD Student at Imperial College London
Project title: *Theoretical basis of high-LET radiation therapy and identification of the clinical and radiological instances where such therapy might be of practical benefit.*
Supervisor: Prof. Roger G. Dale
- 09/2000–11/2002 MSc Medical Physics (Medical Scientist) at University of Glasgow.
MSc Thesis: *Use Of An Anthropomorphic Thorax/Heart Phantom To Investigate Different Cardiac SPECT Procedures.*
Supervisor: Dr. T.E. Hilditch.
- 09/1998–06/2000 MPhys Physics with Medical Technology at The University of Hull (2-1 Honors).
MPhys Thesis: *Utilization of electron density data inherent in a CT scan data for radiotherapy treatment planning.*
Supervisor: Dr. Andy Beavis.
- 09/1992–06/1998 General Physics (Courses 1 to 3) at the University of Seville (part-time).

09/1988–08/1992 Bachelor in Science at ‘Colegio San Antonio Maria Claret’ (Seville).

PROFESSIONAL QUALIFICATIONS

Grade A Training in Medical Science achieving the Institute of Physics and Engineering in Medicine (IPEM) Graduate Diploma (*DipIPEM*).

WORKING EXPERIENCE

- 11/2005– Clinical Scientist trainee (AfC Band 7) completing the higher training scheme in the Department of Radiation Physics and Radiobiology (Charing Cross Hospital, London) in order to obtain state registration status.
- 11/2002–11/2005 Appointed ‘Cyclotron Trust Research Fellow’ at Imperial College London (Division of Medicine).
- 09/2000–11/2002 Grade A Trainee at North Glasgow University Hospitals NHS Trust.
- 09/1991–09/1998 School assistant at ‘San Antonio Maria Claret’ school (Part-time).
-

PAPERS AND CHAPTERS

‘The incorporation of the concept of minimum RBE (RBE_{min}) into the linear-quadratic model and the potential for improved radiobiological analysis of high-LET treatments’. Carabe-Fernandez A, Dale RG and Jones B. *Int J Radiat Biol* 83(1):27–39 (2007).

‘Calculation of high-LET radiotherapy dose required for compensation of overall treatment time extensions’. Jones B, Carabe-Fernandez A, Dale RG. *Br J Radiol* 79(939):254–7 (2006).

‘Conventional wisdom and activities of the middle range’. Jones B, Dale RG, Carabe A. *Br J Radiol* 78(936):1119 (2005).

‘The radiobiology of conventional radiotherapy and its application to radionuclide therapy’. Dale RG, Carabe-Fernandez A. *Cancer Biother Radiopharm* 20(1):47–51 (2005).

‘The Oxygen effect’. Jones B, Carabe-Fernandez A, Dale RG. *In: Radiobiological Modelling in Radiation Oncology*. pp.138–157. Dale RG and Jones B (eds.). The British Institute of Radiology (2007).

‘High-LET Radiotherapy’. Jones B, Dale RG, Carabe-Fernandez A. *In: Radiobiological Modelling in Radiation Oncology*. pp.265–275. Dale RG and Jones B (eds.). The British Institute of Radiology (2007).

AWARDS

Workshop Attendance Bursary Award granted by *Cancer Research UK* to attend the 'BEAMnrc WORKSHOP' on Monte Carlo simulation for radiation transport, October 2007, Ottawa, Canada.

Workshop Attendance Bursary Award granted by *Cancer Research UK* to attend the 'IX INTERNATIONAL WORKSHOP ON RADIATION DAMAGE TO DNA', May 2006, Antalya, Turkey.

ATTENDED MEETINGS AND SEMINARS

- *9th Biennial ESTRO Meeting on Physics and Radiation Technology* - Barcelona, Spain, 8–13 September, 2007

Pre-meeting Workshop on: '*Dose Calculation for External Photon and Electron Beam Therapy, today and in the future*'.

- *UK Research Network on Biomedical Applications of MeV Ion Beams* - University of Surrey, Guildford. 30th July–2nd August, 2007
 - *DNA Repair: Therapeutic Implications* - British Institute of Radiology (London, UK) 3rd March, 2005
 - *UK Research Network on Biomedical Applications of MeV Ion Beams* - Christie Hospital (Manchester) 25th January, 2005
 - *40th PTCOG* - Orsay (France) June 16-18, 2004
 - *Association for Radiation Research 2004 Meeting* - Missenden Abbey (Buckinghamshire, UK) 12th-14th May, 2004
 - *Advances in Radiotherapy Technology - Real or Virtual* - British Institute of Radiology (London, UK) December, 2003
 - *Clinical Radiobiology* - Royal Marsden Hospital (London, UK) 10th July, 2003
 - *38th PTCOG* - Chester (UK) May 14-16, 2003
 - *Association for Radiation Research 2003 Meeting* - Oxford University (UK) February, 2003
-

COMPUTER SKILLS

I have a sound knowledge in a wide cross-section of computer languages and programmes including C++, L^AT_EX Mathematica together with all the Microsoft packages

LANGUAGE KNOWLEDGE

Spanish	Native
English	Good command of the English Language

REFERENCES

Prof. Roger G Dale

Thesis supervisor	Phone: +44 (0) 208 846 1726
Radiation Physics and Radiobiology	Fax: +44 (0) 208 846 7640
Charing Cross Hospital	Email: r.dale@imperial.ac.uk
London W6 8RF	

Prof. Bleddyn Jones

Oncology Department	
Queen Elizabeth University Hospital	Email: B.Jones.1@bham.ac.uk
Birmingham B15 2TH	